Advanced Polymers with Ge=Ge Double Bonds

Dissertation

zur Erlangung des Grades
des Doktors der Naturwissenschaften
der Naturwissenschaftlich-Technisschen Fakultät
der Universität des Saarlandes

von

Anna-Lena Thömmes

Saarbrücken
2025

Tag des Kolloquiums:	29.08.2025
Dekan:	Prof. Dr.-Ing. Dirk Bähre
Berichterstatter:	Prof. Dr. David Scheschkewitz
	Prof. Dr. Dominik Munz
	Prof. Dr. Holger Helten
Vorsitz:	Prof. Dr. Christopher W. M. Kay
Akademischer Mitarbeiter:	Dr. Bernd Morgenstern

The present dissertation was prepared in the time between February 2021 and May 2025 at the Institute for General and Inorganic Chemistry of the Faculty of Natural Sciences and Technology at Saarland University under the supervision of Prof. Dr. David Scheschkewitz.

Die vorliegende Dissertation wurde in der Zeit zwischen Februar 2021 und Mai 2025 am Institut für Allgemeine und Anorganische Chemie der Naturwissenschaftlich-Technischen Fakultät an der Universität des Saarlandes unter der Aufsicht von Prof. Dr. David Scheschkewitz erstellt.

„Und die Ida hatte doch recht.“

– Otto Hahn über Ida Noddack

Zusammenfassung

Der Einbau anorganischer Hauptgruppenelemente in organische π-konjugierte Grundgerüste hat erheblichen Einfluss auf die elektronische Struktur dieser Hybrid-Polymere und somit auf deren Anwendbarkeit in (opto-)elektronischen Bauteilen. Die erstmalige Synthese eines Polymers mit Ge=Ge-Doppelbindungen in einer Metathese schwererer acyclischer Diene (HADMET) bildet einen wichtigen Schritt in Richtung anwendungsspezifischer Materialien. In dieser Arbeit wurden innovative Poly(digermene) mit hoher Löslichkeit und hohen Polymerisationsgraden entwickelt sowie deren Abscheidung in dünnen Filmen. Um mögliche Funktionalisierungsstrategien zu entwickeln, wurde das Schlüsselintermediat stabilisiert, und zwar entweder mit einem N-heterocyclischen Carben (NHC) oder einem cyclischen (Alkyl)(amino)carben (CAAC), wodurch ein präzedenzloses CAAC-Bis(germen) mit Ge=C-Doppelbindungen entstand. Das NHC-Bis(germylen) erlaubt die Synthese von Poly(digermenen) unabhängig von den strukturellen Restriktionen des HADMET-Verfahrens, wodurch sich grundlegend neue Möglichkeiten zur Funktionalisierung und Copolymerisation ergeben. In Modellsystemen erwies sich das sperrige nukleophile CAAC als geeignet für das Endcapping der reaktiven Ge(II)-Zentren, während Heteroallene selektive Rückgrat-Funktionalisierung zeigen. Aus einem so erhaltenen NHC-Bis(acylgermylen) wird ein einzigartiges CAAC-radikal-substituiertes Germylen hergestellt – ein potentieller Prototyp für entsprechende (Poly-)radikale.

Abstract

Inorganic main group elements in inorganic-organic hybrid polymers with covalently doped π-conjugated frameworks exert significant influence on the electronic structure – with implications for the use in (opto-)electronic devices. On the pathway towards purpose-built materials, the recently reported heavier acyclic diene metathesis (HADMET) represents a milestone providing the first polymer with Ge=Ge double bonds. In this thesis, advanced poly(digermene)s with high solubility and high degrees of polymerization are developed and deposited as thin films. Functionalization strategies are elaborated based on the key intermediate of the polymerization, which is either stabilized with a cyclic (alkyl)(amino)carbene (CAAC), providing an unprecedented CAAC-bis(germene) with Ge=C double bonds, or with an N-heterocyclic carbene (NHC). Employing the NHC-bis(germylene) as precursor, a novel route towards poly(digermene)s is developed, which overcomes the structural limitations of the HADMET process and hence unlocks huge potential for the design of functionalized derivatives and copolymers. As demonstrated with model systems, the bulky nucleophilic CAAC might be suitable for end-capping of the reactive Ge(II) centers, whereas heteroallenes could allow for selective backbone functionalization. Radical-fragmentation of an NHC-bis(acylgermylene), thus obtained, yields a unique germylene with a tethered CAAC-radical as potential prototype of corresponding (poly-)radicals.

List of Publications

This thesis has been published in parts in:

- A.-L. Thömmes,* T. Büttner, B. Morgenstern, O. Janka, G. Kickelbick, B.-J. Niebuur, T. Kraus, M. Gallei, D. Scheschkewitz,* Near-Infinite-Chain Polymers with Ge=Ge Double Bonds. *Angew. Chem. Int. Ed.* **2024**, *63*, e202415103.

  https://doi.org/10.1002/anie.202415103

  German Version: Nahezu unendlich lange Polymere mit Ge=Ge-Doppelbindungen. *Angew. Chem.* **2024**, *136*, e202415103.

  https://doi.org/10.1002/ange.202415103

- A.-L. Thömmes, B. Morgenstern, M. Zimmer, D. M. Andrada, D. Scheschkewitz,* σ,π-Conjugated Bis(germylene) Adducts with NHC and CAACs, *Chem. Eur. J.* **2023**, *29*, e202301273.

  https://doi.org/10.1002/chem.202301273

- A.-L. Thömmes, R. Völker, B. Morgenstern, M. Zimmer, D. Munz, C. W. M. Kay, D. Scheschkewitz,* Silagermylenation of C=O bonds and radical fragmentation of CO_2-expanded bis(germylene) by a cyclic (alkyl)(amino)carbene, *Inorg. Chem. Front.* **2025**, *12*, 4835-4843.

  https://doi.org/10.1039/D5QI00678C

The introduction will be submitted as a Review in Angewandte Chemie:

- A.-L. Thömmes,* D. Scheschkewitz,* Conjugated Inorganic-Organic Hybrid Polymers with p-block Elements, *Angew. Chem. Int. Ed.* **2025**, *manuscript in preparation*.

Other publications:

- L. Klemmer, A.-L. Thömmes, M. Zimmer, V. Huch, B. Morgenstern, D. Scheschkewitz,* Metathesis of Ge=Ge double bonds. *Nat. Chem.* **2021**, *13*, 373.

  https://doi.org/10.1038/s41557-021-00639-9

- E. Quraishi,* A.-L. Thömmes,* Regionales Stipendiat:innentreffen 2022 des VCI/FCI in Mainz. *Nachrichten aus der Chemie* **2022**, *70*, 83.

  https://doi.org/10.1002/nadc.20224131488

Acknowledgements/Danksagung

Zunächst gilt mein herzlicher Dank **Prof. Dr. David Scheschkewitz** für die Möglichkeit, meine Doktorarbeit zu dieser interessanten und spannenden Themenstellung unter seiner Betreuung anzufertigen. Ich möchte ihm außerdem besonderen Dank dafür aussprechen, dass er mir stets großes Vertrauen entgegengebracht hat und mir die Freiheit gegeben hat, die Projekte eigeninitiativ und eigenständig zu planen und durchzuführen, wobei er meine Arbeit durch seine Bereitschaft zu kritischen Diskussionen und durch hilfreiche Kritik und Ideen vorangebracht hat. Ich bedanke mich auch für die zahlreichen Möglichkeiten, meine Forschungsergebnisse auf internationalen Konferenzen zu präsentieren.

Ebenfalls möchte ich mich herzlich bei **Prof. Dr. Dominik Munz** bedanken, dass er sich bereit erklärt hat, das Zweitgutachten für diese Arbeit zu erstellen und für die stetige Bereitschaft zu kritischen Diskussionen.

Ich bedanke mich außerdem beim **Fonds der Chemischen Industrie** des Verbands der Chemischen Industrie e. V. für die finanzielle und ideelle Förderung im Rahmen eines Kekulé Promotionsstipendiums.

Thanks to the current and former members of the Scheschkewitz group for constructive, interesting and helpful discussions with many of you and for the good times at conferences and during coffee, beer or noodle & protein breaks. Thank you, **Dr. Carsten Präsang, Ankur, Luisa Giarrana, Peter A. M. Spies, Philipp Grewelinger, Daniel Mühlhausen, Thomas Büttner**, **Marc Hunsicker**, **Nasrina Parvin, Henrike Waller, Dr. Paresh Kumar Majhi**, **Dr. Lukas Klemmer**, **Dr. Nadine Poitiers, Dr. Yvonne Kaiser**, **Dr. Kinga Leszczyńska**, **Dr. Yannic Heider**, **Liane Müller, Michel Bollmann (Böhmi), Tim Wiesmeier, Kashish, Dominika Posse, Emily Elisa Klein, Dr. Andreas Rammo, Dr. Michael Zimmer, Andreas Kell**, **Bianca Ianuzzi**, **Andreas Adolf**, **Eveline Altmeyer**, **Britta Schreiber, Lu Huang, Nadzeya Brezhneva, Robin Völker, Vanessa Grabowski, Leonie Wirtz, Hannah Theis, Wilma Isabel Koblé**.

Prof. Dr. Christopher W. M. Kay möchte ich für die Möglichkeit danken, jederzeit verschiedene EPR-Experimente durchführen zu dürfen und für interessante Diskussionen.

Bei **Dr. Daniel Rauber** möchte ich mich für die Einführung in die DOSY-NMR-Spektroskopie und die ersten Messversuche an meinen Polymeren bedanken.

Prof. Dr. Johann Jauch, Dr. Bart-Jan Niebuur, Prof. Dr. Gregor Jung, Dr. Samuel Pearson und **Prof. Dr. Markus Gallei** danke ich für interessante und aufschlussreiche Diskussionen während meiner Zeit als Doktorandin und während des Studiums.

Dr. Lukas Klemmer möchte ich besonders für die Betreuung meiner Vertiefungsarbeit, während der er meine Faszination für die anorganische Molekülchemie gefördert hat und meine Begeisterung für die Forschung an niederkoordinierten Germanium-Verbindungen geweckt hat, bedanken. Danke für Dein Vertrauen in mich und Dein stetiges Interesse an meiner Forschung.

Danke an **Robin Völker**, der mir sein Vertrauen für die Betreuung während seiner Bachelorarbeit, seines Vertiefungspraktikums und seiner HiWi-Zeit im Arbeitskreis entgegengebracht hat und der in dieser Zeit einige spannende Resultate erzielt hat.

Danke an **Dr. Bernd Morgenstern** für die Kristallstrukturanalytik, inklusive aller Messungen, für die galt „das do woar leider nix, Anna-Lena“, und für deine hochgeschätzte Gründlichkeit. Ich danke Dir sehr für dein unermüdliches Interesse an meiner Arbeit, für zahlreiche interessante fachliche Diskussionen, auch über mehrere Tage hinweg, und für lange Gespräche „zwischen Tür und Angel“.

Dr. Carsten Präsang möchte ich für sein stetiges Interesse an meiner Arbeit und seine fachliche, administrative und menschliche Unterstützung danken, für die Einführung und Betreuung des Glovebox-Teams und dass er immer mit Ruhe und Humor Lösungen für jedes noch so verrückt erscheinende Problem findet.

Den Mitgliedern und Ehemaligen des **JungesChemieForums (JCF) Saar** aus meiner aktiven JCF-Zeit danke ich für die gemeinsame Zeit, die wir mit viel Leben gefüllt haben und durch viele neue Ideen, unterhaltsame gemeinsame Abende inklusive etlicher bereichernder Diskussionen und durch zahlreiche spannende Vorträge und Exkursionen zu einer wertvollen gemacht haben. Ich hoffe, dass der besondere Zusammenhalt im JCF Saar weiterlebt.

Dr. Diego Andrada möchte ich für viele interessante und anregende Diskussionen danken – auch während unserer Läufe – und für den stetigen sportlichen Ansporn durch anspruchsvolle gemeinsame Trainingseinheiten.

Danke **Mara Heitmann**, **Tim Brachmann, Yvonne Ritter, Daniel Mühlhausen**, **Viktoria Kiefer, Stavroula Pachoula, Laura Thilmont** und **Jeremy Arweiler**! Ihr habt die Zeit an der Universität des Saarlandes zu einer spannenden, interessanten und vor allem auch sehr spaßigen Zeit gemacht und mit euch waren die Laborpraktika und Prüfungen eine besonders erlebnisreiche und schöne Erfahrung, die mir immer in guter Erinnerung bleiben wird.

Luisa Giarrana, Ilgin Demirer, Inga-Alexandra Bischoff, Sergi Danés, Julian Messelberger, Jan Rettig, **Enric Sabater Berzal, Dennis Welterlich, Emiliano Martínez-Vollbert, Martí Gimferrer, Dajana Momper und Nicola Marigo** for good times during beers or runs and deep and random discussions about chemistry, life and everything under the sun.

Ganz besonders möchte ich **Simon Petrus Muhm** danken für seine Unterstützung und sein bemerkenswertes Verständnis in sämtlichen Lebenslagen. Ich danke Dir auch ganz besonders für die vielen anregenden und aufschlussreichen Diskussionen. Danke M!

Ein ganz besonderer Dank gilt vor allem dem „Stammtisch“: **Walli, Luise** und **Lauri**! Ich bin Euch unendlich dankbar für Eure immerwährende Freundschaft, für Eure Unterstützung in allen Lebenslagen, für viele bereichernde Gespräche, Eure herzliche Art und auch für Euer Verständnis, wenn ich mal wieder nicht bei Euch, sondern im Labor war.

Meiner gesamten Familie, insbesondere meinen Eltern **Claudia** und **Peter Thömmes** sowie meinem Bruder **Markus Thömmes** möchte ich an dieser Stelle herzlich dafür danken, dass sie mir seit jeher zur Seite stehen und mich immer in jederlei Hinsicht und nach bester Möglichkeit unterstützen. Besonders möchte ich auch meiner Oma **Hildegard Thömmes** danken, die mir mein ganzes bisheriges Leben mit ihrer besonders herzlichen Art bedingungslos zur Seite stand und mir immer wieder bewusst gemacht hat, worauf es ankommt. Ich vermisse Dich.

Table of Contents

Zusammenfassung ..... **IX**

Abstract ..... **XI**

List of Publications ..... **XIII**

Acknowledgements/Danksagung ..... **XV**

Introduction **1**

Single heteroatoms embedded in the main chain 3

Group 13: Poly(gallane)s & recent developments of poly(borane)s 3
Group 14: Rise of the heavier elements in hybrid poly(tetrelane)s 9
Group 15: Recent advances in poly(pnictane)s 19

Diheteroatomic multiple bonds embedded in the main chain 31

Group 13: B=N bridges in conjugated hybrid polymers 31
Group 14: Towards poly(tetrelene)s and poly(ditetrelene)s 38
Group 15: Polymers with P=C and P=P in the conjugation path 43

Aims and Scope **46**

Results and Discussion **48**

Near-Infinite-Chain Polymers with Ge=Ge Double Bonds 48

σ,π-Conjugated Bis(germylene) Adducts with NHC and CAACs 61

Silagermylenation of C=O bonds and radical fragmentation of CO_2-expanded bis(germylene) by a cyclic (alkyl)(amino)carbene 71

Conclusions and Outlook **82**

References **90**

Supporting Information **107**

Near-Infinite-Chain Polymers with Ge=Ge Double Bonds 108

σ,π-Conjugated Bis(germylene) Adducts with NHC and CAACs 203

Silagermylenation of C=O bonds and radical fragmentation of CO_2-expanded bis(germylene) by a cyclic (alkyl)(amino)carbene 247

Introduction

Organic polymers are characterized by their unmatched versatility, as manifest in the variety of applications for almost every aspect of our lives and in the continuously increasing yearly production.[1-7] Conjugated derivatives have become particularly important with regard to applications in (opto-)electronic devices,[8-10] a development that culminated in the award of the Nobel Prize in Chemistry in 2000 to A. J. Heeger, A. G. MacDiarmid and H. Shirakawa “for the discovery and development of conductive polymers”.[11] The advantageous mechanical properties in combination with semiconductivity and high charge carrier mobilities of some organic electronics even outperform the bulk silicon- and germanium-based congeners.[12] Well-known examples of polymer-based electronics include organic light emitting diodes (OLEDs),[13-16] organic solar cells (OSCs),[17-20] organic field effect transistors (OFETs)[21-23] and capacitors,[24] as well as medical and pharmaceutical devices, such as artificial muscles and bio/chemosensors.[25-32] Apart from light weight and (often) flexibility, low-cost production and low toxicity, polymer electronics offer crucial advantages, such as facile processability and disposal as well as possibilities for modular combination and customized structural design. The ongoing expansion of the library of accessible structural motifs increasingly allows for purpose-built materials with specific energy band levels, and adjustable charge generation and transport properties.

In recent years, band gap tuning by covalent doping of organic polymers with typical inorganic main group elements has come to the fore. The incorporation of main group heteroelements apart from the typically applied organic representatives (N, O, S, Se) and tellurium into the main chain of these inorganic-organic hybrid polymers brings about considerable modifications of the electronic and geometric structure and hence offers a variety of possibilities for adjusting the photophysical and electronic properties.[33-40] Band gap tuning is either achieved *directly* through incorporation of the heteroelement as part of the conjugation path or *indirectly* by favorable interaction with the covalently bonded heteroelement in the backbone of the organic π-system. As a consequence of the differences in the electronic structures of the heteroelement motifs, variable types of conjugation have been realized in both cases with implications for the photophysical properties, the reactivities and the adjustability through post-

functionalization. In Group 13, the empty p-orbital of the sp^2-hybridized heteroatom center is crucial for the interaction with the extended π-system, allowing for p,π-conjugation between the inorganic and the organic part. In Group 14, the typically low-lying σ^*-orbitals of sp^3-hybridized moieties act as electron-accepting groups, resulting in σ,π-conjugation. Pnictogen motifs are characterized by lone-pairs of electrons, constituting electron-donating groups for n,π-conjugation.

The introduction of single heteroatoms into the main chain of conjugated polymers is comparably well-established. In the case of Group 13, numerous representatives, most often containing boron, have been reported and reviewed in detail over the past two decades.[41-61] In the following, an overview of the less investigated poly(gallane)s and of the newest developments in the very active field of poly(borane)s is provided. In Group 14 chemistry, the heavier elements are also on the rise,[62] beginning to complement the vast variety of the well-known lighter poly(silane)s.[33,63-70] While the most prominent examples, the poly(silole)s, are hence only briefly introduced with references to corresponding reviews,[65-66,68-69,71-79] a broad overview of the different types of reported germanium-based derivatives is given. Details on recent developments and on the far less investigated poly(stannane)s are provided and ditetrelane-bridged congeners are introduced. Poly(phosphane)s have also been a major research focus in the past decades.[33,80-85] Recently reported derivatives and their post-functionalization are discussed as well as poly(arsane)s, which have been at the center of research more recently.[86]

Conjugated polymers with multiply bonded heteroatom motifs in the main chain are by far less common in comparison. Poly(iminoborane)s containing zwitterionic B=N bonds with partial double bond character are nonetheless quite frequent. In the case of Group 14 and 15, however, there are only very few representatives, including exclusive examples with element-element double bonds, despite the development of a wide range of unsaturated compounds of the heavier p-block elements.[87-103]

Single heteroatoms embedded in the main chain

Group 13: Poly(gallane)s & recent developments of poly(borane)s

The overwhelming majority of studies employ boron as electron-deficient Group 13 element, which is presumably due to the ease of synthesis and enhanced air and moisture stability of the resulting compounds compared to the heavier congeners.

The only known aluminum-based examples at present contain porphyrin or salen ligands employing N–Al–N and O–Al–O moieties, respectively, in the otherwise organic π-conjugated main chain.[104-106] The resulting microporous structures allow for CO_2 capture (~ 8 wt%)[104] and applications as efficient catalysts in the conversion of CO_2 to carbonates. Salen-coordinated gallium oligothiophene copolymers were obtained previously through electropolymerization of the corresponding monomers with thiophene end groups.[107] The O–Ga–O containing polymer with four-coordinate cationic gallium centers served as a precursor for Ga_2S_3 nanoparticles, in contrast to the corresponding neutral five-coordinate derivative. The metal centers, however, do not contribute to the conjugation in these systems and only act as Lewis acidic reaction sites,[108-109] as also known for related boron-based polymers.[110-111]

In poly(gallane)s **1** and **2** with arylene bridges (Figure 1), obtained by transition metal catalyzed C–C coupling of the corresponding bifunctionalized monomers, the gallium centers are directly incorporated into the conjugation path.[112] Despite the small degrees of polymerization (**1**: X_n = 7, **2**: X_n = 10), the comparison of the UV absorption of **1** (λ_{abs} = 275 nm) to those of the corresponding monomer (λ_{abs} = 240 nm), of a monomeric model compound with a biphenyl substituent at gallium (λ_{abs} = 260 nm) and of the dimer (λ_{abs} = 270 nm) revealed a substantial and systematic bathochromic shift. DFT calculations on a molecular model compound confirmed the delocalization of the lowest unoccupied molecular orbital (LUMO) across the gallane center. Incorporating gallium into fluorene scaffolds as in copolymers **3a–g** provokes variable red-shifts of the UV/Vis absorptions (λ_{abs} = 330 to 480 nm) depending on the employed electron-deficient comonomer units.[113] The most red-shifted absorptions were obtained for cyclopentadithiophene (**3e**), ethynylene-substituted benzotriazole (**3f**) and benzothiadiazole (**3g**) linking units. As a result, the fluorescence of **3a-g** covers the whole range of the visible spectrum (Figure 1). In the case of **3e,f**, additional red-shifted

bands assigned to intermolecular transitions were observed in thin films (and a concentrated solution of **3f**), possibly because of the enhanced planarity through the extended π-bridges and intermolecular interactions established through additional S- and N-centered lone-pairs of electrons.

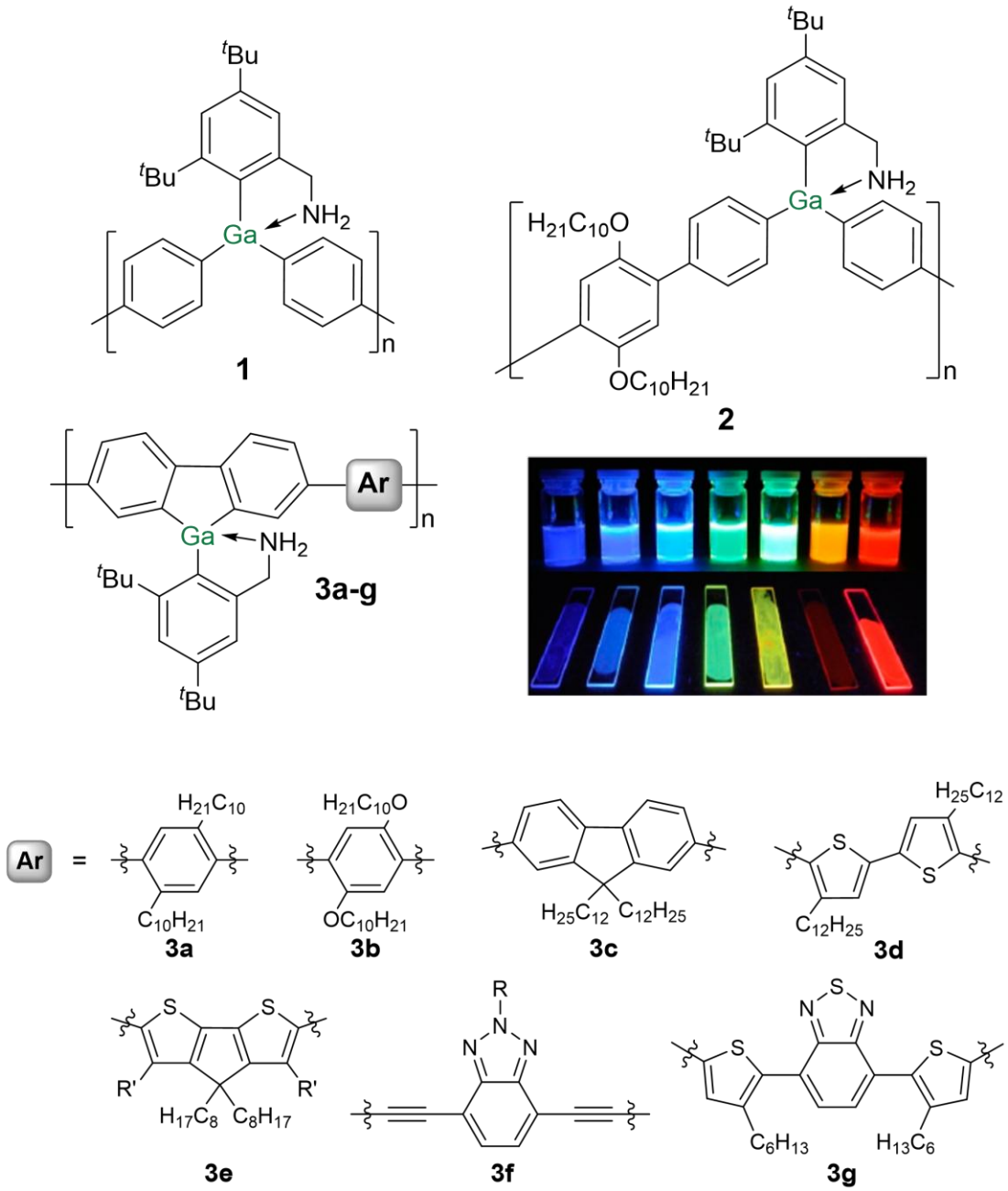

Figure 1. Structures of arylene-bridged poly(gallane)s **1** and **2** and poly(gallafluorene)s **3a-g** (R = 2-decyl-tetradecane). Picture of solutions and thin films of polymers **3a-g** under UV irradiation, adapted with permission from Ref. [113], copyright © 2015 American Chemical Society.

Recently, Ohshita *et al.* investigated the differences in the electronic structures, the resulting optical properties and Lewis base coordination of poly(dithienoborepin)s **4** and **5** with fused dihexoxybenzenes in the backbone (Figure 2).[114] The two regioisomers **4** and **5** were obtained by Stille cross-coupling of the corresponding distannyl- and dihalo-substituted monomers. The Hückel aromatic borepin scaffold with sterically protecting and electron-rich fused thiophene rings shows air and water stability.[115] Both poly(borepin)s exhibit characteristic conjugation along the main chain, manifest in significant bathochromic shifts of the absorption (λ_{abs} = 450 nm) and fluorescence (**4**: λ_{em} = 525, **5**: λ_{em} = 500 nm) compared to the monomers (λ_{abs} = 390 nm, λ_{em} = 420 to 430 nm). Thin films of **4** and **5** evoke additional red-shifts by $\Delta\lambda$ = 10 to 90 nm, presumably due to intermolecular interactions in the solid state. As expected and previously described for structurally related thiophene fused borepin polymers,[115-116] the conjugation path in polymer **5** with the sulfur atoms in β-position to boron, leads along the backbone rather than the boron centers. The frontier orbitals show major contributions of the benzene backbone and, in the LUMO, no discernible contribution at the boron centers is found, in stark contrast to **4** where the sulfur atoms are in α-position to boron. Unsurprisingly, the cross-conjugated position of boron in **5** exerts a smaller influence than the fully π-conjugated position in **4**. As a consequence, cyanide coordination at the boron centers leads to significant changes in the optical properties in the case of **4** (Figure 2), while the spectra of **5** are considerably less affected. For both, **4** and **5**, hypsochromically shifted ($\Delta\lambda$ ~ 100 nm) absorption bands appear after cyanide addition, yet in the case of **4**, their intensity is significantly weakened and an additional broad bathochromically shifted band with an onset at λ_{abs} ~ 650 nm was observed, presumably due to charge transfer transitions from the tetracoordinate boron centers. Accordingly, the fluorescence of cyanide-coordinated **4** is also bathochromically shifted, from green to orange emission ($\Delta\lambda$ = 130 nm, Figure 2), while the emission maximum of **5** is not influenced. The weaker donor pyridine induces similar effects. Notably, UV/Vis absorption and emission vanish completely upon cyanide addition to the corresponding monomers, due to interruption of the conjugation and the lack of similar CT transitions.

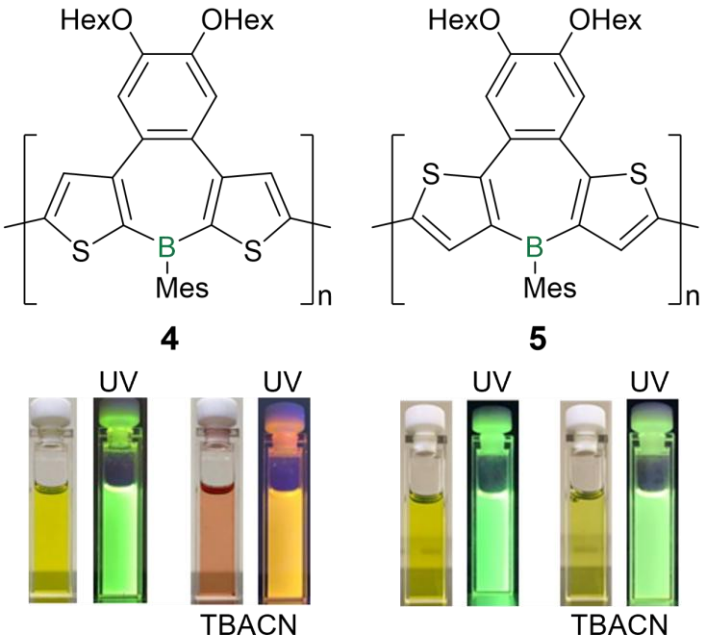

Figure 2. Top: Structures of regioisomeric poly(dithienoborepins)s **4** and **5**. Bottom: Appearances under ambient light and UV light, respectively, before and after addition of two equivalents of tetrabutylammonium cyanide (TBACN), adapted with permission from Ref. [114], copyright © 2021 Royal Society of Chemistry.

Pu and Ren *et al.* reported on the coordination of pyridine derivatives to the boron centers in poly(trithienylborane) networks, in which the boron atoms act as bridging atoms between the 2-positions of thiophene rings and are thus incorporated in the conjugation path.[117] In these cases, the donor coordination provoked a hypsochromic shift of the emission (by $\Delta\lambda$ = 60 nm from λ_{abs} = 660 nm) through inhibition of the conjugation across the previously vacant boron p-orbitals. A cross-linked derivative was applied as a photocatalyst for hydrogen production.

These studies demonstrate the potential of heteroelement-based conjugated polymers for the (potentially reversible) tuning of the band gap: small changes in the chemical environment of the heteroelement, such as the coordination of a nucleophile, exert considerable influence on the optical properties of the materials. The responsiveness of the materials towards such changes can be controlled, for example by using different regioisomers.

Similarly, bora-substitution next to the thiophene rings in 2-position in poly(dithienoborane)s **6a,b** (Figure 3) results in more effective conjugation between the π-system and the empty p-orbitals at the boron centers in comparison to

substitution in 3-position in the corresponding regioisomers **7a,b**.[118] The LUMO levels and thus the energy gap to the mostly unaffected highest occupied molecular orbital (HOMO) are substantially decreased in **6a,b**, resulting in huge bathochromic shifts of the absorption maxima by $\Delta\lambda$ = 100 to 125 nm compared to those of **7a,b**. Although not explicitly discussed by the authors, the somewhat smaller shifts of the fluorescence maxima by $\Delta\lambda$ = 25 to 70 nm and accordingly smaller Stokes shifts in the case of **6a,b** might result from structural relaxation of the excited states of **7a,b**: The aryl substituents at the boron centers (R in Figure 3), which are perpendicular to the thiophene rings in the electronic ground state according to the single crystal X-ray structures of corresponding monomers, could approach a more favorable conformation closer to coplanarity, in line with the slightly broader emission bands of **7a,b** compared to those of **6a,b** (Figure 3). Formal substitution of the *tert*-butyl groups of the supermesityl substituent Mes* (**6a**,**7a**) by CF_3 groups (**6b**,**7b**) allows for a more delicate fine-tuning, providing smaller red-shifts of the absorption and emission in the range of $\Delta\lambda$ = 2 to 50 nm.

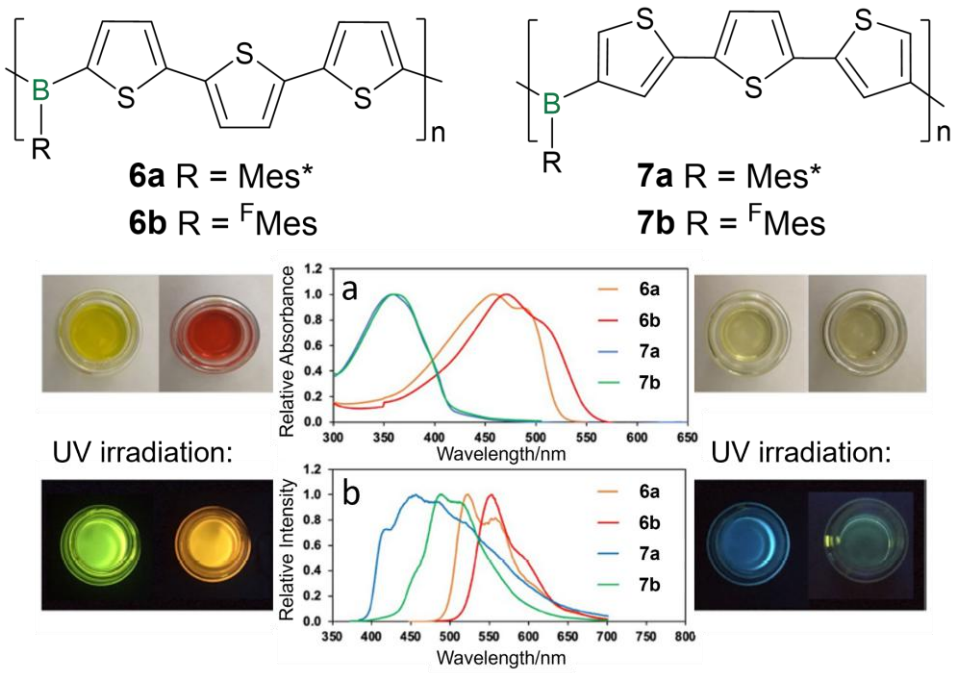

Figure 3. Top: Structures of regioisomeric poly(dithienoborane)s **6a,b** and **7a,b** (Mes* = 2,4,6-tri-*tert*-butylphenyl, FMes = 2,4,6-tris(trifluoromethyl)phenyl). Bottom: Appearances under ambient light and UV light and corresponding representative absorption (a) and fluorescence spectra (b), adapted with permission from Ref. [118], copyright © 2023 Wiley VCH.

Adachi and Ohshita *et al.* employed a sulfur-bridge to enforce coplanarity of the thiophene rings,[119] a generally favorable feature to enable efficient charge transport in semiconducting thin-film materials.[120] In compounds **8** and **9** (Scheme 1), the introduction of the aromatic thiaborin ring results in the stabilization of the HOMO and a hypsochromic shift of the absorption by $\Delta\lambda$ = 30 to 40 nm in comparison to unbridged derivatives.[121-122] Nonetheless, considerable conjugation is established by huge bathochromic shifts of $\Delta\lambda$ = 50 to 180 nm compared to the monomer and model compounds and depending on the presence of the silole moiety, which induces a red-shift by $\Delta\lambda$ = 90 nm from **8** to **9** by further increasing the system's planarity and thereby the conjugation cross section. In addition, the enhanced planarity also induces π-stacking in thin films of the resulting polymers **8** and **9** (Scheme 1) due to π-π and S-S interactions. The aggregate formation was suggested to explain the appearance of additional red-shifted absorption bands and shoulders between λ_{abs} = 500 and 600 nm in the solution and thin film UV/Vis spectra, respectively. In line with that, these absorption bands remained unobserved in solutions of **8** and **9** that had been filtered through 0.2 µm membrane filters. Notably, the corresponding monomers with considerably shorter π-systems showed no indication of intermolecular stacking. While the polymers **8** and **9** exhibit intense green fluorescence in solution (λ_{em} = 530 to 560 nm) and red fluorescence in thin films (λ_{em} = 670 to 690 nm), the monomers only exhibit weak fluorescence at room temperature but blue-green phosphorescence at 77 K. Very recently, the same group reported room temperature phosphorescence in solution and in the solid state through introduction of $BiPh_2$ end groups in the conjugation path of thiophene-substituted boranes to enhance intersystem crossing.[123]

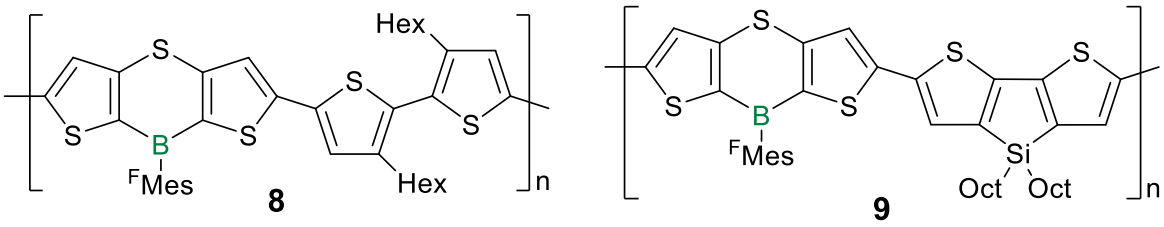

Scheme 1. Structures of alternating dithienoborane copolymers **8** and **9** with bisthiophene and dithienosilole units, respectively, and sulfur-bridges connecting the thiophene rings in the borane units (^{F}Mes = 2,4,6-tris(trifluoromethyl)phenyl).

Group 14: Rise of the heavier elements in hybrid poly(tetrelane)s

Simple poly(silane)s exhibit σ-conjugation due to low-lying σ*-orbitals at the tetracoordinate silicon atoms, resulting in semiconductivity and UV light absorption and emission.[65,124-125] These materials have been known for decades and have been applied in various fields, for instance, as photoresist and adhesion-supporting materials in coatings and microlens arrays, as sensors for the detection of explosives, as radical reaction initiators or as hydrogen storage materials and, most importantly, in conducting or semiconducting devices, such as OLEDs or OSCs.[126-129] The semiconducting properties are, however, dependent on the conformation of the Si–Si bonds, which influences the conjugation along the polymer chain[124-125,130] – in vast contrast to mostly planar π-conjugated materials.

Combinations of σ- and π-conjugation were explored in anticipation of potential fine-tuning of the band gaps by simple changes in the repeat units' structures. In heavier analogues of pyrroles and related compounds, such as fluorenes, the heteroelement influences the HOMO-LUMO gap *indirectly* through σ*-π* mixing of low-lying σ*-orbitals (Figure 4), resulting in smaller band gaps due to a general decrease of the LUMO levels and, to a lesser extent, the HOMO energies.[33,71,131-132] For instance, the formal substitution of the CH_2 group in cyclopentadiene for a SiH_2 group was calculated to lower the LUMO level by 1.29 eV and the HOMO by only 0.44 eV.[71]

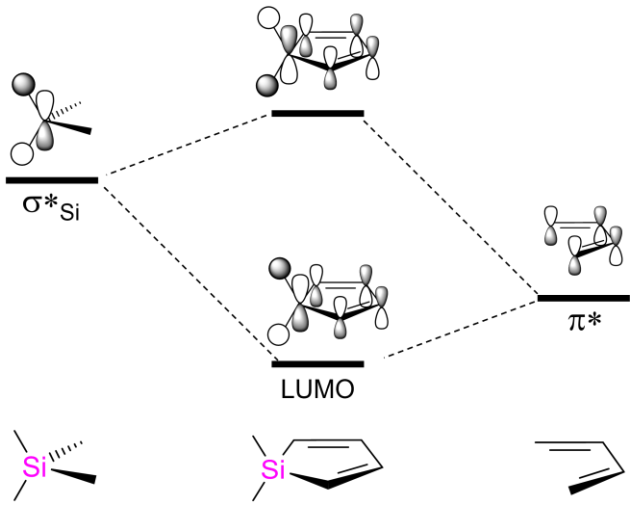

Figure 4. Qualitative orbital correlation diagram for 1,1-dimethylsilole based on PM3 calculations by Tamao *et al.*[71]

Poly(silole)s or derivatives thereof containing phenylene, acetylene or thiophene spacers are the most prominent representatives and have shown superior performance in electronic devices compared to pure organic congeners.[66,68-69,71-74] Numerous examples have been isolated and in some cases applied to OLEDs, OSCs and OFETs due to their high charge carrier mobilities.[75-77] Poly(silole)s typically show blue fluorescence and their rigid propeller-like structure prevents quenching of emission and allows for aggregation-induced fluorescence, rendering them useful as bio/chemosensors.[65,78-79]

Germanium analogues often exhibit even superior electronic properties and a better chemical stability than silicon congeners.[74,133-136] There are different types of poly(germole)s according to the ring positions of the atoms connecting the monomer units. For instance, Tilley *et al.* have reported the ring-bridged poly(2,5-diphenylgermole) **10** (Scheme 2) and related oligomers, which exhibit green fluorescence (λ_{em} = 490 to 500 nm) and absorption in the visible range (λ_{abs} = 400 to 440 nm).[137] The considerable lower LUMO energy induced by the presence of germanium in the backbone results in remarkable bathochromic shifts (by up to $\Delta\lambda$ = 80 nm for the absorption) with increasing chain length, in particular compared to the corresponding monomeric model compounds, which show blue fluorescence (λ_{em} = 450 to 460 nm) and absorb in the UV (λ_{abs} = 360 to 380 nm). The polymer **10** is prepared by nickel-mediated C–C coupling of dihalides of the 2,5-diphenylgermole monomer, in turn obtained through metallacycle transfer of the corresponding zirconacyclopentadiene with $GeCl_4$. This kind of transmetalation chemistry of metalacyclic structures has been applied for the construction of various poly(heterole)s in the following years (*vide infra*). Conveniently, the transmetalation is typically implemented as post-functionalization as, for instance, in the synthesis of poly(2,4-diphenylgermole) **11** for which a titanacyclopentadiene polymer is transmetalated with $GeCl_4$.[138] Random copolymer **12** constitutes an exceptional example in which the repeat units are connected *via* the germanium atoms.[139] It was obtained by polycyclotrimerization of the diacetylene-substituted germole with 1-octyne. In contrast to typical poly(heterole)s, the direct incorporation of the germanium into the conjugation path results in a strongly red-shifted absorption band in the visible range at λ_{abs} ~ 540 nm. While this was taken as a hint towards extended conjugation *via* σ,π-interactions between the arylene bridges and the germole rings across the germanium

centers, the red-shifted band likely originates from aggregation-induced intermolecular transitions. Further evidence for the formation of aggregates was provided by the increased emission intensity in thf solutions at lower temperatures (λ_{em} = 490 nm, λ_{exc} = 410 nm).

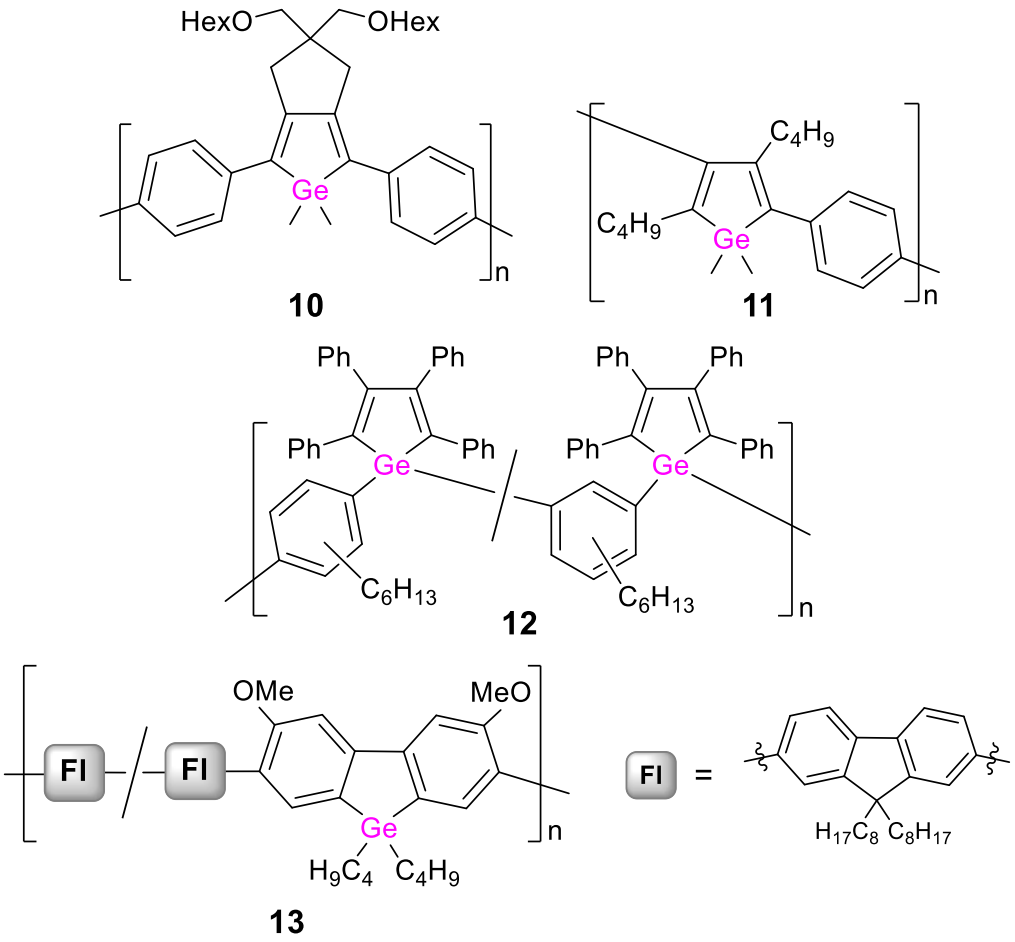

Scheme 2. Representative examples of poly(phenylenegermole)s bridged *via* different positions and a poly(germafluorene).

The incorporation of germanium into a poly(fluorene) was achieved in 2009 *via* Suzuki coupling of a bis(pinacolborane) and a dibrominated germafluorene.[140] The obtained random germafluorene-fluorene copolymer **13** (Scheme 2) exhibits intense characteristically blue fluorescence (λ_{em} = 440 nm), as does the corresponding homopolymer (λ_{em} = 420 nm).[141] While the optical band gaps are relatively large (2.9, 3.0 eV), donor-acceptor copolymers with thiophene-bridged typical benzothiadiazole and diketopyrrolopyrrole acceptor units reduce the gap to 1.6 to 1.8 eV and thus confer reasonable hole mobilities (up to $8 \cdot 10^{-3}$ cm^2 V^{-1} S^{-1}) and power conversion values (up to 2.8%) in OFETs and OSCs. The incorporation of thiophene units has proven

advantageous in poly(dithienogermole)s, which offer a variety of possibilities for fine-tuning the band gap, the charge carrier mobilities and the photophysical properties of corresponding polymer electronics through modification of the substitution pattern at the heteroatom or the thiophene rings and employment of different copolymers.[73-74,133-134,142-150]

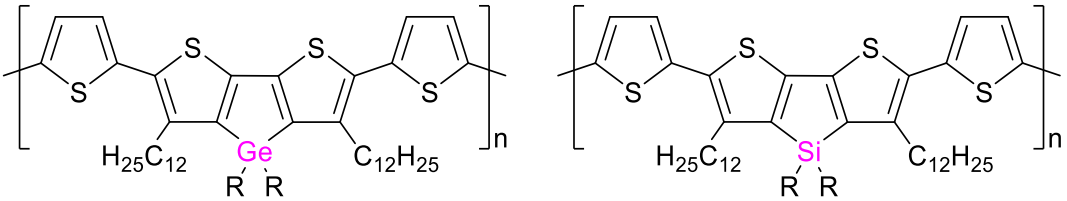

14a R = Bu
14b R = Me

15a R = Bu
15b R = Me

Scheme 3. Poly(dithienogermole)s and poly(dithienosilole)s with thiole spacer units.

In a recent study, the influence of the Group 14 atoms in poly(dithienotetrole)s **14a** and **15a** (Scheme 3) on intersystem crossing (ISC) rates with similar optical absorption properties, oxidation potentials and charge transport mobilities was elucidated.[151] The germole derivative exhibits a smaller ISC rate, presumably due to enhanced coplanarity of the rings, resulting in higher exciton yields in donor-acceptor blends with a fullerene derivative. The increased bond length of the Ge–C bond and therefore reduced steric strain were assumed to account for this structural effect in an earlier work by Kim and Heeney *et al.* on poly(germole) **16** (Scheme 4).[134] Bathochromic shifts of the thin film absorption maxima compared to the corresponding silole derivative were observed, in addition to an increased degree of crystallinity and a higher charge carrier mobility in an OSC device. In both cases, the longest wavelength absorptions (Ge: λ_{abs} = 770 nm, Si: λ_{abs} = 750 nm) lie in the far red of the visible spectrum and were assigned to charge-transfer transitions between the heterole donor part and the benzothiadiazole acceptor unit as well as to intermolecular transitions due to aggregation. End-capping with phenyl groups has been shown to lead to favorable additional intermolecular interactions and with that to enhanced ordering in thin films and thus increased charge carrier mobilities.[147]

Further fine-tuning of the photophysical properties can be achieved through modification of the substitution pattern at the heteroatom, as was shown for **14a,b** and **15a,b**.[152] In fact, methyl substitution results in a substantial bathochromic shift of the

absorption (λ_{abs} = 550 to 560 nm) and the red thin-film emission (λ_{em} = 650 to 710 nm) by $\Delta\lambda$ = 40 to 60 nm compared to the corresponding butyl-substituted derivatives **14a** and **15a** due to less-hindered intermolecular π-stacking in the dimethyl poly(tetrole)s **14b** and **15b**.

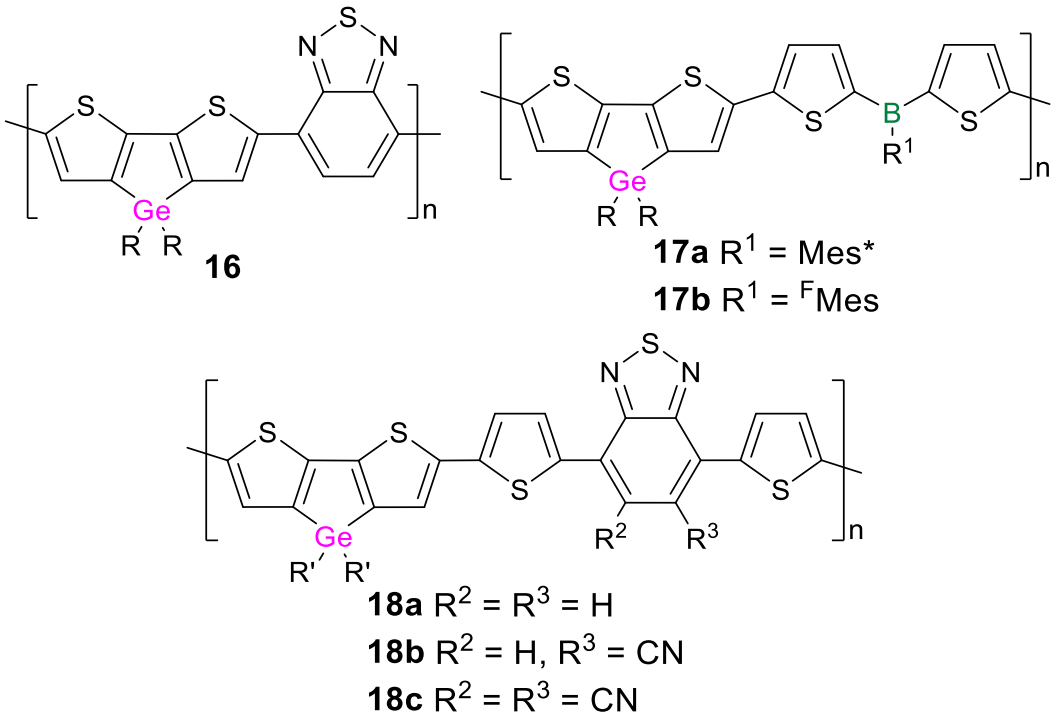

Scheme 4. Poly(dithienogermole)s with different linking units (R = 2-ethylhexyl, R' = 2-octyldodecyl, Mes* = 2,4,6-tri-*tert*-butylphenyl, ^{F}Mes = 2,4,6-tris(trifluoromethyl)phenyl).

Employing dithienylborane instead of benzothiadiazole units as the electron-deficient moieties in donor-acceptor-type polymers **17a,b** provided access to the more blue-shifted range of the spectrum with a hypsochromic shift of the absorption from the far red to λ_{abs} = 540 nm: the polymers exhibit a red instead of blue color and red fluorescence (λ_{em} = 660 to 700 nm).[122] Thiophene-bridged benzothiadiazole/dithienogermole copolymers **18a-c** have been applied in OSC devices by Heeney *et al.* and a comparison reveals that slight changes in the backbone substitution pattern of the acceptor unit can have considerable effects: the monocyano-substituted derivative **18b** provides a device efficiency of 7%, twice as high as with unsubstituted **18a**.[149] Disubstitution in **18c**, however, hampers the exciton generation significantly by further lowering the LUMO to a level at which electron transfer to the additionally employed fullerene acceptor is prevented, resulting in an efficiency of

< 1%. In line with a narrowing of the band gap, the thin film absorption was bathochromically shifted with an increasing number of cyano substituents (**18a**: λ_{abs} = 680 nm, **18b**: λ_{abs} = 790 nm, **18c**: λ_{abs} = 830 nm).

The corresponding tin analogues have been far less investigated in comparison to their lighter congeners. In analogy to the synthesis of poly(germole)s, the first poly(stannole)s, bridged with phenylene or biphenylene linkers in the 2,4- and 2,5-positions of the stannole ring, were obtained by transmetalation of the corresponding titanacyclopentadiene polymer with $SnCl_4$.[153] The LUMO energy levels are lowered by the tin atom in a comparable manner as in an analogous poly(germole), resulting in absorption maxima in the UV range between λ_{abs} = 280 and 290 nm, which tail into the visible region (~ 400 nm) and correspond to similarly large band gaps of ~ 3 eV. Regioregular derivatives **19a,b**, connected exclusively *via* the 2,5-positions of the stannole ring (Scheme 5), were prepared in corresponding post-functionalizations of regioregular titanacyclopentadienes and gave rise to substantially smaller band gaps of ~ 2 eV.[154] Remarkable bathochromic shifts by up to $\Delta\lambda$ = 130 nm compared to corresponding molecular model compounds were observed in these cases as well as in poly(stannole)s **20a-e** with thiophene linkers, corresponding to small band gaps (down to 1.6 eV in thin films).[155-156] The air- and moisture-stable poly(thienylstannole)s were prepared by Stille cross-coupling reactions of diiodothienylstannoles as bifunctionalized monomers with different substituents at the central tin atom and the corresponding distannylthiophenes. The absorption of the *para*-hexylphenyl and *para*-hexyloxyphenyl-substituted derivatives **20a,b** (λ_{abs} = 560 nm) is bathochromically shifted in comparison to **20c,d** (λ_{abs} = 520 to 530 nm), despite much shorter chain lengths of **20a,b** (X_n = 6.3; **20c,d**: X_n = 10–12) and although electron-withdrawing groups at the tin center typically reduce the HOMO-LUMO gap. Notably, **20a-d** showed weak red fluorescence with similar shifts of the emission maxima (**20a,b**: λ_{em} = 720 nm, **20c,d**: λ_{em} = 650 to 660 nm). It was assumed that the additional hexyl groups in the backbone of **20c,d** reduce the planarity of the system and hence diminish effective conjugation. Derivative **20e** contains the solubility enhancing hexyl groups at the thiophene rings as in **20c,d** but less electron-withdrawing phenyl substituents at tin and shorter chain lengths (**20e**: X_n = 9, **20c,d**: X_n = 10–12).[156] The absorption maximum of **20e** (λ_{abs} = 540 nm) lies, however, in between those of **20a,b** and **20c,d**, possibly due to electronic and steric effects of the CF_3 groups: the electron-withdrawing

influence could diminish conjugation along the polymer chain through increased interaction of the π-electrons with the aryl substituents at tin and the steric demand of the CF_3 groups might additionally reduce the planarity of the system.

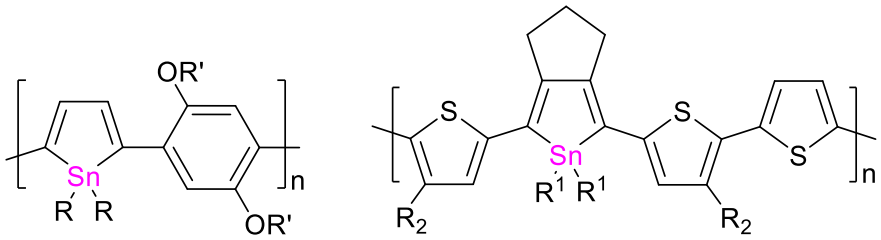

19a R = Me
19b R = Ph

20a R^1 = *p*-Hex-C_6H_4, R^2 = H
20b R^1 = *p*-OHex-C_6H_4, R^2 = H
20c R^1 = *p*-CF_3-C_6H_4, R^2 = Hex
20d R^1 = 3,5-$(CF_3)_2$-C_6H_3, R^2 = Hex
20e R^1 = Ph, R^2 = Hex

Scheme 5. Poly(stannole)s with phenylene and thiophene linking units (R' = 2-ethylhexyl).

The implementation of Si or Ge into the π-conjugation path of poly(amide)s, poly(ester)s, poly(imide)s, poly(azomethine)s and related compounds confers improved solubility in organic solvents as compared to the organic congeners while maintaining good thermal stability and appropriate glass transition temperatures, hence rendering them superior materials for thin-film applications.[157-169] While their syntheses and thermal properties have been extensively investigated during the past decades, the (opto-)electronic properties, crucial for applications in electronic devices, moved into focus more recently. Germanium-doped oligo(urethane)s show blue fluorescence due to the low-lying σ*-orbitals at the tetrelane moieties and resulting σ,π-conjugation along the polymer chain (as discussed above for poly(silole)s), but exhibit relatively large band gaps of ~ 3.8 eV.[170] Although poly(azomethine)s with silylene bridges exhibit similarly large band gaps of 3.1 to 3.5 eV, these poly(germane)s become conductive in the form of thin films.[171] Phenyl groups at the heteroatom or phenylene instead of thiophene bridges give rise to band gaps as small as 2.0 eV,[172-173] resembling those of poly(thiophene) derivatives used in optoelectronics.[174-175]

The σ,π-conjugated poly(biphenylgermane) **21a** (Scheme 6) was just recently employed as a host material in a blue light emitting OLED with an excellent external quantum efficiency of 24%.[176] In combination with an organic cohost and variable

guest compounds, blue, red, green and white emitting devices were obtained with **21a** as the host material.[177] In a comparative study of related poly(biphenyltetrelanes) containing different Group 14 heteroelements (C, Si, Ge, Sn), the germanium-based analogue **21b** exhibited the best device performance, despite smaller hole and electron mobilities than the silicon congener.[178]

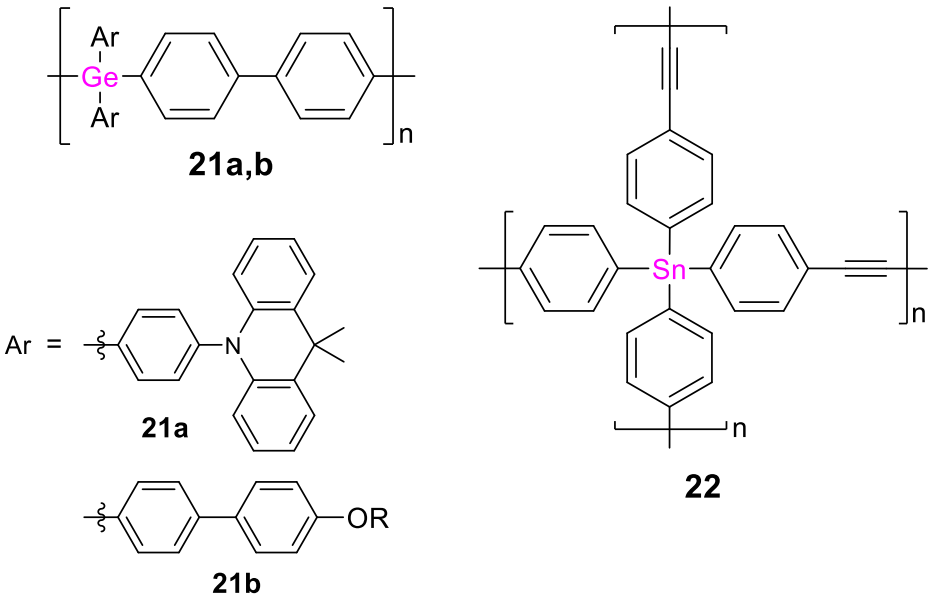

Scheme 6. Representative examples of σ,π-conjugated polymers with germanium atoms embedded in the conjugation path of linear π-conjugated organic polymers and a corresponding poly(stannane) (R = 2-ethylhexyl).

Only recently, poly(stannane) **22** with ethynylene arylene linking units was obtained in a Sonogashira cross-coupling between tetra(ethynylphenyl)stannane and diiodobenzene in a 1:2 ratio.[179] Depending on the reaction conditions, i.e. base and catalyst employed, catalyst load, solvent, temperature and reaction time, **22** was obtained as microporous or non-porous insoluble material with Brunauer–Emmet–Teller surface areas between 2 and 750 $m^2\ g^{-1}$. The largest pore sizes (1.6 to 2.8 nm) were determined with NEt_3 as base (instead of piperidine) and higher catalyst load (2 mol% $Pd(PPh_3)_2Cl_2$) in toluene and the corresponding anisotropically shaped particles were about 500 nm in size according to scanning electron microscopy. Fluorescence maxima (in the solid state and in suspension) were found at λ_{em} = 500 to 540 nm or at λ_{em} = 460 to 480 nm. The preference for either range presumably depends on the macroscopic structure. Although no conclusive trend was discernible, the applied base as well as the catalyst load seem to have considerable impact on the emission. In

comparison to *para*-phenylethynylbenzene with triphenylstannyl end groups as a molecular model compound with intense blue fluorescence (solution: λ_{em} = 410 nm, solid state: λ_{em} = 450 nm), the emission is bathochromically shifted independent of the reaction conditions.

The incorporation of two covalently bonded σ-conjugated Group 14 atoms into π-conjugated polymeric frameworks has been extensively investigated in the case of silicon:[63,180-181] various representatives with alkenyl, alkynyl and aryl bridging units[182-193] as well as furane and thiophene rings were reported in the 1980s and 1990s.[194-198] The UV/Vis absorption is bathochromically shifted with increasing chain lengths, in line with σ,π-conjugation across the silicon centers, resulting in a relatively large range of absorption from λ_{abs} = 240 to 500 nm and emission maxima from λ_{em} = 350 to 620 nm. The absorption of thin films is generally even further red-shifted due to π-stacking. These materials showed relatively high thermal stabilities (~ 200–350 °C), according to thermogravimetric analyses (TGA). The Si–Si bonds can be cleaved under UV irradiation,[182-183,194-195] a feature that was used for the modification of TiO_2 electrode surfaces employed in solar cells.[146,181,193] For instance, poly(disilane) **23** (Scheme 7) and derivatives containing pyridine and pyrazine units as additional TiO_2-coordination sites were successfully attached to the electrode surfaces and proved applicable as dye-sensitizing materials in the solar cells, albeit with low power conversion efficiencies of 0.16–0.89%.[146] Thin films of poly(disilane)s become conductive upon preparation under an oxidizing atmosphere of SbF_5 with conductivities up to 0.2 S cm^{-1}, increasing to 1 S cm^{-1} when exposed to air.[184-185,188]

Germanium analogues **24a-e** with vinylene, thiophene and phenylene units (Scheme 7) showed hypsochromic shifts of the absorption maxima (λ_{abs} = 240 to 260 nm) by $\Delta\lambda$ ~ 10 nm, but slightly higher conductivities (3–4·10^{-4} S cm^{-1}) in comparison to the corresponding silicon congeners (1–2 10^{-4} S cm^{-1}).[199-200] Preparing the films under iodine instead of SbF_5 vapor, results in slightly smaller values (~ 1·10^{-4} S cm^{-1}).

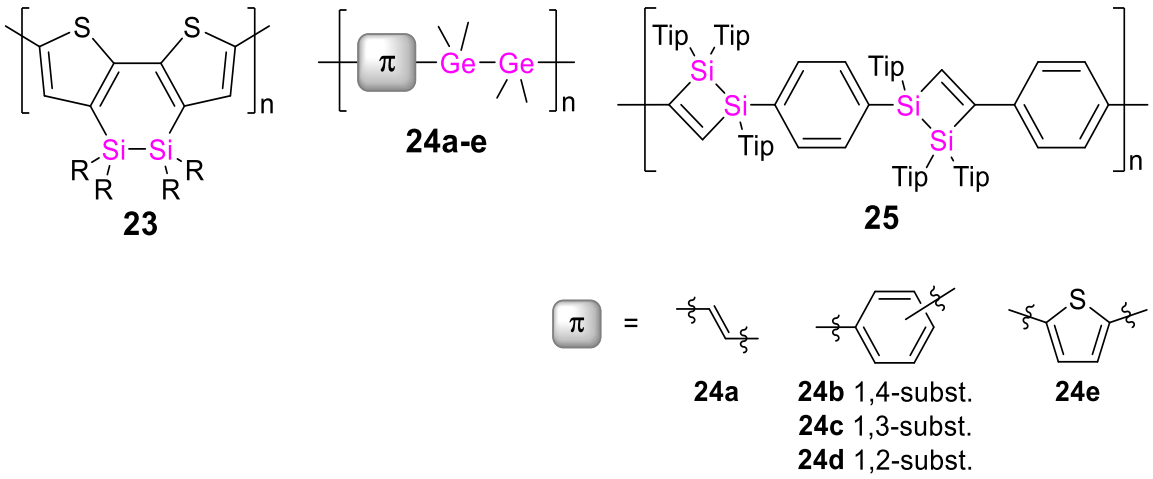

Scheme 7. Representative examples of conjugated polymers with heavier tetrel–tetrel bridges (R = hexyl).

In 2014, Scheschkewitz *et al.* reported the σ,π-conjugated poly(1,2-disilacyclobutene) **25** containing Si–Si units of which only one silicon is incorporated in the conjugation path while the other is in close proximity (Scheme 7).[201] Effective conjugation of the π-electrons across the low-lying σ*-orbitals at the bridging silicon centers was evident from a substantial bathochromic shift of the polymer absorption (λ_{abs} = 310 nm) by $\Delta\lambda$ = 30 nm compared to the bis(1,2-disilacyclobutene) monomer. DFT calculations additionally showed substantial contributions from the adjacent Tip_2Si moiety to the LUMO. Poly(1,2-disilacyclobutene) **25** is obtained by [2+2]-cycloaddition of a *para*-phenylene-bridged tetrasilabutadiene,[202] and 1,4-diethynylbenzene, one of the rare examples of a polymerization protocol employing heavier alkene homologues as polymerization precursor (further elaborated in a subsequent section).

Group 15: Recent advances in poly(pnictane)s

The incorporation of heavier Group 15 element motifs into π-conjugated systems typically results in effective n,π- or σ,π-conjugation, leading to a decrease of the LUMO energies and the HOMO-LUMO gaps and hence in some cases to semiconducting properties. Additionally, the band gaps can be readily fine-tuned by electrophile coordination to the heteroelement and a concomitant change of the oxidation state. Accordingly, the corresponding polymers constitute promising materials for application in (opto-)electronic devices and indeed some poly(phosphole) and poly(arsole) derivatives have been employed in OLEDs, OSCs and OFETs.[33,35-36,38,81-85]

Recently, Gates *et al.* reported an n,π-conjugated poly(*p*-phenylene diethynylenephosphane) statistical copolymer **26** (Figure 5), prepared by nickel-catalyzed coupling of the two π-bridged bis(alkynes) with phenyldichlorophosphane.[203] The phosphorus atoms are incorporated into a π-conjugated linear organic framework consisting of a random sequence of *para*-phenylenediethynylene and fluorenyldiethynylene repeat units. In the presence of Au(I) and Au(III) (employed as Au(tht)Cl and $HAuCl_4 \cdot 3H_2O$, respectively; tht = tetrahydrothiophene), highly blue-fluorescent materials are formed: with Au(I), the corresponding **26**$\cdot(AuCl)_n$ polymeric complex with gold-coordinated phosphorus centers is formed and in the case of Au(III), a presumably cross-linked but insoluble polymer network was obtained. Notably, the fluorescence was exclusively observed in the presence of gold ions but not with any other cation tested (alkali, earth alkali and transition metals). Comparable sensing behavior had been reported earlier for different π-conjugated phosphane-diyne hybrid polymers **27a-e** (Figure 6) in which either a fluorene or a phenylene moiety is contained in the repeat unit.[204-205] The phosphorus atoms in **26** and **27a-e** are prone to oxidation under air or in the presence of H_2O_2, resulting in the formation of the corresponding phosphane oxide polymers, which show intense blue fluorescence in solution (λ_{em} = 330 to 420 nm) and weak yellow-green fluorescence (λ_{em} = 430 to 560 nm) in the solid state. The red-shift of the thin film emission and the concomitant substantial peak broadening compared to the solution state are attributed to aggregate formation.

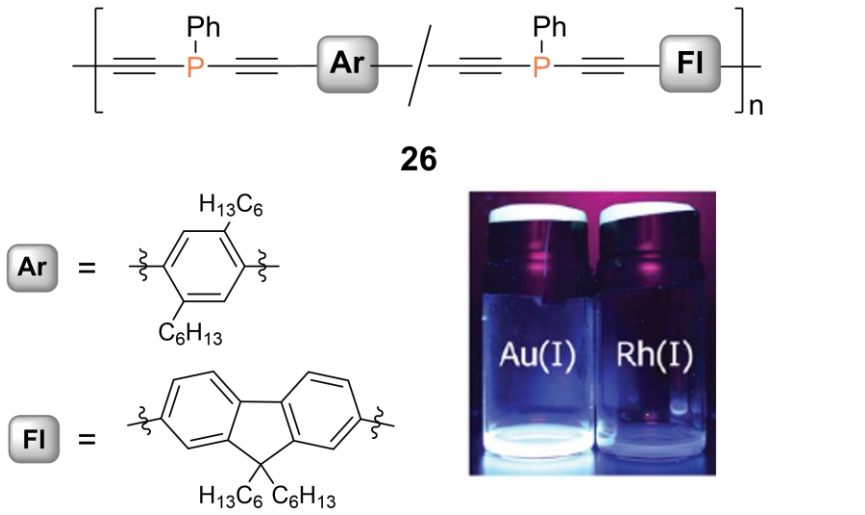

Figure 5. Fluorenyl and phenyl containing poly(diethynylenephosphane) statistical copolymer. Representative picture of solutions of a corresponding molecular model compound exhibiting blue fluorescence in the presence of Au(tht)Cl but not with $[Rh(COD)Cl]_2$, adapted with permission from Ref. [203], copyright © 2020 American Chemical Society.

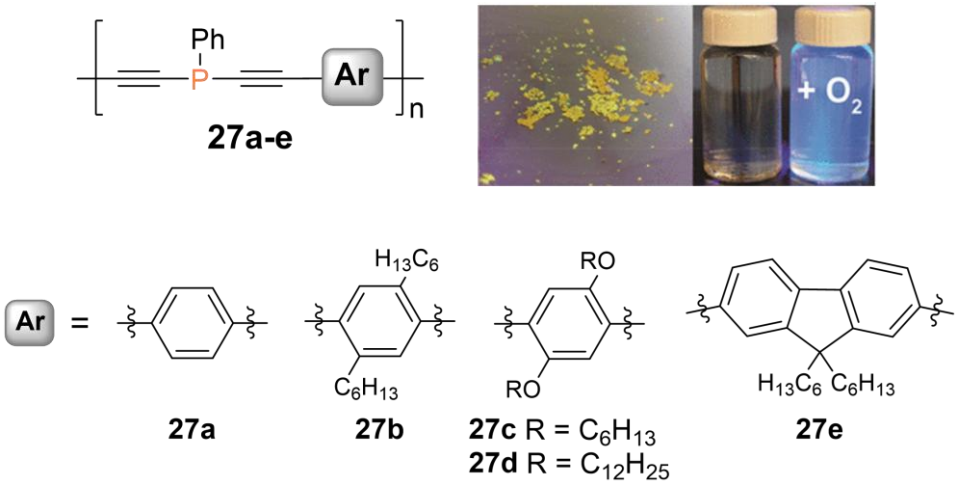

Figure 6. Poly(diethynylenephosphane) copolymers with different phenylene and fluorene spacers. Representative picture of the yellow solid state emission and the solution emission after oxidation of a poly(phosphane), adapted with permission from Ref. [205], copyright © 2017 American Chemical Society

Phosphorus-containing thiophene polymer networks **28a-c** (Scheme 8) were obtained either *via* Stille P–C polycondensation of distannylthiophenes and PCl_3 or by reaction of a dilithiated oligo(thiophene) with PCl_3. Post-functionalization of **28b** with H_2O_2 yielded phosphane oxide derivative **29** and in reactions of **28a-c** with MeOTf the methyl-substituted cations **30a-c** were obtained. Methylated polymers **30b,c** were applied as photocatalysts for the hydrogen evolution reaction. Increasing conversion

rates from the phosphane catalyst (155 µmol h^{-1} g^{-1}) and the phosphane oxide (900 µmol h^{-1} g^{-1}) to the cationic methyl-substituted phosphane (2050 µmol h^{-1} g^{-1}) showcase a strong dependency of the activity on the nature of the phosphorus centers and the possibilities for tailoring polymer properties according to specific requirements through heteroatom incorporation and post-functionalization.[206]

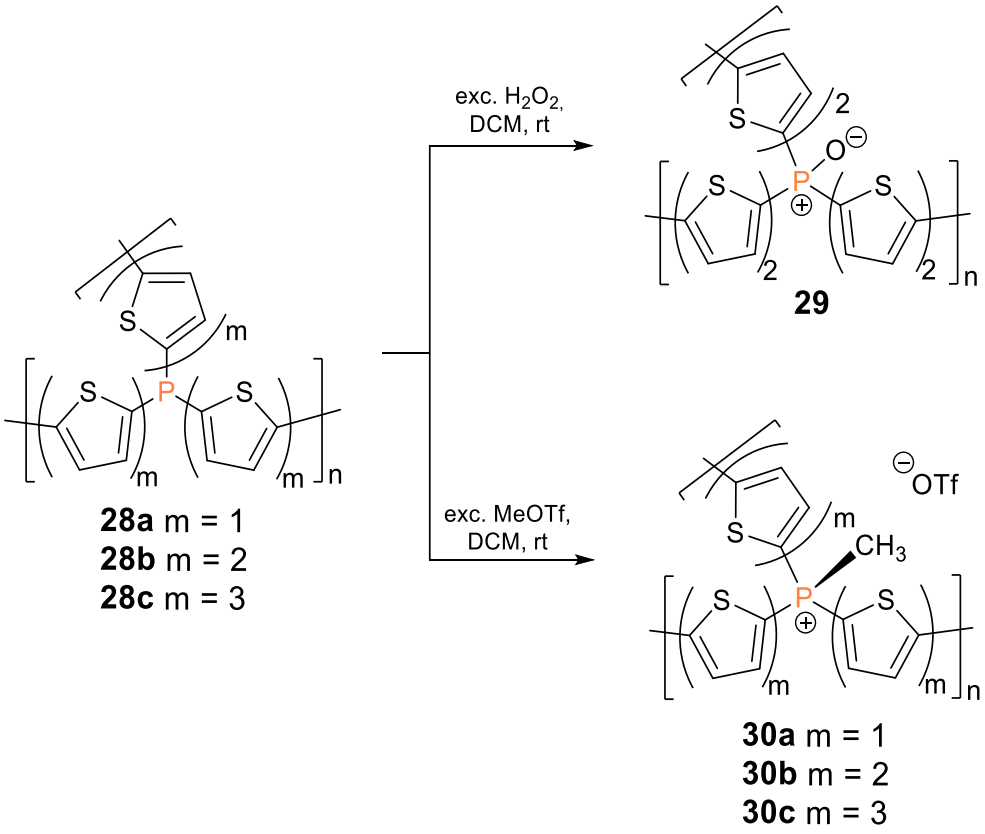

Scheme 8. Post-functionalization of phosphorus-bridged thiophene polymer networks **28a-c** with H_2O_2 and MeOTf provides poly(phosphane oxide) **29** and methyl-substituted cations **30a-c**.

As demonstrated by the "turn-on" fluorescence of the phosphaneoxide polymers by Gates *et al.* (*vide supra*),[204-205] compounds with oxidized P(V) centers are particularly interesting, exhibiting even lower LUMO levels than the corresponding phosphanes. Tomita *et al.* prepared the phosphole-phenylene copolymer **31** and its oxidized analogue **32** (Figure 7) by reactions of the corresponding titanacyclopentadiene polymer with $PhPCl_2$ and $^tBuPCl_2$, respectively.[207] While the phenyl-substituted derivative **31** proved stable in air, oxidation to *tert*-butyl-substituted **32** occured during workup. Both polymers exhibit orange to yellow fluorescence. The photophysical properties of the phenyl-substituted poly(phosphole) **31** were compared to a

monomeric model compound (Figure 7), revealing huge bathochromic shifts of the absorption (λ_{abs} = 520 nm) and emission maxima (λ_{em} = 590 nm) by $\Delta\lambda$ = 120 to 130 nm due to effective π-conjugation along the chain. Notably, *tert*-butyl derivative **32** shows a substantial hypsochromic shift in comparison (λ_{abs} = 450 nm, λ_{em} = 550 nm), which has not been discussed by the authors, but most probably arises from a more effective lowering of the LUMO by the phosphorus in **31** with the electron-withdrawing phenyl substituent.

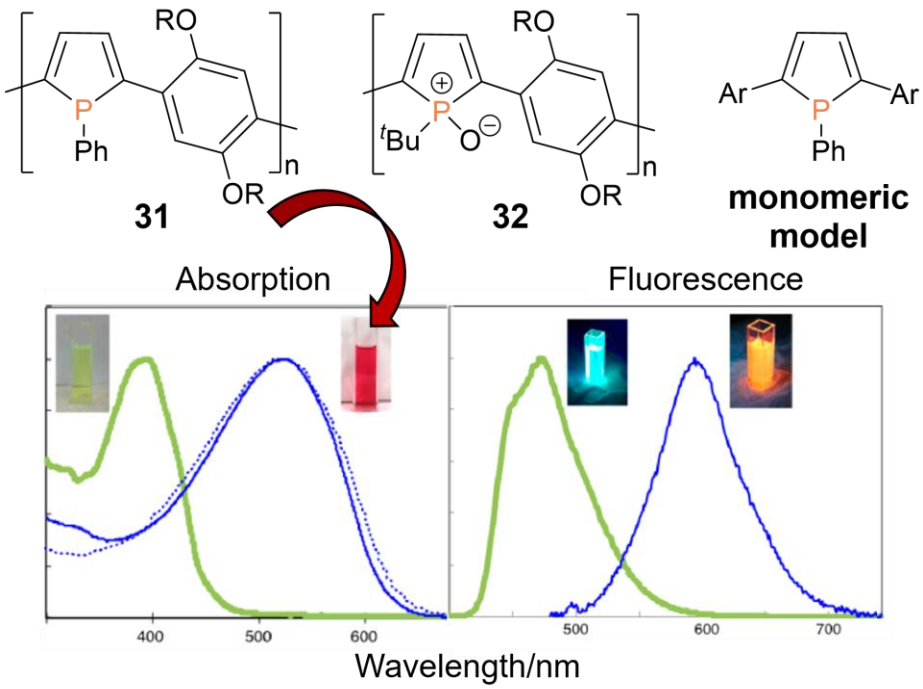

Figure 7. Top: Structure of phenylene-bridged poly(phosphole) **31**, *tert*-butyl-substituted poly(phosphole oxide) **32** and a monomeric model compound (R = 2-ethylhexyl, Ar = 2-methoxyphenyl). Bottom: Absorption and emission spectra of polymer **31** (blue lines) show huge bathochromic shifts compared to the monomeric model compound (green lines) and have been adapted with permission from Ref. [207], copyright © 2015 American Chemical Society.

In contrast to **32**, poly(phosphole oxide) **33** (Figure 8) was obtained in a Stille coupling reaction of the distannyl and the diiodo phosphole oxides in a 1:1 ratio.[208] The UV/Vis absorption (λ_{abs} = 660 nm) shows an even larger red-shift by $\Delta\lambda$ = 270 nm in comparison to the corresponding monomer (λ_{abs} = 390 nm). The weak fluorescence, observed in the mono-, di- and trimer, is correspondingly shifted from blue-green to orange with increasing chain length and even into the NIR region in the case of the polymer. Notably, the absorption maximum of the aryl-substituted oxidized

poly(phosphole) lies in the far red of the visible spectrum – in line with a blue appearance (Figure 8) – and is hence substantially bathochromically shifted ($\Delta\lambda$ = 210 nm) compared to that of phenyl-substituted poly(phosphole) **31** (λ_{abs} = 520 nm).

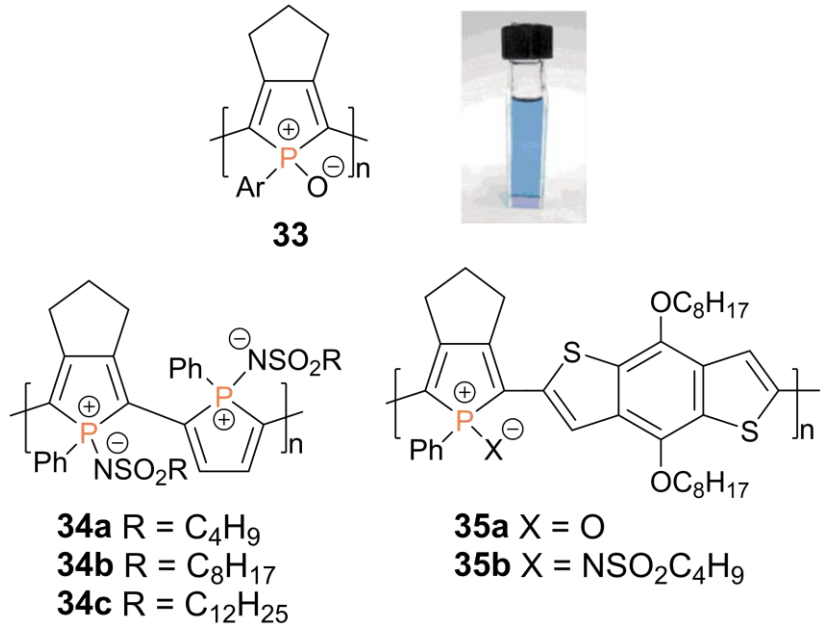

Figure 8. Structurally related poly(phosphole oxide)s and poly(phospholeimide)s (Ar = *p*-dodecyloxyphenyl) and a picture of a solution of poly(phosphole) **33**, adapted with permission from Ref. [208], copyright © 2010 American Chemical Society.

Poly(phospholeimide)s **34a-c** with alkylsulfonylimino-substituted phosphorus atoms (Figure 8) provide an even more distinct decrease of the LUMO levels and smaller HOMO-LUMO gaps with absorption bands reaching into the near infrared region.[209] Considerable red-shifts of the absorption maxima (λ_{abs} = 670 to 680 nm) in comparison to a corresponding phospholeimide monomer (λ_{abs} = 400 nm) demonstrate efficient π-conjugation along the polymer chains. The resulting charge carrier mobilities (up to $6 \cdot 10^{-3}$ cm^2 V^{-1} s^{-1}) are suitable for the use as semiconducting materials. Notably, longer alkyl substituents at the sulfonyl group showed a slightly enhancing effect. Donor-acceptor copolymers **35a,b**, with electron-rich benzodithiophene units in combination with the phosphole oxide moieties exhibit a red-shifted absorption (λ_{abs} = 580 to 600 nm) in solutions and in thin films and have been applied to OSCs.[210] A slightly improved performance is achieved with the oxide (**35a**) in comparison to the imide (**35b**), presumably due to a less bulky environment and hence stronger intermolecular π-π interactions.

Considerable differences in the emission behavior due to different oxidation states of the phosphorus atoms in the polymer chain have also been observed in a comparative study of the electroluminescence in OLEDs.[211] The emissive layers consisted either of poly(phosphafluorene) **36** or its oxidized form **37**, both obtained by Suzuki coupling of the corresponding fluorene and heterofluorene comonomers. P(V) containing polymer **37** with a smaller optical band gap (2.74 eV) compared to **36** (2.81 eV) gives rise to white-light emission, while **36** with P(III) moieties exhibits intense blue emission with maxima at λ_{em} = 420, 450, and 480 nm (Figure 9). Notably, in thin films of poly(oxophosphafluorene)s with phenylene spacer units, intense green-blue fluorescence (λ_{em} = 460 to 470 nm) was also observed.[212] While the longest wavelength absorption of **36** (λ_{abs} = 380 to 400 nm) is comparable to the absorption maximum of **37** (λ_{abs} = 400 nm), the latter exhibits an additional shoulder at 430 nm, attributed by the authors to a β-phase with higher planarity.[211]

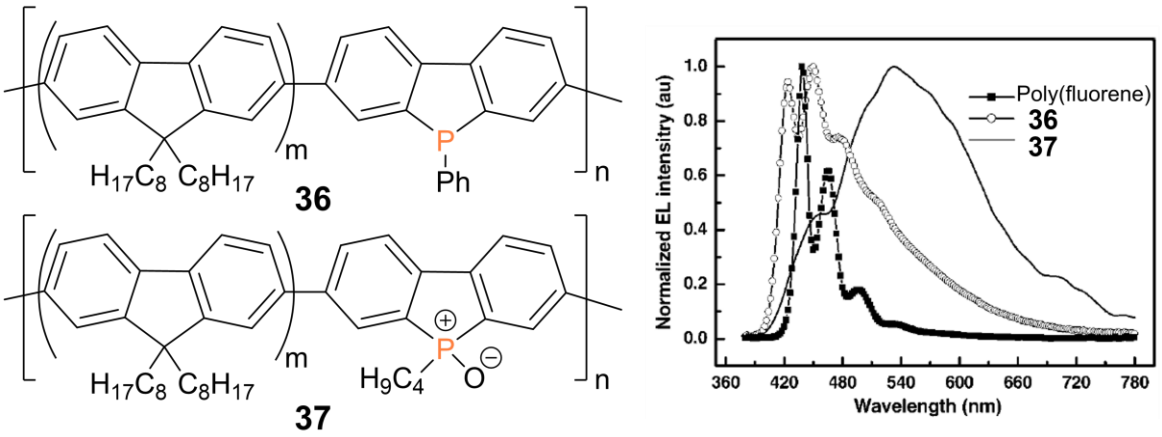

Figure 9. Poly(phosphafluorene) **36** gives rise to blue light emission in an OLED device, while the oxidated poly(phosphafluoreneoxide) **37** exhibits white light emission under the same conditions. Representation of the fluorescence spectra adapted with permission from Ref. [211], copyright © 2008 American Chemical Society.

The incorporation of benzodithiophene units in poly(phosphafluorene)s with either oxo or sulfur functionalities at the phosphorus centers, on the other hand, results in a bathochromic shift of the absorption maxima (λ_{abs} = 470 nm), which is even more pronounced (λ_{abs} = 530 nm) in a gold(I)-coordinated poly(phosphafluorene).[213] Employed in OSC devices, these post-functionalized benzodithiophene phosphafluorene copolymers resulted in low, slightly variable power conversion efficiencies (O: 0.13%, S: 0.60%, Au: 0.26%).

Poly(dithienophosphole oxide) **38** with phenylene bridging units (Scheme 9) was obtained by Stille coupling of the distannylphosphole oxide monomer and *p*-diiodo-2,5-dioctyloxybenzene and showed yellow-green luminescence (λ_{em} = 555 nm), considerably red-shifted compared to the dithienophosphole monomer (λ_{em} = 463 nm).[214] Poly(dithiazolophosphole oxide) **39** with triazole-bridged fluorene units (Scheme 10) is obtained by click reaction of the corresponding fluorenyl-diazide and the phosphole with two ethynylene substituents.[215] Presumably due to poor solubility limiting the chain growth, only short oligomers of **39** were obtained. Benzodithiophene copolymers of dithienophosphole oxides were employed in OSCs providing relatively high power conversion efficiencies of 6 to 7%.[216]

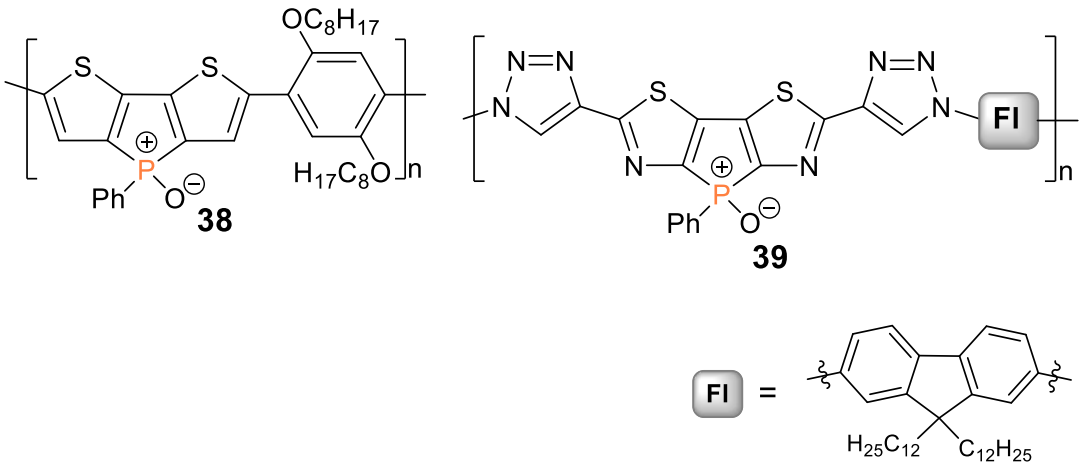

Scheme 9. Representative examples of poly(phosphole oxide)s with fused heterole substituents.

Conjugated polymers with As(III) centers in the main chain should show a lower tendency toward oxidation compared to their phosphorus analogues. Poly(arsane)s have only come to the fore during the last decade,[86] although the first examples had already been reported by Chujo and Naka *et al.* as early as in 2002: the alternating poly(vinylenearsane)s **40a,b** were obtained selectively by free-radical copolymerization of pentamethylcyclopentaarsane or hexaphenylcyclohexaarsane with phenylacetylene (Scheme 10).[217] Notably, phenyl-substituted **40b** is a colorless solid, whereas the methyl-substituted polymer **40a** appears bright yellow. Although the differences between the optical properties of **40a** and **40b** were not discussed by the authors, the yellow color of **40a**, in line with the absorption tailing into the visible range up to $\lambda_{abs,onset}$ = 550 nm, was attributed to n→π* transition along the polymer chain.

Furthermore, **40a** exhibits green-blue luminescence (λ_{em} = 490 nm) with maximum intensity at an excitation wavelength of λ_{exc} = 400 nm. In stark contrast to related phosphorus compounds (*vide supra*), ^{1}H NMR spectroscopy suggests poly(vinylenearsane) **40a** to be stable towards oxidation, even with H_2O_2.

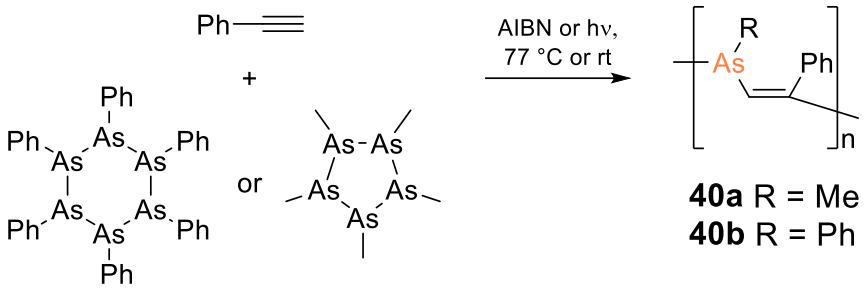

Scheme 10. Free-radical copolymerization of cycloarsanes and phenylacetylene yielded the first arsenic-embedded conjugated polymers **40a,b**.

Most recently, trivalent arsane motifs have been embedded into the π-conjugation path of phenylene and fluorene groups to result in **41a,b** (Scheme 11).[218] The n,π-conjugated polymers were obtained by Suzuki-Miyaura polycondensation of *para*-dibrominated triphenylarsane with the corresponding bis(boronic acid) comonomer. DFT calculations showed that the arsane moiety contributes considerably to a decrease of the LUMO energy.

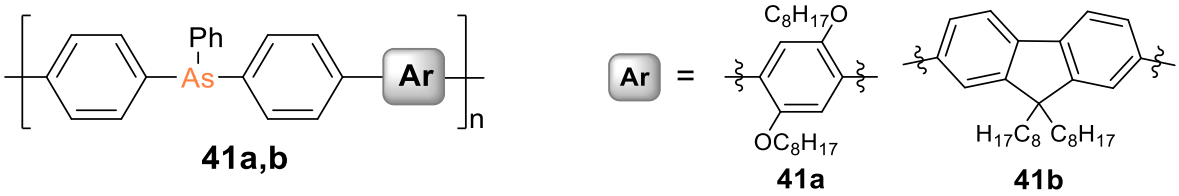

Scheme 11. Structures of poly(triphenylarsane)s **41a,b**.

The observed bathochromic shift of the absorption (λ_{abs} = 340 nm) by $\Delta\lambda$ = 50 nm compared to a model compound of the repeat unit was, however, shown to be mainly caused by an extension of the π-system across the phenyl rings rather than across the arsenic atoms. Blue emission (λ_{em} ~ 400 nm) with considerable quantum yields (17–65%) was observed for both **41a,b**, as well considerably red-shifted compared to the monomeric model system by $\Delta\lambda$ = 60 nm.

The first examples of arsole-based polymers were reported in 2016 independently by the groups of Heeney, Naka and Tomita.[219-221] Tomita *et al.* synthesized arsole-phenylene copolymer **42** (Figure 10) by transmetalative post-functionalization of the corresponding titanacyclopentadiene polymer,[220] a strategy they had already implemented in the syntheses of Group 14 cyclopentadiene polymers and poly(phosphole) derivatives (*vide supra*). The employed diiodoarsane reagent was generated from hexaphenylcyclohexaarsane in a reaction with iodine.[222] Poly(arsole) **42** precipitates from methanol as a dark red solid with similar absorption and fluorescence properties (λ_{abs} = 520 nm, λ_{em} = 600 nm) as its phosphorus analogue **31** (λ_{abs} = 520 nm, λ_{em} = 590 nm).[207]

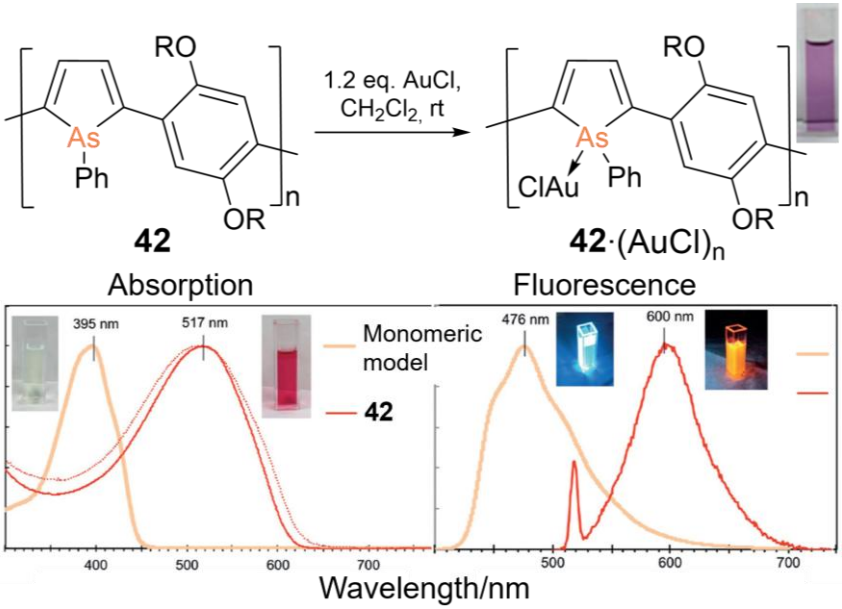

Figure 10. Top: Reaction of poly(arsole) **42** with AuCl (R = 2-ethylhexyl). Bottom: Pictures of solutions of the compounds solutions under daylight and upon UV irradiation as well as the absorption and fluorescence spectra, adapted with permission from Ref. [220], copyright © 2016 Wiley VCH.

Notably, **42** exhibits quasi-reversible oxidation peaks in cyclic voltammetry, whereas the corresponding poly(phosphole) **31** is irreversibly oxidized under the same conditions. In analogy to Gates' poly(phosphane) **26** (*vide supra*),[203] poly(arsole) **42** forms the corresponding **42**·$(AuCl)_n$ polymer with Au(I)-coordinated arsenic centers. The LUMO level and thus the HOMO-LUMO gap are lowered, as experimentally confirmed by bathochromic shifts of $\Delta\lambda$ = 30 nm for both, absorption and emission.

Heeney *et al.* reported the synthesis of the first poly(dithienoarsole) **43a** (Figure 11).[219] The dark blue vinylene-containing copolymer with a remarkably high absorption wavelength of λ_{abs} = 620 nm was employed in an FET and exhibited promising charge carrier mobilities. Subsequently, the corresponding poly(dithienoarsole)s **43b,c** with benzodithiopene units were synthesized and applied to OSC devices with reasonable performance.[223] Poly(dithienoarsole) **43d** with bridging fluorene units was obtained by Suzuki-Miyaura polycondensation,[221] whereas **43a-c** had been synthesized by Stille cross-coupling. In the case of **43d**, a broad absorption band with a maximum at λ_{abs} ~ 450 nm and a shoulder of almost equal intensity at ~ 500 nm were observed. Furthermore, the intense yellow fluorescence of **43d** (λ_{em} ~ 550 nm, Figure 11) slightly red-shifted yet weakened in thin films (λ_{em} ~ 600 nm). Similar red-shifts were observed for the thin film absorption of poly(arsole)s **43a-c**, presumably due to aggregation of the π-systems. This interpretation finds support in the absence of such a red-shift upon deposition in a poly(methylmethacrylate) (PMMA) matrix. In comparison to molecular model compounds, the fluorescence of **43d** showed a remarkably large bathochromic shift by $\Delta\lambda$ ~ 150 nm (Figure 11) as a result of effective extension of the conjugated system along the polymer chain. Due to the remarkably high fluorescence quantum yield of **43d** (44%), and its low tendency towards oxidation, it was applied as a photooxidation catalyst and as highly efficient photosensitizer for singlet oxygen generation.[224] Recent progress was achieved through solubility enhancing formal *para*-alkoxylation of the phenyl substituent at the arsenic centers of poly(dithienoarsole)s **44a-c**, which renders the incorporation of sterically demanding long alkyl chains in 3-position of the thiophene rings (R' in **43a-d**) redundant.[225] This allowed for copolymerization with benzoxadiazole and benzothiadiazole as electron acceptor units in highly planar donor-acceptor copolymers **44b,c**. The resulting decrease of the LUMO levels caused red-shifted absorptions (**44b**: λ_{abs} = 680 nm, **44c**: λ_{abs} = 660 nm) and huge Stokes shifts ($\Delta\lambda$ = 160 to 230 nm) to near infrared emission with maxima at λ_{em} = 840 (**44b**) and 890 nm (**44c**).

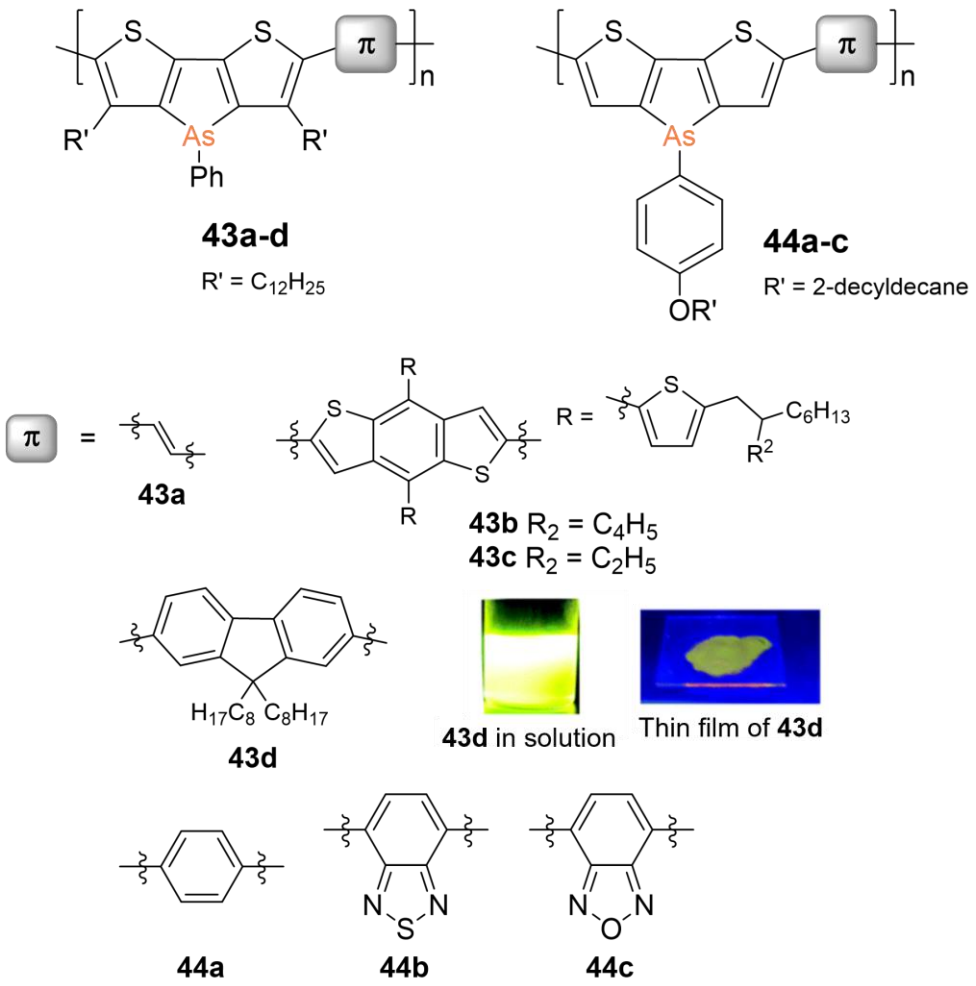

Figure 11. Poly(dithienoarsole)s **43a-d**, with solubility enhancing alkyl groups in 3-position of the thiophene rings and **44a-c** with *para*-alkoxyphenyl substituents at the arsenic centers and pictures of the yellow fluorescence of **43d** in solution and in the solid state, adapted with permission from Ref. [221], copyright © 2016 The Royal Society of Chemistry.

Dithienoarsole homopolymer **45** without additional π-linking units (Scheme 12) was obtained as an insoluble red-colored thin film on an indium tin oxide electrode by electropolymerization of the corresponding dithienoarsole monomer. Intense absorption maxima were observed in the UV/Vis spectrum of the polymer film at λ_{abs} = 390 and 460 nm, and a weaker red-shifted band (λ_{abs} = 630 nm) comparable to the absorption of vinylene copolymer **43a** (λ_{abs} = 620 nm) but at higher wavelengths than the corresponding benzodithiophene and fluorene copolymers **43b-d** and arylene-bridged poly(arsole) **42** (λ_{abs} = 450 to 520 nm).[226] Notably, an alternating arsafluorene-fluorene copolymer **45**, obtained analogously to the poly(dithienoarsole)s by Suzuki-Miyaura polycondensation, exhibits an absorption maximum further in the blue range

(λ_{abs} = 390 nm) and shows amplified spontaneous emission, crucial for the use in photonics, such as lasers.[227-228] Recently, poly(arsole) **46** with 2,3-connectivity of the arsole rings (Scheme 12) was reported to absorb in the same region (λ_{abs} = 500 nm) as 2,5-substituted derivatives, such as **42** (λ_{abs} = 520 nm), and exhibits intense green luminescence (λ_{em} = 520 nm), suggesting considerable influence of the arsane unit on the frontier orbitals of the conjugated system in this bent regioisomer.[229]

The only known conjugated polymer with bismuth directly adjacent to the conjugation path was reported in 2006 by Chujo *et al.*[230] Poly(bismole) **47** (Scheme 12) exhibits blue emission (λ_{em} = 440 nm) and was synthesized from a poly(zirconacyclopentadiene) by post-functionalization *via* lithiation and subsequent reaction with $BiPhBr_2$.

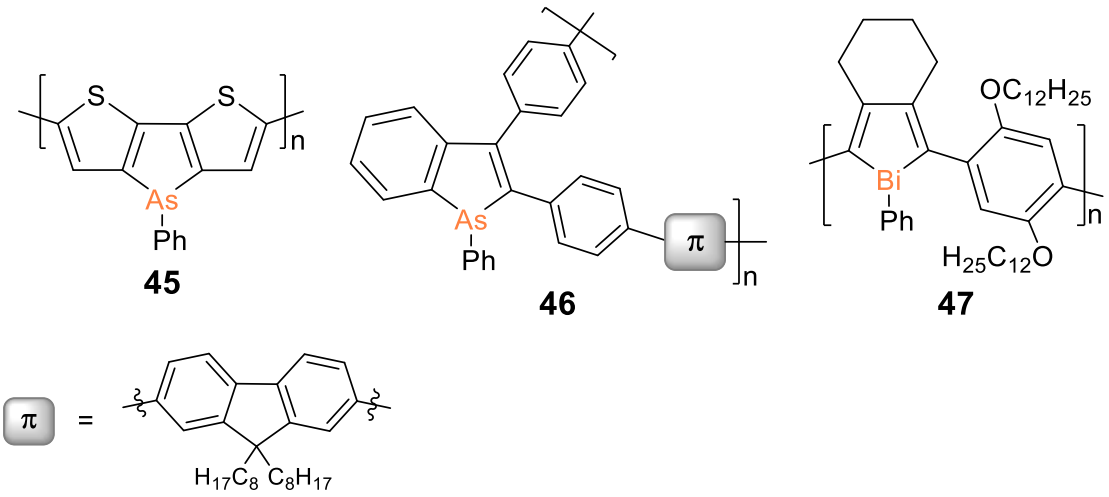

Scheme 12. Structures of poly(dithienoarsole) **45**, 2,3-substituted poly(arsole) **46** (substitution along the polymer chain is regiorandom; for clarity, only one representative constitution of the repeat unit is depicted) and of the only reported poly(bismole) **47**.

Diheteroatomic multiple bonds embedded in the main chain

Group 13: B=N Bridges in conjugated hybrid polymers

The zwitterionic B=N moiety is associated with a much larger HOMO-LUMO gap than corresponding C=C bonds, rendering poly(iminoborane)s promising air-stable materials with dielectric rather than (semi-)conducting properties. This band gap shift provides new possibilities regarding the fine-tuning of the electronic properties of resulting materials for the use in optoelectronic devices, for instance through combination with organic polymers.[231-232] Numerous examples of poly(iminoborane)s with B=N units in the main chain have been reported in recent years.[232]

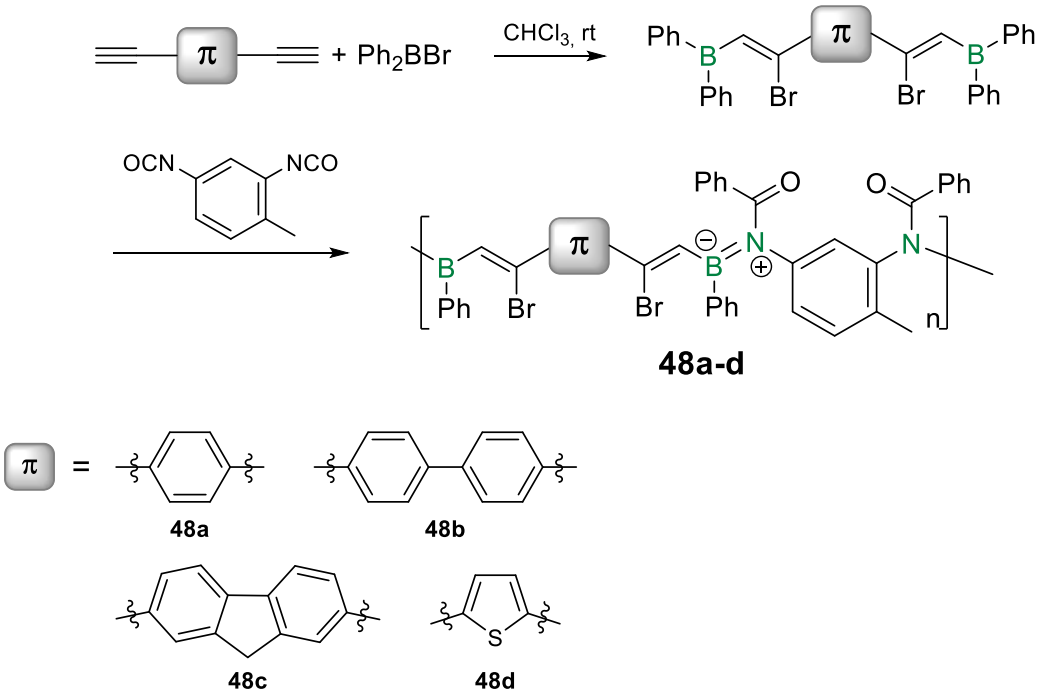

Scheme 13. Representative examples of poly(boronic carbamate)s with variable bridging units.

Chujo *et al.* reported on the syntheses of the first poly(iminoborane)s, applying diisocyanate monomers, which are important building blocks for poly(urethane)s.[233-234] Phenylene-bridged poly(boronic carbamate)s are either obtained by alkoxyboration of a diisocyanate with mesityl dimethyl boronate at 150 °C[235] or as copolymers **48a-d** in a two-step reaction (Scheme 13):[236-237] In the first step, 1,4-diethynylbenzene

undergoes haloboration with Ph_2BBr at room temperature, followed by phenylboration of the subsequently added diisocyanate in the second step. Notably, **48d** with thiophene bridges exhibits green fluorescence in solution. The anticipated extension of the conjugation path length along the polymer chain was, however, not confirmed experimentally, which is not surprising, regarding the highly polar character of the B=N bond. To illustrate this point: in non-aromatic borazine, the so-called “inorganic benzene”, the electrons are as well mainly localized at nitrogen, resulting in only marginal ring currents, in sharp contrast to the well-known aromatic benzene.[238-240]

In recent years, Helten *et al.* investigated potentially π-conjugated linear polymers containing B=N units in the main chain. The bis(borane) adduct of *para*-phenylenediamine was found to undergo spontaneous dehydrocoupling in the presence of aniline to provide the dimer **49** with NBN units bridged by *para*-phenylene groups (Scheme 14).[241] Dissolution of the mono(borane) adduct of *para*-phenylenediamine in thf results as well in gas evolution, indicating the formation of dihydrogen and presumably the corresponding polymer, which was, however, obtained as an insoluble material, eluding further characterization. Solubility enhancing mesityl groups at the boron centers were incorporated by using mesityl dichloroborane in a Si/B metathesis with *N*,*N’*-bis(silyl)-substituted *para*-phenylenediamine. Subsequent end-capping with 4-*tert*-butyl-*N*-trimethylsilylaniline provided poly(iminoborane) **50** with an estimated degree of polymerization of X_n = 33 (Scheme 14).

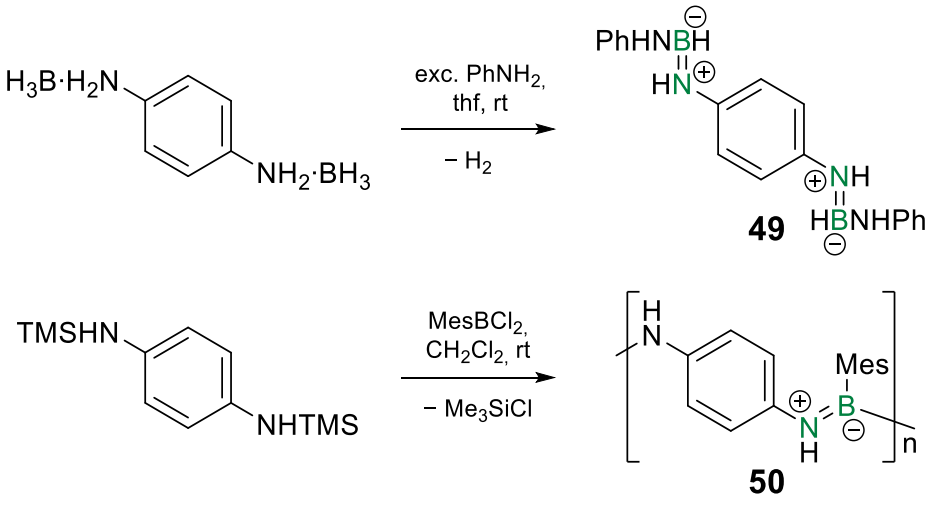

Scheme 14. Spontaneous dehydrocoupling of the bis(borane) adduct of *para*-phenylenediamine to bis(iminoborane) **49** and Si/B exchange polycondensation of disilyl-substituted *para*-phenylenediamine with mesityldichloroborane to poly(iminoborane) **50** (TMS = trimethylsilyl, Mes = 2,4,6-trimethylphenyl).

The sterically demanding mesityl group induces a distinct preference for the *E*,*Z* configuration according to DFT calculations and in line with the crystal structure of a corresponding monomeric diaminoborane. Along the polymer chain of **50**, however, different configurations are encountered according to the observed splitting of characteristic ^{1}H NMR signals upon lowering the temperature and in agreement with DFT calculations on the dimer. The longest wavelength absorptions of dimer **49** and polymer **50** are both observed in the UV at λ_{abs} = 290 and 295 nm, respectively, and only slightly bathochromically shifted by $\Delta\lambda$ = 20 to 30 nm compared to those of the corresponding monomers. This was taken as an indication of extended π-conjugation, although TD-DFT calculations on molecular model compounds additionally confirmed some extent of charge transfer to the boron. Nonetheless, the delocalization across the phenylene linker, the B=N moieties and the terminal phenyl groups was supported by the topologies of HOMO and LUMO according to DFT calculations. Considerable deviations from coplanarity, however, imply a significantly diminished π-conjugation along the polymer chain. The monomeric, oligomeric and polymeric compounds exhibit blue fluorescence (λ_{em} = 420 to 470 nm) with large stokes shifts ($\Delta\lambda$ = 160 nm in the case of polymer **50**), suggesting the relaxation of twisted intramolecular charge transfer excited states and thus emphasizing the possibly prevalent role of charge transfer to the boron centers along the chain rather than π-conjugation.

Iminoborane analogues of poly(*p*-phenylenevinylene) (PPV) and poly(thiophenevinylene) **51-54**, are obtained by two conceptually related strategies (Figure 12). Homopolymer **51** and copolymer **53** can be prepared by both methods, which involve either HBr or TMSBr elimination from *para*-phenylenediamine or the corresponding N-silylated derivative on the one hand side and the appropriate bis(bromoboryl) species on the other.[242-243] In contrast, the thiophene homopolymer **52** and copolymer **54** are only accessible *via* the Si/B metathesis polymerization due to the instability of the silyl-free diaminothiophene precursor.[243-244] The bromoboryl end groups in the resulting polymers were subsequently capped with dimethylamino groups through addition of $TMSNMe_2$. Approximate degrees of polymerization between X_n = 19 and 70 were obtained, with a slight trend towards higher values in the case of the HBr elimination pathway. Poly(iminoborane)s **51-54** give rise to remarkable bathochromic shifts of $\Delta\lambda$ = 60 to 80 nm of the absorption (**51**: λ_{abs} = 340 nm, **52**: λ_{abs} = 390 nm, **53**: λ_{abs} = 360, **54**: λ_{abs} = 370 nm) in comparison to the respective monomers

(Figure 12), which was interpreted as evidence for extended π-conjugation across the B=N double bonds along the polymer chain. Notably, these shifts are considerably larger than in the case of poly(diaminoborane) **50** (*vide supra*), possibly due to the incipient donor-acceptor character in copolymers **51-54**, promoting charge-transfer along the chain. This was particularly emphasized in the case of the aminothiophene-borylbenzene copolymer **54**, for which molecular model compounds showed a tendency towards higher wavelength absorptions in comparison to the corresponding aminophenylene-borylthiophene derivatives.

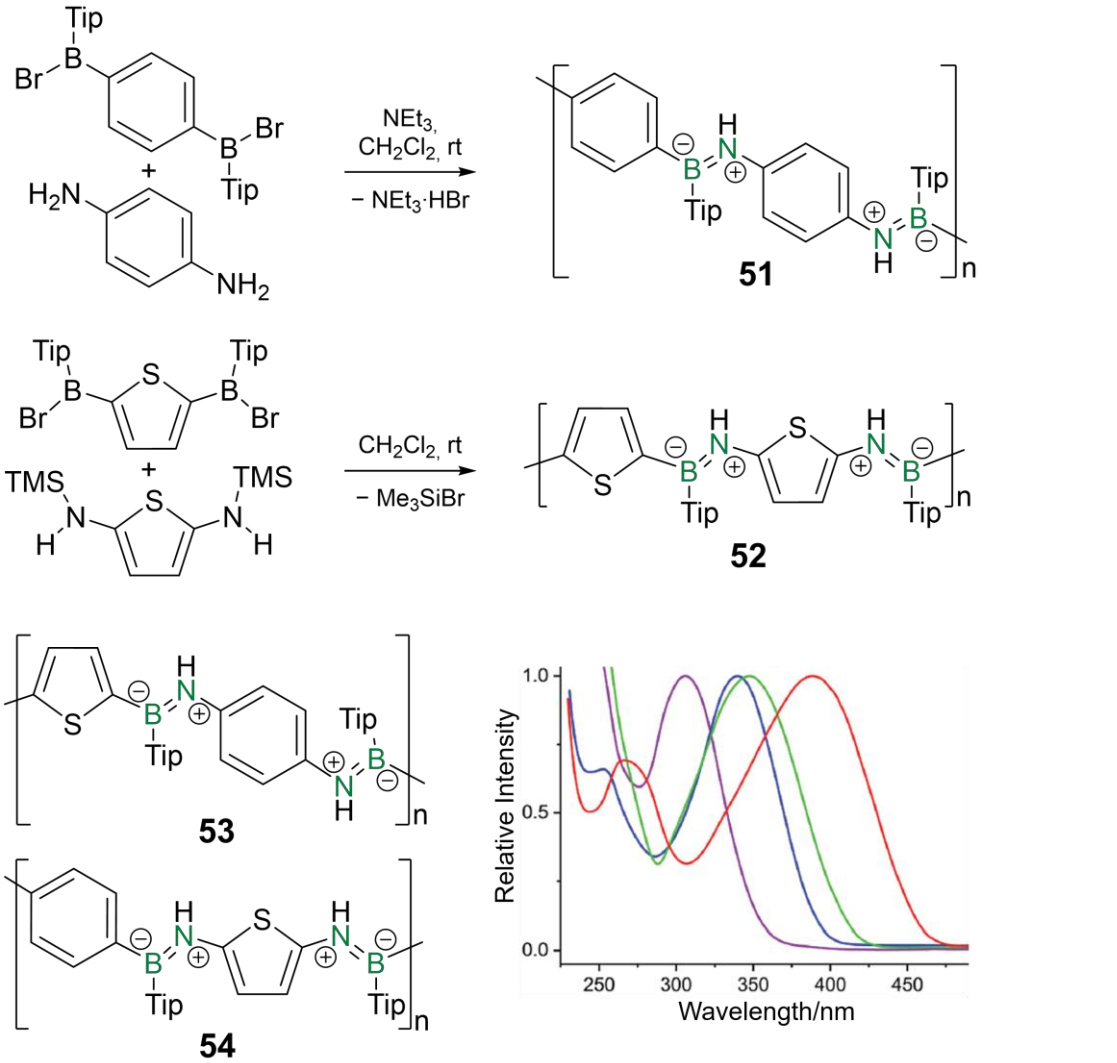

Figure 12. Top: HBr and Me_3SiBr elimination polycondensation methods for the synthesis of iminoborane analogues of poly(*p*-phenylenevinylene) and poly(thiophenevinylene) as applied to **51** and **52** (Tip = 2,4,6-triisopropylphenyl). Bottom: Poly(iminoborane)s with alternating thiophene and phenylene units and absorption spectra of the all-thiophene derivative **52** (red line), the corresponding monomeric system (purple line) and regioisomers of the dimeric models (blue and green lines), adapted with permission from Ref. [244], copyright © 2023 Wiley VCH.

In line with favorable orbital overlap between the organic framework and the B=N units and hence substantial electron transfer, the crystal structures of the monomeric model systems exhibit coplanarity of the π-substituents and the B=N units, which is, however, slightly less pronounced for the dimers. The frontier orbitals of dimers of **51-54** clearly indicate charge transfer from the π-spacer, where the HOMO is located, to the terminal π-ligands, showing major contributions to the LUMO. Systematic red-shifts of the absorption and the fluorescence (in PMMA films) are observed with increasing thiophene content: The all-thiophene polymer **52** exhibits yellowish-green luminescence (λ_{em} = 520 nm), whereas the all-phenylene derivative **51** shows deep-blue fluorescence (λ_{em} = 450 nm). The alternating copolymers **53** (λ_{em} = 460 nm) and **54** (λ_{em} = 500 nm) are characterized by emissions in between those of **51** and **52**, with a tendency towards higher wavelengths for **54** with favorable donor-acceptor matching: the donicity of the nitrogen center is enhanced by the adjacent thiophene and the electron-deficiency of boron by the moderately electron-accepting phenylene linker. Striking hypsochromic shifts of the emission and a substantial intensity increase were observed for solutions of the corresponding dimers upon increasing water content and strongly suggest aggregation-induced emission. Indeed, dynamic light scattering (DLS) measurements of the dimers confirmed the presence of particles with hydrodynamic radii between 130 and 160 nm. A positive solvatochromic effect due to intramolecular charge transfer upon excitation was presumed to counteract the hypsochromic shift, almost canceling it out in the case of the aminothiophene containing dimers of **52** and **54**.

In order to shed more light on the impact of the charge transfer due to the B=N moieties, the implementation of more electrophilic acceptor units, for instance, the well-established benzothiadiazole, might be a promising next step. As a consequence, the multiple bond character of the B=N bonds should be increased and charge-transfer along the polymer chain promoted, with implications for the absorption and emission.

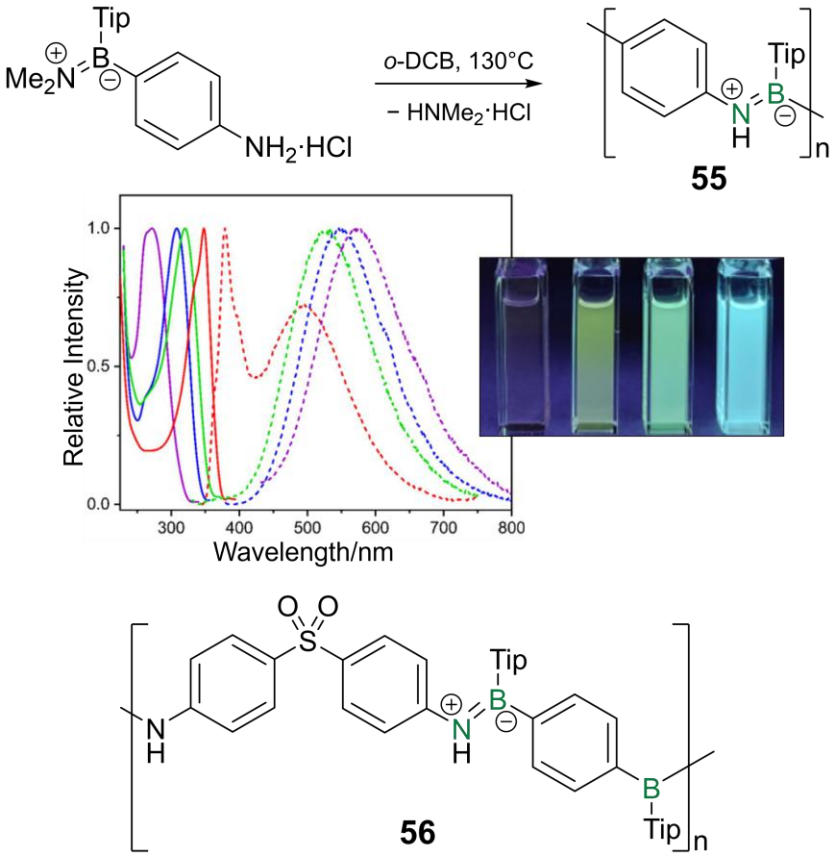

Figure 13. Top: Polymerization of a *para*-aminophenylene iminoborane at elevated temperature providing poly(iminoborane) **55** and absorption (solid lines) and fluorescence spectra (dotted lines) of **55** (red) and of the corresponding monomeric (purple), dimeric (blue) and trimeric (green) model systems, adapted with permission from Ref. [245], copyright © 2025 Wiley VCH. Bottom: Structure of a poly(iminoborane) with sulfoxide bridging units (Tip = 2,4,6-triisopropylphenyl).

Very recently, the same group developed a poly(iminoborane) **55** with a strictly alternating BN sequence (Figure 13), as opposed to the previous examples with BN/NB alternation.[245] Polymer **55** was prepared by heating a solution of a *para*-aminophenylene dimethyliminoborane for several days under the release of dimethylamine. The UV/Vis absorption is bathochromically shifted with increasing chain length (monomer: λ_{abs} = 272 nm, dimer: λ_{abs} = 308 nm, trimer: λ_{abs} = 322 nm, **55**: λ_{abs} = 348 nm), indicating the extension of π-conjugation along the polymer chain. The emission behavior resulting from the alternating BN pattern, however, differs fundamentally from the previous examples: the PPV-analogue **55** exhibits intense green-blue fluorescence in solution (λ_{em} = 380, 490 nm) – hypsochromically shifted compared to the monomeric (λ_{em} = 570 nm), dimeric (λ_{em} = 550 nm) and trimeric (λ_{em} = 530 nm) models – with a remarkable quantum yield of 58%, which is even

approaching the 65% of a PMMA film. A huge Stokes shift by $\Delta\lambda$ = 146 nm and the appearance of two distinct emission bands in solution indicate dual emission behavior due to an additional twisted intramolecular charge transfer, which is theoretically confirmed. This is in line with the absence of the higher energy band in the solid state, where the required structural reorganization in the excited state cannot occur. Instead, the dimer and trimer model systems exhibit aggregation-induced emission, demonstrated by a substantial hypsochromic shift with increasing water content (0% to 70%) in a thf solution of **55** by $\Delta\lambda$ ~ 50 nm. DLS indeed confirmed the formation of aggregates with hydrodynamic radii of 60 nm (dimer), 70 nm (trimer), and 106 nm (polymer **55**).

Different polymers with sulfur-containing bridges and B=N or B–O moieties were recently reported by Helten *et al.*, but only the poly(sulfoxide) **56** with B=N units (Figure 13) showed a significant bathochromic shift of the UV/Vis absorption (λ_{abs} = 320 nm) compared to corresponding monomers ($\Delta\lambda$ = 20 to 40 nm).[246] Notably, acids and bases induce selective degradation of these polymers, which holds considerable promise for application as drug delivery agents.

Group 14: Towards poly(tetrelene)s and poly(ditetrelene)s

While there have been several reports of bridged bis(tetrelene)s and bis(ditetrelene)s with element-carbon and element-element multiple bonds, respectively,[202,247-256] the development of synthetic protocols for higher oligomers and polymers still represents a major challenge. Due to the inherent lability of the heavier double bonds, they are prone to side reactions and typically require careful handling under an inert atmosphere. Furthermore, decreasing solubility with increasing chain length has prevented further chain growth as well as full characterization of presumably polymeric compounds in some cases.

Bis(disilenes) **57a-f** with variable aryl linkers and sterically encumbered 2,4,6-triisopropylphenyl (Tip) ligands were synthesized by Scheschkewitz *et al.* in substitution reactions of a lithium disilenide – an anionic silicon analogue of vinyllithium – with the corresponding dihaloarenes (Scheme 15).[202,250,253] The *para*-phenylene-substituted derivative **57a** served as precursor in a [2+2]-cycloaddition polymerization to the σ,π-conjugated phenylene-bridged poly(1,2-disilacyclobutene) **25** with a Si–Si motif in the repeat unit (*vide supra*). It is worth noting that the *in situ* generated silene TMS_2Si=Ad has also been employed in a polymerization to a poly(disilane) with a $–R_2Si–SiR_2–CH_2–$ repeat unit.[257] In this case, reported by Apeloig *et al.*, the regioselective reaction was either initiated by thermolysis of the silene, releasing radical species, or by addition of a radical initiator. A comparison of the ^{29}Si NMR shifts with molecular model compounds revealed the constitution of the repeat unit.

The Si=Si units in the bis(disilene)s **57a-f** exhibit relatively high deviations from coplanarity with the arylene substituents (dihedral angles: 25 to 75°). Nonetheless, substantial bathochromic shifts by $\Delta\lambda$ = 20 to 70 nm of the absorption maxima (λ_{abs} = 460 to 600 nm) compared to the corresponding monomers were obtained, which were partially attributed to conjugation between the Si=Si bonds across the arylene linkers and partially to intramolecular charge transfer transitions. *Meta*-substitution at the phenylene spacer (**57b**) resulted in an interruption of the conjugation and hence in a hypsochromic shift of the absorption (λ_{abs} = 450 nm)[250] compared to the corresponding *para*-phenylene-bridged tetrasilabutadiene **57a** (λ_{abs} = 510 nm).[202] The biphenyl-, bis(*para*-phenylene)acetylene-, naphthalene- and anthracene-bridged **57c-f** derivatives showed orange to red fluorescence in solution and in the solid state (λ_{em} =

510 to 590 nm).[253] Notably, no fluorescence was observed in the case of the thiophene-, bithiophene- and anthracene-bridged bis(disilene)s **57g–i** with dialkyl-substitution at the terminal silicon atoms and even larger dihedral angles (80–85°) reported by Iwamoto *et al*.[254]

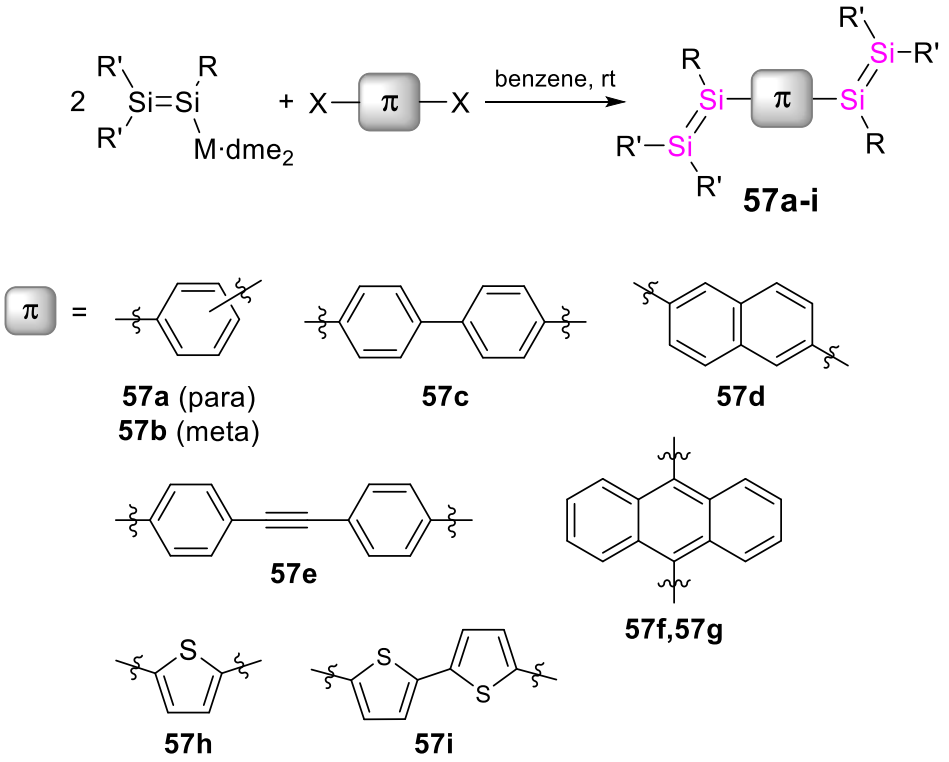

Scheme 15. Synthesis of bis(disilene)s **57a–i** (X = Br or I, **57a–57f**: R = R' = Tip = 2,4,6-triisopropylphenyl, M = Li, **57g–57i**: R = Mes = 2,4,6-trimethylphenyl, R' = 1,1,4,4-tetrakis(trimethylsilyl)-1,4-butyl, M = K).

In contrast to our *para*-phenylene-bridged bis(disilene), the analogue by Tamao *et al.* with *s*-hydrindacene substituents exhibits coplanarity between the Si=Si units and the central phenyl ring, and even the terminal phenyl groups deviate only slightly with a dihedral angle of 9.0° to the central phenyl group.[249] The solubility was, however, insufficient for the synthesis of longer oligomers, a problem that was overcome by the introduction of the hexyloxy groups to the *s*-hydrindacenyl substituents in **58a-d**.[249] Analogous to the insoluble dimer, the synthesis of a mixture of **58a-d** containing up to four Si=Si units occurred from the reaction of a *para*-phenylene-bridged bis(dibromosilane) with a dibromosilane (for end-capping) in a 1:2 ratio under reductive conditions (Figure 14). The efficient π-conjugation along the oligomer chains, resulting from the coplanarity of the phenyl rings and the Si=Si units, is corroborated by

remarkable bathochromic shifts of the UV/Vis absorption maxima (λ_{abs} = 470 to 610 nm) with increasing, albeit limited, chain length (Figure 14): for instance, the tetramer exhibits a red-shift of $\Delta\lambda$ = 145 nm in comparison to the monomer. Furthermore, red fluorescence (λ_{em} = 610 to 670 nm) with increasing wavelengths and quantum yields (10–48%) was observed for the oligomers, in vast contrast to the monomers. The experimentally proposed delocalization of the π-electrons in the oligo(disilenes) was theoretically confirmed by DFT calculations.[202,252] Notably, Tamao's disilenes showed moderate to good air stability in solution and in the solid state, respectively.[249] Consequently and in combination with the observed fluorescence, these disilenes constitute promising compounds for the use in optoelectronic devices – in fact, a remarkably stable *s*-hydrindacene dinaphthyldisilene was applied as the emissive layer in an OLED, albeit with very poor external quantum efficiency (0.014%).[258]

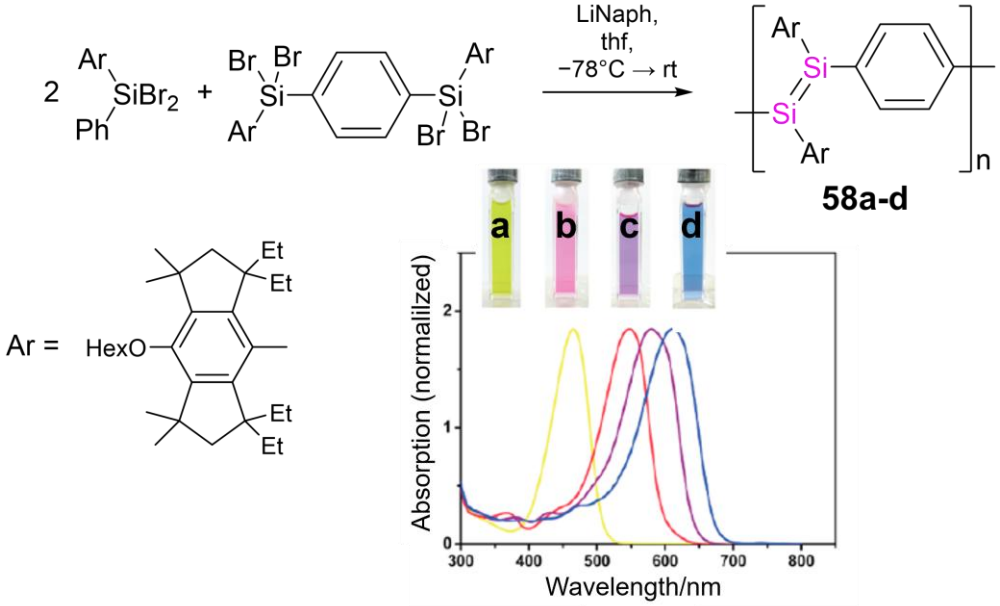

Figure 14. Disilene **58a** (n = 0), bis(disilene) **58b** (n=1), and oligo(disilene)s **58c,d** (n = 2, 3) with disilenyl end groups are obtained through reductive coupling of a bis(dibromosilane) and a dibromosilane in a 1:2 ratio. Inset: Absorption spectra and pictures of solutions of **58a-d**, adapted with permission from Ref. [252], copyright © 2015 American Chemical Society.

The *s*-hydrindacene ligand was further deployed in a coplanar π-conjugated bis(phosphasilene) with comparable air stability, obtained in a reaction of the bridged disilene and a lithium phosphide.[259] Similar to the disilenes, a substantial red-shift of

the absorption (λ_{abs} = 450 nm) compared to the monomer (λ_{abs} = 390 nm) was observed due to the extension of the conjugation. While the absorption of the P=Si dimer is considerably blue-shifted compared to the Si=Si analogue (λ_{abs} = 540 nm), the emission maximum (λ_{em} = 590 nm) differs by only 20 nm. The large Stokes shift in the phosphasilene case was attributed to substantial structural reorganization in the excited state, i.e. twisting about the P–Si bond.

It is worth noting, that the polymerization of arylene-bridged bis(hydrosilanes) on copper and gold surfaces was recently shown to result in the formation of a sub-monolayer of poly(disilene)s coordinated to the metal surface.[260]

While analogous germanium compounds are not known as of today, the recently reported synthesis of a silylenephenylene-bridged bis(digermene) **59** from a lithium digermenide and the dichlorinated *para*-disilylarylene linker provided a breakthrough for the development of polymers with Ge=Ge double bonds: the so-called *heavier acyclic diene metathesis* (HADMET) polymerization of **59** resulted in the formation of poly(digermene) **60** and $Tip_2Ge{=}GeTip_2$ in a net metathesis reaction through thermally induced homolytic cleavage of the Ge=Ge double bonds in the monomer (Scheme 16).[255]

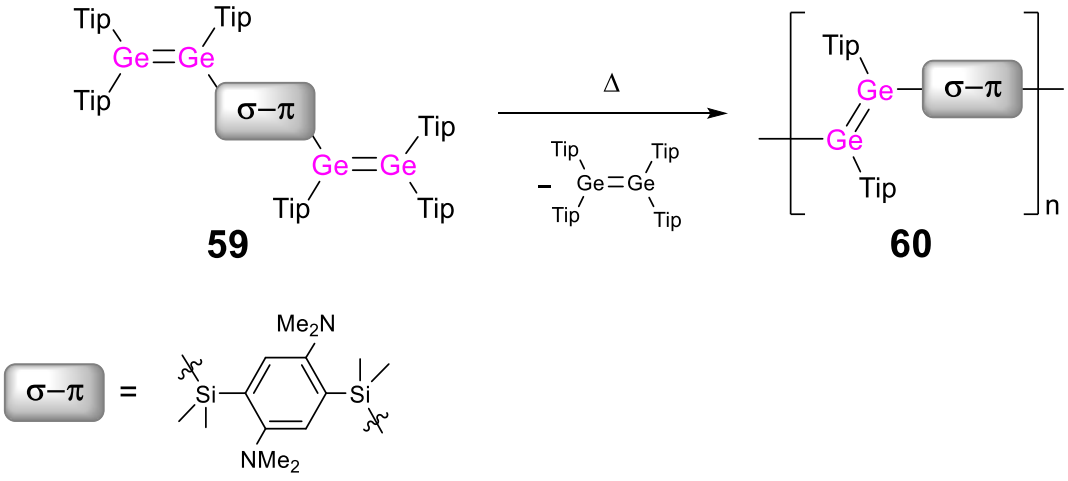

Scheme 16. HADMET polymerization of bis(digermene) **59** provides σ,π-conjugated poly(digermene)s **60**.

The N-donor in the arylene-linker was deliberately included in *ortho*-position to the silyl substituent providing the required intramolecular stabilization of the presumed transient bis(germylene) to avoid undesired side-reactions. The resulting polymer **60**

precipitated as a yellow solid from the reaction mixture and was insoluble in all common organic solvents. Therefore, the degree of polymerization was determined either indirectly by the amount of the released condensation by-product (X_n = 23), by a rough estimation based on the particle sizes (X_n = 26 to 31) obtained in DLS measurements and by ^{13}C CP/MAS NMR end group analysis (X_n = 23). Further analyses, in particular regarding the photophysical and film-forming properties and solution NMR spectroscopy, were prohibited by the poor solubility.

Group 15: Polymers with P=C and P=P in the conjugation path

The first example of a hybrid polymer with an implemented heavier main group multiple bond was the poly(phosphaalkene) **61** reported by Gates *et al.* in 2002 (Scheme 17).[261] It was obtained in a substitution reaction of a *para*-phenylene-bridged bis(disilylphophane) and tetramethylated terephthaloyl chloride, followed by [1,3]-sigmatropic Brook-type rearrangement to form the P=C double bonds. In the solvent-free process, the *para*-arylene-bridged starting materials were melted together as a neat 1:1 mixture for 21 to 34 hours and subsequent precipitation from a thf solution by addition of hexane at low temperature provided **61** as a yellow solid. ^{31}P and ^{29}Si NMR spectra revealed the formation of a *Z/E* isomeric mixture (Z/E ~ 1.1) and ^{31}P NMR end group analysis exhibited degrees of polymerization of X_n = 5 to 21. According to thermogravimetric analysis, the polymer showed reasonable thermal stability up until 190 °C. A slight bathochromic shift of the UV/Vis absorption of $\Delta\lambda$ ~ 15 to 30 nm compared to monomeric and dimeric model compounds supports the presence of π-conjugation in poly(phosphaalkene) **61**. Exclusive formation of the *Z,Z*-form, in which π-conjugation is presumably favored due to the *trans*-conformation of the arylene groups, is achieved by reversing the steric demand of the linking units of the two components: a durylene-bridged bis(phosphane) and unsubstituted terephthaloyl chloride instead of the above mentioned starting materials.[262] Limited solubility of the obtained product prevented further analyses and a determination of the degree of polymerization in this case. Nonetheless, the soluble part of the pure *Z*,*Z*-isomer gives rise to a bathochromically shifted absorption at λ_{abs} = 390 nm compared to the isomeric mixture (λ_{abs} = 330 to 340 nm), corroborating the assumed enhanced π-conjugation.

Protasiewicz *et al.* alternatively used a *para-tert*-butylphenyl-substituted phenylene linker in a phospha-Wittig reaction with variable π-bridged dialdehydes to form poly(phosphaalkene)s.[263] The insolubility of the initially obtained derivatives was addressed by employing a phenylene linker with solubility enhancing hexyloxy groups in *E*-poly(phosphaalkene) **62** (Scheme 18). The degree of polymerization amounted to only X_n = 6, according to end group analysis. The absorption (450 nm) is identical to that of the corresponding dimer, but the P=C groups provoke a bathochromic shift of $\Delta\lambda$ = 20 nm compared to *E*-poly(phenylenevinylene).

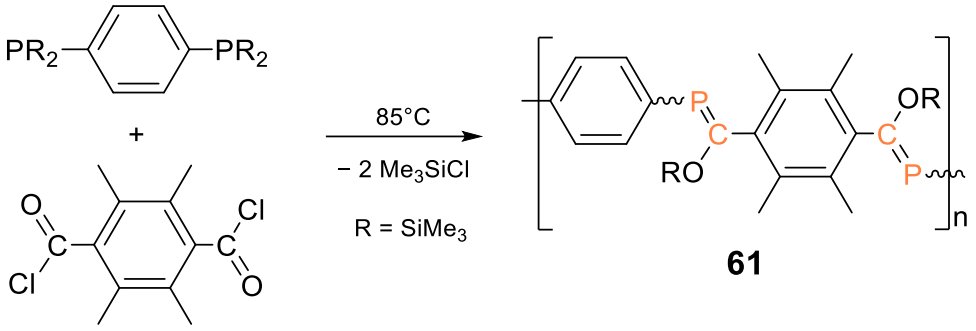

Scheme 17. Reaction of a 1:1 mixture of a phenylene-bridged bis(disilylphophane) and tetramethylated terephthaloyl chloride to poly(phosphaalkene) **61**.

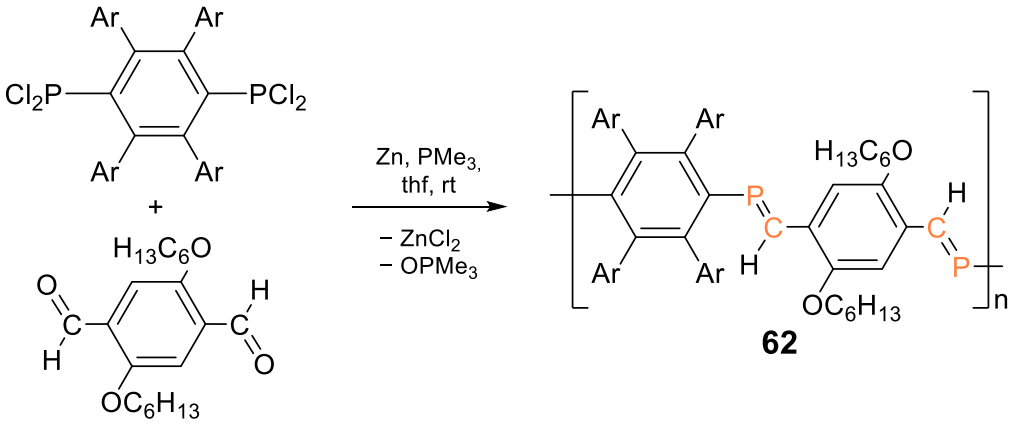

Scheme 18. The phospha-Wittig reaction of an arylene-bridged bis(dichlorophosphane) and dialdehyde yields *E*-poly(phosphaalkene) **62**.

In a conceptually related manner, the corresponding phospha-Wittig reaction provides poly(phosphaalkene)s **63a-c** (Scheme 19) with phenylene, biphenylene or thiophene linking units in combination with an oligo(phenylenevinylene) linker between the P=C bonds and a degree of polymerization of X_n = 4.5 to 6.5.[264] The same arylenevinylene bridged bis(ylide) was used to prepare a poly(diphosphene) **64** with P=P double bonds and X_n = 5.8 *via* photolytic or thermolytic cleavage of PMe_3 and formal oligomerization of the bis(phosphinidene) intermediate. While the absorption of poly(phosphaalkenes)s **63a-c** with an extended π-system as the linking unit are expectedly bathochromically shifted (λ_{abs} = 420 to 450 nm) compared to initially reported **61** and derivatives by Gates *et al.* (λ_{abs} = 330 to 390 nm, *vide supra*),[261-262] the absorption wavelength is not influenced by the chain length as manifest in the comparison with a bis(phosphaalkene) model compound. Nonetheless, poly(phosphaalkene)s **62** and **63a-c** exhibit green-blue fluorescence (λ_{em} = 480 to 550

nm), which is enhanced in comparison to the model compound, and hence indeed corroborating the presence of π-conjugation. Poly(diphosphene) **64** exhibits the π→π* transition in the same region of the absorption spectrum at λ_{abs} = 440 nm and an additional n→π* absorption band at longer wavelength (λ_{abs} = 480 nm).

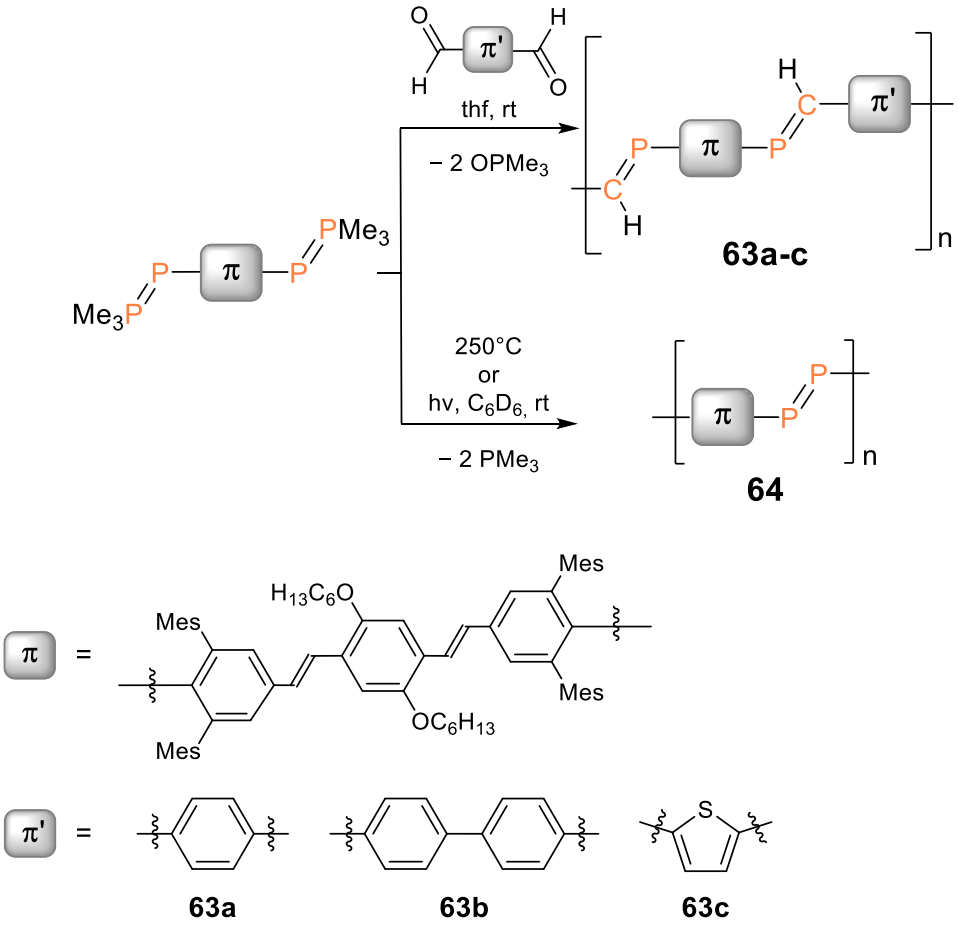

Scheme 19. Phospha-Wittig reaction of an arylenevinylene-bridged bis(diphosphene) with dialdehydes yields poly(phosphaalkene)s **63a-c** and thermolysis or photolysis provides poly(diphosphene) **64**.

Aims and Scope

The advances of the past decades in the incorporation of inorganic main group heteroelements into the main chain of conjugated polymers have showcased significant impact on the band gaps and thus the photophysical properties of the materials. First applications in electronic devices are emerging (*vide supra*). Nonetheless, as yet there are only very few examples with multiple bond motifs involving heavier heteroelements.

The short oligo(disilene)s reported by Tamao *et al.* have been the only extended systems featuring multiple bonds of the heavier Group 14 double bonds in the conjugation path[252] until our recent report on the heavier acyclic diene metathesis (HADMET).[255] Applied to bridged bis(digermene) **59**, the HADMET procedure resulted in the formation of poly(digermene) **60** with Ge=Ge double bonds (Scheme 20), which, however, proved insoluble in all common organic solvents and hence was neither amenable to analysis in solution, nor processible into a thin film, generally required for the application in (opto-)electronic devices.

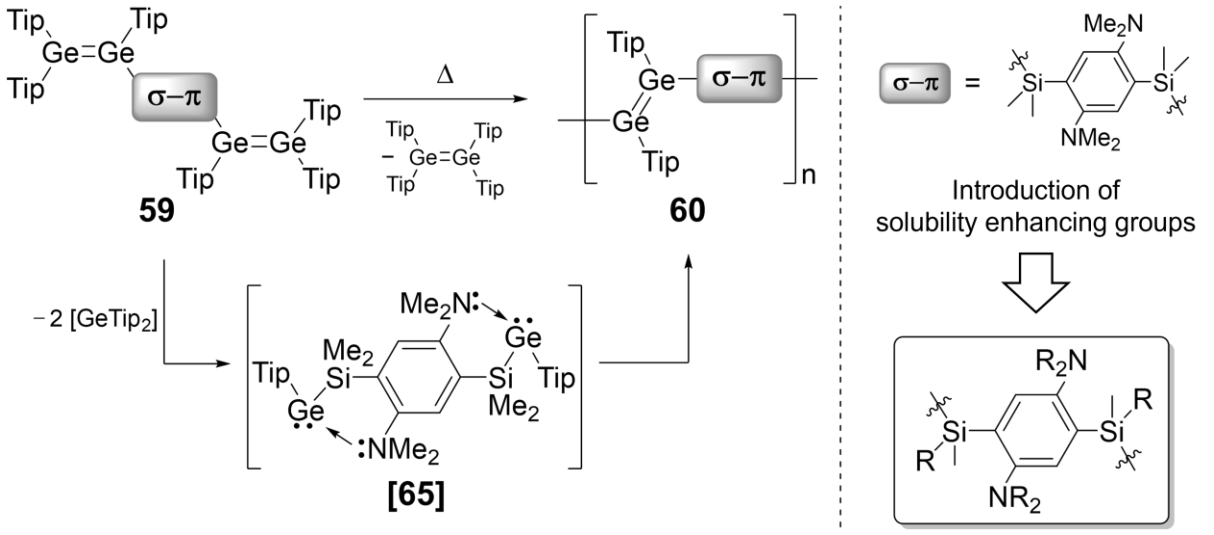

Scheme 20. HADMET polymerization of bis(digermene) **59** to poly(digermene) **60** *via* intermediate bis(germylene) **[65]** and schematic representation of the considered alkyl substitution in the silylenearylene linker for the development of soluble poly(digermene)s (Tip = 2,4,6-triisopropylphenyl).

As the presence of longer alkyl chains is commonly known to enhance solubility, the incorporation of alkyl groups into the repeat unit of the poly(digermene) was considered. The silylene and amino functionalities of the arylene spacer were selected

for an according derivatization with longer alkyl chains (Scheme 20). In the first part of this thesis, the development of synthetic protocols for the required modified monomers and the corresponding HADMET polymerizations is discussed. The structure-function relationship of the resulting poly(digermene)s is explored by applying various methods in solution, in bulk solids and in thin films.

As proposed key intermediate in the Ge=Ge double bond metathesis of bis(digermene) **59**, bis(germylene) **[65]** (Scheme 20) is of particular interest with regard to the elaboration of functionalization strategies for poly(digermene)s. The isolation of **[65]** was envisaged through donor stabilization with N-heterocyclic carbenes (NHCs) and cyclic (alkyl)(amino)carbenes (CAACs), respectively. CAACs could provide stronger σ-donation and in principle allow for considerable π-backdonation (**[65]CAAC**, Scheme 21),[265-274] which may allow for their application as end groups in poly(digermene)s.

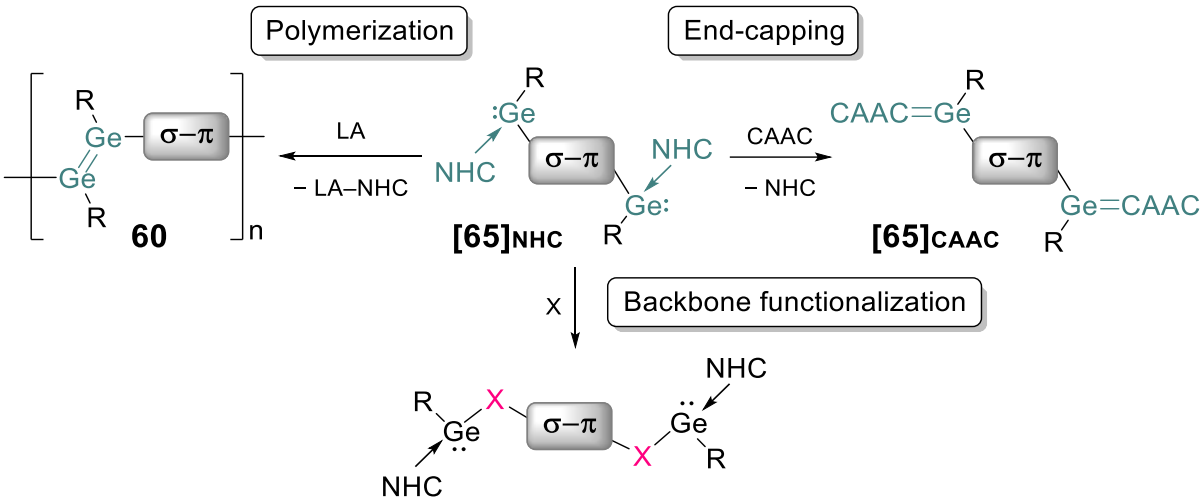

Scheme 21. Versatile reactivity of NHC-bis(germylene) investigated in the present thesis (R = Tip = 2,4,6-triisopropylphenyl, σ–π = 2,5-dimethylaminobenzene-1,4-dimethylsilylene, LA = Lewis acid, X = small electrophile).

In contrast, the versatile reactivity of an NHC-bis(germylene) with typically weak donor-acceptor bonds (**[65]NHC**) is investigated (Scheme 21): A new route towards poly(digermene)s *via* Lewis acid-induced NHC-abstraction is employed and the reactivity towards bulky nucleophiles, such as CAAC, and small electrophiles, on the other hand, is determined. While with CAAC, the formation of stronger carbene-germylene bonds was conceived, small electrophiles, such as CO_2, were going to be investigated for their potential in backbone functionalization under retention of the Ge(II) centers.

Results and Discussion

Near-Infinite-Chain Polymers with Ge=Ge Double Bonds

Anna-Lena Thömmes,* Thomas Büttner, Bernd Morgenstern, Oliver Janka, Guido Kickelbick, Bart-Jan Niebuur, Tobias Kraus, Markus Gallei, David Scheschkewitz,*
Angew. Chem. Int. Ed. **2024**, *63*, e202415103 (1–11).

https://doi.org/10.1002/anie.202415103

German Version: Nahezu unendlich lange Polymere mit Ge=Ge-Doppelbindungen. *Angew. Chem.* **2024**, *136*, e202415103 (1–12).

https://doi.org/10.1002/ange.202415103

The results are additionally concluded and put into context in the "Conclusions and Outlook" chapter of this thesis.

Contributions of the authors:

Anna-Lena Thömmes

Lead: Synthesis and characterization of the compounds, formal analysis, data curation, investigation, methodology, validation, visualization, writing (original draft)
Equal: Conceptualization, funding acquisition, writing (review and editing)

Thomas Büttner

Lead: AFM measurements
Supporting: Data curation, formal analysis, methodology, validation, visualization

Bernd Morgenstern

Lead: X-Ray analysis and crystal structure refinement

Oliver Janka

Lead: Powder X-ray diffractometry and analysis of the corresponding data
Supporting: Validation

Guido Kickelbick

Supporting: Methodology, resources, validation, writing (review and editing)

Bart-Jan Niebuur

Lead: SAXS measurements and analysis of the corresponding data
Supporting: methodology, validation, writing (review and editing)

Tobias Kraus

Supporting: Formal analysis, investigation, methodology, resources, validation, writing (review and editing)

Markus Gallei

Supporting: Formal analysis, validation, writing (review and editing)

David Scheschkewitz

Lead: Project administration, resources, supervision
Equal: Conceptualization, funding acquisition, writing (review and editing)
Supporting: Data curation, formal analysis, investigation, methodology, validation, visualization

GDCh Research Article Angewandte International Edition Chemie www.angewandte.org

Check for updates

How to cite: *Angew. Chem. Int. Ed.* **2024**, *63*, e202415103
doi.org/10.1002/anie.202415103

VIP Conjugated Polymers Very Important Paper

Near-Infinite-Chain Polymers with Ge=Ge Double Bonds

Anna-Lena Thömmes, Thomas Büttner, Bernd Morgenstern, Oliver Janka, Guido Kickelbick, Bart-Jan Niebuur, Tobias Kraus, Markus Gallei, and David Scheschkewitz**

In memory of Ian Manners

Abstract: Despite considerable interest in heteroatom-containing conjugated polymers, there are only few examples with heavier p-block elements in the conjugation path. The recently reported heavier acyclic diene metathesis (HADMET) allowed for the synthesis of a polymer containing Ge=Ge double bonds—albeit insoluble and with limited degree of polymerization. By incorporation of long alkyl chains, we now obtained soluble representatives, which exhibit degrees of polymerization near infinity according to diffusion-ordered NMR spectroscopy (DOSY) and dynamic light scattering (DLS). UV/Vis and NMR data confirm the presence of σ,π-conjugation across the silylene-phenylene linkers between the Ge=Ge double bonds. Favorable intermolecular dispersion interactions lead to ladder-like cylindrical assemblies as confirmed by X-ray diffraction (XRD), small angle X-ray scattering (SAXS) and DLS. AFM and TEM images of deposited thin films reveal lamellar ordering of extended polymer bundles.

[*] A.-L. Thömmes, T. Büttner, Prof. Dr. D. Scheschkewitz
Krupp-Chair for General and Inorganic Chemistry
Saarland University
66123 Saarbrücken, Germany
E-mail: anna-lena.thoemmes@uni-saarland.de
scheschkewitz@mx.uni-saarland.de

Dr. B. Morgenstern, Dr. O. Janka, Prof. Dr. G. Kickelbick
Inorganic Solid-State Chemistry
Saarland University
66123 Saarbrücken, Germany

Dr. B.-J. Niebuur, Prof. Dr. T. Kraus
INM—Leibniz-Institute for New Materials
66123 Saarbrücken, Germany

Prof. Dr. T. Kraus
Colloid and Interface Chemistry
Saarland University
66123 Saarbrücken, Germany

Prof. Dr. M. Gallei
Polymer Chemistry
Saarland University
66123 Saarbrücken, Germany

Introduction

Polymers exhibit considerable advantages compared to many other materials such as high flexibility, light weight, low cost, low toxicity, and facile processability and handling. They are used in various applications, e.g. food conservation, clothes, furniture, encapsulation, membranes, medical implants, and many more.[1] Conjugated polymers are extensively applied in commercial electronic devices[2] and some even outperform silicon and germanium as semiconductors.[3] Bulk conducting polymers can be tuned by alteration of the chemical composition: the incorporation of heteroelements, for instance, is essential to the *indirect* alteration of the band gap through secondary effects without incorporation into the conjugation path. As a technology-critical semiconductor,[4] germanium is frequently employed in this context.[5]

The availability of a variety of stable unsaturated compounds of the heavier p-block elements,[6] inspired new avenues in the design of conjugated systems. The heavy analogues of alkenes exhibit distinct properties due to differences in the topological and electronic structures: the Ge=Ge double bond motif, in stark contrast to the colorless alkenes, absorbs in the visible range in line with the inherently small HOMO–LUMO gap. The entire range of the visible spectrum can be addressed by changing the substituents: while most aryl and alkyl substituted digermenes are bright yellow,[7] variable red-shifts can be achieved by B, Si, Ge and P substitution of the Ge=Ge bond[8–11] or its incorporation into cyclic motifs.[7i,12] Heavier alkenes with residual functionality allow for the incorporation of unsaturated bonding motifs into extended systems.[13] In particular, the nucleophilic heavier analogues of vinyl anions[8,9,14,15] have paved the way for the synthesis of arylene-bridged group 14 oligomers with element-element or element-carbon double bonds in the conjugation path.[10,14,16–20]

Unsaturated motifs of heavier p-block elements in the repeat unit of conjugated polymers exert a *direct* influence on the band gap, but only a handful of such compounds are known[21] due to the inherent preparative challenges associated to heavier main group multiple bonding:[6] typically, meticulous exclusion of air and water is a must to prevent the otherwise facile hydrolysis of the unsaturated motif. Bulky substituents are also required to kinetically stabilize the compounds against secondary intermolecular reactions.

GDCh Research Article Angewandte International Edition Chemie

Pioneering work by the groups of Gates and Protasiewicz on poly(phosphaalkene)s such as **I** with P=C bonds in the conjugation path and polymerization degrees of $X_n = 4.5$ to 21[22] was soon complemented by the isolation of a poly(diphosphene) **II** with P=P bonds and $X_n = 5.8$ (Scheme 1).[23] In contrast, the only examples in case of group 14 had been the short oligo(disilene)s **III** ($X_n = 2$ to 3)[17] until our recent report on the heavier acyclic diene metathesis (HADMET) of a phenylene bridged bis(digermene). The HADMET process results in polymer **IV** with Ge=Ge repeat units in the pathway of a σ,π-conjugated system.[10] Although the degree of polymerization X_n of **IV** between 21 and 31 (depending on the method) is competitive with the P=C and P=P containing materials, its insolubility in all common organic solvents prevented a comprehensive analysis and—even more importantly—was assumed to be the limiting factor during chain growth. We now report on the synthesis of modified heavier acyclic dienes with solubility-increasing alkyl chains at silicon or nitrogen. Their polymerization by the HADMET procedure yields soluble rod-like polymers with essentially unlimited chain lengths. The increased solubility enables the full characterization of these Ge=Ge containing σ,π-conjugated polymers and their deposition as thin films with noteworthy patterns of lamellar bundles.

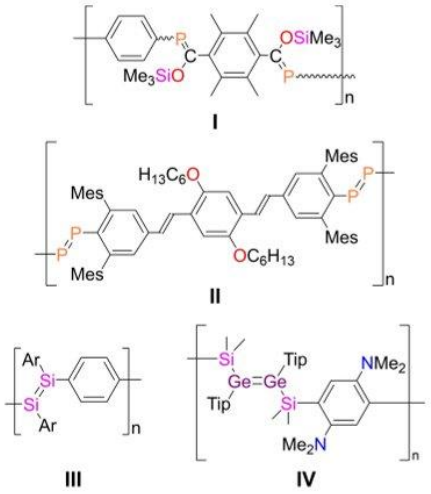

Scheme 1. Reported polymers containing heavier p-block multiple bonds: bridged poly(phosphaalkene) **I**,[22a] poly(diphosphene) **II** (Mes = 2,4,6-trimethylphenyl),[23] disilene oligomers **III**[17] (Ar = 1,1,3,3,5,5,7,7-octaethyl-s-hydrindacen-4-yl) and poly(digermene) **IV** (Tip = 2,4,6-triisopropylphenyl).[10]

Results and Discussion

In order to modify the linking unit between the Ge=Ge moieties for higher solubility, we envisaged the incorporation of longer alkyl chains at either the silylene spacers or at the pending amino groups. Methyloctyl substituted chlorosilane **1a** was synthesized in an analogous manner to the published precursor synthesis[10] by using methyloctyldichlorosilane instead of Me_2SiCl_2 (Figure 1a). Crystallization from a hexane solution yields 62 % of the corresponding bis(chlorosilyl)benzene as a diastereomeric mixture (dr = 1:1) according to heteronuclear NMR spectroscopy and in agreement with the presence of two stereogenic

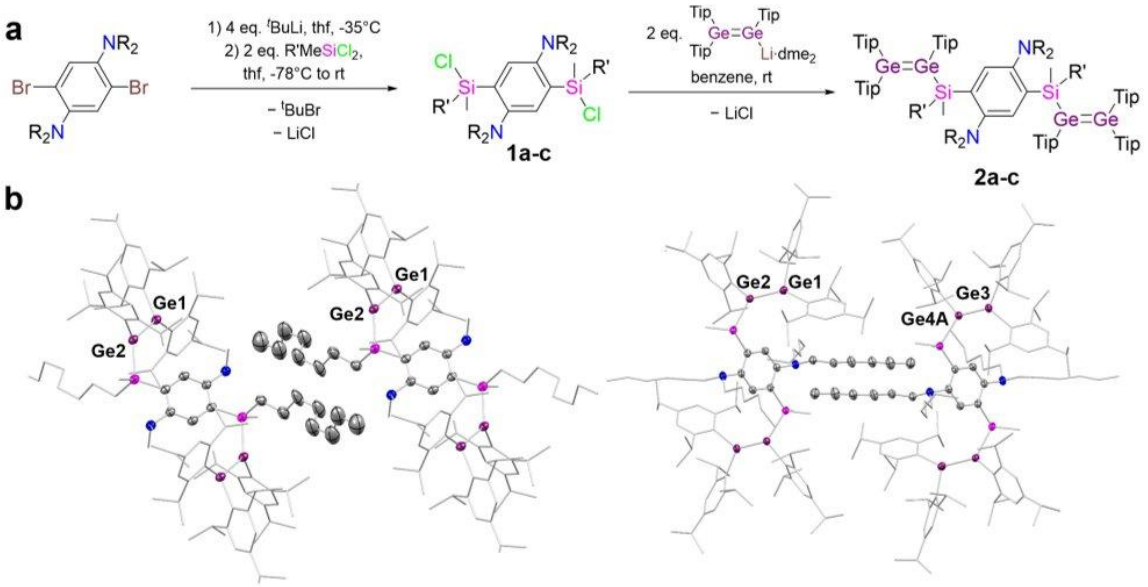

Figure 1. a) Synthesis of bis(chlorosilyl) linkers **1a–c** and substitution reactions with a lithium digermenide to bis(digermene)s **2a–c** (**1a**,**2a**: R=Me, R′=Oct, **1b**,**2b**: R=Hex, R′=Me, **1c**,**2c**:[10] R=R′=Me). b) Adjacent molecules in the single crystal X-ray structures of bis(digermene) monomers **2a** (left) and **2b** (right).

centers at the silicon atoms. X-ray analysis of a colorless crystal reveals the structure of the *meso*-form (for details see Supporting Information).

For adaption of the amino groups, hexyl chains were attached to the nitrogen atoms in an earlier step of the linker synthesis (see Supporting Information). The achiral bis(chlorosilyl) linker **1b** with dihexylamino groups was obtained by reaction of the dilithiated precursor with Me_2SiCl_2 as colorless crystals in 75 % yield (Figure 1a).

Both, **1a** and **1b**, proved indeed suitable for twofold incorporation of the Ge=Ge moiety by treatment with lithium digermenide $Tip_2Ge{=}GeTip(Li{\cdot}dme_2)$ affording bis(digermene)s **2a**,**b** as yellow crystals in isolated yields of 48 % and 61 %, respectively (Figure 1a). The increased steric demand in **2a**,**b** compared to *Si*,*Si*,*N*,*N*-tetramethyl substituted **2c**[10] requires longer reaction times of 48 h. The incorporation of two longer alkyl chains at silicon completely suppresses the formation of the bis(digermene).

In the synthesis of bis(digermene) **2a**, the diastereomeric ratio of the precursor **1a** is retained in the reaction mixture (dr = 1:1). In crystallized samples of **2a**, however, the *meso*-isomer is enriched to a ratio of dr = 1:7 as determined by the intensity of the ^{29}Si NMR signals at 7.28 (rac) and 7.12 ppm (meso). The ^{1}H and ^{13}C NMR spectra of the two bis(digermene)s show similar shifts as those of previously reported silyl-substituted aryldigermenes.[8,10,11d] ^{1}H NMR spectroscopy reveals characteristically downfield shifted singlets due to the protons at the phenylene linker each at 8.28 (**2a**) and 8.36 ppm (**2b**).

X-ray diffraction on single crystals obtained from saturated solutions (**2a**: hexane, RT; **2b**: Et_2O, −23 °C) confirm the molecular structures of **2a** and **2b** in the solid state (Figures 1b and S30, S31 in Supporting Information). The Ge–Ge distances of 2.2923(5) Å (**2a**) and 2.2742(5)/2.2972(9) Å (**2b**) are slightly shorter than the Ge=Ge double bond lengths in the *Si*,*Si*,*N*,*N*-tetramethyl derivative **2c** (2.3038 Å),[10] and in asymmetrically substituted $Tip_2Ge{=}GeTip(SiPh_3)$ (2.3279 Å),[11d] but fit quite well the corresponding distances in tetrakis(trialkylsilyl)substituted digermenes (2.266–2.298 Å).[11a] The substituents at the double bonds are more or less *trans*-bent and twisted as common for digermenes, a manifestation of the shallow bending potential at the heavier double bonds.[6b,24] The values for the *trans*-bent angle θ vary between 15.7(1)° and 35.5(1)°, for the twisting angle τ between 17.9(1)° and 21.8(1)°.

UV/Vis spectra of both bis(digermene) monomers **2a**,**b** exhibit the longest wavelength absorption at 431 nm, in the range of $\pi\rightarrow\pi^*$ transitions of the Ge=Ge double bonds in aryl and silyl digermenes (406 to 438 nm),[7a,c,8,10,11a,d,25] hence confirming the integrity of the double bond in solution. The high extinction coefficients of $\varepsilon = 27800$ (**2a**) and 33400 $L\,mol^{-1}\,cm^{-1}$ (**2b**) are in line with the large absorption cross sections typical of conjugated systems, notably also in hyperconjugated silyl-substituted systems.[26,27] The presence of σ,π-conjugation in **2a**,**b** is confirmed by DFT calculations at the BP86-D3(BJ)/def2-SVP level of theory (Figure 2): the π-orbitals of the Ge=Ge double bonds are represented by in-phase and out-of-phase combinations of both Ge–Ge bonds, with visible mutual σ*-contributions, separated by as much as 0.11 eV (**2a**) and 0.13 eV (**2b**). The corresponding unoccupied π*-orbitals are equally non-degenerate, albeit with smaller separations of 0.03 and 0.08 eV, respectively. The LUMO + 2, located mainly at the aniline linker, exhibit contributions from the σ*-orbitals at the silicon atoms in the conjugation path as well (see Supporting Information).

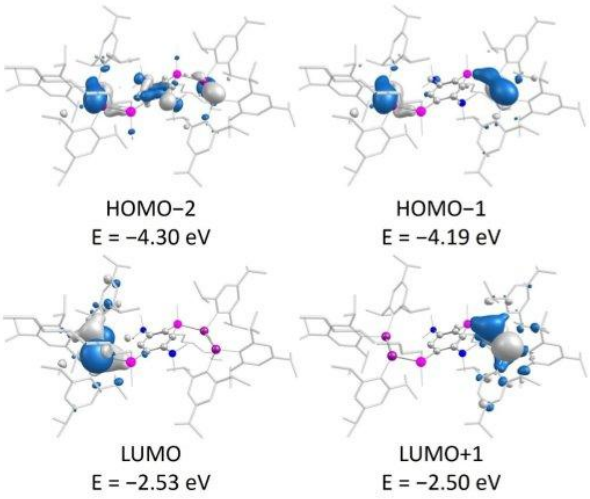

Figure 2. Selected frontier orbitals of bis(digermene) monomer **2a** (contour value 0.036). Hydrogen atoms omitted for clarity.

With these bridged digermenes as monomers in hand, we attempted the HADMET polymerization to the corresponding Ge=Ge-containing polymers (Scheme 2). Heating of **2a**,**b** in solution led to the elimination of $Tip_2Ge{=}GeTip_2$ according to ^{1}H NMR monitoring. The appearance of broad signals in the ^{1}H, ^{13}C and ^{29}Si NMR spectra suggested the formation of the targeted polymers and the sharp signals of the molecular starting materials decrease in intensity. Polymerization of octyl-substituted monomer **2a** is observed at 65 °C in benzene just as it had been in the case of the previously reported *Si*,*Si*,*N*,*N*-tetramethyl derivative **2c**.[10] The hexylamino derivative **2b** requires heating to 105 °C in toluene despite the sterically less demanding environment of the Ge=Ge units. The additional stabilization is most likely due to favorable dispersion interactions between the Tip groups and the alkyl chains, which are increased in the presence of four instead of two long alkyl chains.[28]

For a first estimation of the degree of polymerization X_n, the progress of the step-growth polymerization was monitored by integration of a characteristic ^{1}H NMR signal of the concomitantly formed by-product $Tip_2Ge{=}GeTip_2$.[10] According to Carother's $X_n = (1-p)^{-1}$ correlation between the number-average degree of polymerization X_n and the conversion p of a bifunctional monomer in a condensation polymerization, $X_n = 25$ for $p = 96$ %.[29] This is achieved after 44 h in the case of the previously reported *Si*,*Si*,*N*,*N*-tetramethyl substituted derivative **IV** whose further polymerization is prevented by its low solubility.[10]

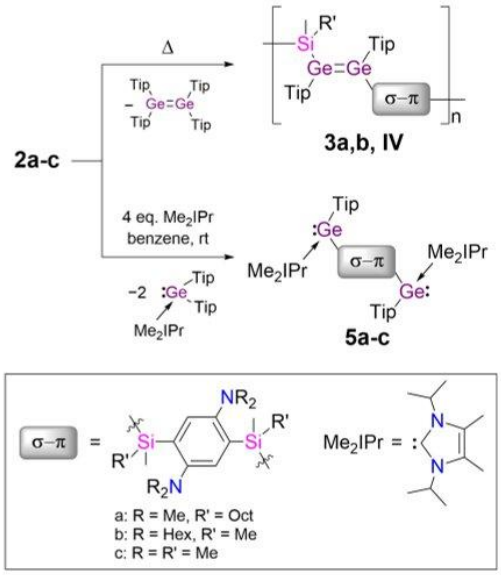

Scheme 2. HADMET polymerization of bis(digermene) monomers **2a–c** yielding soluble poly(digermene)s **3a,b** and previously reported insoluble **IV** and reaction of bis(digermene) monomers **2a–c** with *N*-heterocyclic carbene 1,3-diisopropylimidazol-4,5-dimethyl-2-ylidene (Me_2IPr) providing NHC-bis(germylene) adducts **5a–c** and Tip_2Ge–NHC.

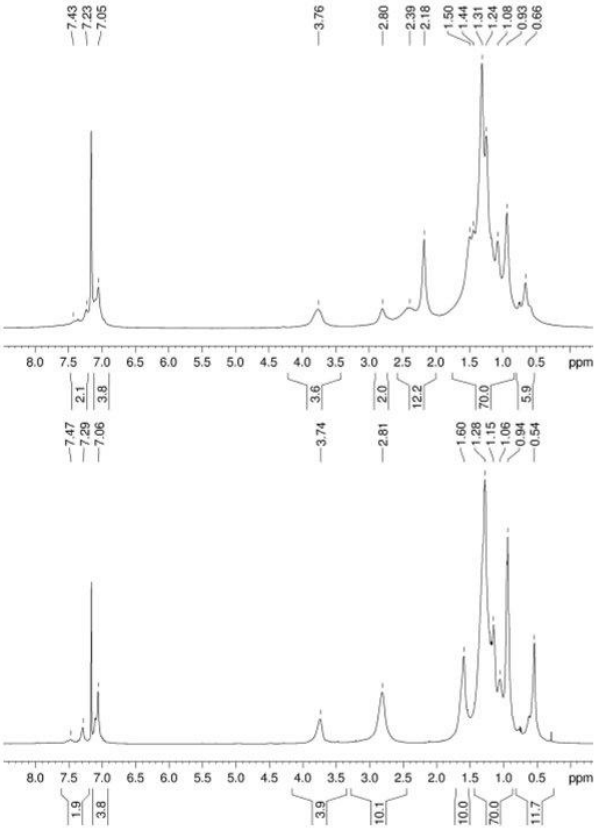

Figure 3. ^{1}H NMR spectra of 76 g L^{-1} C_6D_6 solutions of poly(digermene)s **3a** (top) and **3b** (bottom), corresponding to repeat unit concentrations of c(**3a**) = 74 and c(**3b**) = 68 mol L^{-1}. Given a detection limit of 50 μM, the absence of Tip_2Ge end group signals suggests minimum degrees of polymerizations of 1400.

As expected, the alkylated derivatives indeed exhibit a much higher solubility (vide infra) so that long polymer chains still remain available for further step-growth. In these cases, 96 % conversion and hence $X_n = 25$ is achieved after 18 h (**2a**) and 19 h (**2b**) while the ^{1}H NMR signals of the monomers have completely disappeared after 40 h (Figure S53, Supporting Information). In view of the exponential increase of X_n in step-growth polymerization,[10,29,30] confirmed by plotting X_n over the reaction time (see Supporting Information), the degree of polymerization of the soluble digermene polymers **3a**,**b** must be substantially higher than 25. The inherently large standard deviation close to full conversion (with X_n approaching infinity) is prohibitive regarding an exact value for X_n based on this method.

Despite the high solubility in hydrocarbon and etheric solvents, separation of the polymers **3a**,**b** from the $Tip_2Ge{=}GeTip_2$ by-product is possible by precipitation with acetonitrile from a toluene solution at room temperature (**3a**) and −55 °C (**3b**; for details see Supporting Information). As typical for dissolving polymers,[31] it takes about a day (depending on the desired concentration) at room temperature to obtain slightly viscous yellow solutions of poly(digermenes) **3a**,**b** in different solvents. Most of the broad peaks in the solution ^{1}H NMR spectra (Figure 3) appear at similar shifts as those of the corresponding monomers. Apart from the polymer broadening of the resonances, the main difference between the ^{1}H NMR spectra of **3a**,**b** and of the monomers **2a**,**b** is the significant highfield shift of the resonances of the phenylene linkers by about 1 ppm (**2a**: 8.28, **2b**: 8.36, **3a**: 7.3, **3b**: 7.4 ppm). Considering that the metathetic elimination of the diarylgermylene fragment $GeTip_2$ and its replacement by the Si-bonded germylene terminus of the polymer chain is separated from the phenylene hydrogen atoms by no less than five bonds, the pronounced shielding is a clear indication of a conjugation effect across the polymer chain, namely σ,π-conjugation involving σ*-orbitals at the silylene linkers. The donation of electron density to the Si centers receives further support from the ^{29}Si NMR resonances of both polymers, which are upfield shifted by 8.0 to 10 ppm compared to the corresponding monomer resonances (**2a**: 7.28, 7.12; **2b**: 7.19; **3a**: −0.91; **3b**: −2.76 ppm).

The NMe_2 and SiMe proton resonances of the *Si*-octylated derivative **3a** exhibit small shoulders, which are tentatively attributed to the presence of different diastereomers of the polymer owing to the stereogenic centers at the silicon atoms. Integration of all peaks agrees particularly well with the number of protons in the repeat units hence suggesting a remarkably low amount of Tip_2Ge end groups. In fact, assuming a detection limit of 50 μM, the corresponding peaks should be detectable at polymerization degrees smaller than 1400. Their absence is hence consistent with

the formation of near-infinite polymer chains[32] as suggested by the ^{1}H NMR spectroscopic monitoring of the conversion (vide supra).

The ^{13}C NMR signals of **3a**,**b** at similar chemical shifts as in the monomers are mostly quite broad with the exception of those assigned to the methyl and methylene groups of the longer alkyl side chains. The latter are remarkably sharp, confirming that they are less prone to the electronic influence of polymer chain. ^{13}C and ^{29}Si CP/MAS NMR spectra confirm the structural integrity of the polymers in the solid state (see Supporting Information).

Delocalization along the polymer main chain is further supported by second order perturbation analysis at the BP86/def2-TZVPP level of theory on digermene **4**, serving as model compound for the repeat units of polymers **3a**,**b**. The optimized geometry of **4** agrees well with the experimental one, exhibiting only minor variations in the bond lengths and angles. The π(Ge=Ge) bond (NBO 96, see Supporting Information Figure S70 for NBO plots) donates into the σ*-orbitals of the Si–C bonds (NBO 247: 1.51 kcal mol^{-1}; NBO 249: 2.28 kcal mol^{-1}). The phenylene linker (NBO 142) interacts with the σ*-orbital of the Ge–Si bond (NBO 243: 2.14 kcal mol^{-1}). Additional σ→σ* conjugation is reflected by stabilization energies of 2.54 kcal mol^{-1} and 1.92 kcal mol^{-1}, respectively, for the interactions between the Ge–Si and Ge–Ge σ-bonds (NBOs 93 and 95) and the corresponding σ*-orbitals (NBOs 243 and 245). These conjugative interactions result in relatively low occupancies of the σ- and π-components of the Ge=Ge double bond of 1.92e and 1.85e and the Ge–Si σ-orbital (1.91e).

In line with the yellow color, the UV/Vis longest wavelength absorptions of poly(digermenes) **3a**,**b** in hexane are observed at λ_{max} = 423 nm (**3a**) and 418 nm (**3b**), respectively (Figure 4). These values fall into the typical range of absorptions for π-π* transitions of moderately to untwisted acyclic digermenes (411 to 438 nm).[7c,8–10,11a,d,33,34] TD-DFT calculations on symmetric model digermene **4** at the PBE0/def2-TZVP level of theory confirm the assignment. Compared to model digermene **4** (λ_{max} = 411 nm),[10] they are red-shifted by $\Delta\lambda$ = 12 and 7 nm. The onsets of the peaks at 463 nm (**3a**) and 457 nm (**3b**) correspond to HOMO–LUMO gaps of 2.68 and 2.72 eV, respectively, at the lower end of the range of organic π-conjugated materials typically used in OLEDs, OSCs and OFETs (2.64 to 4.01 eV).[35] Compared to the monomers (both 431 nm) a slight hypsochromic shift is manifest, most likely owing to diminished twisting of the substituents at the Ge=Ge double bond.[11c,33,36] The weak bands at 334 nm (**3a**) and 338 nm (**3b**) as well as the intense UV bands at ~248 nm and ~295 nm (for both **3a**,**b**) arise from charge transfer transitions of the Ge=Ge double bond to the linking unit's π-system, according to TD-DFT calculations (see Supporting Information). They are considerably bathochromically shifted compared to the corresponding bands of model digermene **4** (322 nm, 250 nm)[10] and the σ,π-conjugated monomers (**2a**: 324, 237 nm, **2b**: 322, 237 nm).

As a result of increased stability brought about by σ,π-conjugation, digermene polymers **3a**,**b** do not react with 1,3-diisopropylimidazol-4,5-dimethyl-2-ylidene (Me_2IPr) even at 65 °C—unlike monomers **2a**,**b**. According to heteronuclear NMR spectroscopy, the latter readily react with Me_2IPr at room temperature to form the corresponding bridged bis(germylene)-NHC adducts **5a**,**b** and Tip_2Ge–NHC, in analogy to the previously reported reaction of *Si*,*Si*,*N*,*N*-tetramethyl bis(digermene) **2c** to NHC-bis(germylene) **5c** (Scheme 2).[20] The characteristic ^{13}C NMR resonances of the carbenic carbon atoms of **5a**,**b** are observed between 177.7 and 177.2 ppm as well as particularly broad ^{1}H NMR signals between 6.3 and 5.2 ppm for the CH backbone of the germylene coordinated carbene. The ^{29}Si NMR signals at −7.16 to −9.94 ppm are characteristically upfield shifted by 14 to 17 ppm compared to preceding bis(digermene)s **2a**,**b**, similarly to the reported case of **5c** ($\Delta\delta$ = 15–16 ppm).[20] For the *Si*-octylated derivative **5a**, the presence of several diastereomers in the mixture is expected due to four stereogenic centers, in line with broad multiplets in the corresponding heteronuclear NMR spectra.

Conjugated polymers find applications as semiconducting thin film materials in electronic devices. For efficient charge transport, ordered structures are required.[2,37] We therefore investigated the deposition behavior of polymers **3a**,**b** and the morphology of resulting thin films. Noticeably,

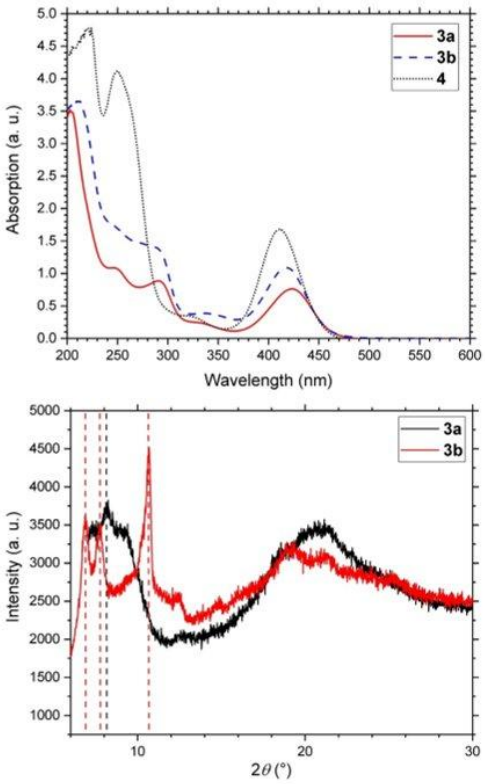

Figure 4. Top: UV/Vis absorption spectra of digermene polymers **3a** (red, solid line; c = 0.4 g L^{-1}), **3b** (blue, dashed line; c = 0.9 g L^{-1}) and molecular model **4**[10] (black; dotted line, $c = 6 \cdot 10^{-4}$ M). Bottom: Powder X-ray diffractograms of poly(digermene)s **3a**,**b**.

powder X-ray diffraction of the bulk samples of polymers **3a**,**b** (Figure 4) revealed partial crystallinity, demonstrating a relatively high level of order. Particularly in the case of the *N*-hexyl derivative **3b**, several distinct reflections of significant intensity are observed at $2\theta = 6.9°$ (1.28 nm), 7.7° (1.15 nm) and 10.7° (0.83 nm). The *Si*-octyl substituted poly(digermene) **3a** appears to show a lower degree of crystallinity as suggested by only one distinct peak protruding at 8.2° (1.08 nm) from the otherwise very broad reflections in smaller 2θ values.

The amorphous contributions to both diffractograms resemble those of ladder structures of amorphous polysilsesquioxanes exhibiting characteristic broad reflections at 2θ ~20° ($d = 0.34$ to 0.53 nm) in addition to those at smaller 2θ angles.[38] The short distance of 0.83 nm is assigned to intramolecular distances between the Ge=Ge units, which is slightly smaller than the value estimated from the single crystal structure of monomer **2b** (1.00 nm). The larger values are assigned to interstrand Ge–Ge distances, fitting the lower end of the corresponding values derived from the molecular solid-state structures (**2a**: 1.15–1.66 nm, **2b**: 1.05–1.69 nm). In line with this, the monomers show relatively short distances between adjacent molecules, in particular between the alkyl chains with H–H distances as short as 2.7651(2) Å (**2a**) and 3.2687(2) Å (**2b**) and the isopropyl groups of the Tip substituents with H–H distances of 1.9347(1) Å (**2a**) and 2.1659(1) Å (**2b**). We assume that the resulting mutual penetration of two molecules via London dispersion interactions between the alkyl branches (Figure 1b) is retained in the polymeric structures **3a**,**b** along individual strands. The resulting ladder structures could account for the larger 2θ values ($d = 0.34$ to 0.53 nm) exhibited in the powder XRD patterns.

The presence of interchain interactions is evident in the formation of highly viscous gels when the polymerization is performed at higher monomer concentrations or upon slow evaporation of the solvent of polymer solutions. In addition to a high degree of polymerization, this is expected to result in an increase of the general stiffness of the compounds and hence in higher glass transition temperatures.[39,40] Indeed, in contrast to the *Si*,*Si*,*N*,*N*-tetramethyl substituted digermene polymer **IV**, which exhibits a T_g of 72 °C,[10] no glass transitions are obtained for **3a**,**b** in the temperature range between −40 °C and 160 °C. The constitutional integrity of the polymers after heating to 160 °C in the solid state was confirmed by ^{1}H NMR spectroscopy of dissolved samples with no discernible changes compared to pristine samples. At higher temperatures, degradation of **3a**,**b** is observed: heating solid samples of **3a**,**b** to 200 °C for 1.5 h results in the appearance of additional sharp ^{1}H NMR signals in solution spectra (**3b**) or the formation of an insoluble solid (**3a**). This is in line with additional exothermic DSC events at onset temperatures of 167 °C (**3a**) and 168 °C (**3b**), respectively (Figure 5).

At room temperature and in the absence of air and moisture, the polymers are stable for at least two years in the solid state and in solution, according to ^{1}H NMR spectroscopy. When exposed to air, rapid degradation of **3a** and **3b** to unknown molecular fragments is observed.

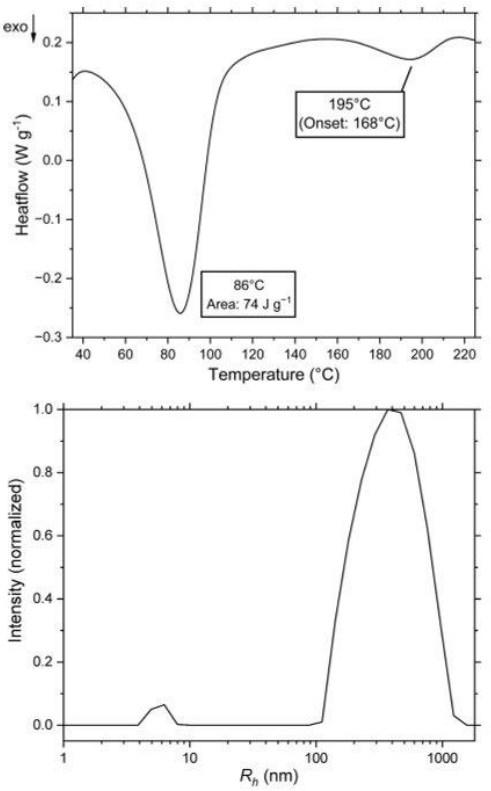

Figure 5. Top: DSC curve of digermene polymer **3b** recorded at 10 K min^{-1}. Bottom: Size distribution profile obtained from DLS measurement of **3a** in benzene at a scattering angle of 25°.

Melting of the samples in NMR tubes was only observed well above the degradation temperatures at 242 °C (**3a**) and 250 °C (**3b**). The melting temperatures exceed by far those of the monomers (**2b**: 160 °C; **2c**: 180 °C), in line with the increased stiffness. According to thermal gravimetric analyses (TGA), the melting processes are accompanied by mass loss. The corresponding onset temperatures (**3a**: 243 °C, **3b**: 249 °C) are substantially higher than for the *Si*,*Si*,*N*,*N*-tetramethyl derivative **IV** (122 °C),[10] confirming the considerable stabilization brought about by the intermolecular dispersive interactions of the alkyl chains and the vastly higher degrees of polymerization in polymers **3a**,**b**. Furthermore, the first cycles of the DSC measurements (Figure 5 and Supporting Information) reveal remarkably intense irreversible exothermal events at 81–82 °C (**3a**) and 86–96 °C (**3b**), tentatively attributed to the increased order by the establishment of additional interchain interactions and hence supramolecular structures. The heat release corresponding to energies of 37–48 J g^{-1} (**3a**) and 74–75 J g^{-1} (**3b**) is in line with heat-induced crystallization processes.[41]

The formation of aggregates of sizes of at least 150 nm is confirmed by small angle X-ray scattering (SAXS) experiments on concentrated (30 to 45 g L^{-1}) solutions of **3a**,**b** in toluene (Figure S86, Supporting Information), showing strong forward scattering. Furthermore, the forward scatter-

ing in the case of *Si*-octylated poly(digermene) **3a** follows a slope close to q^{-1} at intermediate scattering vector values ($q = 0.02$–0.1 Å^{-1}) and for **3b** a trend towards q^{-1} is found. The corresponding mass-fractal dimension of $D_m = 1$, indicative of elongated structures,[42] is consistent with the presence of cylindrical particles.

Hydrodynamic radii obtained with dynamic light scattering (DLS) experiments (Figure 5 and Supporting Information) on 5 g L^{-1} benzene solutions of the polymers show a strong scattering angle dependency, characteristic for large or anisotropically shaped particles above the Rayleigh limit.[43a,e,44] The hydrodynamic radii at $R_h = 5.3$ nm (**3a**) and 4.8 nm (**3b**) correspond to diffusion coefficients (**3a**: $D = 6.8 \cdot 10^{-11}$, **3b**: $D = 7.6 \cdot 10^{-11}$ m^2 s^{-1}) in the range of translational diffusion of high-molecular-weight polymer chains (polystyrenes with $M_w = 30000$ to 200000 g mol^{-1} exhibit values of $D = 8$ to $3 \cdot 10^{-11}$ m^2 s^{-1})[45] and expectedly about one order of magnitude smaller compared to rod-like polymers with correspondingly larger volumes such as cellulose or the tobacco mosaic virus ($D = 1.5 \cdot 10^{-12}$ to $6.0 \cdot 10^{-12}$ m^2 s^{-1}).[44b,46] The peaks at higher radii (**3a**: 389 nm, **3b**: 168 nm) are in line with the presence of supramolecular structures with approximately 10^7–10^8 repeat units per agglomerate (for details see Supporting Information).

Diffusion ordered NMR spectroscopy (DOSY) on 10 g L^{-1} solutions in thf-d_8 provided two different diffusion coefficients for each derivative (for details see Supporting Information). The smaller diffusion coefficients of $D = 4.4 \cdot 10^{-11}$ (**3a**) and $5.2 \cdot 10^{-11}$ m^2 s^{-1} (**3b**) are one order of magnitude smaller than the values obtained for the monomers (**2a**: $D = 5.4 \cdot 10^{-10}$ m^2 s^{-1}, $R_h = 0.84$ nm; **2b**: $D = 5.0 \cdot 10^{-10}$ m^2 s^{-1}, $R_h = 0.91$ nm), accounting for considerably larger volumes, in the same order of magnitude as single polymer strand translational diffusion observed in the DLS experiments (**3a**: $D = 6.8 \cdot 10^{-11}$, **3b**: $D = 7.6 \cdot 10^{-11}$ m^2 s^{-1}). The larger diffusion coefficients (**3a**: $D = 1.3 \cdot 10^{-10}$ m^2 s^{-1}; **3b**: $D = 1.4 \cdot 10^{-10}$ m^2 s^{-1}) are tentatively assigned to slow rotational diffusion processes about rotational axes perpendicular to the main axis of the approximately cylindrically shaped polymer strands. Similar conclusions have been drawn for rod-like particles typically formed by *para*-phenylene-containing repeat units.[43,47] Using a modified version of the Stokes–Einstein equation for cylindrical structures with widths corresponding to the monomers' diameters (see Supporting Information for details), the translational diffusion coefficients allow for a tentative rod length estimation of 2100 nm (**3a**) and 1100 nm (**3b**), respectively. Assuming the rods to consist of unentangled polymer chains with strict linear conformation and a repeat unit length of 1 nm (estimated from the distances between two Ge=Ge moieties in the molecular structures of **2a**,**b**), these lengths suggest degrees of polymerization X_n of similar absolute values. The corresponding molecular weights amount to 2200 and 1400 kg mol^{-1}.

The presence of large cylindrical superstructures of **3a**,**b** in solution and in the solid state due to the attractive dispersion forces between the alkyl side-chains of different polymer strands prompted us to investigate the deposition of highly ordered thin films. A concentrated hexane solution of the *N*-hexylated derivative **3b** (1 g L^{-1}) was spin-coated onto a mica substrate and the surface was scanned using atomic force microscopy (AFM). The resulting image shows the substrate covered by a layer (thickness 12 to 18 nm) of the polymer and randomly distributed crystalline peaks protruding about 14 to 29 nm from the relatively soft amorphous background (Figure 6a). Thinner films with more clearly defined nanostructures, are obtained from less concentrated solutions (0.4 g L^{-1}) by dip-coating and subsequent washing with hexane. A mica substrate coated with *Si*-octylated polymer **3a** (Figure 6b) exhibits a pattern of approximately parallel long strands, confirming the formation of cylindrical superstructures as presumed on the basis of the solution and solid state analytical data.

Close-ups at higher resolution reveal the strands to be about 500 nm in breadth (Figure 6c and Supporting Infor-

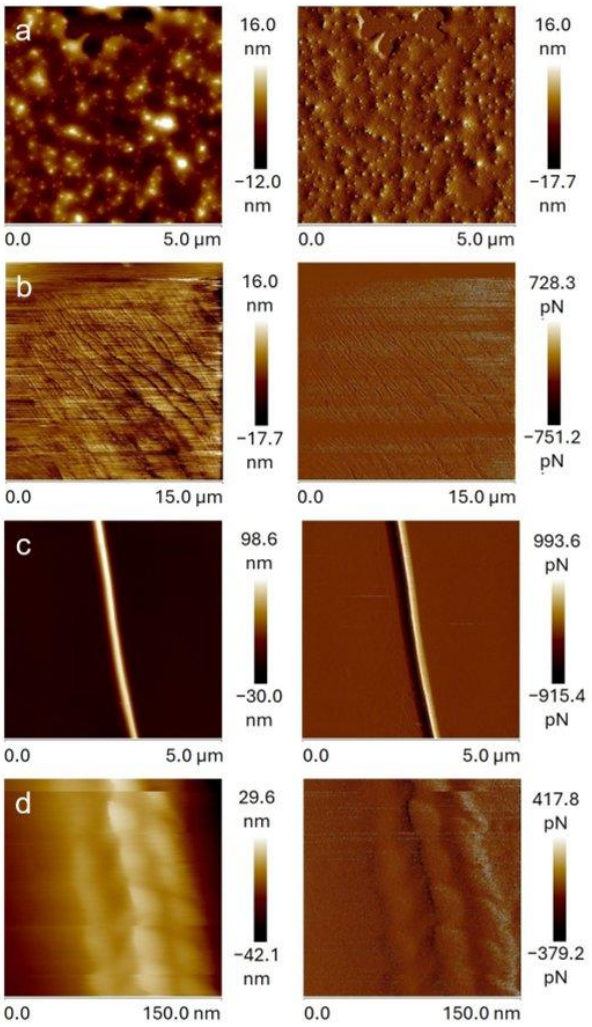

Figure 6. AFM images of a) **3b** spin-coated with a 1 g L^{-1} hexane solution and b-d) **3a** dip-coated with a 0.4 g L^{-1} hexane solution on mica substrates (left: height sensor, right: peak force error).

mation Figure S96). Similar rods formed by the *N*-hexylated derivative on a highly ordered pyrolytic graphite (HOPG) surface are thinner with a width of about 64 nm (Figures S95, S96, Supporting Information). The orientation of these rods in the thin films implies an ordering along the conjugation path parallel to the surface. Notably, the rods are between five and ten times flatter than wide with heights of 97 nm (**3a**) and 6.4 nm (**3b**) (Figure S96, Supporting Information). The agglomerates hence exhibit an almost sheet-like shape consisting of several parallel adjacent fibrils.

At closer view, a plait-like structure of the strands becomes apparent in the case of the *Si*-octylated derivative **3a** (Figure 6d). This repetitive pattern suggests an ordered arrangement of the cylindrical agglomerates and consequently of the underlying polymer chains, in line with regular attractive interactions between the single chains and even between adjacent fibrils as known for instance from polyacrylonitrile fibers.[48]

Transmission electron microscopy (TEM) of both derivatives was performed on samples on holey carbon-coated copper TEM grids, prepared by drop-coating hexane or toluene solutions. In line with the AFM findings, the resulting images (Figure 7a and Supporting Information) show broad bundles of polymers in the case of concentrated solutions (1 g L^{-1}) with an approximate width of 50 nm. More dilute poly(digermene) solutions result in numerous parallel fibrils each of a width of about 3 nm (Figure 7b–d and Supporting Information). The width of individual polymer chains of **3a**,**b** is estimated to about 1.6–1.8 nm on the basis of the DOSY data and the crystal structures of monomers **2a**,**b** (see also Supporting Information). Hence, the observed fibrils most probably show ladder structures consisting of two interlocked polymer strands resulting in a theoretical width < 3.6 nm.

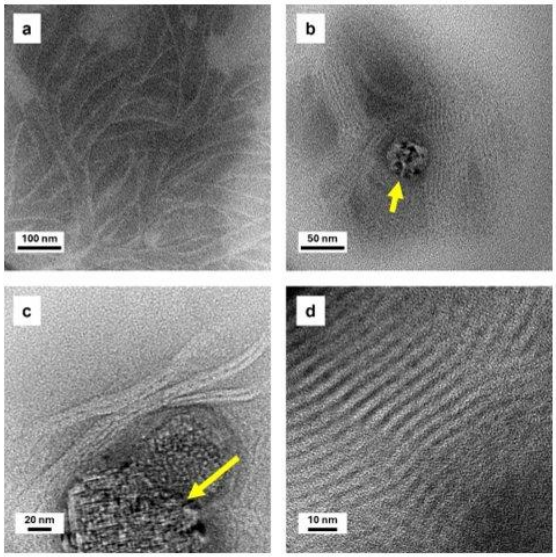

Figure 7. TEM images showing the morphologies of supramolecular structures formed by poly(digermene)s on holey carbon-coated copper grids prepared by drop-coating of polymer solutions of different concentrations: a) **3b** (c = 1 g L^{-1}), b) **3a** (0.1 g L^{-1}), c) **3b** (0.4 g L^{-1}), d) **3a** (0.1 g L^{-1}). Yellow arrows mark areas where mesh-like structures are exhibited.

Their linear parallel alignment corroborates the assumed self-assembly due to distinct interchain interactions and a general rigidity of the linear chains. Cross-linked cylindrical micelles of poly(ferrocenylsilane) block copolymers, for instance, assemble in a parallel manner resulting in supramolecular fibers.[49] Notably, the lamellar substructures in the poly(digermene) films resemble the well-ordered structures of regioregular poly(thiophene)s used in organic solar cells and field effect transistors.[50] The images in Figures 7b,c additionally show regions with mesh-like structures (see also Figure S97, Supporting Information), suggesting an overlay of several crossing fibers. Such patterns may result from a different morphology, e.g. as in fringed micelles where the ends of parallel polymer strands form knots.[48,51,52]

Conclusions

In conclusion, polymers with Ge=Ge double bonds in the conjugation path and extremely high degrees of polymerization have been synthesized and characterized in solution, as bulk solids and in thin films. By equipping the silylene-phenylene bridge between the Ge=Ge moieties with long alkyl chains either at the silyl group or the amino functionality, considerable solubility in different organic solvents is conferred. This allows for essentially unlimited chain growth in the polymerization process following our recently reported HADMET protocol for the metathesis of bis(digermene)s. Substantial intermolecular dispersion interactions between the alkyl groups of adjacent polymer chains lead to the formation of ladder-like cylindrical assemblies in solution and in thin films as apparent from AFM and TEM images and corroborated by diffusion experiments and powder XRD. The thin films exhibit ordered structures of parallel aligned fibrils, consistent with the partial crystallinity of the bulk polymer, which ultimately results in a reasonable thermal stability of the Ge=Ge-containing polymers up to > 160 °C. Characterization of the bis(digermene) monomers supported by DFT calculations confirms substantial σ,π-conjugation across the silylene-phenylene linker and the Ge=Ge units. This is further corroborated by the NMR and UV/Vis data of the yellow polymer solutions. In combination with the absorption in the visible range, due to a small HOMO–LUMO gap, this new class of materials offers interesting perspectives for the application in polymer electronics.

Supporting Information

The authors have cited additional references within the Supporting Information (Ref. [54–77]).

Acknowledgements

We thank the Fonds der Chemischen Industrie for a Kekulé fellowship for A.-L.T. and the German Research Foundation for funding (DFG SCHE 906/9-1). We acknowledge the instrumentation facilities provided by the service center for X-ray analysis established with the financial support from Saarland University and German Research Foundation (INST 256/506-1). We thank Diego M. Andrada for access to his computational cluster. We are grateful for measurements by Michael Zimmer, Elias Gießelmann (Solid State CP/MAS NMR), Josef Zapp (DOSY NMR), Lucas Niedner (DLS), Jörg Schmauch (TEM), Bastian Oberhausen and Jan-Falk Kannengießer (DSC), Mana Mohamed (TGA) and for preliminary experiments by Lukas Klemmer. Open Access funding enabled and organized by Projekt DEAL.

Conflict of Interest

The authors declare no conflict of interest.

Data Availability Statement

The data that support the findings of this study are available in the supplementary material of this article.

Keywords: conjugated polymers · thin films · σ,π-conjugation · self-assembly · dispersion interactions

[1] a) H. F. Brinson, L. C. Brinson, in *Polymer Engineering Science and Viscoelasticity*, Springer, New York **2015**; b) T. D. Clemons, S. I. Stupp, *Prog. Polym. Sci.* **2020**, *111*, 101310; c) M. Zakaria, M. A. R. Bhuiyan, M. S. Hossain, N. M.-M. U. Khan, M. A. Salam, K. Nakane, *Discover Nano* **2024**, *19*, 24; d) Y. Wang, H. Li, A. Rasool, H. Wang, R. Manzoor, G. Zhang, *J. Nanobiotechnol.* **2022**, *24*, 1; e) L. Guo, Y. Wang, M. Steinhart, *Chem. Soc. Rev.* **2021**, *50*, 6333; f) W. Hou, Y. Xiao, G. Han, J.-Y. Lin, *Polymers* **2019**, *11*, 143; g) F. R. R. Teles, L. P. Fonseca, *Mater. Sci. Eng. C* **2008**, *28*, 1530; h) P. Das, P. K. Marvi, S. Ganguly, X. S. Tang, B. Wang, S. Srinivasan, A. R. Rajabzadeh, A. Rosenkranz, *Nano-Micro Lett.* **2024**, *16*, 135; i) E. Tamjid, P. Najafi, M. A. Khalili, N. Shokouhnejad, M. Karimi, N. Sepahdoost, *Discover Nano* **2024**, *19*, 29.

[2] Reviews: a) K. Müllen, U. Scherf, *Macromol. Chem. Phys.* **2023**, *224*, 2200337; b) M. C. Scharber, N. S. Sariciftci, *Adv. Mater. Technol.* **2021**, *6*, 2000857; c) G. Hong, X. Gan, C. Leonhardt, Z. Zhang, J. Seibert, J. M. Busch, S. A. Bräse, *Adv. Mater.* **2021**, *33*, 2005630; d) R. H. Friend, R. W. Gymer, A. B. Holmes, J. H. Burroughes, R. N. Marks, C. Taliani, D. D. C. Bradley, D. A. Dos Santos, J. L. Brédas, M. Lögdlund, W. R. Salaneck, *Nature* **1999**, *397*, 121.

[3] S. Fratini, M. Nikolka, A. Salleo, G. Schweicher, H. Sirringhaus, *Nat. Mater.* **2020**, *19*, 491.

[4] a) R. R. Moskalyk, *Miner. Eng.* **2004**, *17*, 393; b) E. Rosenberg, *Rev. Environ. Sci. Bio/Technol.* **2009**, *8*, 29; c) M. Patel, A. K. Karamalidis, *Sep. Purif. Technol.* **2021**, *275*, 118981.

[5] a) B. L. Lucht, M. A. Buretea, T. Don, *Organometallics* **2000**, *19*, 3469; b) N. Allard, R. B. Aïch, D. Gendron, P.-L. T. Boudreault, C. Tessier, S. Alem, S.-C. Tse, Y. Tao, M. Leclerc, *Macromolecules* **2010**, *43*, 2328; c) I. A. Jessop, A. Mariman, P. A. Sobarzo, R. A. Hauyon, C. Saldías, E. Schott, X. Zarate, F. E. Rodríguez-González, J. Medina, C. M. González-Henríquez, A. Tundidor-Camba, C. A. Terraza, *Eur. Polym. J.* **2021**, *148*, 110373; d) W. Sun, Y. Adachi, J. Ohshita, *Dyes Pigm.* **2022**, *203*, 110333.

[6] Reviews: a) P. P. Power, *J. Chem. Soc. Dalton Trans.* **1998**, 2939; b) P. P. Power, *Chem. Rev.* **1999**, *99*, 3463; c) R. C. Fischer, P. P. Power, *Chem. Rev.* **2010**, *110*, 3877; d) R. C. Fischer, in *Comprehensive Inorganic Chemistry II*, Vol. 2 (Eds.: J. Reedijk, K. Poeppelmeier), Elsevier, Waltham, MA, USA **2013**, pp. 269; e) V. Nesterov, N. C. Breit, S. Inoue, *Chem. Eur. J.* **2017**, *23*, 12014; f) C. Weetman, *Chem. Eur. J.* **2021**, *27*, 1941; g) F. Dankert, C. Hering-Junghans, *Chem. Commun.* **2022**, *58*, 1242; h) S. Fujimori, Y. Mizuhata, N. Tokitoh, *Proc. Jpn. Acad. Ser. B* **2023**, *99*, 480; i) V. Y. Lee, *Molecules* **2023**, *28*, 1558; j) C. Duan, C. Cui, *Chem. Soc. Rev.* **2024**, *53*, 361.

[7] a) S. Masamune, Y. Hanzawa, D. J. Williams, *J. Am. Chem. Soc.* **1982**, *104*, 6136; b) P. B. Hitchcock, M. F. Lappert, S. J. Miles, A. J. Thorne, *J. Chem. Soc. Chem. Commun.* **1984**, *480*; c) J. Park, S. A. Batcheller, S. Masamune, *J. Organomet. Chem.* **1989**, *367*, 39; d) H. Schäfer, W. Saak, M. Weidenbruch, *Organometallics* **1999**, *18*, 3159; e) M. Stender, L. Pu, P. P. Power, *Organometallics* **2001**, *20*, 1820; f) K. L. Hurni, P. A. Rupar, N. C. Payne, K. M. Baines, *Organometallics* **2007**, *26*, 5569; g) T. J. Hadlington, M. Hermann, J. Li, G. Frenking, C. Jones, *Angew. Chem. Int. Ed.* **2013**, *52*, 10199; h) N. Hayakawa, T. Sugahara, Y. Numata, H. Kawaai, K. Yamatani, S. Nishimura, S. Goda, Y. Suzuki, T. Tanikawa, H. Nakai, D. Hashizume, T. Sasamori, N. Tokitoh, T. Matsuo, *Dalton Trans.* **2018**, *47*, 814; i) K. Suzuki, Y. Numata, N. Fujita, N. Hayakawa, T. Tanikawa, D. Hashizume, K. Tamao, H. Fueno, K. Tanakade, T. Matsuo, *Chem. Commun.* **2018**, *54*, 2200.

[8] D. Nieder, L. Klemmer, Y. Kaiser, V. Huch, D. Scheschkewitz, *Organometallics* **2018**, *37*, 632.

[9] X. Zheng, A. E. Crumpton, M. A. Ellwanger, S. Aldridge, *Dalton Trans.* **2023**, *52*, 16591.

[10] L. Klemmer, A.-L. Thömmes, M. Zimmer, V. Huch, B. Morgenstern, D. Scheschkewitz, *Nat. Chem.* **2020**, *13*, 373.

[11] a) M. Kira, T. Iwamoto, T. Maruyama, C. Kabuto, H. Sakurai, *Organometallics* **1996**, *15*, 3767; b) A. Schäfer, W. Saak, M. Weidenbruch, *Z. Anorg. Allg. Chem.* **1998**, *624*, 1405; c) V. Y. Lee, K. McNeice, Y. Ito, A. Sekiguchi, *Chem. Commun.* **2011**, *47*, 3272; d) L. Klemmer, Y. Kaiser, V. Huch, M. Zimmer, D. Scheschkewitz, *Chem. Eur. J.* **2019**, *25*, 12187; e) K. Izod, M. Liu, P. Evans, C. Wills, C. M. Dixon, P. G. Waddell, M. R. Probert, *Angew. Chem. Int. Ed.* **2022**, *61*, e202208851; f) A. Caise, L. P. Griffin, A. Heilmann, C. McManus, J. Campos, S. Aldridge, *Angew. Chem. Int. Ed.* **2021**, *60*, 15606.

[12] a) C. Cui, M. M. Olmstead, P. P. Power, *J. Am. Chem. Soc.* **2004**, *126*, 5062; b) T. Sasamori, T. Sugahara, T. Agou, J.-D. Guo, S. Nagase, R. Streubel, N. Tokitoh, *Organometallics* **2015**, *34*, 2106; c) T. Sugahara, J.-D. Guo, T. Sasamori, Y. Karatsu, Y. Furukawa, A. E. Ferao, S. Nagase, N. Tokitoh, *Bull. Chem. Soc. Jpn.* **2016**, *89*, 1375.

[13] a) C. Präsang, D. Scheschkewitz, *Chem. Soc. Rev.* **2016**, *45*, 900; b) A. Rammo, D. Scheschkewitz, *Chem. Eur. J.* **2018**, *24*, 6866.

[14] a) D. Scheschkewitz, *Chem. Lett.* **2011**, *40*, 2; b) T. Matsuo, N. Hayakawa, *Sci. Technol. Adv. Mater.* **2018**, *19*, 108.

[15] a) D. Scheschkewitz, *Angew. Chem. Int. Ed.* **2004**, *43*, 2965; b) M. Ichinohe, K. Sanuki, S. Inoue, A. Sekiguchi, *Organometallics* **2004**, *23*, 3088; c) M. Ichinohe, K. Sanuki, S. Inoue, A. Sekiguchi, *Silicon Chem.* **2005**, *3*, 111; d) S. Inoue, M. Ichinohe, A. Sekiguchi, *Chem. Lett.* **2005**, *34*, 1564; e) T. Iwamoto, M. Kobayashi, K. Uchiyama, S. Sasaki, S. Nagendran, S. Isobe, M. Kira, *J. Am. Chem. Soc.* **2009**, *131*, 3156; f) L. Zborovsky, R.

Dobrovetsky, M. Botoshansky, D. Bravo-Zhivotovskii, Y. Apeloig, *J. Am. Chem. Soc.* **2012**, *134*, 18229; g) D. Pinchuk, J. Mathew, A. Kaushansky, D. Bravo-Zhivotovskii, Y. Apeloig, *Angew. Chem. Int. Ed.* **2016**, *55*, 10258; h) A. Rit, J. Campos, H. Niu, S. Aldridge, *Nat. Chem.* **2016**, *8*, 1022; i) M. Tian, J. Zhang, H. Yang, C. Cui, *J. Am. Chem. Soc.* **2020**, *142*, 4131; j) P. K. Majhi, V. Huch, D. Scheschkewitz, *Angew. Chem. Int. Ed.* **2021**, *60*, 242.

[16] I. Bejan, D. Scheschkewitz, *Angew. Chem. Int. Ed.* **2007**, *46*, 5783.

[17] a) A. Fukazawa, Y. Li, S. Yamaguchi, H. Tsuji, K. Tamao, *J. Am. Chem. Soc.* **2007**, *129*, 14164; b) L. Li, T. Matsuo, D. Hashizume, H. Fueno, K. Tanaka, K. Tamao, *J. Am. Chem. Soc.* **2015**, *137*, 15026.

[18] N. M. Obeid, L. Klemmer, D. Maus, M. Zimmer, J. Jeck, I. Bejan, A. J. P. White, V. Huch, G. Jung, D. Scheschkewitz, *Dalton Trans.* **2017**, *46*, 8839.

[19] T. Kosai, S. Ishida, T. Iwamoto, *Dalton Trans.* **2017**, *46*, 11271.

[20] A.-L. Thömmes, B. Morgenstern, M. Zimmer, D. M. Andrada, D. Scheschkewitz, *Chem. Eur. J.* **2023**, *29*, e202301273.

[21] A. M. Priegert, B. W. Rawe, S. C. Serin, D. P. Gates, *Chem. Soc. Rev.* **2016**, *45*, 922.

[22] a) V. A. Wright, D. P. Gates, *Angew. Chem. Int. Ed.* **2002**, *41*, 2389; b) R. C. Smith, X. Chen, J. D. Protasiewicz, *Inorg. Chem.* **2003**, *42*, 5468.

[23] R. C. Smith, J. D. Protasiewicz, *J. Am. Chem. Soc.* **2004**, *126*, 2268.

[24] J.-P. Malrieu, G. Trinquier, *J. Am. Chem. Soc.* **1989**, *111*, 5916.

[25] W. Ando, H. Ito, T. Tsumuraya, H. Yoshida, *Organometallics* **1988**, *7*, 1880.

[26] H. Maeda, T. Suzuki, M. Segi, *Photochem. Photobiol. Sci.* **2018**, *17*, 781.

[27] a) M.-C. Fang, A. Watanabe, M. Matsuda, *Jpn. J. Appl. Phys.* **1995**, *34*, 98; b) S. Kyushin, M. Ikarugi, M. Goto, H. Hiratsuka, H. Matsumoto, *Organometallics* **1996**, *15*, 1067; c) S. Kyushin, T. Kitahara, H. Matsumoto, *Chem. Lett.* **1998**, *27*, 471; d) S. Kyushin, T. Matsuura, H. Matsumoto, *Organometallics* **2006**, *25*, 2761; e) S. Kyushin, Y. Suzuki, *Molecules* **2022**, *27*, 2241.

[28] J. P. Wagner, P. R. Schreiner, *Angew. Chem. Int. Ed.* **2015**, *54*, 12274.

[29] W. H. Carother, *Trans. Faraday Soc.* **1936**, *32*, 39.

[30] H. G. Elias, *Makromolecules*, Vol. 2, Wiley-VCH GmbH Verlag, Weinheim, Germany **2006**.

[31] B. A. Miller-Chou, J. L. Koenig, *Prog. Polym. Sci.* **2003**, *28*, 1223.

[32] The model of infinite chains is widely used for the theoretical description of polymers with considerable degrees of polymerisation (see for instance: a) B. Champagne, J.-M. André, *Int. J. Quantum Chem.* **1990**, *38*, 859; b) D. S. Galvão, M. J. Caldas, *J. Chem. Phys.* **1990**, *92*, 2630; c) J. Kürti, H. Kuzmany, *Phys. Rev. B* **1991**, *44*, 597; d) R. Wang, Z.-G. Wang, *Macromolecules* **2014**, *47*, 4094). Polyiodine chains in an experimentally obtained pyrroloperylene-iodine complex have also been referred to as infinite (see e) S. Madhu, H. A. Evans, V. V. T. Doan-Nguyen, J. G. Labram, G. Wu, M. L. Chabinyc, R. Seshadri, F. Wudl, *Angew. Chem. Int. Ed.* **2016**, *55*, 8032). In view of the essentially unlimited chain growth during polymerization, supported by the discussed NMR spectroscopic data, we refer to the poly(digermene) chains herein as *near-infinite.*

[33] M. Kira, *Proc. Jpn. Acad. Ser. B* **2012**, *88*, 167.

[34] T. Iwamoto, J. Okita, N. Yoshida, M. Kira, *Silicon* **2010**, *2*, 209.

[35] J. C. S. Costa, R. J. S. Taveira, C. F. R. A. C. Lima, A. Mendes, L. M. N. B. F. Santos, *Opt. Mater.* **2016**, *58*, 51.

[36] V. Y. Lee, K. McNiece, Y. Ito, A. Sekiguchi, N. Geinik, J. Y. Becker, *Heteroat. Chem.* **2014**, *25*, 313.

[37] a) Y. Lei, P. Deng, M. Lin, X. Zheng, F. Zhu, B. S. Ong, *Adv. Mater.* **2016**, *28*, 6687; b) M. Li, D. K. Mangalore, J. Zhao, J. H. Carpenter, H. Yan, H. Ade, H. Yan, K. Müllen, P. W. M. Blom, W. Pisula, D. M. de Leeuw, K. Asadi, *Nat. Commun.* **2018**, *9*, 451; c) M. Gao, W. Wang, J. Hou, Y. L. Long, *Aggregate* **2021**, *2*, e46.

[38] a) K. A. Andrianov, S. V. Bushin, M. G. Vitovskaya, V. N. Yemel'yanov, P. N. Lavrenko, N. N. Makarova, A. M. Muzafarov, V. Y. Nikolayev, G. F. Kolbina, I. N. Shtennikova, V. N. Tsvetkov, *Polym. Sci. U. S. S. R.* **1977**, *19*, 536; b) C. Liu, Y. Liu, Z. Shen, P. Xie, R. Zhang, J. Yang, F. Bai, *Macromol. Chem. Phys.* **2001**, *202*, 1581; c) K. Deng, T. Zhang, X. Zhang, A. Zhang, P. Xie, R. Zhang, *Macromol. Chem. Phys.* **2006**, *204*, 404; d) X. Zhang, P. Xie, Z. Shen, J. Jiang, C. Zhu, H. Li, T. Zhang, C. C. Han, L. Wan, S. Yan, R. Zhang, *Angew. Chem. Int. Ed.* **2006**, *45*, 3112; e) Z.-X. Zhang, J. Hao, P. Xie, X. Zhang, C. C. Han, R. Zhang, *Chem. Mater.* **2008**, *20*, 1322; f) M. Handke, B. Handke, A. Kowalewska, W. Jastrzebski, *J. Mol. Struct.* **2009**, *254*, 924; g) M. Handke, M. Sitarz, E. Dlugon, *J. Mol. Struct.* **2011**, *993*, 193; h) Z. Chena, Z. Renb, J. Zhanga, W. Fua, Z. Lia, R. Zhang, *React. Funct. Polym.* **2012**, *72*, 503; i) S.-S. Choi, A. S. Lee, S. S. Hwang, K.-Y. Baek, *Macromolecules* **2015**, *48*, 6063; j) W. R. Kang, A. S. Lee, S. Park, S.-H. Park, K.-Y. Baek, K. B. Lee, S.-H. Lee, J.-H. Lee, S. S. Hwang, J. S. Lee, *J. Membr. Sci.* **2015**, *475*, 384; k) M. Pei, A. S. Lee, S. S. Hwang, H. Yang, *J. Mater. Chem. C* **2017**, *5*, 10955; l) S. O. Hwanga, A. S. Leeb, J. Y. Leea, S.-H. Parka, K. I. Junga, H. W. Junga, J.-H. Lee, *Prog. Org. Coat.* **2018**, *121*, 105; m) W. Zhang, X. Wang, Y. Wu, Z. Qi, R. Yang, *Inorg. Chem.* **2018**, *57*, 3883; n) S. Pohl, O. Janka, E. Füglein, G. Kickelbick, *Macromolecules* **2021**, *54*, 3873; o) J. Marchewka, P. Jelen, I. Rutkowska, P. Bezkosty, M. Sitarz, *Materials* **2021**, *14*, 1340.

[39] a) J. H. Gibbs, E. A. DiMarzio, *J. Chem. Phys.* **1958**, *28*, 373; b) M. C. Shen, A. Eisenberg, *Prog. Solid State Chem.* **1967**, *3*, 407; c) V. P. Privalko, Y. S. Lipatov, *J. Macromol. Sci. Phys.* **1974**, *9*, 551; d) C. Müller, *Chem. Mater.* **2015**, *27*, 2740; e) R. Xie, A. R. Weisen, Y. Lee, M. A. Aplan, A. M. Fenton, A. E. Masucci, F. Kempe, M. Sommer, C. W. Pester, R. H. Colby, E. D. Gomez, *Nat. Commun.* **2020**, *11*, 893.

[40] H. Dominninghaus, P. Elsner, P. Eyerer, T. Hirth, *Kunststoffe—Eigenschaften und Anwendungen*, Springer-Verlag Berlin Heidelberg, Germany **2008**.

[41] C. Schick, *Anal. Bioanal. Chem.* **2009**, *395*, 1589.

[42] G. Beaucage, *J. Appl. Crystallogr.* **1996**, *29*, 134.

[43] a) S. R. Aragón, R. Pecora, *J. Chem. Phys.* **1977**, *66*, 2506; b) S. Fujime, K. Kubota, *Biophys. Chem.* **1985**, *23*, 1; c) R. Piazza, V. Degiorgio, *J. Phys. Condens. Matter* **1993**, *5*, B173; d) D. Lehner, H. Lindner, O. Glatter, *Langmuir* **2000**, *16*, 1689; e) F. Babick, in *Micro and Nano Technologies, Characterization of Nanoparticles* (Eds.: V.-D. Hodoroaba, W. E. S. Unger, A. G. Shard), Elsevier **2020**, pp. 137.

[44] a) R. Pecora, *J. Chem. Phys.* **1968**, *48*, 4126; b) E. Loh, E. Ralston, V. N. Schumaker, *Biopolymers* **1979**, *18*, 2549; c) H. Kato, A. Nakamura, S. Kinugasa, *Nanomaterials* **2018**, *8*, 708; d) L. Jin, C. W. Jarand, M. L. Brader, W. F. Reed, *Meas. Sci. Technol.* **2022**, *33*, 045202.

[45] W. Li, H. Chung, C. Daeffler, J. A. Johnson, R. H. Grubbs, *Macromolecules* **2012**, *45*, 9595.

[46] Y. Boluk, C. Danumah, *J. Nanopart. Res.* **2014**, *16*, 2174.

[47] H. G. Elias, *Makromolecules*, Vol. 3, Wiley-VCH GmbH Verlag, Weinheim, Germany **2008**.

[48] C. Kunzmann, G. Schmidt-Bilkenroth, J. Moosburger-Will, S. Horn, *J. Mater. Sci.* **2018**, *53*, 4693.

[49] a) H. Qiu, V. A. Du, M. A. Winnik, I. Manners, *J. Am. Chem. Soc.* **2013**, *135*, 17739; b) D. J. Lunn, O. E. C. Gould, G. R. Whittell, D. P. Armstrong, K. P. Mineart, M. A. Winnik, R. J. Spontak, P. G. Pringle, I. Manners, *Nat. Commun.* **2016**, *7*, 12371.

[50] a) I. Osaka, R. D. McCullough, *Acc. Chem. Res.* **2008**, *41*, 1202; b) R. Zhang, B. Li, M. C. Iovu, M. Jeffries-EL, G. Sauvé, J. Cooper, S. Jia, S. Tristram-Nagle, D. M. Smilgies, D. N. Lambeth, R. D. McCullough, T. Kowalewski, *J. Am. Chem. Soc.* **2006**, *128*, 3480; c) M. C. Iovu, C. R. Craley, M. Jeffries-EL, A. B. Krankowski, R. Zhang, T. Kowalewski, R. D. McCullough, *Macromolecules* **2007**, *40*, 4733.
[51] H. G. Elias, *Makromolecules*, Vol. 1, Wiley-VCH GmbH Verlag, Weinheim, Germany **2005**.
[52] a) D. Braun, H. Cherdron, M. Rehahn, H. Ritter, B. Voit, *Polymer Synthesis: Theory and Practice - Fundamentals, Methods, Experiments*, Springer-Verlag GmbH, Germany **2013**.
[53] Deposition numbers CCDC 2358519 (1,4-bis(chlorodibutylsilyl)-2,5-*N*,*N*,*N*′,*N*′-tetramethylphenylenediamine), 2358520 (1,4-dibromo-2,5-*N*,*N*,*N*′,*N*′-tetrahexylphenylenediamine), 2358523 (1,4-bis(chlorodihexylsilyl)-2,5-*N*,*N*,*N*′,*N*′-tetramethylphenylenediamine), 2358526 (**2b**), 2358527 (**2a**), 2358528 (**1a**), contain the supplementary crystallographic data for this paper. These data are provided free of charge by the joint Cambridge Crystallographic Data Centre and Fachinformationszentrum Karlsruhe Access Structures service.
[54] N. Kuhn, T. Kratz, *Synthesis* **1993**, *1993*, 561.
[55] T. Doornbos, J. Strating, *Org. Prep. Proced.* **1969**, *4*, 287.
[56] G. R. Fulmer, A. J. M. Miller, N. H. Sherden, H. E. Gottlieb, A. Nudelman, B. M. Stoltz, J. E. Bercaw, K. I. Goldberg, *Organometallics* **2010**, *29*, 2176.
[57] G. M. Sheldrick, *Acta Crystallogr. Sect. A* **2008**, *64*, 112.
[58] G. M. Sheldrick, *Acta Crystallogr. Sect. A* **2015**, *71*, 3.
[59] C. B. Hübschle, G. M. Sheldrick, B. Dittrich, *J. Appl. Crystallogr.* **2011**, *44*, 1281.
[60] M. J. Frisch, G. W. Trucks, H. B. Schlegel, G. E. Scuseria, M. A. Robb, J. R. Cheeseman, G. Scalmani, V. Barone, B. Mennucci, G. A. Petersson, H. Nakatsuji, M. Caricato, X. Li, H. P. Hratchian, A. F. Izmaylov, J. Bloino, G. Zheng, J. L. Sonnenberg, M. Hada, M. Ehara, K. Toyota, R. Fukuda, J. Hasegawa, M. Ishida, T. Nakajima, Y. Honda, O. Kitao, H. Nakai, T. Vreven, J. J. A. Montgomery, J. E. Peralta, F. Ogliaro, M. Bearpark, J. J. Heyd, E. Brothers, K. N. Kudin, V. N. Staroverov, R. Kobayashi, J. Normand, K. Raghavachari, A. Rendell, J. C. Burant, S. S. Iyengar, J. Tomasi, M. Cossi, N. Rega, J. M. Millam, M. Klene, J. E. Knox, J. B. Cross, V. Bakken, C. Adamo, J. Jaramillo, R. Gomperts, R. E. Stratmann, O. Yazyev, A. J. Austin, R. Cammi, C. Pomelli, J. W. Ochterski, R. L. Martin, K. Morokuma, V. G. Zakrzewski, G. A. Voth, P. Salvador, J. J. Dannenberg, S. Dapprich, A. D. Daniels, O. Farkas, J. B. Foresman, J. V. Ortiz, J. Cioslowski, D. J. Fox, *Gaussian 16, Revision C.01*, Gaussian, Inc., Wallingford CT **2016**.
[61] a) J. P. Perdew, *Phys. Rev. B* **1986**, *33*, 8822; b) A. D. Becke, *Phys. Rev. A* **1988**, *38*, 3098.
[62] a) A. Schäfer, H. Horn, R. Ahlrichs, *J. Chem. Phys.* **1992**, *97*, 2571; b) A. Schäfer, C. Huber, R. Ahlrichs, *J. Chem. Phys.* **1994**, *100*, 5829; c) F. Weigend, R. Ahlrichs, *Phys. Chem. Chem. Phys.* **2005**, *7*, 3297; d) F. Weigend, *Phys. Chem. Chem. Phys.* **2006**, *8*, 1057.
[63] a) S. Grimme, J. Antony, S. Ehrlich, H. Krieg, *J. Chem. Phys.* **2010**, *132*, 154104; b) S. Grimme, S. Ehrlich, L. Goerigk, *J. Comput. Chem.* **2011**, *32*, 1456.
[64] a) A. E. Reed, R. B. Weinstock, F. Weinhold, *J. Chem. Phys.* **1985**, *83*, 735; b) A. E. Reed, L. A. Curtiss, F. Weinhold, *Chem. Rev.* **1988**, *88*, 899; c) E. D. Glendening, C. R. Landis, F. Weinhold, *J. Comput. Chem.* **2019**, *40*, 2234.
[65] F. Neese, F. Wennmohs, U. Becker, C. Riplinger, *J. Chem. Phys.* **2020**, *152*, 224108.
[66] a) J. P. Perdew, M. Ernzerhof, K. Burke, *J. Chem. Phys.* **1996**, *105*, 9982; b) C. Adamo, V. Barone, *J. Chem. Phys.* **1999**, *110*, 6158.
[67] Chemcraft—graphical software for visualization of quantum chemistry computations. https://www.chemcraftprog.com.
[68] J. Zhou, R. Tang, X. Wang, W. Zhang, X. Zhuang, F. Zhang, *J. Mater. Chem. C* **2016**, *4*, 1159.
[69] C. C. Miller, *Proc. R. Soc. London, Ser. A* **1924**, *106*, 724.
[70] J. H. Dymond, J. Robertston, J. D. Isdale, *Int. J. Thermophys.* **1981**, *2*, 223.
[71] C. S. Johnson, *Prog. Nucl. Magn. Reson. Spectrosc.* **1999**, *34*, 203.
[72] S. Berger, S. Braun, *200 and More NMR Experiments*, Wiley-VCH Verlag GmbH & Co. KGaA, Weinheim **2004**.
[73] E. O. Stejskal, J. E. Tanner, *J. Chem. Phys.* **1965**, *42*, 288.
[74] M. Nilsson, M. A. Connell, A. L. Davis, G. A. Morris, *Anal. Chem.* **2006**, *78*, 3040.
[75] P.-J. Voorter, A. McKay, J. Dai, O. Paravagna, N. R. Cameron, T. Junkers, *Angew. Chem.* **2022**, *134*, e202114536; *Angew. Chem. Int. Ed.* **2022**, *61*, e202114536.
[76] P. J. Mohr, B. N. Taylor, D. B. Newell, *Rev. Mod. Phys.* **2012**, *84*, 1527.

Manuscript received: August 14, 2024
Accepted manuscript online: October 23, 2024
Version of record online: November 16, 2024

σ,π-Conjugated Bis(germylene) Adducts with NHC and CAACs

Anna-Lena Thömmes, Bernd Morgenstern, Michael Zimmer, Diego M. Andrada, David Scheschkewitz, *Chem. Eur. J.* **2023**, *29*, e202301273 (1–9).

https://doi.org/10.1002/chem.202301273

The results are additionally concluded and put into context in the "Conclusions and Outlook" chapter of this thesis.

Contributions of the authors:

Anna-Lena Thömmes

Lead: Synthesis and characterization of the compounds, quantum chemical calculations, formal analysis, investigation, visualization, writing – original draft
Equal: Conceptualization, data curation, funding acquisition, methodology
Supporting: Writing – review & editing

Bernd Morgenstern

Lead: X-Ray analysis and crystal structure refinement

Michael Zimmer

Lead: CP/MAS NMR measurements

Diego M. Andrada

Supporting: Formal analysis and validation of the quantum chemical calculations

David Scheschkewitz

Lead: Supervision, writing – review & editing, funding acquisition, resources, project administration;
Equal: Conceptualization, methodology, data curation

Chemistry–A European Journal
Research Article
doi.org/10.1002/chem.202301273
Chemistry Europe
European Chemical Societies Publishing
www.chemeurj.org

Special Collection

σ,π-Conjugated Bis(germylene) Adducts with NHC and CAACs

Anna-Lena Thömmes,[a] Bernd Morgenstern,[b] Michael Zimmer,[a] Diego M. Andrada,[a] and David Scheschkewitz*[a]

Abstract: Heavier tetrylenes attract attention for their potential in synthesis, catalysis and small molecule activation. The coordination by *N*-heterocyclic carbenes (NHCs) and cyclic (alkyl)(amino)carbenes (CAACs) results in substantial structural and electronic differences although typically only one of these yields stable derivatives for one and the same tetrylene. We now report both NHC- and CAAC-coordination to a bridged bis(germylene) motif. The NHC-coordinated bis(germylene) exhibits pyramidal germanium centers with lone pairs of electrons, while with CAAC an unprecedented stable bis(germene) with two Ge=C bonds is isolated. Spectroscopic and crystallographic evidence as well as DFT calculations confirm the effects of σ,π-conjugation between the two germanium centers in both cases. The coordination of NHC is reversible as the reaction with BPh_3 liberates the transient bis(germylene) and thus provides an alternative low-temperature route towards polymers with Ge=Ge bonds.

Introduction

Heavier low-valent group 14 compounds with their exceptional electronic structures and versatile reactivity continue to be at the focus for their role in synthesis, catalysis and small molecule activation.[1] In particular, heavier carbene analogues (tetrylenes) and their dimers have been studied extensively during the past decades.[2] The kinetic stabilization of otherwise transient derivatives is achieved by bulky substituents, often complemented by the additional thermodynamic stability offered by intra- or intermolecular electron donors.[2b–e] *N*-Heterocyclic carbenes (NHCs) and cyclic (alkyl)(amino)carbenes (CAACs) have been employed as strong σ-donors in a variety of low-valent main group compounds.[3–9] The coordination of NHCs vs. CAACs often leads to drastic differences in (electronic) structure due to the stronger π-acceptor and σ-donor abilities of the latter. This has been evaluated experimentally and theoretically for group 13 and 15 with anionic borafluorenes by the Gilliard group,[10] the diborene carbene adducts by Engels et al.[11] or the carbene phosphinidene adducts by Bertrand et al.[12] In group 14, the considerably shorter Si–C_{CAAC} bond distances in the $(CAAC{\cdot}SiR)_2$ adducts (R=Cl, H, Me)[13] compared to the corresponding NHC adduct $(NHC{\cdot}SiCl)_2$[14] underpin these differences despite the pyramidal coordination environments of both adjacent tetrel(II) centers. In case of dihalosilylenes, predominantly NHC adducts have been reported.[15,16] The corresponding 1:1 adducts with CAAC apparently retain considerable electrophilicity leading to the addition of a second carbene equivalent as, for example, during the formation of Roesky's $(CAAC)_2{\cdot}SiCl_2$ diradical[17] or the addition of an NHC to the only isolated derivative, the equally pyramidal $CAAC{\cdot}SiI_2$.[18,19]

As concerns of germanium, after the groundbreaking isolation of the diiodogermylene-NHC adduct **I** by Arduengo et al. in 1993,[20] numerous pyramidal NHC adducts with germylenes have been reported.[21–27] The first diarylgermylene-NHC adduct **II** was obtained by Baines et al. in 2007 by cleavage of the corresponding digermene by an NHC.[28] All CAAC-adducts of halogermylenes exhibit a pyramidal structure comparable to the corresponding NHC adducts, irrespective of the nature of the halogen and despite the pronounced π-accepting ability of CAACs.[29,30] With the extremely electron-rich digermylenylgermene **III**[31] (Scheme 1), only one tetrylene-CAAC adduct with a genuine Ge=C double bond is known.

Neither NHC nor CAAC adducts of bridged bis(tetrylenes) with organic or inorganic linking units have been reported, presumably because known bis(tetrylenes) are without exception stabilized by internal donation of adjacent n-donor substituents at both tetrel(II) centers.[32–57] The thus reduced electron deficiency is obviously detrimental to formation of adducts with external donors. Recently, we reported the polymerization of the heavier acyclic diene **1** to give Ge=Ge containing polymer **2** via the postulated bis(germylene) **[3]** as

[a] A.-L. Thömmes, Dr. M. Zimmer, Dr. D. M. Andrada, Prof. Dr. D. Scheschkewitz
Chair in General and Inorganic Chemistry
Saarland University
Campus Geb. C4 1, 66123 Saarbrücken (Germany)
E-mail: scheschkewitz@mx.uni-saarland.de
Homepage: http://www.uni-saarland.de/lehrstuhl/scheschkewitz.html

[b] Dr. B. Morgenstern
Inorganic Solid State Chemistry
Saarland University
Campus Geb. C4 1, 66123 Saarbrücken (Germany)

Supporting information for this article is available on the WWW under https://doi.org/10.1002/chem.202301273

Special Collection Part of a Special Collection on the p-block elements.

Chemistry–A European Journal
Research Article
doi.org/10.1002/chem.202301273
Chemistry Europe
European Chemical Societies Publishing

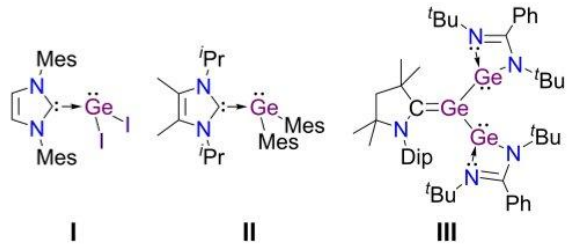

I II III

Scheme 1. Selected examples of germylene carbene adducts (Mes = 2,4,6-trimethylphenyl, Dip = 2,6-diisopropylphenyl).

key intermediate of a procedure dubbed as Heavier Acyclic Diene Metathesis (HADMET; Scheme 2).[58] Trapping of the monogermylene related to **[3]** by Et_3SiH suggested its pronounced electrophilicity at both germanium(II) centers. We therefore became curious about the effect of the σ,π-conjugated linking unit on the interaction of **[3]** with stable carbenes.

Results and Discussion

Indeed, the $GeTip_2$ moieties of **1** are easily substituted by NHC as well as by CAAC donors to afford the corresponding bis(carbene) adducts. As will be shown, the σ,π-conjugation between the germanium(II) centers is a main factor in determining the nature of the interaction of the carbene moieties with the germanium centers.

During the polymerization of the heavier acyclic diene precursor **1**, the dissociation of the Ge=Ge bond is induced thermally by heating to 65 °C.[58] In order to prove the intermediacy of bis(silylgermylene) **[3]**, we repeated the reaction in the presence of Et_3SiH. The bridged bis(silylgermane) was indeed obtained as double Si–H insertion product along with the concomitantly formed silylgermane[58] (Scheme 3). Two ^1H NMR resonances in the characteristic range for Ge–*H* protons at 4.22 and 4.19 ppm indicate the formation of the diastereomeric mixture of the oxidative addition product. In the $^{29}Si/^1H$ HMBC NMR spectrum, cross peaks of the ^1H signals to the $^{29}Si\{^1H\}$ NMR signals of the Et_3Si (4.54, 5.51 ppm) and the Me_2Si moieties (−8.73, −9.08 ppm) confirm the connectivity.

Baines et al. had shown that the dissociation of digermenes can also be initiated by addition of an NHC.[27,28] As a preliminary test, we therefore added four equivalents of Me_2IPr to the linker-separated tetragermadiene **1** at room temperature, which indeed resulted in the clean formation of two products in the 1:2 ratio required by the stoichiometry of the reaction. The bis(germylene)/Me_2IPr adduct **4** (Scheme 4) precipitates from the reaction mixture as a yellow solid in 63% yield. The concomitantly formed, equally yellow NHC-$GeTip_2$ adduct was isolated from the concentrated mother liquor in 38% yield by precipitation with pentane.

The presence of stereochemically active lone pairs at both germanium atoms in **4** is confirmed by the ^1H, $^{13}C\{^1H\}$ and $^{29}Si\{^1H\}$ NMR spectra, which each exhibit two similar sets of signals suggesting a 1:1 diastereomeric mixture. The $^{29}Si\{^1H\}$ signals of equal intensity at −11.07 and −11.19 ppm are in the range of σ,π-conjugated silyl groups (20.9 to −21.2 ppm).[59,60] The slight upfield shift compared to the parent tetragermadiene **1** (4.27 ppm)[58] and silyldigermenes and -germylenes in general (13.5 to −2.7 ppm)[27,58,61,62] is in line with a certain donation of

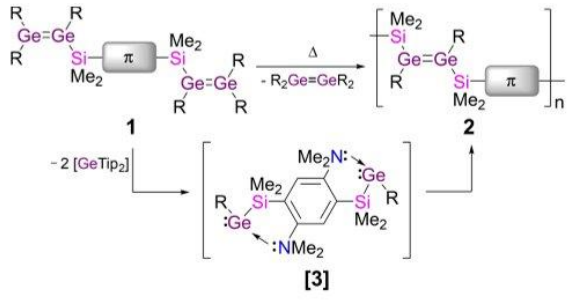

Scheme 2. Previously reported HADMET polymerization of **1** via transient bis(germylene) **[3]** (R=Tip = 2,4,6-triisopropylphenyl, π = *N,N,N′,N′*-tetramethyl-2,5-phenylenediamine).[58]

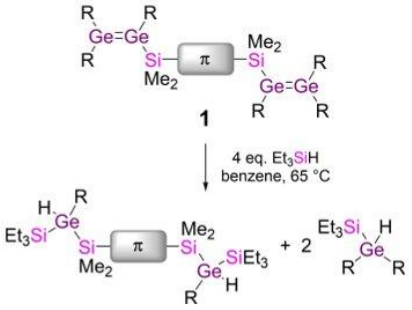

Scheme 3. Silane trapping of bis(germylene) **[3]** released from bis(digermene) **1** (R=Tip = 2,4,6-triisopropylphenyl, π = *N,N,N′,N′*-tetramethyl-2,5-phenylenediamine).

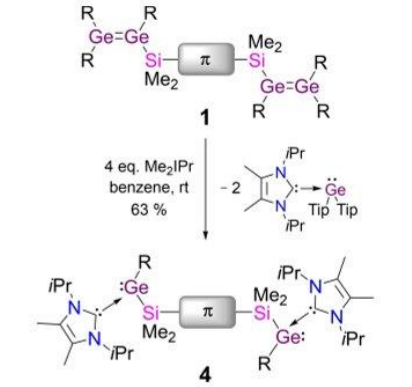

Scheme 4. Synthesis of NHC-stabilized germylene **4** (R=Tip = 2,4,6-triisopropylphenyl, π = *N,N,N′,N′*-tetramethyl-2,5-phenylenediamine).

Chemistry–A European Journal | Research Article doi.org/10.1002/chem.202301273 | Chemistry Europe European Chemical Societies Publishing

the germanium-centered lone pairs of **4** to σ*-orbitals at the $SiMe_2$ bridge. The characteristic ^1H and $^{13}C\{^1H\}$ signals of the Me_2IPr methine groups (5.54 ppm) and the carbenic carbons (177.08, 177.00 ppm) confirm the coordination of Me_2IPr to the germanium centers.[19,20,23,27,28,63–67] The $GeTip_2/Me_2IPr$ adduct shows similar ^1H NMR septets at 5.64 and 5.34 ppm and a $^{13}C\{^1H\}$ resonance at 176.94 ppm for the coordinated Me_2IPr.

As crystallization attempts with bis(germylene) **4** remained unsuccessful, we also synthesized the mono(germylene)/NHC adduct **6** from digermene **5** in an analogous manner (Scheme 5). Similar characteristic resonances as for **4** were observed at 5.73 ppm in the ^1H, at 177.45 ppm in the $^{13}C\{^1H\}$ and at −11.49 ppm in the $^{29}Si\{^1H\}$ NMR spectrum. The ^1H and $^{13}C\{^1H\}$ spectra exhibit two sets of signals for the diastereotopic methyl groups at silicon, the Tip group and the NHC, respectively, in accordance with a pyramidal structure at germanium. Yellow single crystals of the NHC adduct **6** were grown from a pentane solution in 77% yield and analyzed by X-ray diffraction (Figure 1). The compound crystallized as a two component twin and was refined accordingly. There are two very similar molecules of **6** in the asymmetric unit, only one of which is referred to in the following: The relatively short Ge1–C16 bond of 2.070(6) Å is very close to those of the dimesitylgermylene-NHC complexes with IMe_4 (2.067(3) Å) and Me_2IPr (2.078(3) Å),[28] but far longer than typical Ge=C bond lengths (1.77–1.88 Å).[31,68,69] The Ge–Si distance (2.435(2) Å) is somewhat shorter than in an NHC-stabilized cyclic disilylgermylene (2.47, 2.48 Å)[43] and thus in line with partial interaction of the lone pair with the σ*-orbitals of the $SiMe_2$ bridge.

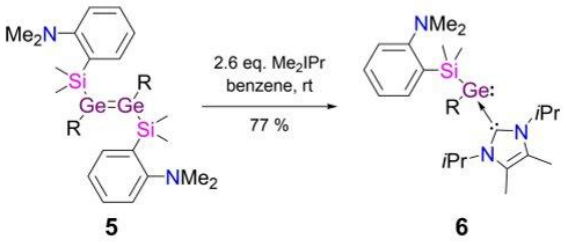

Scheme 5. Synthesis of mono(germylene)/NHC adduct **6** (R=Tip = 2,4,6-triisopropylphenyl).

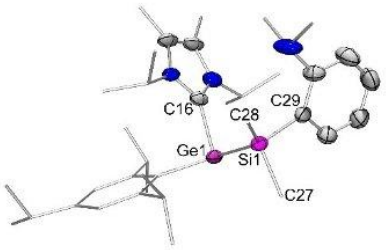

Figure 1. Molecular structure of NHC-germylene adduct **6** in the solid state (second molecule in asymmetric unit and hydrogen atoms omitted for clarity, thermal ellipsoids at 50%).[90] Selected bond lengths [Å] and angles [°]: Ge1–C16 2.070(6), Ge1–Si1 2.435(2), Si1–C27 1.891(6), Si1–C28 1.890(7), Si1–C29 1.900(7), Σ°(Ge1) 311.7(6).

Consequently, the Si–C bonds in **6** (1.89–1.90 Å) are slightly longer than in the disilylgermylenes (1.86–1.89 Å).[43] The substituents at the germanium center are arranged in a pyramidal manner (Σ°(Ge) = 311.7(6)°), which further supports the absence of significant Ge–C double bond character and instead confirms the existence of a stereochemically active lone pair at Ge as in similar compounds.[24] This is fully in line with the observation of diastereomers in case of the bis(NHC) adduct **4** in the multinuclear NMR spectra (see above).

The longest wavelength UV/Vis absorptions of bis(germylene) **4** are surprisingly intense: the broad band at $\lambda_{max} = 395$ nm shows an extinction coefficient of $\varepsilon = 10500\ L\,mol^{-1}\,cm^{-1}$, which is more than twice as large as that of mono(germylene) **6** ($\lambda_{max} = 395$ nm, $\varepsilon = 4000\ L\,mol^{-1}\,cm^{-1}$). Despite the absence of a noticeable red-shift, this intensity increase is even more pronounced than that of π-conjugated tetrasiladienes in comparison with the corresponding disilenes,[70–73] strongly suggesting an intramolecular charge transfer (ICT) process.

In order to shed further light on the electronic structure, we performed DFT calculations at the BP86/def2-SVP level of theory. The HOMO of NHC-germylene adduct **6** is best represented by a lone pair at Ge with dominant s-character and only minor p-orbital admixture ($s^{0.7}p^{0.3}$, Figure 2). The LUMO is mainly located at the NHCs and the anilinyl substituent (Figure 2). TD-DFT calculations at the PBE0/def2-TZVP level of theory indeed support the assignment of the longest wavelength absorption to the HOMO→LUMO excitation and thus an n→π* ICT transition from the germanium center to the surrounding ligands. The postulated σ,π-conjugation via the $SiMe_2$ linker is further supported by visual inspection of the HOMO of **6** (Figure 2), which clearly indicates mixing of the lone pair n-orbital at Ge with the σ*-orbital of the Ge–Si bond. For bis(germylene) **4**, HOMO and HOMO−1 likewise represent one of the lone pairs at the germanium atoms with partial mutual contribution (see Supporting Information). They differ in energy by 0.08 eV, in agreement with a resonance interaction of the two germylene moieties. The decrease of the HOMO–LUMO gaps from germylene **6** (2.40 eV) to bis(germylene) **4** (2.27 eV) is attributed to conjugative destabilization of the HOMO and stabilization of the LUMO (see Supporting Information for energy levels of bis(germylene) **4**), a well-known effect of increasing the conjugation path length of π-conjugated systems[74–76] as well as σ,π-conjugated compounds.[59]

Second order perturbation theory determines the interaction energy of the Ge lone pair (NBO 1) with one of the

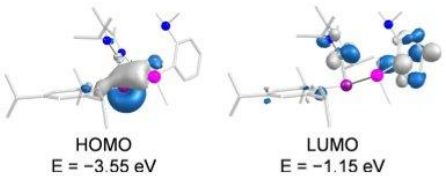

Figure 2. HOMO and LUMO of NHC-germylene **6** (contour value 0.052). Hydrogen atoms omitted for clarity.

Chemistry–A European Journal | Research Article doi.org/10.1002/chem.202301273 | Chemistry Europe European Chemical Societies Publishing

antibonding σ*-orbitals of the $SiMe_2$ moiety (NBO 4) to 7.02 kcal mol^{-1} (Figure 3). The relatively low occupancy of NBO 1 of 1.81 e, together with the partially occupied (0.08 e) Si–C σ*-orbital (NBO 4) substantiate this further. Additionally, the Ge–Si bond (NBO 3) donates into NBO 5, another Si–C σ*-orbital, with an interaction energy of 2.04 kcal mol^{-1} and a reduced occupancy of 1.85 e. Consequently, the Ge–Si bond (NBO 3) is slightly polarized towards silicon (Figure 3) and the negative charge brought about by the NHC coordination is distributed across the aromatic substituents (confirmed by natural population analysis; see Supporting Information).

In line with the pronounced delocalization of the Ge-centered lone pair, neither NHC-bis(germylene) **4** nor Tip_2Ge–Me_2IPr react as Lewis bases when BH_3–thf complex is added to a mixture of both. This is in sharp contrast to the reactivity of Baines' Me_2IPr–$GeMes_2$, which has been reported to form the corresponding BH_3-adduct.[28] While in the case of $GeTip_2$ the higher steric demand of the two Tip compared to two Mes groups is likely responsible, the bridged germylene **4** features the much less bulky silylene linker. The decreased nucleophilicity is thus arguably the result of substantial delocalization of the lone pair across the silicon center and the aromatic bridge.

Sterically encumbered, yet much more Lewis acidic BPh_3 on the other hand readily reacts with mono(germylene) **6** under NHC abstraction, giving rise to previously reported disilyldigermene **5**,[58] the dimerization product of the free germylene, along with Me_2IPr–BPh_3[77] (Scheme 6). Under the same conditions, bis(germylene) **4** provides an alternative and milder route towards poly(digermene) **2**:[58] Reaction of **4** with BPh_3 (Scheme 6) results in the immediate consumption of the starting material and precipitation of an insoluble yellow solid overnight, identified as polymer **2** by $^{13}C\{^1H\}$ and $^{29}Si\{^1H\}$ CP/MAS NMR spectroscopy.[59]

In light of the already pronounced delocalization of the Ge lone pairs in NHC-stabilized **4** into Si-centered σ*-orbitals, we became curious about the competing effect of a CAAC as strong π-acceptor. In contrast to Me_2IPr, cyclic (alkyl)(amino)carbene Me_4CAAC turned out to be inert towards tetragermadiene **1** at room temperature. Heating of **1** to 65 °C in the presence of an excess of Me_4CAAC, however, yields bis(germene) **7** and $Tip_2Ge{=}GeTip_2$ as the only detectable products (Scheme 7). The lower reactivity of Me_4CAAC compared to Me_2IPr is plausibly due to the higher steric congestion brought about by the Dip group at the nitrogen center. This assumption is underpinned by the fact that Dip-substituted 1,3-bis(2,6-diisopropylphenyl)imidazol-2-ylidene does not react at all with tetragermadiene **1**, even at elevated temperatures. Bis(germene) **7** is separated from $Tip_2Ge{=}GeTip_2$ by precipitation from thf as a yellow solid in 47% yield. Its very low solubility in all common organic solvents prevents the characterization by multinuclear NMR in solution. The $^{29}Si\{^1H\}$ CP/MAS NMR, however, exhibits only one singlet at −5.77 ppm, upfield shifted compared to the solution resonance found for the precursor, digermene **1** (4.29 ppm).[77] In the $^{13}C\{^1H\}$ CP/MAS spectrum the carbene carbon peak is found at 194.3 ppm, considerably upfield shifted compared to the solution $^{13}C\{^1H\}$ NMR resonances of free Me_4CAAC (313.6 ppm)[78] and of the CAAC-germene **III** reported by Roesky et al. (219.4 ppm).[31]

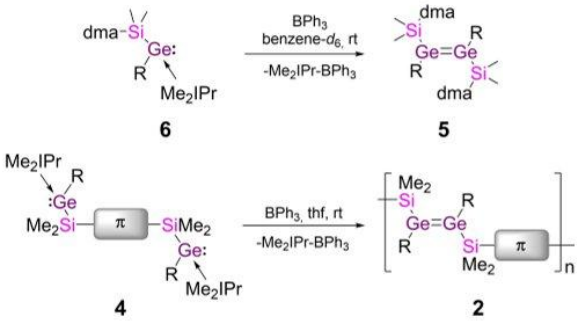

Scheme 6. NHC abstraction with BPh_3 (R=Tip = 2,4,6-triisopropylphenyl, dma = 2-*N*,*N*-dimethylanilinyl, π = *N*,*N*,*N*′,*N*′-tetramethyl-2,5-phenylenediamine).

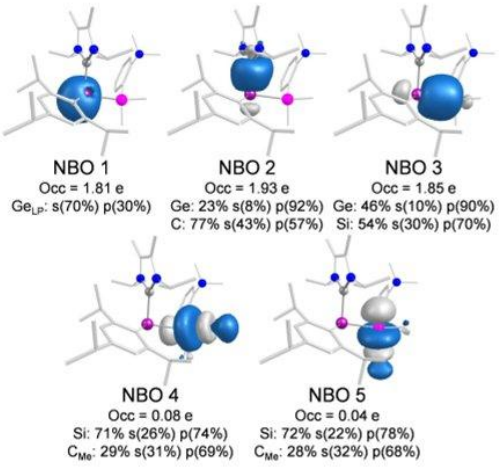

Figure 3. Selected NBOs of NHC-germylene **6** (contour value 0.043). Hydrogen atoms omitted for clarity.

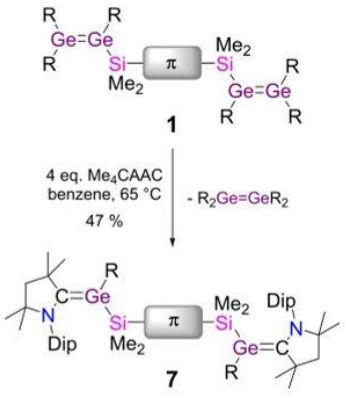

Scheme 7. Synthesis of $(Me_4CAAC)_2$-bis(germene) **7** (R=Tip = 2,4,6-triisopropylphenyl, π = *N*,*N*,*N*′,*N*′-tetramethyl-2,5-phenylenediamine).

Chemistry–A European Journal | Research Article doi.org/10.1002/chem.202301273 | Chemistry Europe European Chemical Societies Publishing

Yellow crystals suitable for X-ray diffraction were directly obtained from a benzene solution of the reaction mixture. The molecular structure in the solid state shows the presence of the *Z*,*Z*-isomer of **7** (Figure 4).

The Ge–C distance of 1.825(2) Å is in the range of known Ge–C double bonds (1.77–1.88 Å).[31,68,69] In fact, it fits particularly well to the Ge–C distances of the conjugated acetylene bridged bis(germenes) reported by Weidenbruch (1.819, 1.819 Å).[79,80] With a sum of the angles of $\Sigma^{\circ}(Ge) = 359.7(2)^{\circ}$ and $\Sigma^{\circ}(C) = 359.6(5)^{\circ}$ there is only a slight deviation from planarity as also shown by the rather small *trans*-bent angles of $\Theta(Ge) = 5.05(7)^{\circ}$ and $\Theta(C) = 5.7(1)^{\circ}$, thus confirming the existence of a $\sigma+\pi$ double bond between Ge and C. In addition, the substituents are only slightly twisted ($\tau = 5.8(1)^{\circ}$), comparable with other nearly planar germenes ($\tau = 3.6^{\circ}$,[31] 5.9°,[81] 4°[82]). Noticeably, the Ge–C bond in **7** is not coplanar to the phenylene linker, but rather exhibits a pronounced dihedral angle of C8–Ge1–Si1–C3 = 78.03(9)°. This geometry allows for an optimal interaction of the π-bond with the antibonding σ*-orbitals of the $SiMe_2$ group. Indeed, the Si–C bonds (1.87–1.90 Å) are slightly longer than in trimethylsilylalkyl and -aryl compounds (1.85–1.89 Å)[83–85] while the Ge1–Si1 distance (2.3699(9) Å) is considerably shorter than in tetragermadiene **1** (2.4007(7) Å).[58]

In the UV/Vis spectrum of bis(germene) **7** a broad absorption band is observed at $\lambda_{max} = 404$ nm, in between the longest absorption wavelengths of the disilylgermene of Haas et al. (368 nm),[69] transient germenes (262 to 325 nm)[86–88] and Weidenbruch's purely π-conjugated bis(germenes) (500–595 nm).[79,80] The extinction coefficient of bis(germene) **7** ($\varepsilon(404\text{ nm}) = 34000\ L\,mol^{-1}\,cm^{-1}$) is almost twice as large as for tetragermadiene **1** ($\varepsilon(426\text{ nm}) = 17600\ L\,mol^{-1}\,cm^{-1}$)[58] and even four times larger than for an acetylene linked π-conjugated bis(germene) ($\varepsilon(500\text{ nm}) = 8000\ L\,mol^{-1}\,cm^{-1}$).[80] These properties are in accordance with the typical large absorption cross-section of strongly conjugated systems and suggest the relevance of σ,π-conjugation in this system. The experimental results are further underpinned by DFT computations at the BP86/def2-SVP level of theory. The experimentally found *Z*,*Z*-isomer is more stable than the *E*,*Z* isomer and the *E*,*E* isomer by 2.05 kcal mol^{-1} and 6.61 kcal mol^{-1}, respectively, and was therefore used for further calculations. TD-DFT (BP86/def2TZVPP) identifies three bands at 437, 427 and 422 nm as due to the HOMO→LUMO+1 and HOMO−1→LUMO+2 transitions. Transitions from HOMO/HOMO−1 to the π*-orbital of the *para*-phenylene linker (LUMO+3) also contribute significantly to these bands. Accordingly, HOMO and HOMO−1, representing the π-orbitals of the C=Ge double bonds, show considerable contribution of the σ*-orbital of the silyl linker as judged from visual inspection (Figure 5). They are not degenerate but separated by 0.08 eV. An identical separation is found between LUMO+1 and LUMO+2, the corresponding orbitals of π*-symmetry. The LUMO consists mainly of the π*-orbital of the *para*-phenylene linker and visibly shows admixture of the σ*(Si)-orbital. The energy gaps between HOMO−1 and LUMO+1 and HOMO and LUMO+2, each amount to only 2.10 eV. The occupied π-orbitals of the phenylene linker, HOMO−12 and HOMO−13 display a *para*-quinoid appearance including the $SiMe_2$ groups (Figure 5). For example, the frontier orbitals of the *para*-phenylenediamine radical cation show a similar pattern with respect to the amino groups as part of the π-system.[89]

NBO analysis was performed on mono(germene) **8** as a model compound for comparison with the mono(germylene)/NHC adduct **6**. The optimized structure of **8** exhibits considerable deviation from planarity at the germanium center ($\Sigma^{\circ}(Ge) = 350.9^{\circ}$), in stark contrast to the bis(germene) **7** ($\Sigma^{\circ}(Ge) = 359.6^{\circ}$). Consequently, the Ge=C double bond is substantially stabilized electronically via the $SiMe_2$-phenylene bridge, confirming the presence of conjugative interaction. Despite the slight pyramidalization at the germanium center,

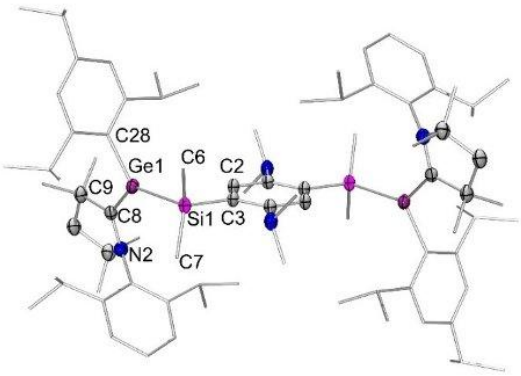

Figure 4. Molecular structure of bis(germene) **7** in the solid state (H atoms, co-crystallized benzene and disordered atoms omitted for clarity, thermal ellipsoids at 50%).[90] Selected bond lengths [Å] and angles [°]: Ge1–C8 1.825(2), Ge1–Si1 2.3699(9), Si1–C3 1.898(2), Si1–C6 1.879(3), Si1–C7 1.870(3), Σ°(Ge1) 359.7(2), Σ°(C8) 359.6(5), Θ(Ge1) 5.05(7), Θ(C8) 5.7(1), τ 5.8(1), Ge1–Si1–C3–C2 1.5(1), C8-Ge1–Si1–C3 78.03(9).

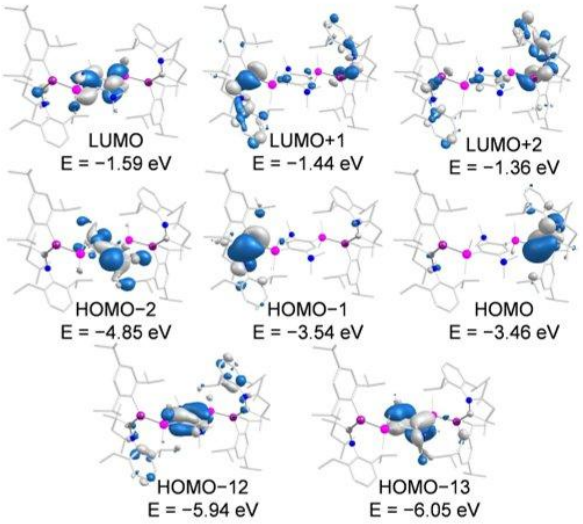

Figure 5. Selected frontier orbitals of bis(germene) **7** (contour value 0.036). Hydrogen atoms omitted for clarity.

Chemistry–A European Journal | Research Article doi.org/10.1002/chem.202301273 | Chemistry Europe European Chemical Societies Publishing

the NBOs still confirm significant double bond character between Ge and C in mono(germene) **8** (NBO 1 and NBO 2; Figure 6) with a Wiberg bond index of 1.35.

The σ,π-conjugation in **7** gains further support from the NBO analysis of model compound **8**, which quantifies the interaction of the Ge–C π-bond (NBO 2, Figure 6) and the σ*-orbital of the Si–C_{dma} bond (NBO 4) to 3.43 kcal mol^{-1} (Figure 6). Notably, NBO 2 shows a slightly higher occupation of 1.85 e compared to 1.81 e of the Ge lone pair in the corresponding germylene-NHC adduct **6**. Owing to distinct donation, the σ* of the Si–C_{dma} bond (NBO 4) is occupied by 0.08 e. In line with the somewhat decreased delocalization in the CAAC adduct **8**, the Ge–Si σ-bond is slightly polarized towards germanium (NBO 3; Figure 6), in contrast to the NHC adduct **6** (NBO 3; Figure 3).

Consistent with distinct backdonation towards the carbene, monogermene **8** features a negative charge of −0.33 e at the CAAC substituent (see Supporting Information),[31] in stark contrast to the monogermylene/NHC adduct **6** with a positively charged NHC ligand (+0.32 e). Thus, unlike the case of the corresponding NHC adduct, the pronounced π-accepting ability of the CAAC enables the formation of Ge=C double bonds. The σ,π-conjugation across the silylphenylene linker provides the required electronic stabilization although to a lesser extent than in the bis(germylene)/NHC adduct **4**, presumably due to the stronger and hence more localized binding of the CAAC moiety.

In order to provide experimental evidence for the stronger bonds of the CAAC to the germylene fragments in comparison with those of the NHCs, NHC stabilized bis(germylene) **4** was treated with an excess of Me_4CAAC. Indeed, the reaction readily occurred even at room temperature to give bis(germene) **7** (Scheme 8). The much lower temperature and hence milder conditions compared to the reaction of **1** with CAAC, resulted in an increased yield of 57% (49% from **1**, Scheme 7).

Conclusion

In conclusion, exchange of the $GeTip_2$ moiety in a bridged bis(digermene) provides the first NHC- and CAAC-stabilized bis(germylenes). While the Me_2IPr-germylene adduct exhibits pyramidal structures with a lone pair and a vacant p-orbital at the germanium centers, with Me_4CAAC the first example of a CAAC-based bis(germene) – featuring Ge=C double bonds – is formed. This is in stark contrast to most other known CAAC/germylene adducts which, despite the pronounced π-accepting ability of CAACs, have pyramidal structures.[29,30] The stronger bond between the germylene moiety and Me_4CAAC in comparison to Me_2IPr is demonstrated by the facile exchange reaction at room temperature. In both cases, for the NHC and the CAAC adducts with the bis(germylene), significant interaction between the unsaturated germanium centers through σ,π-conjugation across the linking unit is confirmed by crystallographic, spectroscopic and computational evidence. The hence decreased nucleophilicity of the lone pair prevents the reaction with BH_3-thf even for the NHC adduct. With the bulkier BPh_3, on the other hand, NHC abstraction is readily achieved, offering an alternative route to the recently reported polymer with Ge=Ge double bonds.[58] In addition, the generation of the transient bis(germylene) under mild conditions promises the wide application of such species in small molecule activation and catalysis.

Experimental Section

General considerations

All manipulations were carried out under a protective atmosphere of argon applying standard Schlenk or glovebox techniques. The glassware was pre-dried in oven at 125 °C and heated in vacuo prior to use. Solvents were dried and degassed by reflux over sodium/benzophenone under argon (thf, benzene) or taken from a solvent purification system (Innovative technology PureSolv MD7; diethylether, hexane, pentane). C_6D_6 and thf-d_8 were dried over potassium mirror and distilled under argon prior to use. Me_4CAAC,[91] Me_2IPr,[92] 1,3-bis(2,6-diisopropylphenyl)imidazol-2-

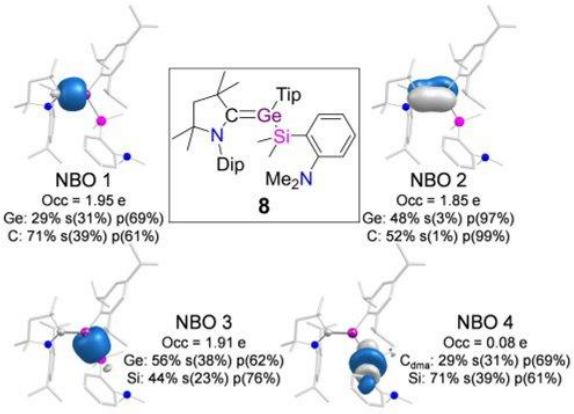

Figure 6. Structure of model germene **8** and selected NBOs (contour value 0.052). Hydrogen atoms omitted for clarity.

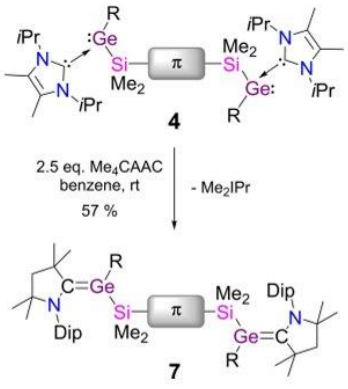

Scheme 8. Exchange reaction of NHC-bis(germylene) **4** with Me_4CAAC yielding the bis(germylene)/CAAC adduct **7**.

Chemistry–A European Journal | Research Article doi.org/10.1002/chem.202301273 | Chemistry Europe European Chemical Societies Publishing

ylidene[93] and digermenes **1** and **5**[58] were prepared according to the published procedures. All other chemicals were obtained commercially and used as received. The NMR spectra were recorded on a Bruker Avance III HD 400 spectrometer (^{1}H: 400.13 MHz, ^{13}C: 100.61 MHz, ^{29}Si: 79.49) or on a Bruker Avance III HD 300 at 300 K (^{1}H: 300.13 MHz, ^{13}C: 75.56 MHz, ^{29}Si: 59.6 MHz). The ^{1}H and ^{13}C{^{1}H} NMR spectra were referenced to the residual proton and natural abundance ^{13}C resonances of the deuterated solvent and chemical shifts were reported relative to $SiMe_4$ (C_6D_6: $\delta^1H = 7.16$ ppm and $\delta^{13}C = 128.06$ ppm, thf-d_8: $\delta^1H = 1.78$, 3.58 ppm and $\delta^{13}C = 67.21$, 25.31 ppm).[94] The ^{29}Si NMR chemical shifts were referenced to external $SiMe_4$. The following abbreviations were used for the multiplicities: s – singlet, d – doublet, t – triplet, sept – septet, m – multiplet, brs – broad singlet. Solid state CP/MAS NMR spectra were recorded on a Bruker Avance III 400 WB at 13 kHz (^{13}C{^{1}H}: 100.61 MHz, ^{29}Si{^{1}H: 79.49 MHz). UV/Vis spectra were recorded on a Shimdazu UV-2600 spectrometer in quartz cells with a path length of 0.1 cm. Melting points were determined under argon in sealed NMR tubes and are uncorrected. The molten samples were examined by NMR spectroscopy to confirm whether decomposition had occurred upon melting. Elemental analyses were performed in triplicate for each sample using Leco CHN900 analyzer and mean values are given below for each compound. Crystallographic data was collected using a Bruker D8 Venture diffractometer with a microfocus sealed tube and a Photon II detector. Monochromated $Mo_{K\alpha}$ radiation ($\lambda = 0.71073$) was used. Data were collected at 133(2) K and corrected for absorption effects using the multi-scan method. The structure was solved by direct methods using SHELXT[95] and was refined by full matrix least squares calculations on F2 (SHELXL2018)[96] in the graphical user interface Shelxle.[97]

Synthesis of bis(germylene)/Me$_2$IPr adduct 4: Bis(digermene) **1** (1.5 g, 803 µmol) and Me_2IPr (579 mg, 3.21 mmol) are dissolved in 18.5 mL of benzene. Stirring for eight hours at room temperature is followed by filtration. Washing of the yellow solid with 2 mL of benzene yields bis(germylene)/Me_2IPr adduct **4** (624 mg, 63 %).* All volatiles are removed from the mother liquor in vacuo and the residue is dissolved in pentane. The yellow crystalline solid formed from this solution is separated by filtration and dried in vacuo to give $Tip_2Ge\cdot Me_2IPr$ (402 mg, 38 %).

* contains 0.6 wt.% of free Me_2IPr

NMR data of bis(germylene)/Me_2IPr adduct **4**:

^{1}H NMR (400.13 MHz, thf-d_8, 300 K, TMS): δ = 7.12, 7.06 (each s, overall 2H, Ph*H*), 6.79 (s, 4H, Tip*H*), 5.54 (brs, 4H, C*H*(CH$_3$)$_2$ of Me_2IPr), 3.88 (brs, 4H, C*H*(CH$_3$)$_2$ of Tip), 2.73 (sept, 2H, C*H*(CH$_3$)$_2$ of Tip), 2.47 (s, 12H, N(C*H*$_3$)$_2$), 2.17 (s, 12H, Me_2IPr–CC*H*$_3$), 1.29 (d, 12H, CH(C*H*$_3$)$_2$ of Me_2IPr), 1.17 (d, 12H, CH(C*H*$_3$)$_2$ of Me_2IPr), 1.03 (d, 12H, CH(C*H*$_3$)$_2$ of Tip), 0.90 (d, 12H, CH(C*H*$_3$)$_2$ of Tip), 0.78, 0.76 (each d, overall 12H, CH(C*H*$_3$)$_2$ of Tip), 0.53, 0.52 (d, s, overall 12H, Si(C*H*$_3$)$_2$) ppm. **^{13}C{^{1}H} NMR** (100.61 MHz, thf-d_8, 300 K, TMS): δ = 177.08, 177.00 (Me_2IPr–*C*), 155.93 (Ph*C*). 154.51, 151.67, 146.13, 142.49 (Tip*C*), 129.02, 128.85 (Me_2IPr–*C*CH$_3$), 126.75, 126.73 (Ph*C*), 120.72 (Tip*C*), 53.88 (CH(CH$_3$)$_2$ of Me_2IPr), 47.40 (N(CH$_3$)$_2$), 34.94 (*C*H(CH$_3$)$_2$ of Tip), 24.56, 24.47, 21.58, 21.55, (CH(*C*H$_3$)$_2$ of Tip), 20.58, 20.52 (CH(CH$_3$)$_2$ of Me_2IPr), 10.19 (Me_2IPr–*C*CH$_3$), 4.58, 4.48, 3.68, 3.55 (Si(CH$_3$)$_2$) ppm. **^{29}Si{^{1}H} NMR** (79.49 MHz, thf-d_8, 300 K, TMS): δ = −11.08, −11.21 ppm. **UV/Vis** (*n*-hexane/thf = 80/20): λ_{max} = 332 nm (ε = 15500 L mol^{-1} cm^{-1}), 395 nm (ε = 10500 L mol^{-1} cm^{-1}). **Elemental analysis**: Calcd. for ($C_{66}H_{112}Ge_2N_6Si_2$): C, 66.55; H, 9.48; N, 7.06. Found: C, 66.94; H, 8.76; N, 6.55. **Mp.**: 162 °C (decomposition).

NMR data of $Tip_2Ge\cdot Me_2IPr$:

^{1}H NMR (400.13 MHz, thf-d_8, 300 K, TMS): δ = 7.22 (s, 1H, Tip*H*), 7.17 (s, 1H, Tip*H*, overlapping with residual protons from C_6D_6), 5.64 (sept, 1H, C*H*(CH$_3$)$_2$ of Me_2IPr), 5.34 (sept, 1H, C*H*(CH$_3$)$_2$ of Me_2IPr), 4.59 (sept, 1H, C*H*(CH$_3$)$_2$ of Tip), 4.10 (sept, 1H, C*H*(CH$_3$)$_2$ of Tip), 4.00 (sept, 1H, C*H*(CH$_3$)$_2$ of Tip), 3.59 to 3.47 (m, 1H, C*H*(CH$_3$)$_2$ of Tip), 2.89 (sept, 2H, C*H*(CH$_3$)$_2$ of Tip), 1.76 (dd, 6H, CH(C*H*$_3$)$_2$ of Tip), 1.56 (d, 6H, CH(C*H*$_3$)$_2$ of Me_2IPr), 1.48, 1.45 (each d, overall 6H, CH(C*H*$_3$)$_2$ of Tip), 1.34 to 1.30 (m, 18H, CH(C*H*$_3$)$_2$ of Me_2IPr and Tip), 1.25 to 1.20 (m, 9H, CH(C*H*$_3$)$_2$ of Tip)m 1.15 (d, 3H, CH(C*H*$_3$)$_2$ of Tip), 1.02 (d, 6H, CH(C*H*$_3$)$_2$ of Tip) ppm. **^{13}C{^{1}H} NMR** (100.61 MHz, thf-d_8, 300 K, TMS): δ = 176.94 (Me_2IPr–*C*), 156.76, 156.18, 155.78, 153.81, 151.20, 149.85, 147.44, 146.23 (Tip*C*), 128.18, 127.94 (*C*CH3 of Me_2IPr), 126.22, 125.30, 121.39 (Tip*C*), 120.84 (*C*CH$_3$of Me_2IPr), 120.51 (Tip*C*), 53.01, 52.05 (*C*H(CH$_3$)$_2$ of Me_2IPr), 37.70, 35.47, 34.76, 33.76, 33.42 (*C*H(CH$_3$)$_2$ of Tip), 26.61, 26.54, 25.99, 25.81, 25.45, 25.30, 24.70 to 24.47, 24.17, 23.97 (CH(*C*H$_3$)$_2$ of Tip), 21.61, 20.86, 20.77, 20.22 (CH(*C*H$_3$)$_2$ of Me_2IPr), 10.24, 10.08 (*C*CH$_3$ of Me_2IPr) ppm. **UV/Vis** (*n*-hexane): λ_{max} = 313 (ε = 4700 L mol^{-1} cm^{-1}), 361 (ε = 5900 L mol^{-1} cm^{-1}), 407 (ε = 5400 L mol^{-1} cm^{-1}). **Elemental analysis**: Calcd. for ($C_{41}H_{66}GeN_2$): C, 74.66; H, 10.09; N, 4.25. Found: C, 72.50; H, 9.25; N, 4.30. **Mp.**: 136 °C (partial formation of $Tip_2Ge{=}GeTip_2$).

Synthesis of germylene/Me$_2$IPr adduct 6: Digermene **5** (420 mg, 411 µmol) and Me_2IPr (193 mg, 1.07 mmol) are dissolved in 9 mL of benzene. The resulting yellow solution is stirred at room temperature for overnight. After addition of another 9 mL of benzene, the reaction mixture is filtered. All volatile parts are removed in vacuo and the resulting red oil is dissolved in pentane. Yellow crystals of **6** are obtained from this solution at room temperature (211 mg, 77 %).*

* contains 5 wt.% of free Me_2IPr

^{1}H NMR (400.13 MHz, C_6D_6, 300 K, TMS): δ = 7.99 (dd, 1H, Me_2N–Ph*H*) 7.27 to 7.20 (ddd, 1H, Me_2N–Ph*H*), 7.11 (s, 2H, Tip*H*), 7.09–7.05 (m, 2H, Me_2N–Ph*H*), 5.74 (sept, 2H, C*H*(CH$_3$)$_2$ of Me_2IPr), 4.24 (sept, 2H, C*H*(CH$_3$)$_2$ of Tip), 2.90 (sept, 1H, C*H*(CH$_3$)$_2$ of Tip), 2.63 (s, 6H, N(C*H*$_3$)$_2$), 1.56 (s, 6H, NHC–C*H*$_3$), 1.33, 1.33, 1.31 (each d, overall 12H, CH(C*H*$_3$)$_2$ of Me_2IPr), 1.13 (d, 6H, CH(C*H*$_3$)$_2$ of Tip), 1.04 (d, 6H, CH(C*H*$_3$)$_2$ of Tip), 0.97, 0.90 (each s, overall 6H, Si(C*H*$_3$)$_2$), 0.80 (d, 6H, CH(C*H*$_3$)$_2$ of Tip) ppm. **^{13}C{^{1}H} NMR** (100.61 MHz, C_6D_6, 300 K, TMS): δ = 177.45 (Me_2IPr–*C*), 161.27 (Ph*C*), 154.72, 150.83, 146.45, 142.91 (Tip*C*), 137.82, 136.03 (Ph*C*), 128.96 (Me_2IPr–*C*CH$_3$), 125.81, 124.05 (Ph*C*), 120.92 (Tip*C*), 53.34 (*C*H(CH$_3$)$_2$ of Me_2IPr), 47.36 (N(CH$_3$)$_2$), 36.67, 34.72 (*C*H(CH$_3$)$_2$ of Tip), 25.63, 25.17 (CH(*C*H$_3$)$_2$ of Tip), 21.41, 20.57 (CH(*C*H$_3$)$_2$ of Me_2IPr), 9.99 (Me_2IPr–*C*CH$_3$), 4.45, 4.06 (Si(CH$_3$)$_2$) ppm. **^{29}Si{^{1}H} NMR** (79.49 MHz, C_6D_6, 300 K, TMS): δ = −11.49 ppm. **UV/Vis** (*n*-hexane/thf = 80/20): λ_{max} = 329 nm (ε = 6000 L mol^{-1} cm^{-1}), 395 nm (ε = 4000 L mol^{-1} cm^{-1}). **Elemental analysis**: Calcd. for ($C_{36}H_{59}GeN_3Si$): C, 68.14; H, 9.37; N, 6.62. Found: C, 67.96; H, 9.04; N, 6.67. **Mp.**: 135 °C.

Synthesis of bis(germylene)/Me$_4$CAAC adduct 7: Bis(digermene) **1** (1.05 g, 565 µmol) and Me_4CAAC (740 mg, 2.59 mmol) are dissolved in 10 mL of benzene. The red solution is heated to 65 °C overnight. The solvent is distilled off in vacuo and the residue is stirred in 6 mL of thf at 65 °C for a few minutes. The soluble parts are filtered off and the residue is washed three times with overall 12 mL of thf. Bis(germene) **7** is obtained as a yellow solid, which is dried in vacuo (368 mg, 47 %). Single crystals of **7** are obtained directly from the reaction mixture in C_6D_6.

^{13}C{^{1}H} CP/MAS NMR (100.61 MHz, 300 K, 13 kHz, TMS): δ = 194.31 (Me_4CAAC–*C*), 157.13, 154.17, 148.62, 142.93, 141.52, 139.42, 133.66, 126.05, 123.84, 122.27, 119.60 (Ph*C*, Tip*C* and Dip*C*), 66.32 (N(CH$_3$)$_2$), 58.44 (C_q of Me_4CAAC), 49.82 (CH(CH$_3$)$_2$ of Tip and Dip), 47.20 (C_q of Me_4CAAC), 37.75, 35.26, 34.18, 33.09 (*C*H(CH$_3$)$_2$ of Tip and Dip), 25.51 (*C*H$_3$ of Tip and Dip), 0.81 (Si(CH$_3$)$_2$). **^{29}Si{^{1}H} CP/MAS NMR** (79.49 MHz, 300 K, 13 kHz, TMS): δ = −5.77 ppm. **UV/Vis** (*n*-hexane/thf = 80/20): λ_{max} = 404 nm (ε = 34000 L mol^{-1} cm^{-1}). **Elemental anal-**

Chemistry–A European Journal | Research Article doi.org/10.1002/chem.202301273 | Chemistry Europe European Chemical Societies Publishing

ysis: Calcd. for ($C_{84}H_{134}Ge_2N_4Si_2$): C, 71.99; H, 9.64, N, 4.00. Found: C, 71.68; H, 9.22; N, 4.26. **Mp.**: 220 °C (decomposition).

Supporting Information

Detailed experimental, analytical and computational data are contained in the Supporting Information. Additional references cited within the Supporting Information.[98–105]

Supplementary crystallographic data see Ref. [90].

Acknowledgements

We thank the Fonds der Chemischen Industrie for a Kekulé fellowship for A.-L.T. We also acknowledge the instrumentation facilities provided by the service center for X-ray analysis established with the financial support from Saarland University and German Research Foundation (INST 256/506-1). Open Access funding enabled and organized by Projekt DEAL.

Conflict of Interests

The authors declare no conflict of interest.

Data Availability Statement

The data that support the findings of this study are available in the supplementary material of this article.

Keywords: carbene homologues · conjugation · cyclic (alkyl)(amino)carbenes · *N*-heterocyclic carbenes · subvalent compounds

[1] a) C. Präsang, D. Scheschkewitz, *Chem. Soc. Rev.* **2016**, *45*, 900; b) V. Nesterov, N. C. Breit, S. Inoue, *Chem. Eur. J.* **2017**, *23*, 12014; c) A. Rammo, D. Scheschkewitz, *Chem. Eur. J.* **2018**, *24*, 6866; d) C. Weetman, *Chem. Eur. J.* **2021**, *27*, 1941; e) F. Hanusch, L. Groll, S. Inoue, *Chem. Sci.* **2021**, *12*, 2001; f) F. Dankert, C. Hering-Junghans, *Chem. Commun.* **2022**, *58*, 1242.

[2] a) W. P. Neumann, *Chem. Rev.* **1991**, *91*, 311; b) N. N. Zemlyanskii, I. V. Borisova, M. S. Nechaev, V. N. Khrustalev, V. V. Lunin, M. Y. Antipin, Y. A. Ustynyuk, *Russ. Chem. Bull. Int. Ed.* **2004**, *53*, 980; c) Y. Mizuhata, T. Sasamori, N. Tokitoh, *Chem. Rev.* **2009**, *109*, 3479; d) M. Asay, C. Jones, M. Driess, *Chem. Rev.* **2011**, *111*, 354; e) C. Shan, S. Yao, M. Driess, *Chem. Soc. Rev.* **2020**, *49*, 6733; f) J. A. Cabeza, P. García-Álvarez, C. J. Laglera-Gándara, *Eur. J. Inorg. Chem.* **2020**, *2020*, 784; g) N. Sen, S. Khan, *Chem. Asian J.* **2021**, *16*, 705; h) R. J. Somerville, J. Campos, *Eur. J. Inorg. Chem.* **2021**, *2021*, 3488; i) M. Ghosh, N. Sen, S. Khan, *ACS Omega* **2022**, *7*, 6449; j) T. Y. Lai, J. C. Fettinger, P. P. Power, *Organometallics* **2022**, *41*, 1590; k) P. M. Keil, A. Soyemi, K. Weisser, T. Szilvási, C. Limberg, T. J. Hadlington, *Angew. Chem.* **2023**, *62*, e202218141; *Angew. Chem. Int. Ed.* **2023**, *135*, e202218141.

[3] D. Bourissou, O. Guerret, F. P. Gabbaı, G. Bertrand, *Chem. Rev.* **2000**, *100*, 39.

[4] M. N. Hopkinson, C. Richter, M. Schedler, F. Glorius, *Nature* **2014**, *510*, 485.

[5] M. Soleilhavoup, G. Bertrand, *Acc. Chem. Res.* **2015**, *48*, 256.

[6] M. Melaimi, R. Jazzar, M. Soleilhavoup, G. Bertrand, *Angew. Chem.* **2017**, *129*, 10180; *Angew. Chem. Int. Ed.* **2017**, *56*, 10046.

[7] A. Doddi, M. Peters, M. Tamm, *Chem. Rev.* **2019**, *119*, 6994.

[8] P. Bellotti, M. Koy, N. Hopkinson, F. Glorius, *Nat. Chem. Rev.* **2021**, *5*, 711.

[9] S. Kumar Kushvaha, A. Mishra, H. W. Roesky, K. Chandra Mondal, *Chem. Asian J.* **2022**, *17*, e202101301.

[10] K. E. Wentz, A. Molino, S. L. Weisflog, A. Kaur, D. A. Dickie, D. J. D. Wilson, R. J. Gilliard, *Angew. Chem.* **2021**, *133*, 13175; *Angew. Chem. Int. Ed.* **2021**, *60*, 13065.

[11] E. Welz, J. Böhnke, R. D. Dewhurst, H. Braunschweig, B. Engels, *J. Am. Chem. Soc.* **2018**, *140*, 12580.

[12] O. Back, M. Henry-Ellinger, C. D. Martin, D. Martin, G. Bertrand, *Angew. Chem.* **2013**, *125*, 2675; *Angew. Chem. Int. Ed.* **2013**, *52*, 2939.

[13] a) K. C. Mondal, H. W. Roesky, B. Dittrich, N. Holzmann, M. Hermann, G. Frenking, A. Meents, *J. Am. Chem. Soc.* **2013**, *135*, 15990; b) C. Mohapatra, S. Kundu, A. N. Paesch, R. Herbst-Irmer, D. Stalke, D. M. Andrada, G. Frenking, H. W. Roesky, *J. Am. Chem. Soc.* **2016**, *138*, 10429; c) S. Kundu, P. P. Samuel, A. Luebben, D. M. Andrada, G. Frenking, B. Dittrich, H. W. Roesky, *Dalton Trans.* **2017**, *46*, 7947.

[14] Y. Wang, Y. Xie, P. Wei, R. B. King, H. F. Schaefer, P. V. R. Schleyer, G. H. Robinson, *Science* **2008**, *321*, 1069.

[15] R. S. Ghadwal, H. W. Roesky, S. Merkel, J. Henn, D. Stalke, *Angew. Chem.* **2009**, *121*, 5793; *Angew. Chem. Int. Ed.* **2009**, *48*, 5683.

[16] A. C. Filippou, O. Chernov, G. Schnakenburg, *Angew. Chem.* **2009**, *121*, 5797; *Angew. Chem. Int. Ed.* **2009**, *48*, 5687.

[17] K. C. Mondal, H. W. Roesky, M. C. Schwarzer, G. Frenking, I. Tkach, H. Wolf, D. Kratzert, R. Herbst-Irmer, B. Niepötter, D. Stalke, *Angew. Chem.* **2013**, *125*, 1845; *Angew. Chem. Int. Ed.* **2013**, *52*, 1801.

[18] Y. Li, Y.-C. Chan, Y. Li, I. Purushothaman, S. De, P. Parameswaran, C. W. So, *Inorg. Chem.* **2016**, *55*, 9091.

[19] S. Khan, H. W. Roesky, *Chem. Eur. J.* **2019**, *25*, 1636.

[20] A. J. Arduengo, H. V. R. Dias, J. C. Calabrese, F. A. Davidson, *Inorg. Chem.* **1993**, *32*, 1541.

[21] P. A. Rupar, M. C. Jennings, K. M. Baines, *Organometallics* **2008**, *27*, 5043.

[22] A. J. Ruddy, P. A. Rupar, K. J. Bladek, C. J. Allan, J. C. Avery, K. M. Baines, *Organometallics* **2010**, *29*, 1362.

[23] J. Baumgartner, C. Marschner, *Rev. Inorg. Chem.* **2013**, *34*, 119.

[24] G. Prabusankar, A. Sathyanarayana, P. Suresh, C. N. Babu, K. Srinivas, B. P. R. Metla, *Coord. Chem. Rev.* **2014**, *269*, 96.

[25] V. Nesterov, D. Reiter, P. Bag, P. Frisch, R. Holzner, A. Porzelt, S. Inoue, *Chem. Rev.* **2018**, *118*, 9678.

[26] J. Hlina, J. Baumgartner, C. Marschner, L. Albers, T. Müller, *Organometallics* **2013**, *32*, 3404.

[27] A. Jana, V. Huch, H. S. Rzepa, D. Scheschkewitz, *Angew. Chem.* **2015**, *127*, 291; *Angew. Chem. Int. Ed.* **2015**, *54*, 289.

[28] P. A. Rupar, M. C. Jennings, P. J. Ragogna, K. M. Baines, *Organometallics* **2007**, *26*, 4109.

[29] Y. Li, K. C. Mondal, H. W. Roesky, H. Zhu, P. Stollberg, R. Herbst-Irmer, D. Stalke, D. M. Andrada, *J. Am. Chem. Soc.* **2013**, *135*, 12422.

[30] C. Gendy, J. M. Rautinen, A. Mailman, H. M. Tuononen, *Chem. Eur. J.* **2021**, *27*, 14405.

[31] Y. Li, K. C. Mondal, J. Lübben, H. Zhu, B. Dittrich, I. Purushothaman, P. Parameswaran, H. W. Roesky, *Chem. Commun.* **2014**, *50*, 2986.

[32] P. B. Hitchcock, M. F. Lappert, A. J. Thorne, *J. Chem. Soc. Chem. Commun.* **1990**, *22*, 1587.

[33] H. Braunschweig, P. B. Hitchcock, M. F. Lappert, L. J.-M. Pierssens, *Angew. Chem.* **1994**, *106*, 1181; *Angew. Chem. Int. Ed. Engl.* **1994**, *33*, 1156.

[34] W. Wang, S. Inoue, S. Yao, M. Driess, *J. Am. Chem. Soc.* **2010**, *132*, 15890.

[35] S.-H. Zhang, C.-W. So, *Organometallics* **2011**, *30*, 2059.

[36] S. Krupski, J. V. Dickschat, A. Hepp, T. Pape, F. E. Hahn, *Organometallics* **2012**, *31*, 2078.

[37] W. Wang, S. Inoue, S. Enthaler, M. Driess, *Angew. Chem.* **2012**, *124*, 6271; *Angew. Chem. Int. Ed.* **2012**, *51*, 6167.

[38] W. Wang, S. Inoue, E. Irran, M. Driess, *Angew. Chem.* **2012**, *124*, 3751; *Angew. Chem. Int. Ed.* **2012**, *51*, 3691.

[39] J. V. Dickschat, D. Heitmann, T. Pape, F. E. Hahn, *J. Organomet. Chem.* **2013**, *744*, 160.

[40] R. K. Siwatch, D. Yadav, G. Mukherjee, G. Rajaraman, S. Nagendran, *Inorg. Chem.* **2013**, *52*, 13384.

[41] D. Gallego, S. Inoue, B. Blom, M. Driess, *Organometallics* **2014**, *33*, 6885.

[42] C. Cui, M. M. Olmstead, J. C. Fettinger, G. H. Spikes, P. P. Power, *J. Am. Chem. Soc.* **2005**, *127*, 17530.

Chemistry–A European Journal | Research Article doi.org/10.1002/chem.202301273 | Chemistry Europe European Chemical Societies Publishing

[43] Y.-P. Zhou, S. Raoufmoghaddam, T. Szilvási, M. Driess, *Angew. Chem.* **2016**, *128*, 13060; *Angew. Chem. Int. Ed.* **2016**, *55*, 12868.
[44] S. Bestgen, N. H. Rees, J. M. Goicoechea, *Organometallics* **2018**, *37*, 4147.
[45] P. Garg, D. Dange, C. Jones, *Eur. J. Inorg. Chem.* **2020**, *2020*, 4037.
[46] P. Garg, D. Dange, C. Jones, *Dalton Trans.* **2021**, *50*, 9118.
[47] M. Dehmel, M. A. Wünsche, H. Görls, R. Kretschmer, *Eur. J. Inorg. Chem.* **2021**, *2021*, 4806.
[48] M.-P. Lücke, S. Yao, M. Driess, *Chem. Sci.* **2021**, *12*, 2909.
[49] S.-C. Huo, Y. Li, D.-X. Zhang, Q. Zhou, Y. Yang, H. W. Roesky, *Chem. Asian J.* **2022**, *17*, e202200141.
[50] Y. Xiong, S. Dong, S. Yao, C. Dai, J. Zhu, S. Kemper, M. Driess, *Angew. Chem.* **2022**, *134*, e202209250; *Angew. Chem. Int. Ed.* **2022**, *61*, e202209250.
[51] B. Gehrhus, P. B. Hitchcock, M. F. Lappert, *Z. Anorg. Allg. Chem.* **2005**, *631*, 1383.
[52] A. V. Zabula, F. E. Hahn, T. Pape, A. Hepp, *Organometallics* **2007**, *26*, 1972.
[53] F. E. Hahn, A. V. Zabula, T. Pape, A. Hepp, *Eur. J. Inorg. Chem.* **2007**, *2007*, 2405.
[54] F. E. Hahn, A. V. Zabula, T. Pape, A. Hepp, *Z. Anorg. Allg. Chem.* **2008**, *634*, 2397.
[55] F. E. Hahn, A. V. Zabuka, T. Pape, A. Hepp, R. Tonner, R. Haunschild, G. Frenking, *Chem. Eur. J.* **2008**, *14*, 10716.
[56] S. Yao, M. Brym, K. Merz, M. Driess, *Organometallics* **2008**, *27*, 3601.
[57] F. E. Hahn, A. V. Zabula, T. Pape, F. Hupka, *Z. Anorg. Allg. Chem.* **2009**, *635*, 1341.
[58] L. Klemmer, A.-L. Thömmes, M. Zimmer, V. Huch, B. Morgenstern, D. Scheschkewitz, *Nat. Chem.* **2020**, *13*, 373.
[59] H. Maeda, T. Suzuki, M. Segi, *Photochem. Photobiol. Sci.* **2018**, *17*, 781.
[60] A. Pöcheim, G. A. Özpınar, T. Müller, J. Baumgartner, C. Marschner, *Chem. Eur. J.* **2020**, *26*, 17252.
[61] D. Nieder, L. Klemmer, Y. Kaiser, V. Huch, D. Scheschkewitz, *Organometallics* **2018**, *37*, 632.
[62] L. Klemmer, Y. Kaiser, V. Huch, M. Zimmer, D. Scheschkewitz, *Chem. Eur. J.* **2019**, *25*, 12187.
[63] D. Nieder, C. B. Yildiz, A. Jana, M. Zimmer, V. Huch, D. Scheschkewitz, *Chem. Commun.* **2016**, *52*, 2799.
[64] D. Dhara, V. Huch, D. Scheschkewitz, A. Jana, *Inorganics* **2018**, *6*, 6.
[65] A. Jana, V. Huch, D. Scheschkewitz, *Angew. Chem.* **2013**, *125*, 12401; *Angew. Chem. Int. Ed.* **2013**, *52*, 12179.
[66] A. Jana, I. Omlor, V. Huch, H. S. Rzepa, D. Scheschkewitz, *Angew. Chem.* **2014**, *126*, 10112; *Angew. Chem. Int. Ed.* **2014**, *53*, 9953.
[67] D. Nieder, V. Huch, C. B. Yildiz, D. Scheschkewitz, *J. Am. Chem. Soc.* **2016**, *138*, 13996.
[68] R. C. Fischer, P. P. Power, *Chem. Rev.* **2010**, *110*, 3877.
[69] M. Haas, M. Leypold, D. Schnalzer, A. Torvisco, H. Stueger, *Organometallics* **2015**, *34*, 5291.
[70] I. Bejan, D. Scheschkewitz, *Angew. Chem.* **2007**, *119*, 5885; *Angew. Chem. Int. Ed.* **2007**, *46*, 5783.
[71] N. M. Obeid, L. Klemmer, D. Maus, M. Zimmer, J. Jeck, I. Bejan, A. J. P. White, V. Huch, G. Jung, D. Scheschkewitz, *Dalton Trans.* **2017**, *46*, 8839.
[72] A. Fukazawa, Y. Li, S. Yamaguchi, H. Tsuji, K. Tamao, *J. Am. Chem. Soc.* **2007**, *129*, 14164.
[73] L. Li, T. Matsuo, D. Hashizume, H. Fueno, K. Tanaka, K. Tamao, *J. Am. Chem. Soc.* **2015**, *137*, 15026.
[74] Y. Fu, M. Li, W. Shen, *Mol. Simul.* **2009**, *35*, 1279.
[75] B.-G. Kim, X. Ma, C. Chen, Y. Le, E. W. Coir, H. Hashemi, Y. Aso, P. F. Green, J. Kieffer, J. Kim, *Adv. Funct. Mater.* **2012**, *23*, 439.
[76] N. Yin, L. Wang, Y. Lin, J. Yi, L. Yan, J. Dou, H.-B. Yang, X. Zhao, C.-Q. Ma, *Beilstein J. Org. Chem.* **2016**, *12*, 1788.
[77] H. Cui, J. Zhang, C. Cui, *Organometallics* **2013**, *32*, 1.
[78] C. Müller, D. M. Andrada, I.-A. Bischoff, M. Zimmer, V. Huch, N. Steinbrück, A. Schäfer, *Organometallics* **2019**, *38*, 1052.
[79] F. Meiners, W. Saak, M. Weidenbruch, *Organometallics* **2000**, *19*, 2835.
[80] B. Pampuch, W. Saak, M. Weidenbruch, *J. Organomet. Chem.* **2006**, *691*, 3540.
[81] M. Lazraq, J. Escudié, C. Couret, J. Satgé, M. Draeger, R. Dammel, *Angew. Chem.* **1988**, *100*, 885; *Angew. Chem. Int. Ed. Engl.* **1988**, *27*, 828.
[82] N. Tokitoh, K. Kishikawa, R. Okazaki, *J. Chem. Soc. Chem. Commun.* **1995**, *1995*, 1425.
[83] A. F. Pozharskii, O. V. Ryabtsova, V. A. Ozeryanskii, A. V. Degtyarev, O. N. Kazheva, G. G. Alexandrov, O. A. Dyachenko, *J. Org. Chem.* **2003**, *68*, 10109.
[84] R. Gajda, A. Katrusiak, *Cryst. Growth Des.* **2008**, *8*, 211.
[85] A. K. Wolf, J. Glinnemann, L. Fink, E. Alig, M. Bolte, M. U. Schmidt, *Acta Crystallogr. Sect. B* **2010**, *66*, 229.
[86] J. Escudie, H. Ranaivonjatovo, *Adv. Organomet. Chem.* **1999**, *44*, 113.
[87] V. N. Khabashesku, S. E. Boganov, D. Antic, O. M. Nefedov, J. Michl, *Organometallics* **1996**, *15*, 4714.
[88] N. P. Toltl, W. J. Leigh, *J. Am. Chem. Soc.* **1998**, *120*, 1172.
[89] D. M. Chipman, Q. Sun, G. N. R. Tripathi, *J. Chem. Phys.* **1992**, *97*, 8073.
[90] Deposition Numbers 2236120 (**6**) and 2236118 (**7**) contain the supplementary crystallographic data for this paper. These data are provided free of charge by the joint Cambridge Crystallographic Data Centre and Fachinformationszentrum Karlsruhe Access Structures service.
[91] a) C. Müller, D. M. Andrada, I.-A. Bischoff, M. Zimmer, V. Huch, N. Steinbrück, A. Schäfer, *Organometallics* **2019**, *38*, 1052; b) C. M. Weinstein, G. P. Junor, D. R. Tolentino, R. Jazzar, M. Melaimi, G. Bertrand, *J. Am. Chem. Soc.* **2018**, *140*, 9255.
[92] N. Kuhn, T. Kratz, *Synthesis* **1993**, *1993*, 561.
[93] A. J. Arduengo, R. Krafczyk, R. Schmutzler, H. A. Craig, J. R. Goerlich, W. J. Marshall, M. Unverzagt, *Tetrahedron* **1999**, *55*, 14523.
[94] G. R. Fulmer, A. J. M. Miller, N. H. Sherden, H. E. Gottlieb, A. Nudelman, B. M. Stoltz, J. E. Bercaw, K. I. Goldberg, *Organometallics* **2010**, *29*, 2176.
[95] G. M. Sheldrick, *Acta Crystallogr. Sect. A* **2015**, *71*, 3.
[96] G. M. Sheldrick, *Acta Crystallogr. Sect. C* **2015**, *71*, 3.
[97] C. B. Hübschle, G. M. Sheldrick, B. Dittrich, *J. Appl. Crystallogr.* **2011**, *44*, 1281.
[98] Gaussian 09, Revision A.02, M. J. Frisch, G. W. Trucks, H. B. Schlegel, G. E. Scuseria, M. A. Robb, J. R. Cheeseman, G. Scalmani, V. Barone, G. A. Petersson, H. Nakatsuji, X. Li, M. Caricato, A. Marenich, J. Bloino, B. G. Janesko, R. Gomperts, B. Mennucci, H. P. Hratchian, J. V. Ortiz, A. F. Izmaylov, J. L. Sonnenberg, D. Williams-Young, F. Ding, F. Lipparini, F. Egidi, J. Goings, B. Peng, A. Petrone, T. Henderson, D. Ranasinghe, V. G. Zakrzewski, J. Gao, N. Rega, G. Zheng, W. Liang, M. Hada, M. Ehara, K. Toyota, R. Fukuda, J. Hasegawa, M. Ishida, T. Nakajima, Y. Honda, O. Kitao, H. Nakai, T. Vreven, K. Throssell, J. A. Montgomery, Jr., J. E. Peralta, F. Ogliaro, M. Bearpark, J. J. Heyd, E. Brothers, K. N. Kudin, V. N. Staroverov, T. Keith, R. Kobayashi, J. Normand, K. Raghavachari, A. Rendell, J. C. Burant, S. S. Iyengar, J. Tomasi, M. Cossi, J. M. Millam, M. Klene, C. Adamo, R. Cammi, J. W. Ochterski, R. L. Martin, K. Morokuma, O. Farkas, J. B. Foresman, D. J. Fox, Gaussian, Inc., Wallingford CT, **2016**.
[99] a) J. P. Perdew, *Phys. Rev. B* **1986**, *33*, 8822; b) A. D. Becke, *Phys. Rev. A* **1988**, *38*, 3098.
[100] a) A. Schäfer, H. Horn, R. Ahlrichs, *J. Chem. Phys.* **1992**, *97*, 2571; b) A. Schäfer, C. Huber, R. Ahlrichs, *J. Chem. Phys.* **1994**, *100*, 5829; c) F. Weigend, R. Ahlrichs, *Phys. Chem. Chem. Phys.* **2005**, *7*, 3297; d) F. Weigend, *Phys. Chem. Chem. Phys.* **2006**, *8*, 1057.
[101] S. Grimme, J. Antony, S. Ehrlich, H. Krieg, *J. Chem. Phys.* **2010**, *132*, 154104.
[102] NBO 7.0. E. D. Glendening, J. K. Badenhoop, A. E. Reed, J. E. Carpenter, J. A. Bohmann, C. M. Morales, P. Karafiloglou, C. R. Landis, F. Weinhold, Theoretical Chemistry Institute, University of Wisconsin, Madison **2018**.
[103] F. Neese, F. Wennmohs, U. Becker, C. Riplinger, *J. Chem. Phys.* **2020**, *152*, 224108.
[104] a) J. P. Perdew, M. Ernzerhof, K. Burke, *J. Chem. Phys.* **1996**, *105*, 9982; b) C. Adamo, V. Barone, *J. Chem. Phys.* **1999**, *110*, 6158.
[105] Chemcraft – graphical software for visualization of quantum chemistry computations. http://www.chemcraftprog.com.

Manuscript received: April 21, 2023
Accepted manuscript online: April 28, 2023
Version of record online: May 19, 2023

Silagermylenation of C=O bonds and radical fragmentation of CO_2-expanded bis(germylene) by a cyclic (alkyl)(amino)carbene

Anna-Lena Thömmes, Robin Völker, Bernd Morgenstern, Michael Zimmer, Dominik Munz, Christopher W. M. Kay, David Scheschkewitz*, *Inorg. Chem. Front.* **2025**.

https://doi.org/10.1039/D5QI00678C

The results are additionally concluded and put into context in the "Conclusions and Outlook" chapter of this thesis.

Contributions of the authors:

Anna-Lena Thömmes

Lead: Synthesis and characterization of the compounds, quantum chemical calculations, formal analysis, data curation, investigation, methodology, validation, visualization, writing (original draft)
Equal: Conceptualization, funding acquisition, writing (review and editing)

Robin Völker

Supporting: Synthesis and characterization of the compounds

Bernd Morgenstern

Lead: X-Ray analysis and crystal structure refinement

Michael Zimmer

Lead: VT-NMR spectroscopic measurements

Dominik Munz

Equal: Funding acquisition
Supporting: Validation, writing (review and editing)

Christopher W. M. Kay

Supporting: Resources, validation, writing (review and editing)

David Scheschkewitz

Lead: Project administration, supervision
Equal: Conceptualization, funding acquisition, resources, writing (review and editing)
Supporting: Data curation, formal analysis, investigation, methodology, validation, visualization

INORGANIC CHEMISTRY
FRONTIERS

RESEARCH ARTICLE

View Article Online
View Journal

Cite this: DOI: 10.1039/d5qi00678c

Silagermylenation of C=O bonds and radical fragmentation of CO_2-expanded bis(germylene) by a cyclic (alkyl)(amino)carbene†

Anna-Lena Thömmes, [a] Robin Völker, [a] Bernd Morgenstern,[b] Michael Zimmer,[a] Dominik Munz, [c] Christopher W. M. Kay [d,e] and David Scheschkewitz *[a]

The transformation of the greenhouse gas CO_2 into value-added products represents a major contemporary challenge. Low-valent p-block compounds typically react at the oxygen termini of CO_2 due to the oxophilicity of the metal centers. We now report on the selective activation of CO_2 and ethyl isocyanate at the central carbon atom by an N-heterocyclic carbene (NHC)-stabilized *para*-silylenephenylene-bridged bis(germylene). During the net silagermylenation, the C=X (X = O, NEt) bonds are inserted into the Ge–Si bonds through cooperativity of the low-valent metal center and the electrophilic silyl backbone. The germanium(II) centers are retained in the products, as is confirmed by multinuclear NMR data, IR spectroscopy and X-ray analysis and supported by DFT calculations. Attempts to substitute the NHCs by cyclic (alkyl)(amino)carbenes (CAACs) resulted in a germylene-CAAC radical by homolytic cleavage of the Si–O bonds as evidenced by single crystal X-ray diffraction and continuous-wave EPR spectroscopy.

Received 7th March 2025,
Accepted 13th April 2025

DOI: 10.1039/d5qi00678c

rsc.li/frontiers-inorganic

Introduction

Small molecules are elementary, easily accessible and inexpensive potential chemical feedstocks, and as such their transformation into value-added products is extensively investigated, particularly in the case of the greenhouse gas CO_2. In recent years, heavier p-block compounds have been demonstrated to activate small molecules without the support of the typically applied transition metals.[1] In low-valent Group 14 chemistry, heavier alkene and alkyne analogues have been applied to CO_2 activation[2,3] as well as various silylenes and even bis(silylene)s.[4] Whereas silylenes exclusively react under participation of the lone-pair and the vacant p orbital at the low-valent silicon in these reactions, the few reports on CO_2 reactivity of the heavier congeners[5,6] suggest a pronounced dependency on the nature of the substituents.

Despite the plethora of stable germylenes,[7] reports on their reactivity towards CO_2 are surprisingly scarce. Sita *et al.* have reported the metathesis of a homoleptic amino-substituted germylene and CO_2 to provide bis(siloxy)germylene dimer **I** (Scheme 1).[5a] Only very recently, a gallyl-substituted germylene has been shown to reduce CO_2 to CO through insertion of an oxygen atom into the Ge–Ga bond to give galloxy derivative

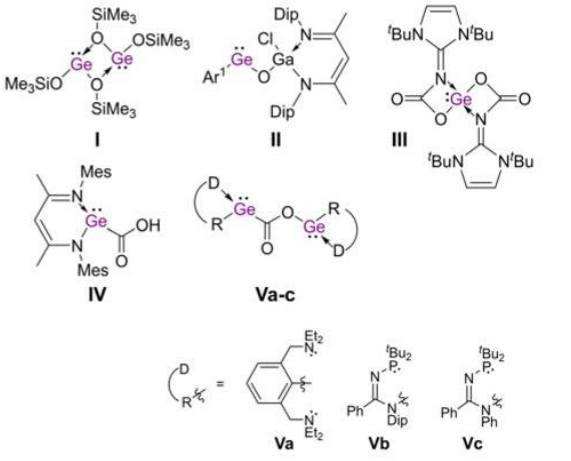

Scheme 1 Selected products of reactions of germylenes and digermynes with CO_2 (Ar^1 = 2,6-(2,6-^{i}Pr$_2$C$_6$H$_3$)$_2$C$_6$H$_3$, Dip = 2,6-^{i}Pr$_2$C$_6$H$_3$, Mes = 2,4,6-Me$_3$C$_6$H$_2$).

[a]*Krupp-Chair for General and Inorganic Chemistry, Saarland University, 66123 Saarbrücken, Germany. E-mail: scheschkewitz@mx.uni-saarland.de*
[b]*Inorganic Solid-State Chemistry, Saarland University, 66123 Saarbrücken, Germany*
[c]*Coordination Chemistry, Saarland University, 66123 Saarbrücken, Germany*
[d]*Physical Chemistry and Chemistry Education, Saarland University, 66123 Saarbrücken, Germany*
[e]*London Centre for Nanotechnology, University College London, London WC1H 0AH, UK*

†Electronic supplementary information (ESI) available: Details on the synthetic procedures and analyses, SC-XRD, NMR and IR spectroscopic data and DFT calculations. CCDC 2427550 (**2b**) and 2427551 (**3**). For ESI and crystallographic data in CIF or other electronic format see DOI: https://doi.org/10.1039/d5qi00678c

II.[5b] In contrast, in the reaction of an N-heterocyclic imino (NHI) di-substituted germylene, the carbonyl group adds in a [2 + 2]-cycloaddition across the Ge–N bonds to provide four-coordinate germylene **III**.[5c] The only known examples for reactions of the germanium center at the CO_2 carbon atom are hydrogermylenation reactions with heteroleptic hydrido germylenes, in which carboxy germylenes with Ge–C bonds, such as **IV**, are obtained instead.[5d,e] Such germylenes afford methanol and formic acid derivatives in stoichiometric reactions with suitable reactions[5e,f] and have also been proposed as intermediates of the rare examples of catalytic CO_2 derivatization by main-group systems.[5g] Certain digermynes undergo related insertion reactions of the C=O bond, forming germylenyl esters **Va–c**.[3]

Bis(tetrylene)s with linking units, spatially separating the two tetrylene centers, are of particular interest, for instance, as bidentate ligands or for the activation of small molecules.[1d,8] In our heavier acyclic diene metathesis (HADMET) polymerization, bis(germylene)s even constitute transient intermediates to σ,π-conjugated Ge=Ge-containing polymers.[9] A corresponding stabilized NHC-adduct has been isolated and employed as alternative precursor to poly(digermene)s.[10] Hence, we became interested in the derivatization of this NHC-bis(germylene). While simple substitution of the NHC occurs with a nucleophilic and sterically demanding CAAC,[10] we anticipated a fundamentally different reactivity with small electrophiles. Here we report on the activation of carbon dioxide and ethyl isocyanate through selective insertion reactions into the Ge–Si bonds of the silylenearylene-bridged NHC-bis(germylene) under retention of the germanium(II) functionalities. The CO_2 insertion product is shown to undergo CAAC-induced radical fragmentation.

Results and discussion

Exposure of a benzene suspension of yellow NHC-bis(germylene) **1** to CO_2 at room temperature results in immediate dissolution and decolorization. Multinuclear NMR spectroscopy of the crude reaction mixture confirms quantitative conversion to a new product to which we tentatively assign the constitution of silyl ester **2a** (Scheme 2), where the carboxy groups have been inserted into the Ge–Si bonds, based on NMR spectroscopic analysis. Notably, the silagermylenation of CS_2 has very recently been reported to result in the corresponding silyl dithioester.[11] Silyl ester **2a** is isolated as an off-white powder by removing the solvent under vacuum.

A characteristic $^{13}C\{^1H\}$ NMR low-field resonance at 173.2 ppm due to the carbenic carbon atoms as well as a broad septet in the ^1H NMR spectrum at 5.69 ppm arising from the N-bonded isopropyl groups suggest NHC-coordination to the Ge(II) centers.[10,12,13] In comparison to organic esters (158 to 177 ppm),[14] the carbonyl carbon resonance at 204.9 ppm of **2a** is similarly downfield-shifted as oxycarbonyl germylenes **Va–c** (206 to 209 ppm).[3] Furthermore, the considerable deviation from the corresponding shifts of organic

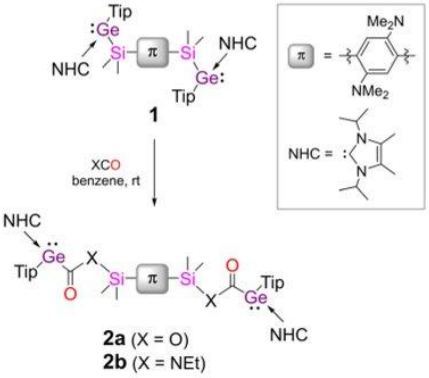

Scheme 2 Reactions of NHC-bis(germylene) **1** with CO_2 and ethyl isocyanate, respectively, to carboxy- and amide-functionalized NHC-bis(germylene)s **2a,b** (Tip = 2,4,6-triisopropylphenyl).

germylenyl esters (~177 ppm)[15] and oxycarbonyl silanes (184 to 192 ppm)[16] speaks against the formation of the corresponding product with reversed regioselectivity, *i.e.* with Ge–O and Si–C bonds (Scheme S1, ESI†), and corroborates the suggested constitution of **2a**.

In line with a more electronegative environment, the $^{29}Si\{^1H\}$ NMR peaks at 2.09 and 2.05 ppm are considerably downfield shifted compared to the germylenyl substituted silicon atoms of the starting material **1** (−11.07, −11.19 ppm).[10] Such low-field shifts are indeed characteristic for silanoles, silyl ethers and silyl esters with Si–O bonds (−3 to 34 ppm)[17] in contrast to the corresponding alkyl silanes (−11 to −3 ppm)[18] and in particular to acyl silanes, including esters (−30 to −7 ppm).[16a,19] The two $^{29}Si\{^1H\}$ NMR peaks with equal intensities in addition to two sets of signals for the phenylene, the NMe_2 and $SiMe_2$ groups in the $^{13}C\{^1H\}$ and ^1H NMR spectra suggest the presence of a 1 : 1 diastereomeric mixture of the racemate and the *meso*-form. Similar results have been obtained for NHC-bis(germylene) **1**[10] and corroborate NHC-coordination to the germylene centers in a pyramidal manner, thus giving rise to Ge-centered chirality. The peak separations are slightly smaller in the case of **2a**, in line with the larger spatial separation of the respective nuclei from the germanium stereocenters. Further evidence for the presence of the ester functionality is provided by a characteristic band in the IR spectrum at 1613 cm^{-1}, just between the C=O stretching vibrations in germylenyl esters **Vb,c** (1581, 1593 cm^{-1})[3b] and acyl digermenes (1649 to 1653 cm^{-1}).[20]

The formation of silyl ester **2a** *vs.* the alternative germylenyl ester (Scheme S1, ESI†) is rationalized by the formation of Si–O bonds (BDE ~ 191 kcal mol^{-1}),[21] which are substantially stronger than Ge–O bonds (BDE ~ 158 kcal mol^{-1}).[21] Accordingly, DFT-calculations for both isomers confirm the silyl ester **2a** to be favored by ΔG = 11.4 kcal mol^{-1} (see ESI†).

Unfortunately, crystallization attempts from pentane, hexane, benzene and thf remained unsuccessful, in part presumably due to the limited stability of **2a** in solution. In par-

View Article Online
Inorganic Chemistry Frontiers Research Article

ticular in thf, precipitation of NHC–CO_2 [22] concomitant with the formation of a mixture of unidentified products is already observed after a few hours. We therefore turned our attention to ethyl isocyanate as an isolobal imine analogue of CO_2 in the anticipation that the additional organic substituent could facilitate crystallization without compromising the reactivity.

The reaction of NHC-bis(germylene) **1** with two equivalents of EtNCO in benzene at room temperature (Scheme 2) indeed gives rise to very similar NMR spectroscopic data, in line with the formation of the corresponding bis(amide) **2b**. The characteristic $^{13}C\{^1H\}$ and ^1H NMR peaks of the coordinated NHCs are observed at 172.6 ppm and 5.73 ppm, and the carbonyl carbon resonances at 212.2 and 211.9 ppm. The latter peaks are slightly downfield-shifted with respect to **2a** (204.9 ppm), as is typically observed for amides and imides in comparison to the corresponding esters.[14b,23] The low-field shift of the $^{29}Si\{^1H\}$ NMR resonances at −6.3 and −6.4 ppm in comparison to germylenyl silane **1** (−11.07, −11.19 ppm)[10] is considerably less pronounced than in the case of **2a** (2.09, 2.05 ppm). This is in perfect agreement with the substitution of the O- for an *N*-substituent at silicon as previously observed for silylamines ($PhMe_2SiNR_2$: −5 to −1 ppm)[17e] in comparison to the corresponding silanole ($PhMe_2SiOH$: 7 ppm), for instance.[17d]

The appearance of two $^{13}C\{^1H\}$ carbonyl carbon resonances for **2b** in addition to the somewhat larger separation of the two $^{29}Si\{^1H\}$ NMR peaks in comparison to **2a** hints towards the presence of rotational isomers due to the newly introduced amide moieties. Hindered rotation about the C–N bond is further corroborated by low-temperature NMR spectra: the $^{29}Si\{^1H\}$ peak ratio changes from 1.5 : 1 at room temperature to 2.4 : 1 at −60 °C, suggesting one of the conformations of the zwitterionic form of the amide functionalities in **2b** (Scheme 3) to be thermodynamically favored.

Most probably, the interaction of the $SiMe_2$ group with the formally negatively charged oxygen center in the *E*-conformer is favorable compared to the germylene lone-pair in the *Z*-conformer, also on steric grounds. Equally characteristic for the presence of rotamers is the distinct increase of the peak separation at low temperature (40 Hz at −60 °C, 9.3 Hz at rt), corresponding to an estimated rotational barrier of $\Delta G^{\ddagger} \sim 60$ kJ mol^{-1} (see ESI†). Similar to dimethylbenzamide (62 kJ mol^{-1}),[24a] the rotation in **2b** is slightly less hindered than in *N*,*N*-dialkyl formamides and acetamides (68 to 88 kJ mol^{-1}),[24] which suggests competing interactions of the lone-pairs at the nitrogen and the germanium centers with the carbonyl group. Even the $SiMe_2$, the aryl protons of the Tip groups and the NHCs' isopropyl methine groups give rise to peak splitting in the ^1H NMR spectrum at −60 °C, despite a larger spatial separation from the C–N bonds (see ESI†).

In stark contrast to this and as expected for a diastereomeric mixture, **2a** does not show coalescence behavior. Notably, in the ^1H NMR spectrum of **2a** accidental isochrony of the diastereomers' peaks is exhibited in thf-d_8 as opposed to C_6D_6. It is therefore not surprising, that the thf-d_8 spectra of **2b** show no additional peak splitting either. Given the structural similarities and the common synthetic origin, however, the presence of different diastereomers is assumed for **2b** as well. Corresponding investigations in C_6D_6 are nonetheless prohibited by its poor solubility.

As in the case of organic amides,[25] the diminished C=O bond strength due to the interaction with the nitrogen lone-pair is reflected in the IR spectrum: the C=O stretching frequency of **2b** (1548 cm^{-1}) is considerably red-shifted compared to ester **2a** (1613 cm^{-1}).

The molecular structure of the *meso*-form of **2b**, obtained by X-ray diffraction on a single crystal (Fig. 1), indeed confirms coordination of the carbene to the germylene center with a characteristically elongated Ge–C single bond (2.078(2) Å). While this is in line with silyl–aryl and diaryl NHC-germylenes (2.067 to 2.078 Å; $\Sigma^{\circ}_{Ge} = 308.4°$ to 317.7°),[10,12] the pyramidalization in **2b** ($\Sigma^{\circ}_{Ge1} = 296.0(2)°$) is slightly increased in comparison. In contrast, the angles are considerably less acute than in intramolecularly stabilized oxycarbonyl germylenes **Va,b** and the related CS_2 insertion product of a silyl germylene ($\Sigma^{\circ}_{Ge1} = 253.4°$ to 282.8°).[3,11] With the smaller pyramidalization, enhanced interaction of the germanium lone-pair with the carbonyl moiety is possible, thus diminishing the donation of the nitrogen lone-pairs to the carbonyl groups: the N2–C10 bond (1.382(3) Å) lies at the upper end of the range constituted by considerably conjugated amides and anilines (1.31 to 1.38 Å).[26] The partial zwitterionic character in amides as opposed to esters results in an elongated C=O double bond length of 1.239(2) Å compared to germylenyl oxycarbonyl germylenes **Va,b** (1.19, 1.20 Å).[3] Notably, the coordination

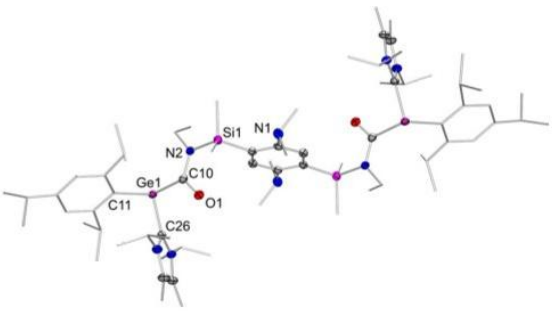

Fig. 1 Molecular structure of amide-functionalized NHC-bis(germylene) **2b** in the solid state (co-crystallized solvent molecules and hydrogen atoms omitted for clarity, thermal ellipsoids at 50%). Selected bond lengths [Å] and angles [°]: Ge1–C26 2.078(2), Ge1–C10 2.066(2), N2–C10 1.382(3), C10–O1 1.239(2), Σ°(Ge1) 296.0(2), Σ°(N2) 360.0(5), Si1–N2–C10–O1 9.1(2).

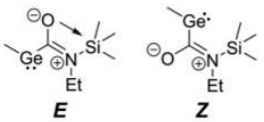

Scheme 3 Schematic representation of the *E*- and *Z*-conformations of the zwitterionic form of the amide moieties in **2b**.

View Article Online
Research Article Inorganic Chemistry Frontiers

environment of the nitrogen centers are perfectly planar ($\Sigma^{\circ}_{N2} = 360.0(5)^{\circ}$) and the carbonyl group only slightly deviates (Si1–N2–C10–O1 9.1(2)°) from the presumably favored *E*-conformation (*vide supra*).

According to DFT calculations for **2b** at the BP86-D3(BJ)/def2-TZVPP//BP86-D3(BJ)/def2-SVP level of theory, the HOMO and HOMO−1 (Fig. 2) are best represented by lone-pairs at the germanium atoms with π-contributions from the amide functionalities. In line with pronounced interaction between the germylene lone-pairs and the carbonyl groups, HOMO−4 and HOMO−5 exhibit contributions from the carbonyl groups as well as from the germanium and the nitrogen atoms (see ESI†). The LUMO is located at the arylene linker with little admixture from the adjacent silylene moieties. The unoccupied π orbitals at higher energy (LUMO+1 and LUMO+2) are predominantly located at the NHC ligands, suggesting σ,π-interaction only between the π-system of the linker and the $SiMe_2$ groups. In fact, the in-phase and out-of-phase combinations of the pairwise occurring orbitals at both sides of the bridging unit are degenerate, confirming the absence of extended conjugation between the germylene centers.

The activation of the C=X (X = N, O) bonds is presumably achieved through cooperativity of the nucleophilic germylene lone-pair and the electrophilic silyl backbone in bis(germylene) **1**, driven by the formation of strong Si–X bonds. This has been confirmed theoretically by Gonnade and Sen *et al.* for the silagermylenation of CS_2.[11] Notably, neither the CAAC-stabilized bis(germene) analogue of **1** with Ge=C bonds[10] nor the corresponding bis(digermene) with Ge=Ge bonds[9a] react similarly with CO_2, corroborating the importance of the nucleophilicity-enhancing NHC-donor.

Since the reaction of NHC-bis(germylene) **1** with $CAAC^{Me}$, as the stronger σ-donor and π-acceptor, yields the corresponding bis(germene),[10] we attempted the generation of Ge=C double bonds in the corresponding reaction of bis(carboxygermylene) **2a** as well. Surprisingly, however, treatment of **2a** with two equivalents of $CAAC^{Me}$ affords NHC-germylene **3** comprising a tethered radical center, albeit in a very low yield of 11% (Scheme 4). The constitution of **3** is confirmed by single crystal X-ray crystallography and continuous-wave EPR spectroscopy (Fig. 3). The obtained *g*-factor (2.0035) is slightly

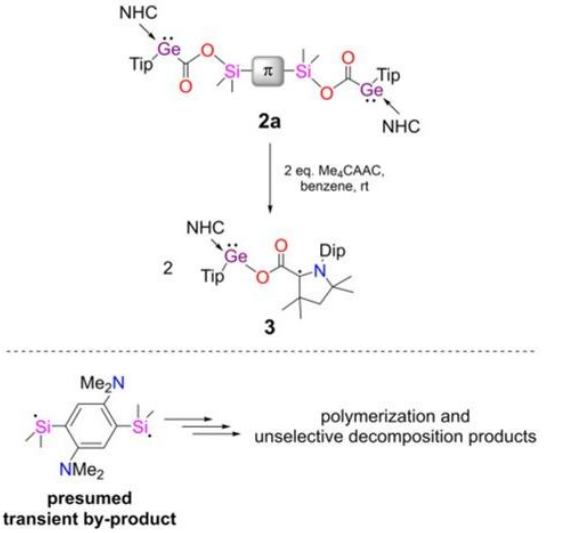

Scheme 4 Synthesis of paramagnetic NHC-germylene **3** (NHC = 1,3-diisopropylimidazol-4,5-dimethyl-2-ylidene, $CAAC^{Me}$ = 1-(2,6-diisopropylphenyl)-3,3,5,5-tetramethyl-pyrrolidin-2-ylidene).

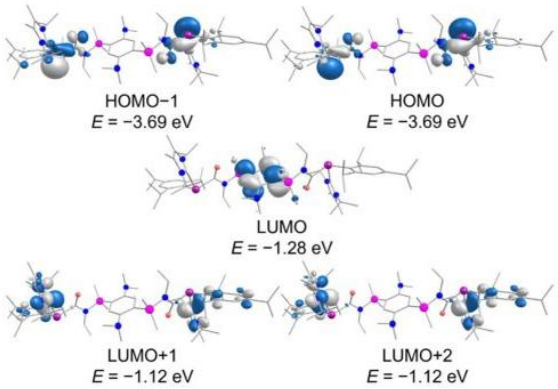

Fig. 2 Selected frontier orbitals of amide-functionalized NHC-bis(germylene) **2b** (contour value 0.036). Hydrogen atoms omitted for clarity.

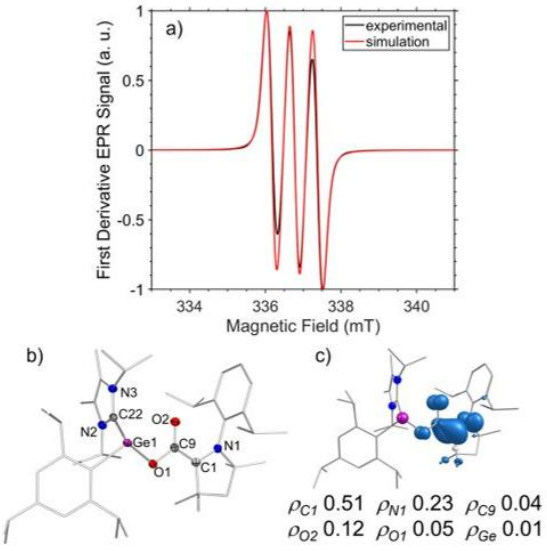

Fig. 3 (a) Experimental and simulated continuous-wave EPR spectra of a C_6D_6 solution of **3** (simulation parameters: g = 2.0035, $A(^{14}N)$ = 6.0 G). (b) Molecular structure of NHC-germylene radical **3** in the solid state (co-crystallized solvent molecules and hydrogen atoms omitted for clarity, thermal ellipsoids at 50%). Selected bond lengths [Å] and angles [°]: Ge1–O1 1.9528(7), C9–O1 1.339(1), C9–O2 1.238(1), C1–N1 1.376(1), C1–C9 1.441(1), Σ°(Ge1) 288.2(1). (c) Calculated Mulliken spin densities and spin density plot (contour value 0.0038).

smaller than in germylenyl substituted CAAC-radicals (2.0070, 2.0075; $A(^{14}N)$ = 5.0, 5.3 G),[27] in line with a larger distance of the unpaired electron from the germanium. Furthermore, no ^{73}Ge coupling is observed and the ^{14}N coupling ($A(^{14}N)$ = 6.0 G), manifest in a triplet splitting, is only slightly increased, hence suggesting the spin-density to be predominantly located on the substituent.

Accordingly, the molecular structure of **3** (Fig. 3) exhibits an elongated C═O bond (1.238(1) Å) compared to oxycarbonyl germylenes **Va,b** (1.19, 1.20 Å)[3] and even similar to amide **2b** (1.239(2) Å). The short C1–C9 bond length of 1.441(1) Å confirms partial double bond character, in stark contrast to $CAAC^{Me}$–CO_2 (1.52 Å),[28] but in agreement with the delocalization of the unpaired electron across the carbonyl group and the CAAC substituent. The C1–N1 distance (1.376(1) Å) is similar to reported germylenyl substituted CAAC-radicals (1.37 Å).[27] Considerable pyramidalization ($\Sigma^{\circ}_{Ge1} = 288.2(1)^{\circ}$), comparable to a reported siloxy aryl NHC-germylene ($\varepsilon^{\circ}_{Ge1} = 283.7^{\circ}$),[29] suggests the presence of a lone-pair at germanium and no significant contribution from the unpaired electron. This is further confirmed by the Ge1–O1 (1.9528(7) Å) and C9–O1 distances (1.339(1) Å), which are comparable to germylenyl oxycarbonyl germylenes **Va,b** (Ge–O: 1.96 Å, C–O: 1.33 to 1.34 Å).[3]

In line with the experimental data, the Mulliken spin densities obtained at the UB3LYP-D3(BJ)/def2-TZVPP//UB3LYP-D3(BJ)/def2-SVP level of theory are highest at the carbene fragment (Fig. 3). The computed *g*-value of 2.0033 and the ^{14}N coupling constant of $A(^{14}N)$ = 4.2 G validate the accuracy of the computational model.

Apparently, germylene **3** is formed *via* CAAC-induced homolytic cleavage of the Si–O bonds in **2a**. Hence, most likely, a highly reactive silicon centered diradical by-product is formed, whose unselective decomposition and/or polymerization prevent its identification (Scheme 4). While CAACs are known to stabilize main group radicals,[30] they are, however, typically obtained through reduction or hydrogen abstraction. Substitution induced synthesis has only been reported in two cases for silicon and diborane centered diradicals.[31] With the carboxy group as an additional spacer separating the radical center from the Ge(II) moiety in **3**, as opposed to the directly connected CAAC-germylenes,[27] analogous diradicals could be envisaged. We are currently investigating more economic pathways towards such (poly-)radical germylenes, avoiding the use of the relatively complicated linking unit of **2a**.

Conclusions

In conclusion, the silagermylenation reactions of CO_2 and EtNCO with a *para*-silylenephenylene-bridged NHC-bis(germylene) are reported. These highly atom-economic transformations constitute a convenient strategy for the selective backbone functionalization with acyl groups under retention of the low-valent germylenes' integrity. In particular, this may facilitate the synthesis and characterization of structurally derived functionalized poly(digermene)s. In a reaction of the obtained carboxy germylene with $CAAC^{Me}$, structural evidence for an unprecedented germylene with a tethered radical is provided, which may serve as a prototype for related (poly-)radicals in future investigations.

Author contributions

A.-L. T. and D. S. conceptualized the project. D. S. held the project administration and supervision. A.-L. T. (lead) and R. V. (supporting) synthesized and isolated the compounds and collected the NMR, IR, and EPR spectroscopic data. A.-L. T. performed the quantum chemical calculations and carried out the visualization and analysis of the data. B. M. performed the single crystal X-ray analyses and the refinement of the structures. M. Z. performed the VT-NMR spectroscopic measurements. D. S., D. M. and A.-L. T. acquired funding for the project. A.-L. T. (original draft + review and editing) and D. S. (review and editing) wrote the manuscript. C. W. M. K. and D. M. validated the spectroscopic data and the quantum chemical calculations and contributed to the revision and editing of the manuscript.

Data availability

The data supporting this article have been included as part of the ESI.†

Conflicts of interest

There are no conflicts to declare.

Acknowledgements

We thank the Fonds der Chemischen Industrie for a Kekulé fellowship for A.-L. T. and the German Research Foundation for funding ("Solar-Driven Chemistry: Light-Induced Small Molecule Fixation by Diradicals"; DFG SCHE 906/9-1). We acknowledge the instrumentation facilities provided by the service center for X-ray analysis established with the financial support from Saarland University and the German Research Foundation (INST 256/506-1 and INST 256/582-1). We thank Prof. Stella Stopkowicz for access to the computational cluster.

References

1 Reviews: (*a*) R. Akhtar, K. Gaurav and S. Khan, Applications of low-valent compounds with heavy group-14 elements, *Chem. Soc. Rev.*, 2024, **53**, 6150–6243; (*b*) S. Sinha and J. Jiang, Main group elements in electrochemical hydrogen evolution and carbon dioxide reduction, *Chem. Commun.*, 2023, **59**, 11767–11779; (*c*) M. Pérez-Jiménez, H. Corona,

F. de la Cruz-Martínez and J. Campos, Donor-Acceptor Activation of Carbon Dioxide, *Chem. – Eur. J.*, 2023, **29**, e202301428; (*d*) A. Saddington, S. Yao and M. Driess, Recent advances in low-valent silicon chemistry, in *Advances in Inorganic Chemistry*, ed. K. Meyer and R. van Eldik, Academic Press, 2023, vol. 82, pp. 119–156; (*e*) F. Dankert and C. Hering-Junghans, Heavier group 13/15 multiple bond systems: synthesis, structure and chemical bond activation, *Chem. Commun.*, 2022, **58**, 1242–1262; (*f*) S. Fujimori and S. Inoue, Small Molecule Activation by Two-Coordinate Acyclic Silylenes, *Eur. J. Inorg. Chem.*, 2020, 3131–3142; (*g*) C. Shan, S. Yao and M. Driess, Where silylene–silicon centres matter in the activation of small molecules, *Chem. Soc. Rev.*, 2020, **49**, 6733–6754; (*h*) Y. Su and R. Kinjo, Small molecule activation by boron-containing Heterocycles, *Chem. Soc. Rev.*, 2019, **48**, 3613–3659; (*i*) R. L. Melen, Frontiers in molecular p-block chemistry: From structure to reactivity, *Science*, 2019, **363**, 479–484; (*j*) T. J. Hadlington, M. Driess and C. Jones, Low-valent group 14 element hydride chemistry: towards catalysis, *Chem. Soc. Rev.*, 2018, **47**, 4176–4197; (*k*) C. Weetman and S. Inoue, The Road Travelled: After Main-Group Elements as Transition Metals, *ChemCatChem*, 2018, **10**, 4213–4228; (*l*) T. Chu and G. I. Nikonov, Oxidative Addition and Reductive Elimination at Main-Group Element Centers, *Chem. Rev.*, 2018, **118**, 3608–3680; (*m*) X. Wang, C. Xia and L. Wu, Homogeneous carbon dioxide reduction with p-block element-containing reductants, *Green Chem.*, 2018, **20**, 5415–5426; (*n*) S. Yadav, S. Saha and S. S. Sen, Compounds with Low-Valent p-Block Elements for Small Molecule Activation and Catalysis, *ChemCatChem*, 2016, **8**, 486–501; (*o*) B. Blom and M. Driess, Recent Advances in Silylene Chemistry: Small Molecule Activation En-Route Towards Metal-Free Catalysis, in *Functional Molecular Silicon Compounds II. Structure and Bonding*, ed. D. Scheschkewitz, Springer International Publishing, 2014, vol. 156, pp. 85–123.

2 (*a*) N. Wiberg, W. Niedermayer, K. Polborn and P. Mayer, Reactivity of the Isolable Disilene R*PhSi=SiPhR* (R*=Si*t*Bu$_3$), *Chem. – Eur. J.*, 2002, **8**, 2730–2739; (*b*) D. Gau, R. Rodriguez, T. Kato, N. Saffon-Merceron, A. de Cózar, F. P. Cossío and A. Baceiredo, Synthesis of a Stable Disilyne Bisphosphine Adduct and Its Non-Metal-Mediated CO_2 Reduction to CO, *Angew. Chem., Int. Ed.*, 2011, **50**, 1092–1096, (*Angew. Chem.*, 2011, **123**, 1124–1128); (*c*) J. Li, M. Hermann, G. Frenking and C. Jones, The Facile Reduction of Carbon Dioxide to Carbon Monoxide with an Amido-Digermyne, *Angew. Chem., Int. Ed.*, 2012, **51**, 8611–8614, (*Angew. Chem.*, 2012, **124**, 8739–8742); (*d*) D. Wendel, T. Szilvási, D. Henschel, P. J. Altmann, C. Jandl, S. Inoue and B. Rieger, Precise Activation of Ammonia and Carbon Dioxide by an Iminodisilene, *Angew. Chem., Int. Ed.*, 2018, **57**, 14575–14579, (*Angew. Chem.*, 2018, **130**, 14783–14787); (*e*) A. Kostenko and M. Driess, Geometrically Compelled Disilene with λ^4-Coordinate SiII Atoms, *J. Am. Chem. Soc.*, 2018, **140**, 16962–16966.

3 (*a*) A. Caise, L. P. Griffin, C. McManus, A. Heilmann and S. Aldridge, Reversible Uptake of CO_2 by Pincer Ligand Supported Dimetallynes, *Angew. Chem., Int. Ed.*, 2022, **61**, e202117496, (*Angew. Chem.*, 2022, **134**, e202117496); (*b*) J. Fan, S. Quek, M.-C. Yang, Z.-F. Zhang, M.-D. Su and C.-W. So, Reversible CO_2 activation by a *N*-phosphinoamidinato digermyne, *Chem. Commun.*, 2022, **58**, 1033–1036.

4 (*a*) P. Jutzi, D. Eikenberg, A. Möhrke, B. Neumann and H.-G. Stammler, Decamethylsilicocene Chemistry: Unprecedented Multistep Reactions of a Silicon(II) Compound with the Heterocumulenes CO_2, COS, CS_2, and RNCS (R = Methyl, Phenyl), *Organometallics*, 1996, **15**, 753–759; (*b*) S. Yao, Y. Xiong, M. Brym and M. Driess, An Isolable Silanoic Ester by Oxygenation of a Stable Silylene, *J. Am. Chem. Soc.*, 2007, **129**, 7268–7269; (*c*) X. Liu, X.-Q. Xiao, Z. Xu, X. Yang, Z. Li, Z. Dong, C. Yan, G. Lai and M. Kira, Reactions of an Isolable Dialkylsilylene with Carbon Dioxide and Related Heterocumulenes, *Organometallics*, 2014, **33**, 5434–5439; (*d*) K. Junold, M. Nutz, J. A. Baus, C. Burschka, C. Fonseca Guerra, F. M. Bickelhaupt and R. Tacke, The Donor-Stabilized Silylene Bis[*N*,*N*′-diisopropylbenzamidinato(−)]silicon(II): Synthesis, Electronic Structure, and Reactivity, *Chem. – Eur. J.*, 2014, **20**, 9319–9329; (*e*) F. M. Mick, J. A. Baus, M. Nutz, C. Burschka, J. Poater, F. M. Bickelhaupt and R. Tacke, Reactivity of the Donor-Stabilized Silylenes [*i*PrNC(Ph)N*i*Pr]$_2$Si and [*i*PrNC(N*i*,Pr$_2$)N*i*Pr]$_2$Si: Activation of CO_2 and CS_2, *Chem. – Eur. J.*, 2015, **21**, 16665–16672; (*f*) D. Wendel, A. Porzelt, F. A. D. Herz, D. Sarkar, C. Jandl, S. Inoue and B. Rieger, From Si(II) to Si(IV) and Back: Reversible Intramolecular Carbon–Carbon Bond Activation by an Acyclic Iminosilylene, *J. Am. Chem. Soc.*, 2017, **139**, 8134–8137; (*g*) A. V. Protchenko, P. Vasko, D. C. Huan Do, J. Hicks, M. Á. Fuentes, C. Jones and S. Aldridge, Reduction of Carbon Oxides by an Acyclic Silylene: Reductive Coupling of CO, *Angew. Chem., Int. Ed.*, 2019, **58**, 1808–1812, (*Angew. Chem.*, 2019, **131**, 1822–1826); (*h*) M.-P. Luecke, E. Pens, S. Yao and M. Driess, An Isolable Bis(Silanone-Borane) Adduct, *Chem. – Eur. J.*, 2020, **26**, 4500–4504; (*i*) Y. Xiong, S. Yao, A. Ruzicka and M. Driess, Distinctly different reactivity of bis(silylenyl)- *versus* phosphanyl-silylenyl-substituted o-dicarborane towards O_2, N_2O and CO_2, *Chem. Commun.*, 2021, **57**, 5965–5968.

5 (*a*) L. R. Sita, J. R. Babcock and R. Xi, Facile Metathetical Exchange between Carbon Dioxide and the Divalent Group 14 Bisamides M[N(SiMe$_3$)$_2$]$_2$ (M = Ge and Sn), *J. Am. Chem. Soc.*, 1996, **118**, 10912–10913; (*b*) A. Bücker, C. Wölper and S. Schulz, Activation of heteroallenes by metal-substituted electron-rich tetrylenes, *Polyhedron*, 2024, **247**, 116702; (*c*) L. Groll, J. A. Kelly and S. Inoue, Reactivity of NHI-Stabilized Heavier Tetrylenes towards CO_2 and N_2O, *Chem. – Asian J.*, 2024, **19**, e202300941; (*d*) A. Jana, D. Ghoshal, H. W. Roesky, I. Objartel, G. Schwab and D. A. Stalke, A Germanium(II) Hydride as an Effective Reagent for Hydrogermylation Reactions, *J. Am. Chem. Soc.*,

2009, **131**, 1288–1293; (*e*) G. Tan, W. Wang, B. Bloma and M. Driess, Mechanistic studies of CO_2 reduction to methanol mediated by an N-heterocyclic germylene hydride, *Dalton Trans.*, 2014, **43**, 6006–6011; (*f*) A. Jana, G. Tavčar, H. W. Roesky and M. John, Germanium(II) hydride mediated reduction of carbon dioxide to formic acid and methanol with ammonia borane as the hydrogen source, *Dalton Trans.*, 2010, **39**, 9487–9489; (*g*) T. J. Hadlington, C. E. Kefalidis, L. Maron and C. Jones, Efficient Reduction of Carbon Dioxide to Methanol Equivalents Catalyzed by Two-Coordinate Amido-Germanium(II) and -Tin(II) Hydride Complexes, *ACS Catal.*, 2017, **7**, 1853–1859.

6 (*a*) J. R. Babcock, L. Liable-Sands, A. L. Rheingold and L. R. Sita, Syntheses, Structural Characterizations, and Heterocumulene Metathesis Studies of New Monomeric Bis (triorganosilylamido)tin(II) Derivatives, *Organometallics*, 1999, **18**, 4437–4441; (*b*) A. Jana, H. W. Roesky, C. Schulzke and A. Döring, Reactions of Tin(II) Hydride Species with Unsaturated Molecules, *Angew. Chem., Int. Ed.*, 2009, **48**, 1106–1109, (*Angew. Chem.*, 2009, **121**, 1126–1129); (*c*) D. A. Dickie, E. N. Coker and R. A. Kemp, Formation of a Reversible, Intramolecular Main-Group Metal–CO_2 Adduct, *Inorg. Chem.*, 2011, **50**, 11288–11290; (*d*) S. Weiß, M. Widemann, K. Eichele, H. Schubert and L. Wesemann, Low valent lead and tin hydrides in reactions with heteroallenes, *Dalton Trans.*, 2021, **50**, 4952–4958; (*e*) A. V. Protchenko, M. Á. Fuentes, J. Hicks, C. McManus, R. Tirfoin and S. Aldridge, Reactions of a diborylstannylene with CO_2 and N_2O: diboration of carbon dioxide by a main group bis(boryl) complex, *Dalton Trans.*, 2021, **50**, 9059–9067; (*f*) D. Sarkar, L. Groll, D. Munz, F. Hanusch and S. Inoue, Ligand Assisted CO_2 Activation and Catalytic Valorization by an NHI-Stabilized Stannylene, *ChemCatChem*, 2022, **14**, e202201048.

7 Reviews: (*a*) W. P. Neumann, Germylenes and Stannylenes, *Chem. Rev.*, 1991, **91**, 311–334; (*b*) N. N. Zemlyanskii, I. V. Borisova, M. S. Nechaev, V. N. Khrustalev, V. V. Lunin, M. Y. Antipin and Y. A. Ustynyuk, Divalent silicon, germanium, and tin compounds with element-heteroatom bonds, *Russ. Chem. Bull. Int. Ed.*, 2004, **53**, 980–1006; (*c*) Y. Mizuhata, T. Sasamori and N. Tokitoh, Stable Heavier Carbene Analogues, *Chem. Rev.*, 2009, **109**, 3479–3511; (*d*) M. Asay, C. Jones and M. Driess, *N*-Heterocyclic, Carbene Analogues with Low-Valent Group 13 and Group 14 Elements: Syntheses, Structures, and Reactivities of a New Generation of Multitalented Ligands, *Chem. Rev.*, 2011, **111**, 354–396; (*e*) J. A. Cabeza and P. García-Álvarez, Polydentate Amidinato-Silylenes, -Germylenes and -Stannylenes, *Chem. – Eur. J.*, 2024, **30**, e202400786.

8 Reviews: (*a*) N. Mukherjee and M. Majumdar, Diverse Functionality of Molecular Germanium: Emerging Opportunities as Catalysts, *J. Am. Chem. Soc.*, 2024, **146**, 24209–24232; (*b*) X. Gao, Y. He and J. Cui, Charting the frontiers of Bis-germylene chemistry, *J. Organomet. Chem.*, 2024, **1012**, 123146; (*c*) S. Yao, A. Saddington, Y. Xiong and M. Driess, Chelating Bis-silylenes As Powerful Ligands To Enable Unusual Low-Valent Main-Group Element Functions, *Acc. Chem. Res.*, 2023, **56**, 475–488.

9 (*a*) L. Klemmer, A.-L. Thömmes, M. Zimmer, V. Huch, B. Morgenstern and D. Scheschkewitz, Metathesis of Ge=Ge double bonds, *Nat. Chem.*, 2020, **13**, 373–377; (*b*) A.-L. Thömmes, T. Büttner, B. Morgenstern, O. Janka, G. Kickelbick, B.-J. Niebuur, T. Kraus, M. Gallei and D. Scheschkewitz, Near-Infinite-Chain Polymers with Ge=Ge Double Bonds, *Angew. Chem., Int. Ed.*, 2024, **63**, e202415103, (Nahezu unendlich lange Polymere mit Ge=Ge-Doppelbindungen, *Angew. Chem.*, 2024, **136**, e202415103).

10 A.-L. Thömmes, B. Morgenstern, M. Zimmer, D. M. Andrada and D. Scheschkewitz, σ,π-Conjugated Bis (germylene) Adducts with NHC and CAACs, *Chem. – Eur. J.*, 2023, **29**, e202301273.

11 V. S. Ajithkumar, N. Khilari, P. B. Ghanwat, G. Venugopal, D. Koley and S. S. Sen, Activation of carbon disulfide by a hypersilyl germylene, *Dalton Trans.*, 2024, **53**, 10814–10818.

12 (*a*) K. L. Hurni, P. A. Rupar, N. C. Payne and K. M. Baines, Stabilization of a Transient Diorganogermylene by an N-Heterocyclic Carbene, *Organometallics*, 2007, **26**, 4109–4111; (*b*) A. J. Ruddy, P. A. Rupar, K. J. Bladek, C. J. Allan, J. C. Avery and K. M. Baines, On the Bonding in N-Heterocyclic Carbene Complexes of Germanium(II), *Organometallics*, 2010, **29**, 1362–1367.

13 (*a*) A. Jana, V. Huch and D. Scheschkewitz, NHC-Stabilized Silagermenylidene: A Heavier Analogue of Vinylidene, *Angew. Chem., Int. Ed.*, 2013, **52**, 12179–12182, (NHC-Stabilisiertes Silagermenyliden: ein schweres Analogon von Vinyliden, *Angew. Chem.*, 2013, **125**, 12401–12404); (*b*) A. Jana, V. Huch, H. S. Rzepa and D. Scheschkewitz, A Multiply Functionalized Base-Coordinated GeII Compound and Its Reversible Dimerization to the Digermene, *Angew. Chem., Int. Ed.*, 2015, **54**, 289–292, (Eine mehrfach funktionalisierte Basen-koordinierte GeII-Verbindung und ihre reversible Dimerisierung zum Digermen, *Angew. Chem.*, 2015, **127**, 291–295); (*c*) D. Nieder, C. B. Yildiz, A. Jana, M. Zimmer, V. Huch and D. Scheschkewitz, Dimerization of a marginally stable disilenyl germylene to tricyclic systems: evidence for reversible NHC-coordination, *Chem. Commun.*, 2016, **52**, 2799–2802; (*d*) D. Nieder, V. Huch, C. B. Yildiz and D. Scheschkewitz, Regiodiscriminating Reactivity of Isolable NHC-Coordinated Disilenyl Germylene and Its Cyclic Isomer, *J. Am. Chem. Soc.*, 2016, **138**, 13996–14005.

14 (*a*) A. B. Terent'ev, V. I. Dostovalova and R. K. Freidlina, Carbon-13 N.m.r. Spectra of Branched Carboxylic Acids and their Derivatives, *Org. Magn. Reson.*, 1977, **9**, 301–307; (*b*) K. L. Williamson, M. U. Hasan and D. R. Clutter, Conformational Analysis by NMR. ^{13}C Nuclear Magnetic Resonance Spectra of Saturated and Unsaturated Carboxylic Acids and Their Corresponding Esters and Anhydrides, *J. Magn. Reson.*, 1978, **30**, 367–383.

15 N. N. Zemlyansky, I. V. Borisova, V. N. Khrustalev, M. Y. Antipin, Y. A. Ustynyuk, M. S. Nechaev and

V. V. Lunin, New Stable Germylenes, Stannylenes, and Related Compounds. 3. Stable Monomers $XGeOCH_2CH_2NMe_2$ (X = Cl, OCOMe) with Only One Intramolecular Coordination Metal–Nitrogen Bond: Synthesis and Structure, *Organometallics*, 2003, **22**, 5441–5446.

16 (*a*) K. Igawa, N. Kokan and K. Tomooka, Asymmetric Synthesis of Chiral Silacarboxylic Acids and Their Ester Derivatives, *Angew. Chem., Int. Ed.*, 2010, **49**, 728–731; (*b*) K. Igawa, Y. Kawasaki, S. Nozaki, N. Kokan and K. Tomooka, Ozone Oxidation of Silylalkene: Mechanistic Study and Application for the Synthesis of Silacarboxylic Acid Derivatives, *J. Org. Chem.*, 2020, **85**, 4165–4171.

17 Ph_3SiOH (−13 ppm)[17d] constitutes an exception to the general trend and was omitted from the discussion for clarity; (*a*) J. Schraml, V. Chvalovský, M. Mägi and E. Lippmaa, The role of electronic and steric effects in ^{29}Si-NMR spectra of compounds with Si–O–C group, *Collect. Czech. Chem. Commun.*, 1981, **46**, 377–390; (*b*) I. Zicmane, E. Liepins, L. M. Ignatovich and E. Lukevics, A ^{13}C, ^{17}O, ^{19}Si NMR study of some silicon, germanium and tin acyloxyderivatives, *J. Organomet. Chem.*, 1991, **417**, 355–362; (*c*) P. Lassacher, A. G. Brook and A. J. Lough, Reactions of Silenes: A New Silene to Silene Thermal Rearrangement, *Organometallics*, 1995, **14**, 4359–4365; (*d*) Y. Okada, M. Oba, A. Arai, K. Tanaka, K. Nishiyama and W. Ando, Diorganotelluride-Catalyzed Oxidation of Silanes to Silanols under Atmospheric Oxygen, *Inorg. Chem.*, 2010, **49**, 383–385; (*e*) A. I. Ojeda-Amador, J. Munarriz, P. Alamán-Valtierra, V. Polo, R. Puerta-Oteo, M. V. Jiménez, F. J. Fernández-Alvarez and J. J. Pérez-Torrente, Mechanistic Insights on the Functionalization of CO_2 with Amines and Hydrosilanes Catalyzed by a Zwitterionic Iridium Carboxylate-Functionalized Bis-NHC Catalyst, *ChemCatChem*, 2019, **11**, 5524–5535.

18 S. Fortier, Y. Zhang, H. K. Sharma and K. H. Pannell, Formation of Silicon–Carbon Bonds by Photochemical Irradiation of $(\eta^5\text{-}C_5H_5)Fe(CO)_2SiR_3$ and $(\eta^5\text{-}C_5H_5)Fe(CO)_2Me$ to Obtain R_3SiMe, *Organometallics*, 2010, **29**, 1041–1044.

19 P. C. Bulman Page, S. S. Klair and S. Rosenthal, Synthesis and Chemistry of Acyl Silanes, *Chem. Soc. Rev.*, 1990, **19**, 147–195.

20 L. Klemmer, Y. Kaiser, V. Huch, M. Zimmer and D. Scheschkewitz, Persistent Digermenes with Acyl and α-Chlorosilyl Functionalities, *Chem. – Eur. J.*, 2019, **25**, 12187–12195.

21 Y.-R. Luo, *Comprehensive Handbook of Chemical Bond Energies*, Taylor & Francis, Boca Raton, 2007, vol. 1, pp. 455–480.

22 X. Wang, J. Zhang, L. Wang and L. Deng, High-Spin Iron(II) Alkynyl Complexes with N-Heterocyclic Carbene Ligation: Synthesis, Characterization, and Reactivity Study, *Organometallics*, 2015, **34**, 2775–2782.

23 M. U. Hasan, ^{13}C NMR Spectra of some Amides and Imides. Effect of Inductive and Mesomeric Interactions, Cyclization and Hydrogen Bonding on ^{13}C NMR Chemical Shifts, *Org. Magn. Reson.*, 1980, **14**, 447–450.

24 (*a*) L. W. Reeves, R. C. Shaddick and K. N. Shaw, Nuclear Magnetic Resonance Studies of Multi-site Chemical Exchange. III. Hindered Rotation in Dimethylacetamide, Dimethyl Trifluoroacetamide, and Dimethyl Benzamide, *Can. J. Chem.*, 1971, **49**, 3683–3691; (*b*) M. Feigel, Rotation Barriers of Amides in the Gas Phase, *J. Phys. Chem.*, 1983, **87**, 3054–3058; (*c*) V. S. Dimitrov and J. A. Ladd, Dynamic NMR: comparison of the experimental barriers to internal rotation in *N*,*N*-dimethylformamide with those calculated by the ab initio SCF MO method, *J. Mol. Struct.*, 1987, **159**, 107–112.

25 (*a*) T. Threlfall, The infrared spectra of amides. Part 1. The stretching vibrations of primary carboxamides, *Vib. Spectrosc.*, 2022, **121**, 103386; (*b*) H. F. Shurvell, Spectra-Structure Correlations in the Mid- and Far-infrared, in *Handbook of Vibrational Spectroscopy*, ed. P. Griffiths and J. M. Chalmers, John Wiley & Sons, Chichester, 2006, vol. 1, pp. 1783–1816.

26 (*a*) M. Chen, B. Lei, X. Wang, H. Rong, H. Song and Z. Mo, A Silylene-Stabilized Germanium Analogue of Alkynylaluminum, *Angew. Chem., Int. Ed.*, 2022, **61**, e202204495, (*Angew. Chem.*, 2022, **134**, e202204495); (*b*) R. S. C. Charman, N. J. Evans, L. E. English, S. E. Neale, P. Vasko, M. F. Mahon and D. J. Liptrot, The structures and reactivity of NHC-supported copper(I) triphenylgermyls, *Chem. Sci.*, 2024, **15**, 584–593; (*c*) L. K. Saunders, H. Nowell, L. E. Hatcher, H. J. Shepherd, S. J. Teat, D. R. Allan, P. R. Raithby and C. C. Wilson, Exploring short strong hydrogen bonds engineered in organic acid molecular crystals for temperature dependent proton migration behaviour using single crystal synchrotron X-ray diffraction (SCSXRD), *CrystEngComm*, 2019, **21**, 5249–5260; (*d*) J. R. Holden, C. Dickinson and C. M. Bock, The Crystal Structure of 2,4,6-Trinitroaniline, *J. Phys. Chem.*, 1972, **76**, 3597–3602.

27 A. Pratap Singh, P. P. Samuel, H. W. Roesky, M. C. Schwarzer, G. Frenking, N. S. Sidhu and B. A. Dittrich, A Singlet Biradicaloid Zinc Compound and Its Nonradical Counterpart, *J. Am. Chem. Soc.*, 2013, **135**, 7324–7329.

28 M. M. Siddiqui, S. K. Sarkar, S. Sinhababu, P. N. Ruth, R. Herbst-Irmer, D. Stalke, M. Ghosh, M. Fu, L. Zhao, D. Casanova, G. Frenking, B. Schwederski, W. Kaim and H. W. Roesky, Isolation of Transient Acyclic Germanium(I) Radicals Stabilized by Cyclic Alkyl(amino) Carbenes, *J. Am. Chem. Soc.*, 2019, **141**, 1908–1912.

29 D. Sarkar, C. Weetman, S. Dutta, E. Schubert, C. Jandl, D. Koley and S. Inoue, N-Heterocyclic Carbene-Stabilized Germa-acylium Ion: Reactivity and Utility in Catalytic CO_2 Functionalizations, *J. Am. Chem. Soc.*, 2020, **142**, 15403–15411.

30 (*a*) C. D. Martin, M. Soleilhavoup and G. Bertrand, Carbene-stabilized main group radicals and radical ions, *Chem. Sci.*, 2013, **4**, 3020–3030; (*b*) S. Kundu, S. Sinhababu, V. Chandrasekhar and H. W. Roesky, Stable cyclic (alkyl)(amino)carbene (cAAC) radicals with main group substituents, *Chem. Sci.*, 2019, **10**, 4727–4741; (*c*) K. Breitwieser, H. Bahmann, R. Weiss and D. Munz, Gauging Radical

View Article Online
Inorganic Chemistry Frontiers Research Article

Stabilization with Carbenes, *Angew. Chem., Int. Ed.*, 2022, **61**, e202206390, (*Angew. Chem.*, 2022, **134**, e202206390).

31 (*a*) K. C. Mondal, H. W. Roesky, M. C. Schwarzer, G. Frenking, I. Tkach, H. Wolf, D. Kratzert, R. Herbst-Irmer, B. Niepötter and D. Stalke, Conversion of a Singlet Silylene to a stable Biradical, *Angew. Chem., Int. Ed.*, 2013, **52**, 1801–1805, (Umwandlung eines Singulett-Silylens in ein stabiles Biradikal, *Angew. Chem.*, 2013, **125**, 1845–1850); (*b*) J. Böhnke, T. Dellermann, M. A. Celik, I. Krummenacher, R. D. Dewhurst, S. Demeshko, W. C. Ewing, K. Hammond, M. Heß, E. Bill, E. Welz, M. I. S. Röhr, R. Mitrić, B. Engels, F. Meyer and H. Braunschweig, Isolation of diborenes and their 90°-twisted diradical congeners, *Nat. Commun.*, 2018, **9**, 1197.

Conclusions and Outlook

The isolation of the first digermenide, a digerma analogue of vinyllithium, reported in 2018 by the Scheschkewitz group[275] provided access to heteroleptic digermenes of the type $A_2Ge=GeAB$.[276] The asymmetric substitution pattern compromised the double bond stability, resulting in the thermally induced homolytic cleavage of the Ge=Ge double bonds and the formation of the homoleptic digermene $Tip_2Ge=GeTip_2$. Although this was a clear indication of a metathetic exchange, neither the corresponding RTipGe moieties (R = silyl or acyl substituents), nor their dimerization products were observed due to insufficient stability of the germylenes. Subsequently, an *ortho*-aniline substituent was implemented in silyldigermenes **66a,b** to provide the required stabilization through donor-acceptor interaction with the vacant p-orbital at the Ge(II) center in the intermediate germylenes **[67a,b]** and hence allowed for the formation of 1,2-disilyldigermenes **68a,b** concomitant with $Tip_2Ge=GeTip_2$ (Scheme 22).[255]

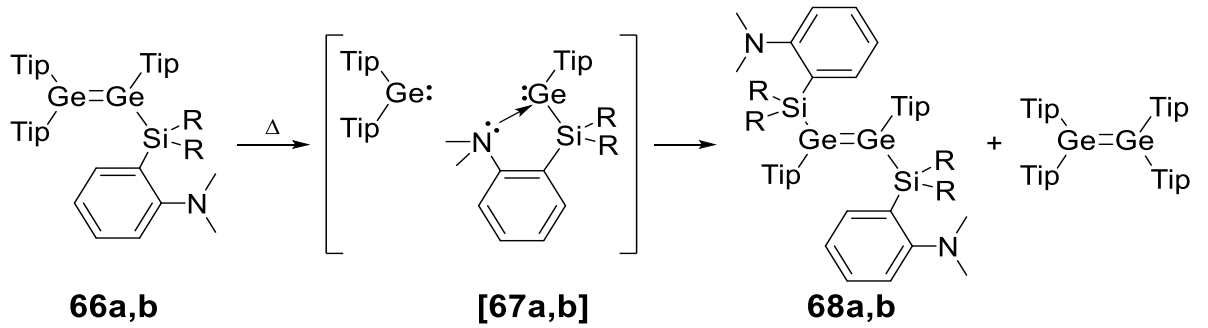

66a,b **[67a,b]** **68a,b**

Scheme 22. Ge=Ge Double bond metathesis of heteroleptic digermenes **66a,b** to homoleptic 1,2-disilyldigermenes **68a,b** *via* intermediate germylenes **[67a,b]** and Tip_2Ge (**66a,67a,68a**: R = Me, **66b,67b,68b**: R = Ph).

Applied to the analogous bis(digermene) **59** with a 2,5-diaminophenylene linker, this so-called *heavier acyclic diene metathesis* (HADMET) procedure resulted in the formation of poly(digermene) **60** (Scheme 23).[255] The obtained poly(digermene) **60** appeared, however, as an insoluble yellow solid with limited chain length and hence eluded characterization with common solution-based methods and the deposition as thin film for potential applications in electronic devices. Consequently, the development of soluble derivatives through the incorporation of longer alkyl chains into the repeat unit was one central goal of this PhD thesis.

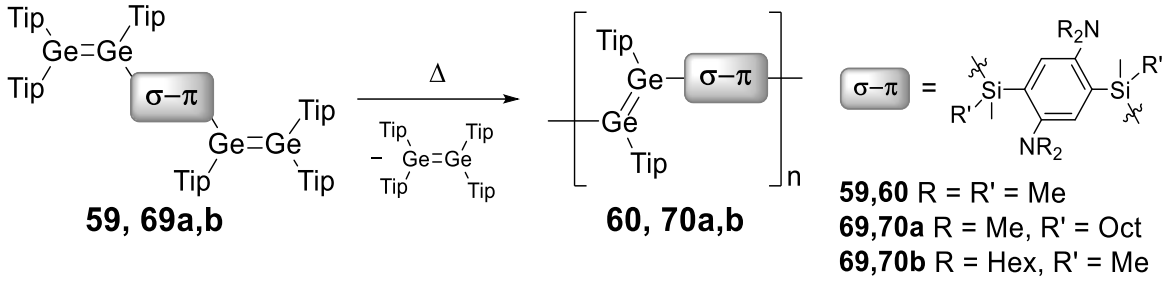

Scheme 23. HADMET polymerization of bis(digermene)s **59** and **69a,b** to σ,π-conjugated poly(digermene) **60** and soluble derivatives **70a,b** (Tip = 2,4,6-triisopropylphenyl).

Preliminary results had shown, that the introduction of two butyl or hexyl chains at each silyl group in the bis(chlorosilane)s precursors suppresses the subsequent substitution reaction with the digermenide to provide the bis(digermene) monomers. In order to minimize the steric and electronic influence on the centers of the substitution reaction and still maintain the principal structure of the repeat units, two alternative strategies have been devised: the substitution of only one methyl group at the silicon atoms by an octyl group and the derivatization with hexyl chains at the amino groups. The resulting monomers **69a,b** exhibit similar NMR shifts and UV/Vis absorption as the tetramethyl-substituted derivative **59** and provided poly(digermene)s **70a,b** in analogous HADMET reactions (Scheme 23). On the basis of DLS measurements and diffusion ordered NMR spectroscopy (DOSY), high degrees of polymerization of X_n = 2100 (**70a**) and 1100 (**70b**) were estimated, supported by the absence of end group signals in the NMR spectra and in line with Carother's correlation for the conversion of bifunctional monomers. The extremely high degrees of polymerization in comparison to the previously reported insoluble derivative **60** (X_n = 23–31, depending on the method)[255] resulted in a dramatic increase of the thermal stability according to TGA measurements with mass losses only at 240–250 °C in comparison to 120 °C in the case of tetramethyl-substituted **60**. Notably, DSC and NMR measurement revealed that degradation is already initiated prior to the actual mass loss. Comparisons of the UV/Vis absorption bands (λ_{max} ~ 420 nm) and the NMR data with a monomeric model compound exhibit characteristic (bathochromic) shifts, indicating the presence of σ,π-conjugation along the polymer chains, which was also supported by DFT calculations.

The high solubility of **70a,b** in different organic solvents enabled the deposition as thin films from polymer solutions. Atomic force microscopy (AFM) and transmission

electron microscopy (TEM) revealed the self-assembly to well-ordered supramolecular cylindrical structures with a lamellar substructure (Figure 15), a feature that has been found to be advantageous for charge transfer in well-established poly(thiophene)s.[277-278] The aggregation of the polymer chains is presumably caused by interchain dispersion interactions between the alkyl chains of the linking units as suggested by the single-crystal X-ray data of the bis(digermene) monomers (Figure 15) in combination with powder X-ray diffractometry of the polymer solids as well as DLS and small angle scattering (SAXS) measurements of solutions of **70a,b**.

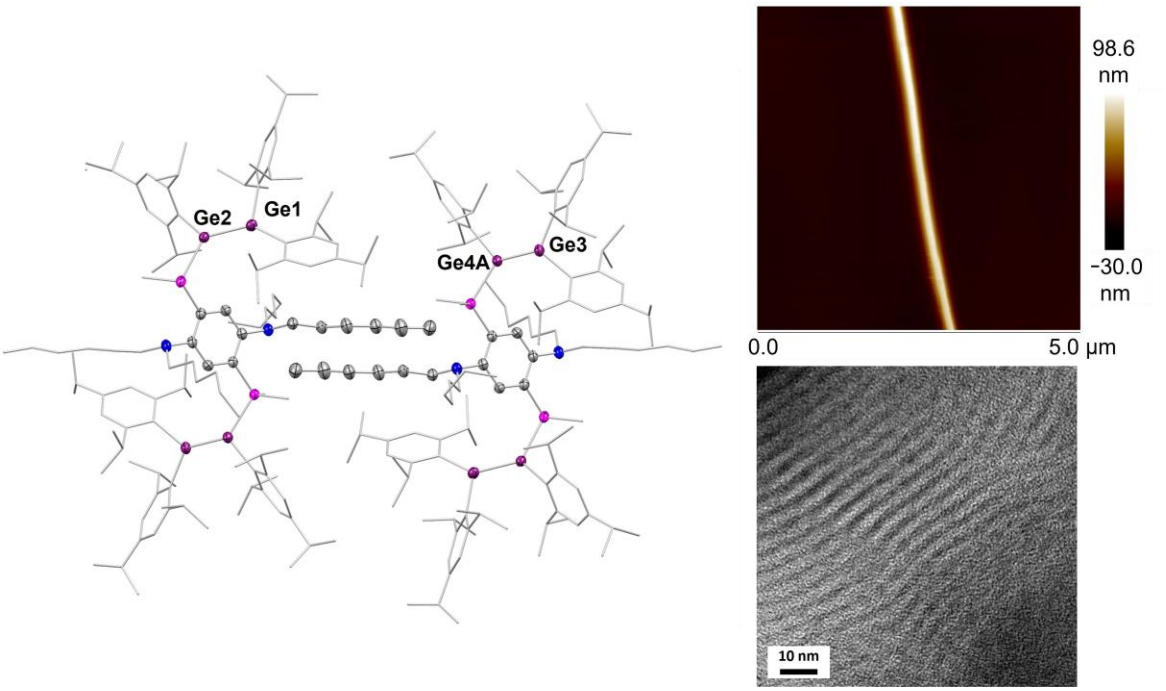

Figure 15. Adjacent molecules in the X-ray structure of bis(digermene) **69b** and representative AFM (top) and TEM (bottom) images of thin films of poly(digermene) **70a** showcasing the self-assembly to cylindrical aggregates and the lamellar substructure.

Poly(digermene)s **70a,b** represent the first examples of processible polymers with multiple bonds of heavier Group 14 elements. The combination of the absorption in the visible range, σ,π-conjugation along the chain and the elucidated self-assembly behavior – advantageous features for charge generation and transport – with high solubilities and thermal stabilities renders the poly(digermene)s promising materials for application in (opto-)electronic devices. For further fine-tuning of the mechanical and electronic properties as well as the aggregation and deposition behavior, different substitution patterns at the amino and silylene groups might be considered. Simple

exchange of the alkyl groups for π-substituents may establish π-stacking between the polymer chains, whereas sterically encumbered groups, such as *tert*-butyl or Tip, might inhibit the interchain interactions and the corresponding self-assembly. Delicate control over the intermolecular interactions should allow for the implementation of self-healing properties and engineering of charge transport in thin films.

Bis(germylene) **[65]** with highly reactive amphiphilic Ge(II) moieties was proposed as the key intermediate in the HADMET polymerization of bis(digermene)s. Accordingly, strategies for the isolation of stabilized derivatives and the development of functionalization methods are of particular interest. When triethylsilane was added to bis(digermene) **59** under HADMET conditions, silyl-substituted bis(germane) **71** is obtained (Scheme 24), confirming the intermediacy of **[65]** in the polymerization since silanes are known to selectively react with germylenes in the presence of digermenes.[279-280] Bis(germylene) **[65]** and derivatives **[72a,b]**, corresponding to the modified soluble poly(digermene)s, were isolated in the form of NHC- and CAAC-adducts **73a-c** and **74** through reactions of the carbenes with bis(digermene)s **59** and **69a,b**, respectively (Scheme 24). The double bond cleavage was readily induced at ambient temperature by the NHC with sterically less demanding substituents than in the employed CAAC. Accordingly, the reaction with the comparatively bulky CAAC only occurred at elevated temperature, i.e. upon thermal generation of bis(germylene) **[65]**, despite the higher HOMO energy of the carbene in comparison to the NHC.

The pronounced π-acceptor ability of the CAAC resulted in the formation of genuine Ge=C double bonds in bis(germene) **74**. Notably, there is only one other example of a CAAC-germene[281] and no reported bridged derivatives, as CAAC-germylenes typical exhibit pyramidal coordination of the carbene.[282-283] CAAC-ligands are well-known to stabilize paramagnetic species,[284-286] hence rendering bis(germene) **74** a potential precursor for a stable diradical with two spatially separated unpaired electrons. First follow-up experiments, beyond the scope of the present thesis, to form the corresponding dianion by reduction of **74** proved indeed promising: The formation of a triplet diradical was indicated by the appearance of a half-field signal in the frozen solution EPR spectrum of the reaction mixture in addition to the corresponding intense signals from the spin-allowed transitions at ambient temperature. In the context of polymers, the observed reactivity with a CAAC is a first step towards the development

of poly(germene)s with Ge=C double bonds, which might be obtained in analogous reactions of bis(digermene)s with just recently reported bridged bis(CAAC)s.[287-288]

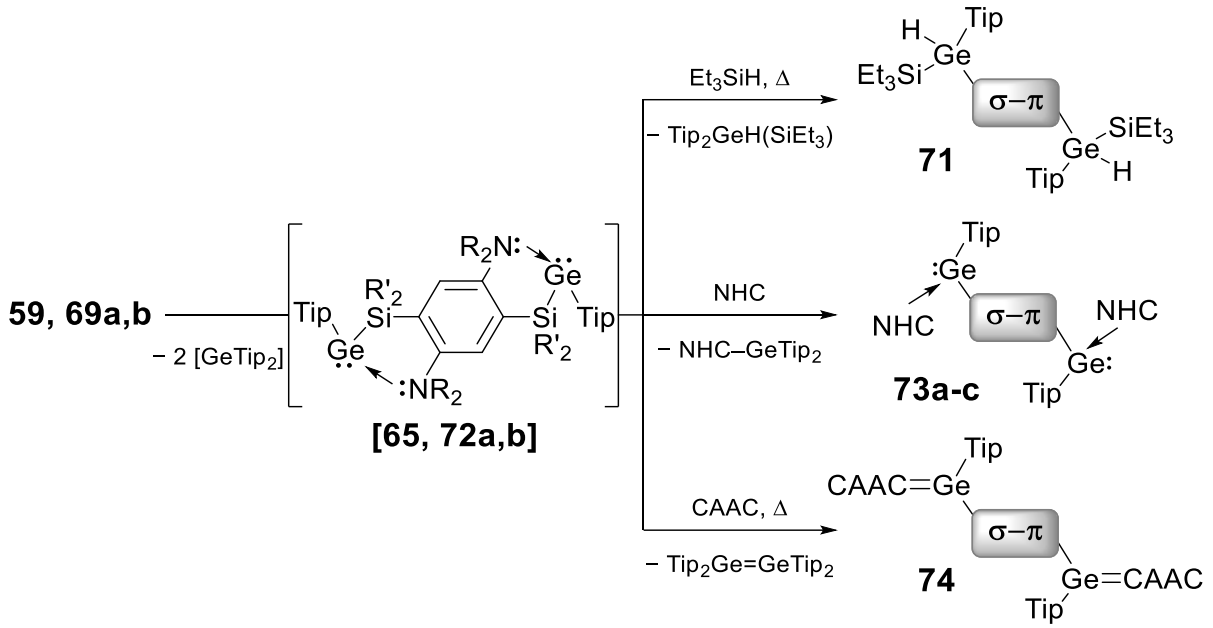

Scheme 24. Trapping of transient bis(germylene)s **[65]** and **[72a,b]** through reactions of bis(digermene)s **59** and **69a,b** with a silane and carbenes (R = Tip = 2,4,6-triisopropylphenyl, **[63], 71, 73a, 74**: R = R' = Me, **72a, 73b**: R = Me, R' = Oct, **72b, 73c**: R = Hex, R' = Me, NHC = 1,3-diisopropylimidazol-4,5-dimethyl-2-ylidene, CAAC = 1-(2,6-diisopropylphenyl)-3,3,5,5-tetramethyl-pyrrolidin-2-ylidene).

The NHC-adducts **73a-c** exhibit a fundamentally different bonding situation in comparison to the CAAC-adduct **74**, maintaining the integrity of the germanium lone-pairs through weaker donor-acceptor interaction between the NHCs and the vacant p-orbitals. The exchange reaction of NHC-bis(germylene) **73a** with the CAAC (Scheme 25) additionally demonstrates the higher bond strength of the germylene–carbene bonds in bis(germene) **74** and the potential use of CAAC for a control of the degree of polymerization by end-capping. Based on the comparably weak bonds in the NHC-adducts, a novel route towards poly(digermene)s *via* NHC-abstraction with triphenylborane was developed (Scheme 25). Notably, the reversible reaction, i.e. controlled degradation of poly(digermene)s **70a,b** by reaction with the NHC, was not achieved, even at elevated temperatures. This is a manifestation of the remarkable electronic and steric stabilization in the σ,π-conjugated polymers, in particular in comparison to a structurally related molecular 1,2-disilyldigermene, which readily reacts with the NHC to form the carbene-stabilized germylene.

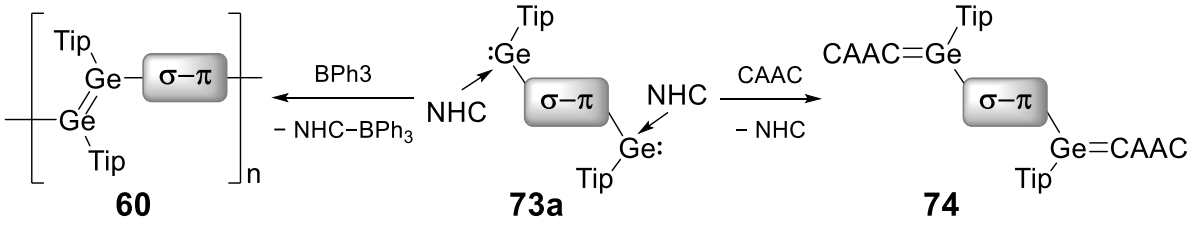

60 **73a** **74**

Scheme 25. Formation of poly(digermene) **60** *via* NHC abstraction from NHC-bis(germylene) **73a** and carbene exchange reaction to CAAC-bis(germene) **74** (Tip = 2,4,6-triisopropylphenyl, σ–π = 2,5-dimethylaminobenzene-1,4-dimethylsilylene, NHC = 1,3-diisopropylimidazol-4,5-dimethyl-2-ylidene, CAAC = 1-(2,6-diisopropylphenyl)-3,3,5,5-tetramethyl-pyrrolidin-2-ylidene).

The employed silylenearylene spacer units have been custom-designed to enable the HADMET process through a well-balanced stabilization of the intermediate bis(germylene)s: the amino substituent is in *ortho*-position to the silylene group in order to facilitate the interaction with the germylene upon forming a favorable five-membered ring. Eluding the necessity of the intramolecular stabilization, the polymerization *via* NHC-abstraction should consequently enable a variety of derivatizations. For instance, the amino ligands might be omitted or replaced by any other functional group, such as phosphino, boryl, alkyl or aryl groups, to tailor the electronic structure and induce properties and reactivities for specific purposes, e.g. interactions with Lewis acids or bases for post-functionalization or the implementation of reversible interchain interactions. Furthermore, the synthesis of a phenylene-bridged poly(digermene), omitting the R_2Si groups, might be possible by employing the corresponding bis(digermene) in the new route, which was isolated in our group some years ago.[289] Substitution of the silylene group for a Group 13 or Group 15 motif should establish p-π- and n-π-conjugation, respectively, between the heteroelement motif, the Ge=Ge units and the arylene linker, and the introduction of a methylene linker should interrupt the conjugation. Diborane(4) bridges might even allow for photoswitchable conjugation considering the previously observed severe structural reorganization in the excited state of diboranes(4).[290] Furthermore, copolymers with variable bridging units and Ge=E (E = Group 13 or 14 element) bonds could be envisioned.

Since the poly(digermene)s exhibit considerably higher chemical stabilities than structurally related molecular compounds, the introduction of functional groups is envisaged through modified precursors, i.e. prior to the polymerization. With the aim of further developing the polymers at hand and the huge potential, NHC-bis(germylene)s

offer as precursors for poly(digermene)s, the third part of the present thesis was devoted to investigations on the reactivity of NHC-adduct **73a**. In contrast to the sterically demanding nucleophilic CAAC, which provided bis(germene) **74** in an exchange reaction (*vide supra*), small electrophiles proved suitable for selective backbone functionalization: The readily available, simple building blocks carbon dioxide and ethyl isocyanate were employed in insertion reactions of one of the C=X (X = O, N) bonds into the Ge–Si bonds in NHC-bis(germylene) **73a** (Scheme 26). The cooperativity of the electrophilic silylene linker with accessible σ^*-orbitals and the nucleophilic germanium lone-pairs resulted in an inversion of the conventional reactivity of low-valent p-block compounds at the oxygen termini of CO_2.[291-314] Notably, the incorporation of the carboxy and amide functionalities in **75a,b** resulted in the interruption of the σ,π-conjugation and a concomitant color change from bright yellow to colorless. The integrity of the NHC-stabilized Ge(II) centers is maintained in the acyl-extended NHC-bis(germylene)s **75a,b**, rendering them promising precursors for poly(digermene)s with accordingly adapted properties.

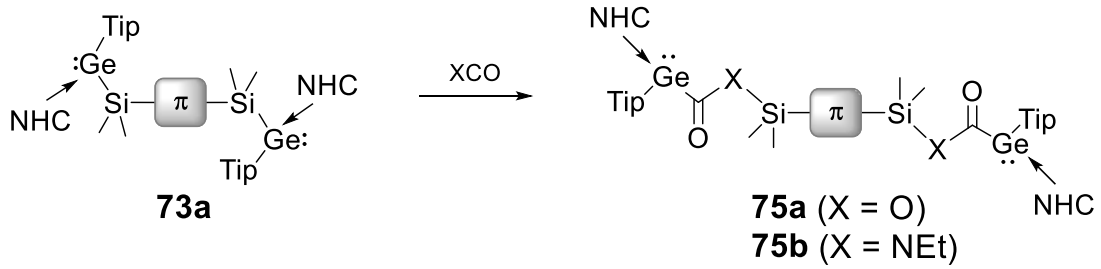

73a **75a** (X = O) **75b** (X = NEt)

Scheme 26. Investigated reactivity of NHC-bis(germylene) **73a** with heteroallenes to acyl-substituted NHC-bis(germylene)s **75a,b** (Tip = 2,4,6-triisopropylphenyl, π = 2,5-(tetramethyldiamino)-*p*-phenylene, NHC = 1,3-diisopropylimidazol-4,5-dimethyl-2-ylidene).

Acyl-substituted germanes show a tendency to form transient radicals upon cleavage of the Ge–C(=O) bonds and are therefore used as photoinitiators, for instance for the polymerization-based curing of (dental) composites[315-319] and grafting-from surface-modification of nanoparticles.[320-321] The susceptibility of Ge–C(=O) bonds to homolytic cleavage is also manifest in an unconventional substitution-induced radical fragmentation of acyl-functionalized NHC-bis(germylene) **75a**: upon CAAC-addition, the stable CAAC-centered radical **76** tethered to an NHC-germylene *via* a carboxy group is formed (Scheme 27). The corresponding spacer fragment was not observed

due to the inherently high reactivity and resulting unselective decomposition of the presumably formed silicon-centered diradical. While polyradicals have been extensively investigated for more than 50 years[322-326] and exhibit beneficial properties, for example for the use in small molecule activation and as molecular switches, there are only a few reports on CAAC-based diradical(oid)s.[327-332] The effective separation of the unpaired electron at the CAAC substituent and the Ge(II) center by the carboxy moiety in **76** should be advantageous for the formation of related polyradicals with two or more CAAC–CO_2 ligands.

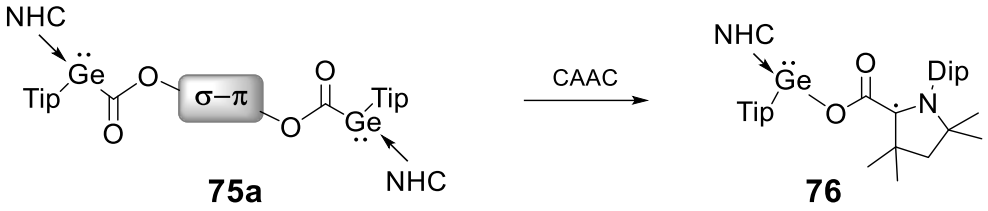

Scheme 27. Formation of NHC-germylene **76** with a tethered CAAC-radical from acyl-substituted NHC-bis(germylene) **75a** (Tip = 2,4,6-triisopropylphenyl, σ–π = 2,5-dimethylaminobenzene-1,4-dimethylsilylene, NHC = 1,3-diisopropylimidazol-4,5-dimethyl-2-ylidene, CAAC = 1-(2,6-diisopropylphenyl)-3,3,5,5-tetramethyl-pyrrolidin-2-ylidene).

In summary, this work represents a rare contribution on the border line of inorganic (low-coordinate) main group chemistry and materials chemistry. The development of processable polymers with Ge=Ge double bonds allowed for a detailed analysis of the structure-function relationship and the deposition as thin films of this new class of inorganic-organic hybrid polymers with embedded heteroatoms. Based on the key intermediate of the HADMET polymerization, which was isolated in the form of carbene-stabilized bis(germylene)s, a new route towards poly(digermene)s was elaborated. Deliberate selective functionalization of an NHC-adduct provided a CAAC-bis(germene) with Ge=C double bonds and – upon activation of heteroallenes – acyl-substituted NHC-bis(germylene)s as potential derivatized monomers. These findings will have implications for the development of related (co-)polymers with Ge=Ge and Ge=C bonds and the synthesis of novel p-block element (poly-)radicals for instance for the use in electronic devices, in small molecule activation and as molecular switches.

References

[1] Y. Ito, S. Okamura, B. Rånby, Macromolecular Concept and Strategy for Humanity in Science, Technology and Industry, Springer Science & Business Media, **1996**.

[2] A. C. Grimsdale, K. Leok Chan, R. E. Martin, P. G. Jokisz, A. B. Holmes, *Chem. Rev.* **2009**, *109*, 897-1091.

[3] H. Morawetz, in *Encycl. Polym. Sci. Eng.* (Ed.: H. Mark), John Wiley & Sons, **2014**, pp. 1-30.

[4] R. Geyer, J. R. Jambeck, K. L. Law, *Sci. Adv.* **2017**, *3*, e1700782.

[5] H.-Q. Peng, W. Zhu, W.-J. Guo, Q. Li, S. Ma, C. Bucher, B. Liu, X. Ji, F. Huang, J. L. Sessler, *Prog. Polym. Sci.* **2023**, *137*, 101635.

[6] L. Li, L. Han, H. Hu, R. Zhang, *Mater. Adv.* **2023**, *4*, 726-746.

[7] J. Yi, G. Zhang, H. Yu, H. Yan, *Nat. Rev. Mater.* **2024**, *9*, 46-62.

[8] K. Müllen, U. Scherf, *Macromol. Chem. Phys.* **2023**, *224*, 2200337.

[9] M. C. Scharber, N. S. Sariciftci, *Adv. Mater. Technol.* **2021**, *6*, 2000857.

[10] R. M. Pankow, B. C. Thompson, *Polymer* **2020**, *207*, 122874.

[11] The Nobel Prize in Chemistry 2000. NobelPrize.org. Nobel Prize Outreach AB 2025. Sat. 29 Mar 2025. https://www.nobelprize.org/prizes/chemistry/2000/summary/

[12] S. Fratini, M. Nikolka, A. Salleo, G. Schweicher, H. Sirringhaus, *Nat. Mater.* **2020**, *19*, 491-502.

[13] J. H. Burroughes, D. D. Bradley, A. Brown, R. Marks, K. Mackay, R. H. Friend, P. L. Burns, A. B. Holmes, *Nature* **1990**, *347*, 539-541.

[14] A. Kraft, A. C. Grimsdale, A. B. Holmes, *Angew. Chem. Int. Ed.* **1998**, *37*, 402-428.

[15] R. H. Friend, R. Gymer, A. Holmes, J. Burroughes, R. Marks, C. Taliani, D. Bradley, D. D. Santos, J.-L. Bredas, M. Lögdlund, W. Salaneck, *Nature* **1999**, *397*, 121-128.

[16] G. Hong, X. Gan, C. Leonhardt, Z. Zhang, J. Seibert, J. M. Busch, S. Bräse, *Adv. Mater.* **2021**, *33*, 2005630.

[17] Y.-S. Zimmermann, A. Schäffer, C. Hugi, K. Fent, P. F.-X. Corvini, M. Lenz, *Environ. Int.* **2012**, *49*, 128-140.

[18] K. Zhou, R. Zhang, J. Liu, M. Li, X. Yu, R. Xing, Y. Han, *ACS Appl. Mater. Interfaces* **2015**, *7*, 25352-25361.

[19] S. M. Haque, J. A. Ardila-Rey, Y. Umar, H. Rahman, A. A. Mas' ud, F. Muhammad-Sukki, R. Albarracín, *Polymers* **2018**, *10*, 307.

[20] E. K. Solak, E. Irmak, *RSC Adv.* **2023**, *13*, 12244-12269.

[21] A. Tsumura, H. Koezuka, T. Ando, *Appl. Phys. Lett.* **1986**, *49*, 1210-1212.

[22] X. Guo, Y. Xu, S. Ogier, T. N. Ng, M. Caironi, A. Perinot, L. Li, J. Zhao, W. Tang, R. A. Sporea, *IEEE Trans. Electron Devices* **2017**, *64*, 1906-1921.

[23] J. Yang, Z. Zhao, S. Wang, Y. Guo, Y. Liu, *Chem* **2018**, *4*, 2748-2785.

[24] H. Li, Y. Zhou, Y. Liu, L. Li, Y. Liu, Q. Wang, *Chem. Soc. Rev.* **2021**, *50*, 6369-6400.

[25] E. Smela, *Adv. Mater.* **2003**, *15*, 481-494.

[26] T. Sen, S. Mishra, N. G. Shimpi, *RSC Adv.* **2016**, *6*, 42196-42222.

[27] X. Wang, F. Li, Y. Guo, *Front. Chem.* **2020**, *8*, 586702.

[28] M. R. Karim, M. M. Alam, M. O. Aijaz, A. M. Asiri, F. S. AlMubaddel, M. M. Rahman, *RSC Adv.* **2020**, *10*, 12224-12233.

[29] M. Eskandari, F. Faridbod, *New J. Chem.* **2018**, *42*, 15655-15662.

[30] S. K. Pandey, K.-H. Kim, K.-T. Tang, *Trends Anal. Chem.* **2012**, *32*, 87-99.

[31] S. Maiti, B. Mandal, M. Sharma, S. Mukherjee, A. K. Das, *Chem. Commun.* **2020**, *56*, 9348-9351.

[32] P. Vahdatiyekta, M. Zniber, J. Bobacka, T.-P. Huynh, *Anal. Chim. Acta* **2022**, *1221*, 340114.

[33] M. Hissler, P. W. Dyer, R. Réau, *Coord. Chem. Rev.* **2003**, *244*, 1-44.

[34] X. He, T. Baumgartner, *RSC Adv.* **2013**, *3*, 11334-11350.

[35] S. M. Parke, M. P. Boone, E. Rivard, *Chem. Commun.* **2016**, *52*, 9485-9505.

[36] A. M. Priegert, B. W. Rawe, S. C. Serin, D. P. Gates, *Chem. Soc. Rev.* **2016**, *45*, 922-953.

[37] H. Helten, in *Encycl. Inorg. Bioinorg. Chem.* (Ed.: R. A. Scott), John Wiley & Sons, Inc., **2017**, pp. 1-27.

[38] F. Vidal, F. Jäkle, *Angew. Chem. Int. Ed.* **2019**, *58*, 5846-5870.

[39] Z. Zhang, Z. Liu, C. Xue, H. Chen, X. Han, Y. Ren, *Commun. Chem.* **2023**, *6*, 271.

[40] S. Ito, M. Gon, K. Tanaka, *Eur. J. Inorg. Chem.* **2024**, *27*, e202400180.

[41] C. D. Entwistle, T. B. Marder, *Angew. Chem. Int. Ed.* **2002**, *41*, 2927-2931.

[42] C. D. Entwistle, T. B. Marder, *Chem. Mater.* **2004**, *16*, 4574-4585.

[43] F. Jäkle, *Coord. Chem. Rev.* **2006**, *250*, 1107-1121.

[44] N. Matsumi, Y. Chujo, *Polym. J.* **2008**, *40*, 77-89.

[45] F. Jäkle, *Chem. Rev.* **2010**, *110*, 3985-4022.

[46] K. Tanaka, Y. Chujo, *Macromol. Rapid Commun.* **2012**, *33*, 1235-1255.

[47] F. Jäkle, in *Synthesis and Application of Organoboron Compounds, Vol. 49* (Eds.: E. Fernández, A. Whiting), Springer International Publishing, Cham, **2015**, pp. 297-325.

[48] Y. Ren, F. Jäkle, *Dalton Trans.* **2016**, *45*, 13996-14007.

[49] Y. Ren, F. Jäkle, in *Main Group Strategies towards Functional Hybrid Materials*, **2017**, pp. 79-110.

[50] H. Helten, *Chem. Asian J.* **2019**, *14*, 919-935.

[51] N. Chauhan, N. Hosmane, M. Mozafari, *Mater. Today Chem.* **2019**, *14*, 100184.

[52] J. He, F. Rauch, M. Finze, T. B. Marder, *Chem. Sci.* **2021**, *12*, 128-147.

[53] X. Yin, J. Liu, F. Jäkle, *Chem. Eur. J.* **2021**, *27*, 2973-2986.

[54] S. Ito, M. Gon, K. Tanaka, Y. Chujo, *Polym. Chem.* **2021**, *12*, 6372-6380.

[55] A. Dhiman, L. Giribabu, R. Trivedi, *Chem. Rec.* **2021**, *21*, 1738-1770.

[56] H. Helten, in *Comprehensive Organometallic Chemistry IV* (Eds.: G. Parkin, K. Meyer, D. O'hare), Elsevier, Oxford, **2022**, pp. 71-134.

[57] D. Shimoyama, F. Jäkle, *Aggregate* **2022**, *3*, e149.

[58] J. Miao, Y. Wang, J. Liu, L. Wang, *Chem. Soc. Rev.* **2022**, *51*, 153-187.

[59] C. Liu, L. Yin, Y. Li, *J. Mater. Chem. C* **2024**.

[60] F. Zhao, M. An, N. Wang, X. Yin, *Chem. Eur. J.* **2025**, *31*, e202403810.

[61] S. Ito, K. Tanaka, *Polym. Chem.* **2025**, *16*, 2046-2057.

[62] M. Gon, K. Tanaka, *Smart Mol.* **2025**, e20240064.

[63] J. Ohshita, A. Kunai, *Acta Polym.* **1998**, *49*, 379-403.

[64] S. Yamaguchi, K. Tamao, in *Silicon-Containing Polymers: The Science and Technology of Their Synthesis and Applications* (Eds.: R. G. Jones, W. Ando, J. Chojnowski), Springer Netherlands, Dordrecht, **2000**, pp. 461-498.

[65] K. Tamao, S. Yamaguchi, *J. Organomet. Chem.* **2000**, *611*, 5-11.

[66] S. Yamaguchi, K. Tamao, *J. Organomet. Chem.* **2002**, *653*, 223-228.

[67] A. S. Abd-El-Aziz, C. E. Carraher Jr., C. U. Pittman Jr., M. Zeldin, *Macromolecules Containing Metal and Metal-Like Elements: Group IVA Polymers*, John Wiley & Sons, Inc., **2005**.

[68] J. Chen, Y. Cao, *Macromol. Rapid Commun.* **2007**, *28*, 1714-1742.

[69] J. Ohshita, *Macromol. Chem. Phys.* **2009**, *210*, 1360-1370.

[70] S. M. Budy, D. Y. Son, *J. Inorg. Organomet. Polym. Mater.* **2018**, *28*, 1673-1687.

[71] S. Yamaguchi, K. Tamao, *J. Chem. Soc., Dalton Trans.* **1998**, 3693-3702.

[72] S. Yamaguchi, K. Tamao, *Chem. Lett.* **2005**, *34*, 2-7.

[73] M. Nakashima, M. Miyazaki, Y. Ooyama, Y. Fujita, S. Murata, Y. Kunugi, J. Ohshita, *Polym. J.* **2016**, *48*, 645-651.

[74] C. K. Lo, B. R. Gautam, P. Selter, Z. Zheng, S. D. Oosterhout, I. Constantinou, R. Knitsch, R. M. W. Wolfe, X. Yi, J.-L. Brédas, F. So, M. F. Toney, V. Coropceanu, M. R. Hansen, K. Gundogdu, J. R. Reynolds, *Chem. Mater.* **2018**, *30*, 2995-3009.

[75] A. C. Arias, J. D. MacKenzie, I. McCulloch, J. Rivnay, A. Salleo, *Chem. Rev.* **2010**, *110*, 3-24.

[76] Y. Huang, E. J. Kramer, A. J. Heeger, G. C. Bazan, *Chem. Rev.* **2014**, *114*, 7006-7043.

[77] P. Bujak, I. Kulszewicz-Bajer, M. Zagorska, V. Maurel, I. Wielgus, A. Pron, *Chem. Soc. Rev.* **2013**, *42*, 8895-8999.

[78] M. Wang, G. Zhang, D. Zhang, D. Zhu, B. Z. Tang, *J. Mater. Chem.* **2010**, *20*, 1858-1867.

[79] J. Liu, J. W. Lam, B. Z. Tang, *J. Inorg. Organomet. Polym. Mater.* **2009**, *19*, 249-285.

[80] M. Hissler, P. W. Dyer, R. Reau, in *New Aspects in Phosphorus Chemistry V. Topics in Current Chemistry, Vol. 250* (Ed.: J. Majoral), Springer, Berlin, Heidelberg, **2005**, pp. 127-163.

[81] T. Baumgartner, R. Réau, *Chem. Rev.* **2006**, *106*, 4681-4727.

[82] T. Baumgartner, *Acc. Chem. Res.* **2014**, *47*, 1613-1622.

[83] D. Joly, P. A. Bouit, M. Hissler, *J. Mater. Chem. C* **2016**, *4*, 3686-3698.

[84] M. A. Shameem, A. Orthaber, *Chem. Eur. J.* **2016**, *22*, 10718-10735.

[85] A. Ghorai, S. Banerjee, *Prog. Polym. Sci.* **2023**, *138*, 101646.

[86] H. Imoto, K. Naka, *Polymer* **2022**, *241*, 124464.

[87] P. P. Power, *J. Chem. Soc., Dalton Trans.* **1998**, 2939-2951.

[88] P. P. Power, *Chem. Rev.* **1999**, *99*, 3463-3504.

[89] H. Roesky, D. A. Atwood, in *Structure and Bonding, Vol. 103* (Ed.: D. Mingos), Springer Verlag Berlin Heidelberg, **2002**.

[90] T. Sasamori, N. Tokitoh, *Dalton Trans.* **2008**, 1395-1408.

[91] R. C. Fischer, P. P. Power, *Chem. Rev.* **2010**, *110*, 3877-3923.

[92] R. Fischer, in *Comprehensive Inorganic Chemistry II, Vol. 2* (Eds.: J. Reedijk, K. Poeppelmeier), Elsevier: Amsterdam, **2013**, pp. 269-287.

[93] V. Nesterov, N. C. Breit, S. Inoue, *Chem. Eur. J.* **2017**, *23*, 12014-12039.

[94] A. Rammo, D. Scheschkewitz, *Chem. Eur. J.* **2018**, *24*, 6866-6885.

[95] A. Agarwal, S. K. Bose, *Chem. Asian J.* **2020**, *15*, 3784-3806.

[96] C. Weetman, *Chem. Eur. J.* **2021**, *27*, 1941-1954.

[97] F. Dankert, C. Hering-Junghans, *Chem. Commun.* **2022**, *58*, 1242-1262.

[98] S. Fujimori, Y. Mizuhata, N. Tokitoh, *Proc. Jpn. Acad., Ser. B* **2023**, *99*, 480-512.

[99] V. Y. Lee, *Molecules* **2023**, *28*, 1558.

[100] M. Karni, Y. Apeloig, in *Organogermanium Compounds* (Ed.: V. Y. Lee), John Wiley & Sons, **2023**, pp. 1-102.

[101] V. Y. Lee, in *Organogermanium Compounds* (Ed.: V. Y. Lee), John Wiley & Sons, **2023**, pp. 435-475.

[102] K. V. Zaitsev, in *Organogermanium Compounds* (Ed.: V. Y. Lee), John Wiley & Sons, **2023**, pp. 103-193.

[103] C. Duan, C. Cui, *Chem. Soc. Rev.* **2024**, *53*, 361-379.

[104] Y. Xie, T.-T. Wang, X.-H. Liu, K. Zou, W.-Q. Deng, *Nat. Commun.* **2013**, *4*, 1960.

[105] M. Chen, X. Liu, Y. Yang, W. Xu, K. Chen, R. Luo, *ACS Appl. Mater. Interfaces* **2023**, *15*, 8263-8274.

[106] X. Zhang, H. Zhang, B. Qiu, D. Zhu, S. Zhang, Y. Bian, J. Wang, D. Li, S. Wang, W. Mai, J. Chen, T. Li, *Fuel* **2023**, *331*, 125828.

[107] M. L. Mejía, G. Reeske, B. J. Holliday, *Chem. Commun.* **2010**, *46*, 5355-5357.

[108] K. Y. Hwang, H. Kim, Y. S. Lee, M. H. Lee, Y. Do, *Chem. Eur. J.* **2009**, *15*, 6478-6487.

[109] A. V. Eroshin, A. A. Otlyotov, I. A. Kuzmin, P. A. Stuzhin, Y. A. Zhabanov, *Int. J. Mol. Sci.* **2022**, *23*, 939.

[110] S. Ohtani, N. Yamada, M. Gon, K. Tanaka, Y. Chujo, *Polym. Chem.* **2021**, *12*, 2752-2759.

[111] M. Gon, K. Tanaka, Y. Chujo, *Polym. J.* **2023**, *55*, 723-734.

[112] T. Matsumoto, Y. Onishi, K. Tanaka, H. Fueno, K. Tanaka, Y. Chujo, *Chem. Commun.* **2014**, *50*, 15740-15743.

[113] T. Matsumoto, K. Tanaka, Y. Chujo, *Macromolecules* **2015**, *48*, 1343-1351.

[114] Y. Adachi, F. Arai, M. Sakabe, J. Ohshita, *Polym. Chem.* **2021**, *12*, 3471-3477.

[115] D. R. Levine, M. A. Siegler, J. D. Tovar, *J. Am. Chem. Soc.* **2014**, *136*, 7132-7139.

[116] Y. Adachi, J. Ohshita, *Organometallics* **2018**, *37*, 869-881.

[117] X. Han, C. Xue, Z. Zhao, M. Peng, Q. Wang, H. Liu, N. Yu, C. Pu, Y. Ren, *ACS Macro Lett.* **2023**, *12*, 961-967.

[118] A. F. Alahmadi, X. Yin, R. A. Lalancette, F. Jäkle, *Chem. Eur. J.* **2023**, *29*, e202203619.

[119] Y. Adachi, M. Sakabe, T. Nomura, J. Ohshita, *Polym. J.* **2023**, *55*, 489-496.

[120] L. Dou, Y. Liu, Z. Hong, G. Li, Y. Yang, *Chem. Rev.* **2015**, *115*, 12633-12665.

[121] X. Yin, F. Guo, R. A. Lalancette, F. Jäkle, *Macromolecules* **2016**, *49*, 537-546.

[122] Y. Adachi, Y. Ooyama, Y. Ren, X. Yin, F. Jäkle, J. Ohshita, *Polym. Chem.* **2018**, *9*, 291-299.

[123] Y. Adachi, S. Terao, Y. Kanematsu, J. Ohshita, *Chem. Asian J.* **2024**, *19*, e202301142.

[124] R. D. Miller, J. Michl, *Chem. Rev.* **1989**, *89*, 1359-1410.

[125] H. A. Fogarty, D. L. Casher, R. Imhof, T. Schepers, D. W. Rooklin, J. Michl, *Pure Appl. Chem.* **2003**, *75*, 999-1020.

[126] R. West, *J. Organomet. Chem.* **1986**, *300*, 327-346.

[127] S. Hayase, *Prog. Polym. Sci.* **2003**, *28*, 359-381.

[128] H. Jamshidi, A. Rahimi, *Phosphorus, Sulfur Silicon Relat. Elem.* **2006**, *181*, 2565-2576.

[129] V. B. Kumar, E. M. Leitao, *Appl. Organomet. Chem.* **2020**, *34*, e5402.

[130] A. Bande, J. Michl, *Chem. Eur. J.* **2009**, *15*, 8504-8517.

[131] Y. Yamaguchi, *Synth. Met.* **1996**, *82*, 149-153.

[132] S. Yamaguchi, R.-Z. Jin, K. Tamao, M. Shiro, *Organometallics* **1997**, *16*, 2486-2488.

[133] J. Ohshita, M. Miyazaki, D. Tanaka, Y. Morihara, Y. Fujita, Y. Kunugi, *Polym. Chem.* **2013**, *4*, 3116-3122.

[134] J. S. Kim, Z. Fei, S. Wood, D. T. James, M. Sim, K. Cho, M. J. Heeney, J. S. Kim, *Adv. Energy Mater.* **2014**, *4*, 1400527.

[135] Y. Adachi, Y. Ooyama, N. Shibayama, J. Ohshita, *Dalton Trans.* **2016**, *45*, 13817-13826.

[136] Y. Adachi, T. Nabeya, T. Nomura, K. Kondo, K. Kawakami, Y. Ooyama, J. Ohshita, *Dalton Trans.* **2019**, *48*, 16671-16678.

[137] B. L. Lucht, M. A. Buretea, T. D. Tilley, *Organometallics* **2000**, *19*, 3469-3475.

[138] W.-M. Zhou, I. Tomita, *Polym. Bull.* **2008**, *61*, 603-609.

[139] C. C. Law, J. Chen, J. W. Lam, H. Peng, B. Z. Tang, *J. Inorg. Organomet. Polym.* **2004**, *14*, 39-51.

[140] R. Chen, R. Zhu, C. Zheng, S. Liu, Q. Fan, W. Huang, *Sci. China, Ser. B: Chem.* **2009**, *52*, 212-218.

[141] N. Allard, R. B. Aïch, D. Gendron, P.-L. T. Boudreault, C. Tessier, S. Alem, S.-C. Tse, Y. Tao, M. Leclerc, *Macromolecules* **2010**, *43*, 2328-2333.

[142] J. Ohshita, Y.-M. Hwang, T. Mizumo, H. Yoshida, Y. Ooyama, Y. Harima, Y. Kunugi, *Organometallics* **2011**, *30*, 3233-3236.

[143] C. M. Amb, S. Chen, K. R. Graham, J. Subbiah, C. E. Small, F. So, J. R. Reynolds, *J. Am. Chem. Soc.* **2011**, *133*, 10062-10065.

[144] D. Gendron, P.-O. Morin, P. Berrouard, N. Allard, B. R. Aich, C. N. Garon, Y. Tao, M. Leclerc, *Macromolecules* **2011**, *44*, 7188-7193.

[145] J. Shaw, H. Zhong, C. P. Yau, A. Casey, E. Buchaca-Domingo, N. Stingelin, D. Sparrowe, W. Mitchell, M. Heeney, *Macromolecules* **2014**, *47*, 8602-8610.

[146] J. Ohshita, M. Miyazaki, M. Nakashima, D. Tanaka, Y. Ooyama, T. Sasaki, Y. Kunugi, Y. Morihara, *RSC Adv.* **2015**, *5*, 12686-12691.

[147] U. Koldemir, S. R. Puniredd, M. Wagner, S. Tongay, T. D. McCarley, G. D. Kamenov, K. Müllen, W. Pisula, J. R. Reynolds, *Macromolecules* **2015**, *48*, 6369-6377.

[148] V. Gupta, L. F. Lai, R. Datt, S. Chand, A. J. Heeger, G. C. Bazan, S. P. Singh, *Chem. Commun.* **2016**, *52*, 8596-8599.

[149] A. Casey, S. D. Dimitrov, P. Shakya-Tuladhar, Z. Fei, M. Nguyen, Y. Han, T. D. Anthopoulos, J. R. Durrant, M. Heeney, *Chem. Mater.* **2016**, *28*, 5110-5120.

[150] J. Ohshita, Y. Adachi, R. Sagisaka, M. Nakashima, Y. Ooyama, Y. Kunugi, *Synth. Met.* **2017**, *227*, 87-92.

[151] F. J. Hernández, Z. Fei, C. Osborne, R. Crespo-Otero, M. Heeney, S. D. Dimitrov, *J. Phys. Chem. C* **2022**, *126*, 1036-1045.

[152] Z. Fei, Y. Kim, J. Smith, E. B. Domingo, N. Stingelin, M. A. McLachlan, K. Song, T. D. Anthopoulos, M. Heeney, *Macromolecules* **2012**, *45*, 735-742.

[153] W.-M. Zhou, I. Tomita, *J. Inorg. Organomet. Polym. Mater.* **2009**, *19*, 113-117.

[154] Y. Matsumura, M. Sugihara, S. E. Tan, T. Sato, K. Hayashi, H. Nishiyama, W. M. Zhou, S. Inagi, I. Tomita, *Macromol. Rapid Commun.* **2019**, *40*, 1800929.

[155] I.-M. Ramirez y Medina, M. Rohdenburg, P. Rusch, D. Duvinage, N. C. Bigall, A. Staubitz, *Mater. Adv.* **2021**, *2*, 3282-3293.

[156] J. Linshoeft, E. J. Baum, A. Hussain, P. J. Gates, C. Näther, A. Staubitz, *Angew. Chem. Int. Ed.* **2014**, *53*, 12916-12920.

[157] M. Bruma, B. Schulz, *J. Macromol. Sci., Polym. Rev.* **2001**, *41*, 1-40.

[158] C. Terraza, L. Tagle, A. Leiva, J. Vega, *Polym. Bull.* **2004**, *52*, 101-107.

[159] C. Terraza, L. Tagle, A. Leiva, *Polym. Bull.* **2005**, *55*, 277-285.

[160] L. Tagle, C. Terraza, A. Leiva, F. Devilat, *J. Appl. Polym. Sci.* **2008**, *110*, 2424-2431.

[161] C. Terraza, L. Tagle, A. Leiva, L. Poblete, F. Concha, *J. Appl. Polym. Sci.* **2008**, *109*, 303-308.

[162] L. Tagle, C. Terraza, A. Leiva, P. Alvarez, *J. Appl. Polym. Sci.* **2009**, *114*, 1080-1085.

[163] C. Terraza, L. Tagle, A. Leiva, *Polym. Bull.* **2009**, *63*, 663-672.

[164] L. Tagle, C. Terraza, A. Leiva, N. Yazigi, L. Lopez, *J. Appl. Polym. Sci.* **2010**, *117*, 1526-1534.

[165] A. Tundidor-Camba, C. Terraza, L. Tagle, D. Coll, P. Ortiz, *J. Appl. Polym. Sci.* **2012**, *124*, 1036-1041.

[166] C. Terraza, L. Tagle, D. Mejías, A. Tundidor-Camba, P. Ortiz, D. Muñoz, F. Alvarez, C. González-Henríquez, *Polym. Bull.* **2013**, *70*, 773-788.

[167] C. Terraza, L. Tagle, C. Contador, A. Tundidor-Camba, C. González-Henríquez, *Polym. Bull.* **2014**, *71*, 1101-1115.

[168] A. Tundidor-Camba, C. A. Terraza, L. H. Tagle, D. Coll, I. Ojeda, M. Pino, *RSC Adv.* **2015**, *5*, 23057-23066.

[169] L. Tagle, C. Terraza, A. Tundidor-Camba, D. Coll, *Polym. Bull.* **2017**, *74*, 263-281.

[170] I. A. Jessop, A. Mariman, P. A. Sobarzo, R. A. Hauyon, C. Saldías, E. Schott, X. Zarate, F. E. Rodríguez-González, J. Medina, C. M. González-Henríquez, A. Tundidor-Camba, C. A. Terraza, *Eur. Polym. J.* **2021**, *148*, 110373.

[171] A. Tundidor-Camba, C. M. González-Henríquez, M. A. Sarabia-Vallejos, L. H. Tagle, R. A. Hauyón, P. A. Sobarzo, A. González, P. A. Ortiz, E. M. Maya, C. A. Terraza, *RSC Adv.* **2018**, *8*, 1296-1312.

[172] P. A. Sobarzo, I. A. Jessop, A. P. Mariman, A. F. González, C. Saldías, E. Schott, X. Zarate, R. A. Hauyon, G. Recabarren-Gajardo, C. M. González-Henríquez, A. Tundidor-Camba, C. A. Terraza, *Eur. Polym. J.* **2020**, *130*, 109658.

[173] P. A. Sobarzo, A. González, I. A. Jessop, R. A. Hauyon, J. Medina, L. E. Garcia, X. Zarate, C. González-Henríquez, E. Schott, A. Tundidor-Camba, C. A. Terraza, *Eur. Polym. J.* **2022**, *181*, 111712.

[174] C. O. Sánchez, P. Sobarzo, N. Gatica, *New J. Chem.* **2015**, *39*, 7979-7987.

[175] J. Sun, Z. Zhang, X. Yin, J. Zhou, L. Yang, R. Geng, F. Zhang, R. Zhu, J. Yu, W. Tang, *J. Mater. Chem. A* **2018**, *6*, 2549-2554.

[176] M.-K. Hung, K.-W. Tsai, S. Sharma, J.-Y. Wu, S.-A. Chen, *Angew. Chem. Int. Ed.* **2019**, *58*, 11317-11323.

[177] M.-K. Hung, S.-T. Chung, S. Sharma, K.-W. Tsai, J.-Y. Wu, S.-A. Chen, *ACS Appl. Mater. Interfaces* **2022**, *14*, 55873-55885.

[178] M.-K. Hung, K.-W. Tsai, S. Sharma, J. Lei, J.-Y. Wu, S.-A. Chen, *ACS Appl. Mater. Interfaces* **2019**, *11*, 36895-36904.

[179] A. C. Uptmoor, R. Ilyas, S. M. Elbert, I. Wacker, R. R. Schröder, M. Mastalerz, J. Freudenberg, U. H. F. Bunz, *Chem. Eur. J.* **2018**, *24*, 1674-1680.

[180] S. M. Budy, D. Y. Son, *J. Inorg. Organomet. Polym. Mater.* **2018**, *28*, 1673-1687.

[181] Y. Adachi, D. Tanaka, Y. Ooyama, J. Ohshita, *Inorganics* **2018**, *6*, 3.

[182] M. Ishikawa, N. Hongzhi, K. Matsusaki, K. Nate, T. Inoue, H. Yokono, *J. Polym. Sci., Part B: Polym. Lett. Ed.* **1984**, *22*, 669-671.

[183] K. Nate, M. Ishikawa, H. Ni, H. Watanabe, Y. Saheki, *Organometallics* **1987**, *6*, 1673-1679.

[184] J. Ohshita, K. Furumori, M. Ishikawa, T. Yamanaka, *Organometallics* **1989**, *8*, 2084-2085.

[185] M. Ishikawa, Y. Hasegawa, T. Hatano, A. Kunai, T. Yamanaka, *Organometallics* **1989**, *8*, 2741-2742.

[186] S. Ijadi-Maghsoodi, Y. Pang, T. J. Barton, *J. Polym. Sci., Part A: Polym. Chem.* **1990**, *28*, 955-965.

[187] R. West, S. Hayase, T. Iwahara, *J. Inorg. Organomet. Polym.* **1991**, *1*, 545-565.

[188] J. Ohshita, A. Matsuguchi, K. Furumori, R. F. Hong, M. Ishikawa, T. Yamanaka, T. Koike, J. Shioya, *Macromolecules* **1992**, *25*, 2134-2140.

[189] M.-C. Fang, A. Watanabe, M. Matsuda, *Polymer* **1996**, *37*, 163-169.

[190] M.-C. Fang, A. Watanabe, M. Matsuda, *Macromolecules* **1996**, *29*, 6807-6813.

[191] J. Ohshita, K. Sugimoto, A. Kunai, Y. Harima, K. Yamashita, *J. Organomet. Chem.* **1999**, *580*, 77-81.

[192] J.-H. Kim, Y.-T. Park, *Bull. Korean Chem. Soc.* **2006**, *27*, 869-874.

[193] D. Tanaka, J. Ohshita, Y. Ooyama, T. Mizumo, Y. Harima, *J. Organomet. Chem.* **2012**, *719*, 30-35.

[194] H. H. Hong, W. P. Weber, *Polym. Bull.* **1989**, *22*, 363-369.

[195] J. Ohshita, D. Kanaya, M. Ishikawa, T. Koike, T. Yamanaka, *Macromolecules* **1991**, *24*, 2106-2107.

[196] P. F. van Hutten, R. E. Gill, J. K. Herrema, G. Hadziioannou, *J. Phys. Chem.* **1995**, *99*, 3218-3224.

[197] J. K. Herrema, J. Wildeman, R. E. Gill, R. H. Wieringa, P. F. van Hutten, G. Hadziioannou, *Macromolecules* **1995**, *28*, 8102-8116.

[198] H. Ago, T. Kuga, T. Yamabe, K. Tanaka, A. Kunai, M. Ishikawa, *Chem. Mater.* **1997**, *9*, 1159-1165.

[199] T. Hayashi, Y. Uchimaru, N. P. Reddy, M. Tanaka, *Chem. Lett.* **1992**, 647-650.

[200] K. Mochida, S. Maeyama, M. Wakasa, H. Hayashi, *Polyhedron* **1998**, *17*, 3963-3967.

[201] M. Majumdar, I. Bejan, V. Huch, A. J. White, G. R. Whittell, A. Schäfer, I. Manners, D. Scheschkewitz, *Chem. Eur. J.* **2014**, *20*, 9225-9229.

[202] I. Bejan, D. Scheschkewitz, *Angew. Chem. Int. Ed.* **2007**, *46*, 5783-5786.

[203] H. K. Mackenzie, B. W. Rawe, K. Samedov, H. T. Walsgrove, A. Uva, Z. Han, D. P. Gates, *J. Am. Chem. Soc.* **2020**, *142*, 10319-10324.

[204] B. W. Rawe, D. P. Gates, *Angew. Chem. Int. Ed.* **2015**, *54*, 11438-11442.

[205] B. W. Rawe, M. R. Scott, C. M. Brown, H. K. MacKenzie, D. P. Gates, *Macromolecules* **2017**, *50*, 8916-8927.

[206] Z. Zhang, B. Zhang, X. Han, H. Chen, C. Xue, M. Peng, G. Ma, Y. Ren, *Chem. Sci.* **2023**, *14*, 2990-2998.

[207] Y. Matsumura, M. Ueda, K. Fukuda, K. Fukui, I. Takase, H. Nishiyama, S. Inagi, I. Tomita, *ACS Macro Lett.* **2015**, *4*, 124-127.

[208] A. Saito, Y. Matano, H. Imahori, *Org. Lett.* **2010**, *12*, 2675-2677.

[209] Y. Matano, H. Ohkubo, Y. Honsho, A. Saito, S. Seki, H. Imahori, *Org. Lett.* **2013**, *15*, 932-935.

[210] Y. Matano, H. Ohkubo, T. Miyata, Y. Watanabe, Y. Hayashi, T. Umeyama, H. Imahori, *Eur. J. Inorg. Chem.* **2014**, *2014*, 1620-1624.

[211] R.-F. Chen, R. Zhu, Q.-L. Fan, W. Huang, *Org. Lett.* **2008**, *10*, 2913-2916.

[212] Y. Makioka, T. Hayashi, M. Tanaka, *Chem. Lett.* **2004**, *33*, 44-45.

[213] H. Cao, N. Bauer, S. Bi, D. Li, W. You, P. A. Rupar, *Eur. Polym. J.* **2018**, *104*, 157-163.

[214] T. Baumgartner, W. Bergmans, T. Kárpáti, T. Neumann, M. Nieger, L. Nyulászi, *Chem. Eur. J.* **2005**, *11*, 4687-4699.

[215] X. He, A. Y. Y. Woo, J. Borau-Garcia, T. Baumgartner, *Chem. Eur. J.* **2013**, *19*, 7620-7630.

[216] K. H. Park, Y. J. Kim, G. B. Lee, T. K. An, C. E. Park, S.-K. Kwon, Y.-H. Kim, *Adv. Funct. Mater.* **2015**, *25*, 3991-3997.

[217] K. Naka, T. Umeyama, Y. Chujo, *J. Am. Chem. Soc.* **2002**, *124*, 6600-6603.

[218] H. Kihara, H. Imoto, K. Naka, *Polym. J.* **2023**, *55*, 555-563.

[219] J. P. Green, Y. Han, R. Kilmurray, M. A. McLachlan, T. D. Anthopoulos, M. Heeney, *Angew. Chem. Int. Ed.* **2016**, *55*, 7148-7151.

[220] Y. Matsumura, M. Ishidoshiro, Y. Irie, H. Imoto, K. Naka, K. Tanaka, S. Inagi, I. Tomita, *Angew. Chem. Int. Ed.* **2016**, *55*, 15040-15043.

[221] T. Kato, H. Imoto, S. Tanaka, M. Ishidoshiro, K. Naka, *Dalton Trans.* **2016**, *45*, 11338-11345.

[222] T. Kato, S. Tanaka, K. Naka, *Chem. Lett.* **2015**, *44*, 1476-1478.

[223] J. P. Green, H. Cha, M. Shahid, A. Creamer, J. R. Durrant, M. Heeney, *Dalton Trans.* **2019**, *48*, 6676-6679.

[224] S. Tanaka, T. Enoki, H. Imoto, Y. Ooyama, J. Ohshita, T. Kato, K. Naka, *Macromolecules* **2020**, *53*, 2006-2013.

[225] C. Takahara, M. Nakamura, Y. Aoyama, T. Yanagihara, S. Ito, K. Tanaka, H. Imoto, K. Naka, *Macromolecules* **2023**, *56*, 6758-6763.

[226] H. Imoto, C. Yamazawa, S. Hayashi, M. Aono, K. Naka, *ChemElectroChem* **2018**, *5*, 3357-3360.

[227] V. H. K. Fell, A. Mikosch, A.-K. Steppert, W. Ogieglo, E. Senol, D. Canneson, M. Bayer, F. Schoenebeck, A. Greilich, A. J. C. Kuehne, *Macromolecules* **2017**, *50*, 2338-2343.

[228] D. S. Wiersma, *Nat. Phys.* **2008**, *4*, 359-367.

[229] K. Ishijima, S. Tanaka, H. Imoto, K. Naka, *Chem. Eur. J.* **2021**, *27*, 4676-4682.

[230] Y. Morisaki, K. Ohashi, H. S. Na, Y. Chujo, *J. Polym. Sci., Part A: Polym. Chem.* **2006**, *44*, 4857-4863.

[231] M. Côté, P. D. Haynes, C. Molteni, *Phys. Rev. B* **2001**, *63*, 125207.

[232] H. Helten, *Chem. Eur. J.* **2016**, *22*, 12972-12982.

[233] L. Maisonneuve, O. Lamarzelle, E. Rix, E. Grau, H. Cramail, *Chem. Rev.* **2015**, *115*, 12407-12439.

[234] J. O. Akindoyo, M. D. H. Beg, S. Ghazali, M. R. Islam, N. Jeyaratnam, A. R. Yuvaraj, *RSC Adv.* **2016**, *6*, 114453-114482.

[235] N. Matsumi, Y. Chujo, *Macromolecules* **1998**, *31*, 3802-3806.

[236] N. Matsumi, K. Kotera, K. Naka, Y. Chujo, *Macromolecules* **1998**, *31*, 3155-3157.

[237] N. Matsumi, K. Kotera, Y. Chujo, *Macromolecules* **2000**, *33*, 2801-2806.

[238] G. Monaco, R. Zanasi, S. Pelloni, P. Lazzeretti, *J. Chem. Theory Comput.* **2010**, *6*, 3343-3351.

[239] G. Monaco, R. Zanasi, *Phys. Chem. Chem. Phys.* **2016**, *18*, 11800-11812.

[240] R. Báez-Grez, R. Pino-Rios, *RSC Adv.* **2022**, *12*, 7906-7910.

[241] T. Lorenz, A. Lik, F. A. Plamper, H. Helten, *Angew. Chem. Int. Ed.* **2016**, *55*, 7236-7241.

[242] T. Lorenz, M. Crumbach, T. Eckert, A. Lik, H. Helten, *Angew. Chem. Int. Ed.* **2017**, *56*, 2780-2784.

[243] M. Maier, J. Chorbacher, A. Hellinger, J. Klopf, J. Günther, H. Helten, *Chem. Eur. J.* **2023**, *29*, e202302767.

[244] J. Chorbacher, M. Maier, J. Klopf, M. Fest, H. Helten, *Macromol. Rapid Commun.* **2023**, *44*, 2300278.

[245] J. Chorbacher, J. Klopf, A. Friedrich, M. Fest, J. S. Schneider, B. Engels, H. Helten, *Angew. Chem. Int. Ed.* **2025**, *64*, e202416088.

[246] M. Maier, F. Brosge, J. S. Schneider, J. Bachmann, S. Schmidt, C. Bolm, H. Helten, *Macromolecules* **2024**, *57*, 6370-6378.

[247] D. Scheschkewitz, *Chem. Lett.* **2011**, *40*, 2-11.

[248] T. Matsuo, N. Hayakawa, *Sci. Technol. Adv. Mater.* **2018**, *19*, 108-129.

[249] A. Fukazawa, Y. Li, S. Yamaguchi, H. Tsuji, K. Tamao, *J. Am. Chem. Soc.* **2007**, *129*, 14164-14165.

[250] J. Jeck, I. Bejan, A. J. White, D. Nied, F. Breher, D. Scheschkewitz, *J. Am. Chem. Soc.* **2010**, *132*, 17306-17315.

[251] M. Majumdar, V. Huch, I. Bejan, A. Meltzer, D. Scheschkewitz, *Angew. Chem. Int. Ed.* **2013**, *52*.

[252] L. Li, T. Matsuo, D. Hashizume, H. Fueno, K. Tanaka, K. Tamao, *J. Am. Chem. Soc.* **2015**, *137*, 15026-15035.

[253] N. M. Obeid, L. Klemmer, D. Maus, M. Zimmer, J. Jeck, I. Bejan, A. J. P. White, V. Huch, G. Jung, D. Scheschkewitz, *Dalton Trans.* **2017**, *46*, 8839-8848.

[254] T. Kosai, S. Ishida, T. Iwamoto, *Dalton Trans.* **2017**, *46*, 11271-11281.

[255] L. Klemmer, A.-L. Thömmes, M. Zimmer, V. Huch, B. Morgenstern, D. Scheschkewitz, *Nat. Chem.* **2021**, *13*, 373-377.

[256] A.-L. Thömmes, B. Morgenstern, M. Zimmer, D. M. Andrada, D. Scheschkewitz, *Chem. Eur. J.* **2023**, *29*, e202301273.

[257] D. Bravo-Zhivotovskii, S. Melamed, V. Molev, N. Sigal, B. Tumanskii, M. Botoshansky, G. Molev, Y. Apeloig, *Angew. Chem. Int. Ed.* **2009**, *48*, 1834-1837.

[258] K. Tamao, M. Kobayashi, T. Matsuo, S. Furukawa, H. Tsuji, *Chem. Commun.* **2012**, *48*, 1030-1032.

[259] B. Li, T. Matsuo, D. Hashizume, H. Fueno, K. Tanaka, K. Tamao, *J. Am. Chem. Soc.* **2009**, *131*, 13222-13223.

[260] L. Liu, H. Klaasen, M. C. Witteler, B. Schulze Lammers, A. Timmer, H. Kong, H. Mönig, H.-Y. Gao, J. Neugebauer, H. Fuchs, A. Studer, *Nat. Chem.* **2021**, *13*, 350-357.

[261] V. A. Wright, D. P. Gates, *Angew. Chem. Int. Ed.* **2002**, *41*, 2389-2392.

[262] V. A. Wright, B. O. Patrick, C. Schneider, D. P. Gates, *J. Am. Chem. Soc.* **2006**, *128*, 8836-8844.

[263] R. C. Smith, X. Chen, J. D. Protasiewicz, *Inorg. Chem.* **2003**, *42*, 5468-5470.

[264] R. C. Smith, J. D. Protasiewicz, *J. Am. Chem. Soc.* **2004**, *126*, 2268-2269.

[265] O. Back, B. Donnadieu, P. Parameswaran, G. Frenking, G. Bertrand, *Nat. Chem.* **2010**, *2*, 369-373.

[266] M. Soleilhavoup, G. Bertrand, *Acc. Chem. Res.* **2015**, *48*, 256-266.

[267] S. Roy, K. C. Mondal, H. W. Roesky, *Acc. Chem. Res.* **2016**, *49*, 357-369.

[268] S. Kumar Kushvaha, A. Mishra, H. W. Roesky, K. Chandra Mondal, *Chem. Asian J.* **2022**, *17*, e202101301.

[269] K. C. Mondal, H. W. Roesky, B. Dittrich, N. Holzmann, M. Hermann, G. Frenking, A. Meents, *J. Am. Chem. Soc.* **2013**, *135*, 15990-15993.

[270] O. Back, M. Henry-Ellinger, C. D. Martin, D. Martin, G. Bertrand, *Angew. Chem. Int. Ed.* **2013**, *52*, 2939-2943.

[271] C. Mohapatra, S. Kundu, A. N. Paesch, R. Herbst-Irmer, D. Stalke, D. M. Andrada, G. Frenking, H. W. Roesky, *J. Am. Chem. Soc.* **2016**, *138*, 10429-10432.

[272] S. Kundu, P. P. Samuel, A. Luebben, D. M. Andrada, G. Frenking, B. Dittrich, H. W. Roesky, *Dalton Trans.* **2017**, *46*, 7947-7952.

[273] E. Welz, J. Böhnke, R. D. Dewhurst, H. Braunschweig, B. Engels, *J. Am. Chem. Soc.* **2018**, *140*, 12580-12591.

[274] K. E. Wentz, A. Molino, S. L. Weisflog, A. Kaur, D. A. Dickie, D. J. D. Wilson, R. J. Gilliard Jr., *Angew. Chem. Int. Ed.* **2021**, *60*, 13065-13072.

[275] D. Nieder, L. Klemmer, Y. Kaiser, V. Huch, D. Scheschkewitz, *Organometallics* **2018**, *37*, 632-635.

[276] L. Klemmer, Y. Kaiser, V. Huch, M. Zimmer, D. Scheschkewitz, *Chem. Eur. J.* **2019**, *25*, 12187-12195.

[277] R. Zhang, B. Li, M. C. Iovu, M. Jeffries-El, G. Sauvé, J. Cooper, S. Jia, S. Tristram-Nagle, D. M. Smilgies, D. N. Lambeth, R. D. McCullough, T. Kowalewski, *J. Am. Chem. Soc.* **2006**, *128*, 3480-3481.

[278] I. Osaka, R. D. McCullough, *Acc. Chem. Res.* **2008**, *41*, 1202-1214.

[279] K. Kishikawa, N. Tokitoh, R. Okazaki, *Chem. Lett.* **1998**, *27*, 239-240.

[280] T. Iwamoto, J. Okita, N. Yoshida, M. Kira, *Silicon* **2010**, *2*, 209-216.

[281] Y. Li, K. C. Mondal, J. Lübben, H. Zhu, B. Dittrich, I. Purushothaman, P. Parameswaran, H. W. Roesky, *Chem. Commun.* **2014**, *50*, 2986-2989.

[282] Y. Li, K. C. Mondal, H. W. Roesky, H. Zhu, P. Stollberg, R. Herbst-Irmer, D. Stalke, D. M. Andrada, *J. Am. Chem. Soc.* **2013**, *135*, 12422-12428.

[283] C. Gendy, J. Mikko Rautiainen, A. Mailman, H. M. Tuononen, *Chem. Eur. J.* **2021**, *27*, 14405-14409.

[284] C. D. Martin, M. Soleilhavoup, G. Bertrand, *Chem. Sci.* **2013**, *4*, 3020-3030.

[285] S. Kundu, S. Sinhababu, V. Chandrasekhar, H. W. Roesky, *Chem. Sci.* **2019**, *10*, 4727-4741.

[286] K. Breitwieser, H. Bahmann, R. Weiss, D. Munz, *Angew. Chem. Int. Ed.* **2022**, *61*, e202206390.

[287] B. M. Puerta Lombardi, E. R. Pezoulas, R. A. Suvinen, A. Harrison, Z. S. Dubrawski, B. S. Gelfand, H. M. Tuononen, R. Roesler, *Chem. Commun.* **2022**, *58*, 6482-6485.

[288] B. M. Puerta Lombardi, M. R. Faas, D. West, R. A. Suvinen, H. M. Tuononen, R. Roesler, *Nat. Commun.* **2024**, *15*, 3417.

[289] D. Nieder, PhD thesis, Saarland University (Germany), **2017**.

[290] Y. Kaiser, A. Grandjean, V. Huch, M. Zimmer, G. Jung, D. Scheschkewitz, *Z. Anorg. Allg. Chem.* **2020**, *646*, 816-827.

[291] P. Jutzi, D. Eikenberg, A. Möhrke, B. Neumann, H.-G. Stammler, *Organometallics* **1996**, *15*, 753-759.

[292] S. Yao, Y. Xiong, M. Brym, M. Driess, *J. Am. Chem. Soc.* **2007**, *129*, 7268-7269.

[293] X. Liu, X.-Q. Xiao, Z. Xu, X. Yang, Z. Li, Z. Dong, C. Yan, G. Lai, M. Kira, *Organometallics* **2014**, *33*, 5434-5439.

[294] F. M. Mück, J. A. Baus, M. Nutz, C. Burschka, J. Poater, F. M. Bickelhaupt, R. Tacke, *Chem. Eur. J.* **2015**, *21*, 16665-16672.

[295] D. Wendel, A. Porzelt, F. A. D. Herz, D. Sarkar, C. Jandl, S. Inoue, B. Rieger, *J. Am. Chem. Soc.* **2017**, *139*, 8134-8137.

[296] A. V. Protchenko, P. Vasko, D. C. H. Do, J. Hicks, M. Á. Fuentes, C. Jones, S. Aldridge, *Angew. Chem. Int. Ed.* **2019**, *58*, 1808-1812.

[297] M.-P. Luecke, E. Pens, S. Yao, M. Driess, *Chem. Eur. J.* **2020**, *26*, 4500-4504.

[298] Y. Xiong, S. Yao, A. Ruzicka, M. Driess, *Chem. Commun.* **2021**, *57*, 5965-5968.

[299] L. R. Sita, J. R. Babcock, R. Xi, *J. Am. Chem. Soc.* **1996**, *118*, 10912-10913.

[300] A. Bücker, C. Wölper, S. Schulz, *Polyhedron* **2024**, *247*, 116702.

[301] L. Groll, J. A. Kelly, S. Inoue, *Chem. Asian J.* **2024**, *19*, e202300941.

[302] J. R. Babcock, L. Liable-Sands, A. L. Rheingold, L. R. Sita, *Organometallics* **1999**, *18*, 4437-4441.

[303] A. Jana, H. W. Roesky, C. Schulzke, A. Döring, *Angew. Chem. Int. Ed.* **2009**, *48*, 1106-1109.

[304] D. A. Dickie, E. N. Coker, R. A. Kemp, *Inorg. Chem.* **2011**, *50*, 11288-11290.

[305] S. Weiß, M. Widemann, K. Eichele, H. Schubert, L. Wesemann, *Dalton Trans.* **2021**, *50*, 4952-4958.

[306] A. V. Protchenko, M. Á. Fuentes, J. Hicks, C. McManus, R. Tirfoin, S. Aldridge, *Dalton Trans.* **2021**, *50*, 9059-9067.

[307] D. Sarkar, L. Groll, D. Munz, F. Hanusch, S. Inoue, *ChemCatChem* **2022**, *14*, e202201048.

[308] N. Wiberg, W. Niedermayer, K. Polborn, P. Mayer, *Chem. Eur. J.* **2002**, *8*, 2730-2739.

[309] D. Gau, R. Rodriguez, T. Kato, N. Saffon-Merceron, A. de Cózar, F. P. Cossío, A. Baceiredo, *Angew. Chem. Int. Ed.* **2011**, *50*, 1092-1096.

[310] J. Li, M. Hermann, G. Frenking, C. Jones, *Angew. Chem. Int. Ed.* **2012**, *51*, 8611-8614.

[311] D. Wendel, T. Szilvási, D. Henschel, P. J. Altmann, C. Jandl, S. Inoue, B. Rieger, *Angew. Chem. Int. Ed.* **2018**, *57*, 14575-14579.

[312] A. Kostenko, M. Driess, *J. Am. Chem. Soc.* **2018**, *140*, 16962-16966.

[313] A. Caise, L. P. Griffin, C. McManus, A. Heilmann, S. Aldridge, *Angew. Chem. Int. Ed.* **2022**, *61*, e202117496.

[314] J. Fan, S. Quek, M.-C. Yang, Z.-F. Zhang, M.-D. Su, C.-W. So, *Chem. Commun.* **2022**, *58*, 1033-1036.

[315] A. Kowalska, J. Sokolowski, K. Bociong, in *Polymers, Vol. 13*, **2021**.

[316] B. Ganster, U. K. Fischer, N. Moszner, R. Liska, *Macromolecules* **2008**, *41*, 2394-2400.

[317] N. Moszner, U. K. Fischer, B. Ganster, R. Liska, V. Rheinberger, *Dent. Mater.* **2008**, *24*, 901-907.

[318] N. Moszner, F. Zeuner, I. Lamparth, U. K. Fischer, *Macromol. Mater. Eng.* **2009**, *294*, 877-886.

[319] C. Haslinger, L. P. Leutgeb, M. Haas, S. Baudis, R. Liska, *ChemPhotoChem* **2022**, *6*, e202200108.

[320] M. Müller, M. Drusgala, R. C. Fischer, A. Torvisco, W. Kern, M. Haas, C. Bandl, *ACS Appl. Mater. Interfaces* **2023**, *15*, 31836-31848.

[321] M. W. Müller, M. Drusgala, R. C. Fischer, W. Kern, M. Haas, C. Bandl, *Appl. Surf. Sci.* **2024**, *661*, 160035.

[322] M. Abe, *Chem. Rev.* **2013**, *113*, 7011-7088.

[323] S. González-Gallardo, F. Breher, in *Comprehensive Inorganic Chemistry II, Vol. 2* (Eds.: J. Reedijk, K. Poeppelmeier), Elsevier, Amsterdam, **2013**, pp. 413-455.

[324] X. Hu, W. Wang, D. Wang, Y. Zheng, *J. Mater. Chem. C* **2018**, *6*, 11232-11242.

[325] T. Y. Gopalakrishna, W. Zeng, X. Lu, J. Wu, *Chem. Commun.* **2018**, *54*, 2186-2199.

[326] A. Hinz, J. Bresien, F. Breher, A. Schulz, *Chem. Rev.* **2023**, *123*, 10468-10526.

[327] K. C. Mondal, H. W. Roesky, M. C. Schwarzer, G. Frenking, I. Tkach, H. Wolf, D. Kratzert, R. Herbst-Irmer, B. Niepötter, D. Stalke, *Angew. Chem. Int. Ed.* **2013**, *52*, 1801-1805.

[328] A. P. Singh, P. P. Samuel, H. W. Roesky, M. C. Schwarzer, G. Frenking, N. S. Sidhu, B. Dittrich, *J. Am. Chem. Soc.* **2013**, *135*, 7324-7329.

[329] K. C. Mondal, B. Dittrich, B. Maity, D. Koley, H. W. Roesky, *J. Am. Chem. Soc.* **2014**, *136*, 9568-9571.

[330] M. M. Hansmann, M. Melaimi, D. Munz, G. Bertrand, *J. Am. Chem. Soc.* **2018**, *140*, 2546-2554.

[331] M. K. Nayak, P. Sarkar, B. J. Elvers, S. Mehta, F. Zhang, N. Chrysochos, I. Krummenacher, T. Vijayakanth, R. S. Narayanan, R. Dolai, B. Roy, V. Malik, H. Rawat, A. Mondal, R. Boomishankar, S. K. Pati, H. Braunschweig, C. Schulzke, P. Ravat, A. Jana, *Chem. Sci.* **2022**, *13*, 12533-12539.

[332] M. K. Nayak, B. J. Elvers, S. Mehta, I. Krummenacher, A. Mondal, H. Braunschweig, C. Schulzke, P. Ravat, A. Jana, *Chem. Commun.* **2024**, *60*, 1739-1742.

Supporting Information

Near-Infinite-Chain Polymers with Ge=Ge Double Bonds

And German Version:

Nahezu unendlich lange Polymere mit Ge=Ge-Doppelbindungen

Supporting Information

Anna-Lena Thömmes,* Thomas Büttner, Bernd Morgenstern, Oliver Janka, Guido Kickelbick, Bart-Jan Niebuur, Tobias Kraus, Markus Gallei, David Scheschkewitz*

Table of contents

1. General Remarks 110
2. Synthetic Procedures 111
3. Characterization of dibromophenylene and chlorosilane precursors 121
4. Characterization of bis(digermene) monomers 138
4.1 NMR spectroscopy 138
4.2 X-Ray crystallographic data 143
4.3 UV/Vis absorption spectroscopy 149
4.4 DFT calculations 152
4.5 NMR spectroscopy of reactions with Me_2IPr 164
5. Characterization of digermene polymers 168
5.1 ^1H NMR spectroscopy monitoring of the polymerization process 168
5.2 Solution NMR spectroscopy 171
5.3 Solid state CP/MAS NMR spectroscopy 174
5.4 DFT calculations for model digermenes 177
5.5 Natural bond order (NBO) analysis 179
5.6 TD-DFT calculations 181
5.7 UV/Vis absorption spectroscopy 182
5.8 Powder X-ray diffraction (PXRD) 187
5.9 Differential scanning calorimetry (DSC) 188
5.10 Thermogravimetric analysis (TGA) 190
5.11 Small angle X-ray scattering (SAXS) 191
5.12 Dynamic Light Scattering (DLS) 192
5.13 Diffusion ordered NMR spectroscopy (DOSY) 193
5.14 Atomic force microscopy (AFM) 198
5.15 Transmission electron microscopy (TEM) 200
References 201

1. General Remarks

All manipulations were carried out under a protective atmosphere of argon applying standard Schlenk or glovebox techniques. The glassware was pre-dried in an oven at 125 °C and heated in vacuo prior to use. Solvents were taken from a solvent purification system (Innovative technology PureSolv MD7; diethylether, hexane, pentane, thf, benzene, toluene). Benzene-d_6, thf-d_8 and toluene-d_8 were dried over potassium mirror and distilled under argon prior to use. 1,3-bis(2,6-diisopropyl)imidazol-2-ylidene (Me_2IPr)[S1], lithium digermenide $Tip_2Ge{=}GeTipLi{\cdot}dme_2$[S2], 1,4-Dibromo-2,5-*N*,*N*,*N'*,*N'*-tetrahexylphenylenediamine and 2,5-dibromo-*N*,*N*,*N'*,*N'*-tetramethylbenzene-1,4-diamine[S3] were prepared according to published procedures. All other chemicals were obtained commercially and used as received. The NMR spectra were recorded on a Bruker Avance III HD 400 spectrometer at 300 K (^{1}H: 400.13 MHz, ^{13}C: 100.61 MHz, ^{29}Si: 79.49). The ^{1}H and ^{13}C{^{1}H} NMR spectra were referenced to the residual proton and natural abundance ^{13}C resonances of the deuterated solvent and chemical shifts were reported relative to SiMe4 (benzene-d_6: δH = 7.16 ppm and δC = 128.06 ppm, thf-d_8: δH = 1.78, 3.58 ppm and δC = 67.21, 25.31 ppm).[S4] The ^{29}Si NMR chemical shifts were referenced to external $SiMe_4$. The following abbreviations were used for the multiplicities: s – singlet, d – doublet, t – triplet, sept – septet, m – multiplet, brs – broad singlet. Solid state CP/MAS NMR spectra were acquired on a Bruker AV400 WB spectrometer with a broadband probe from 40 to 160 MHz. UV/Vis spectra were recorded on a Shimdazu UV-2600 spectrometer in quartz cells with a path length of 0.1 cm. Melting points were determined under argon in sealed NMR tubes and are uncorrected. The molten samples were examined by NMR spectroscopy to confirm whether decomposition had occurred upon melting. Elemental analyses were performed in triplicate for each sample using Leco CHN900 analyzer and mean values are given below for each compound. Single crystal X-ray diffraction (SC-XRD) was performed on a Bruker X8 Apex diffractometer (sh4388_a) or on a Bruker D8 Venture diffractometer with a microfocus sealed tube and S2 a Photon II detector. Graphite-monochromated Mo Kα radiation (λ = 0.71073 Å) was used. Data were corrected for absorption effects using the multi-scan method. The structures were solved by direct methods using SHELXS-97[S5] (sh4293a, sh4295, sh4432) or SHELXT[S5] and refined by full matrix least squares calculations on F2 (SHELXL2018)[S6] in the graphical user interface Shelxle.[S7] Computations were carried out with the Gaussian 16.C01 program package.[S8] Structural optimizations and frequency analyses were performed at the BP86-D3(BJ)/def2-SVP level of theory[S9,S10] including the dispersion correction by Grimme with Becke-Johnson damping.[S11] NBO analyses were run with the NBO 7.0 program[S12] at the BP86/def2-TZVP level of theory.[S9,S10] For TD-DFT calculations, the ORCA quantum chemistry program package (Version 4.2.1)[S13] was used and the PBE0/def2-TZVP functional[S14] and basis set[S10] were employed. Pictures of Kohn-Sham and NBO orbitals were displayed with ChemCraft.[S15]

2. Synthetic Procedures

2.1 Synthesis of 1,4-dibromo-2,5-*N,N,N',N'*-tetrahexylphenylenediamine

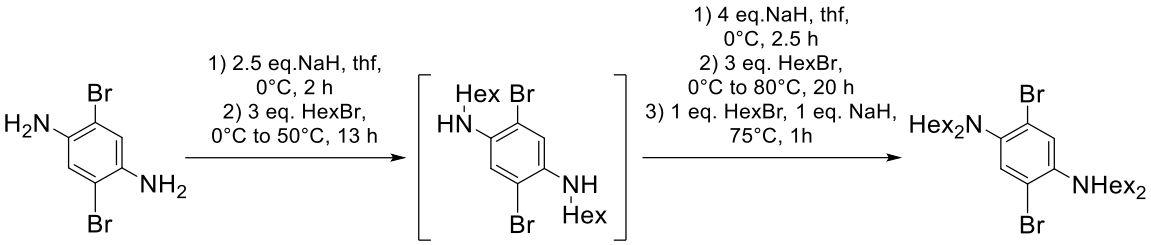

1,4-dibromo-2,5-*N,N,N',N'*-tetrahexylphenylenediamine was synthesized according to modified literature procedures.[S3,S16] 1,4-Dibromo-2,5-*N,N,N',N'*-tetrahexylphenylenediamine (7.8 g, 29.3 mmol, 1 eq.) is dissolved in 220 mL of thf and cooled to 0°C before addition to NaH (1.76 g, 73.3 mmol, 2.5 eq.) at 0°C *via* cannula. The grey suspension is stirred at 0°C for two hours turning violet before 1-hexylbromide (12.6 mL, 87.9 mmol, 3 eq.) is added dropwise at 0°C. The reaction mixture is heated to 50°C for 13 hours. ^{1}H NMR spectroscopy of an aliquot taken from the reaction mixture confirms full conversion to the 1,4-dibromo-2,5-*N,N'*-dihexylphenylenediamine:

^{1}H NMR (400.13 MHz, C_6D_6, 300 K, TMS): δ = 6.92 (s, 2H, Ph*H*), 3.72 (brs, 2H, N*H*), 2.62 (t, J = 7.0 Hz, 4H, NC*H*$_2$(CH$_2$)$_4$CH$_3$), 1.29 to 1.07 (m, 18H, NCH$_2$(C*H*$_2$)$_4$CH$_3$), 0.87 (t, J = 7.1 Hz, 6H, N(CH$_2$)$_5$C*H*$_3$) ppm.

The resulting brownish suspension is subsequently cooled to 0°C and added to NaH (1.76 g, 73.3 mmol, 2.5 eq.) at 0°C. After another 2.5 hours at 0°C 1-hexylbromide (12.6 mL, 87.9 mmol, 3 eq.) is added dropwise at 0°C. The mixture is heated to 50°C for 14 h, but ^{1}H NMR spectroscopy of an aliquot shows no conversion. Heating is hence continued at 80°C for 20 h resulting in 79% conversion according to ^{1}H NMR spectroscopy. After further addition of 1-hexylbromide (4.1 mL, 29.3 mmol, 1 eq.), heating to 75°C for 16.5 hours (no further conversion) and subsequent addition of NaH (703 mg, 29.3 mmol, 1 eq.) at 0°C and heating to 75°C for one hour, full conversion is achieved. The resulting brownish suspension is quenched with 260 mL of demineralized water. After addition of 150 mL of diethyl ether the phases are separated. The aqueous phase is extracted three times with each 150 mL of diethyl ether. The combined organic phases are dried over $MgSO_4$ and the solvent is removed under reduced pressure. The crude product is purified by flash chromatography (DCM/hexane = 3:97). After removing the solvent under reduced pressure residual 1-hexylbromide is removed at 120°C under high vacuum. Tetrahexylated 1,4-dibromo-2,5-*N,N,N',N'*-tetrahexylphenylenediamine is obtained as a colorless solid (11.8 g, 19.5 mmol, 67%). Colorless crystals are obtained from a hexane solution.

^{1}H NMR (400.13 MHz, C_6D_6, 300 K, TMS): δ = 7.53 (s, 2H, Ph*H*), 2.88 (brt, J = 7.5 Hz, 8H, NC*H*$_2$(CH$_2$)$_4$CH$_3$), 1.42 (brquin, J = 7.5 Hz, 8H, NCH$_2$C*H*$_2$(CH$_2$)$_3$CH$_3$), 1.27 to 1.08 (m, 24H, N(CH$_2$)$_2$(C*H*$_2$)$_3$CH$_3$), 0.86 (t, J = 7.2 Hz, 12H, (CH$_2$)$_5$C*H*$_3$) ppm. **^{13}C{^{1}H} NMR** (100.61 MHz, C_6D_6, 300 K, TMS): δ = 146.95 (Ph*C*-N), 129.35, 121.79 (Ph*C*-H and Ph*C*-Br), 53.78 (N*C*H$_2$(CH$_2$)$_4$CH$_3$), 31.97 (NCH$_2$*C*H$_2$(CH$_2$)$_3$CH$_3$), 27.37, 27.18, 23.08 (N(CH$_2$)$_2$(*C*H$_2$)$_3$CH$_3$), 14.30 (N(CH$_2$)$_5$*C*H$_3$) ppm. **Elemental analysis:** Calcd. for

($C_{30}H_{54}Br_2N_2$): C, 59.80.14; H, 9.03; N, 4.65. Found: C, 59.78; H, 8.43; N, 4.48. **Mp.:** 48°C.

2.2 Synthesis of 2,5-bis(chloromethyloctylsilyl)-*N,N,N',N'*-tetramethylbenzene-1,4-diamine (1a)

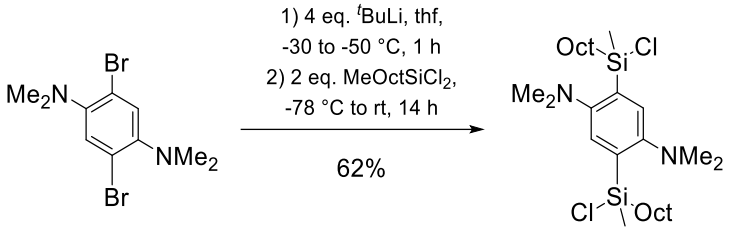

1a

1,4-Dibromo-2,5-*N,N,N',N'*-tetramethylphenylenediamine (7.94 g, 24.7 mmol, 1 eq.) is dissolved in 380 mL of thf and cooled to −78 °C before *t*-butyllithium (1.7 M in pentane, 58.1 mL, 98.8 mmol, 4 eq.) is added dropwise. The resulting bright yellow solution is stirred for 1 hour at −50 to −30 °C and subsequently added to a solution of methyloctyldichlorosilane (11.5 mL, 49.4 mmol, 2 eq.) in 50 mL of thf *via* cannula at −78 °C. After an additional 14 hours of stirring at ambient temperature all volatile species are removed *in vacuo* and the residue is dissolved in 300 mL of hexane. Filtration via a frit equipped with celite and subsequent concentration of the filtrate and storing at −20 °C leads to the formation of colorless crystals of **1a** (5.39 g, 9.88 mmol, 40 %). Additional batches are crystallized from the mother liquor (3.01 g, 5.51 mmol, 22%).

^{1}H NMR (400.13 MHz, C_6D_6, 300 K, TMS): δ = 8.14, 8.13 (each s, overall 2H, Ph*H*), 2.35 (s, 12H, N(CH_3)$_2$), 1.71 to 1.45 (m, 4H, SiCH_2(CH$_2$)$_6$CH$_3$), 1.34 to 1.22 (m, 20H, SiCH$_2$(CH_2)$_5$CH$_2$CH$_3$), 1.16 to 1.10 (m, 4H, Si(CH$_2$)$_6$CH_2CH$_3$), 0.89, 0.89 (each t, J = 6.8, 6.8 Hz, overall 6H, Si(CH$_2$)$_7$CH_3), 0.69, 0.67 (each s, overall 6H, SiCH_3) ppm. **^{13}C{^{1}H} NMR** (100.61 MHz, C_6D_6, 300 K, TMS): δ = 158.72 (Ph*C*-N), 139.42, 139.40 (Ph*C*-SiMeOct), 129.53, 129.49 (Ph*C*H), 46.87 (N(*C*H$_3$)$_2$), 33.52, 33.51, 32.31, 29.70, 29.65, 24.00, 23.07 (SiCH$_2$(*C*H$_2$)$_6$CH$_3$), 19.07, 19.04 (Si*C*H$_2$(CH$_2$)$_6$CH$_3$), 14.39 (Si(CH$_2$)*C*H$_3$), 2.67 (Si*C*H$_3$) ppm. **^{29}Si{^{1}H} NMR** (79.49 MHz, C_6D_6, 300 K, TMS): δ = *The signals strongly overlap hence preventing separate integration.* 17.01, 16.97 ppm. **Elemental analysis:** Calcd. for ($C_{28}H_{54}Cl_2N_2Si_2$): C, 61.61; H, 9.97; N, 5.13. Found: C, 59.86; H, 9.24; N, 5.11. **Mp.:** 83-84°C**.**

2.3 Synthesis of 2,5-bis(chlorodimethylsilyl)-*N*,*N*,*N'*,*N'*-tetrahexylbenzene-1,4-diamine (1b)

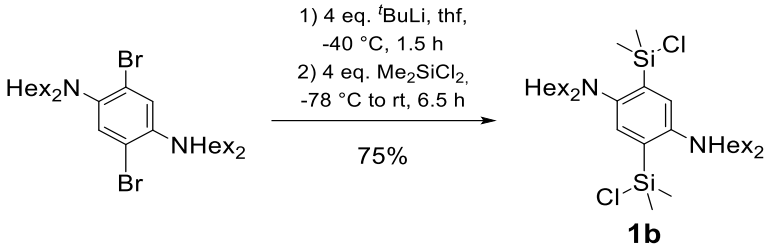

1,4-Dibromo-2,5-*N*,*N*,*N'*,*N'*-tetrahexylphenylenediamine (6.22 g, 10.3 mmol, 1 eq.) is dissolved in 160 mL of thf and cooled to −78 °C before *t*-butyllithium (1.7 M in pentane, 24.2 mL, 41.2 mmol, 4 eq.) is added dropwise. The resulting bright yellow solution is stirred at −40°C for 1.5 hours and subsequently added to a solution of dimethyldichlorosilane (5.0 mL, 41.2 mmol, 4 eq.) in 44 mL of thf *via* cannula at −78 °C. The mixture is allowed to warm up to room temperature and after additional stirring for 6.5 hours all volatile species are removed *in vacuo*. The residue is filtrated from 230 mL of hexane through a frit equipped with celite and the solvent is removed *in vacuo*. Colorless crystals of **1b** (5.32 g, 7.76 mmol, 75 %) are obtained from a concentrated solution in pentane.

^{1}H NMR (400.13 MHz, C_6D_6, 300 K, TMS): δ = 8.07 (s, 2H, Ph*H*), 2.85 to 2.81 (m, 8H, NCH_2(CH$_2$)$_4$CH$_3$), 2.89 to 2.83 (m, 8H, NCH$_2$CH_2(CH$_2$)$_3$CH$_3$), 1.23 to 1.04 (m, 24H, N(CH$_2$)$_2$(CH_2)$_3$CH$_3$), 0.83 (t, J = 6.8 Hz, 12H, N(CH$_2$)$_5$CH_3), 0.81 (s, 12H, Si(CH_3)$_2$) ppm. **^{13}C{^{1}H} NMR** (100.61 MHz, C_6D_6, 300 K, TMS): δ = 156.16 (Ph*C*N), 138.99 (Ph*C*SiMe$_2$), 131.52 (Ph*C*H), 56.11 (N*C*H$_2$(CH$_2$)$_4$CH$_3$), 32.00 (NCH$_2$*C*H$_2$(CH$_2$)$_3$CH$_3$), 27.67, 27.16 (NCH$_2$(*C*H$_2$)$_3$CH$_2$CH$_3$), 23.03 (N(CH$_2$)$_4$*C*H$_2$CH$_3$), 14.24 (N(CH$_2$)$_5$*C*H$_3$), 4.70 (Si(*C*H$_3$)$_2$) ppm. **^{29}Si{^{1}H} NMR** (79.49 MHz, C_6D_6, 300 K, TMS): δ = 18.57 ppm. **Elemental analysis:** Calcd. for ($C_{34}H_{66}Cl_2N_2Si_2$): C, 64.82; H, 10.56; N, 4.45. Found: C, 61.97; H, 9.62; N, 4.51. **Mp.:** 42°C**.**

2.4 Synthesis of *Si*-octylated digermene monomer 2a

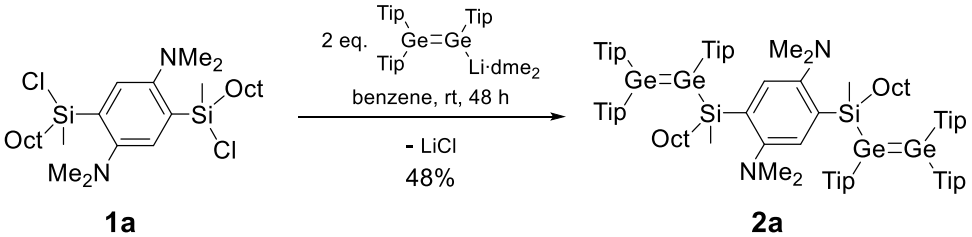

Bis(chlorosilane) **1a** (1.04 g, 1.90 mmol, 1 eq.) and lithium digermenide Tip$_2$Ge=GeTip(Li·dme$_2$) (4.10 g, 3.80 mmol, 2 eq.) are dissolved in 15.0 mL of benzene. After 48 hours all volatile species are removed in vacuo to obtain a yellow solid which is dissolved in 30 mL of hexane and filtrated. Concentrating the solution and storing it at room temperature yields yellow crystals of **2a** (1.66 g, 834 µmol, 44%) suitable for X-ray crystallography. From the mother liquor another batch of yellow crystals of **2a** is obtained (167 mg, 83.9 µmol, 4%).

^{1}H NMR (400.13 MHz, C_6D_6, 300 K, TMS): δ = 8.28 (s, 2H, Ph*H*), 7.09 (brs, 4H, Tip*H*), 7.05 (s, 4H, Tip*H*), 7.01 (s, 4H, Tip*H*), 3.85 (brs, 4H, C*H*$(CH_3)_2$ of Tip), 3.74, 3.69 (each sept, J = 6.7 Hz, overall 8H, C*H*$(CH_3)_2$ of Tip), 2.85 to 2.67 (m, 6H, C*H*$(CH_3)_2$ of Tip), 2.36 (s, 12H, N(C*H*$_3)_2$), 1.35 to 1.26 (m, 36H, Si(C*H*$_2)_7CH_3$ and CH(C*H*$_3)_2$ of Tip), 1.25 to 1.21 (m, 30H, Si(C*H*$_2)_7CH_3$ and CH(C*H*$_3)_2$ of Tip), 1.19 to 1.15 (m, 28H, Si(C*H*$_2)_7CH_3$ and CH(C*H*$_3)_2$ of Tip), 1.12 to 1.01 (m, 24H, Si(C*H*$_2)_7CH_3$ and CH(C*H*$_3)_2$ of Tip), 0.94 to 0.85 (m, 24H, Si$(CH_2)_7$C*H*$_3$ and CH(C*H*$_3)_2$ of Tip), 0.76, 0.75 (each s, overall 6H, SiC*H*$_3$) ppm. **^{13}C{^{1}H} NMR** (100.61 MHz, C_6D_6, 300 K, TMS): δ = *(R,S) isomer:* 158.20, 152.68, 152.61, 149.73, 149.69, 149.65, 146.17, 145.69, 141.37, 138.09 (Tip*C* and Ph*C*), 132.81 (Ph*C*H), 122.41, 122.33, 121.89 (Tip*C*), 47.10 (N*C*H_3), 37.53, 37.22, 34.84, 34.56 (*C*H$(CH_3)_2$ of Tip), 32.42, 31.98, 30.04, 29.76, 26.20 (Si$(CH_2)_2$(*C*$H_2)_5CH_3$), 24.47, 24.38, 24.35, 24.30, 24.26, 24.22, 24.19, 24.15 (CH(*C*$H_3)_2$ of Tip and Si$(CH_2)_2$(*C*$H_2)_5CH_3$), 23.15, 23.07 (Si*C*H_2*C*H_2(C$H_2)_5CH_3$), 19.05 (Si*C*H_2(C$H_2)_6CH_3$), 14.42, 14.37 (Si*C*H_2(C$H_2)_6CH_3$), 0.81 (Si*C*H_3) ppm; *(R,R) isomer:* 158.20, 155.49, 154.33, 153.78, 153.67, 153.52, 153.27, 152.47, 152.13, 150.06, 147.40, 147.28, 146.65, 145.44, 143.19 (Tip*C* and Ph*C*), 132.83 (Ph*C*H), 122.81, 121.80, 121.43, 121.19, 120.59, 120.05 (Tip*C*), 47.10 (N*C*H_3), 37.91, 37.73, 36.69, 36.15, 35.34, 35.04, 34.79, 34.77, 34.63, 34.57 (*C*H$(CH_3)_2$ of Tip), 34.28, 32.48, 29.95, 25.74, 25.66 (Si$(CH_2)_2$(*C*$H_2)_5CH_3$), 25.12, 25.05, 24.90, 24.86, 24.77, 24.66, 24.59, 24.58, 24.56, 24.41, 24.31, 24.22, 24.16, 24.11 (CH(*C*$H_3)_2$ of Tip and Si$(CH_2)_2$(*C*$H_2)_5CH_3$), 23.19, 23.14 (Si*C*H_2*C*H_2(C$H_2)_5CH_3$), 19.08, 19.06, 19.03 (Si*C*H_2(C$H_2)_6CH_3$), 14.42, 14.38 (Si*C*H_2(C$H_2)_6CH_3$), 0.80 (Si*C*H_3) ppm. **^{29}Si{^{1}H} NMR** (79.49 MHz, C_6D_6, 300 K, TMS): δ = 7.28, 7.12 ppm. **UV/Vis** (*n*-hexane): λ_{max} = 431 nm (ε = 32800 L mol^{-1} cm^{-1}), 324 nm (ε = 11900 L mol^{-1} cm^{-1}). **Elemental analysis:** Calcd. for ($C_{118}H_{192}Ge_4N_2Si_2$): C, 71.38; H, 9.75; N, 1.41. Found: C, 70.93; H, 9.60; N, 1.38. **Mp.:** 160°C (under formation of $Tip_2Ge{=}GeTip_2$ and unselective decomposition products).

2.5 Synthesis of *N*-hexylated digermene monomer 2b

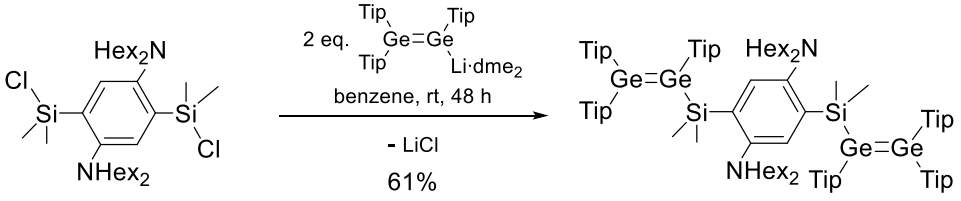

1b **2b**

Bis(chlorosilane) **1b** (1.35 g, 2.15 mmol, 1 eq.) and lithium digermenide $Tip_2Ge{=}GeTip(Li{\cdot}dme_2)$ (4.04 g, 4.29 mmol, 2 eq.) are dissolved in 17.5 mL of benzene. After 48 hours all volatile species are removed *in vacuo* to obtain a yellow solid which is dissolved in 60 mL of hexane and filtrated. Concentrating the solution and storing it at −23°C yields yellow crystals of **1c** (1.77 g, 855 µmol, 40%) suitable for X-ray crystallography. From the mother liquor another batch of yellow crystals of **2b** is obtained (941 mg, 455 µmol, 21%).

^{1}H NMR (400.13 MHz, C_6D_6, 300 K, TMS): δ = 8.36 (s, 2H, Ph*H*), 7.11 (s, 2H, Tip*H*), 7.06 (s, 2H, Tip*H*), 7.00 (s, 2H, Tip*H*), 3.91, 3.82 (each sept, overall 8H, J = 6.7 Hz, C*H*$(CH_3)_2$ of Tip), 3.65 (sept, 4H, J = 6.7 Hz, C*H*$(CH_3)_2$ of Tip), 2.83 to 2.65 (m, 14H, N*C*H_2 and C*H*$(CH_3)_2$ of Tip), 1.50 (brs, 8H, NCH_2*C*H_2(C$H_2)_3CH_3$), 1.38 to 1.07 (m, 24H,

$N(CH_2)_2(CH_2)_3CH_3$) overlapping with 1.22, 1.21, 1.14 (each d, overall 84H, $CH(CH_3)_2$ of Tip), 0.96 to 0.91 (m, 48H, $Si(CH_3)_2$, $N(CH_2)_5CH_3$, $CH(CH_3)_2$ of Tip) ppm. **$^{13}C\{^1H\}$ NMR** (100.61 MHz, C_6D_6, 300 K, TMS): δ = 156.76, 154.03, 152.87, 152.65, 149.72, 149.53, 146.03, 145.77, 141.30, 138.58 (Tip*C* and Ph*C*), 134.71(Ph*C*H), 122.41, 122.32, 121.73 (Tip*C*), 57.04 ($NCH_2(CH_2)_4CH_3$), 37.82, 37.43, 34.74, 34.54, 34.50 ($CH(CH_3)_2$ of Tip), 32.47 ($NCH_2CH_2(CH_2)_3CH_3$), 28.41, 27.73, 24.30, 24.25, 24.15, 24.10 ($CH(CH_3)_2$ of Tip), 23.12 ($N(CH_2)_2(CH_2)_3CH_3$), 14.44 ($N(CH_2)_5CH_3$), 4.83 ($SiCH_3$) ppm. **$^{29}Si\{^1H\}$ NMR** (79.49 MHz, C_6D_6, 300 K, TMS): δ = 7.19 ppm. **UV/Vis** (*n*-hexane): λ_{max} = 431 nm (ε = 33400 L mol^{-1} cm^{-1}), 322 nm (ε = 11700 L mol^{-1} cm^{-1}). **Elemental analysis:** Calcd. for ($C_{126.6}H_{210.5}Ge_4N_2Si_2$ (including 0.65 eq. of cocrystallized Et_2O)): C, 71.79; H, 10.04; N, 1.32. Found: C, 70.36; H, 9.58; N, 1.22. **Mp.:** 180°C (under formation of $Tip_2Ge{=}GeTip_2$ and unselective decomposition products).

2.6 Synthesis of 1,4-bis(chlorodihexylsilyl)-2,5-*N*,*N*,*N'*,*N'*-tetramethyl-phenylenediamine

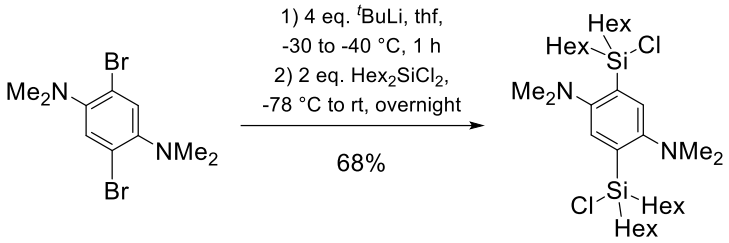

1,4-Dibromo-2,5-*N*,*N*,*N'*,*N'*-tetrahexylphenylenediamine (2.00 g, 6.21 mmol, 1 eq.) is dissolved in 100 mL of thf and cooled to −78 °C before *t*-butyllithium (1.9 M in pentane, 13.2 mL, 25.1 mmol, 4 eq.) is added dropwise. The resulting solution is stirred for 1 hour at −40 to −30 °C and subsequently added to a solution of dihexyldichlorosilane (3.48 mL, 12.4 mmol, 2 eq.) in 30 mL of thf *via* cannula at −78 °C. After stirring overnight at ambient temperature all volatile species are removed *in vacuo* and the residue is suspended in 20 mL of hexane followed by filtration. Concentration of the filtrate and storing at −20 °C leads to the formation of colorless crystals of 1,4-Dibromo-2,5-*N*,*N*,*N'*,*N'*-tetrahexylphenylenediamine (2.66 g, 4.15 mmol, 67%)*.

*13mol% of the monobrominated derivative 1-bromodihexylsilyl-4-chlorodihexylsilyl-2,5-*N*,*N*,*N'*,*N'*-tetramethyl-phenylenediamine are contained in the crystallized product mixture.

^1H NMR (400.13 MHz, C_6D_6, 300 K, TMS): δ = 8.28 (each s, overall 0.26H, Ph*H* of Br_2 derivative), 8.18 (s, 2H, Ph*H*), 2.42 (s, 12H, $N(CH_3)_2$), 1.73 to 1.62, 1.54 to 1.43 (each m, each 4H, $SiCH_2(CH_2)_4CH_3$), 1.36 to 1.13 (m, 32H, $SiCH_2(CH_2)_4CH_3$), 0.85 (t, J = 7.1 Hz, 12H, $Si(CH_2)_5CH_3$) ppm. **$^{13}C\{^1H\}$ NMR** (100.61 MHz, C_6D_6, 300 K, TMS): δ = 158.72 (Ph*C*-N), 138.58 (Ph*C*-$SiHex_2$), 129.87 (Ph*C*H), 46.98 ($N(CH_3)_2$), 33.27, 31.85, 24.02, 23.01 ($SiCH_2(CH_2)_4CH_3$), 18.10 ($SiCH_2(CH_2)_4CH_3$), 14.35 ($Si(CH_2)_5CH_3$). **$^{29}Si\{^1H\}$ NMR** (79.49 MHz, C_6D_6, 300 K, TMS): δ = 21.60 (Br_2 derivative), 19.59 (Cl_2 derivative) ppm. **Elemental analysis:** Calcd. for ($C_{34}H_{66}Cl_{1.74}Br_{0.26}N_2Si_2$ (87mol% Si_2 derivative and 13mol% Br_2 derivative): C, 63.74; H, 10.39; N, 4.37. Found: C, 62.68; H, 8.63; N, 4.21. **Mp.:** 56°C.

2.7 Reaction of dihexyldichlorosilane with digermenide

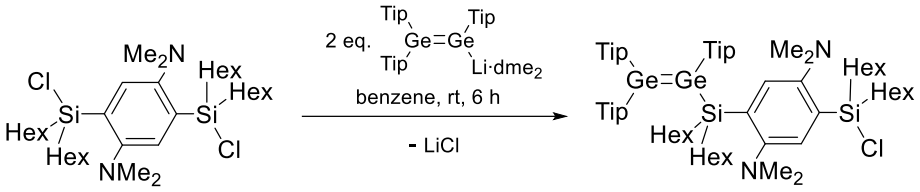

A solution of lithium digermenide $Tip_2Ge{=}GeTip(Li{\cdot}dme_2)$ (50 mg, 50.4 µmol, 2 eq.) in 0.25 mL of benzene is added to a solution of 1,4-Dibromo-2,5-*N*,*N*,*N'*,*N'*-tetrahexylphenylenediamine* (15.9 mg, 24.8 mmol, 1 eq.) in 0.25 mL of benzene. After six hours 81% conversion to the mono(digermene) is confirmed by ^{1}H NMR spectroscopy and no changes are observed after nine hours.

*13mol% of the monobrominated derivative 1-bromodihexylsilyl-4-chlorodihexylsilyl-2,5-*N*,*N*,*N'*,*N'*-tetramethyl-phenylenediamine are contained in the crystallized product mixture.

^{1}H NMR (400.13 MHz, C_6D_6, 300 K, TMS): δ = *Several peaks are overlapping with peaks of residual bis(chlorosilane) and $Tip_2Ge{=}GeTipLi{\cdot}dme_2$, leading to higher integration in some cases as seen in the spectrum. For clarity not all integrals are given here.* 8.19, 8.09 (each s, each 1H, Ph*H*), 7.05, 7.04 (each s, Tip*H*), 7.00, 6.98 (each s, overall 4H, Tip*H*), 3.91 to 3.79, 3.76 to 3.59 (m, C*H*$(CH_3)_2$ of Tip), 2.95 to 2.66 (m, C*H*$(CH_3)_2$ of Tip), 2.56, 2.33 (each s, each 6H, N(C*H*$_3)_2$), 1.72 to 1.08 (m, Si$(CH_2)_4$C*H*$_2$CH$_3$ and CH(C*H*$_3)_2$ of Tip), 0.97 to 0.84 (m, Si$(CH_2)_5$C*H*$_3$) ppm.

2.8 Synthesis of 1,4-bis(chlorodibutylsilyl)-2,5-*N*,*N*,*N'*,*N'*-tetramethyl-phenylenediamine

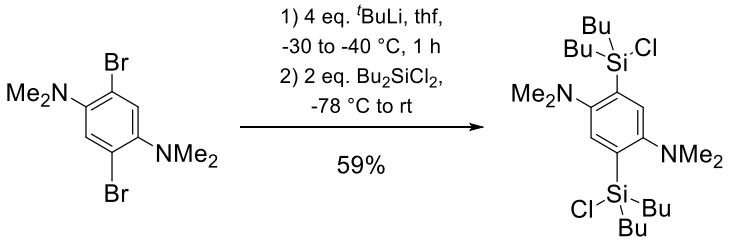

1,4-Dibromo-2,5-*N*,*N*,*N'*,*N'*-tetrahexylphenylenediamine (2.00 g, 6.21 mmol, 1 eq.) is dissolved in 100 mL of thf and cooled to −78 °C before *t*-butyllithium (1.9 M in pentane, 13.2 mL, 25.1 mmol, 4 eq.) is added dropwise. The resulting bright yellow solution is stirred for 1 hour at −50 to −30 °C and subsequently added to a solution of dibutyldichlorosilane (2.68 mL, 12.5 mmol, 2 eq.) in 30 mL of thf *via* cannula at −78 °C. After stirring overnight at ambient temperature all volatile species are removed *in vacuo* and the residue is suspended in 20 mL of hexane followed by filtration. Concentration of the filtrate and storing at −20 °C leads to the formation of colorless crystals of 1,4-Dibromo-2,5-*N*,*N*,*N'*,*N'*-tetrabutylphenylenediamine (1.89 g, 3.65 mmol, 59 %).

^{1}H NMR (400.13 MHz, C_6D_6, 300 K, TMS): δ = 8.16 (s, 2H, Ph*H*), 2.39 (s, 12H, N(C*H*$_3)_2$), 1.69 to 1.56, 1.49 to 1.37 (each m, each 4H, SiC*H*$_2(CH_2)_2CH_3$), 1.36 to 1.22, 1.20 to 1.05 (each m, each 8H, $SiCH_2(CH_2)_2CH_3$), 0.81 (t, J = 7.3 Hz, 12H, Si$(CH_2)_5$C*H*$_3$) ppm. **^{13}C{^{1}H} NMR** (100.61 MHz, C_6D_6, 300 K, TMS): δ = 158.70 (Ph*C*-

N), 138.51 (Ph*C*-SiBu$_2$), 129.85 (Ph*C*H), 46.94 (N(*C*H$_3$)$_2$), 26.49, 26.13 (SiCH$_2$(*C*H$_2$)$_4$CH$_3$), 17.75 (Si*C*H$_2$(CH$_2$)$_2$CH$_3$), 13.89 (Si(CH$_2$)$_3$*C*H$_3$). **^{29}Si{^{1}H} NMR** (79.49 MHz, C_6D_6, 300 K, TMS): δ = 19.61 ppm. **Elemental analysis:** Calcd. for ($C_{26}H_{50}Cl_2N_2Si_2$): C, 60.31; H, 9.73; N, 5.41. Found: C, 59.35; H, 8.19; N, 5.47. **Mp.:** 81°C**.**

2.9 Reaction of dibutyldichlorosilane with a digermenide

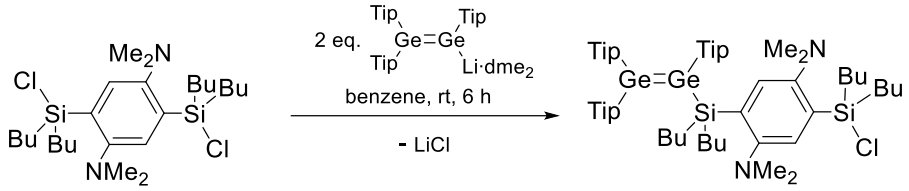

A solution of lithium digermenide Tip$_2$Ge=GeTip(Li·dme$_2$) (50 mg, 50.4 µmol, 2 eq.) in 0.25 mL of benzene is added to a solution of 1,4-Dibromo-2,5-*N*,*N*,*N'*,*N'*-tetrabutylphenylenediamine (13.1 mg, 25.3 mmol, 1 eq.) in 0.25 mL of benzene. After six hours full conversion to the mono(digermene) is confirmed by ^{1}H NMR spectroscopy.

^{1}H NMR (400.13 MHz, C_6D_6, 300 K, TMS): δ = *Several peaks are overlapping with peaks of residual Tip$_2$Ge=GeTipLi·dme$_2$, leading to higher integration in some cases as seen in the spectrum. For clarity not all integrals are given here.* 8.14, 8.07 (each s, each 1H, Ph*H*), 7.05 (s, Tip*H*), 7.01, 6.99 (each s, each 2H, Tip*H*), 3.90 to 3.59 (m, C*H*(CH$_3$)$_2$ of Tip), 2.86 to 2.68 (m, C*H*(CH$_3$)$_2$ of Tip), 2.52, 2.29 (each s, each 6H, N(C*H*$_3$)$_2$), 1.68 to 1.06 (m, Si(CH$_2$)$_2$C*H*$_2$CH$_3$ and CH(C*H*$_3$)$_2$ of Tip), 0.95 (d, CH(C*H*$_3$)$_2$ of Tip), 0.89 (t, Si(CH$_2$)$_3$C*H*$_3$), 0.82 (t, 6H, Si(CH$_2$)$_3$C*H*$_3$) ppm.

2.10 Synthesis of *Si*-octylated digermene polymer 3a

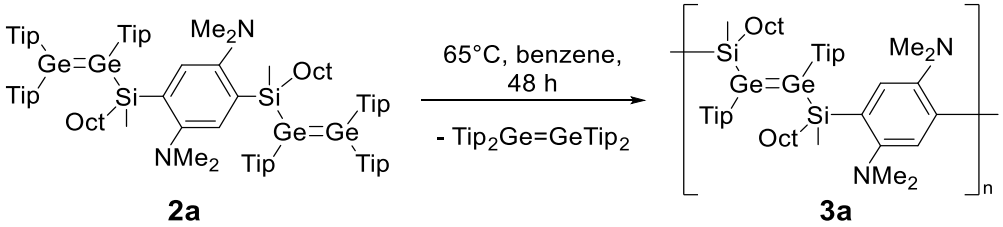

2a **3a**

A solution of bis(digermene) **2a** (1.61 g, 811 µmol, dr = 1:7) in 16 mL of benzene is stirred at 65°C for 48 hours. Removing all volatile species *in vacuo* yields a yellow solid which is subsequently dissolved in 180 mL of toluene. Addition of 50 mL of acetonitrile leads to precipitation of digermene polymer **3a** as a yellow solid from the yellow solution. The suspension is left to settle overnight before the solid is separated from the mother liquor by filtration. Removing the solvent *in vacuo* yields Tip$_2$Ge=GeTip$_2$ (535 mg, 558 µmol). Drying of the yellow solid provides digermene polymer **3a** (627 mg).

^{1}H NMR (400.13 MHz, C_6D_6, 300 K, TMS): δ = 7.4 to 7.2 (brm, 2H, Ph*H*), 7.1 (brm, 4H, Tip*H*), 3.8 (brs, 4H, C*H*(CH$_3$)$_2$ of Tip), 2.8 (brs, 2H, C*H*(CH$_3$)$_2$ of Tip), 2.4 to 2.2 (brm, 12H, N(C*H*$_3$)$_2$), 1.5 to 0.9 (m, 70H, Si(C*H*$_2$)$_5$C*H*$_3$ and C*H*(CH$_3$)$_2$ of Tip), 0.7 (brm, 6H, SiC*H*$_3$) ppm. **^{13}C{^{1}H} NMR** (100.61 MHz, C_6D_6, 300 K, TMS): δ = 157.0, 153.5, 149.5,

141.2, 137.0 (Tip*C* and Ph*C*), 129.0 (Ph*C*H), 121.2 (Tip*C*), 46.7 (N*C*H_3), 37.7, 34.8, 34.3 (*C*H(CH_3)$_2$ of Tip), 32.5, 30.0, 29.8 (Si(CH_2)$_2$(*C*H_2)$_5$$CH_3$), 24.9, 24.4 (CH(*C*$H_3$)$_2$ of Tip and Si(CH_2)$_2$(*C*H_2)$_5$$CH_3$), 23.2 (Si$CH_2$*C*$H_2$($CH_2$)$_5$$CH_3$), 18.5 (Si*C*$H_2$($CH_2$)$_6$$CH_3$), 14.4 (Si($CH_2$)*C*$H_3$), 0.0 (Si*C*$H_3$) ppm. **^{29}Si{^{1}H} NMR** (79.49 MHz, C_6D_6, 300 K, TMS): δ = −0.91 ppm. **^{13}C{^{1}H} CP/MAS NMR** (100.65 MHz, 300K, 13 kHz, TMS): δ = 157.0, 153.3, 149.2, 141.4, 137.5, 129.1, 121.0 (Tip*C* and Ph*C*), 46.7 (N*C*H_3), 37.6, 34.8 (*C*H(CH_3)$_2$ of Tip), 32.5, 29.6 (Si(CH_2)$_2$(*C*H_2)$_5$$CH_3$), 24.5 (CH(*C*$H_3$)$_2$ of Tip and Si*C*H_2(CH_2)$_6$$CH_3$), 14.4 (Si($CH_2$)$_7$*C*$H_3$), 0.3 (Si*C*$H_3$) ppm. **^{29}Si{^{1}H} CP/MAS NMR** (79.53 MHz, 300K, 13kHz, TMS): δ = −1.77 ppm. **UV/Vis** (*n*-hexane): λ_{max} = 423, 334, 291, 247 nm. **Elemental analysis:** Calcd. for ($C_{58}H_{100}Ge_2N_2Si_2$ (repeat unit)): C, 67.84; H, 9.82; N, 2.73; Ge, 14.15; Si 5.47. Found: C, 67.09; H, 8.88; N, 2.56. **Mp.:** 242°C (under unselective degradation).

2.11 Synthesis of *N*-hexylated digermene polymer 3b

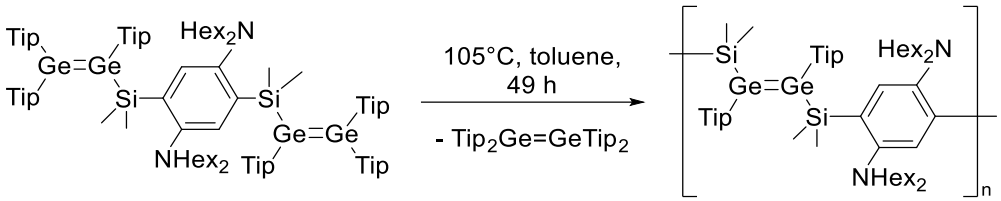

2b **3b**

A solution of bis(digermene) **2b** (1.92 g, 929 µmol) in 19 mL of toluene is stirred at 105°C for 49 hours. Removing all volatile species *in vacuo* yields a yellow solid which is subsequently dissolved in 40 mL of toluene. The solution is added dropwise to a mixture of 286 mL of toluene and 234 mL of acetronitrile at −55°C resulting in the precipitation of digermene polymer **3b** as a yellow solid from the yellow solution. The solid is separated from the mother liquor by filtration. Removing the solvent of the mother liquor yields $Tip_2Ge=GeTip_2$ (592 mg, 618 µmol) and drying of the yellow solid provides digermene polymer **3b** (533 mg).

^{1}H NMR (400.13 MHz, C_6D_6, 300 K, TMS): δ = 7.5 to 7.3 (brm, 2H, Ph*H*), 7.1 (brm, 4H, Tip*H*), 3.7 (brs, 4H, C*H*(CH_3)$_2$ of Tip), 2.8 (brs, 10H, C*H*(CH_3)$_2$ of Tip and NC*H*$_2$(CH_2)$_4$$CH_3$), 1.6 (brs, 10H, C*H*($CH_3$)$_2$ of Tip and NCH_2C*H*$_2$(CH_2)$_3$$CH_3$), 1.3 to 0.9 (brm, 70H, CH(C*H*$_3$)$_2$ of Tip and N(CH_2)$_2$(C*H*$_2$)$_3$C*H*$_3$), 0.5 (brs, 12H, SiC*H*$_3$) ppm. **^{13}C{^{1}H} NMR** (100.61 MHz, C_6D_6, 300 K, TMS): δ = 153.6, 152.8, 149.5, 141.0, 137.5 (Tip*C* and Ph*C*), 131.8 (Ph*C*H), 121.3 (Tip*C*), 54.5 (N*C*H_2(CH_2)$_4$$CH_3$), 37.7, 34.7 (*C*H($CH_3$)$_2$ of Tip), 32.5 (NCH_2*C*H_2(CH_2)$_3$$CH_3$), 27.4, 26.0, 24.9, 24.6 (CH(*C*H_3)$_2$ of Tip), 24.3, 23.1 (N(CH_2)$_2$(*C*H_2)$_3$$CH_3$), 14.5 (N($CH_2$)$_5$*C*$H_3$), 3.1 (Si*C*$H_3$) ppm. **^{29}Si{^{1}H} NMR** (79.49 MHz, C_6D_6, 300 K, TMS): δ = −2.76 ppm. **^{13}C{^{1}H} CP/MAS NMR** (100.65 MHz, 300K, 13 kHz, TMS): δ = 153.7, 149.4, 137.6, 132.8, 121.3 (Tip*C* and Ph*C*), 55.0 (N*C*H_2(CH_2)$_4$$CH_3$), 37.6, 34.7 (*C*H($CH_3$)$_2$ of Tip), 32.3 (NCH_2*C*H_2(CH_2)$_3$$CH_3$), 27.7, 24.0 (CH(*C*$H_3$)$_2$ of Tip and N(CH_2)$_2$(*C*H_2)$_3$$CH_3$), 14.4 (N($CH_2$)$_5$*C*$H_3$), 3.8, 0.4 (Si*C*$H_3$) ppm. **^{29}Si{^{1}H} CP/MAS NMR** (79.53 MHz, 300K, 13kHz, TMS): δ = −3.65 ppm. **UV/Vis** (*n*-hexane): λ_{max} = 418, 338, 298, 249 nm. **Elemental analysis:** Calcd. for ($C_{64}H_{112}Ge_2N_2Si_2$ (repeat unit)): C, 69.19; H, 10.16; N, 2.52; Ge, 13.07; Si, 5.06. Found: C, 67.74; H, 8.60; N, 2.36. **Mp.:** 250 °C (under unselective degradation).

2.12 Reaction of digermene polymer 3a with Me_2IPr

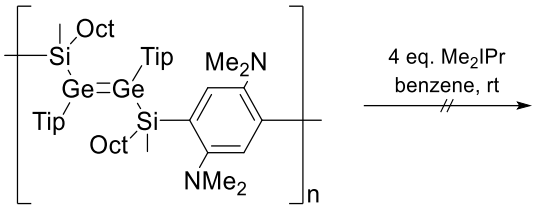

2b

A solution of polymer **3a** (obtained from 50.0 mg (25.2 µmol) of bis(digermene) **1c**) and $Tip_2Ge{=}GeTip_2$ is dissolved in 0.5 mL of C_6D_6 and added to Me_2IPr (9.1 mg, 50.4 µmol, 2 eq.). The integrity of the polymer and $Tip_2Ge{=}GeTip_2$ is confirmed by NMR spectroscopy after 18.5 hours at room temperature and after subsequent heating to 65 °C for 14 hours.

2.13 Reaction of digermene polymer 3b with Me_2IPr

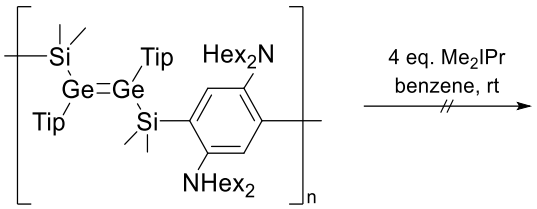

2c

A solution of polymer **3b** (obtained from 50.0 mg (24.2 µmol) of bis(digermene) **1c**) and $Tip_2Ge{=}GeTip_2$ is dissolved in 0.5 mL of toluene-d_8 and added to Me_2IPr (8.7 mg, 48.4 µmol, 2 eq.). The integrity of the polymer and $Tip_2Ge{=}GeTip_2$ is confirmed by NMR spectroscopy after 18.5 hours at room temperature and after subsequent heating to 65 °C for 14 hours.

1.14 Reaction of bis(digermene) 2a with Me_2IPr

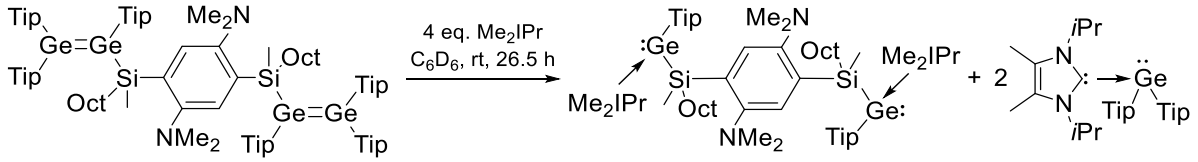

2a **5a**

Me_2IPr (10.9 mg, 60.4 µmol, 4 eq.) is dissolved in 0.5 mL of C_6D_6 and added to bis(digermene) **2a** (30.0 mg, 15.1 µmol, 1 eq.). Full conversion of bis(digermene) **2a** to the bis(germylene)-NHC adduct and Tip_2Ge-Me_2IPr[S17] is confirmed by heteronuclear NMR spectroscopy after 26.5 hour.

^{1}H NMR (400.13 MHz, C_6D_6, 300 K, TMS): δ = 7.45 to 7.27 (m, 2H, Ph*H*), 7.12 to 7.10 (m, 4H, Tip*H*), 5.92 to 5.61 (m, 4H, C*H*$(CH_3)_2$ of Me_2IPr, overlapping with signals of Tip_2Ge-Me_2IPr), 4.39 to 4.14 (m, 4H, C*H*$(CH_3)_2$ of Tip), 4.05 to 3.90 (m, 2H, C*H*$(CH_3)_2$ of Tip, overlapping with signals of Tip_2Ge-Me_2IPr), 2.79 to 2.72 (m, 12H, N(CH_3)$_2$), 1.73 (s, 12H, Me_2IPr-CCH_3, overlapping with signals of Tip_2Ge-Me_2IPr), 1.66 to 1.60 (m, 12H, CH(CH_3)$_2$ of Me_2IPr, overlapping with signals of Tip_2Ge-Me_2IPr), 1.48 (d, 12H, CH(CH_3)$_2$ of Me_2IPr, overlapping with signals of Tip_2Ge-Me_2IPr), 1.26 to 1.11, 1.06 to

0.84 (each m, overall 34H, Si(CH_2)$_7$CH_3 and CH(CH_3)$_2$ of Tip, overlapping with signals of Tip$_2$Ge-Me$_2$IPr), 0.76 to 0.64 (m, 6H, SiCH_3) ppm. **^{13}C{^{1}H} NMR** (100.61 MHz, C_6D_6, 300 K, TMS): δ = 177.68 to 177.20 (very weak multiplet, Me$_2$IPr-*C*), 154.68, 153.55, 153.29, 150.08, 146.46 to 146.28, 143.21, 141.01 (Tip*C* and Ph*C*), 125.80, 122.81, 121.81 (*C*CH3 of Me$_2$IPr), 121.44, 121.10 (Tip*C* and Ph*C*), 53.50 (broad, *C*H(CH$_3$)$_2$ of Me$_2$IPr), 47.70 (N*C*H$_3$), 37.89, 35.20 (Si(*C*H$_2$)$_7$CH$_3$), 34.73, 34.62, 32.59 to 32.38 (*C*H(CH$_3$)$_2$ of Tip), 31.97, 30.27, 30.09 (Si(*C*H$_2$)$_7$CH$_3$), 25.30 (Si(*C*H$_2$)$_7$CH$_3$), 25.12, 24.85 (CH(*C*H$_3$)$_2$ of Tip), 24.60 (Si(*C*H$_2$)$_7$CH$_3$), 24.45, 24.41, 24.30, 24.26, 24.21, 24.18 to 24.14, 23.17, 23.05 (CH(*C*H$_3$)$_2$ of Tip and Si(*C*H$_2$)$_7$CH$_3$), 14.43, 14.35 (Si(CH$_2$)$_7$*C*H$_3$), 10.06 (Me$_2$IPr-C*C*H$_3$), 2.37 to 0.96 (very weak multiplet, Si*C*H$_3$). **^{29}Si{^{1}H} NMR** (79.49 MHz, C_6D_6, 300 K, TMS): −7.16 (broad) ppm.

2.15 Reaction of bis(digermene) 2b with Me$_2$IPr

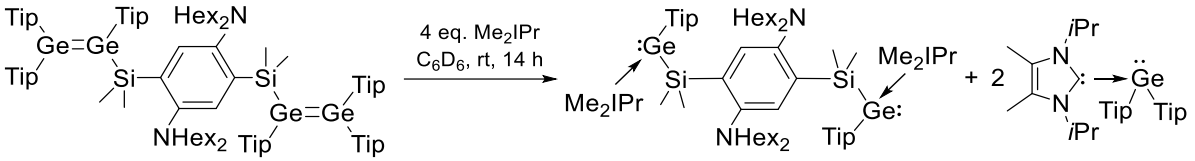

2b **5b**

Me$_2$IPr (17.5 mg, 96.8 µmol, 4 eq.) is dissolved in 0.2 mL of C_6D_6 and added to a solution of bis(digermene) **2b** (50.0 mg, 24.2 µmol, 1 eq.) in 0.3 mL of C_6D_6. Complete consumption of bis(digermene) **2b** is confirmed by ^{1}H NMR spectroscopy after 1 hour and full conversion to the bis(germylene)-NHC adduct and Tip$_2$Ge-Me$_2$IPr[S17] is revealed by heteronuclear NMR spectroscopy after 14 hours.

^{1}H NMR (400.13 MHz, C_6D_6, 300 K, TMS): δ = 7.66, 7.57 (each s, 2H, Ph*H*), 7.09 (s, 4H, Tip*H*), 6.33 to 5.20 (brm, 2.5H (should be 4H, but peak is exceptionally broad), C*H*(CH$_3$)$_2$ of Me$_2$IPr, overlapping with signals of Tip$_2$Ge-Me$_2$IPr), 4.68 to 3.76 (m, 4H, C*H*(CH$_3$)$_2$ of Tip, overlapping with signals of Tip$_2$Ge-Me$_2$IPr), 3.38 to 3.18, 3.17 to 3.00 (each m, each 4H, NC*H*$_2$), 2.95 to 2.84 (m, 2H, C*H*(CH$_3$)$_2$ of Tip, overlapping with signals of Tip$_2$Ge-Me$_2$IPr), 1.69 (s, 12H, Me$_2$IPr-CC*H*$_3$, overlapping with signals of Tip$_2$Ge-Me$_2$IPr), 1.35 to 1.31 (m, 12H, CH(C*H*$_3$)$_2$ of Me$_2$IPr, overlapping with signals of Tip$_2$Ge-Me$_2$IPr), 1.26 to 1.13, 1.05 to 0.90 (each m, overall 88H, N(C*H*$_2$)$_5$*C*H$_3$, CH(C*H*$_3$)$_2$ of Tip, overlapping with signals of Tip$_2$Ge-Me$_2$IPr), 0.79 (m, 12H, Si(C*H*$_3$)$_2$, overlapping with signals of Tip$_2$Ge-Me$_2$IPr) ppm. **^{13}C{^{1}H} NMR** (100.61 MHz, C_6D_6, 300 K, TMS): δ = 177.57, 177.55 (Me$_2$IPr-*C*), 153.50, 153.31, 153.25, 151.11, 151.09, 150.05, 146.28, 143.17, 141.49, 132.14, 131.96 (Tip*C* and Ph*C*), 125.84, 125.82 (*C*CH3 of Me$_2$IPr), 122.81, 121.79 (Tip*C* and Ph*C*), 55.36, 55.26 (*C*H(CH$_3$)$_2$ of Me$_2$IPr), 53.51 (N*C*H$_2$(CH$_2$)$_4$CH$_3$), 37.91, 37.73, 34.67, 34.61, 32.64, 32.61 (*C*H(CH$_3$)$_2$ of Tip), 31.98 (NCH$_2$*C*H$_2$(CH$_2$)$_3$CH$_3$), 28.13, 27.09, 27.02, 25.21, 25.12, 24.86, 24.69, 24.66, 24.40, 24.31, 24.22, 24.10 (CH(*C*H$_3$)$_2$ of Tip), 23.38 (N(CH$_2$)$_2$(*C*H$_2$)$_3$CH$_3$), 14.47, 14.38 (N(CH$_2$)$_5$*C*H$_3$), 10.22 (Me$_2$IPr-C*C*H$_3$), 5.37, 5.31, 4.30, 4.12 (Si(*C*H$_3$)$_2$) ppm. **^{29}Si{^{1}H} NMR** (79.49 MHz, C_6D_6, 300 K, TMS): −9.83, −9.94 ppm.

3. Characterization of dibromophenylene and chlorosilane precursors

3.1 X-Ray crystallographic data

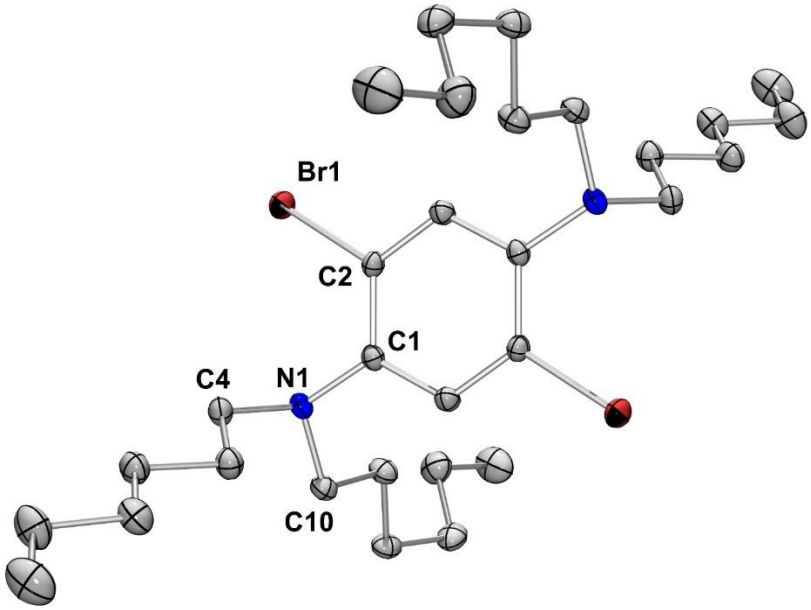

Figure S1. Molecular structure of 1,4-dibromo-2,5-*N*,*N*,*N'*,*N'*-tetrahexylphenylenediamine in the solid state.[S31] Hydrogen atoms omitted for clarity. Thermal ellisoids are shown at 50% probability. Selected bond lengths (in Å) and angles (in °): Br1-C2 1.897(1), C1-N1-C4 113.68(8), C1-N1-C10 116.51(9), C4-N1-C10 114.17(9), $\Sigma°_N$ 344.4(3).

All non H-atoms were located in the electron density maps and refined anisotropically. C-bound H atoms were placed in positions of optimized geometry and treated as riding atoms. Their isotropic displacement parameters were coupled to the corresponding carrier atoms by a factor of 1.2 (CH, CH_2) or 1.5 (CH_3).

Table S1. Crystal Data and Structure Refinement for 1,4-dibromo-2,5-*N*,*N*,*N'*,*N'*-tetrahexylphenylenediamine (CCDC 2358520).[S31]

Identification code	sh4388_a	
Empirical formula	C30 H54 Br2 N2	
Formula weight	602.57	
Temperature	132(2) K	
Wavelength	0.71073 Å	
Crystal system	Triclinic	
Space group	P-1	
Unit cell dimensions	a = 7.7250(4) Å	α= 112.1870(10)°.
	b = 9.5301(5) Å	β= 98.2070(10)°.
	c = 11.6862(6) Å	γ = 97.0940(10)°.
Volume	773.56(7) Å^3	
Z	1	
Density (calculated)	1.293 mg/m^3	
Absorption coefficient	2.639 mm^{-1}	
F(000)	318	
Crystal size	0.44 x 0.34 x 0.19 mm^3	
Theta range for data collection	1.923 to 30.548°	
Index ranges	-11≤h≤11, -13≤k≤13, -16≤l≤16	
Reflections collected	18891	
Independent reflections	4727 [R(int) = 0.0195]	
Completeness to theta = 25.242°	99.8 %	
Absorption correction	Semi-empirical from equivalents	
Max. and min. transmission	0.7461 and 0.6020	
Refinement method	Full-matrix least-squares on F^2	
Data / restraints / parameters	4727 / 0 / 156	
Goodness-of-fit on F^2	1.076	
Final R indices [I>2σ(I)]	R1 = 0.0198, wR2 = 0.0501	
R indices (all data)	R1 = 0.0224, wR2 = 0.0508	
Extinction coefficient	n/a	
Largest diff. peak and hole	0.460 and -0.309 e · Å^{-3}	

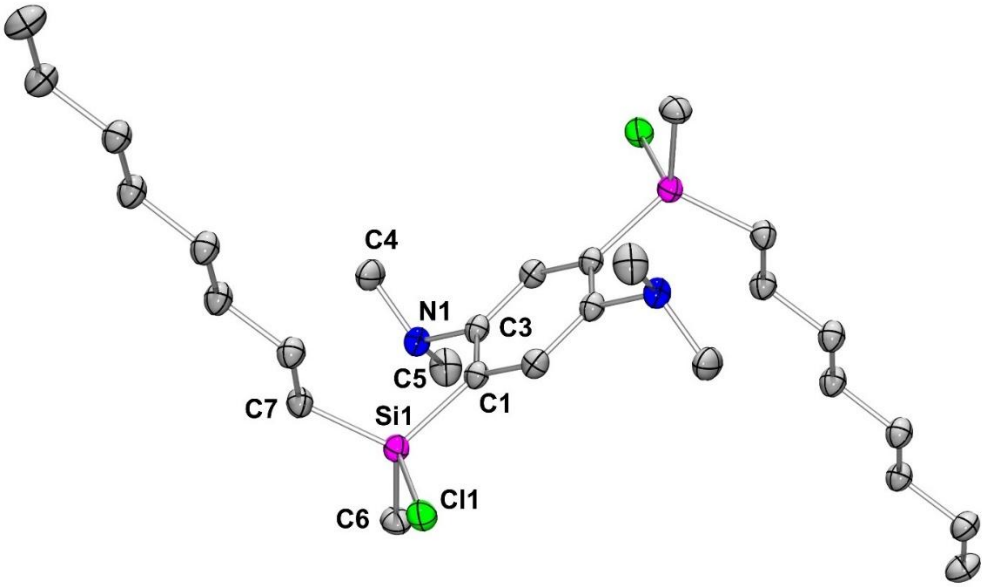

Figure S2. Molecular structure of bis(chlorosilyl)diaminobenzene **1a** in the solid state.[S31] Hydrogen atoms omitted for clarity. Thermal ellisoids are shown at 50% probability. Selected bond lengths (in Å) and angles (in °): Si1-Cl1 2.1207(6), Si1-C1 1.875(2), Si1-C6 1.864(2), Si1-C7 1.857(2), N1-C3 1.449(2), N1-C5 1.465(2), N1-C4 1.466(2), C1-Si1-Cl1 105.95(6), C1-Si1-C6 115.48(8), C1-Si1-C7 112.34(7), C7-Si1-C6 113.69(8), C3-N1-C4 111.7(1), C3-N1-C5 112.5(1), C4-N1-C5 110.6(1), $\Sigma°_{Si1}$ 341.5(2), $\Sigma°_{N1}$ 334.8(3).

All non H-atoms were located in the electron density maps and refined anisotropically. C-bound H atoms were placed in positions of optimized geometry and treated as riding atoms. Their isotropic displacement parameters were coupled to the corresponding carrier atoms by a factor of 1.2 (CH, CH_2) or 1.5 (CH_3).

Table S2. Crystal Data and Structure Refinement for **1a** (CCDC 2358528).[S31]

Identification code	sh5557_a	
Empirical formula	C28 H54 Cl2 N2 Si2	
Formula weight	545.81	
Temperature	130(2) K	
Wavelength	0.71073 Å	
Crystal system	Triclinic	
Space group	$P\bar{1}$	
Unit cell dimensions	a = 6.8159(2) Å	α= 74.5480(10)°.
	b = 8.9406(3) Å	β= 83.2020(10)°.
	c = 13.9887(4) Å	γ = 82.5440(10)°.
Volume	811.55(4) $Å^3$	
Z	1	
Density (calculated)	1.117 mg/m^3	
Absorption coefficient	0.292 mm^{-1}	
F(000)	298	
Crystal size	0.180 x 0.160 x 0.080 mm^3	
Theta range for data collection	2.376 to 27.138°	
Index ranges	-8≤h≤8, -11≤k≤11, -17≤l≤17	
Reflections collected	16669	
Independent reflections	3450 [R(int) = 0.0302]	
Completeness to theta = 25.242°	96.3 %	
Absorption correction	Semi-empirical from equivalents	
Max. and min. transmission	0.7455 and 0.6722	
Refinement method	Full-matrix least-squares on F^2	
Data / restraints / parameters	3450 / 0 / 158	
Goodness-of-fit on F^2	1.047	
Final R indices [I>2σ(I)]	R1 = 0.0360, wR2 = 0.0923	
R indices (all data)	R1 = 0.0424, wR2 = 0.0973	
Extinction coefficient	n/a	
Largest diff. peak and hole	0.402 and -0.392 e · $Å^{-3}$	

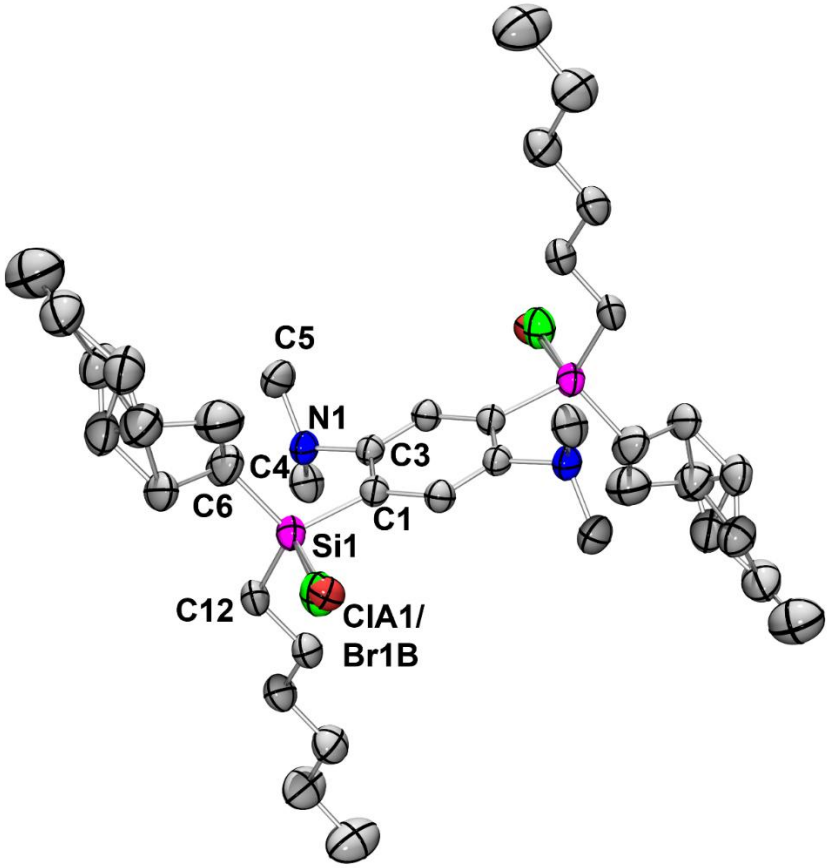

Figure S3. Molecular structure of 1,4-Dibromo-2,5-*N*,*N*,*N'*,*N'*-tetrahexylphenylenediamine in the solid state.[S31] Hydrogen atoms omitted for clarity. Thermal ellisoids are shown at 50% probability. Selected bond lengths (in Å) and angles (in °): Si1-Cl1A 2.122(3), Si1-Br1B 2.243(9), Si1-C1 1.888(2), Si1-C6 1.867(2), Si1-C12 1.880(2), N1-C3 1.458(2), N1-C5 1.473(3), N1-C4 1.469(3), C1-Si1-Cl1A 105.4(1), C1-Si1-Br1B 102.7(5), C1-Si1-C6 114.4(1), C1-Si1-C12 111.5(1), C12-Si1-C6 114.4(1), C3-N1-C4 113.1(2), C3-N1-C5 111.5(2), C4-N1-C5 110.8(2), Σ°(Si1) 340.3(3), Σ°(N1) 335.4(6).

All non H-atoms were located in the electron density maps and refined anisotropically. C-bound H atoms were placed in positions of optimized geometry and treated as riding atoms. Their isotropic displacement parameters were coupled to the corresponding carrier atoms by a factor of 1.2 (CH, CH_2) or 1.5 (CH_3). *Disorder*: The Si1 bonded Cl1a atom shares its position with Br1b (fvar 2: 0.91/0.09) and a part of the Si1 bonded hexyl residue is split over two positions (fvar 3: 0.83/0.17). DFIX restraints 2.09(0.01) Å and 2.24(0.01) Å were used for the Si1-Cl1a and Si1-Br1b distances, respectively.

Table S3. Crystal Data and Structure Refinement for 1,4-Dibromo-2,5-*N*,*N*,*N'*,*N'*-tetrahexylphenylenediamine (CCDC 2358523).[S31]

Identification code	sh4293a	
Empirical formula	C34 H66 Br0.18 Cl1.82 N2 Si2	
Formula weight	638.10	
Temperature	232(2) K	
Wavelength	0.71073 Å	
Crystal system	Triclinic	
Space group	$P\bar{1}$	
Unit cell dimensions	a = 8.559(6) Å	α= 103.51(3)°.
	b = 10.729(8) Å	β= 107.34(3)°.
	c = 12.406(10) Å	γ = 104.27(2)°.
Volume	994.1(13) Å^3	
Z	1	
Density (calculated)	1.066 mg/m^3	
Absorption coefficient	0.418 mm^{-1}	
F(000)	349	
Crystal size	0.412 x 0.335 x 0.267 mm^3	
Theta range for data collection	1.823 to 28.865°	
Index ranges	-10≤h≤11, -14≤k≤13, -16≤l≤15	
Reflections collected	16279	
Independent reflections	5110 [R(int) = 0.0236]	
Completeness to theta = 25.242°	100.0 %	
Absorption correction	Semi-empirical from equivalents	
Max. and min. transmission	0.7458 and 0.6822	
Refinement method	Full-matrix least-squares on F^2	
Data / restraints / parameters	5110 / 96 / 223	
Goodness-of-fit on F^2	1.041	
Final R indices [I>2σ(I)]	R1 = 0.0493, wR2 = 0.1375	
R indices (all data)	R1 = 0.0691, wR2 = 0.1524	
Extinction coefficient	n/a	
Largest diff. peak and hole	0.482 and -0.537 e · Å^{-3}	

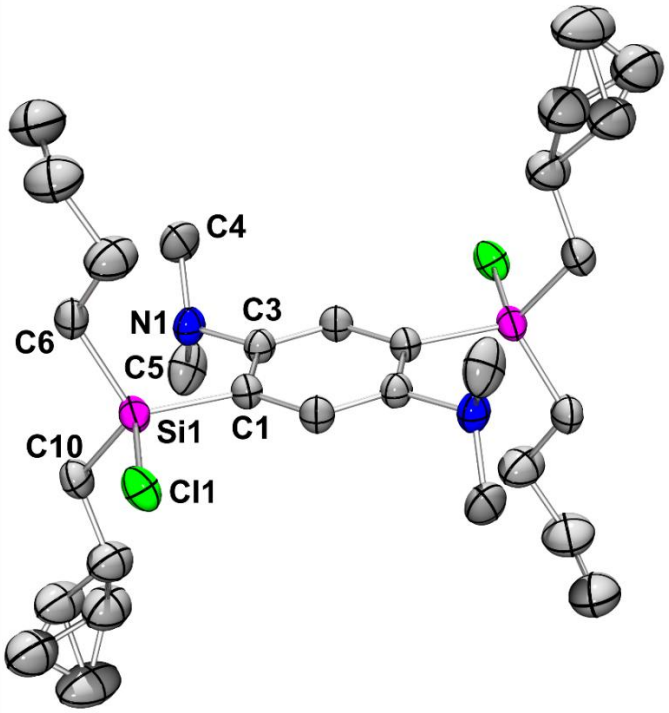

Figure S4. Molecular structure of 1,4-Dibromo-2,5-*N*,*N*,*N'*,*N'*-tetrabutylphenylenediamine in the solid state.[S31] Hydrogen atoms omitted for clarity. Thermal ellisoids are shown at 50% probability. Selected bond lengths (in Å) and angles (in °): Si1-Cl1 2.131(3), Si1-C1 1.891(3), Si1-C6 1.852(3), Si1-C10 1.863(3), N1-C3 1.459(2), N1-C5 1.461(3), N1-C4 1.451(3), C1-Si1-Cl1 103.11(8), C1-Si1-C6 117.9(1), C1-Si1-C10 113.66(8), C10-Si1-C6 110.1(1), C3-N1-C4, 112.5(2), C3-N1-C5 113.6(2), C4-N1-C5 110.6(2), $\Sigma°_{Si1}$ 341.7(1), $\Sigma°_{N1}$ 336.7(6).

All non H-atoms were located in the electron density maps and refined anisotropically. C-bound H atoms were placed in positions of optimized geometry and treated as riding atoms. Their isotropic displacement parameters were coupled to the corresponding carrier atoms by a factor of 1.2 (CH, CH_2) or 1.5 (CH_3). *Disorder*: A part of the butyl-residue on Si1 is split over two positions (fvar 2: 0.90/0.10).

Table S4. Crystal Data and Structure Refinement for 1,4-bis(chlorodibutylsilyl)-2,5-*N*,*N*,*N'*,*N'*-tetramethylphenylenediamine (CCDC 2358519).[S31]

Identification code	sh4295	
Empirical formula	C26 H50 Cl2 N2 Si2	
Formula weight	517.76	
Temperature	213(2) K	
Wavelength	0.71073 Å	
Crystal system	Triclinic	
Space group	$P\bar{1}$	
Unit cell dimensions	a = 8.272(12) Å	α= 67.38(3)°.
	b = 9.672(15) Å	β= 72.18(4)°.
	c = 11.654(17) Å	γ = 69.63(4)°.
Volume	791(2) Å^3	
Z	1	
Density (calculated)	1.087 mg/m^3	
Absorption coefficient	0.297 mm^{-1}	
F(000)	282	
Crystal size	0.541 x 0.517 x 0.292 mm^3	
Theta range for data collection	1.932 to 27.404°	
Index ranges	-10≤h≤9, -12≤k≤12, -14≤l≤14	
Reflections collected	12881	
Independent reflections	3520 [R(int) = 0.0158]	
Completeness to theta = 25.242°	100.0 %	
Absorption correction	Semi-empirical from equivalents	
Max. and min. transmission	0.7455 and 0.6928	
Refinement method	Full-matrix least-squares on F^2	
Data / restraints / parameters	3520 / 66 / 169	
Goodness-of-fit on F^2	1.070	
Final R indices [I>2σ(I)]	R1 = 0.0392, wR2 = 0.1085	
R indices (all data)	R1 = 0.0443, wR2 = 0.1134	
Extinction coefficient	n/a	
Largest diff. peak and hole	0.587 and -0.246 e · Å^{-3}	

3.2 NMR spectroscopy

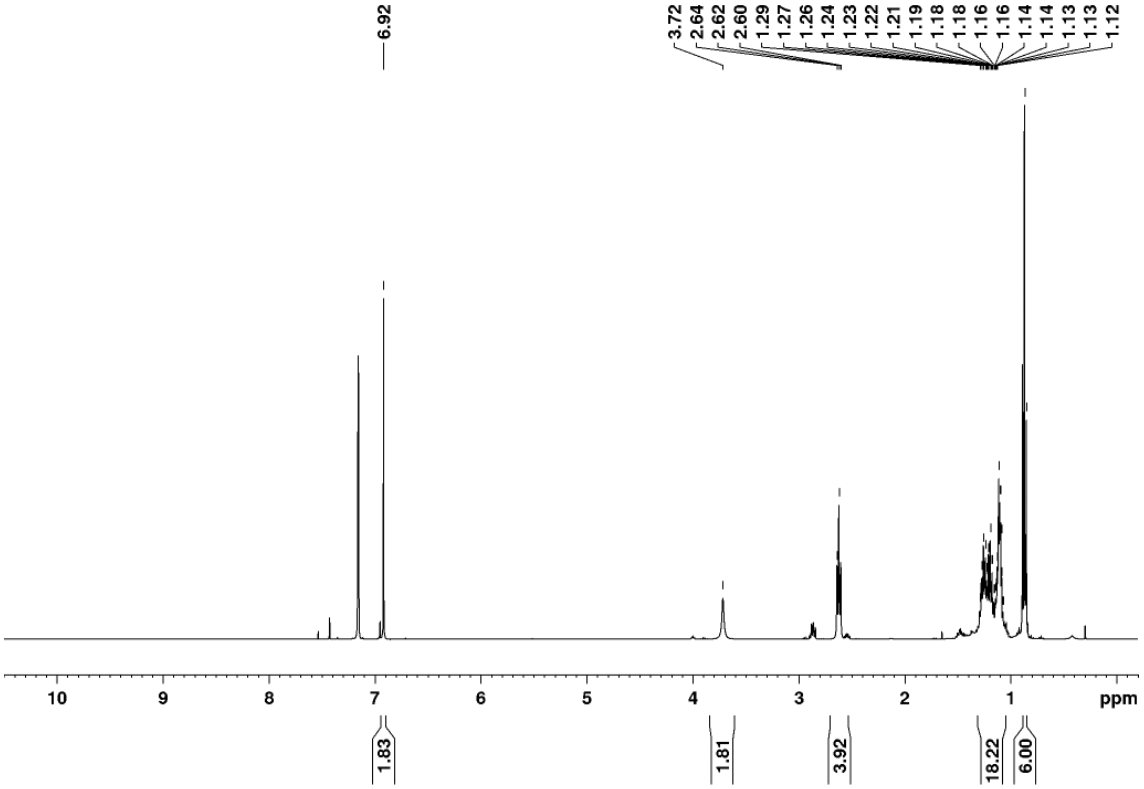

Figure S5. ^{1}H NMR spectrum of the reaction mixture containing 1,4-dibromo-2,5-*N*,*N*'-dihexylphenylenediamine.

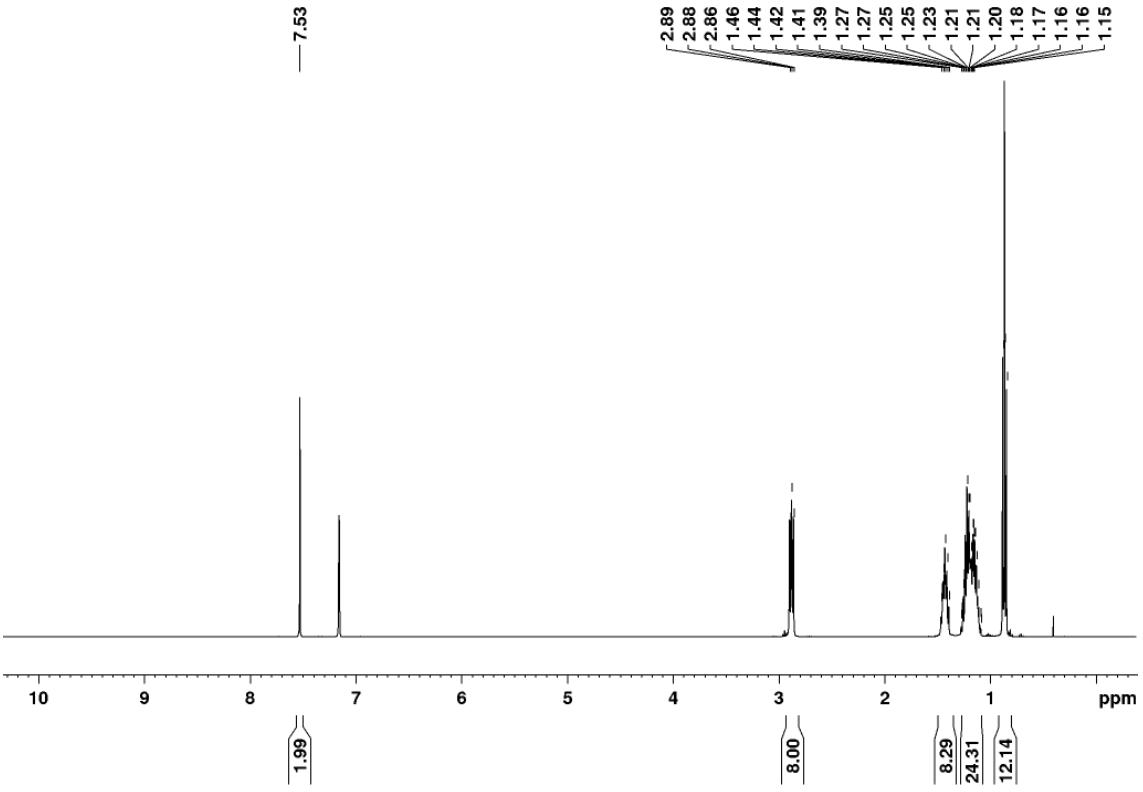

Figure S6. ^{1}H NMR spectrum of tetrahexylated diamine 1,4-dibromo-2,5-*N*,*N*,*N*',*N*'-tetrahexylphenylenediamine.

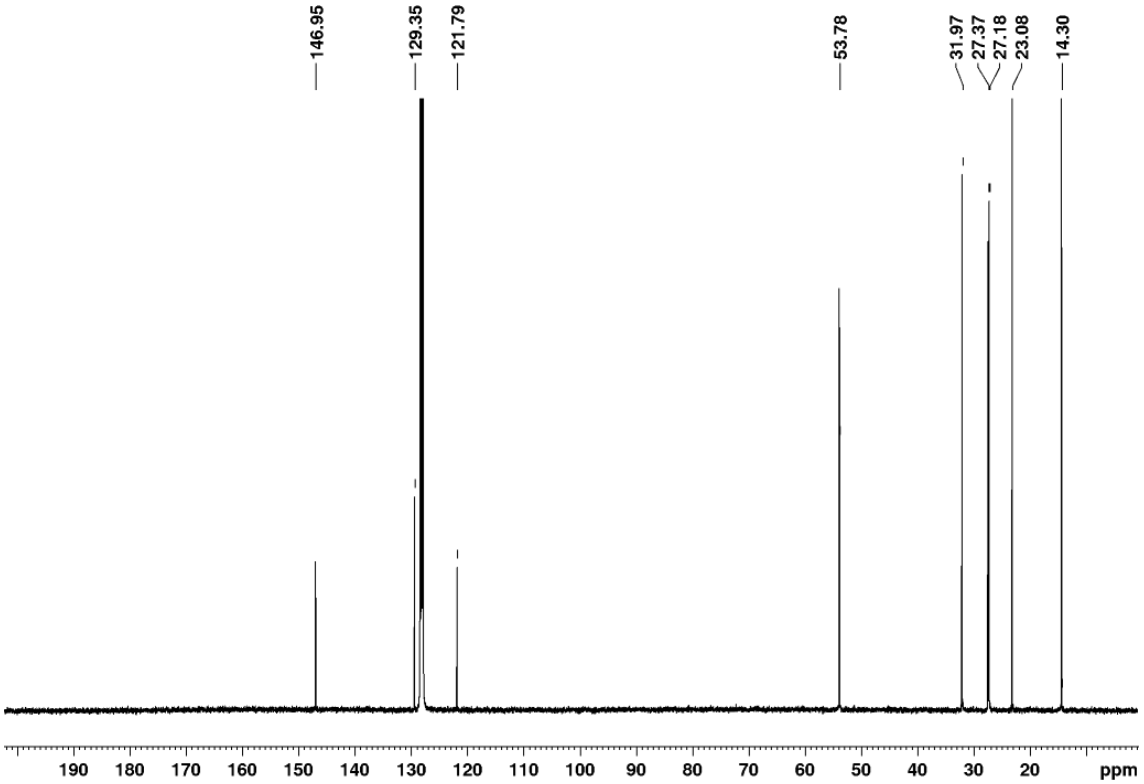

Figure S7. ^{13}C NMR spectrum of tetrahexylated diamine 1,4-dibromo-2,5-*N*,*N*,*N'*,*N'*-tetrahexylphenylenediamine.

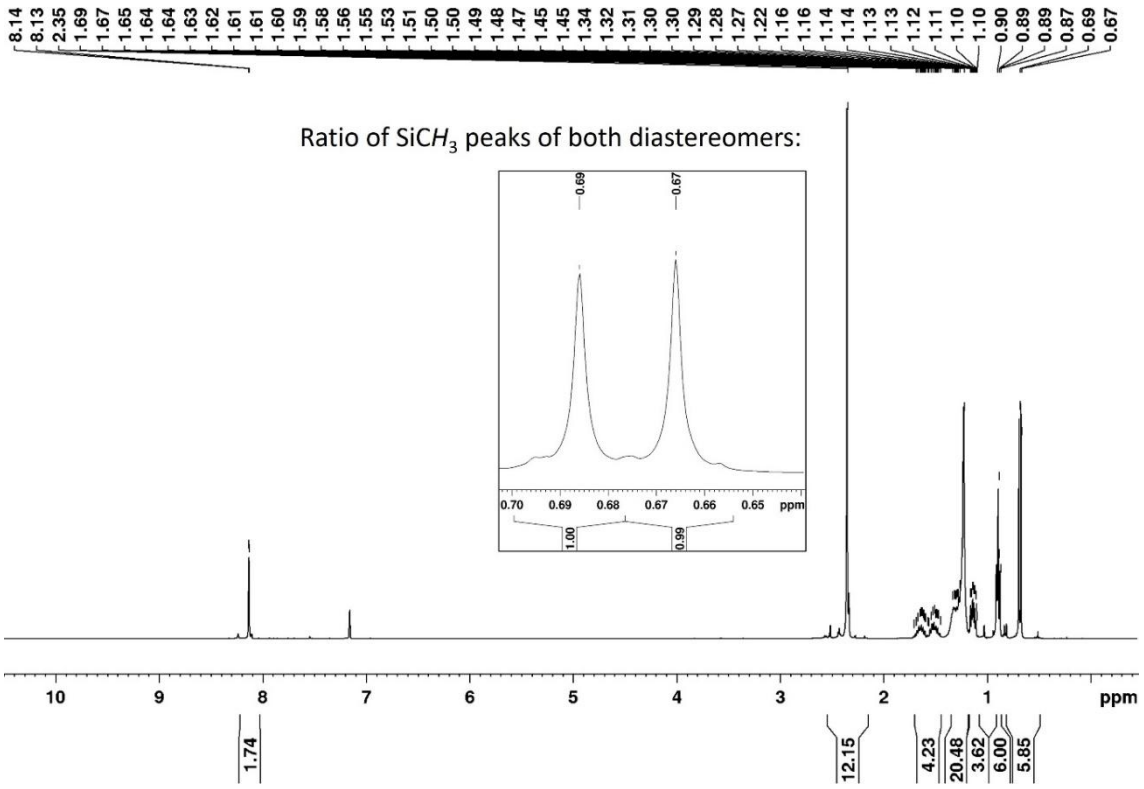

Figure S8. ^{1}H NMR spectrum of methyloctylchlorosilane **1a**.

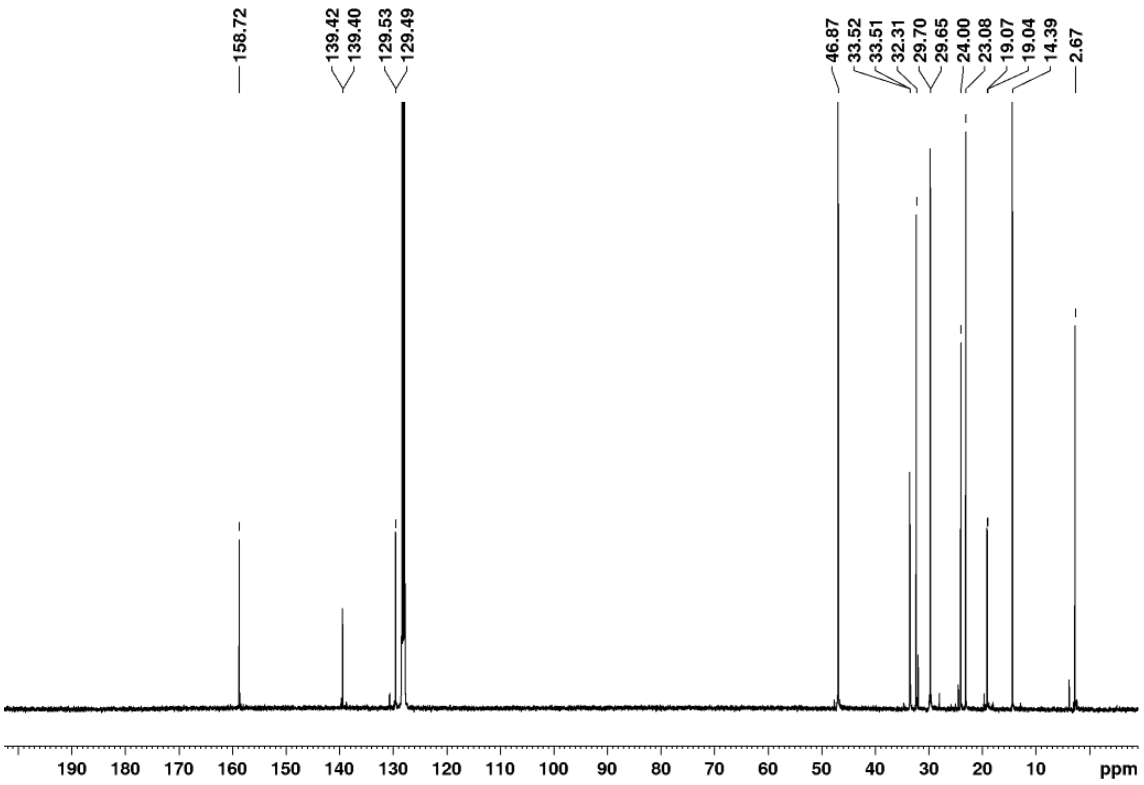

Figure S9. $^{13}C\{^{1}H\}$ NMR spectrum of methyloctylchlorosilane **1a**.

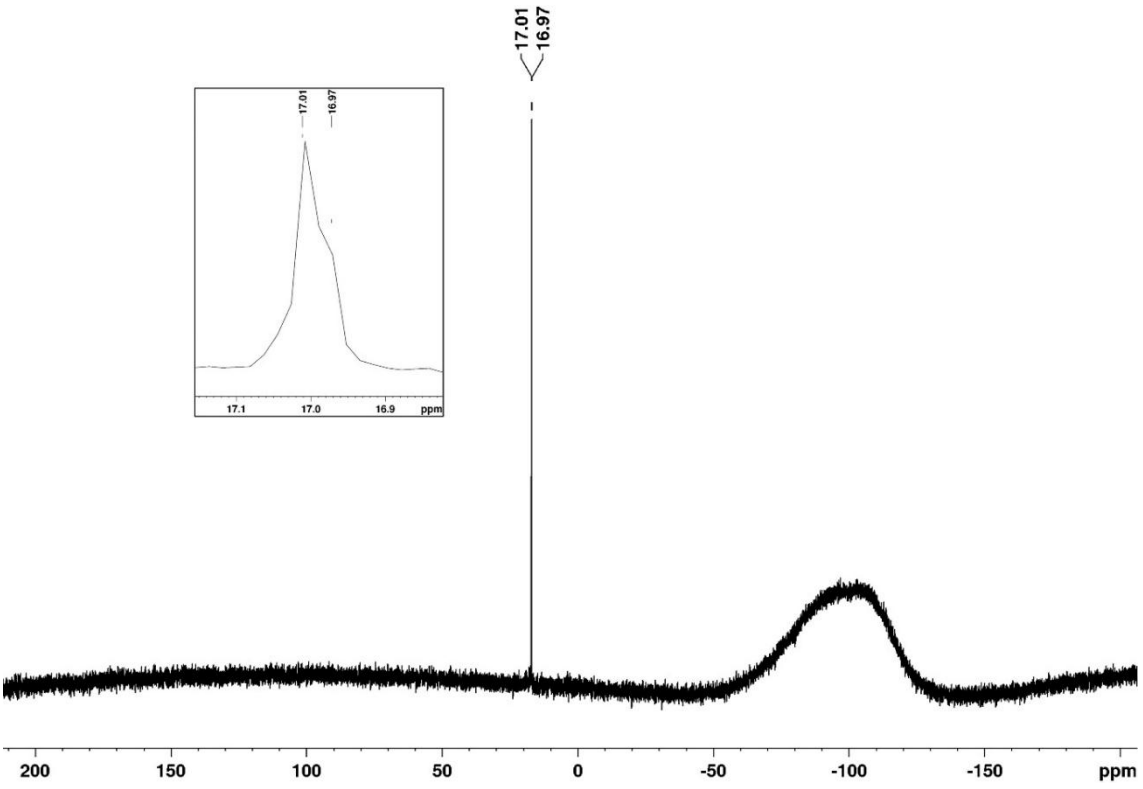

Figure S10. $^{29}Si\{^{1}H\}$ NMR spectrum of methyloctylchlorosilane **1a**.

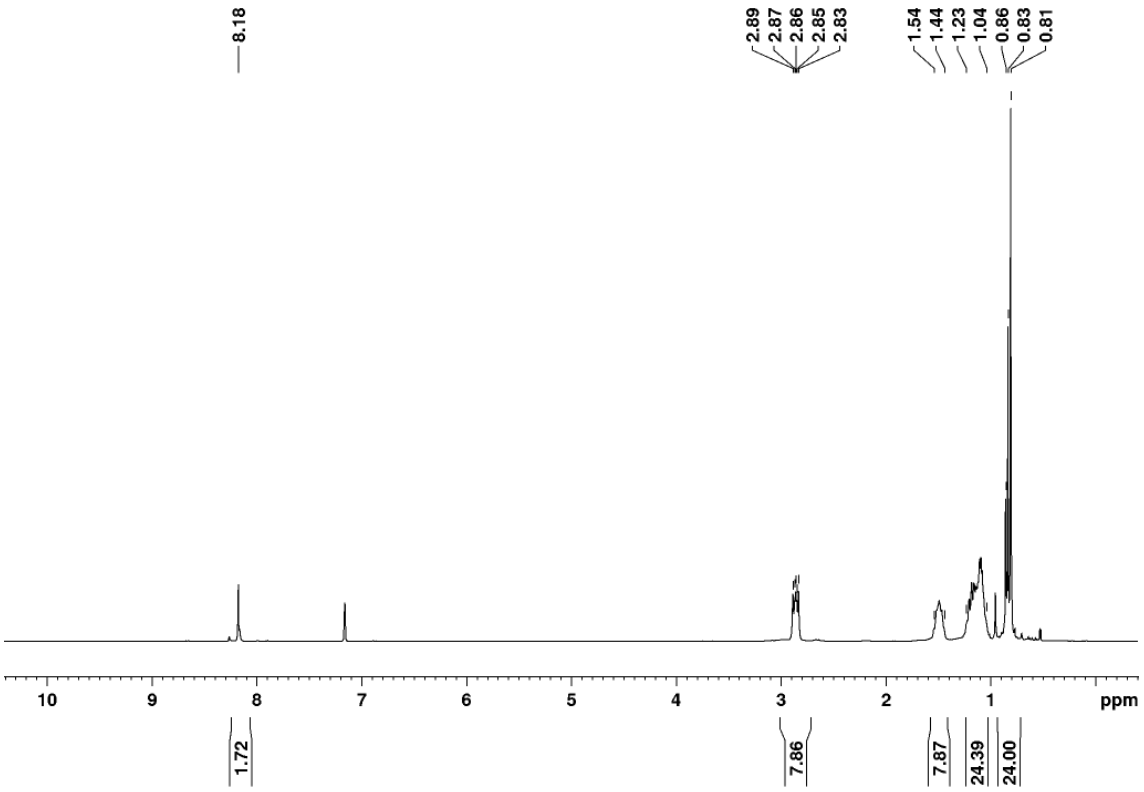

Figure S11. ^{1}H NMR spectrum of 2,5-bis(chlorodimethylsilyl)-*N,N,N',N'*-tetrahexylbenzene-1,4-diamine **1b**.

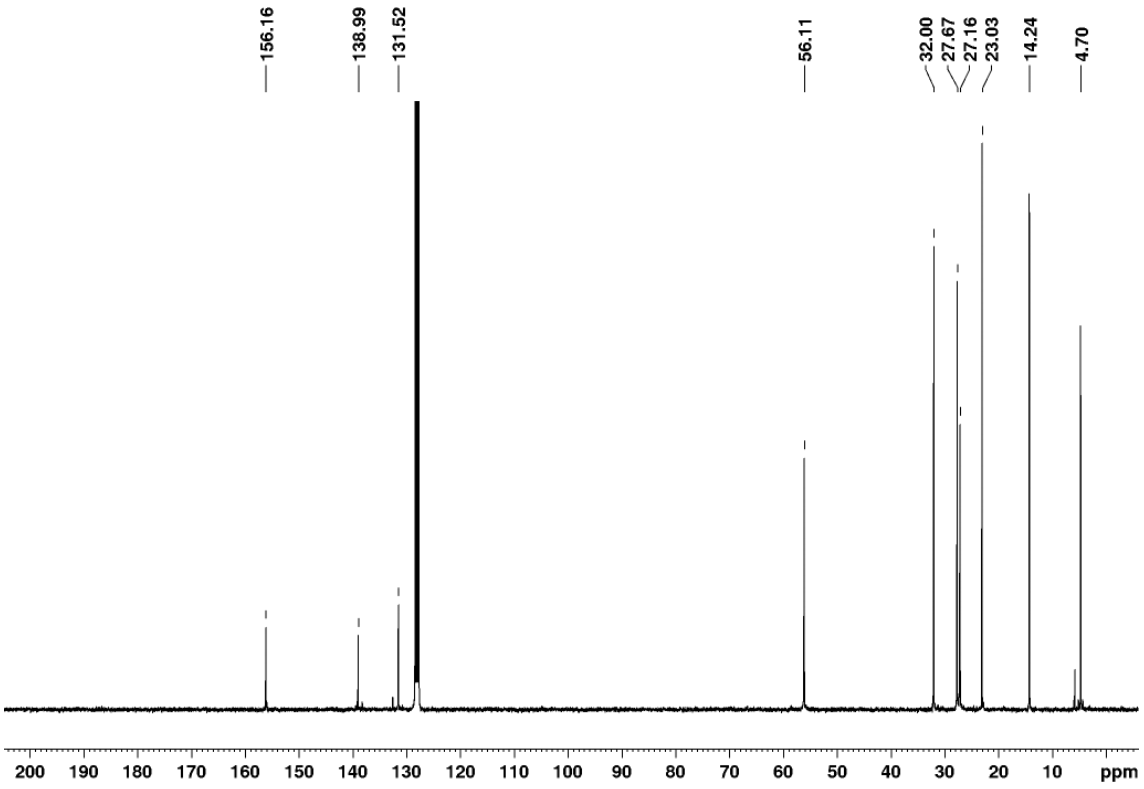

Figure S12. ^{13}C{^{1}H} NMR spectrum of 2,5-bis(chlorodimethylsilyl)-*N,N,N',N'*-tetrahexylbenzene-1,4-diamine **1b**.

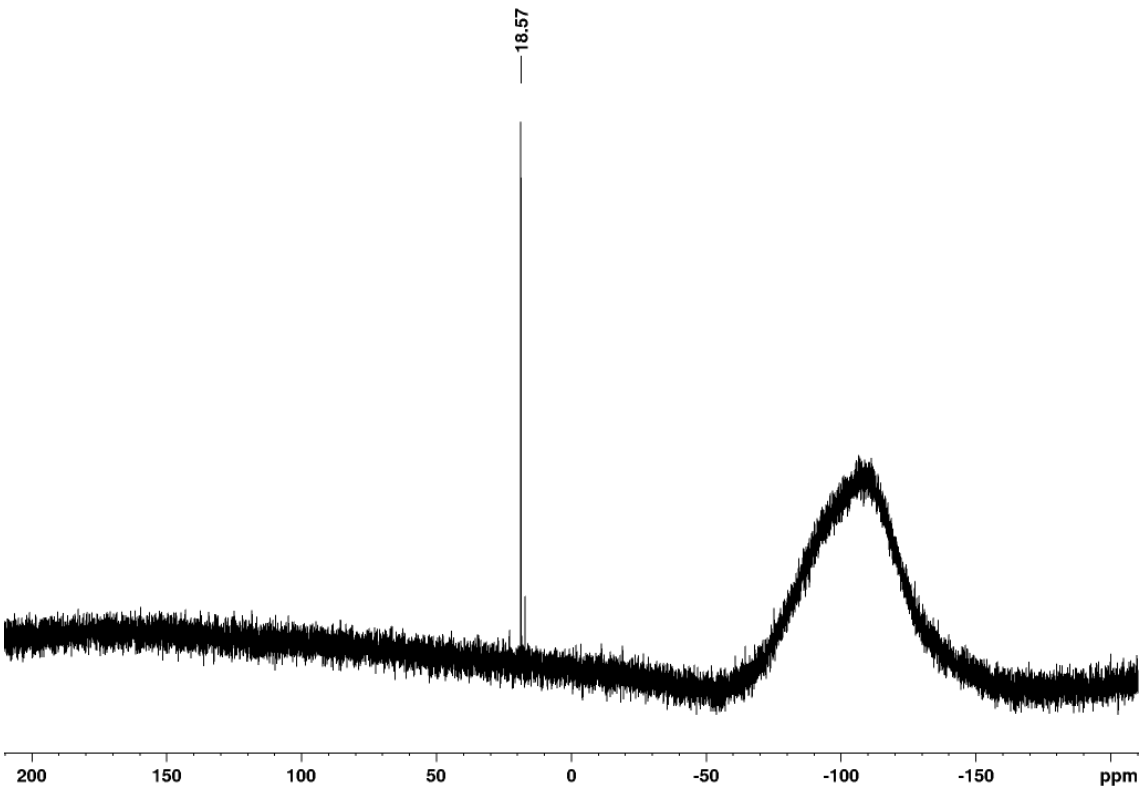

Figure S13. $^{29}Si\{^{1}H\}$ NMR spectrum of bis(chlorosilyl)diaminobenzene **1b**.

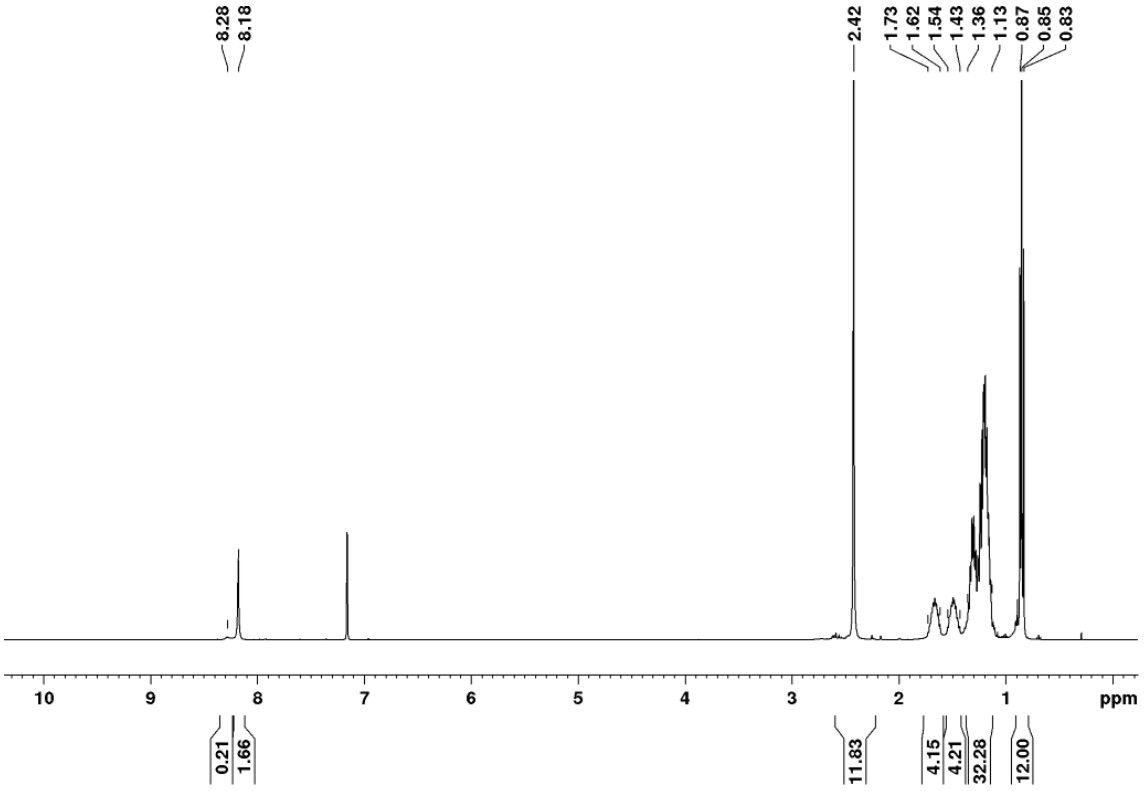

Figure S14. ^{1}H NMR spectrum of 1,4-bis(chlorodihexylsilyl)-2,5-*N*,*N*,*N'*,*N'*-tetramethyl-phenylenediamine (containing 13mol% 1,4-bis(bromodihexylsilyl)-2,5-*N*,*N*,*N'*,*N'*-tetramethyl-phenylenediamine).

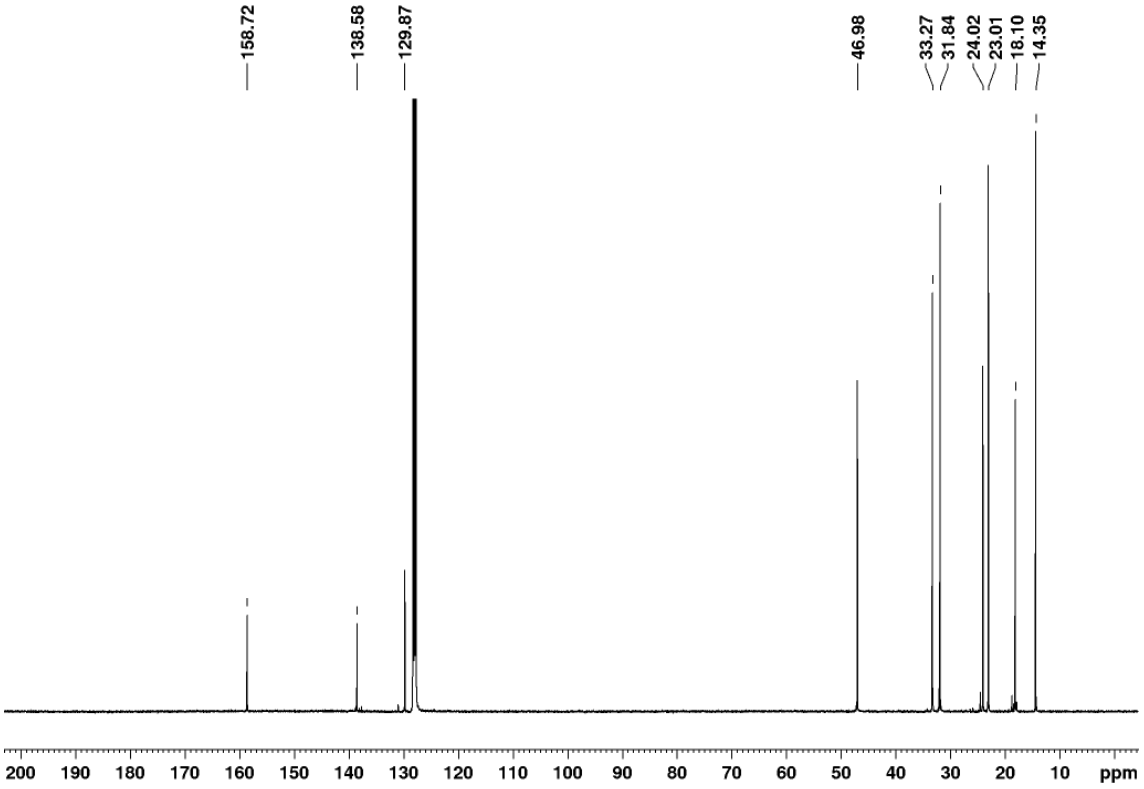

Figure S15. ^{13}C NMR spectrum of 1,4-bis(chlorodihexylsilyl)-2,5-*N*,*N*,*N'*,*N'*-tetramethyl-phenylenediamine.

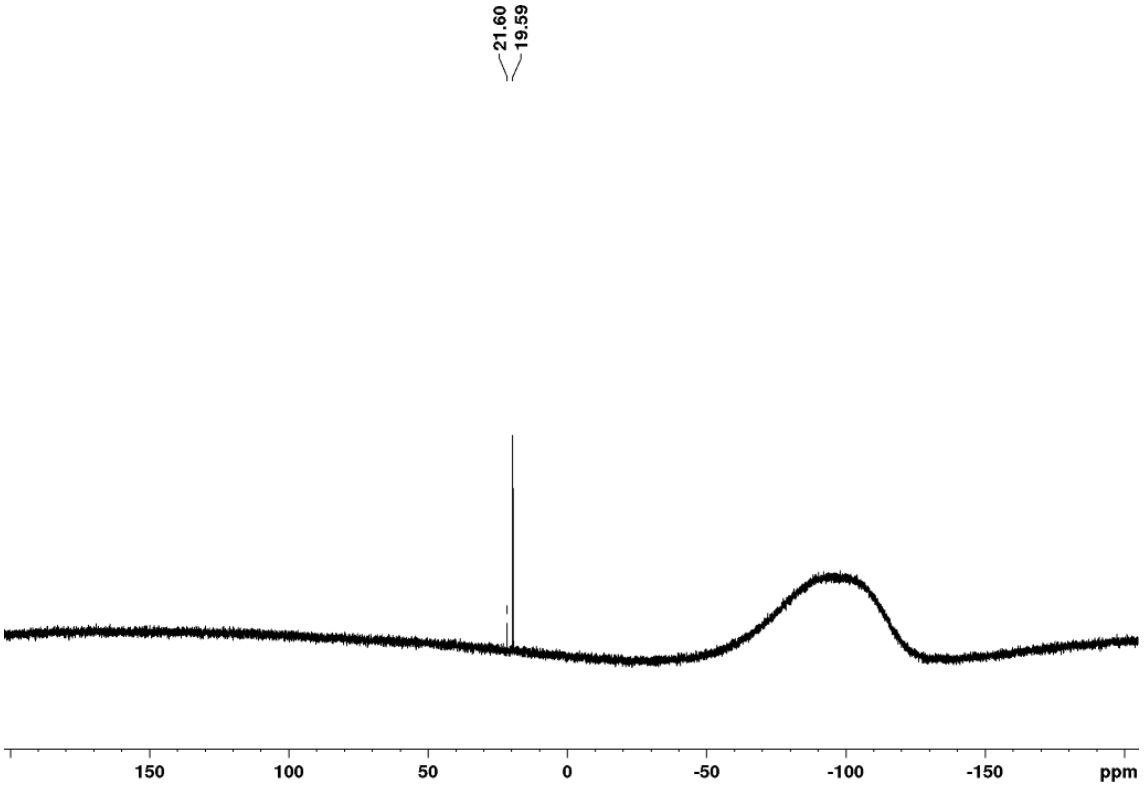

Figure S16. ^{29}Si NMR spectrum of 1,4-bis(chlorodihexylsilyl)-2,5-*N*,*N*,*N'*,*N'*-tetramethyl-phenylenediamine (containing 13mol% 1,4-bis(bromodihexylsilyl)-2,5-*N*,*N*,*N'*,*N'*-tetramethyl-phenylenediamine).

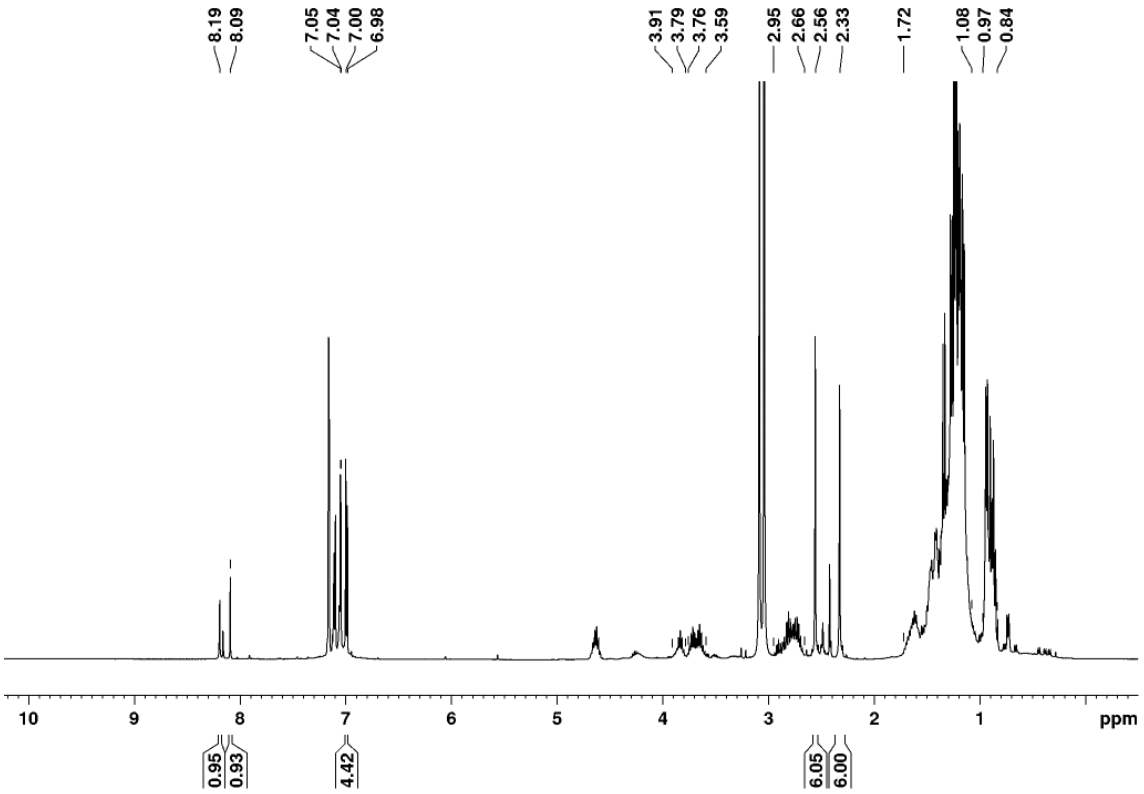

Figure S17. ^{1}H NMR spectrum of the reaction of 1,4-bis(chlorodihexylsilyl)-2,5-*N*,*N*,*N'*,*N'*-tetramethyl-phenylenediamine with $Tip_2Ge{=}GeTipLi{\cdot}dme_2$.

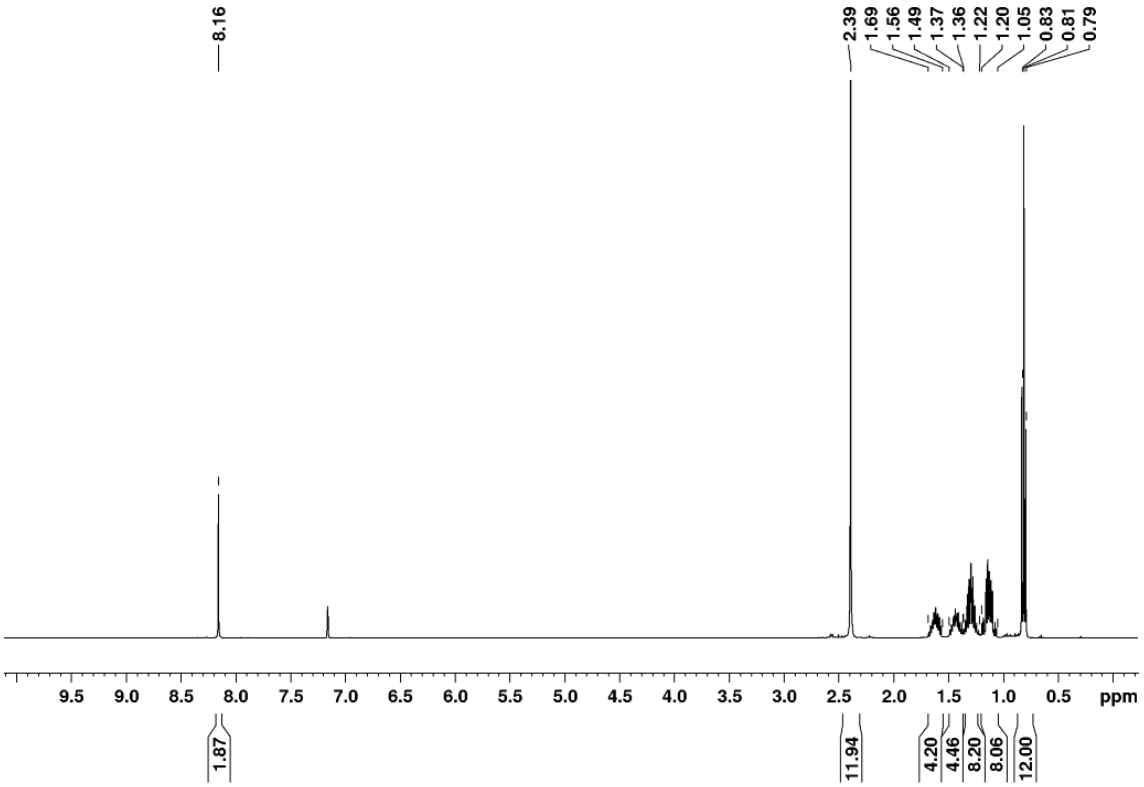

Figure S18. ^{1}H NMR spectrum of 1,4-bis(chlorodibutylsilyl)-2,5-*N*,*N*,*N'*,*N'*-tetramethyl-phenylenediamine.

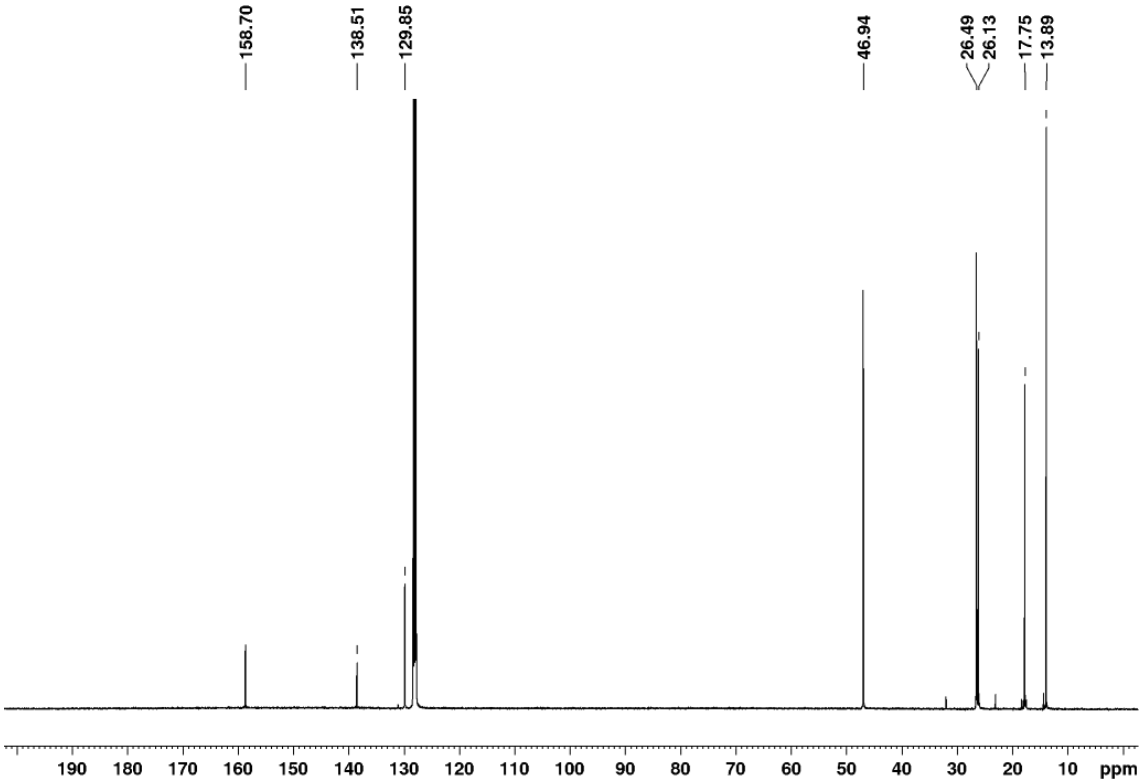

Figure S19. ^{13}C NMR spectrum of 1,4-bis(chlorodibutylsilyl)-2,5-*N*,*N*,*N'*,*N'*-tetramethyl-phenylenediamine.

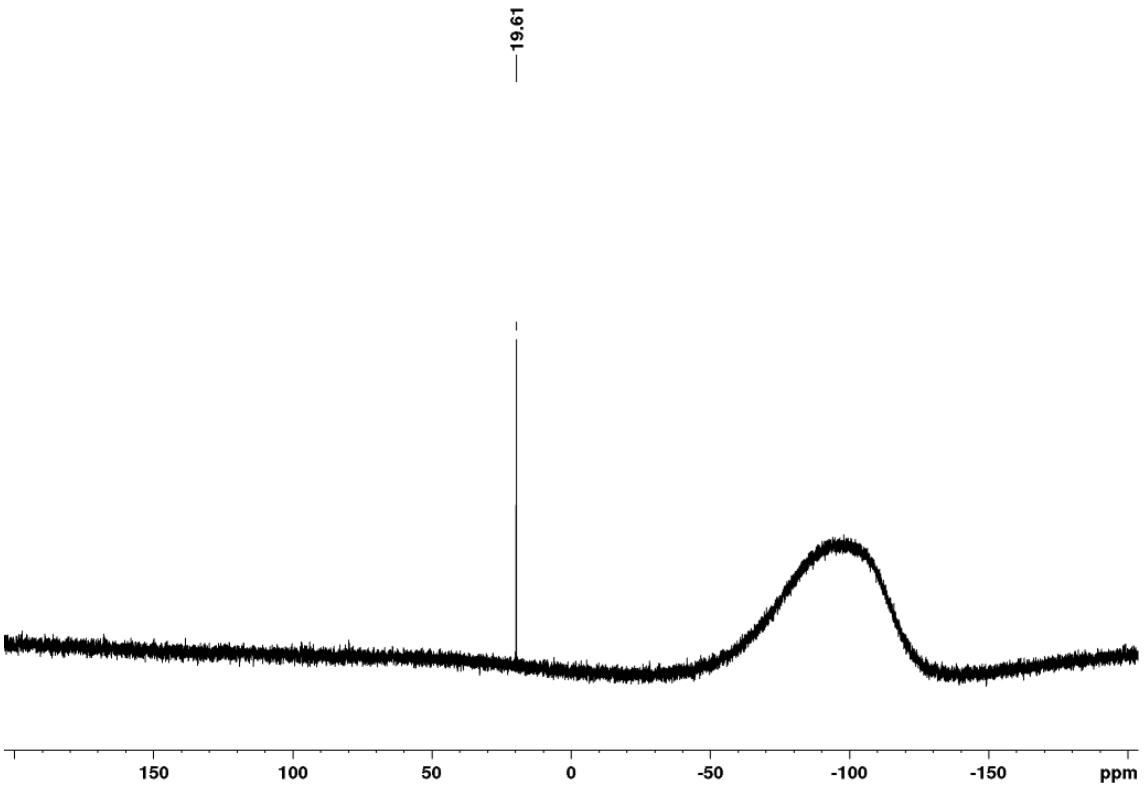

Figure S20. ^{29}Si NMR spectrum of 1,4-bis(chlorodibutylsilyl)-2,5-*N*,*N*,*N'*,*N'*-tetramethyl-phenylenediamine.

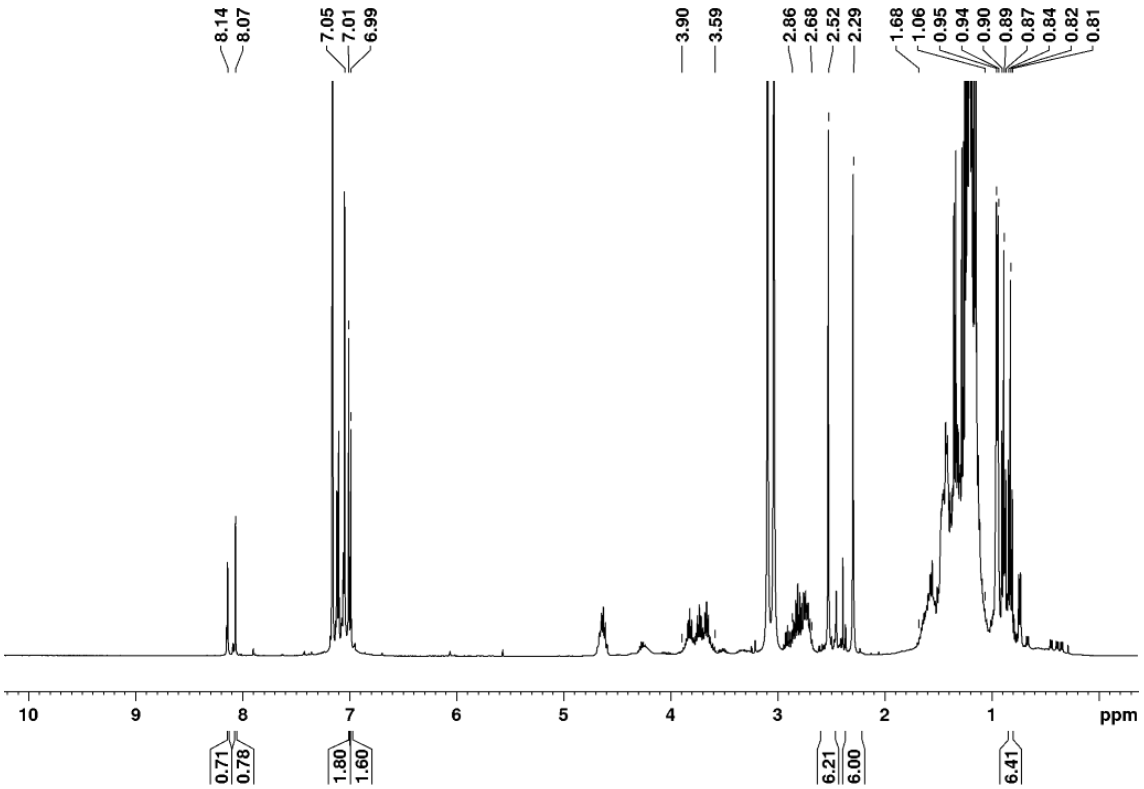

Figure S21. ^{1}H NMR spectrum of the reaction of 1,4-bis(chlorodibutylsilyl)-2,5-*N*,*N*,*N'*,*N'*-tetramethyl-phenylenediamine with $Tip_2Ge{=}GeTipLi{\cdot}dme_2$.

4. Characterization of bis(digermene) monomers

4.1 NMR spectroscopy

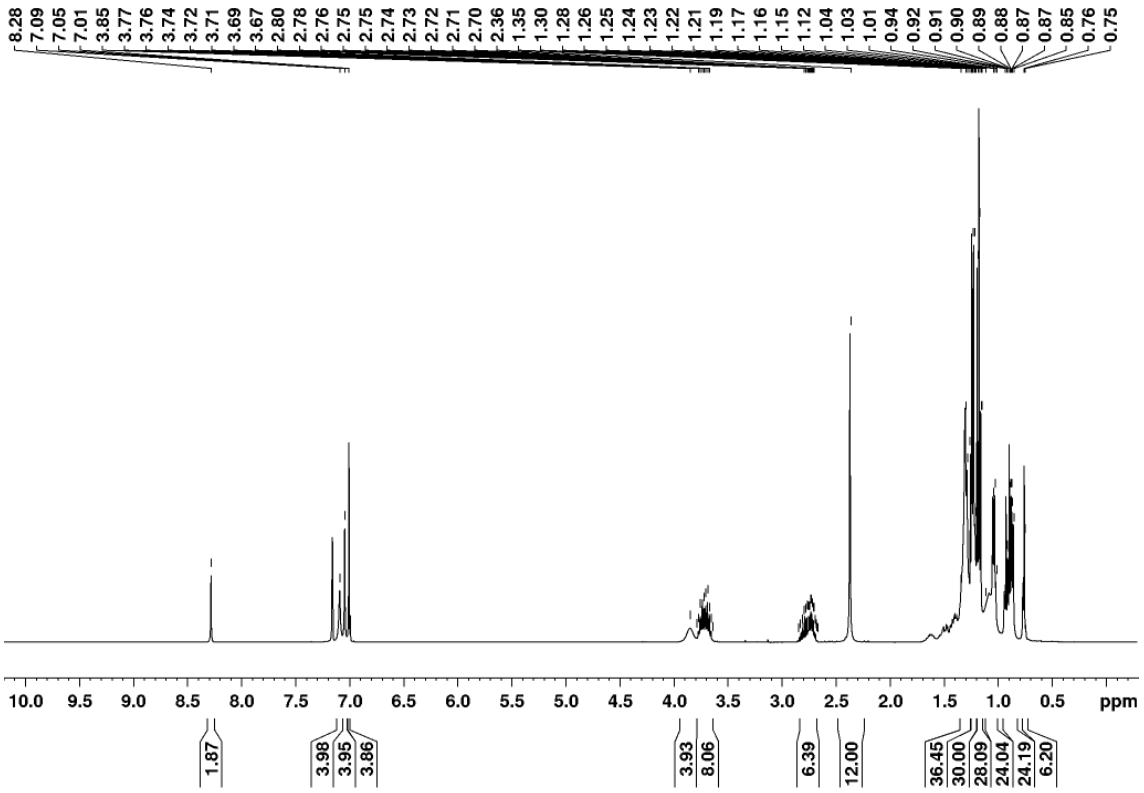

Figure S22. ^{1}H NMR spectrum of *Si*-octylated bis(digermene) **2a** in C_6D_6.

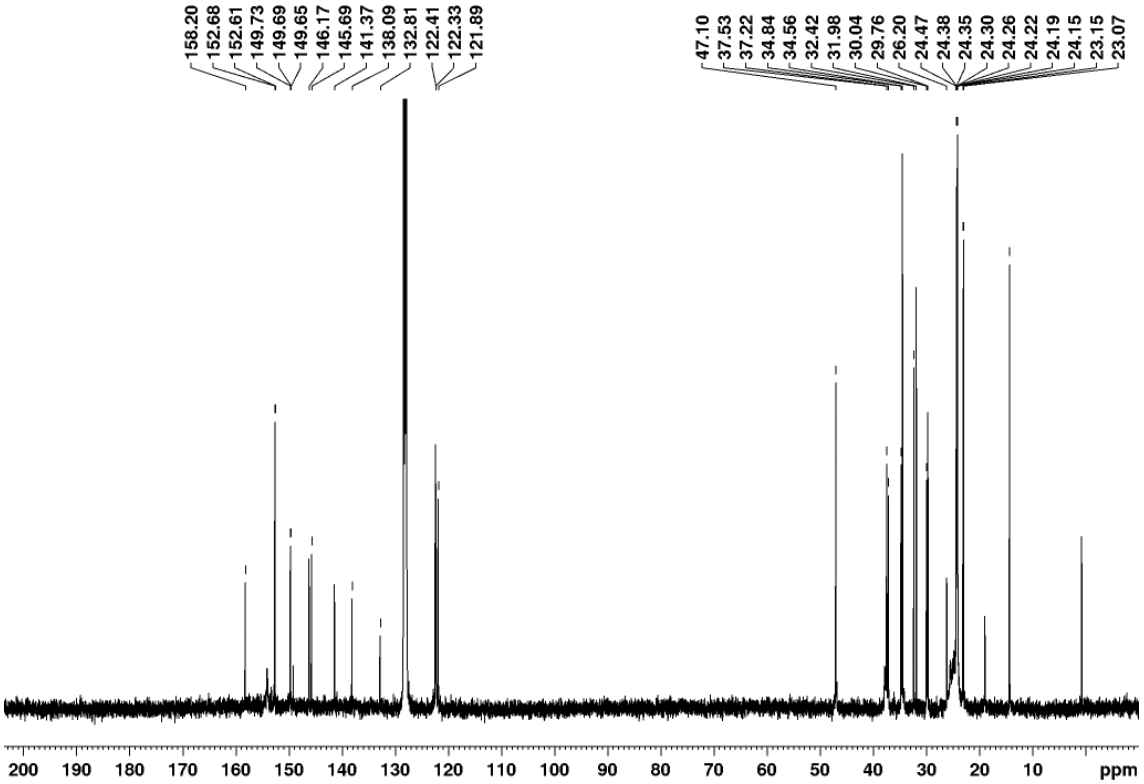

Figure S23. ^{13}C NMR spectrum of *Si*-octylated bis(digermene) **2a** in C_6D_6 (due to low amount of *(R,R)* isomer in the isolated crystalline sample, only signals of the *(R,S)* isomer are exhibited).

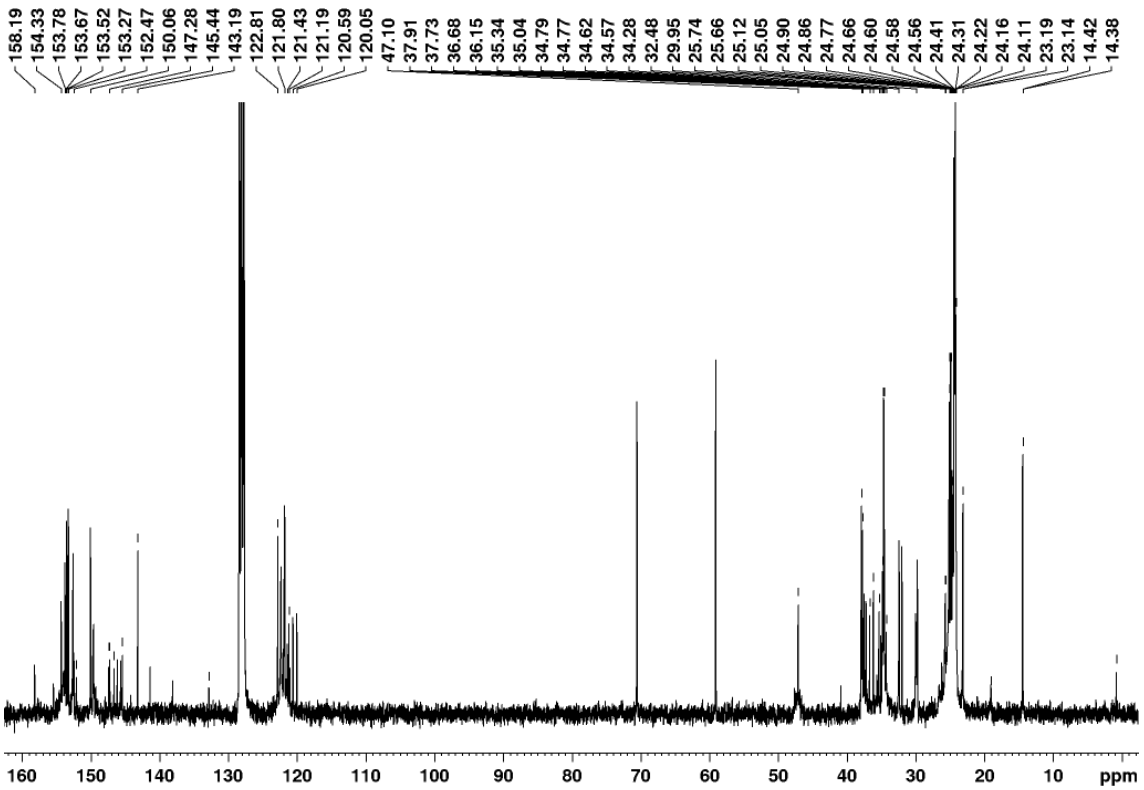

Figure S24. ^{13}C NMR spectrum of reaction mixture containing a diastereomeric mixture of *Si*-octylated bis(digermene) **2a** in C_6D_6 (only signals from *(R,R)* isomer picked).

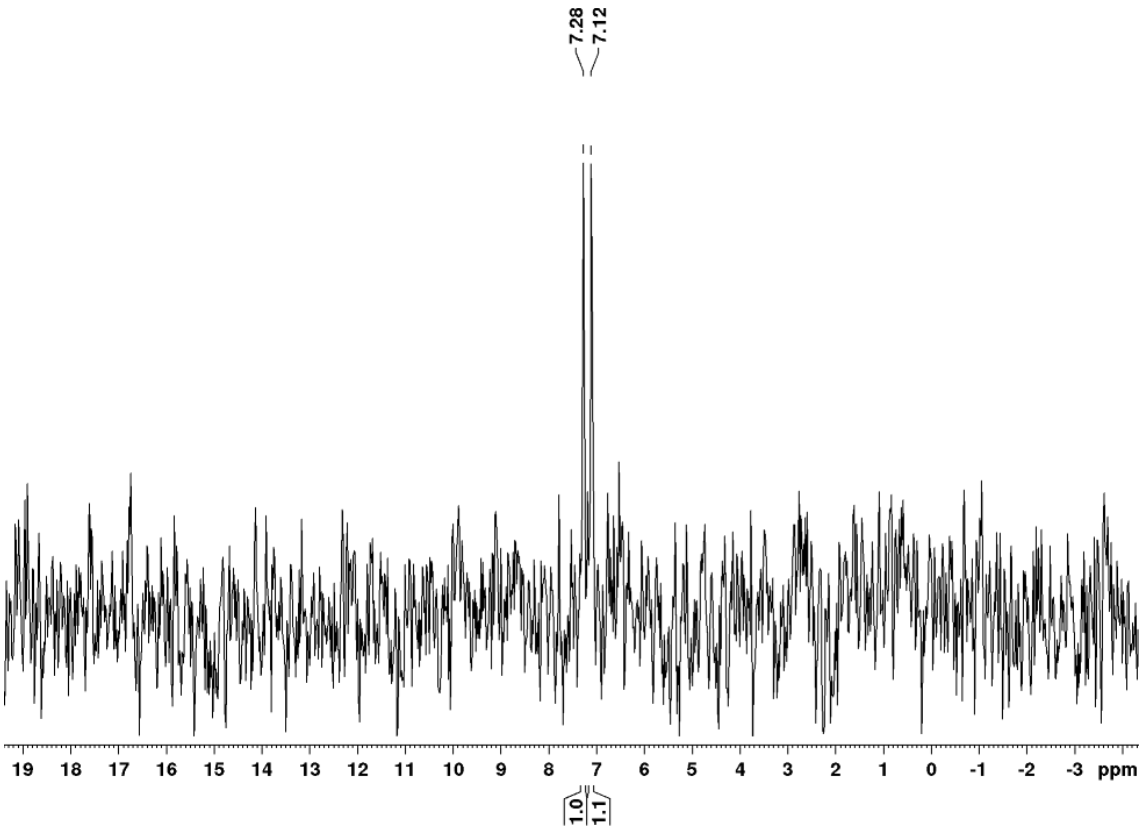

Figure S25. ^{29}Si NMR spectrum of the reaction mixture containing a diastereomeric mixture of *Si*-octylated bis(digermene) **2a** in C_6D_6.

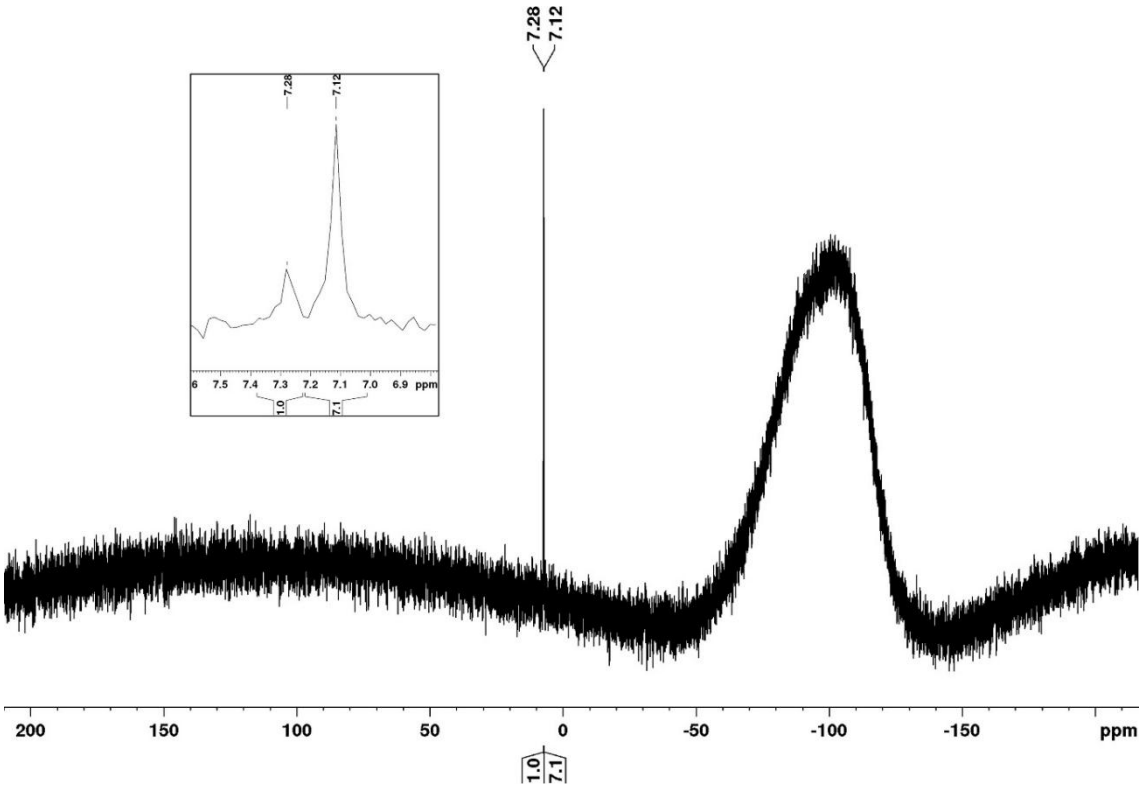

Figure S26. ^{29}Si NMR spectrum of isolated crystalline *Si*-octylated bis(digermene) **2a** in C_6D_6.

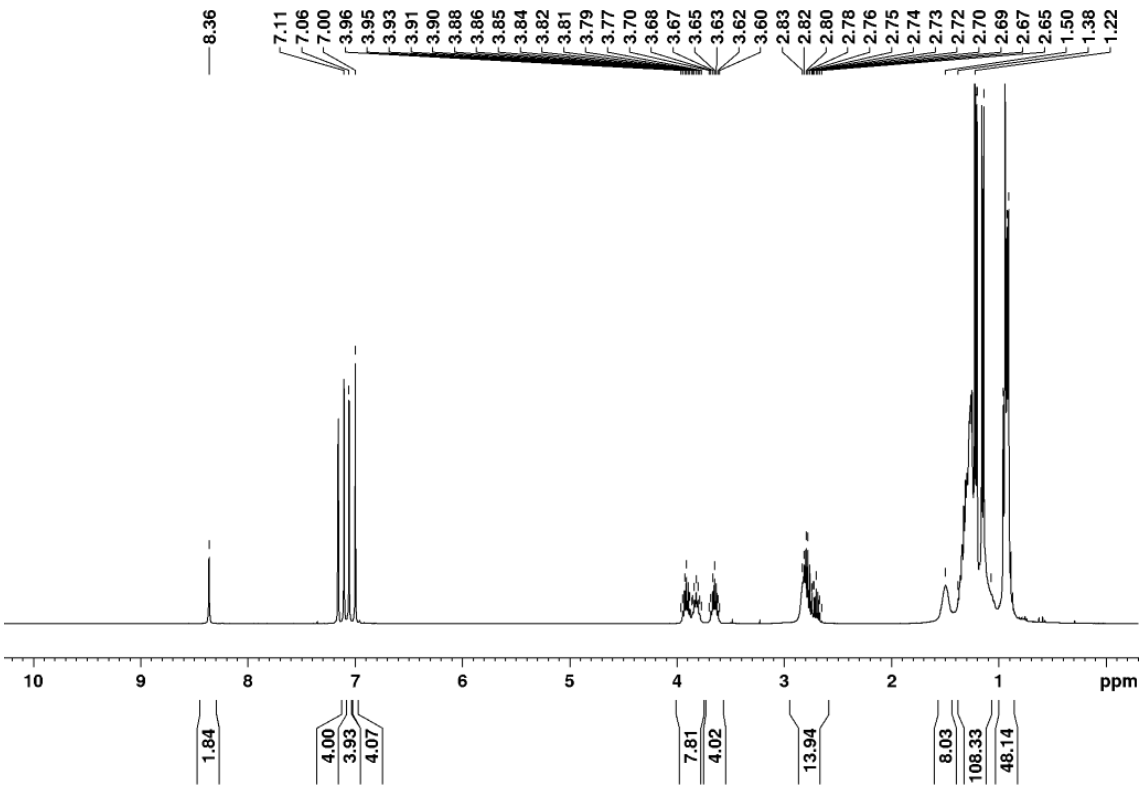

Figure S27. ^{1}H NMR spectrum of *N*-hexylated bis(digermene) **2b** in C_6D_6.

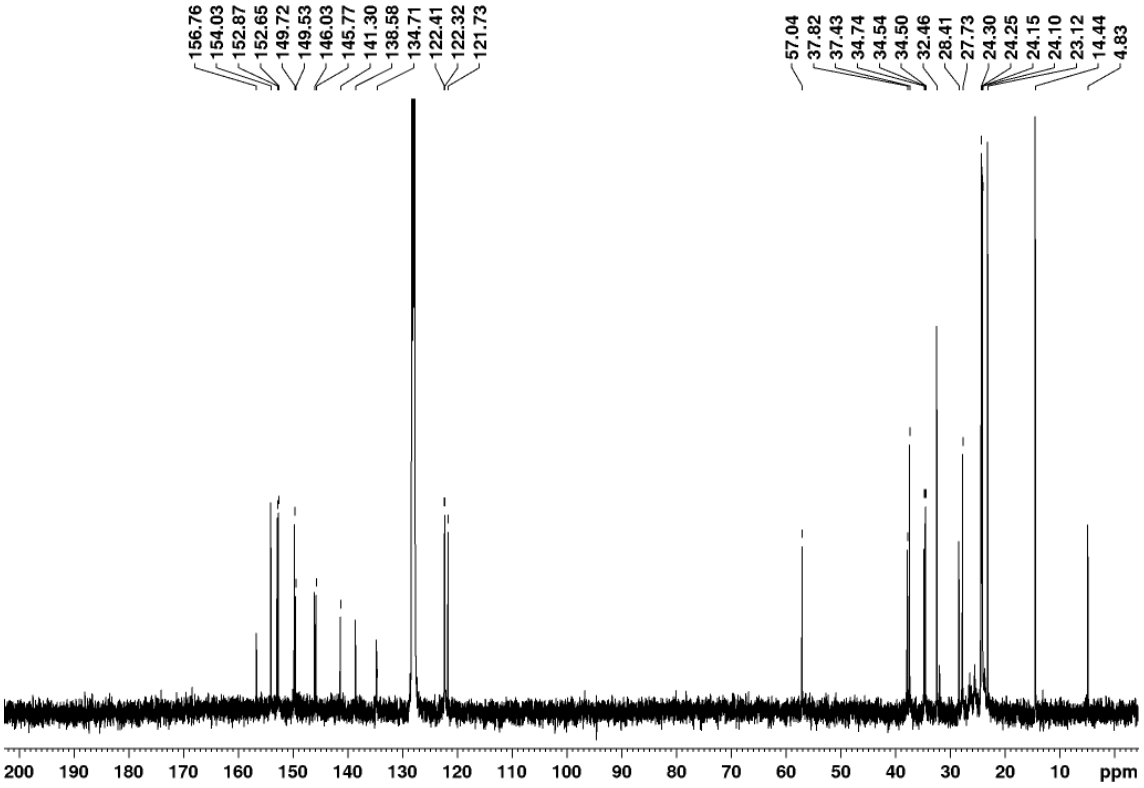

Figure S28. ^{13}C NMR spectrum of *N*-hexylated bis(digermene) **2b** in C_6D_6.

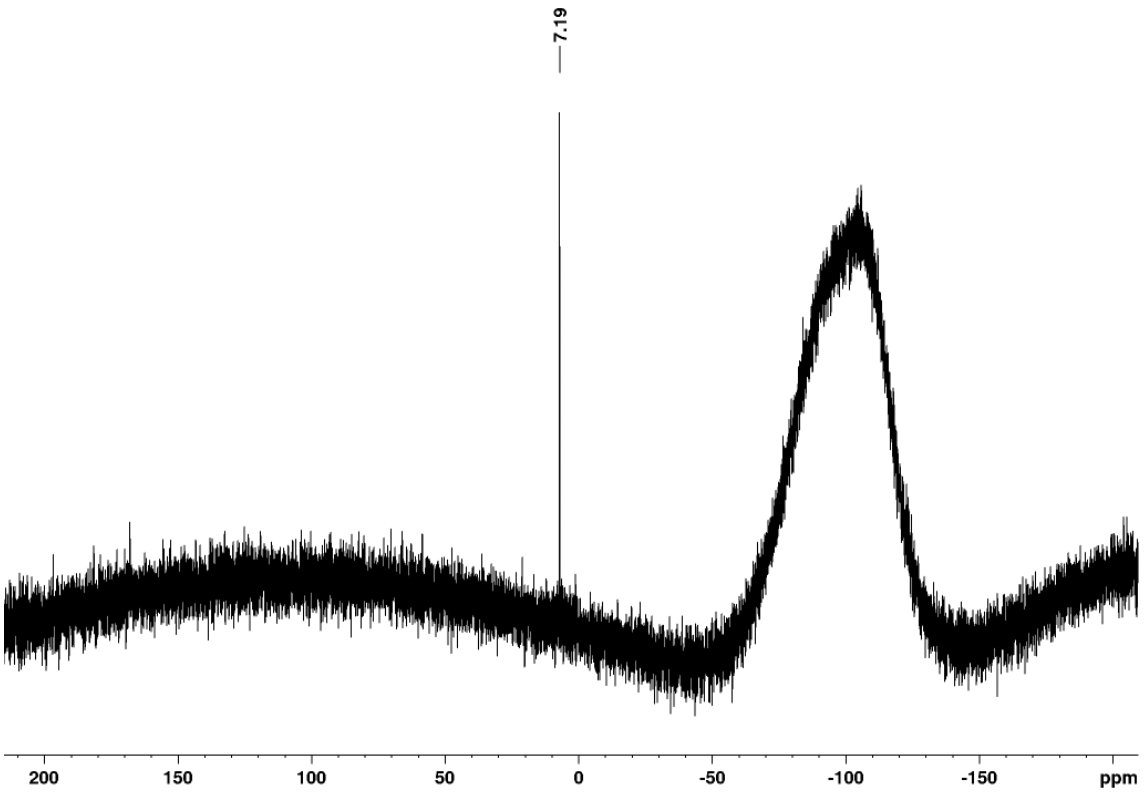

Figure S29. ^{29}Si NMR spectrum of *N*-hexylated bis(digermene) **2b** in C_6D_6.

4.2 X-Ray crystallographic data

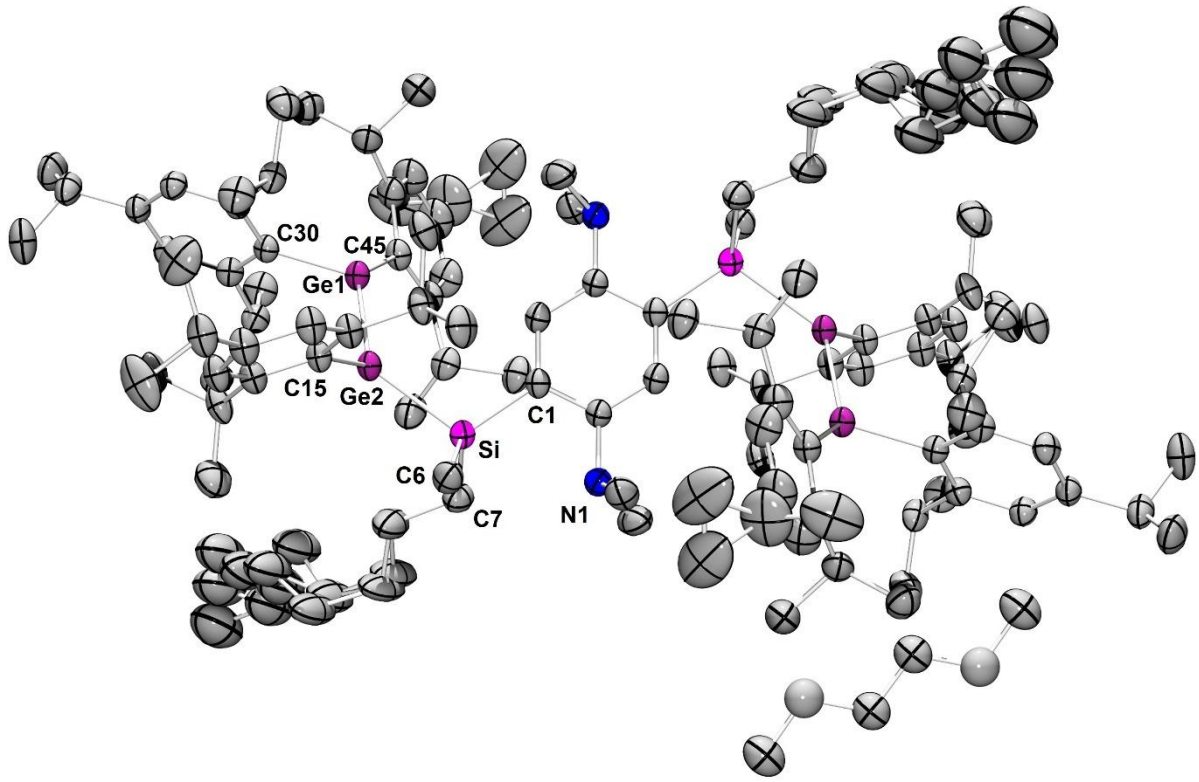

Figure S30. Molecular structure of **2a** in the solid state.[S31] Hydrogen atoms omitted for clarity. Thermal ellipsoids are shown at 50% probability. Selected bond lengths (in Å) and angles (in °): Ge1-Ge2 2.2923(5), Ge2-Si 2.4012(8), Si-C1, 1.882(3), Si-C6 1.876(3), Si-C7 1.883(3), C30-Ge1-Ge2 111.73(8), C45-Ge1-Ge2 129.07(9), C30-Ge1-C45 107.5(1), C15-Ge2-Si 110.35(8), C15-Ge2-Ge1 109.67(8), Si-Ge2-Ge1 130.50(2), $\Sigma°_{Ge1}$ 348.3(3), $\Sigma°_{Ge2}$ 350.5(2), θ_{Ge1} 30.5(1), θ_{Ge2} 27.9(1), τ 20.0(1), Ge1-Ge2-Si-C1 32.9(1).

All non H-atoms were located in the electron density maps and refined anisotropically. C-bound H atoms were placed in positions of optimized geometry and treated as riding atoms. Their isotropic displacement parameters were coupled to the corresponding carrier atoms by a factor of 1.2 (CH, CH_2) or 1.5 (CH_3). *Disorder*: One n-octyl group (fvar 2: 0.64/0.36) and an isopropyl group of a tip ligand (fvar 3: 0.62/0.38) are split over two positions.

Table S5. Crystal data and structure refinement for **2a** (CCDC 2358527).[S31]

Identification code	sh4432	
Empirical formula	C124 H206 Ge4 N2 Si2	
Formula weight	2071.44	
Temperature	133(2) K	
Wavelength	0.71073 Å	
Crystal system	Triclinic	
Space group	$P\bar{1}$	
Unit cell dimensions	a = 12.2406(7) Å	α= 94.353(2)°.
	b = 14.1129(8) Å	β= 99.823(2)°.
	c = 20.2371(11) Å	γ = 113.435(2)°.
Volume	3120.4(3) $Å^3$	
Z	1	
Density (calculated)	1.102 mg/m^3	
Absorption coefficient	1.017 mm^{-1}	
F(000)	1120	
Crystal size	0.251 x 0.176 x 0.060 mm^3	
Theta range for data collection	1.918 to 29.672°	
Index ranges	-17≤h≤16, -18≤k≤19, -28≤l≤28	
Reflections collected	83207	
Independent reflections	17429 [R(int) = 0.0662]	
Completeness to theta = 25.242°	99.5 %	
Absorption correction	Semi-empirical from equivalents	
Max. and min. transmission	0.7459 and 0.5897	
Refinement method	Full-matrix least-squares on F^2	
Data / restraints / parameters	17429 / 174 / 685	
Goodness-of-fit on F^2	1.018	
Final R indices [I>2σ(I)]	R1 = 0.0526, wR2 = 0.1195	
R indices (all data)	R1 = 0.0939, wR2 = 0.1391	
Extinction coefficient	n/a	
Largest diff. peak and hole	0.577 and -0.770 e · $Å^{-3}$	

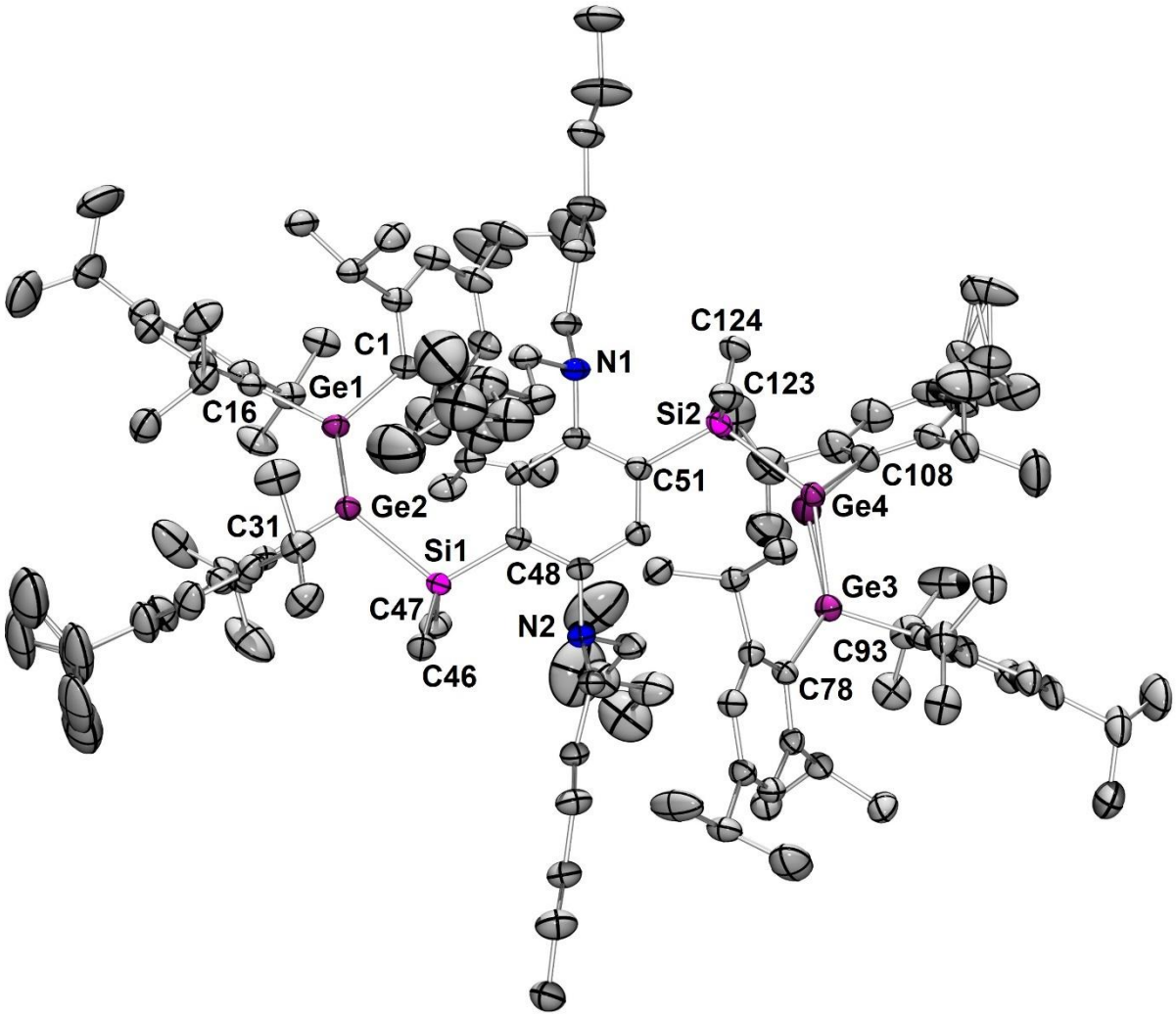

Figure S31. Molecular structure of **2b** in the solid state.[S31] Hydrogen atoms omitted for clarity. Thermal ellipsoids are shown at 50% probability. Selected bond lengths (in Å) and angles (in °): Ge1-Ge2 2.2742(5), Ge3-Ge4 2.2972(9), Ge2-Si1 2.3975(9), Ge4-Si2 2.399(1), Si1-C48 1.887(3), Si2-C51 1.885(3), Si1-C46 1.876(4), Si2-C124 1.874(4), Si1-C47 1.864(4), Si2-C123 1.871(4), C16-Ge1-C1 106.8(1), C16-Ge1-Ge2 124.6(1), C1-Ge1-Ge2 125.5(1), C31-Ge2-Si1 109.62(9), Si1-Ge2-Ge1 121.17(3), C31-Ge2-Ge1 114.76(9), C108-Ge4-Si2 110.1(1), Si2-Ge4-Ge3 132.32(4), C108-Ge4-Ge3 111.3(1), C78-Ge3-C93 107.3(1), C78-Ge3-Ge4 127.87(9), C93-Ge3-Ge4 114.4(1), Σ°_{Ge1} 356.9(3), Σ°_{Ge2} 345.6(2), Σ°_{Ge3} 349.6(3), Σ°_{Ge4} 353.7(2), θ_{Ge1} 15.7(1), θ_{Ge2} 35.5(1), θ_{Ge4} 22.4(1), θ_{Ge3} 28.9(1), $\tau_{Ge1\text{-}Ge2}$ 21.8(1), $\tau_{Ge3\text{-}Ge4}$ 17.9(1), Ge1-Ge2-Si1-C48 67.7(1), Ge3-Ge4-Si2-C51 33.2(1).

All non H-atoms were located on the electron density maps and refined anisotropically. C-bound H atoms were placed in positions of optimized geometry and treated as riding atoms. Their isotropic displacement parameters were coupled to the corresponding carrier atoms by a factor of 1.2 (CH, CH_2) or 1.5 (CH_3). *Disorder*: The isopropyl groups C120A/B-C122A/B, C43A/B-C45A/B and a part of the hexane residue C62A/B-C65A/B are split over two positions. Their occupancy factors refined to 71 %, 62 % and 62 %, respectively for the main compound. Additionally, Ge(4)A/B was split over two positions with a occupancy factor of 91 % for the main residue.

Table S6. Crystal data and structure refinement for **2b** (CCDC 2358526).[S31]

Identification code	sh4644_a	
Empirical formula	C124 H204 Ge4 N2 Si2	
Formula weight	2069.42	
Temperature	133(2) K	
Wavelength	0.71073 Å	
Crystal system	Triclinic	
Space group	$P\bar{1}$	
Unit cell dimensions	a = 14.9254(9) Å	α= 100.047(2)°.
	b = 17.7684(11) Å	β= 96.879(2)°.
	c = 26.3340(14) Å	γ = 113.435(2)°.
Volume	6169.6(6) $Å^3$	
Z	2	
Density (calculated)	1.114 mg/m^3	
Absorption coefficient	1.029 mm^{-1}	
F(000)	2236	
Crystal size	0.272 x 0.264 x 0.117 mm^3	
Theta range for data collection	1.967 to 26.733°	
Index ranges	-18≤h≤18, -22≤k≤22, -33≤l≤33	
Reflections collected	250761	
Independent reflections	26200 [R(int) = 0.0821]	
Completeness to theta = 25.242°	99.9 %	
Absorption correction	Semi-empirical from equivalents	
Max. and min. transmission	0.7455 and 0.6881	
Refinement method	Full-matrix least-squares on F^2	
Data / restraints / parameters	26200 / 296 / 1335	
Goodness-of-fit on F^2	1.026	
Final R indices [I>2σ(I)]	R1 = 0.0531, wR2 = 0.1283	
R indices (all data)	R1 = 0.0734, wR2 = 0.1409	
Extinction coefficient	n/a	
Largest diff. peak and hole	1.510 and -1.096 e · $Å^{-3}$	

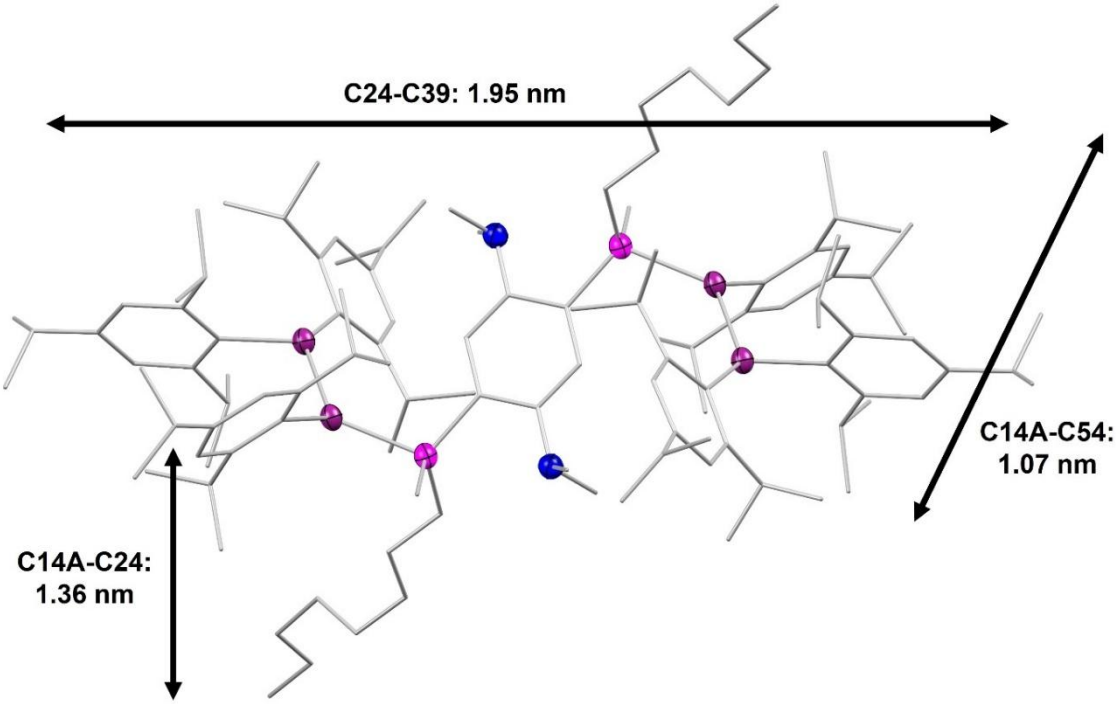

Figure S32. Dimensions of the molecular structure of *Si*-octylated bis(digermene) **2a** used for the determination of the corresponding volume and radius.

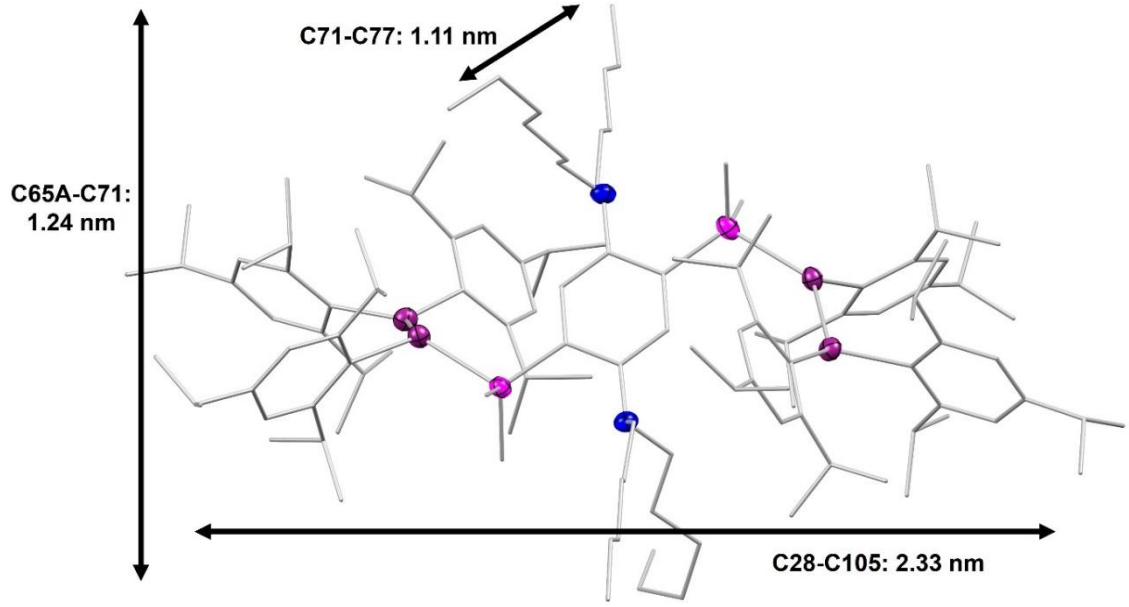

Figure S33. Dimensions of the molecular structure of *N*-hexylated bis(digermene) **2b** used for the determination of the corresponding volume and radius.

Estimation of monomer volumes and radii from the dimensions of the X-ray molecular structures:

Volume: $\mathrm{V} = x_1 \cdot x_2 \cdot x_3$

With x_1, x_2, x_3 being the distances outlined in schemes S32 and S33.

V_{2a} = 2.84 nm^3

V_{2b} = 3.21 nm^3

Radii: $\mathrm{R} = \sqrt[3]{\frac{3}{4\pi}\mathrm{V}}$

R_{2a} = 0.88 nm

R_{2b} = 0.92 nm

Intramolecular Ge-Ge distances for the estimation of the dimensions of the repeat units:

2a: Ge1-Ge2' 9.8219(7) Å

→ diameter of repeat unit ~ 0.98 nm

→ volume: V = 0.49 nm^3

2b: Ge2-Ge3: 9.9051(4) Å, Ge1-Ge4A: 10.012(1) Å

→ diameter of repeat unit ~ 1.00 nm

→ volume: V = 0.52 nm^3

4.3 UV/Vis absorption spectroscopy

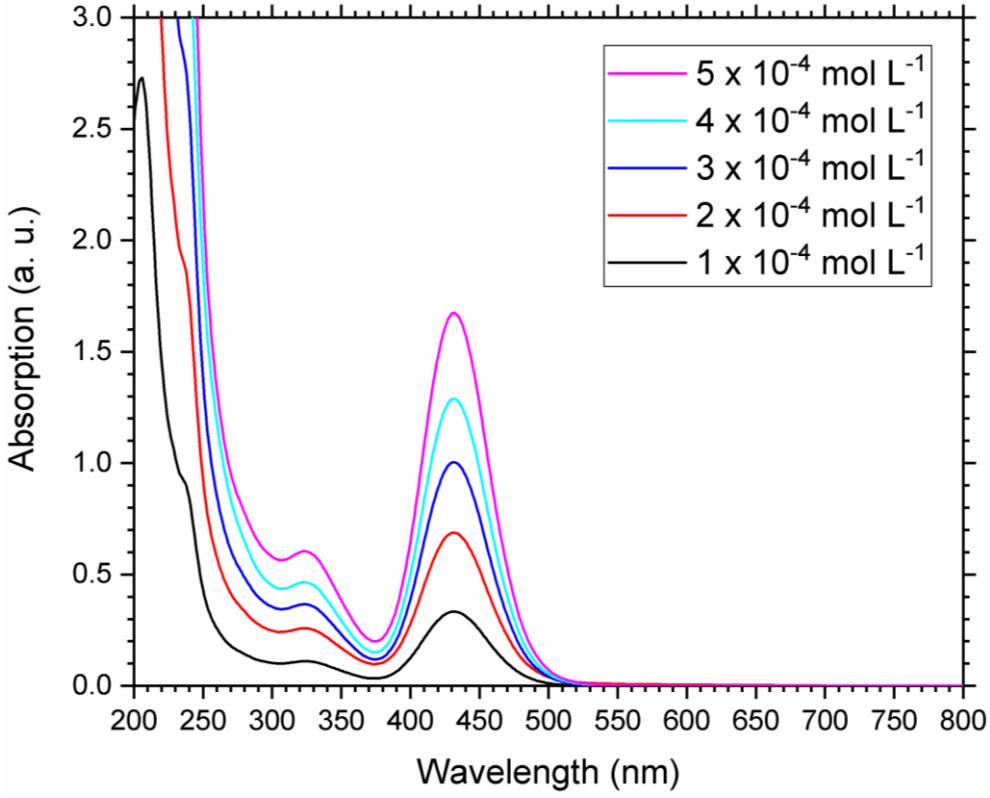

Figure S34. UV/Vis spectra of *Si*-octylated bis(digermene) **2a** at different concentrations.

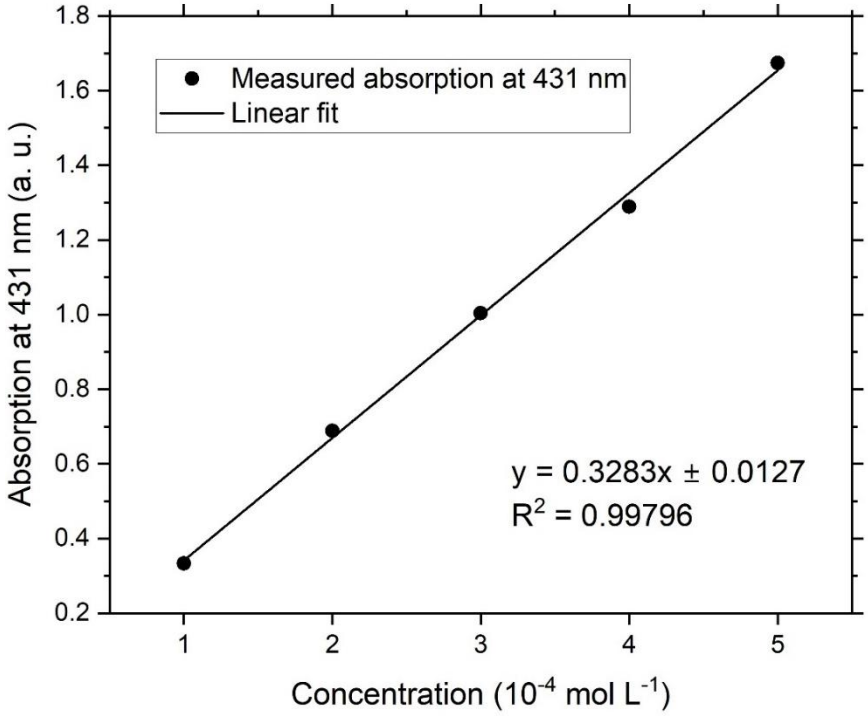

Figure S35. Determination of ε (32800 L mol^{-1} cm^{-1}) of **2a** by linear regression of absorbance at 431 nm against concentration.

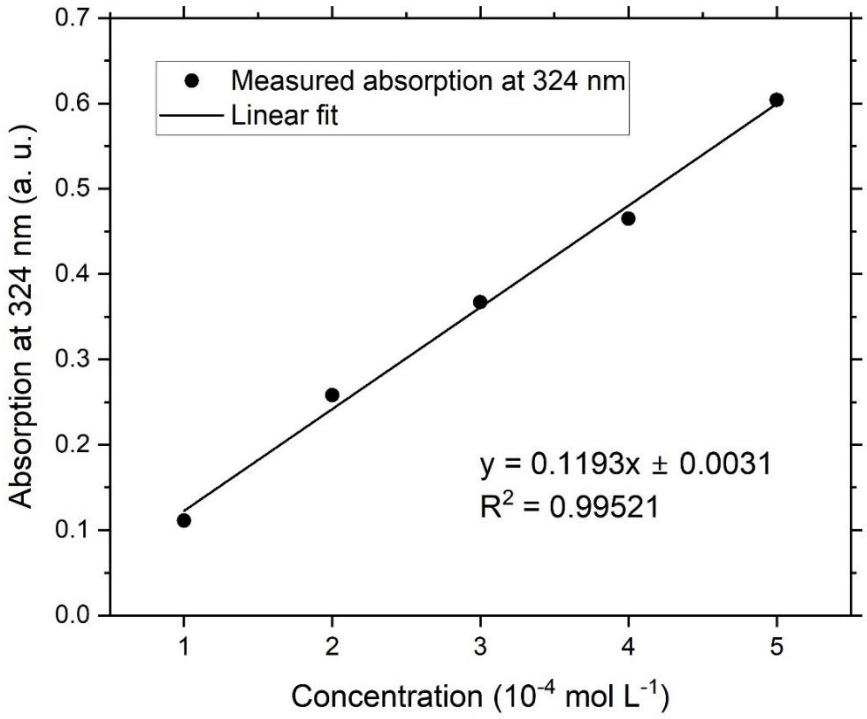

Figure S36. Determination of ε (11900 L mol^{-1} cm^{-1}) of **2a** by linear regression of absorbance at 324 nm against concentration.

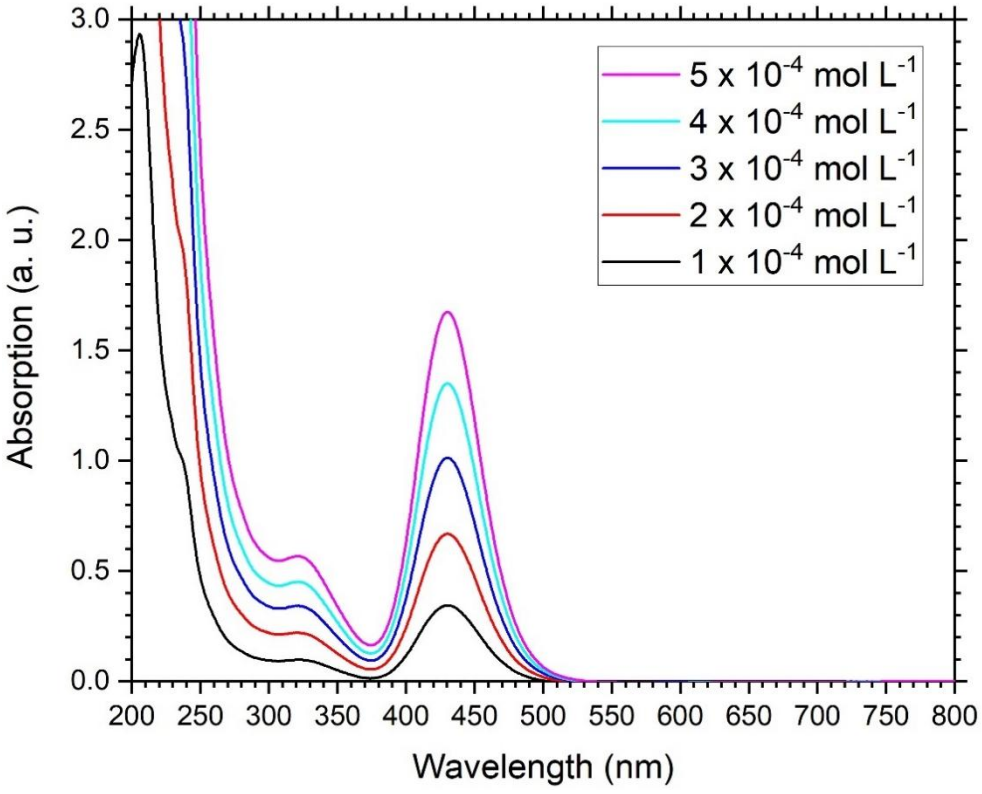

Figure S37. UV/Vis spectra of *N*-hexylated bis(digermene) **2b** at different concentrations.

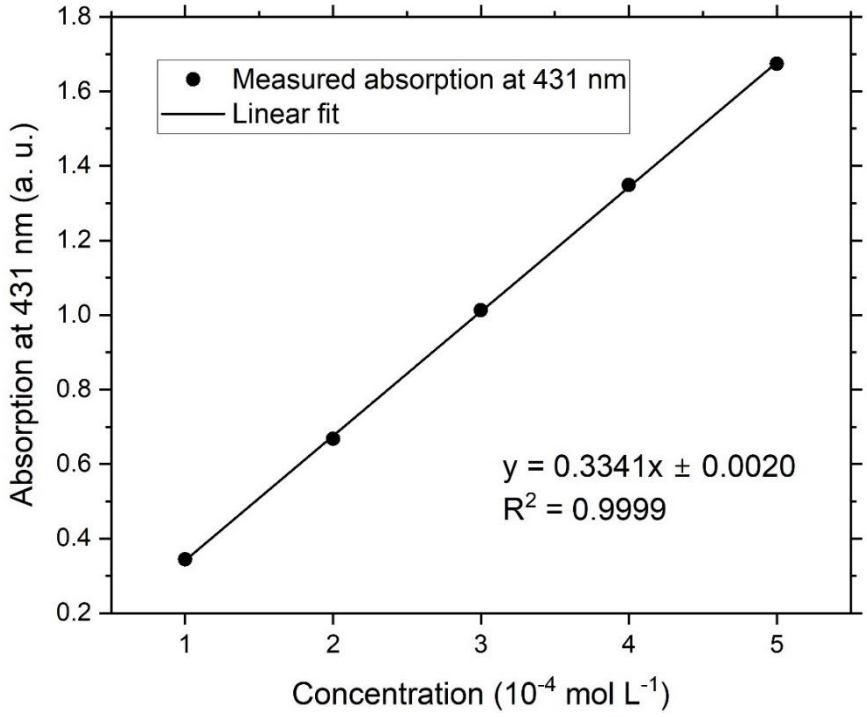

Figure S38. Determination of ε (33400 L mol^{-1} cm^{-1}) of **2b** by linear regression of absorbance at 431 nm against concentration.

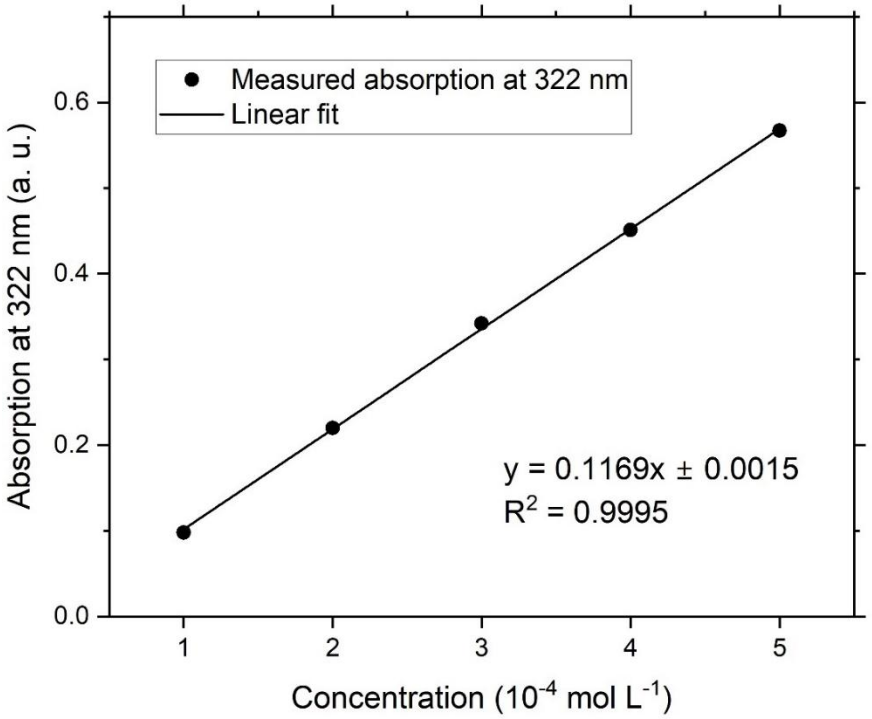

Figure S39. Determination of ε (11700 L mol^{-1} cm^{-1}) of **2b** by linear regression of absorbance at 322 nm against concentration.

4.4 DFT calculations

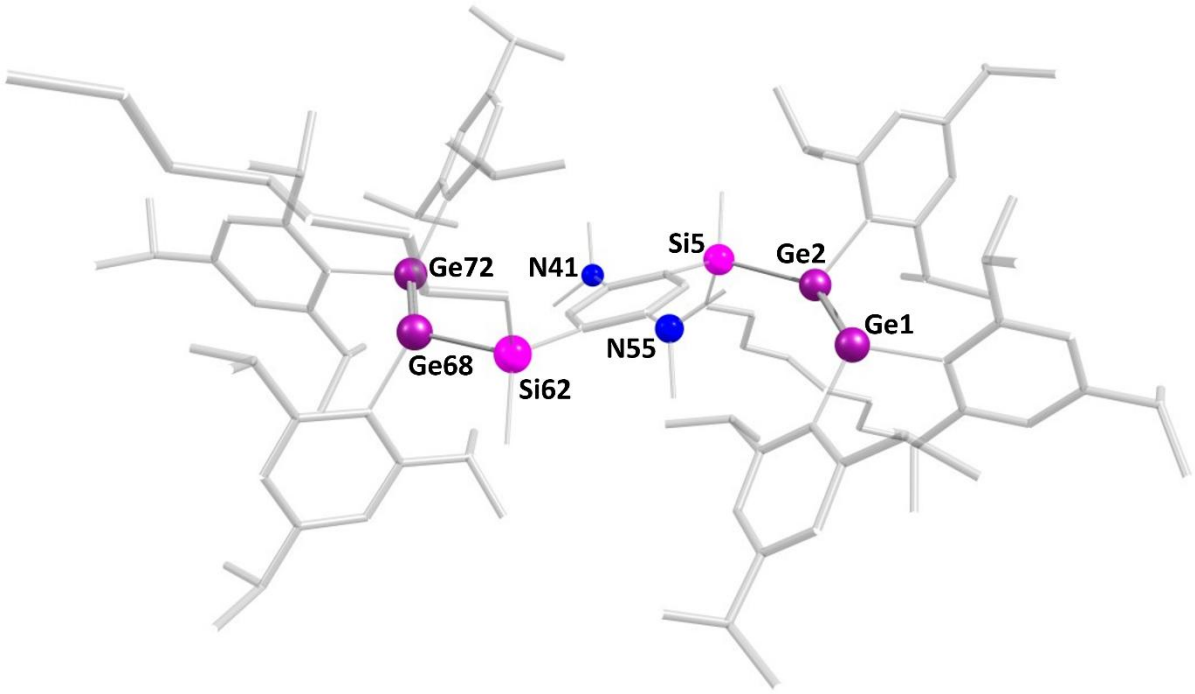

Figure S40. Optimized structure of *Si*-octylated bis(digermene) **2a**.

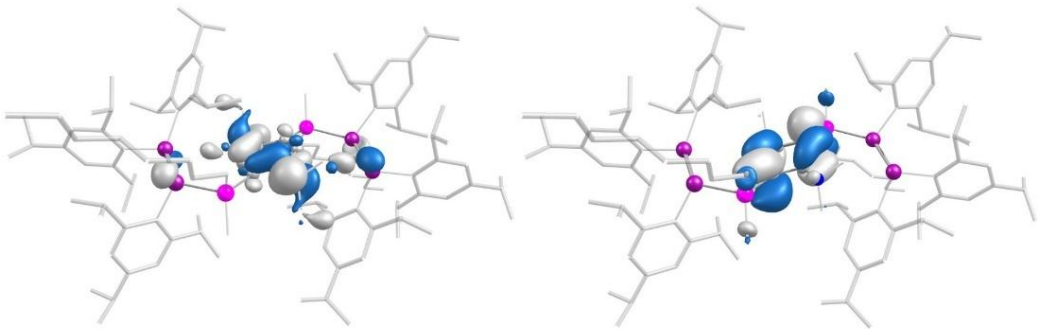

Figure S41. Selected frontier orbitals of *Si*-octylated bis(digermene) **2a** (contour value 0.036).

Table S7. Atomic coordinates of the optimized structure of *Si*-octylated bis(digermene) **2a**.

32	-4.856150397	0.945754999	0.748948297
32	-4.520675183	-1.121398093	-0.248539162
6	-6.825033882	1.294898639	0.941213758
6	-3.972571106	2.663192246	0.238484651
14	-2.426268214	-2.115443813	-0.979024589
6	-5.648938716	-2.441719756	0.731676099
6	-7.509190478	0.958602242	2.139550662

6	-7.535590337	1.942070910	-0.110257436
6	-3.115188581	2.824578580	-0.890179666
6	-4.227909252	3.786512221	1.080211746
6	-0.996739369	-1.127112001	-0.210220899
6	-2.514083448	-3.987706215	-0.621421205
6	-2.446478330	-1.905524331	-2.874861892
6	-5.132342884	-3.189128586	1.829377027
6	-6.986134170	-2.662479815	0.299599595
6	-8.871204821	1.297260521	2.274457062
6	-6.824222653	0.238594884	3.296587721
6	-8.894158889	2.260421260	0.069201612
6	-6.875108973	2.304510985	-1.436029883
6	-2.595936294	4.101915080	-1.171025219
6	-2.729192672	1.681447410	-1.828195443
6	-3.688389630	5.045642378	0.750537167
6	-5.031561775	3.678442056	2.376004594
6	0.270982650	-1.068337062	-0.855084954
6	-1.249192531	-0.223930110	0.841959522
6	-3.845012390	-2.092885547	-3.478236485
6	-5.957404072	-4.146791364	2.451686296
6	-3.731295210	-2.943293977	2.389104377
6	-7.768957293	-3.638443468	0.945146371
6	-7.589869265	-1.886281832	-0.867503384
6	-9.582192661	1.952618598	1.256589079
6	-7.502809553	-1.104412620	3.611659543
6	-6.723800528	1.116164922	4.557431920
6	-6.720883968	3.824214010	-1.618693910
6	-7.588115836	1.657560815	-2.635027904
6	-2.866995402	5.226880664	-0.372870755
6	-1.248606350	1.734426843	-2.240577431
6	-3.636502510	1.630667678	-3.072800319
6	-4.225437756	4.164737151	3.595189065
6	-6.392011685	4.391274830	2.288608775
7	0.574563707	-1.993897376	-1.886820916
6	1.188080205	-0.068832563	-0.466941692
6	-0.325283356	0.767357251	1.241808111
6	-3.913151322	-1.902690407	-4.999389428
6	-7.273717609	-4.391488946	2.024371778
6	-3.747581852	-1.878986690	3.499715504
6	-3.022084828	-4.218236653	2.874171829
6	-7.595959936	-2.742286083	-2.147349190
6	-8.982615894	-1.320555935	-0.549584784
6	-11.060566731	2.279161797	1.417409146
6	-2.178216564	6.550235418	-0.681540428
6	0.740920339	-3.392676758	-1.488970399
6	1.531324244	-1.574563629	-2.892607999
6	0.932949894	0.845949439	0.575686897
7	-0.629088020	1.665354157	2.294572592
6	-5.341957914	-1.923861979	-5.566542009
6	-8.152516816	-5.404688173	2.746035241
6	-11.917884464	1.432670645	0.455295328

6	-11.339035886	3.784375255	1.247781109
6	-0.760652665	6.549948604	-0.067654994
6	-2.976099812	7.785061109	-0.237154107
14	2.364594903	1.894019123	1.260397182
6	-0.747807131	3.081730994	1.948361658
6	-1.622517973	1.241953444	3.263594366
6	-6.207536580	-0.741882934	-5.103585503
6	-9.282101482	-4.695176890	3.519846920
6	-8.710168193	-6.475066795	1.789697660
32	4.447286644	1.049384420	0.340341478
6	2.361191277	3.776915110	0.937865352
6	2.527276700	1.662308101	3.145924328
6	-7.651573819	-0.758434465	-5.625765198
32	4.828831892	-0.984280584	-0.711943307
6	5.352924530	2.453458903	-0.750262291
6	3.949719735	1.952027967	3.644269657
6	-7.796041378	-0.554807526	-7.141258141
6	6.790530150	-1.174255164	-1.087105650
6	4.138393099	-2.768029795	-0.131828339
6	4.663033161	3.156793147	-1.779487323
6	6.708415546	2.777374282	-0.465212499
6	4.156608359	1.756318858	5.151887474
6	-9.255268862	-0.529044141	-7.608702313
6	7.328266311	-0.806403034	-2.348569770
6	7.647368395	-1.733195299	-0.095783561
6	3.409059493	-2.991340757	1.070944376
6	4.409463256	-3.874214296	-0.993585404
6	5.339189735	4.173767566	-2.482175764
6	3.234022751	2.800190240	-2.187781491
6	7.339650925	3.807887828	-1.187179842
6	7.487897180	2.050995744	0.627414618
6	5.620269745	1.903643460	5.599508111
6	8.696801917	-1.028657357	-2.605026369
6	6.477217054	-0.173408280	-3.445092050
6	9.005923982	-1.938871488	-0.397665059
6	7.142154091	-2.124480789	1.289790194
6	3.046119271	-4.309051994	1.414067720
6	2.997271083	-1.874945162	2.027979254
6	4.022785910	-5.169991765	-0.606515292
6	5.073216465	-3.710103942	-2.359993918
6	6.672406199	4.518346893	-2.201038148
6	3.219482071	1.745849896	-3.307348318
6	2.372951045	4.012787137	-2.578816490
6	7.518094838	2.884515164	1.921861012
6	8.896010904	1.629982558	0.181233631
6	6.550046025	0.813935459	5.043436518
6	9.551961665	-1.599421619	-1.648883700
6	6.980804826	1.232367150	-3.811528604
6	6.368593951	-1.064852609	-4.695343935
6	7.109456229	-3.650068577	1.488374038
6	7.922508390	-1.424127041	2.414724197

6	3.346380236	-5.413274867	0.601103523
6	1.529371209	-1.999467575	2.471767361
6	3.941732032	-1.797124536	3.242723245
6	4.208202823	-4.295455611	-3.492085572
6	6.498408697	-4.289112871	-2.393822129
6	7.387314608	5.592418935	-3.010306121
6	8.028245889	0.972038201	5.428203222
6	11.031476376	-1.805476784	-1.944017933
6	2.869121530	-6.808590281	0.979026606
6	8.472143632	4.966402942	-3.909980963
6	7.968158871	6.703656973	-2.116516682
6	8.334427158	0.788445298	6.922099965
6	11.901364820	-0.876421846	-1.073861947
6	11.448089633	-3.280041465	-1.788607931
6	1.638748749	-7.198859719	0.133382476
6	3.983430315	-7.864760441	0.875633399
6	9.827289836	0.903171026	7.248733299

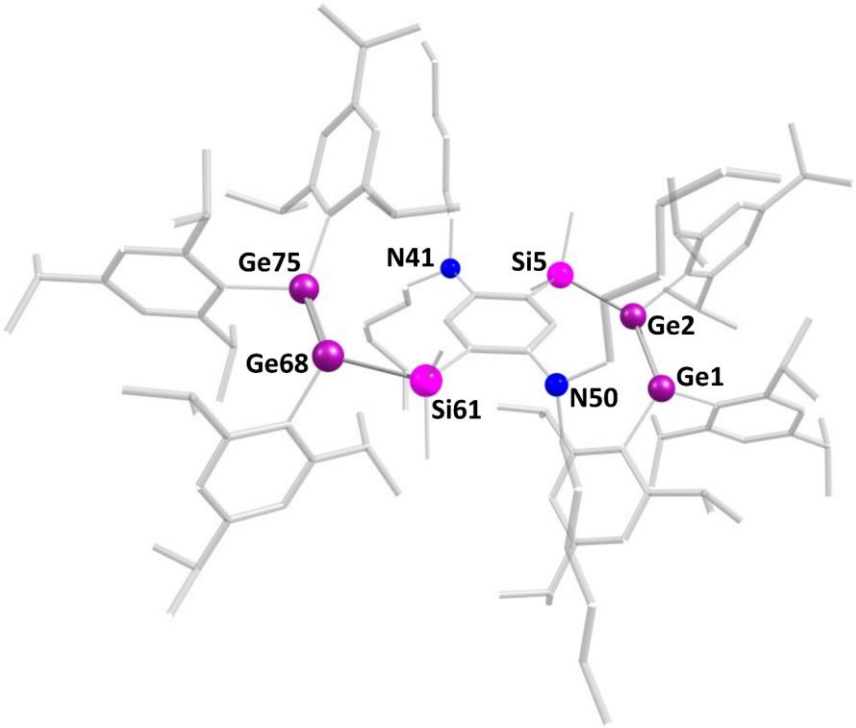

Figure S42. Optimized structure of *N*-hexylated bis(digermene) **2b**.

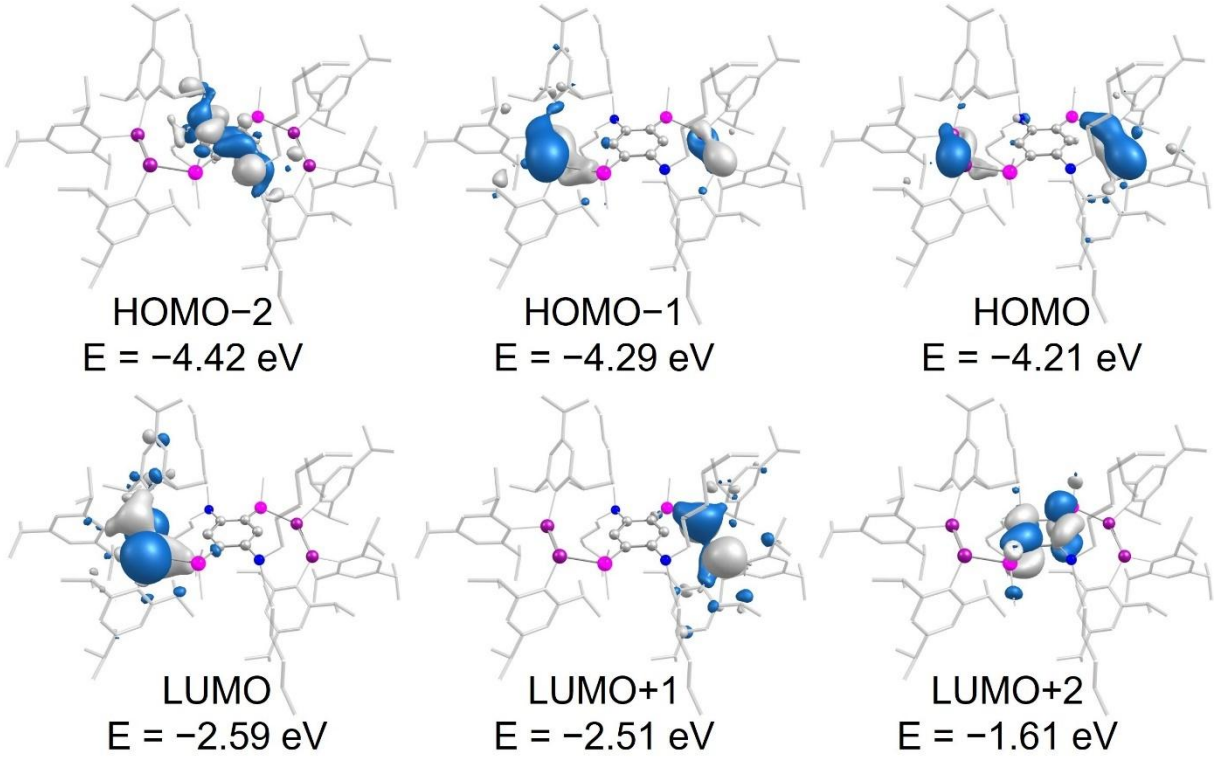

Figure S43. Selected frontier orbitals of *N*-hexylated bis(digermene) **2b** (contour value 0.036).

Table S8. Atomic coordinates of the optimized structure of *N*-hexylated bis(digermene) **2b**.

32	4.955430000	-0.770342000	-0.182387000
32	4.280602000	1.297032000	-0.988278000
6	4.075821000	-2.534992000	-0.515502000
6	6.904598000	-0.998920000	-0.622099000
14	2.057422000	2.222432000	-1.192518000
6	5.598714000	2.668013000	-0.391739000
6	2.973650000	-2.739185000	-1.394810000
6	4.648050000	-3.657808000	0.151561000
6	7.907562000	-0.654783000	0.322504000
6	7.287145000	-1.563330000	-1.874126000
6	2.127605000	4.083820000	-0.791316000
6	1.724296000	2.055639000	-3.052125000
6	0.858884000	1.216895000	-0.111019000
6	6.745524000	2.917465000	-1.193358000
6	5.394055000	3.423603000	0.798368000
6	2.515834000	-4.050869000	-1.625995000
6	2.264803000	-1.608758000	-2.137196000
6	4.164299000	-4.950486000	-0.125899000
6	5.759372000	-3.518081000	1.189955000
6	9.260622000	-0.906097000	0.015489000
6	7.576729000	-0.023023000	1.671115000
6	8.649716000	-1.799636000	-2.133689000
6	6.272195000	-1.931279000	-2.953696000
1	1.846092000	4.289895000	0.259423000
1	1.439792000	4.646889000	-1.454541000
1	3.154922000	4.472279000	-0.951716000
1	2.558511000	2.522765000	-3.617283000
1	0.775016000	2.553253000	-3.324519000
1	1.658804000	0.994422000	-3.357925000
6	1.344766000	0.401592000	0.937908000
6	-0.527804000	1.142321000	-0.424509000
6	7.647591000	3.929446000	-0.808988000
6	6.992064000	2.134072000	-2.478404000
6	6.325881000	4.418212000	1.148151000
6	4.237855000	3.120848000	1.747297000
1	1.669747000	-4.199911000	-2.315722000
6	3.101031000	-5.173257000	-1.015732000
1	2.629729000	-0.650802000	-1.711739000
6	0.742192000	-1.649271000	-1.940491000
6	2.615388000	-1.619177000	-3.637894000
1	4.621624000	-5.817385000	0.380000000
1	5.946896000	-2.429944000	1.325597000
6	5.322873000	-4.051642000	2.566088000
6	7.081246000	-4.151897000	0.724199000
1	10.038847000	-0.641110000	0.751078000
6	9.654455000	-1.485523000	-1.200878000
1	6.471823000	0.118784000	1.688071000
6	7.947178000	-0.935513000	2.854448000
6	8.220308000	1.365317000	1.822211000

1	8.935018000	-2.240567000	-3.103046000
1	5.287072000	-1.562908000	-2.602596000
6	6.553737000	-1.223191000	-4.290345000
6	6.151110000	-3.454412000	-3.138954000
1	2.423890000	0.414703000	1.167403000
6	0.514849000	-0.481013000	1.659872000
7	-1.085059000	1.989681000	-1.424253000
6	-1.339778000	0.234930000	0.285430000
1	8.537506000	4.126574000	-1.428309000
6	7.457321000	4.689941000	0.356697000
1	6.434492000	1.176142000	-2.367472000
6	6.387093000	2.876089000	-3.685214000
6	8.466230000	1.768833000	-2.700179000
1	6.173674000	4.988725000	2.077695000
1	3.429227000	2.661898000	1.133443000
6	3.649893000	4.360008000	2.439542000
6	4.647777000	2.063150000	2.783676000
6	2.609469000	-6.583430000	-1.310037000
1	0.294009000	-2.530126000	-2.444727000
1	0.271202000	-0.746023000	-2.377215000
1	0.466720000	-1.682612000	-0.868962000
1	3.694936000	-1.444445000	-3.808035000
1	2.055583000	-0.830129000	-4.181704000
1	2.348598000	-2.594029000	-4.097148000
1	5.111374000	-5.141095000	2.536570000
1	4.406186000	-3.539436000	2.919280000
1	6.121011000	-3.887481000	3.320237000
1	6.969842000	-5.247698000	0.580382000
1	7.880328000	-3.988785000	1.476948000
1	7.423422000	-3.709706000	-0.231515000
6	11.123923000	-1.735431000	-1.512243000
1	9.043157000	-1.109935000	2.898530000
1	7.454438000	-1.924938000	2.782369000
1	7.642692000	-0.470954000	3.815788000
1	9.328404000	1.291612000	1.857044000
1	7.889125000	1.853442000	2.761734000
1	7.947877000	2.026678000	0.979453000
1	6.558452000	-0.122114000	-4.168610000
1	5.773046000	-1.479363000	-5.037246000
1	7.532372000	-1.523426000	-4.720143000
1	7.105799000	-3.892345000	-3.501288000
1	5.361810000	-3.695106000	-3.881473000
1	5.881030000	-3.953821000	-2.188408000
7	1.015496000	-1.347987000	2.689697000
6	-0.860521000	-0.568452000	1.331811000
6	-1.276961000	3.387840000	-1.005369000
6	-2.187312000	1.443687000	-2.223997000
1	-2.411041000	0.188480000	0.040619000
6	8.479887000	5.735935000	0.780397000
1	6.874913000	3.863219000	-3.831025000
1	5.301137000	3.056488000	-3.536741000

1	6.511223000	2.288895000	-4.619920000
1	8.882559000	1.252049000	-1.812494000
1	9.092187000	2.661136000	-2.914652000
1	8.567572000	1.081743000	-3.564523000
1	2.701779000	4.096476000	2.952989000
1	3.439810000	5.175987000	1.719505000
1	4.335486000	4.761342000	3.215754000
1	4.910289000	1.106500000	2.288434000
1	3.815255000	1.864346000	3.484380000
1	5.523434000	2.403140000	3.374473000
1	3.106126000	-7.256174000	-0.575327000
6	1.088744000	-6.725879000	-1.118975000
6	3.044788000	-7.026583000	-2.721514000
1	11.699612000	-1.448231000	-0.603932000
6	11.605271000	-0.841761000	-2.672415000
6	11.403005000	-3.224251000	-1.792073000
6	1.471814000	-2.635309000	2.140405000
6	1.976159000	-0.747968000	3.618281000
14	-2.063393000	-1.592094000	2.396722000
1	-0.451113000	3.652097000	-0.315244000
1	-2.217911000	3.483670000	-0.410971000
6	-1.325146000	4.393218000	-2.155235000
1	-3.087740000	2.085099000	-2.111621000
1	-2.487441000	0.454582000	-1.828034000
6	-1.834914000	1.263239000	-3.703941000
1	9.206603000	5.834034000	-0.056931000
6	7.841207000	7.117799000	1.010894000
6	9.261065000	5.259932000	2.022067000
1	0.772350000	-7.782185000	-1.245253000
1	0.526963000	-6.121077000	-1.861214000
1	0.777906000	-6.389498000	-0.109811000
1	4.144923000	-6.955563000	-2.842900000
1	2.580327000	-6.381061000	-3.497098000
1	2.738572000	-8.074672000	-2.924112000
1	11.427946000	0.230623000	-2.452303000
1	11.064368000	-1.083083000	-3.612000000
1	12.690229000	-0.983421000	-2.862281000
1	12.486876000	-3.401940000	-1.955174000
1	10.867673000	-3.569585000	-2.701849000
1	11.070330000	-3.860411000	-0.946538000
1	2.441777000	-2.514938000	1.592768000
1	0.736590000	-2.939160000	1.367979000
6	1.602100000	-3.753321000	3.177629000
1	2.977251000	-0.575459000	3.137059000
1	2.156259000	-1.489322000	4.425662000
6	1.467582000	0.552512000	4.245242000
32	-4.304820000	-1.200947000	1.518350000
6	-2.064353000	-1.023984000	4.206096000
6	-1.826715000	-3.480664000	2.440228000
1	-0.389111000	4.337447000	-2.753869000
1	-2.149691000	4.121930000	-2.850170000

6	-1.559219000	5.818372000	-1.646645000
1	-0.900356000	0.665296000	-3.756317000
1	-1.591446000	2.245617000	-4.166317000
6	-2.951507000	0.569611000	-4.490942000
1	7.290290000	7.461591000	0.111648000
1	7.122156000	7.095088000	1.857014000
1	8.615073000	7.875853000	1.254142000
1	9.742700000	4.277930000	1.838910000
1	10.050614000	5.988983000	2.302285000
1	8.584050000	5.141431000	2.894652000
1	2.498751000	-3.589834000	3.815508000
1	0.727363000	-3.721620000	3.863110000
6	1.709067000	-5.121491000	2.498771000
1	0.403492000	0.416969000	4.533742000
1	1.468701000	1.360692000	3.481744000
6	2.288684000	0.993700000	5.462033000
32	-5.019215000	0.561577000	0.156808000
6	-5.023762000	-2.874350000	0.687078000
1	-2.905217000	-1.500122000	4.752334000
1	-2.161620000	0.072682000	4.306914000
1	-1.109382000	-1.339002000	4.673036000
1	-1.223220000	-3.855928000	1.593947000
1	-2.810589000	-3.992417000	2.403559000
1	-1.317033000	-3.767547000	3.381465000
1	-0.698690000	6.132573000	-1.011713000
1	-2.444175000	5.807072000	-0.974134000
6	-1.784065000	6.850313000	-2.755850000
1	-3.193145000	-0.397294000	-3.997426000
1	-3.883503000	1.172556000	-4.421591000
6	-2.616672000	0.326416000	-5.972371000
1	2.470247000	-5.060193000	1.691487000
1	0.747152000	-5.343682000	1.982435000
6	2.065272000	-6.276810000	3.436980000
1	3.371330000	0.935208000	5.212346000
6	1.944326000	2.412935000	5.932839000
1	2.139104000	0.274239000	6.299259000
6	-4.634920000	2.515281000	0.400562000
6	-6.991727000	0.379363000	-0.131939000
6	-4.255240000	-3.643402000	-0.232055000
6	-6.328354000	-3.314928000	1.047509000
1	-0.904084000	6.866332000	-3.439900000
1	-2.645791000	6.525989000	-3.384418000
6	-2.047669000	8.266974000	-2.228293000
1	-2.538302000	1.306744000	-6.494337000
1	-3.471580000	-0.204689000	-6.449057000
6	-1.323693000	-0.472423000	-6.226552000
1	3.017610000	-6.038825000	3.965490000
1	1.294015000	-6.368948000	4.236546000
6	2.214606000	-7.619475000	2.708812000
1	0.872677000	2.443155000	6.232004000
1	2.031968000	3.109187000	5.066356000

6	2.817722000	2.938881000	7.083885000
6	-5.136842000	3.424382000	-0.581971000
6	-3.928364000	3.037927000	1.521148000
6	-7.497859000	-0.235569000	-1.308481000
6	-7.895552000	0.902259000	0.835538000
6	-4.799165000	-4.835024000	-0.752214000
6	-2.893085000	-3.175229000	-0.736121000
6	-6.830771000	-4.511446000	0.503740000
6	-7.171889000	-2.528179000	2.045567000
1	-1.187046000	8.587720000	-1.598359000
1	-2.923231000	8.237872000	-1.540186000
6	-2.293557000	9.298267000	-3.334140000
1	-1.197057000	-0.597419000	-7.324485000
1	-0.444918000	0.124933000	-5.895222000
6	-1.284792000	-1.846783000	-5.547999000
1	2.983123000	-7.509767000	1.909764000
1	1.265416000	-7.852757000	2.175151000
6	2.590146000	-8.783088000	3.631548000
1	2.390239000	3.898850000	7.448543000
1	2.754925000	2.235013000	7.945107000
6	4.287857000	3.157502000	6.701731000
6	-5.003901000	4.809150000	-0.372893000
6	-5.826399000	2.966609000	-1.868075000
6	-3.834450000	4.434067000	1.691028000
6	-3.263047000	2.161504000	2.579291000
6	-8.890412000	-0.306002000	-1.503185000
6	-6.581835000	-0.821256000	-2.380388000
6	-9.280665000	0.814600000	0.593655000
6	-7.416542000	1.584167000	2.115825000
1	-4.213659000	-5.427627000	-1.473675000
6	-6.081093000	-5.287419000	-0.399120000
1	-2.468758000	-2.510210000	0.047471000
6	-3.046310000	-2.298898000	-1.989053000
6	-1.887370000	-4.312560000	-0.977132000
1	-7.842887000	-4.841307000	0.784512000
1	-6.827324000	-1.471644000	1.976875000
6	-8.671727000	-2.530383000	1.721935000
6	-6.887512000	-3.008423000	3.481540000
1	-1.419912000	9.373568000	-4.016455000
1	-2.482590000	10.310380000	-2.920230000
1	-3.172166000	9.020975000	-3.955311000
1	-0.362452000	-2.403419000	-5.813646000
1	-2.154035000	-2.471827000	-5.846322000
1	-1.306830000	-1.762153000	-4.442296000
1	2.693168000	-9.736478000	3.073005000
1	1.821027000	-8.937713000	4.418338000
1	3.554876000	-8.591863000	4.148668000
1	4.869565000	3.580916000	7.546445000
1	4.785708000	2.212130000	6.400996000
1	4.376822000	3.860396000	5.845639000
1	-5.401046000	5.507447000	-1.128385000

6	-4.379826000	5.340815000	0.768996000
1	-5.671129000	1.867784000	-1.949238000
6	-5.207821000	3.602222000	-3.127975000
6	-7.344205000	3.228377000	-1.835255000
1	-3.306283000	4.821121000	2.575493000
1	-3.275874000	1.118304000	2.201441000
6	-4.063277000	2.182930000	3.895479000
6	-1.788362000	2.542555000	2.805463000
1	-9.275627000	-0.785468000	-2.418151000
6	-9.800188000	0.219422000	-0.568077000
1	-5.535675000	-0.640334000	-2.035935000
6	-6.768272000	-2.341873000	-2.508292000
6	-6.746817000	-0.129832000	-3.745535000
1	-9.985473000	1.224048000	1.336869000
1	-6.320455000	1.417858000	2.174587000
6	-8.019924000	0.958613000	3.384752000
6	-7.642913000	3.106591000	2.075603000
6	-6.661745000	-6.550101000	-1.021805000
1	-2.061766000	-1.904785000	-2.312041000
1	-3.707961000	-1.434814000	-1.777583000
1	-3.487387000	-2.873122000	-2.830230000
1	-1.875487000	-5.037780000	-0.139501000
1	-0.863810000	-3.903314000	-1.090435000
1	-2.118378000	-4.876862000	-1.905314000
1	-9.132313000	-3.530127000	1.872512000
1	-8.850211000	-2.215917000	0.674360000
1	-9.208862000	-1.819338000	2.381967000
1	-7.172410000	-4.074576000	3.607011000
1	-7.455355000	-2.409332000	4.224966000
1	-5.807202000	-2.917936000	3.724280000
6	-4.350437000	6.846958000	0.992963000
1	-4.111184000	3.452808000	-3.172100000
1	-5.397854000	4.694821000	-3.169172000
1	-5.651263000	3.157744000	-4.043342000
1	-7.829380000	2.835455000	-2.752764000
1	-7.548985000	4.318760000	-1.781663000
1	-7.825586000	2.742886000	-0.966746000
1	-3.580525000	1.551141000	4.668815000
1	-5.092493000	1.801413000	3.745280000
1	-4.136504000	3.215240000	4.297634000
1	-1.294831000	1.812192000	3.477473000
1	-1.687384000	3.544239000	3.273127000
1	-1.222459000	2.544090000	1.854086000
6	-11.303281000	0.123178000	-0.793488000
1	-6.032820000	-2.772027000	-3.218964000
1	-7.784176000	-2.587024000	-2.885322000
1	-6.638180000	-2.843800000	-1.532847000
1	-6.023606000	-0.541993000	-4.479555000
1	-6.579190000	0.962889000	-3.678833000
1	-7.766884000	-0.287633000	-4.155281000
1	-7.791931000	-0.123716000	3.446903000

1	-9.123103000	1.078352000	3.422222000
1	-7.604015000	1.446066000	4.291452000
1	-7.236871000	3.584682000	2.991501000
1	-8.725087000	3.350262000	2.013140000
1	-7.135166000	3.565305000	1.205192000
1	-5.846868000	-7.021173000	-1.616036000
6	-7.115138000	-7.568261000	0.040618000
6	-7.806698000	-6.200593000	-1.994058000
1	-4.415219000	7.319985000	-0.013655000
6	-5.599562000	7.280504000	1.789687000
6	-3.060775000	7.348138000	1.661605000
1	-11.791268000	0.654502000	0.054058000
6	-11.777058000	-1.343416000	-0.760109000
6	-11.731769000	0.826286000	-2.095314000
1	-7.949786000	-7.167404000	0.653862000
1	-6.285649000	-7.826173000	0.730394000
1	-7.473729000	-8.504779000	-0.435928000
1	-8.649657000	-5.717343000	-1.456015000
1	-8.200158000	-7.111314000	-2.493289000
1	-7.464178000	-5.494567000	-2.777684000
1	-6.531521000	6.958836000	1.281923000
1	-5.632854000	8.383552000	1.914342000
1	-5.594209000	6.819590000	2.800224000
1	-2.978103000	6.991264000	2.709838000
1	-3.043871000	8.457068000	1.692438000
1	-2.160175000	7.005334000	1.113541000
1	-11.318049000	-1.929056000	-1.584748000
1	-12.879845000	-1.409378000	-0.872795000
1	-11.495643000	-1.833638000	0.193991000
1	-11.290426000	0.329151000	-2.985010000
1	-11.402829000	1.885543000	-2.105898000
1	-12.835488000	0.804071000	-2.214384000

4.5 NMR spectroscopy of reactions with Me_2IPr

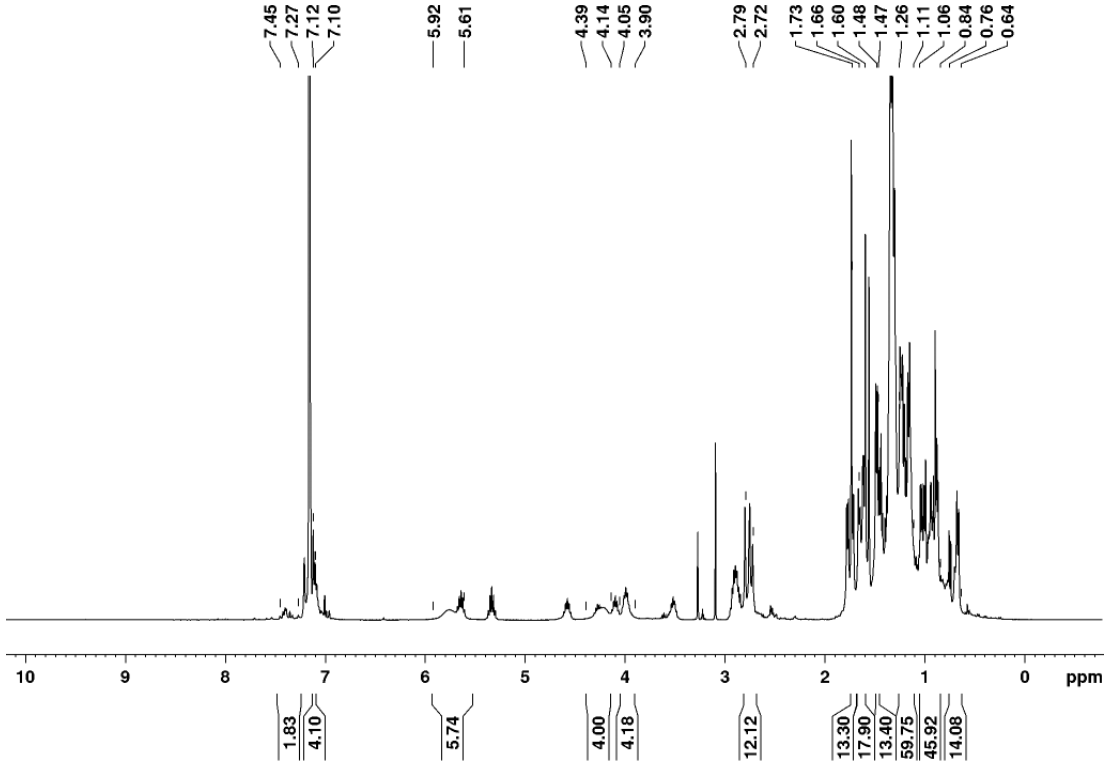

Figure S44. ^{1}H NMR spectrum of the reaction of *Si*-octylated bis(digermene) **2a** with four equivalents of Me_2IPr in C_6D_6 – containing bridged NHC-bis(germylene) adduct (only peaks assigned to this species are picked for clarity) and $Tip_2Ge{=}GeTip_2$.

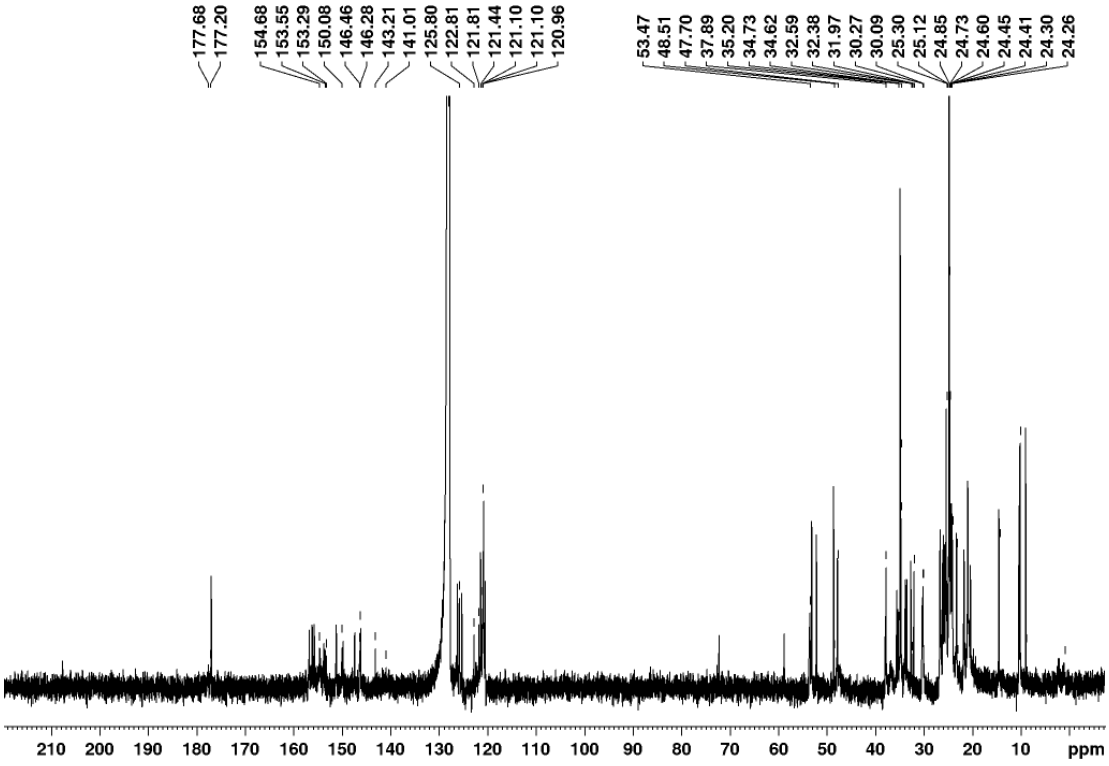

Figure S45. ^{13}C NMR spectrum of the reaction of *Si*-octylated bis(digermene) **2a** with four equivalents of Me_2IPr in C_6D_6 – containing the corresponding bridged NHC-bis(germylene) adduct (only peaks assigned to this species are picked for clarity) and $Tip_2Ge{=}GeTip_2$.

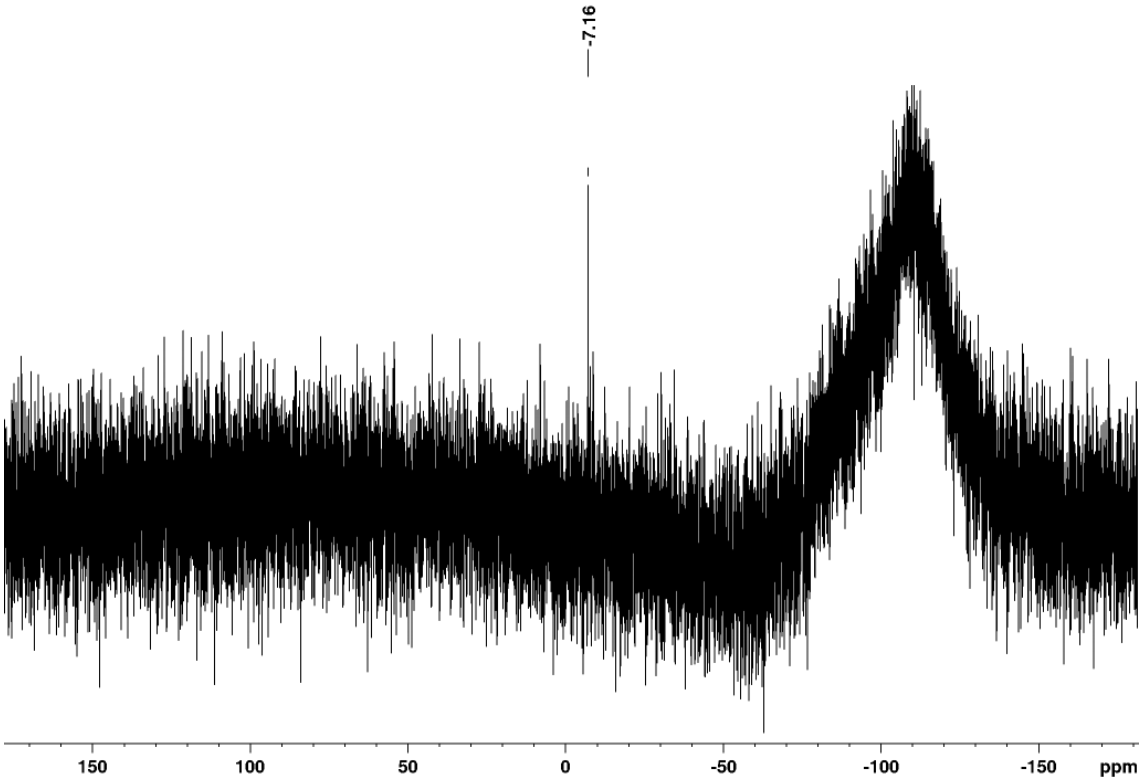

Figure S46. ^{29}Si NMR spectrum of the reaction of *Si*-octylated bis(digermene) **2a** with four equivalents of Me_2IPr in C_6D_6 providing the NHC-bis(germylene) adduct and $Tip_2Ge{=}GeTip_2$.

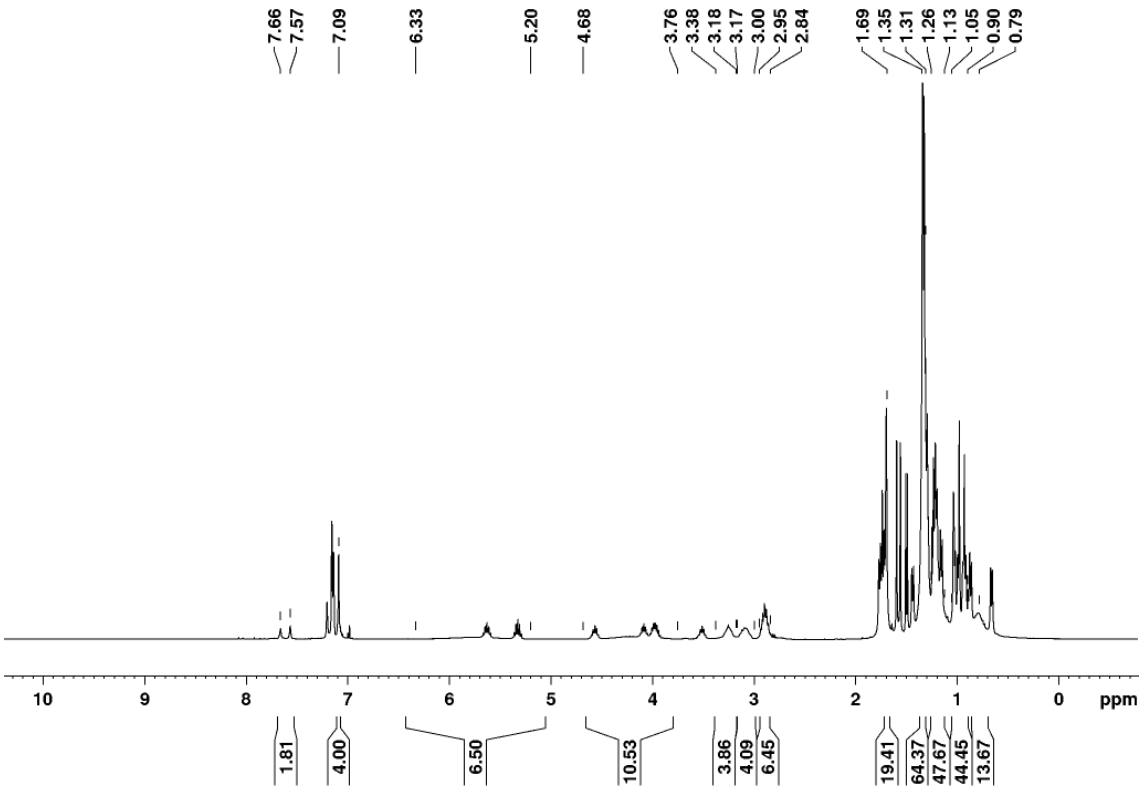

Figure S47. ^{1}H NMR spectrum of the reaction of *Si*-octylated bis(digermene) **2a** with four equivalents of Me_2IPr in C_6D_6 – containing bridged NHC-bis(germylene) adduct (only peaks assigned to this species are picked for clarity) and $Tip_2Ge{=}GeTip_2$.

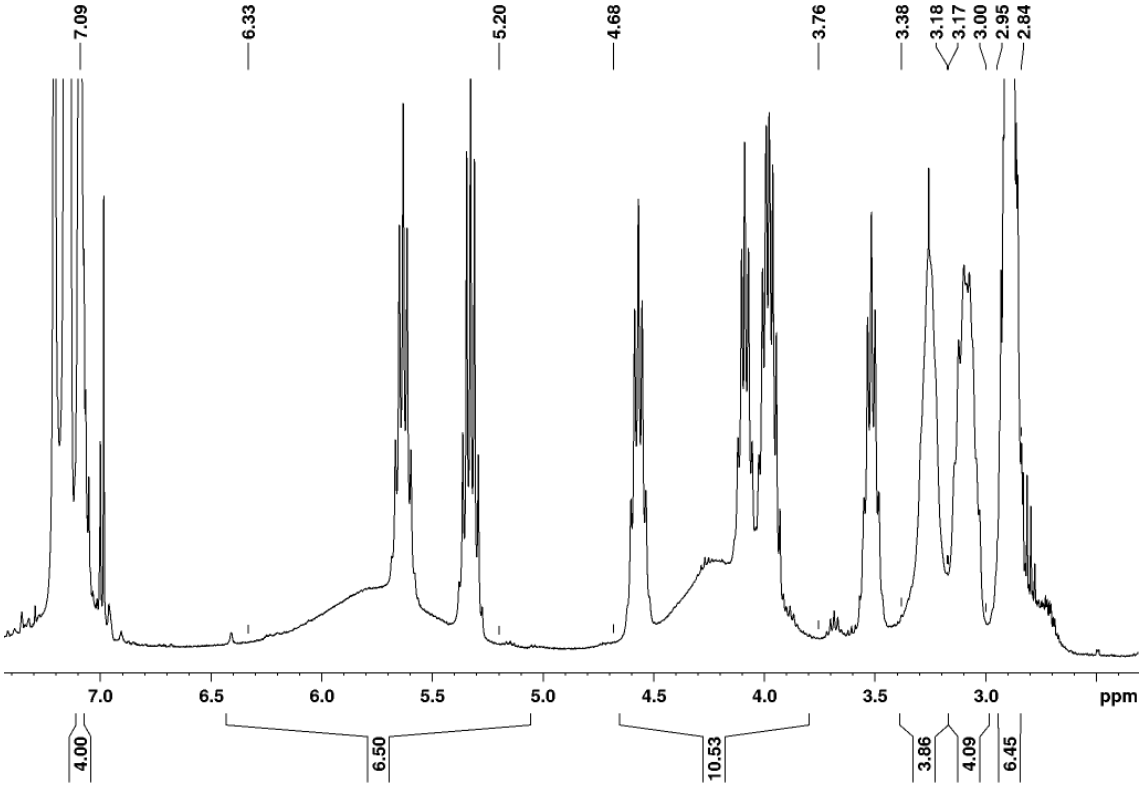

Figure S48. Section from the ^{1}H NMR spectrum of the reaction of *N*-hexylated bis(digermene) **2b** with four equivalents of Me_2IPr in C_6D_6 showing the exceptionally broad multiplets assigned to the isopropyl groups of the coordinated Me_2IPr and the Tip substituents of the bridged NHC-germylene adduct.

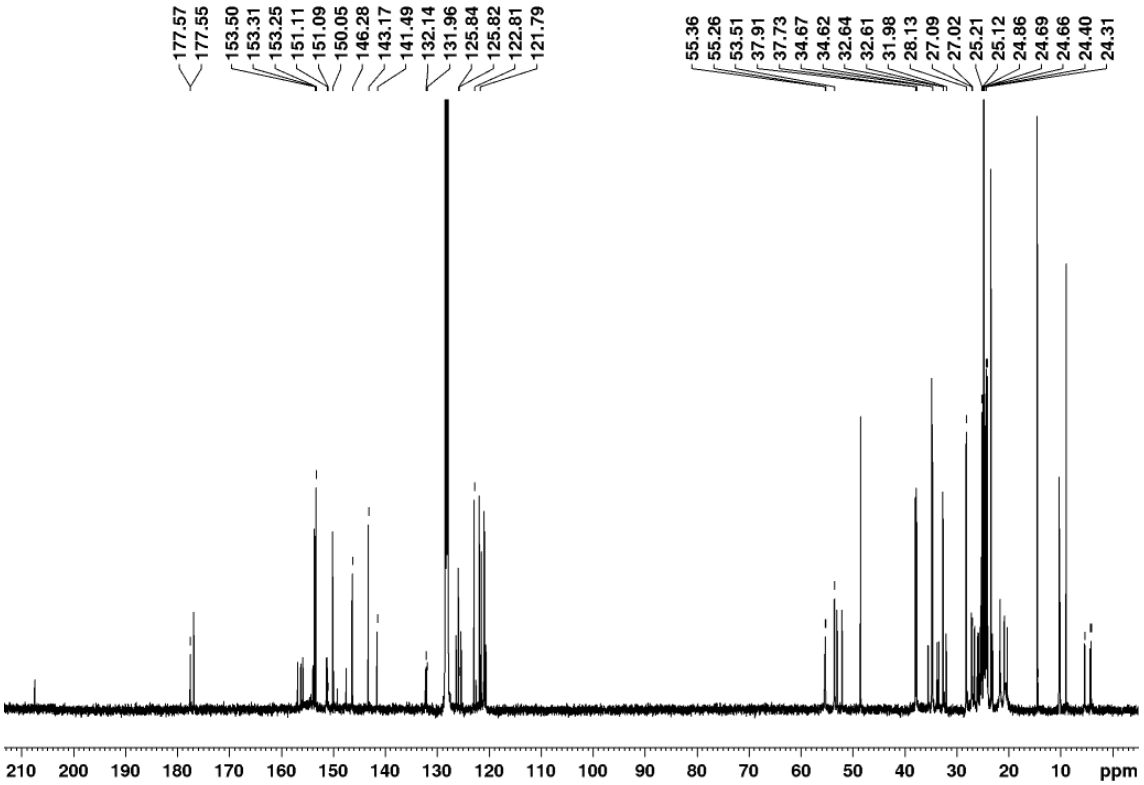

Figure S49. ^{13}C NMR spectrum of the reaction of *N*-hexylated bis(digermene) **2b** with four equivalents of Me_2IPr in C_6D_6 – containing the corresponding bridged NHC-bis(germylene) adduct (only peaks assigned to this species are picked for clarity) and $Tip_2Ge{=}GeTip_2$.

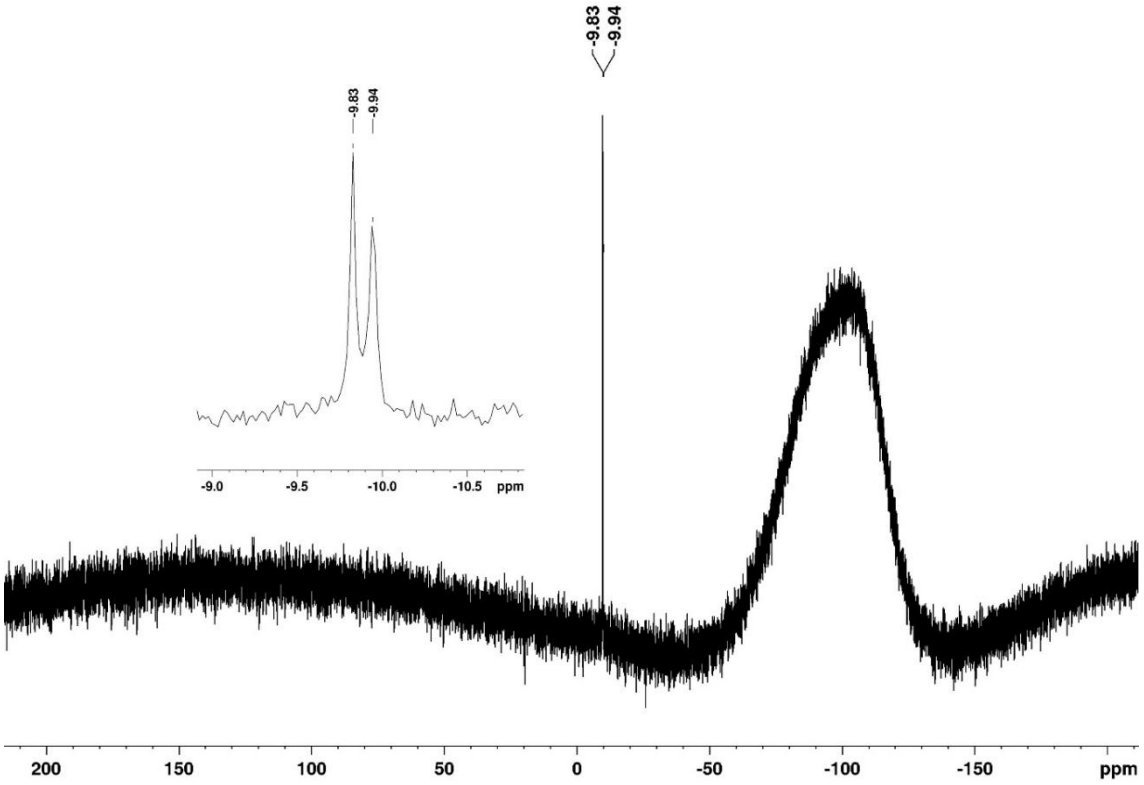

Figure S50. ^{29}Si NMR spectrum of the reaction of *N*-hexylated bis(digermene) **2b** with four equivalents of Me_2IPr in C_6D_6 providing the NHC-bis(germylene) adduct and $Tip_2Ge{=}GeTip_2$.

5. Characterization of digermene polymers

5.1 ^{1}H NMR spectroscopy monitoring of the polymerization process

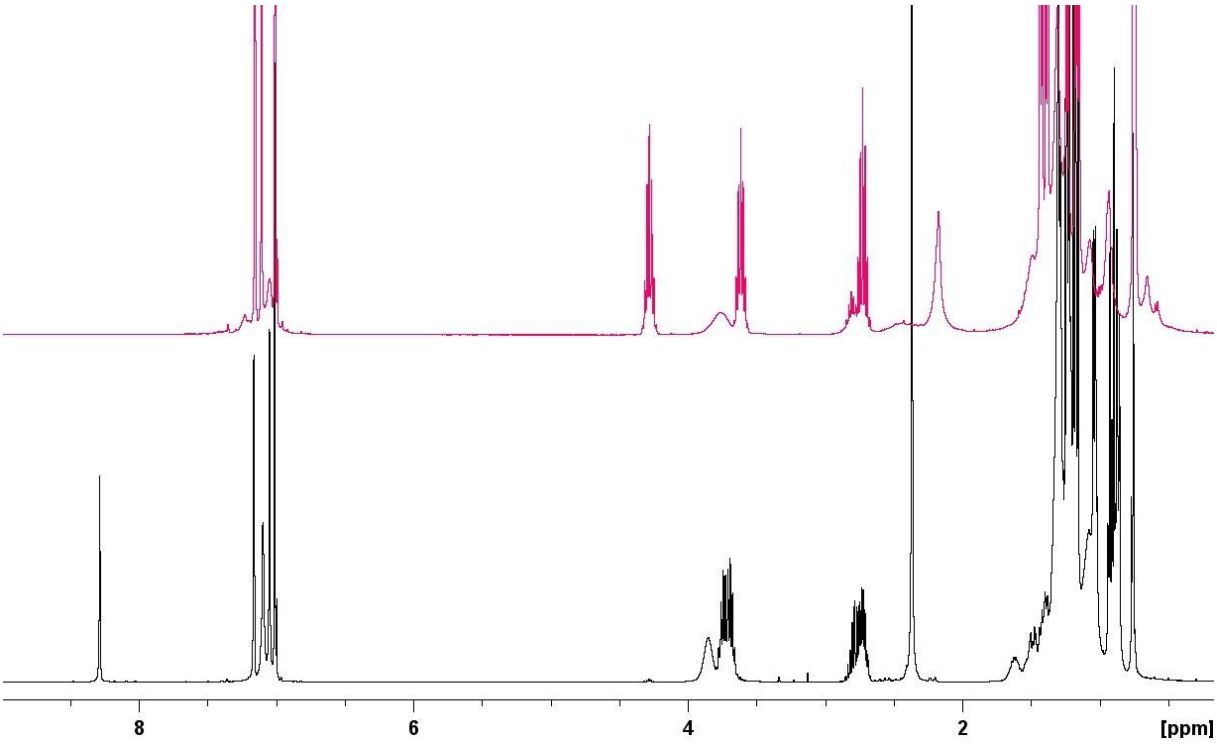

Figure S51. Reaction mixture of the polymerization of *Si*-octylated bis(digermene) **2a** after 48 h (top) and 0 h (bottom).

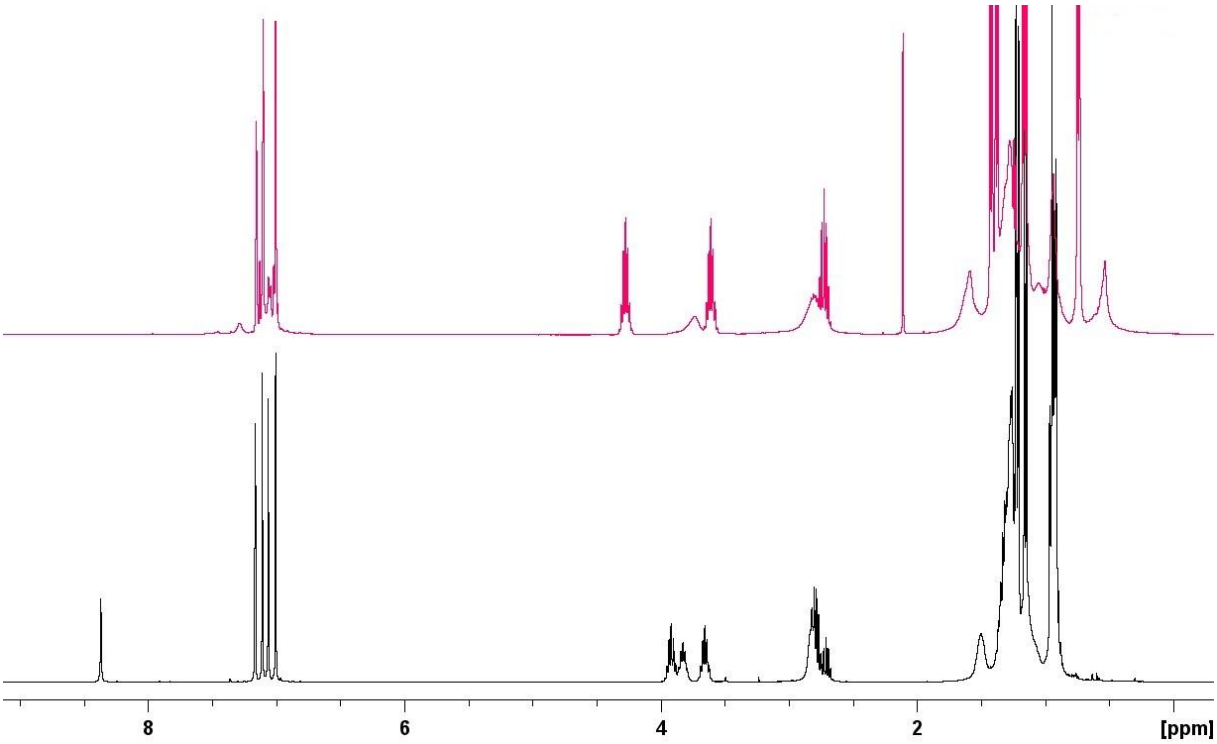

Figure S52. Reaction mixture of the polymerization of *N*-hexylated bis(digermene) **2b** after 48 h (top) and 0 h (bottom).

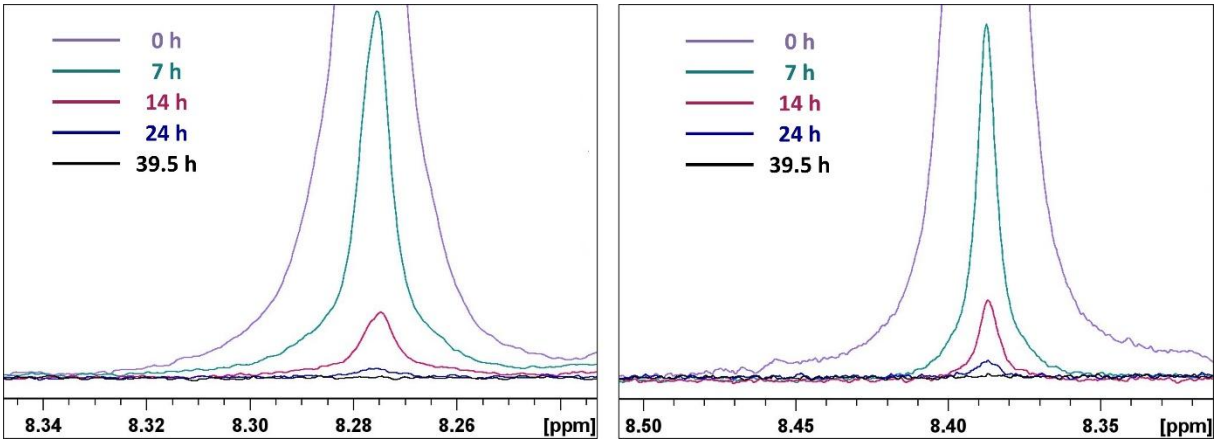

Figure S53. Descending ^{1}H NMR signal of the phenylene protons of monomers **2a** (left) and **2b** (right) at various times during polymerization at 65°C and 105°C, respectively.

Determination of the conversion and degree of polymerization according to Carothers theory:[S18,S19]

Carothers correlation of the degree of polymerization X_n and the conversion p of a bifunctional monomer in a condensation polymerization:

$$X_n = (1-p)^{-1} \quad \text{(S1)}$$

$$p = N_{t,c} \cdot N_0^{-1} \quad \text{(S2)}$$

$N_{t,c}$: number of co-condensate molecules released during the metathesis reaction (in this case: $Tip_2Ge{=}GeTip_2$) at time t; N_0: initial number of monomer molecules

N_0 is set to 1 by referencing the integration of the multiplets in the monomer spectra (at time t = 0 min) at 4.01 to 3.53 ppm (**2a**) and 3.96 to 3.67 ppm (**2b**) to 12H and 8H, respectively. The resulting integration of the solvent peak (**2a**: 7.16 ppm for benzene-d_6, **2b**: 2.08 ppm for toluene-d_8) is taken as reference for all spectra at time t. $N_{t,c}$ is then determined by integration of a Tip-iPr septett of $Tip_2Ge{=}GeTip_2$ representing 4H (**2a**: 4.3865 - 4.1661, **2b**: 4.317 - 4.121 ppm) and devision by 4.

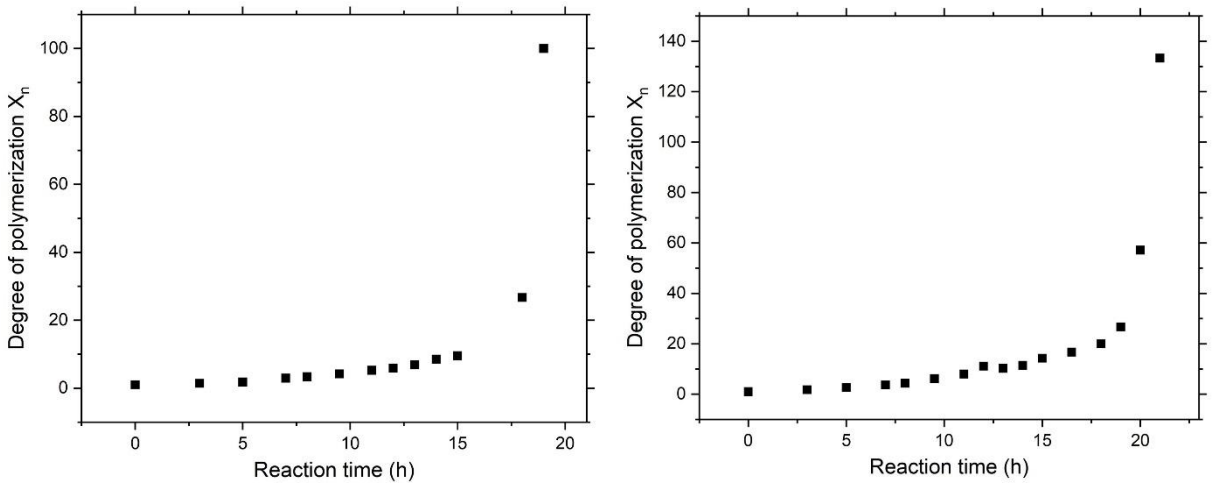

Figure S54. Plot of number average degree of polymerization X_n against reaction time for **3a** (left) and **3b** (right).

Table S9. Reaction times, conversion p and resulting degree of polymerization X_n calculated as outlined above for polymers **3a** and **3b**.

3a			**3b**		
Reaction time (h)	**p (%)**	**X_n**	**Reaction time (h)**	**p (%)**	**X_n**
0	0	1.00	0	0	1.00
3	29.3	1.41	3	44.0	1.79
5	44.5	1.80	5	63.0	2.70
7	66.0	2.94	7	72.8	3.67
8	70.0	3.33	8	77.0	4.35
9.5	76.3	4.21	9.5	83.8	6.15
11	81.0	5.26	11	87.5	8.00
12	83.0	5.88	12	91.0	11.1
13	85.5	6.90	13	90.3	10.3
14	88.3	8.51	14	91.3	11.4
15	89.5	9.52	15	93.0	14.3
18	96.3	26.7	16.5	94.0	16.7
19	99.0	100	18	95.0	20.0
			19	96.3	26.7
			20	98.3	57.1
			21	99.3	133

5.2 Solution NMR spectroscopy

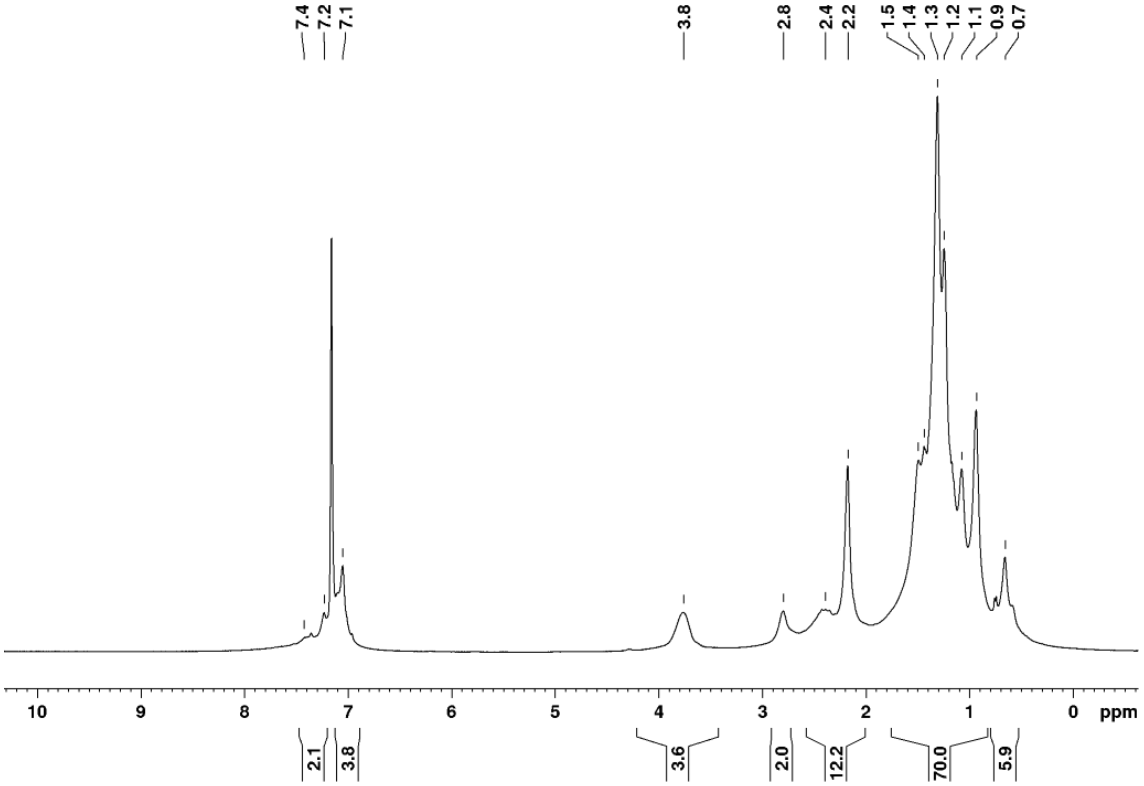

Figure S55. ^{1}H NMR spectrum of *Si*-octylated digermene polymer **3a** in C_6D_6.

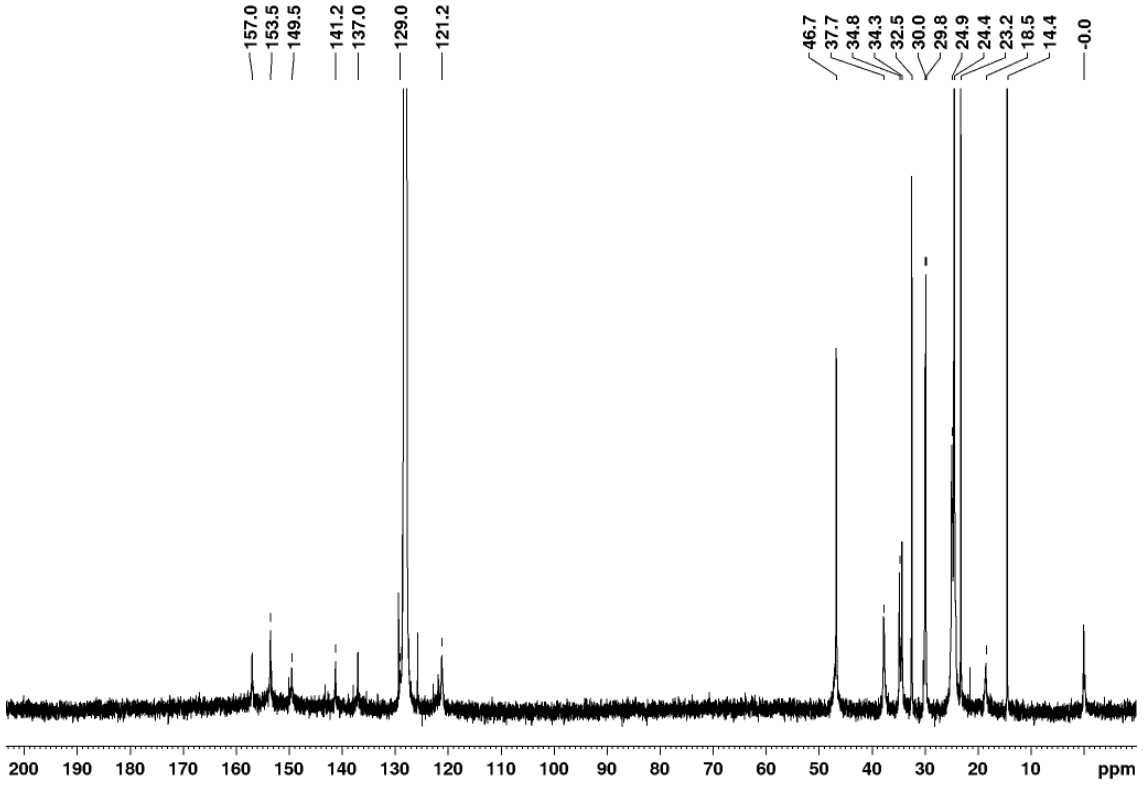

Figure S56. ^{13}C NMR spectrum of *Si*-octylated digermene polymer **3a** in C_6D_6.

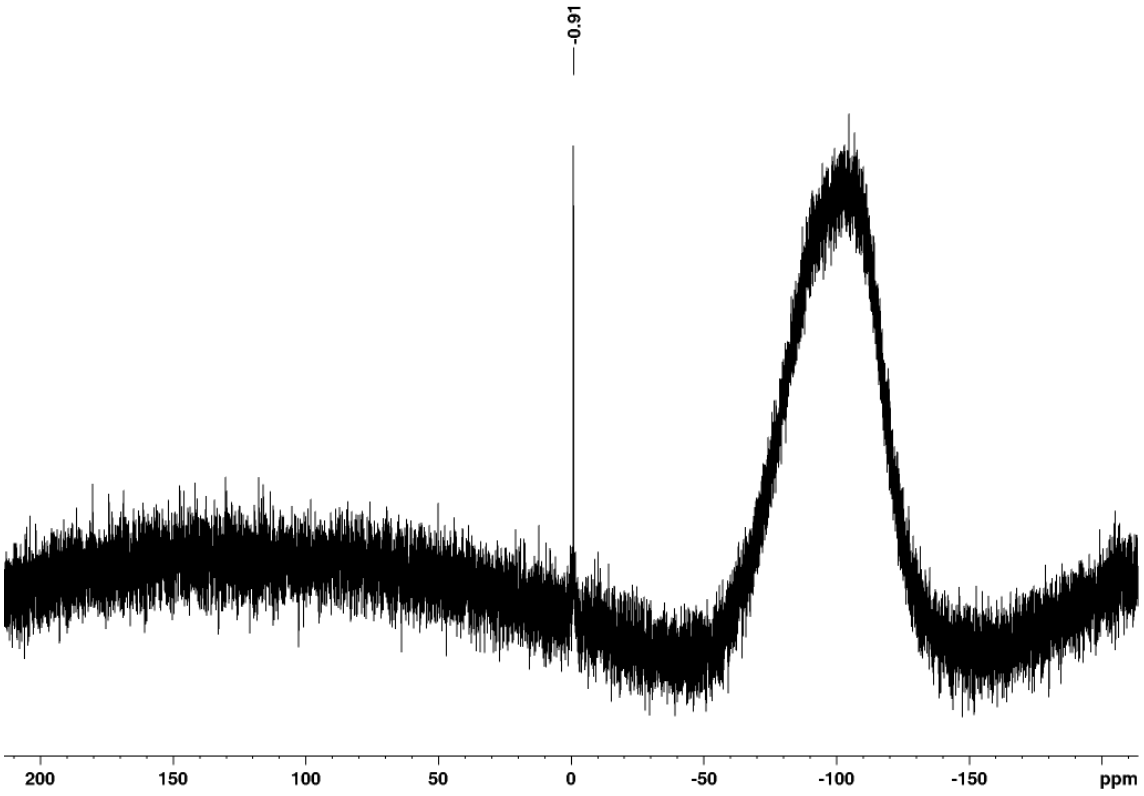

Figure S57. ^{29}Si NMR spectrum of *Si*-octylated digermene polymer **3a** in C_6D_6.

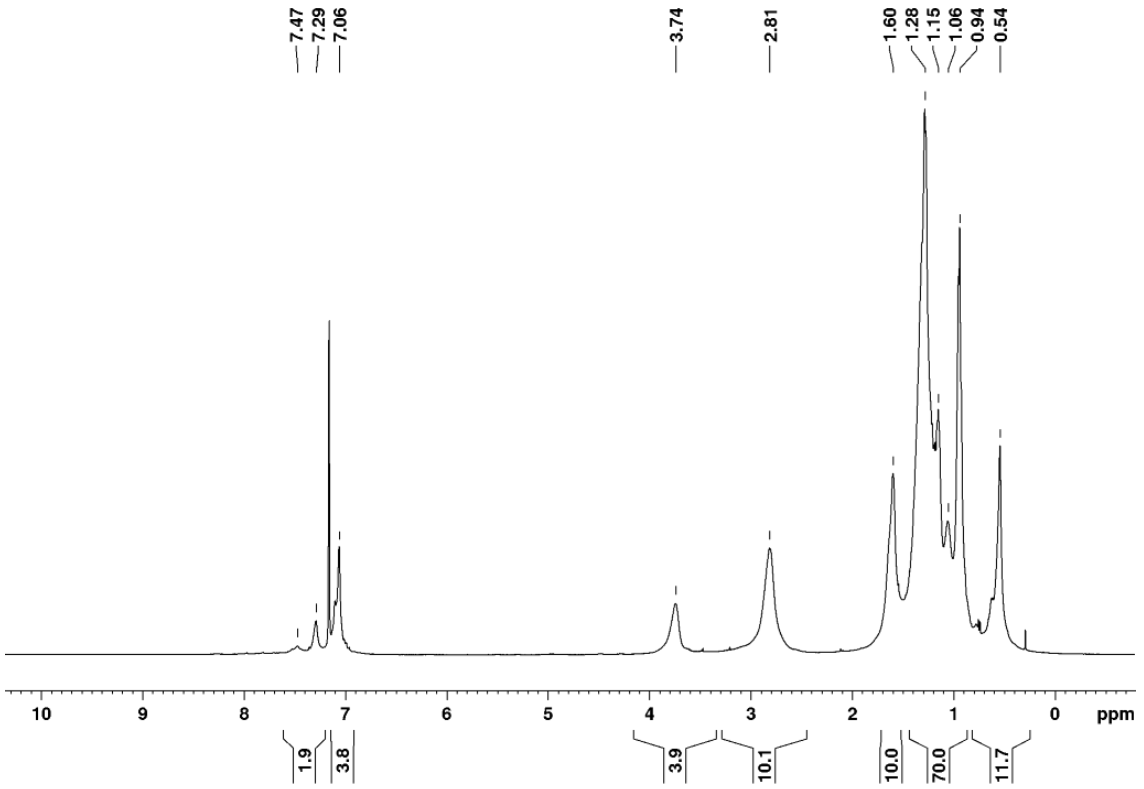

Figure S58. ^{1}H NMR spectrum of *N*-hexylated digermene polymer **3b** in C_6D_6.

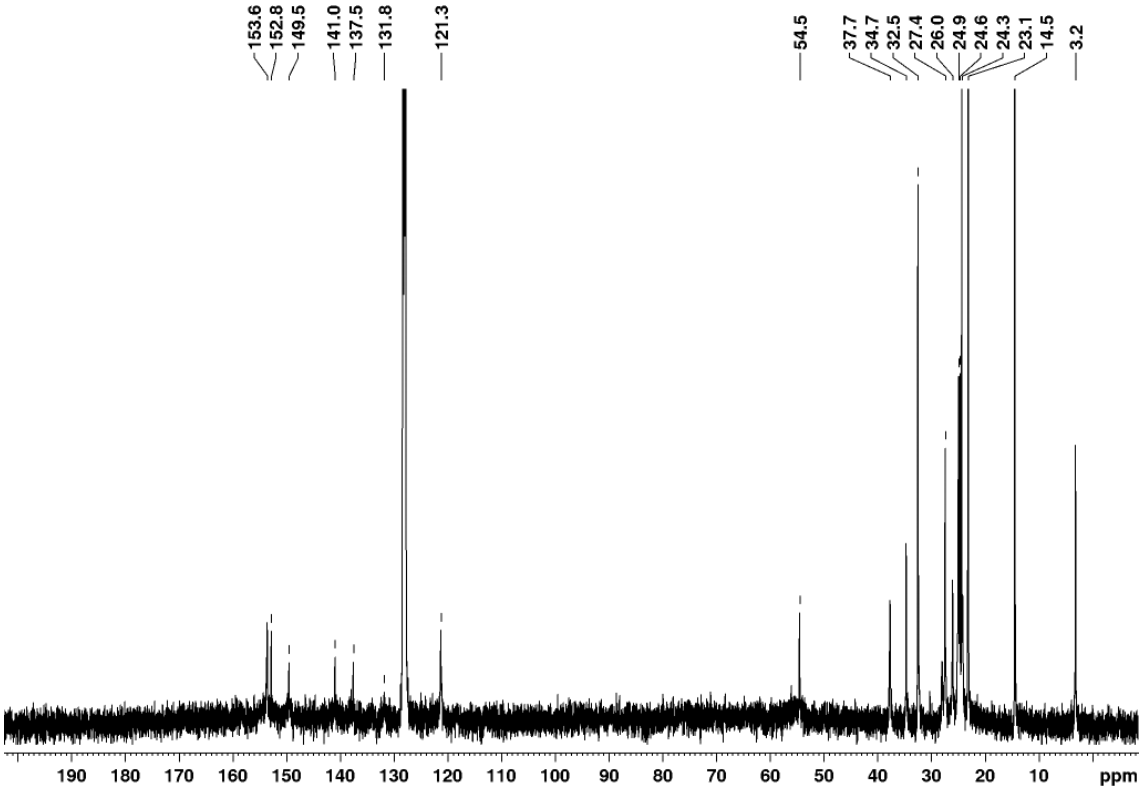

Figure S59. ^{13}C NMR spectrum of *N*-hexylated digermene polymer **3b** in C_6D_6.

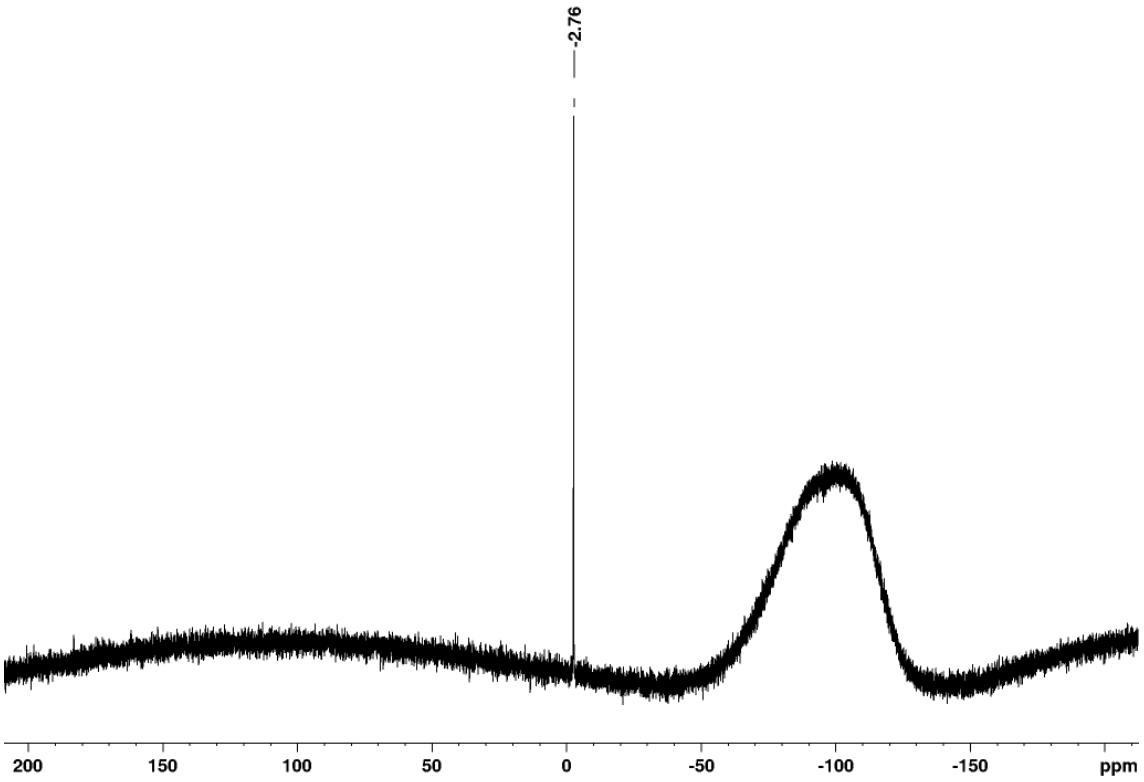

Figure S60. ^{29}Si NMR spectrum of *N*-hexylated digermene polymer **3b** in C_6D_6.

5.3 Solid state CP/MAS NMR spectroscopy

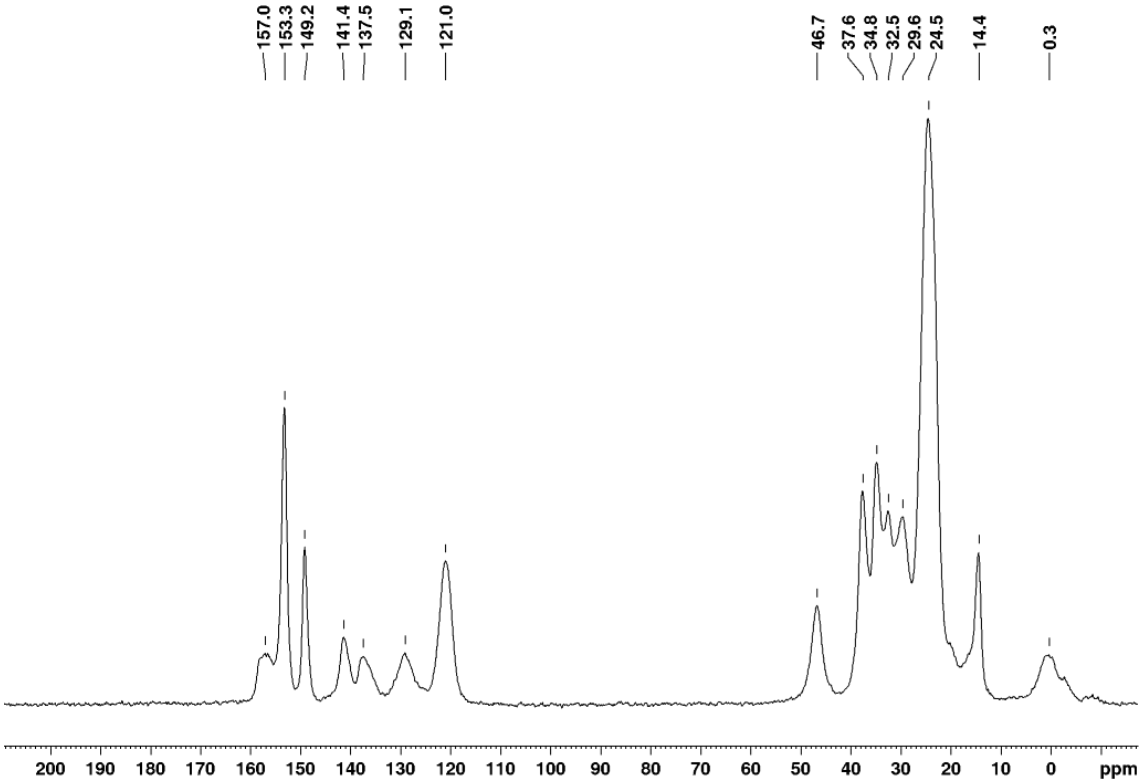

Figure S61. $^{13}C\{^{1}H\}$ CP/MAS NMR spectrum of *Si*-octylated digermene polymer **3a**.

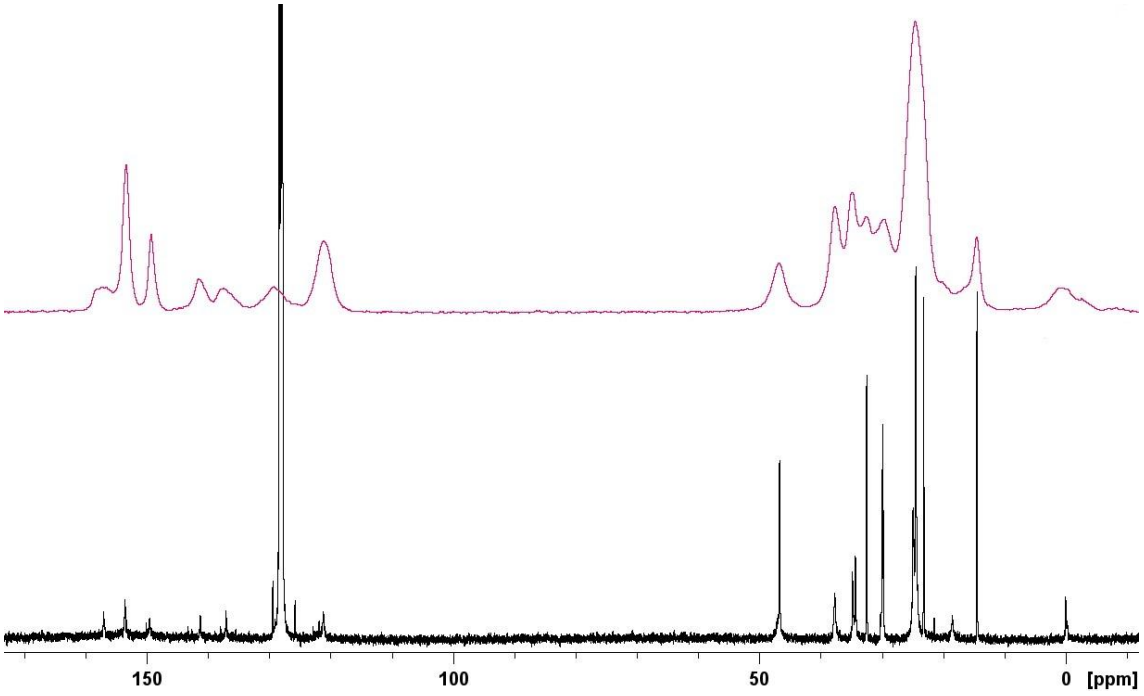

Figure S62. Comparison of the $^{13}C\{^{1}H\}$ CP/MAS NMR and $^{13}C\{^{1}H\}$ solution NMR (bottom) spectra of *Si*-octylated digermene polymer **3a**.

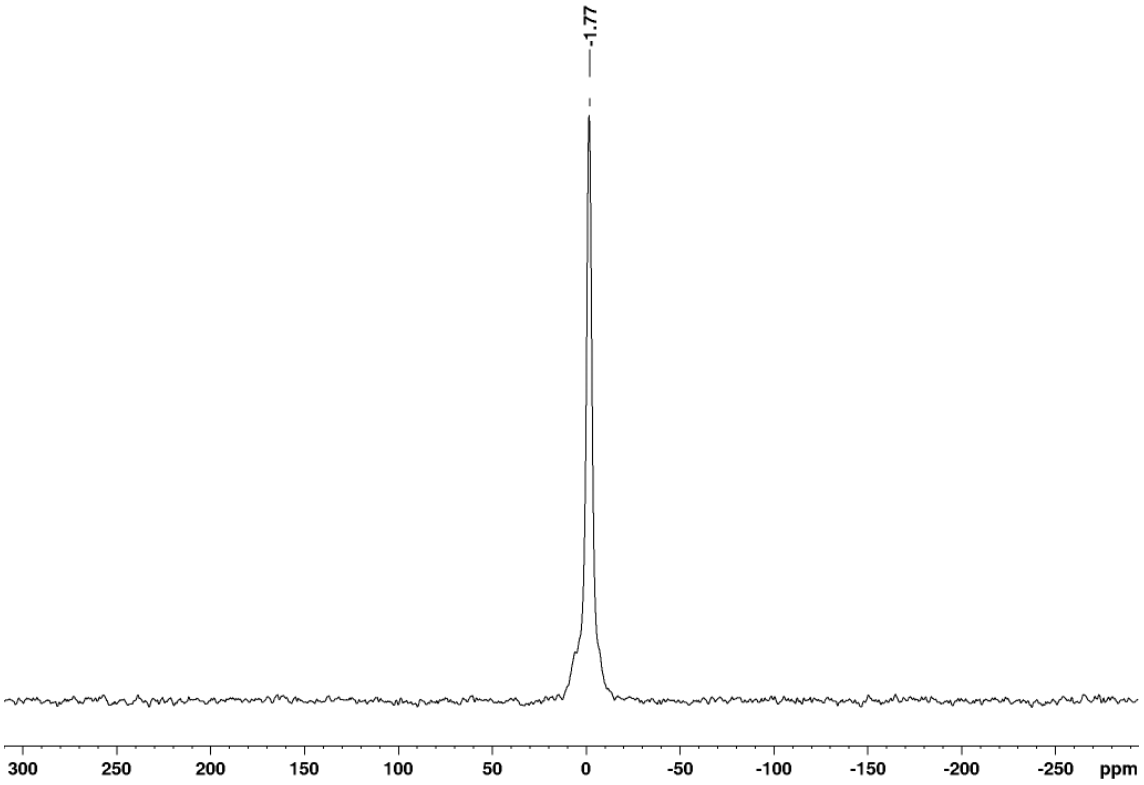

Figure S63. $^{29}Si\{^{1}H\}$ CP/MAS NMR spectrum of *Si*-octylated digermene polymer **3a**.

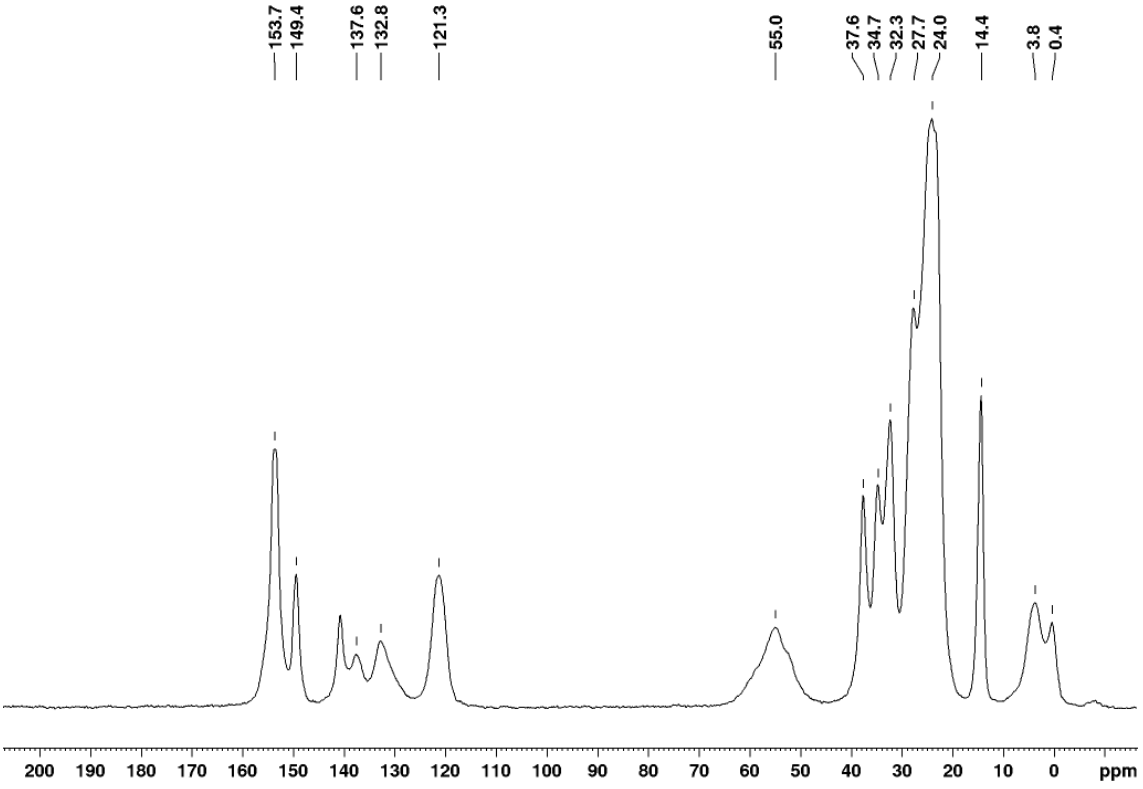

Figure S64. 13C{1H} CP/MAS NMR spectrum of *N*-hexylated digermene polymer **3b**.

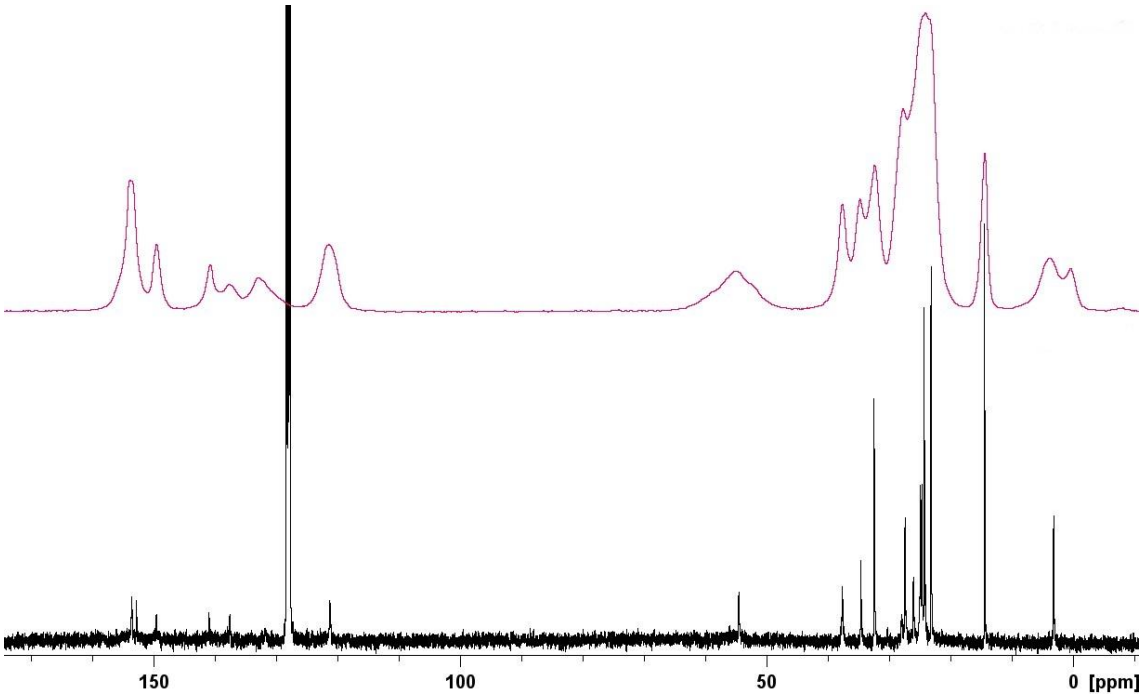

Figure S65. Comparison of the $^{13}C\{^{1}H\}$ CP/MAS NMR and $^{13}C\{^{1}H\}$ solution NMR (bottom) spectra of *N*-hexylated digermene polymer **3b**.

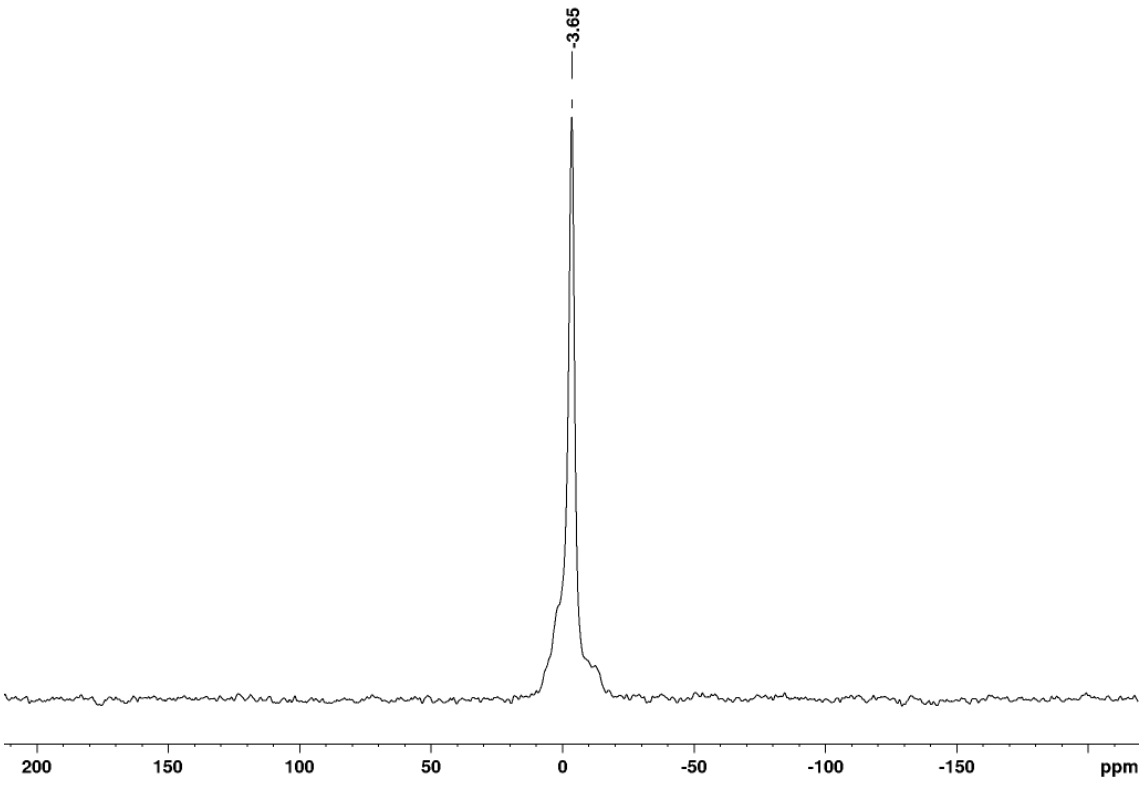

Figure S66. $^{29}Si\{^{1}H\}$ CP/MAS NMR spectrum of *N*-hexylated digermene polymer **3b**.

5.4 DFT calculations for model digermenes

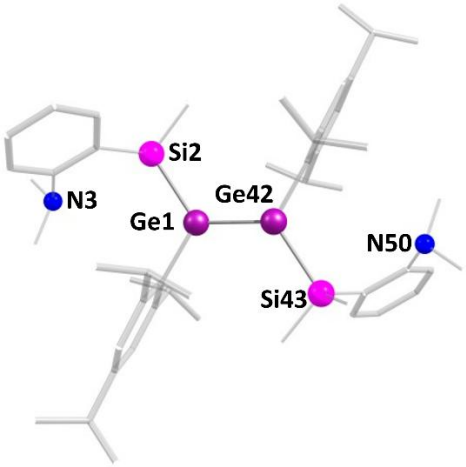

Figure S67. Optimized structure of model disilyldigermene **4**.

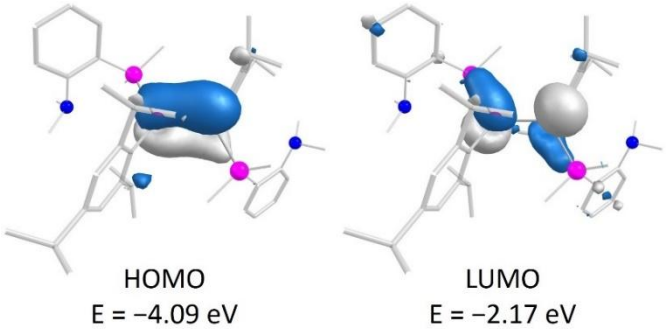

Figure S68. HOMO and LUMO of model disilyldigermene **4** (contour value 0.043); HOMO-LUMO gap = 1.92 eV. Hydrogen atoms omitted for clarity.

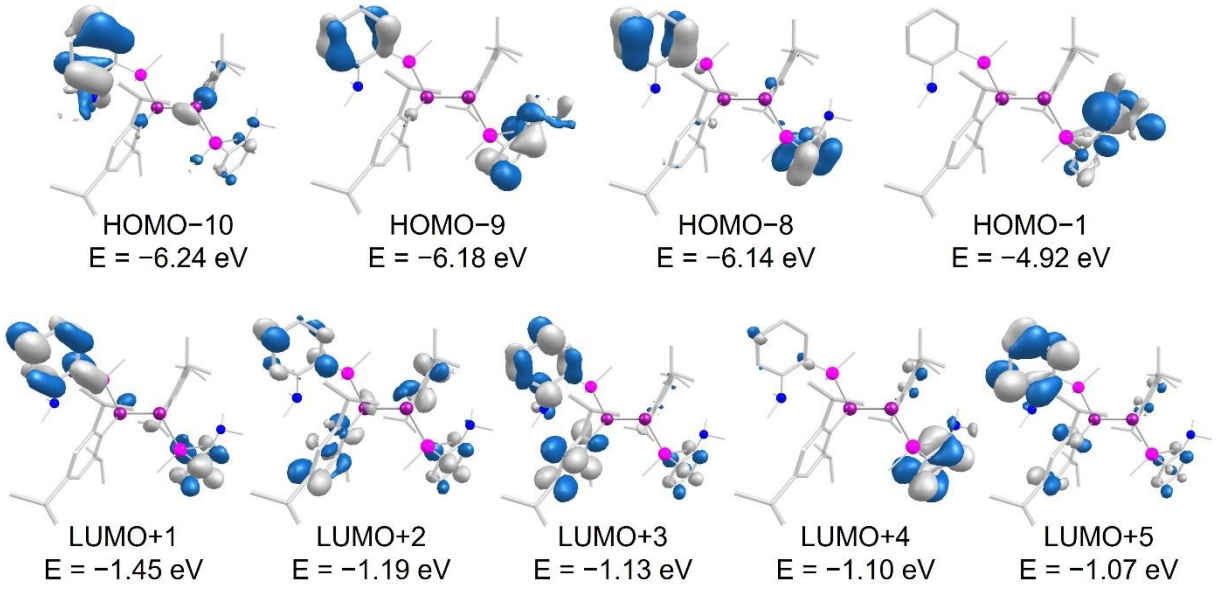

Figure S69. Selected frontier orbitals of model disilyldigermene **4** (contour value 0.036). Hydrogen atoms omitted for clarity.

Table S10. Atomic coordinates of the optimized structure of model disilyldigermene **4**.

32	-0.931234941	0.420610679	-0.389511608
14	-1.283661570	2.772641183	-0.657947003
7	-4.180765231	1.933530195	-1.626885886
6	-2.489527978	-0.780290454	-0.196658165
6	-3.287185749	-0.781494830	0.976745629
6	-4.381198915	-1.665933331	1.054731724
6	-4.701189402	-2.544863456	0.002829941
6	-3.885160555	-2.539199413	-1.143460736
6	-2.780720280	-1.675637515	-1.261750203
6	-2.934912455	0.103844126	2.168697523
6	-2.023933318	-0.658792797	3.147443490
6	-4.157302110	0.690370174	2.888413703
6	-5.906901830	-3.471394123	0.095844626
6	-5.794711438	-4.439793383	1.288698745
6	-7.222265600	-2.668884606	0.142327650
6	-1.911241811	-1.677006497	-2.519622087
6	-2.312740485	-0.534434636	-3.473933083
6	-2.973741730	3.249971878	0.067476081
6	-4.197373756	2.714424319	-0.422561064
6	-5.404060727	2.965074436	0.265437885
6	-5.419361676	3.758918363	1.423441952
6	-4.223342764	4.308738071	1.909342498
6	-3.018667238	4.047992755	1.234720687
6	-4.273946556	2.756712593	-2.834480561
6	-5.134067129	0.828647428	-1.667324686
6	0.069365836	3.624790949	0.363446013
6	-0.980162156	3.280570902	-2.464361568
6	-1.860575195	-3.022411082	-3.255367988
6	4.242942653	1.581340087	-1.335688478
6	4.779798841	2.473534316	-0.389162089
6	4.174395827	2.542079423	0.878765064
6	2.597783800	-0.182616531	-2.120115199
6	5.999538223	3.325059447	-0.718004017
6	7.246557640	2.445499182	-0.937299545
6	2.445653369	1.808984774	2.606836361
6	3.034996573	0.706806811	3.509540251
6	2.727991212	-3.249267257	0.099764148
6	3.520771334	-4.505274586	-1.866961957
6	2.485353347	-4.087729140	-1.014111422
6	4.661101071	-2.763838462	2.676792906
6	5.328572958	-0.941198370	1.241260899
32	0.957568574	-0.250265173	0.718165850
14	1.253651198	-2.594086550	1.103288939
6	2.539304571	0.846819401	0.243022121
6	-0.317707232	-3.460365084	0.485267885
6	1.328920804	-2.911961397	2.975190278
6	3.136198203	0.758950646	-1.043667321
6	3.061517545	1.746992331	1.210632935
6	4.065149702	-2.831445692	0.340492858

7	4.340066591	-1.990963723	1.475714758
6	5.103105973	-3.249683466	-0.519110663
6	1.636763504	0.554094528	-3.067179811
6	3.703147029	-0.901849983	-2.908140203
6	2.530138004	3.186922700	3.276224293
6	4.835630290	-4.083022712	-1.616911980
6	5.745579447	4.252667651	-1.921309217

5.5 Natural bond order (NBO) analysis

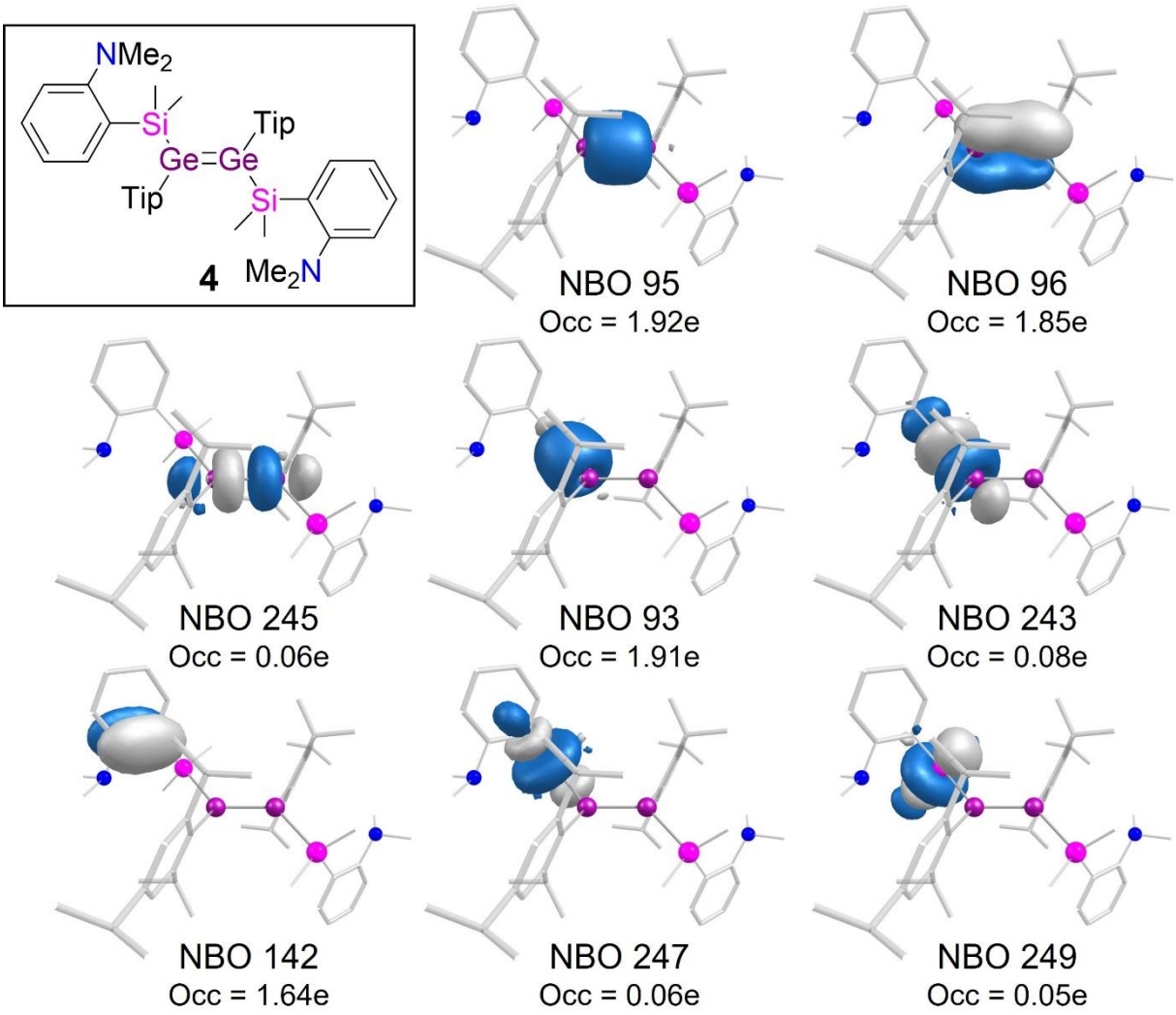

Figure S70. Selected natural bond orbitals (NBOs) of model disilyldigermene **4**.

Table S11. Occupancies and stabilization energies of and between selected NBOs.

Donor NBO	**Occupancy** (e)	**Acceptor NBO**	**Occupancy** (e)	**Stabilization energy** (kcal mol^{-1})
π(Ge=Ge)		**σ*(Si-C)**		
96	1.85	247	0.06	1.51
		249	0.05	2.28
		248*	0.03	0.50
π(C=$C_{aniline}$)		**σ*(Ge-Si)**		
142	1.64	243	0.08	2.14
σ(Ge-Ge)		**σ*(Ge-Si)**		
95	1.92	243	0.08	2.54
σ(Ge-Si)		**σ*(Ge-Ge)**		
93	1.91	245	0.06	1.92
		σ*(Ge-Si)		
		243	0.08	1.65

* σ*(Si-C) of the second methyl group at silicon (comparable to NBO 249)

5.6 TD-DFT calculations

Table S12. Selected absorption bands and assigned transitions from the TD-DFT calculation for disilyldigermene **4** in hexane as a model for the polymers repeat units.

λ_{exp} (nm)	λ_{calc} (nm)	Oscillator strength	Assignment (Contribution)
411	404.5	0.288407724	HOMO → LUMO (85%)
322	324.3	0.037874428	HOMO → LUMO+4 (29%) HOMO → LUMO+5 (24%) HOMO → LUMO+2 (21%)
250	276.3	0.283754397	HOMO-1 → LUMO+1 (84%)
	255.0	0.135298937	HOMO−1 → LUMO+2 (50%) HOMO−8 → LUMO (9%) HOMO−1 → LUMO+4 (7%)
	253.9	0.138684614	HOMO−8 → LUMO (34%) HOMO−1 → LUMO+2 (9%) HOMO−9 → LUMO (5%) HOMO−10 → LUMO (5%)
	249.0	0.149080380	HOMO−1 → LUMO+5 (42%) HOMO−1 → LUMO+3 (13%) HOMO−10 → LUMO (10%) HOMO−9 → LUMO (5%)

5.7 UV/Vis absorption spectroscopy

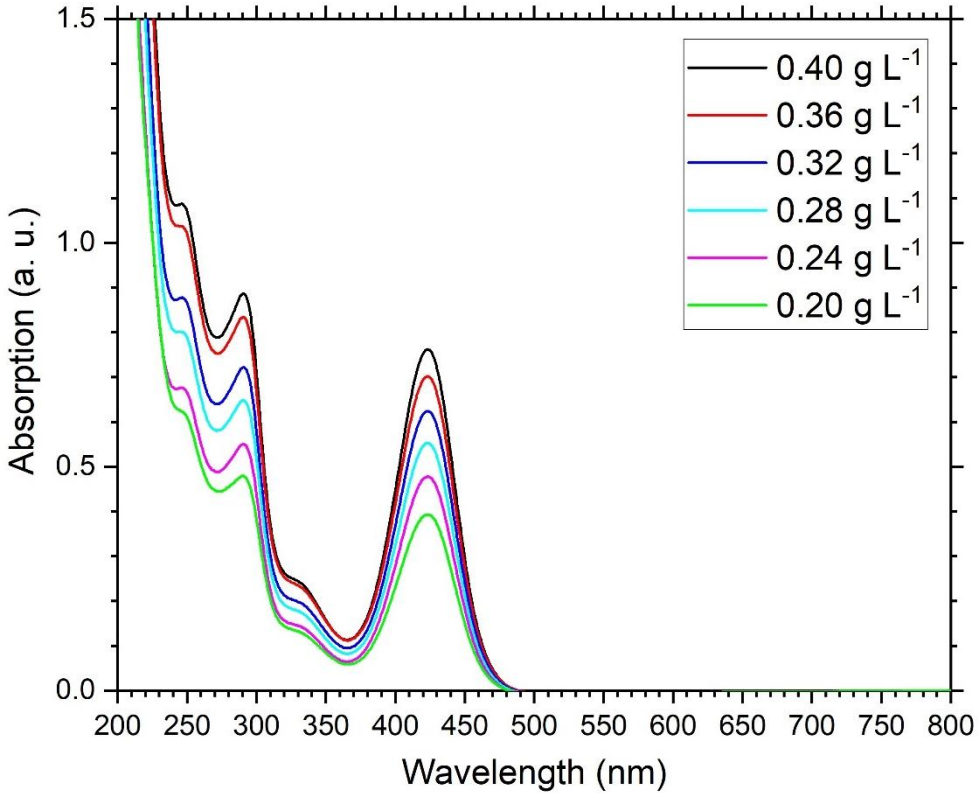

Figure S71. UV/Vis spectra of *Si*-octylated digermene polymer **3a** at different concentrations.

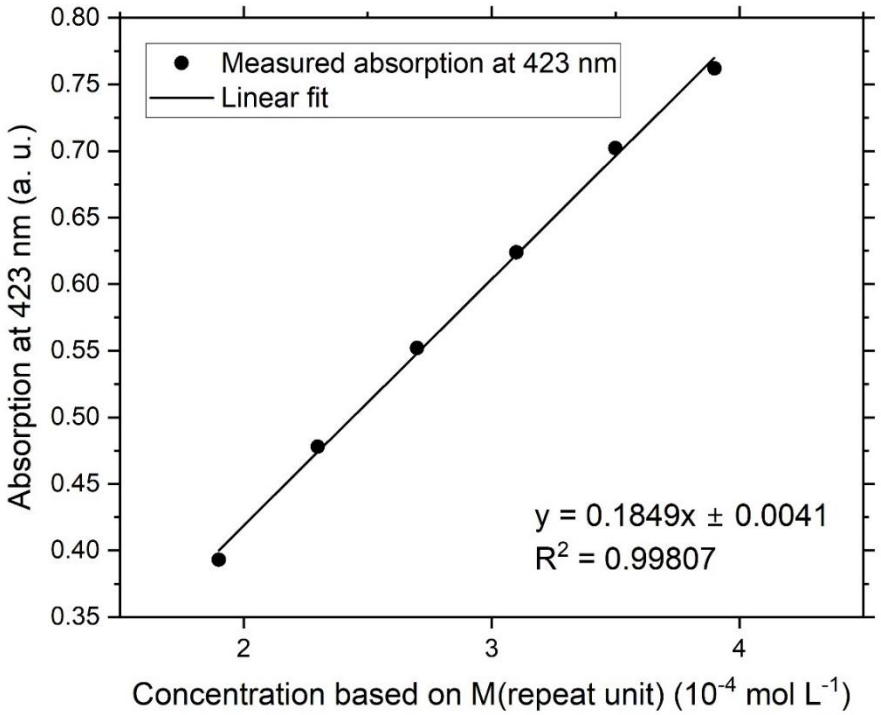

Figure S72. Determination of the extinction coefficient per repeat unit ε (18500 L mol^{-1} cm^{-1}) of **3a** by linear regression of absorbance at 423 nm against concentration.

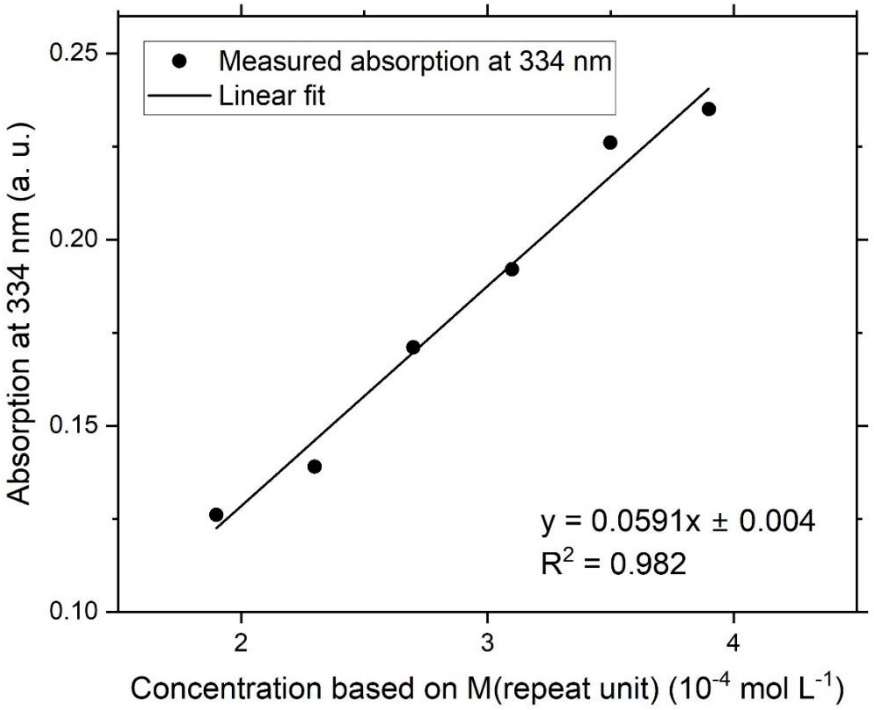

Figure S73. Determination of extinction coefficient per repeat unit ε (5900 L mol^{-1} cm^{-1}) of **3a** by linear regression of absorbance at 334 nm against concentration.

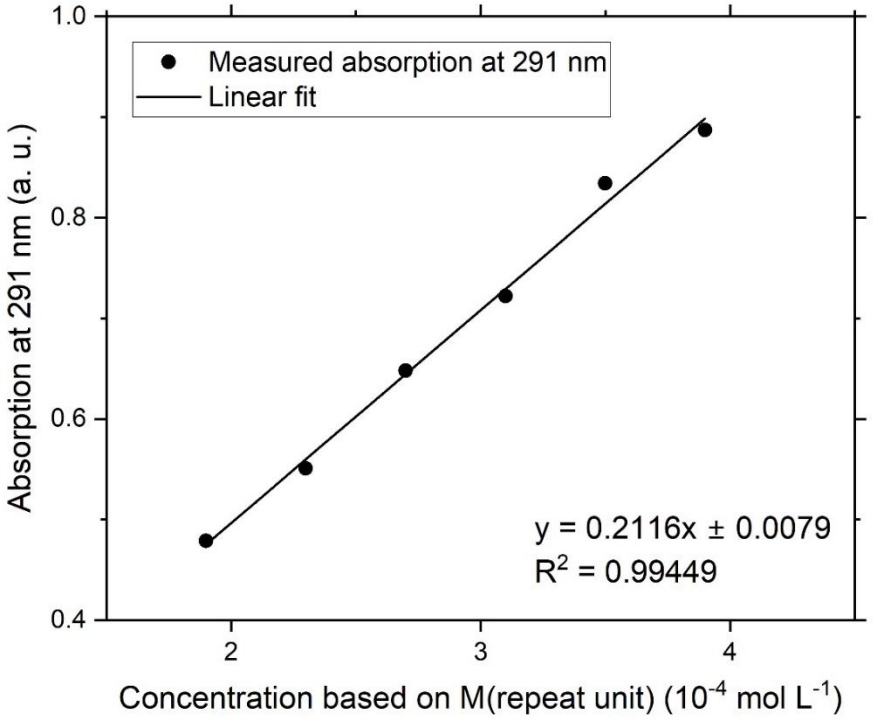

Figure S74. Determination of extinction coefficient per repeat unit ε (21200 L mol^{-1} cm^{-1}) of **3a** by linear regression of absorbance at 291 nm against concentration.

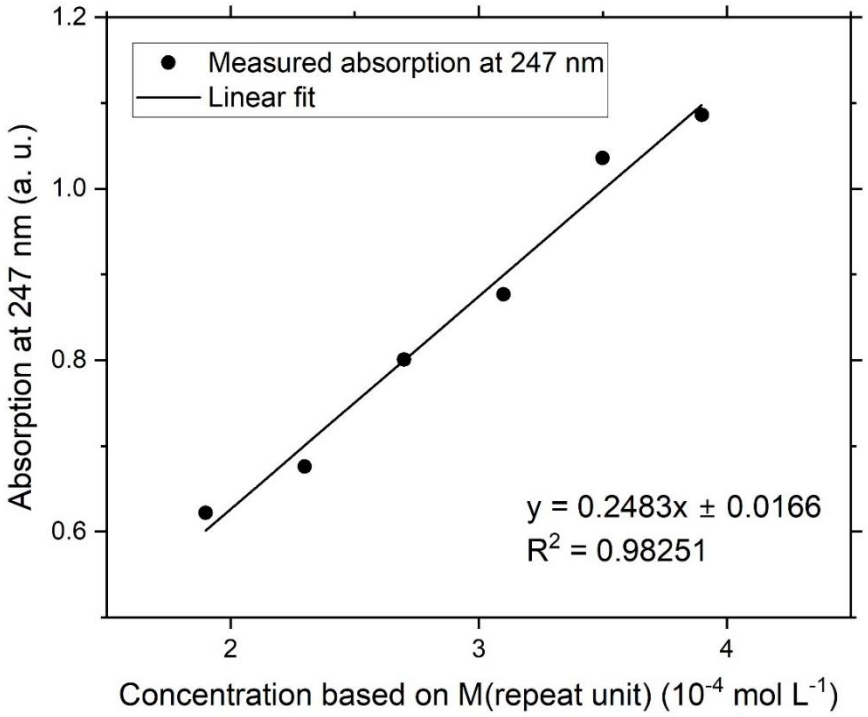

Figure S75. Determination of extinction coefficient per repeat unit ε (24800 L mol^{-1} cm^{-1}) of **3a** by linear regression of absorbance at 247 nm against concentration.

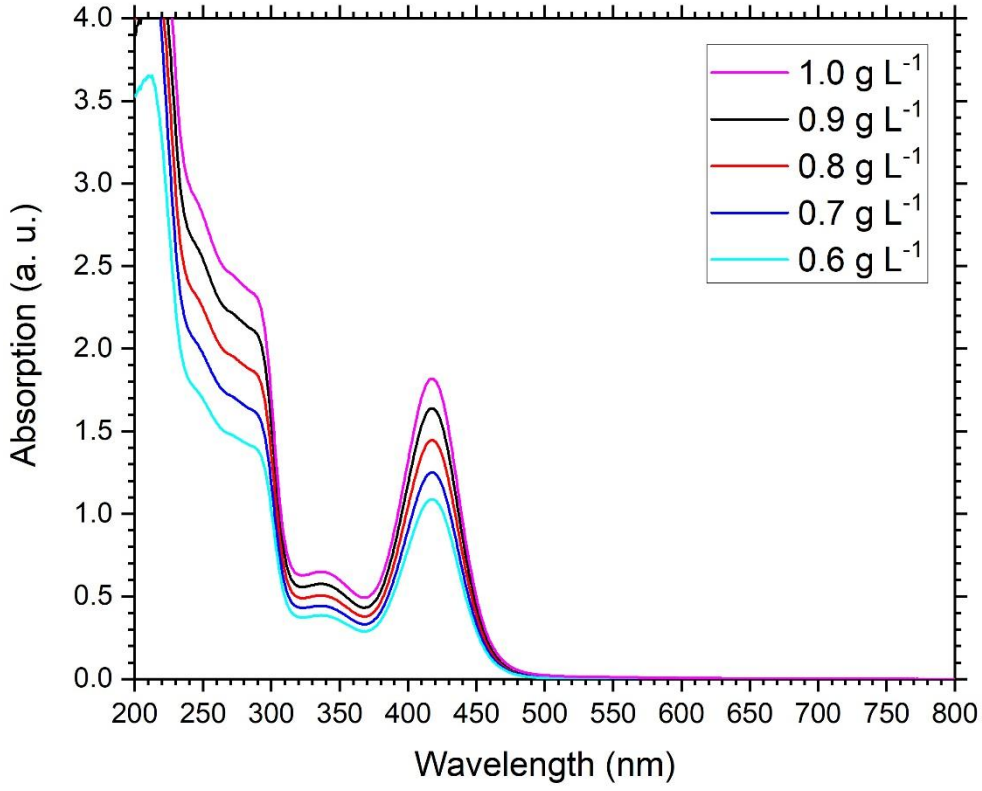

Figure S76. UV/Vis spectra of *N*-hexylated digermene polymer **3b** at different concentrations.

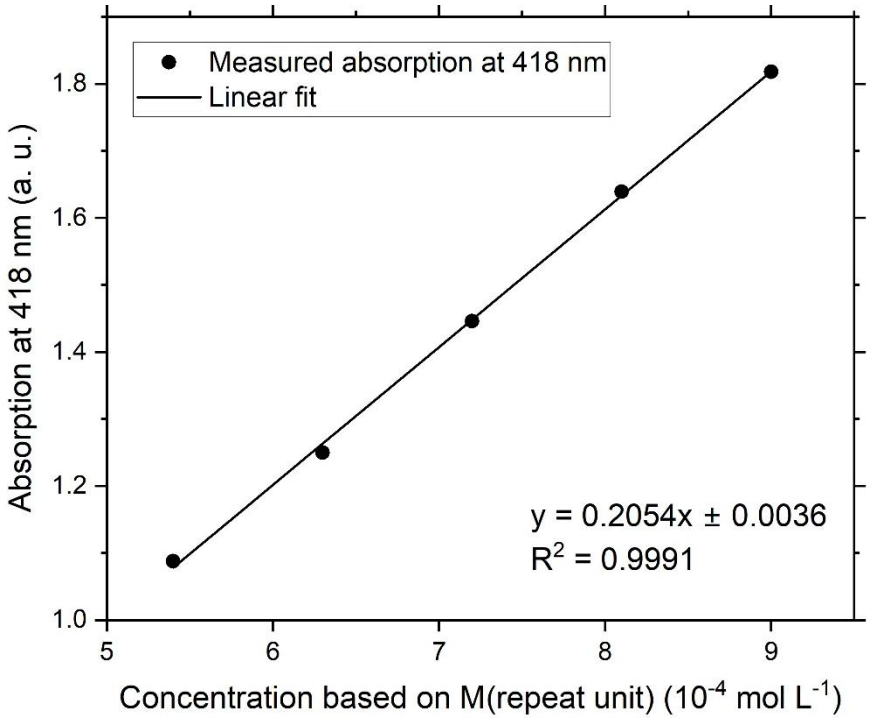

Figure S77. Determination of extinction coefficient per repeat unit ε (20500 L mol^{-1} cm^{-1}) of **3b** by linear regression of absorbance at 418 nm against concentration.

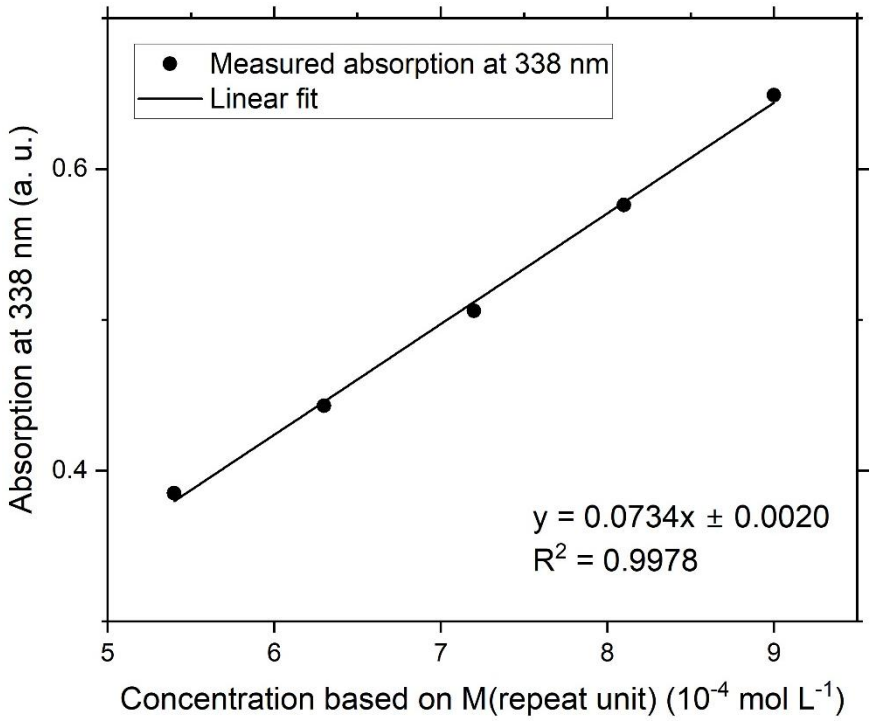

Figure S78. Determination of extinction coefficient per repeat unit ε (7300 L mol^{-1} cm^{-1}) of **3b** by linear regression of absorbance at 338 nm against concentration.

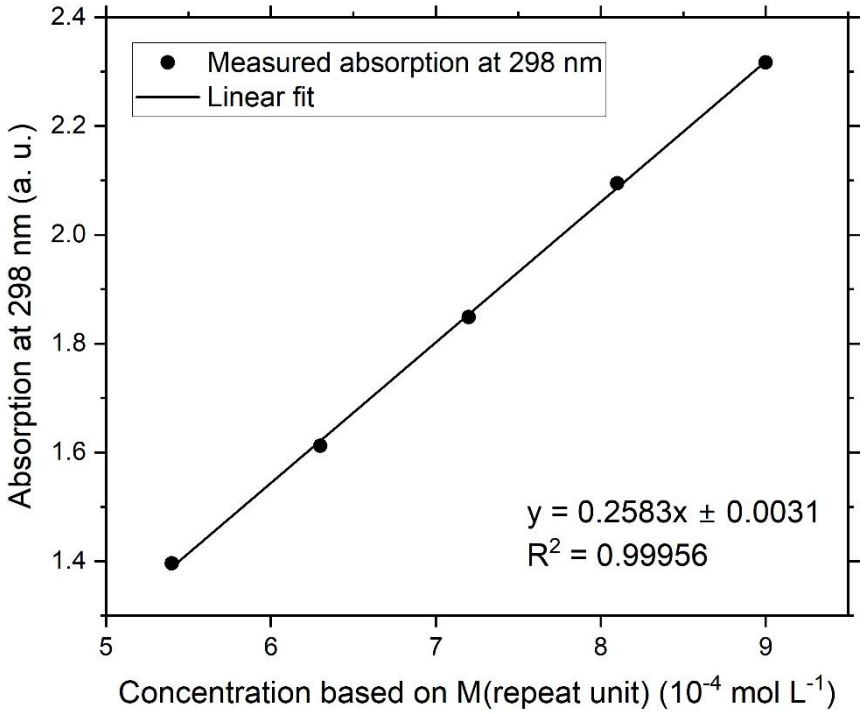

Figure S79. Determination of extinction coefficient per repeat unit ε (25800 L mol^{-1} cm^{-1}) of **3b** by linear regression of absorbance at 298 nm against concentration.

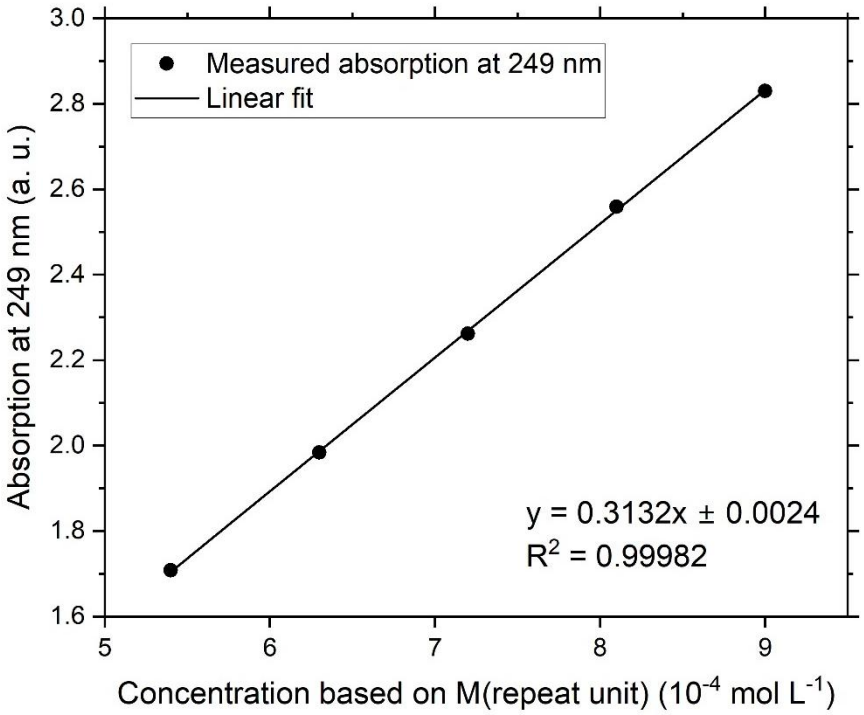

Figure S80. Determination of extinction coefficient per repeat unit ε (31300 L mol^{-1} cm^{-1}) of **3b** by linear regression of absorbance at 249 nm against concentration.

5.8 Powder X-ray diffraction (PXRD)

Powder X-ray diffraction (PXRD) patterns of the pulverized samples were recorded at room temperature on a D8-A25-Advance diffractometer (Bruker, Karlsruhe, Germany) in Bragg-Brentano *θ*-*θ*-geometry (goniometer radius 280 mm) with Cu K_α-radiation (λ = 154.0596 pm). A 12 µm Ni foil working as K_β filter and a variable divergence slit were mounted at the primary beam side. A LYNXEYE detector with 192 channels was used at the secondary beam side. Experiments were carried out in a 2*θ* range of 5 to 70° with a step size of 0.013° and a total scan time of 1h or (after heating) in a 2*θ* range of 7 to 120° with a step size of 0.013° and a total scan time of 2h.

Table S13. 2θ values of the reflections and corresponding distances d obtained in the powder XRD analyses of digermene polymers **3a,b**.

3a		**3b**	
2θ (°)	d (nm)	2θ (°)	d (nm)
8.2	1.08	6.9	1.28
		7.7	1.15
		10.7	0.83
16-26	0.53 – 0.34 (amorphous)	16-26	0.53 – 0.34 (amorphous)

5.9 Differential scanning calorimetry (DSC)

Differential scanning calorimetry (DSC) was performed with a DSC 204 F1 Phoenix calorimeter (NETZSCH-Gerätebau GmbH, Selb, Germany) using aluminium crucibles with pierced lids under nitrogen flow (40 – 60 mL min^{-1}) applying heating rates of 10 to 20 K min^{-1}.

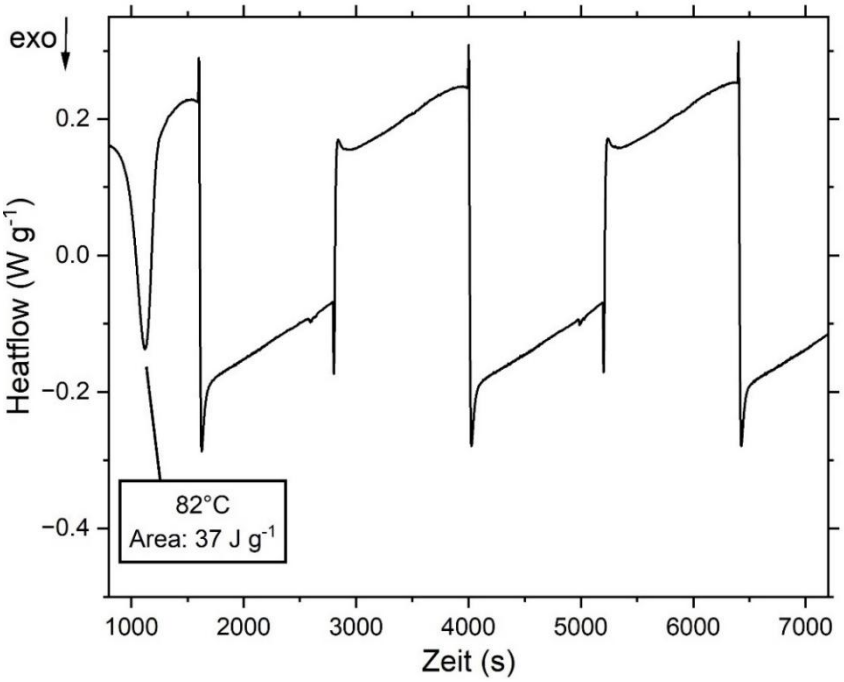

Figure S81. DSC data of *Si*-octylated digermene polymer **3a** showing the heatflow over time at a heating and cooling rate of 10 K min^{-1} for 3 heating and cooling cycles (temperature range: −40 to 160°C).

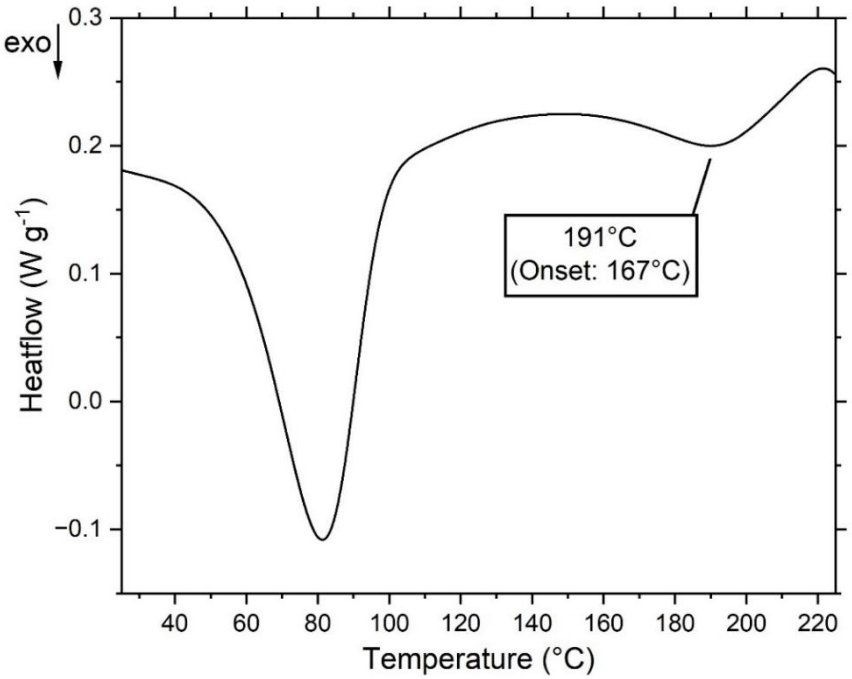

Figure S82. DSC data of *Si*-octylated digermene polymer **3a** showing the heatflow over temperature at a heating rate of 10 K min^{-1}.

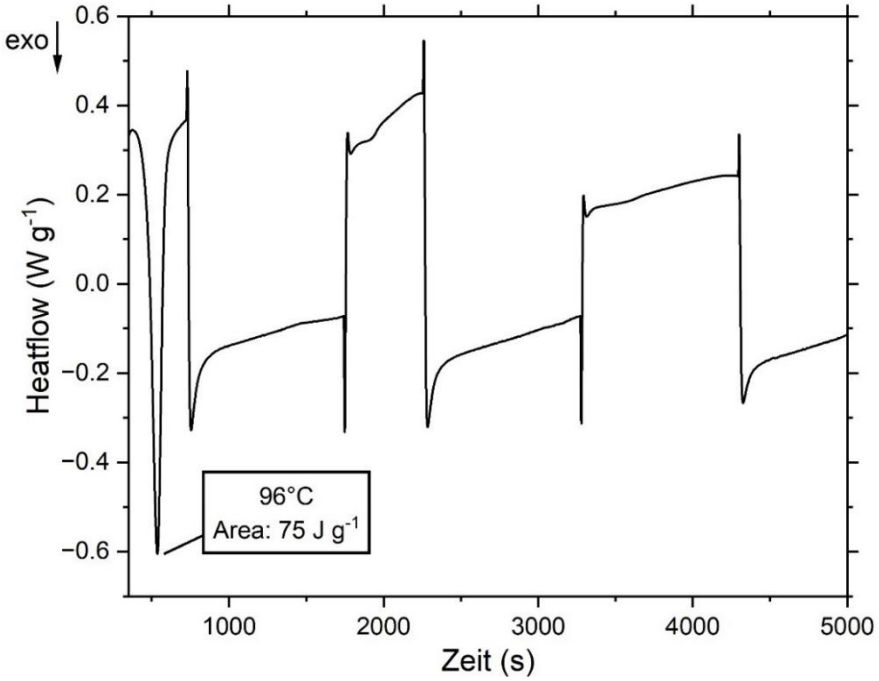

Figure S83. DSC data of *N*-hexylated digermene polymer **3b** showing the heatflow over time at heating rates of 20 K min^{-1} (1^{st} and 2^{nd} cycle) and 10 K min^{-1} (3^{rd} cycle) and a cooling rate of 10 K min^{-1} in all three cycles (temperature range: −10 to 160°C).

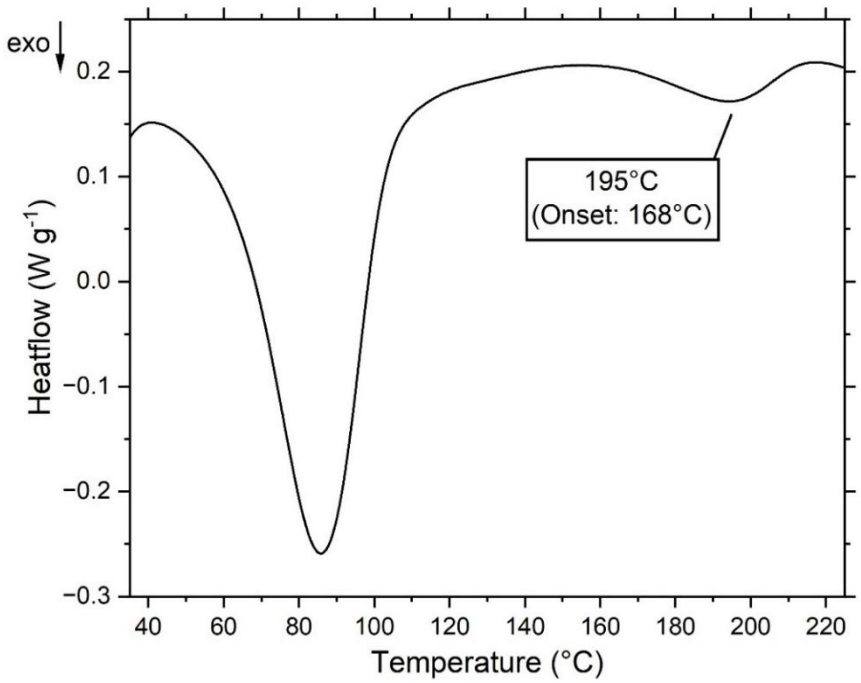

Figure S84. DSC data of *N*-hexylated digermene polymer **3b** showing the heatflow over temperature at a heating rate of 10 K min^{-1}; slight negative heatflow above 220

5.10 Thermogravimetric analysis (TGA)

A Netzsch TG 209 F1 Iris (Netzsch–Gerätebau GmbH, Selb, Germany) was used for thermogravimetric analysis (TGA). Measurements were conducted in aluminum oxide crucibles, heating from room temperature to 1000°C under nitrogen atmosphere with a rate of 10 K/min. The lids were pierced immediately before measurement.

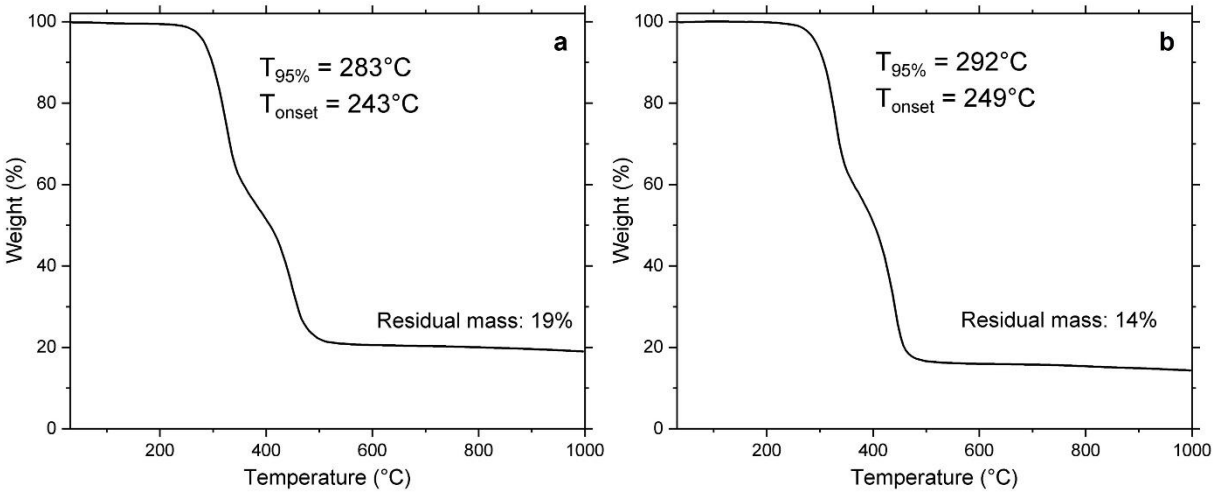

Figure S85. TGA curves of digermene polymers **3a** (a) and **3b** (b).

5.11 Small angle X-ray scattering (SAXS)

Small-angle X-ray scattering experiments were performed on a Xeuss 2.0 system (Xenocs, Grenoble, France). A copper K_α X-ray source (wavelength $\lambda = 0.154$ nm) was used as the incident beam, collimated and focused on the sample with a spot size of 0.25 mm^2. 2D scattering intensity patterns were recorded using a Pilatus 300 K detector with pixel sizes of 172 × 172 μm^2. Measurements were performed at sample-to-detector distances (SDDs) of 2.49 and 0.38 m, calibrated using a silver behenate standard, with acquisition times of 3 and 1.5 h, respectively. This resulted in an accessible range of momentum transfers q of 0.005 – 1.3 $Å^{-1}$ with *q* being the momentum transfer given by $q = 4\pi \sin(\theta/2)/\lambda$, where θ is the scattering angle. As no signs of anisotropic scattering were observed, the scattering patterns were azimuthally averaged to obtain the scattered intensity I(q).The measurements were performed on 35 or 40 g L^{-1} solutions of **3a,b** in toluene.

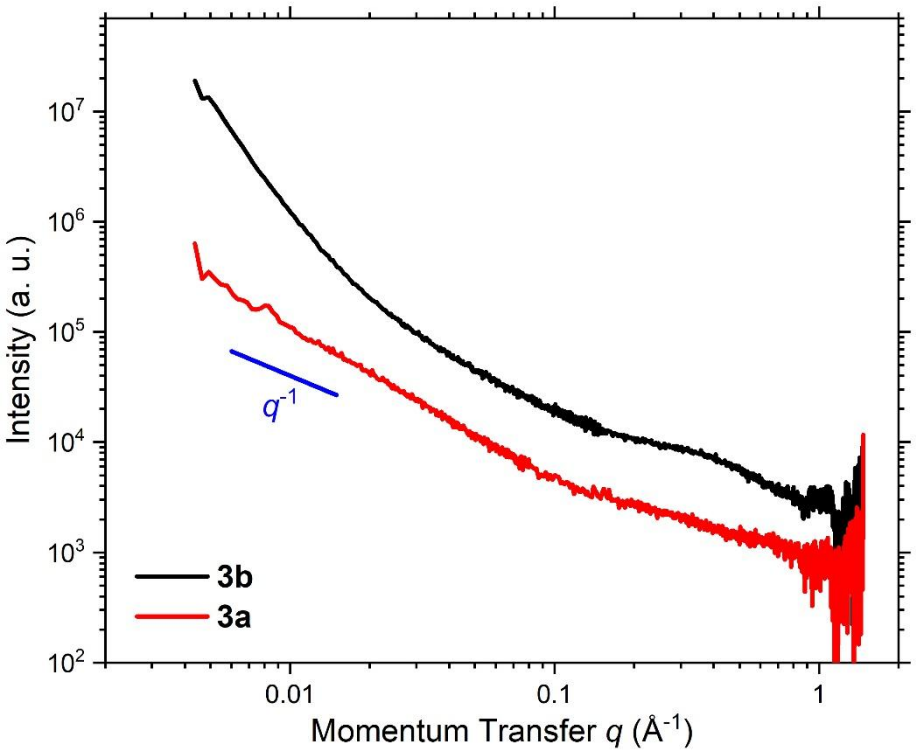

Figure S86. SAXS data obtained from 35 or 40 g L^{-1} solutions of **3a,b** in toluene.

5.12 Dynamic Light Scattering (DLS)

Dynamic light scattering (DLS) was recorded using an ALV/CGS-3 compact goniometer system from ALV (Langen, Germany) with ALV/LSE-5003 electronics and ALV-5000/EPP correlator at a wavelength of 632.8 nm (HeNe laser) and an APD-based single photon detector. The evaluation was performed by autocorrelation with the g2(t) function. For each measurement 5 runs of 10 s were performed. The measurements were performed on 5 g L^{-1} solutions of **3a** and **3b**, respectively, in benzene at detection angles of 25°, 50° or 90°. Due to a systematic underestimation of the hydrodynamic radii for large particles above the Rayleigh limit,[21] the larger values (marked in green in table S16) should represent the actual sizes of the investigated particles best and are therefore used for evaluation in the results and discussion section of the manuscript. Corresponding diffusion coefficients are obtained using the Stokes-Einstein equation[S21] and the viscosity of benzene of η(benzene) = 0.601 mPa s.[S22]

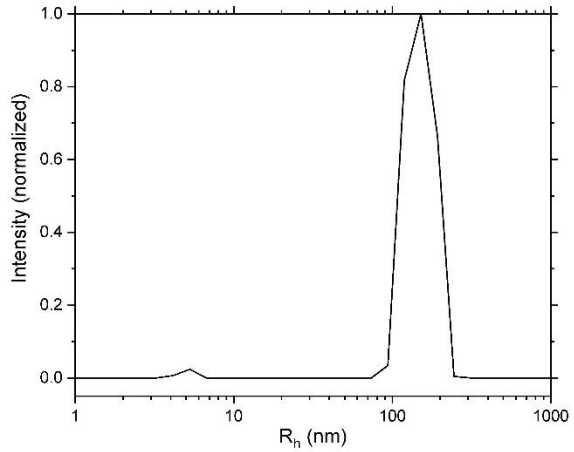

Figure S87. Size distribution profile obtained from DLS measurements of **3b** in benzene at a scattering angle of 90°.

Table S14. Mean values for the hydrodynamic radii R_h obtained from DLS measurements of the polymers, averaged over 2 to 4 single measurements.

	3a		**3b**	
Scattering angle	**$R_{h,large}$ (nm)**	**$R_{h,small}$ (nm)**	**$R_{h,large}$ (nm)**	**$R_{h,small}$ (nm)**
90°	226.9	11.6*	143.4	4.75
50°	282.2	4.02	168.4	3.41
25°	389.4	5.26	159.3	5.82**

*strongly overlapping with peak at higher radii and therefore presumably overestimated
**large standard deviation of 4.8 and in some runs no signal at all; signal intensity weak

The larger hydrodynamic radii (**3a**: 389 nm, **3b**: 168 nm) correspond to volumes of 246568398 nm^3 (**3a**) and 19861701 nm^3 (**3b**) considering spherical shapes for a first approximation. With the corresponding volumes of the repeat units (**3a**: 0.49 nm^3, **3b**: 0.52 nm^3; see X-Ray crystallographic data of bis(digermene) monomers) an amount of $4 \cdot 10^7$ (**3b**) to $5 \cdot 10^8$ (**3a**) repeat units per agglomerate are estimated.

5.13 Diffusion ordered NMR spectroscopy (DOSY)

NMR spectra for the determination of diffusion coefficients were recorded of solutions of polymers **3a,b** (10 g L^{-1}) or of monomers **2a,b** (18 mmol L^{-1}) in thf-d_8 on an AVANCE Neo 500 routine spectrometer (Bruker, Billerica, USA) equipped with a 5 mm TCI Prodigy Cryo probe with a z-gradient. Gradient strengths between 1.18 and 56.2 G cm^{-1} were applied in 16 (for the monomers) or 84 (for the polymers) steps with a rectangular gradient pulse shape. The spinner was turned off because of the sensitivity towards vertical position changes.[S23] The probe was manually shimmed and tuned after every change of the sample and the samples were only measured after one hour of tempering time in the spectrometer. Pulse durations were determined manually, together with a rough estimate of the longitudinal relaxation time *T1*.[S24] The relaxation delay was subsequently chosen as 5 to 7 times *T1*. Manual phase and automatic baseline correction was applied to the raw spectra, which were then integrated. Peak intensities *I* were normalized in all cases to the intensities at the lowest gradient strengths I_0. For the monomers plotting $\ln(I/I_0)$ versus *Q* according to the Stejskal-Tanner equation (S3)[S23,S25] results in straight lines, from which diffusion coefficients *D* are readily obtained as the slopes. For the analysis of the exponential drop of the peak intensity with increasing *Q* in the polymer cases a biexponential version of the Stejskal-Tanner equation (S4)[S26] was required in the polymer cases in order to obtain reasonable fits of the respective data, resulting in two different values for *D*. For the molecular species, the Stokes-Einstein equation[S21] was used to determine the hydrodynamic radii R_{sph}. For the estimation of the dimensions of the polymer strands, a modified version of this equation was used (see below). For the viscosity of thf-d_8: η(thf-d_8): 0.48 mPa s[S27] was used.

Modified version of the Stejskal-Tanner equation:[S23,S25]

$$\ln\frac{I}{I_0} = -D\gamma^2\delta^2 g^2\left(\Delta - \frac{\delta}{3} - \frac{\tau}{2}\right) = -DQ \qquad \text{(S3)}$$

Biexponential version with weighting factors a and b:

$$\frac{I}{I_0} = a \cdot e^{-D_1\gamma^2\delta^2 g^2\left(\Delta-\frac{\delta}{3}-\frac{\tau}{2}\right)} + b \cdot e^{-D_2\gamma^2\delta^2 g^2\left(\Delta-\frac{\delta}{3}-\frac{\tau}{2}\right)} = a\cdot e^{-D_1 Q} + b \cdot e^{-D_2 Q} \qquad \text{(S4)}$$

γ: Gyromagnetic ratio of the nucleus (^{1}H: 267522000 T^{-1} s^{-1})[S28]

δ: Diffusion gradient pulse length (s)

g: Gradient strength (G cm^{-1})

Δ: Diffusion delay (s)

τ: Gradient interspacing (s)

Table S15. Parameters applied to the DOSY NMR measurements.

	3a	**3b**	**2a**	**2b**
δ (s)	0.005	0.005	0.00156	0.0016
Δ (s)	0.1	0.1	0.1	0.1
τ (s)	0.000216	0.000216	0,00021586	0.000216

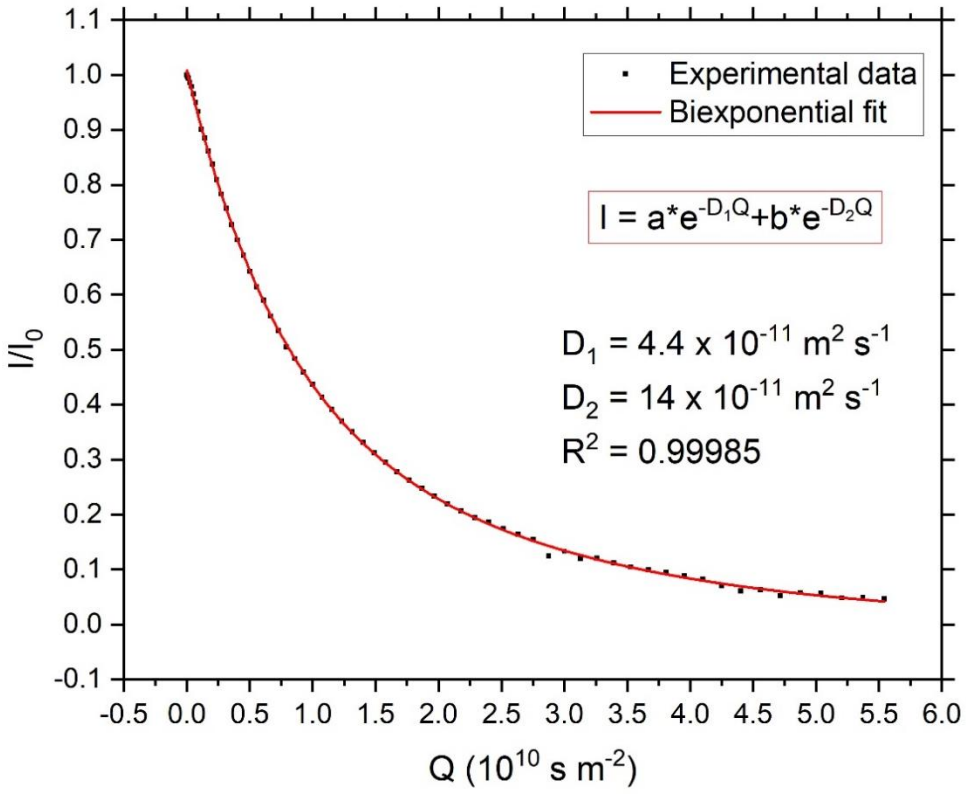

Figure S88. DOSY NMR data of *Si*-octylated digermene polymer **3a** and biexponential fit according to Stejskal-Tanner equation (S4).

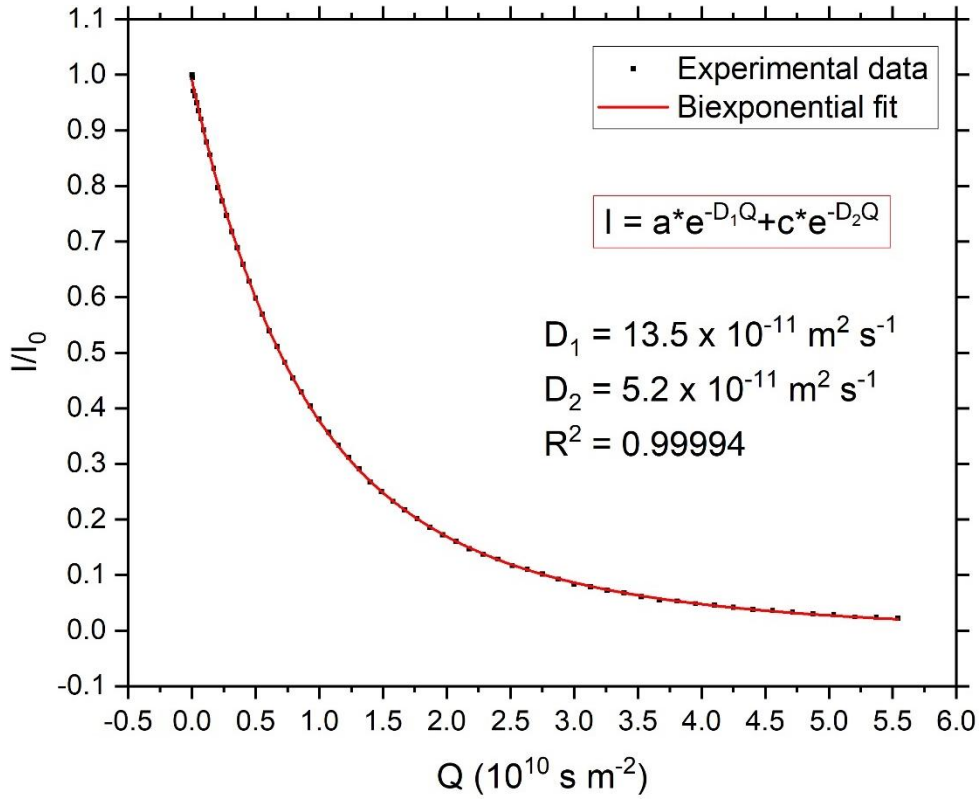

Figure S89. DOSY NMR data of *N*-octylated digermene polymer **3b** and biexponential fit according to Stejskal-Tanner equation (S4).

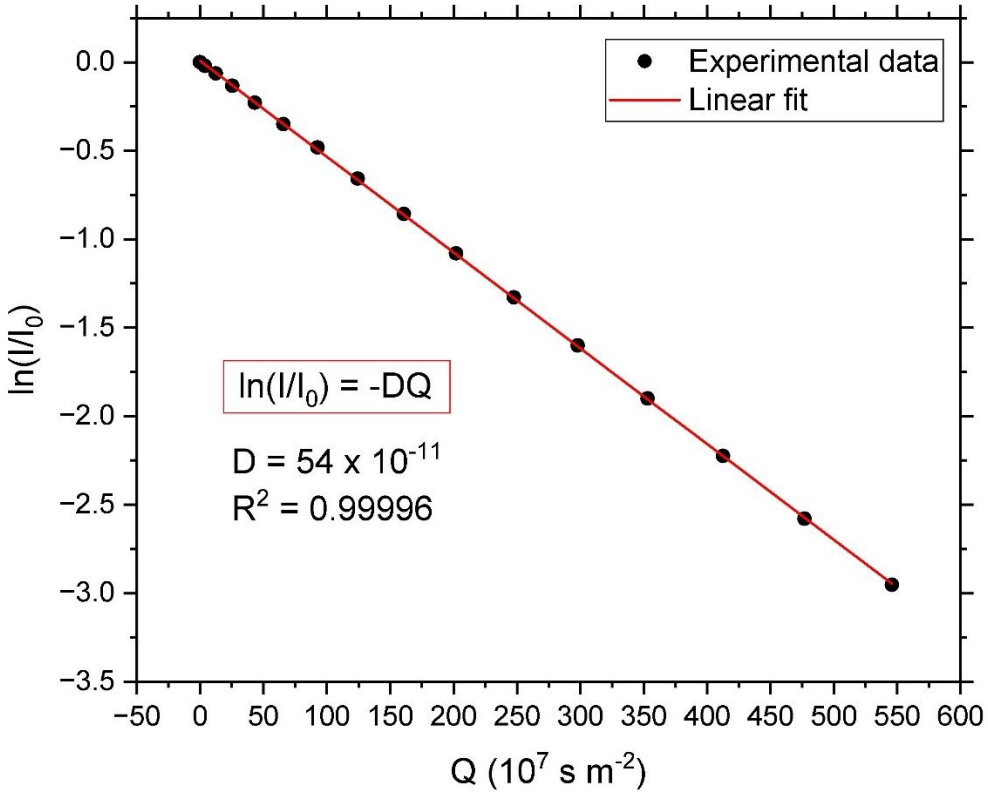

Figure S90. DOSY NMR data of *Si*-octylated bis(digermene) **2a** and linear fit according to Stejskal-Tanner equation (S3).

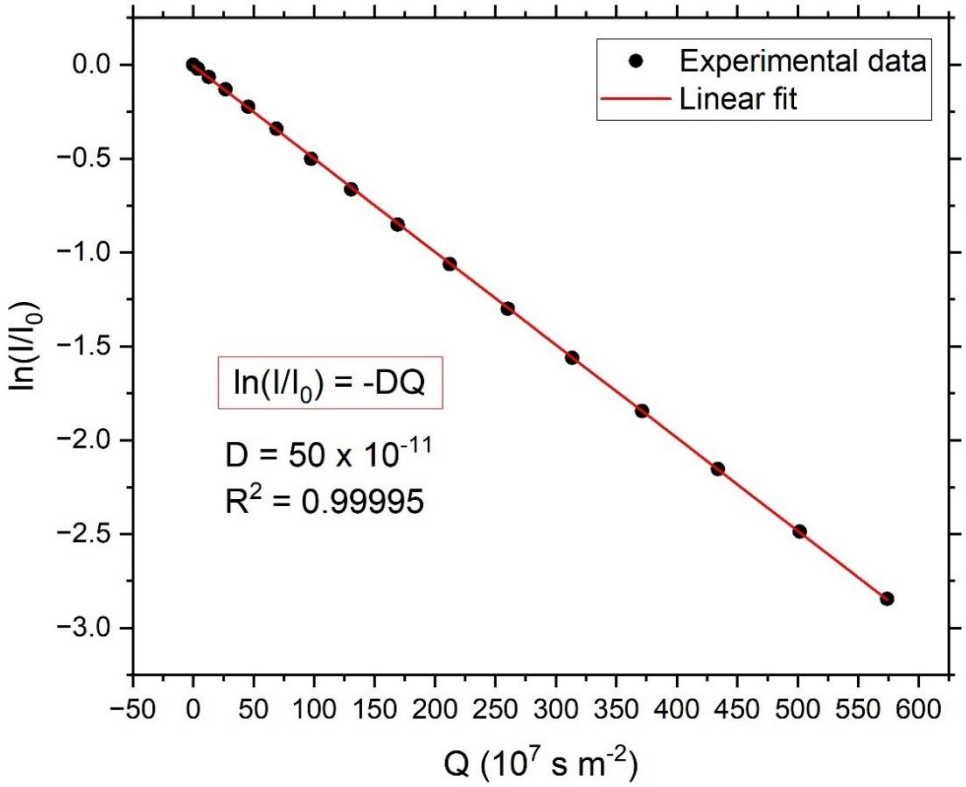

Figure S91. DOSY NMR data of *N*-octylated bis(digermene) **2b** and linear fit according to Stejskal-Tanner equation (S3).

Estimation of the rod lengths L_{rod}, i.e. the lengths of the polymer strands:

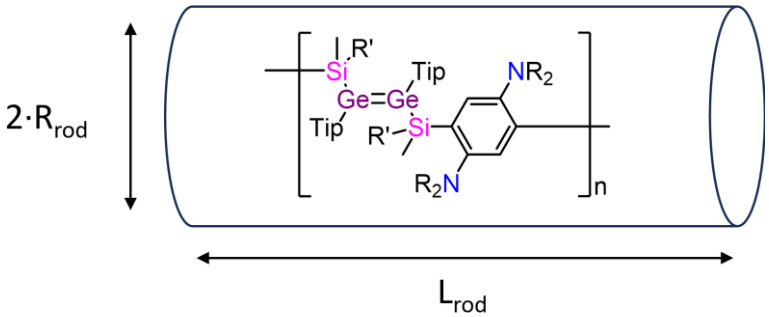

Figure S92. Schematic illustration of the cylindrically shaped polymer chains with corresponding dimension parameters.

In contrast to cylindrical particles the hydrodynamic radii of spherical particles, like the molecular bis(digermene) monomers, can be determined using the Stokes-Einstein equation (S5):[S21,S29]

$$R_{sph} = \frac{k_B T}{6\pi\eta D} \qquad (S5)$$

k_B: Boltzmann constant, T: temperature, η: viscosity of the solvent

Hence, based on the assumption that a cylindrical particle with radius R_{rod} and length L_{rod} (Figure S92) and a spherical particle with radius R_{sph} with the same diffusion coefficients exhibit the same frictional volumes, the corresponding expressions are equalized in equation (S6):[S29]

$$V_{sphere} = V_{cylinder} \rightarrow \frac{4}{3}\pi R_{sph}^3 = \pi R_{rod}^2 L_{rod} \quad \text{(S6)}$$

Rearranging and substituting R_{sph} by equation (S5) provides equation (S7) for the calculation of the length of a polymer chain L_{rod} as a function of the diffusion coefficients D (as obtained by the DOSY measurements) and the widths of the polymer strands R_{rod}, assuming that the diffusion coefficients obtained for the polymers correspond to single polymer strands. The widths of the polymer strands R_{rod} then correspond to the radii of the monomers, as obtained by DOSY measurements of the same (see above).

$$L_{rod} = \frac{4R_{sph}^3}{3R_{rod}^2} = \frac{4}{3R_{rod}^2}\left(\frac{k_B T}{6\pi\eta D}\right)^3 \quad \text{(S7)}$$

Table S16. Diffusion coefficients obtained from DOSY measurements of digermene polymers **3a,b** in thf-d_8 with resulting chains lengths L_{rod} and hydrodynamic radii R_{rod} determined from DOSY measurements of bis(digermene) monomers **2a,b**.

	D (10^{-11} m^2 s^{-1})	**L_{rod} (nm)**	**R_{rod} (nm)**[a]
3a	4.4	2100	0.84
	14		
3b	5.2	1100	0.91
	13		

[a] Determined from the diffusion coefficients obtained for the corresponding monomers.

5.14 Atomic force microscopy (AFM)

AFM Atomic force microscopy (AFM) was performed on a Bruker Dimension Icon in a glovebox under an atmosphere of argon. Vibration isolation was achieved by a Herzan TS-140+40 active isolation table. Atomic force micrographs were recorded in tapping mode with either a Bruker SNL-10A probe with a nominal force constant of k = 0.35 N m^{-1} or a Bruker ScanAsyst-Air probe with a nominal force constant of k = 0.4 N m^{-1} and were uncalibrated. Images were recorded with 512 × 512 data points and a scan rate of 1 Hz. Data was processed with Nanoscope Analysis 1.40 software. The samples were prepared either by spin-coating of a concentrated (1 g L^{-1}) solution of the compounds in hexane or by dip-coating of a dilute (0.4 g L^{-1}) solution and subsequent rinsing with 1 mL of hexane on mica or hopg substrates.

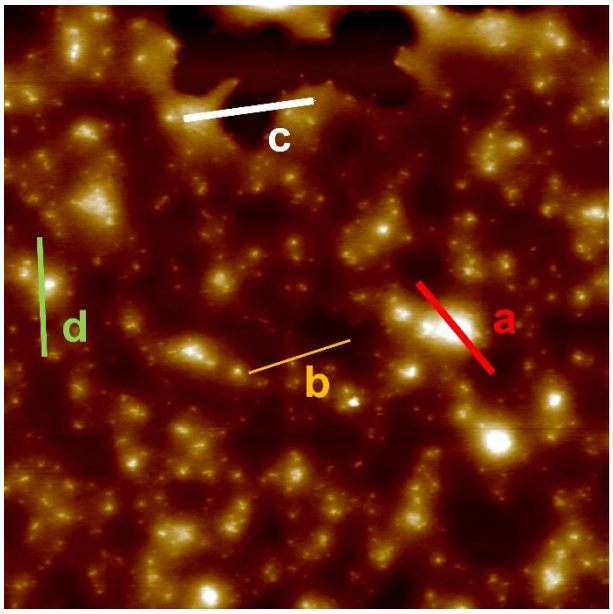

Figure S93. AFM image of digermene polymer **3b** on a mica surface spin-coated with a concentrated (1 g L^{-1}) solution of **3b** and marked traces used to obtain height profiles.

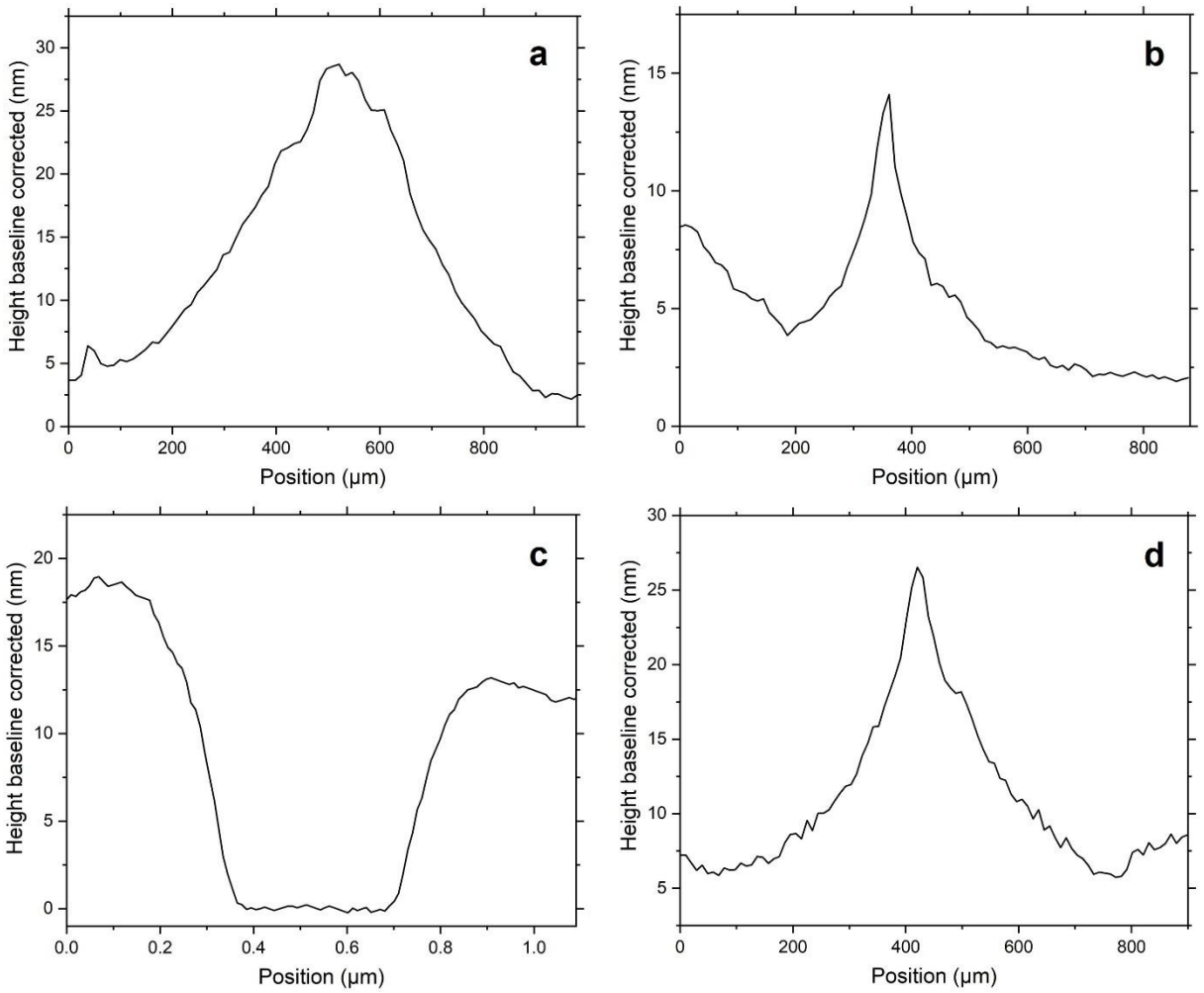

Figure S94. Height profiles extracted from the AFM image of **3b** on a mica surface spin-coated with a concentrated (1 g L^{-1}) solution of **3b**. (a) to (d) according to Figure S93.

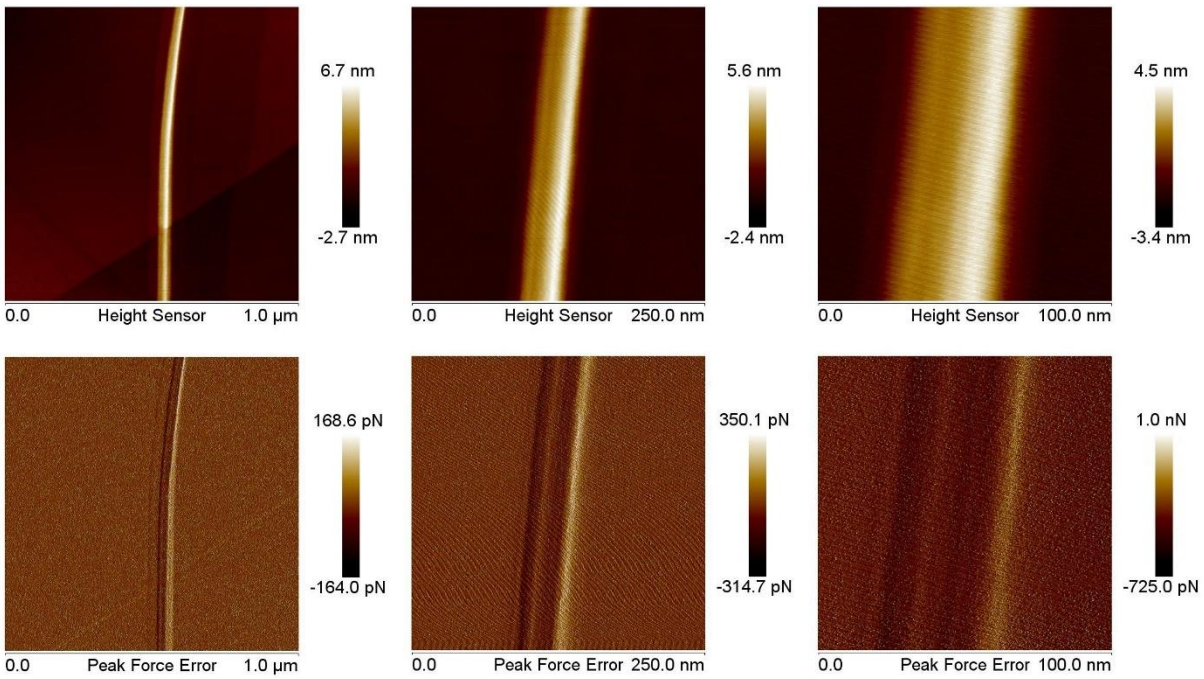

Figure S95. AFM images of **3b** on a highly oriented pyrolytic graphite (HOPG) substrate dip-coated with a dilute (0.4 g L^{-1}) hexane solution.

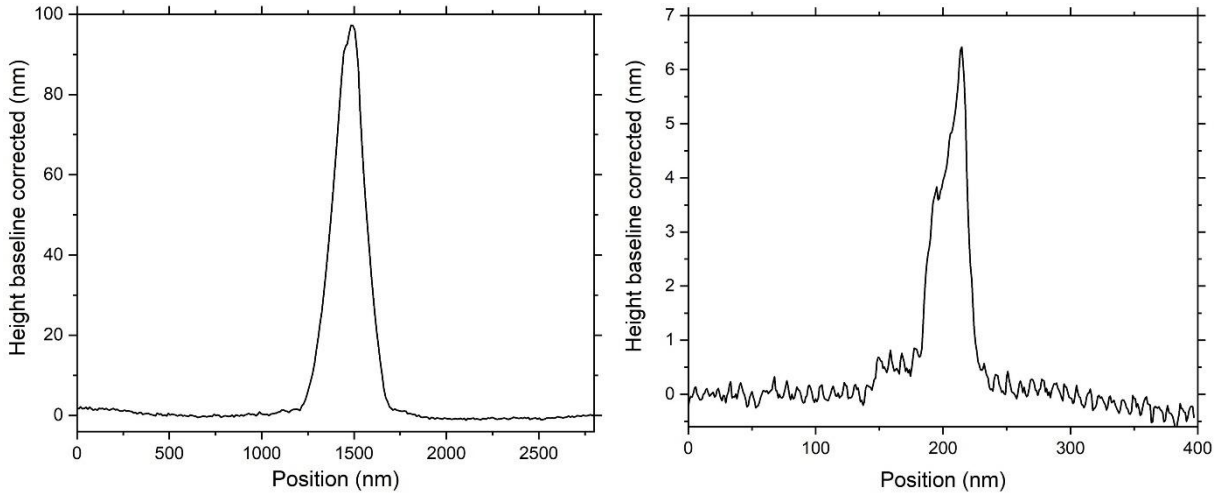

Figure S96. Height profiles of rods in the surfaces of thin films of (left) **3a** with a height of 97 nm and a width of 500 nm, and (right) **3b** with a height of 6.4 nm and a width of 64 nm, extracted from the AFM images.

5.15 Transmission electron microscopy (TEM)

High-resolution transmission electron microscopy (HR-TEM) measurements were conducted on a JEOL ARM 200 TEM/STEM at 200 kV equipped with a Cs-corrector (CEOS GmbH). TEM images of thin films of both digermene polymers were recorded of coated holey carbon-coated copper TEM grids, which were prepared by applying 0.1 g/L to 1 g/L hexane or toluene solutions onto the grids and.

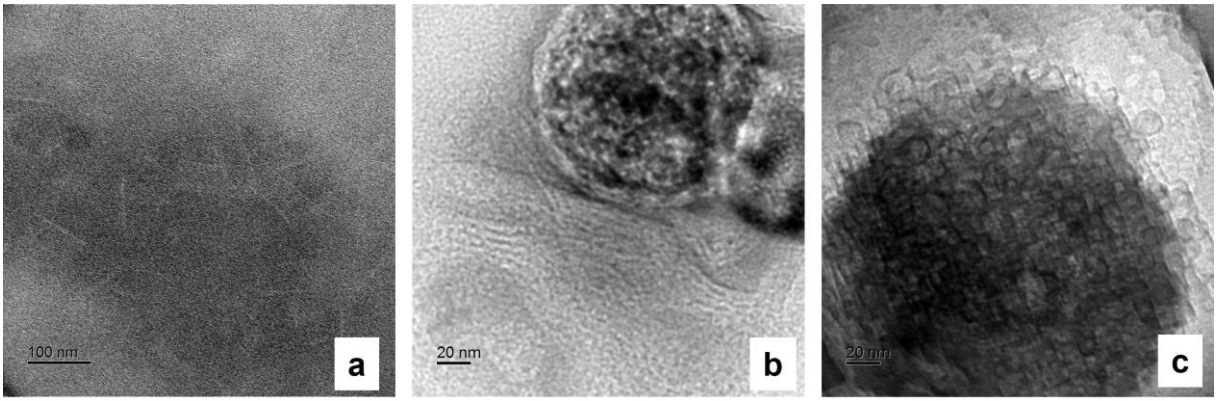

Figure S97. TEM images of (a) **3a** prepared by drop-casting of a 1 g L^{-1} solution in toluene; (b),(c) **3b** prepared by drop-coating of a 0.4 g L^{-1} solution in hexane.

References

[S1] N. Kuhn, T. Kratz, *Synthesis* **1993**, *1993*, 561.

[S2] D. Nieder, L. Klemmer, Y. Kaiser, V. Huch, D. Scheschkewitz, *Organometallics* **2018**, *37*, 632.

[S3] T. Doornbos, J. Strating, *Org. Prep. Proced.* **1969**, *4*, 287.

[S4] G. R. Fulmer, A. J. M. Miller, N. H. Sherden, H. E. Gottlieb, A. Nudelman, B. M. Stoltz, J. E. Bercaw, K. I. Goldberg, *Organometallics* **2010**, *29*, 2176.

[S5] G. M. Sheldrick, *Acta Crystallogr. Sect. A* **2008**, *64*, 112.

[S6] G. M. Sheldrick, *Acta Crystallogr. Sect. A* **2015**, 71, 3.

[S7] C. B. Hübschle, G. M. Sheldrick, B. Dittrich, *J. Appl. Crystallogr.* **2011**, *44*, 1281.

[S8] M. J. Frisch, G. W. Trucks, H. B. Schlegel, G. E. Scuseria, M. A. Robb, J. R. Cheeseman, G. Scalmani, V. Barone, B. Mennucci, G. A. Petersson, H. Nakatsuji, M. Caricato, X. Li, H. P. Hratchian, A. F. Izmaylov, J. Bloino, G. Zheng, J. L. Sonnenberg, M. Hada, M. Ehara, K. Toyota, R. Fukuda, J. Hasegawa, M. Ishida, T. Nakajima, Y. Honda, O. Kitao, H. Nakai, T. Vreven, J. J. A. Montgomery, J. E. Peralta, F. Ogliaro, M. Bearpark, J. J. Heyd, E. Brothers, K. N. Kudin, V. N. Staroverov, R. Kobayashi, J. Normand, K. Raghavachari, A. Rendell, J. C. Burant, S. S. Iyengar, J. Tomasi, M. Cossi, N. Rega, J. M. Millam, M. Klene, J. E. Knox, J. B. Cross, V. Bakken, C. Adamo, J. Jaramillo, R. Gomperts, R. E. Stratmann, O. Yazyev, A. J. Austin, R. Cammi, C. Pomelli, J. W. Ochterski, R. L. Martin, K. Morokuma, V. G. Zakrzewski, G. A. Voth, P. Salvador, J. J. Dannenberg, S. Dapprich, A. D. Daniels, O. Farkas, J. B. Foresman, J. V. Ortiz, J. Cioslowski, D. J. Fox, Gaussian 16, Revision C.01. Gaussian, Inc., Wallingford CT, **2016**.

[S9] a) J. P. Perdew, *Phys. Rev. B* **1986**, *33*, 8822; b) A. D. Becke, *Phys. Rev. A* **1988**, *38*, 3098.

[S10] a) A. Schäfer, H. Horn, R. Ahlrichs, *J. Chem. Phys.* **1992**, *97*, 2571; b) A. Schäfer, C. Huber, R. Ahlrichs, *J. Chem. Phys.* **1994**, *100*, 5829; c) F. Weigend, R. Ahlrichs, *Phys. Chem. Chem. Phys.* **2005**, *7*, 3297; d) F. Weigend, *Phys. Chem. Chem. Phys.* **2006**, *8*, 1057.

[S11] (a) S. Grimme, J. Antony, S. Ehrlich, H. Krieg, *J. Chem. Phys.* **2010**, *132*, 154104; (b) S. Grimme, S. Ehrlich, L. Goerigk, *J. Comput. Chem.* **2011**, *32*, 1456.

[S12] (a) A. E. Reed, R. B. Weinstock, F. Weinhold, *J. Chem. Phys.* **1985**, *83*, 735; (b) A. E. Reed, L. A. Curtiss, F. Weinhold, *Chem. Rev.* **1988**, *88*, 899; (c) E. D. Glendening, C. R. Landis, F. Weinhold, *J. Comp. Chem.* **2019**, *40*, 2234.

[S13] F. Neese, F. Wennmohs, U. Becker, C. Riplinger, *J. Chem. Phys.* **2020**, *152*, 224108.

[S14] a) J. P. Perdew, M. Ernzerhof, K. Burke, *J. Chem. Phys.* **1996**, *105*, 9982; b) C. Adamo, V. Barone, *J. Chem. Phys.* **1999**, *110*, 6158.

[S15] Chemcraft - graphical software for visualization of quantum chemistry computations. https://www.chemcraftprog.com

[S16] J. Zhou, R. Tang, X. Wang, W. Zhang, X. Zhuang, F. Zhang, *J. Mater. Chem. C* **2016**, *4*, 1159.

[S17] A.-L. Thömmes, B. Morgenstern, M. Zimmer, D. M. Andrada, D. Scheschkewitz, *Chem. Eur. J.* **2023**, *29*, e202301273.

[S18] W. H. Carother, *Trans. Faraday Soc.* **1936**, *32*, 39.

[S19] L. Klemmer, A.-L. Thömmes, M. Zimmer, V. Huch, B. Morgenstern, D. Scheschkewitz, *Nat. Chem.* **2020**, *13*, 373.

[S20] a) F. Babick, in *Micro and Nano Technologies, Characterization of Nanoparticles* (Eds.: V.-D. Hodoroaba, W. E. S. Unger, A. G. Shard), Elsevier **2020**, pp. 137; b) S. R. Aragón, R. Pecora, *J. Chem. Phys.* **1977**, *66*, 2506; c) E. Loh, E. Ralston, V. N. Schumaker, *Biopolymers* **1979**, *18*, 2549; d) H. Kato, A. Nakamura, S. Kinugasa, *Nanomaterials* **2018**, *8*, 708; e) L. Jin, C. W. Jarand, M. L. Brader, W. F. Reed, *Meas. Sci. Technol.* **2022**, *33*, 045202.
[S21] C. C. Miller, Proc. R. Soc. London, Ser. A **1924**, *106*, 724.
[S22] J. H. Dymond, J. Robertston, J. D. Isdale, *Int. J. Thermophys.* **1981**, *2*, 223.
[S23] C. S. Johnson, *Prog. Nucl. Magn. Reson. Spectrosc.* **1999**, *34*, 203.
[S24] S. Berger, S. Braun, 200 and More NMR Experiments, Wiley-VCH Verlag GmbH & Co. KGaA, Weinheim, **2004**.
[S25] E. O. Stejskal, J. E. Tanner, *J. Chem. Phys.* **1965**, *42*, 288.
[S26] M. Nilsson, M. A. Connell, A. L. Davis, G. A. Morris, *Anal. Chem.* **2006**, *78*, 3040.
[S27] P.-J. Voorter, A. McKay, J. Dai, O. Paravagna, N. R. Cameron, T. Junkers, *Angew. Chem.* **2022**, *134*, e202114536; *Angew. Chem. Int. Ed.* **2022**, *61*, e202114536.
[S28] P. J. Mohr, B. N. Taylor, D. B. Newell, *Rev. Mod. Phys.* **2012**, *84*, 1527.
[S29] H. G. Elias, *Makromolecules*, Vol. 3, Wiley-VCH GmbH Verlag, Weinheim, Germany **2008**.
[S30] Deposition numbers CCDC 2358520 (1,4-dibromo-2,5-*N*,*N*,*N'*,*N'*-tetrahexylphenylenediamine), 2358528 (**1a**), 2358523 (1,4-bis(chlorodihexylsilyl)-2,5-*N*,*N*,*N'*,*N'*-tetramethylphenylenediamine), 2358519 (1,4-bis(chlorodibutylsilyl)-2,5-*N*,*N*,*N'*,*N'*-tetramethylphenylenediamine), 2358527 (**2a**) and 2358526 (**2b**) contain the supplementary crystallographic data for this paper. These data are provided free of charge by the joint Cambridge Crystallographic Data Centre and Fachinformationszentrum Karlsruhe Access Structures service.

σ,π-Conjugated Bis(germylene) Adducts with NHC and CAACs

Supporting Information

Anna-Lena Thoemmes, Bernd Morgenstern, Michael Zimmer, Diego M. Andrada, David Scheschkewitz*

Table of Contents

1. Synthetic methods and analytical data 204

1.1. General considerations 204
1.2. Reaction of bis(digermene) 1 with triethylsilane 204
1.3. Synthesis of dimeric bis(germylene)/Me_2IPr adduct 4 205
1.4. Synthesis of monomeric germylene/Me_2IPr adduct 6 206
1.5. Attempted reaction of bis(digermene) 1 with Me_2IDip 206
1.6. Attempted reaction of bis(germylene)/Me_2IPr adduct 4 with BH_3-thf 207
1.7. Reaction of germylene/Me_2IPr adduct 6 with BPh_3 207
1.8. Reaction of bis(germylene)/Me_2IPr adduct 4 with BPh_3 207
1.9. Synthesis of bis(germylene)/Me_4CAAC adduct 7 208
1.10. Reaction of bis(germylene)/Me_2IPr adduct 4 with Me_4CAAC 208

2. NMR data 209

3. UV/Vis spectra 217

4. Crystallographic data 223

4.1. Me_2IPr-germylene 6 (CCDC-2236120) 223
4.2. Me_4CAAC-bis(germylene) 7 (CCDC-2236118) 225

5. DFT calculations 227

References 246

1. Synthetic methods and analytical data

1.1. General considerations

All manipulations were carried out under a protective atmosphere of argon applying standard Schlenk or glovebox techniques. The glassware was pre-dried in oven at 125 °C and heated in vacuo prior to use. Solvents were dried and degassed by reflux over sodium/benzophenone under argon (thf, benzene) or taken from a solvent purification system (Innovative technology PureSolv MD7; diethylether, hexane, pentane). Benzene-d_6 and thf-d_8 were dried over potassium mirror and distilled under argon prior to use. Me_4CAAC[S1], Me_2IPr[S2], 1,3-bis(2,6-diisopropylphenyl)imidazol-2-ylidene[S3] and digermenes **1** and **5**[S4] were prepared according to the published procedures. All other chemicals were obtained commercially and used as received. The NMR spectra were recorded on a Bruker Avance III HD 400 spectrometer at 300 K (^{1}H: 400.13 MHz, ^{13}C: 100.61 MHz, ^{29}Si: 79.49) or on a Bruker Avance III HD 300 (^{1}H: 300.13 MHz, ^{13}C: 75.56 MHz, ^{29}Si: 59.6 MHz). The ^{1}H and ^{13}C{^{1}H} NMR spectra were referenced to the residual proton and natural abundance ^{13}C resonances of the deuterated solvent and chemical shifts were reported relative to $SiMe_4$ (benzene-d_6: δH = 7.16 ppm and δC = 128.06 ppm, thf-d_8: δH = 1.78, 3.58 ppm and δC = 67.21, 25.31 ppm).[S5] The ^{29}Si NMR chemical shifts were referenced to external $SiMe_4$. The following abbreviations were used for the multiplicities: s – singlet, d – doublet, t – triplet, sept – septet, m – multiplet, brs – broad singlet. UV/Vis spectra were recorded on a Shimdazu UV-2600 spectrometer in quartz cells with a path length of 0.1 cm. Melting points were determined under argon in sealed NMR tubes and are uncorrected. The molten samples were examined by NMR spectroscopy to confirm whether decomposition had occurred upon melting. Elemental analyses were performed in triplicate for each sample using Leco CHN900 analyzer and mean values are given below for each compound. Crystallographic data was collected using a Bruker D8 Venture diffractometer with a microfocus sealed tube and a Photon II detector. Monochromated $Mo_{K\alpha}$ radiation (λ = 0.71073) was used. Data were collected at 133(2) K and corrected for absorption effects using the multi-scan method. The structure was solved by direct methods using SHELXT[S6] and was refined by full matrix least squares calculations on F2 (SHELXL2018)[S7] in the graphical user interface Shelxle.[S8]

1.2. Reaction of bis(digermene) 1 with triethylsilane

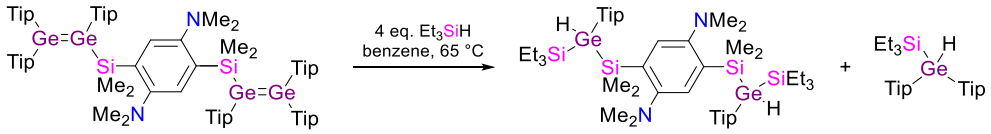

1

To a solution of bis(digermene) **1** (28.9 mg, 15.5 µmol, 1 eq.) in 0.4 mL of benzene-d_6 triethylsilane (0.01 mL, 62.6 µmol, 4 eq.) is added. The resulting orange solution is heated to 65 °C overnight to give a yellow solution. All volatile species are removed in vacuo and the formation of the bis(silylgermane) and the mono(silylgermane)[S4] is confirmed by multinuclear NMR spectroscopy.

Bis(silylgermane):

^{1}H NMR (300.13 MHz, C_6D_6, 300 K, TMS): δ = 7.43, 7.42 (each s, overall 2H, Ph*H*), 7.09 (s, 4H, Tip*H*), 4.23, 4.20 (each s, overall 2H, Ge*H*), 3.43 (sept, 4H, C*H*(CH$_3$)$_2$ of Tip), 2.86-2.67 (m, 2H, C*H*(CH$_3$)$_2$ of Tip), 2.26, 2.24 (each s, overall 12H, N(C*H*$_3$)$_2$), 1.24 to 1.21, 1.18 to 1.13, 1.07 to 0.95 (each m, overall 66H, C*H*$_2$ and C*H*$_3$ of SiEt$_3$ and C*H*$_3$ of Tip), 0.80, 0.79, 0.77 (each s, overall 12H, Si(C*H*$_3$)$_2$) ppm. **^{29}Si{^{1}H} NMR** (59.6 MHz, C_6D_6, 300 K, TMS): δ = 4.56, 4.52 (*Si*Et$_3$), −8.71, −9.07 (*Si*Me$_2$) ppm.

Mono(silylgermane):

^{1}H NMR (300.13 MHz, C_6D_6, 300 K, TMS): δ = 7.09 (s, 4H, Tip*H*), 5.58 (s, 1H, Ge*H*), 3.43 (sept, 2H, C*H*(CH$_3$)$_2$ of Tip), 2.86-2.67 (m, 4H, C*H*(CH$_3$)$_2$ of Tip), 1.24 to 1.21, 1.18 to 1.13, 1.07 to 0.95 (each m, overall 51H, C*H*$_2$ and C*H*$_3$ of SiEt$_3$ and C*H*$_3$ of Tip) ppm. **^{29}Si{^{1}H} NMR** (59.6 MHz, C_6D_6, 300 K, TMS): δ = 5.01 ppm.

1.3. Synthesis of dimeric bis(germylene)/Me$_2$IPr adduct 4

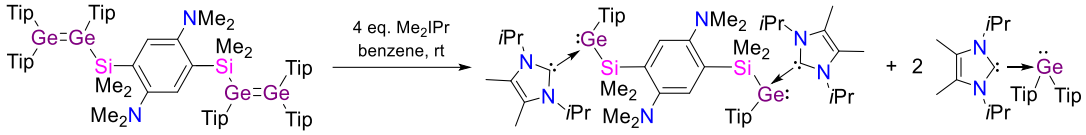

1 **4**

Bis(digermene) **1** (1.5 g, 803 µmol, 1 eq.) and Me$_2$IPr (579 mg, 3.21 mmol, 4 eq.) are dissolved in 18.5 mL of benzene. Stirring for eight hours at room temperature is followed by filtration. The yellow solid is washed with 2 mL of benzene to yield the bis(germylene)/Me$_2$IPr adduct **4** (624 mg, 504 µmol, 63%).* The solvent of the mother liquor is removed in vacuo and the residue is redissolved in pentane. The yellow crystalline solid formed from this solution is separated by filtration and dried in vacuo to give Tip$_2$Ge·Me$_2$IPr (402 mg, 609 µmol, 38%).

*0.6wt% of free Me$_2$IPr contained

Bis(germylene)/Me$_2$IPr adduct **4**:

^{1}H NMR (400.13 MHz, thf-d_8, 300 K, TMS): δ = 7.12, 7.06 (each s, overall 2H, Ph*H*), 6.79 (s, 4H, Tip*H*), 5.54 (brs, 4H, C*H*(CH$_3$)$_2$ of Me$_2$IPr), 3.88 (brs, 4H, C*H*(CH$_3$)$_2$ of Tip), 2.73 (sept, 2H, C*H*(CH$_3$)$_2$ of Tip), 2.47 (s, 12H, N(C*H*$_3$)$_2$), 2.17 (s, 12H, Me$_2$IPr-CC*H*$_3$), 1.29 (d, 12H, CH(C*H*$_3$)$_2$ of Me$_2$IPr), 1.17 (d, 12H, CH(C*H*$_3$)$_2$ of Me$_2$IPr), 1.03 (d, 12H, CH(C*H*$_3$)$_2$ of Tip), 0.90 (d, 12H, CH(C*H*$_3$)$_2$ of Tip), 0.78, 0.76 (each d, overall 12H, CH(C*H*$_3$)$_2$ of Tip), 0.53, 0.52 (d, s, overall 12H, Si(C*H*$_3$)$_2$) ppm. **^{13}C{^{1}H} NMR** (100.61 MHz, thf-d_8, 300 K, TMS): δ = 177.08, 177.00 (Me$_2$IPr-*C*), 155.93 (Ph*C*). 154.51, 151.67, 146.13, 142.49 (Tip*C*), 129.02, 128.85 (Me$_2$IPr-*C*CH$_3$), 126.75, 126.73 (Ph*C*), 120.72 (Tip*C*), 53.88 (*C*H(CH$_3$)$_2$ of Me$_2$IPr), 47.40 (N(*C*H$_3$)$_2$), 34.94 (*C*H(CH$_3$)$_2$ of Tip), 24.56, 24.47, 21.58, 21.55, (CH(*C*H$_3$)$_2$ of Tip), 20.58, 20.52 (CH(*C*H$_3$)$_2$ of Me$_2$IPr), 10.19 (Me$_2$IPr-C*C*H$_3$), 4.58, 4.48, 3.68, 3.55 (Si(*C*H$_3$)$_2$) ppm. **^{29}Si{^{1}H} NMR** (79.49 MHz, thf-d_8, 300 K, TMS): δ = −11.08, −11.21 ppm. **UV/Vis** (*n*-hexane/thf (80:20)): λ_{max} = 332 nm (ε = 15500 L mol^{-1} cm^{-1}), 395 nm (ε = 10500 L mol^{-1} cm^{-1}). **Elemental analysis:** Calcd. for (C$_{66}$H$_{112}$Ge$_2$N$_6$Si$_2$): C, 66.55; H, 9.48; N, 7.06. Found: C, 66.94; H, 8.76; N, 6.55. **Mp.:** 162 °C (decomposition).

Tip$_2$Ge·Me$_2$IPr:

^{1}H NMR (400.13 MHz, thf-d_8, 300 K, TMS): δ = 7.22 (s, 1H, Tip*H*), 7.17 (s, 1H, Tip*H*, overlapping with residual protons from benzene-d_6), 5.64 (sept, 1H, C*H*(CH$_3$)$_2$ of Me$_2$IPr), 5.34 (sept, 1H, C*H*(CH$_3$)$_2$ of Me$_2$IPr), 4.59 (sept, 1H, C*H*(CH$_3$)$_2$ of Tip), 4.10 (sept, 1H, C*H*(CH$_3$)$_2$ of Tip), 4.00 (sept, 1H, C*H*(CH$_3$)$_2$ of Tip), 3.59 to 3.47 (m, 1H, C*H*(CH$_3$)$_2$ of Tip), 2.89 (sept, 2H, C*H*(CH$_3$)$_2$ of Tip), 1.76 (dd, 6H, CH(C*H*$_3$)$_2$ of Tip), 1.56 (d, 6H, CH(C*H*$_3$)$_2$ of Me$_2$IPr), 1.48, 1.45 (each d, overall 6H, CH(C*H*$_3$)$_2$ of Tip), 1.34 to 1.30 (m, 18H, CH(C*H*$_3$)$_2$ of Me$_2$IPr and Tip), 1.25 to 1.20 (m, 9H, CH(C*H*$_3$)$_2$ of Tip)m 1.15 (d, 3H, CH(C*H*$_3$)$_2$ of Tip), 1.02 (d, 6H, CH(C*H*$_3$)$_2$ of Tip) ppm. **^{13}C{^{1}H} NMR** (100.61 MHz, thf-d_8, 300 K, TMS): δ = 176.94 (Me$_2$IPr-*C*), 156.76, 156.18, 155.78, 153.81, 151.20, 149.85, 147.44, 146.23 (Tip*C*), 128.18, 127.94 (*C*CH3 of Me$_2$IPr), 126.22, 125.30, 121.39 (Tip*C*), 120.84 (*C*CH$_3$of Me$_2$IPr), 120.51 (Tip*C*), 53.01, 52.05 (*C*H(CH$_3$)$_2$ of Me$_2$IPr), 37.70, 35.47, 34.76, 33.76, 33.42 (*C*H(CH$_3$)$_2$ of Tip), 26.61, 26.54, 25.99, 25.81, 25.45, 25.30, 24.70 to 24.47, 24.17, 23.97 (CH(*C*H$_3$)$_2$ of Tip), 21.61, 20.86, 20.77, 20.22 (CH(*C*H$_3$)$_2$ of Me$_2$IPr), 10.24, 10.08 (C*C*H$_3$ of Me$_2$IPr) ppm. **UV/Vis** (*n*-hexane): λ_{max} = 313 (ε = 4700 L mol^{-1} cm^{-1}), 361 (ε = 5900 L mol^{-1} cm^{-1}), 407 (ε = 5400 L mol^{-1} cm^{-1}). **Elemental analysis:** Calcd. for (C$_{41}$H$_{66}$GeN$_2$): C, 74.66; H, 10.09; N, 4.25. Found: C, 72.50; H, 9.25; N, 4.30. **Mp.:** 136 °C (partial formation of Tip$_2$Ge=GeTip$_2$).

1.4. Synthesis of monomeric germylene/Me$_2$IPr adduct 6

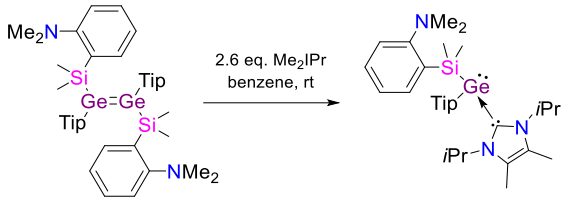

5 **6**

Digermene **5** (420 mg, 411 µmol, 0.5 eq.) and Me$_2$IPr (193 mg, 1.07 mmol, 1.3 eq.) are dissolved in 9 mL of benzene. The resulting yellow solution is stirred at room temperature for overnight. After addition of another 9 mL of benzene the reaction mixture is filtrated. All volatile parts are removed in vacuo and the resulting red oil is dissolved in pentane. Yellow crystals of **6** are obtained from this solution (211 mg, 317 mmol, 77%).*

*5wt% of free Me$_2$IPr contained

^{1}H NMR (400.13 MHz, C_6D_6, 300 K, TMS): δ = 7.99 (dd, 1H, Me$_2$N-Ph*H*) 7.27 to 7.20 (ddd, 1H, Me$_2$N-Ph*H*), 7.11 (s, 2H, Tip*H*), 7.09-7.05 (m, 2H, Me$_2$N-Ph*H*), 5.74 (sept, 2H, C*H*(CH$_3$)$_2$ of Me$_2$IPr), 4.24 (sept, 2H, C*H*(CH$_3$)$_2$ of Tip), 2.90 (sept, 1H, C*H*(CH$_3$)$_2$ of Tip), 2.63 (s, 6H, N(C*H*$_3$)$_2$), 1.56 (s, 6H, NHC-*C*H$_3$), 1.33, 1.33, 1.31 (each d, overall 12H, CH(C*H*$_3$)$_2$ of Me$_2$IPr), 1.13 (d, 6H, CH(C*H*$_3$)$_2$ of Tip), 1.04 (d, 6H, CH(C*H*$_3$)$_2$ of Tip), 0.97, 0.90 (each s, overall 6H, Si(C*H*$_3$)$_2$), 0.80 (d, 6H, CH(C*H*$_3$)$_2$ of Tip) ppm. **^{13}C{^{1}H} NMR** (100.61 MHz, C_6D_6, 300 K, TMS): δ = 177.45 (Me$_2$IPr-*C*), 161.27 (Ph*C*), 154.72, 150.83, 146.45, 142.91 (Tip*C*), 137.82, 136.03 (Ph*C*), 128.96 (Me$_2$IPr-*C*CH$_3$), 125.81, 124.05 (Ph*C*), 120.92 (Tip*C*), 53.34 (*C*H(CH$_3$)$_2$ of Me$_2$IPr), 47.36 (N(CH$_3$)$_2$), 36.67, 34.72 (*C*H(CH$_3$)$_2$ of Tip), 25.63, 25.17 (CH(*C*H$_3$)$_2$ of Tip), 21.41, 20.57 (CH(*C*H$_3$)$_2$ of Me$_2$IPr), 9.99 (Me$_2$IPr-C*C*H$_3$), 4.45, 4.06 (Si(*C*H$_3$)$_2$) ppm. **^{29}Si{^{1}H} NMR** (79.49 MHz, C_6D_6, 300 K, TMS): δ = −11.49 ppm. **UV/Vis** (*n*-hexane/thf, 80/20): λ_{max} = 329 nm (ε = 6000 L mol^{-1} cm^{-1}), 395 nm (ε = 4000 L mol^{-1} cm^{-1}). **Elemental analysis:** Calcd. for ($C_{36}H_{59}GeN_3Si$): C, 68.14; H, 9.37; N, 6.62. Found: C, 67.96; H, 9.04; N, 6.67. **Mp.:** 135 °C.

1.5. Attempted reaction of bis(digermene) 1 with Me$_2$IDip

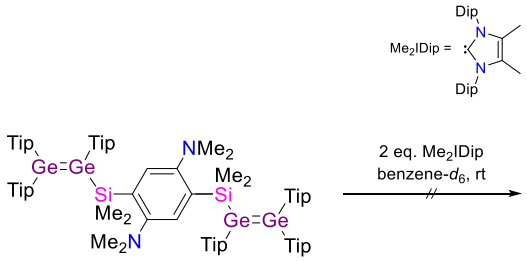

1

To a solution of bis(digermene) **1** (50.0 mg, 26.8 µmol, 1 eq.) in 0.25 mL of benzene-d_6 a solution of Me$_2$IDip (20.8 mg, 53.6 µmol, 2 eq.) in 0.25 mL of benzene-d_6 is added. The resulting red solution is transferred into an NMR tube and the reaction process is tracked by ^{1}H NMR spectroscopy. After 3.5 hours at room temperature no conversion is observed. Heating to 65 °C for 17 hours only results in the formation of Tip$_2$Ge=GeTip$_2$ and poly(digermene) **2** as also occurs in the absence of Me$_2$IDip at this temperature.

1.6. Attempted reaction of bis(germylene)/Me_2IPr adduct 4 with BH_3-thf

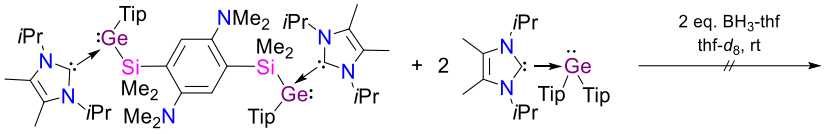

4

To a solution of bis(digermene) **1** (50.0 mg, 26.8 µmol, 1 eq.) in 0.5 mL of benzene-d_6 in an NMR tube is added Me_2IPr (19.3 mg, 107 µmol, 4 eq.). Complete conversion to the germylene/Me_2IPr adducts **4** and $Tip_2Ge{\cdot}Me_2$IPr is confirmed by ^{1}H NMR spectroscopy. After 18 hours at room temperature BH_3-thf (1 M in thf, 0.05 mL, 53.5 µmol, 2 eq.) is added to the formed germylene/Me_2IPr adducts **4** and $Tip_2Ge{\cdot}Me_2$IPr. The reaction process is tracked by ^{1}H and ^{11}B NMR spectroscopy. No reaction occurs during 4 days.

1.7. Reaction of germylene/Me_2IPr adduct 6 with BPh_3

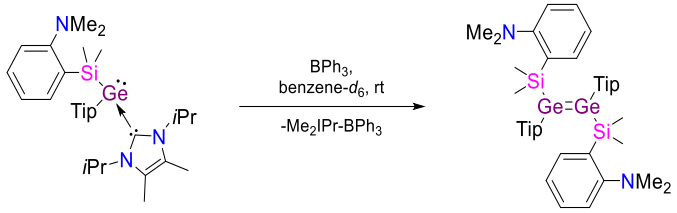

6 5

A solution of germylene/Me_2IPr adduct **6** is formed through addition of Me_2IPr (12.2 mg, 67.7 µmol, 1.5 eq.) to a solution of digermene **5** (20.5 mg, 22.6 µmol, 0.5 eq.) in benzene-d_6. Full conversion is confirmed by multinuclear NMR spectroscopy. To the yellow solution of germylene **6** BPh_3 (16.4 mg, 67.8 µmol, 1.5 eq.) is added. Complete conversion to digermene **5** is confirmed by multinuclear NMR spectroscopy after one hour.

1.8. Reaction of bis(germylene)/Me_2IPr adduct 4 with BPh_3

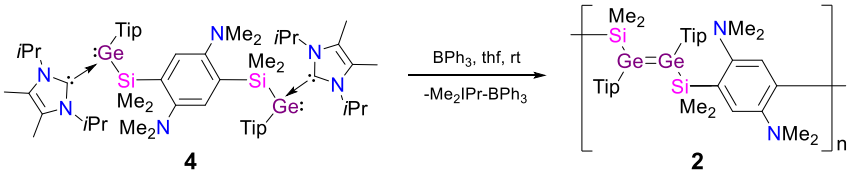

4 2

BPh_3 (78.5 mg, 324 µmol, 1.6 eq.) is dissolved in 0.8 ml of thf and added dropwise to a suspension of bis(germylene)/Me_2IPr adduct **4** (250 mg, 203 µmol, 1 eq.) in 2.5 mL of thf. From the resulting orange solution a yellow solid precipitates after circa 30 minutes. After concentrating the solvent to half the amount the mother liquor is filtrated off and dried in vacuo. A mixture of poly(digermene) **2**[S4] and Me_2IPr-BPh_3[S9] complex (overall 23 mg) is obtained.

1.9. Synthesis of bis(germylene)/Me$_4$CAAC adduct 7

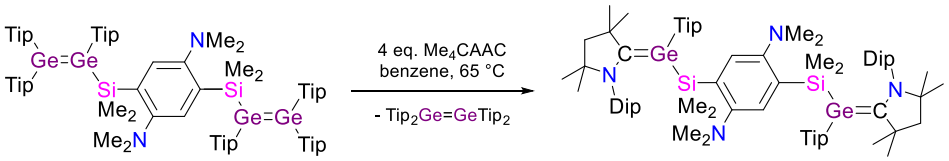

1 **7**

Bis(digermene) **1** (1.05 g, 565 µmol, 1 eq.) and Me$_4$CAAC (740 mg, 2.59 mmol, 4 eq.) are dissolved in 10 mL of benzene. The red solution is heated to 65 °C overnight. The solvent is removed and the residue is stirred in 6 mL of thf at 65 °C for a few minutes. The soluble parts are filtered off and the residue is washed three times with overall 12 mL of thf. Bis(germene) **7** is obtained as a yellow solid which is dried in vacuo (368 mg, 263 µmol, 47%). An additional fraction (22.0 mg, 15.7 µmol, 3%) is obtained from the mother liquor. Single crystals of **7** are obtained directly from the reaction mixture in benzene-d_6 or from the mother liquor.

^{13}C{^{1}H} CP/MAS NMR (100.61 MHz, 300 K, 13 kHz, TMS): δ = 194.31 (Me$_4$CAAC-*C*), 157.13, 154.17, 148.62, 142.93, 141.52, 139.42, 133.66, 126.05, 123.84, 122.27, 119.60 (Ph*C*, Tip*C* and Dip*C*), 66.32 (N(*C*H$_3$)$_2$), 58.44 (C$_q$ of Me$_4$CAAC), 49.82 (*C*H(CH$_3$)$_2$ of Tip and Dip), 47.20 (C$_q$ of Me$_4$CAAC), 37.75, 35.26, 34.18, 33.09 (*C*H(CH$_3$)$_2$ of Tip and Dip), 25.51 (*C*H$_3$ of Tip and Dip), 0.81 (Si(*C*H$_3$)$_2$). **^{29}Si{^{1}H} CP/MAS NMR** (79.49 MHz, 300 K, 13 kHz, TMS): δ = −5.77 ppm. **UV/Vis** (*n*-hexane/thf, 80/20): λ$_{max}$ = 404 nm (ε = 34000 L mol^{-1} cm^{-1}). **Elemental analysis:** Calcd. for (C$_{84}$H$_{134}$Ge$_2$N$_4$Si$_2$): C, 71.99; H, 9.64, N, 4.00. Found: C, 71.68; H, 9.22; N, 4.26. **Mp.:** 220 °C (decomposition).

1.10.Reaction of bis(germylene)/Me$_2$IPr adduct 4 with Me$_4$CAAC

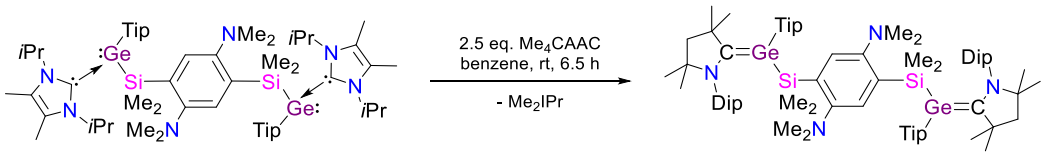

4 **7**

Me$_4$CAAC (48.2 mg, 169 µmol, 2.5 eq.) is dissolved in 0.5 ml of benzene and added dropwise to a suspension of bis(germylene)/Me$_2$IPr adduct **4** (83.2 mg, 67.6 µmol, 1 eq.) in 0.5 mL of benzene. After 6.5 hours the solvent of the resulting bright red solution is removed in vacuo and filtrated from 1 mL of thf. The residual yellow solid is washed two times with overall 2 mL of thf and dried in vacuo to yield bis(germene) **7** (53.6 mg, 38.6 µmol, 57%).

2. NMR data

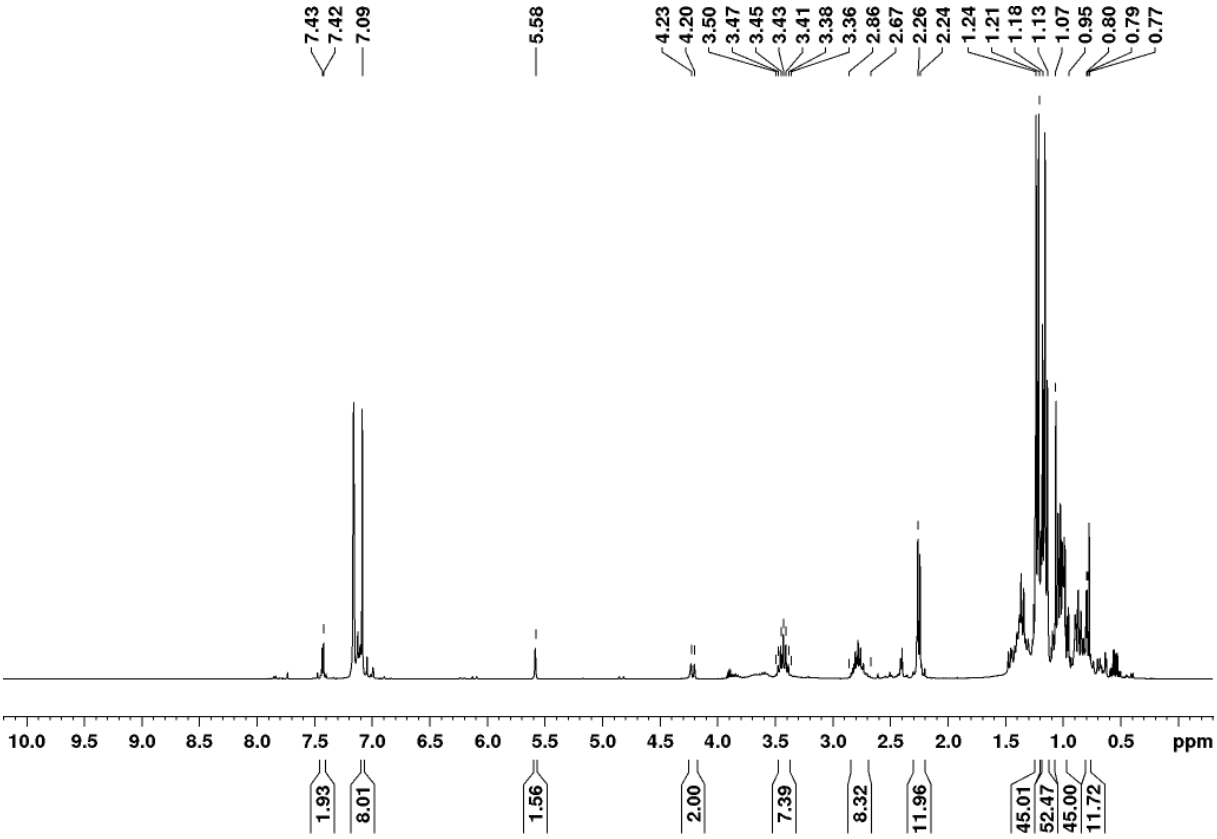

Figure S1. ^{1}H NMR spectrum of a 1:1.5 mixture of the bis(silylgermane) and the mono(silylgermane) from silane trapping of bis(germylene) **[3]** in benzene-d_6.

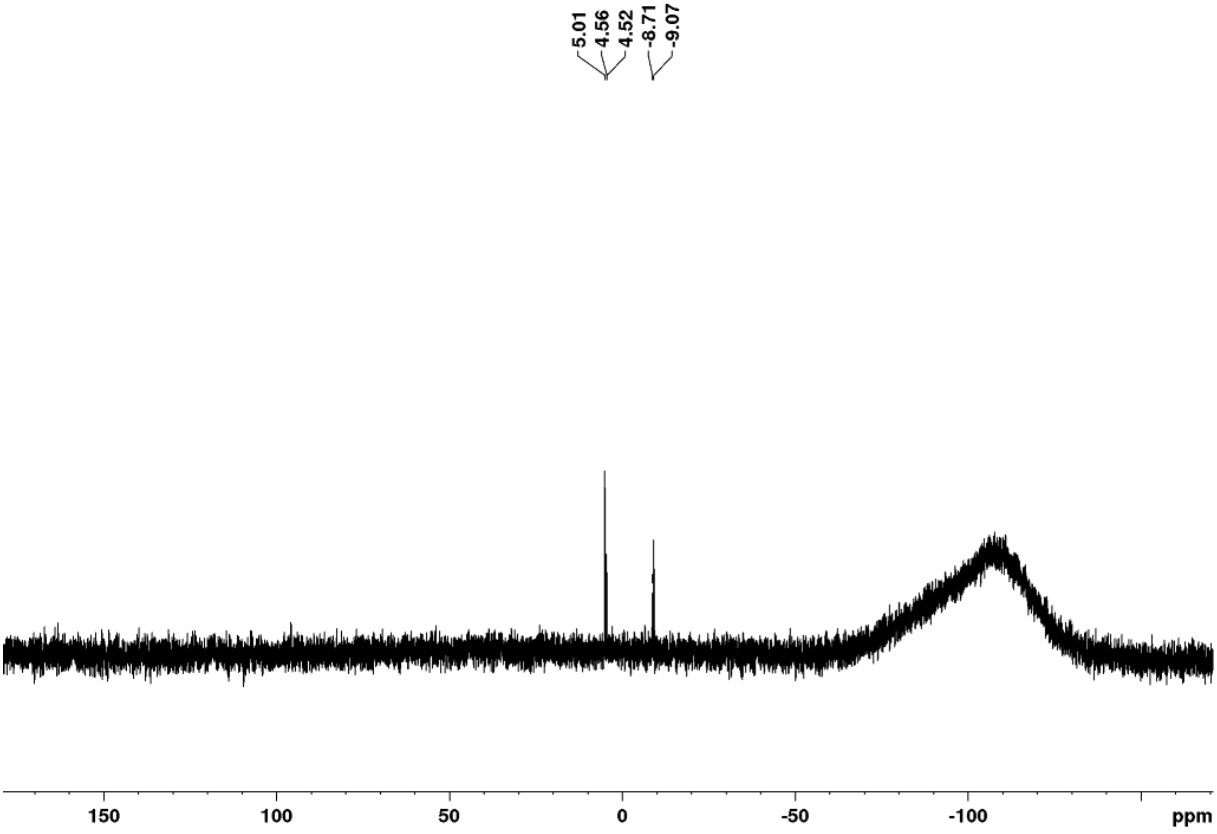

Figure S2. ^{29}Si{^{1}H} NMR spectrum of a 1:1.5 mixture of the bis(silylgermane) and the mono(silylgermane) from silane trapping of bis(germylene) **[3]** in benzene-d_6.

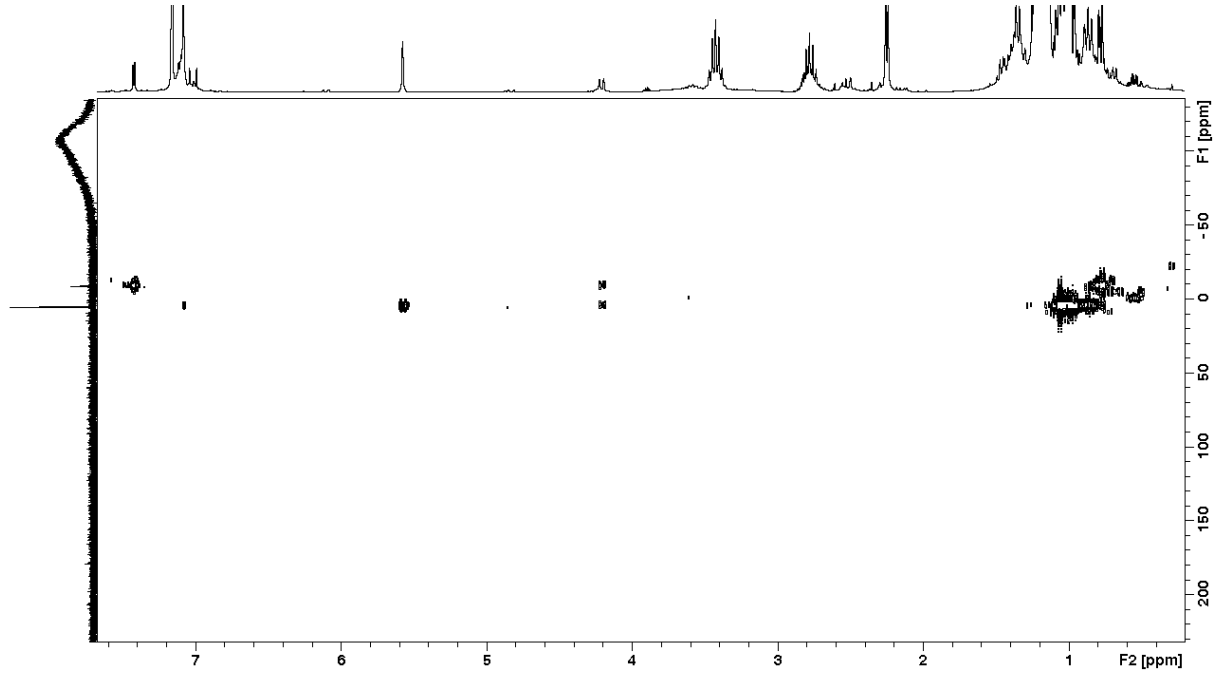

Figure S3. $^{29}Si/^{1}H$ HMBC NMR spectrum of a 1:1.5 mixture of the bis(silylgermane) and the mono(silylgermane) from silane trapping of bis(germylene) **[3]** in benzene-d_6.

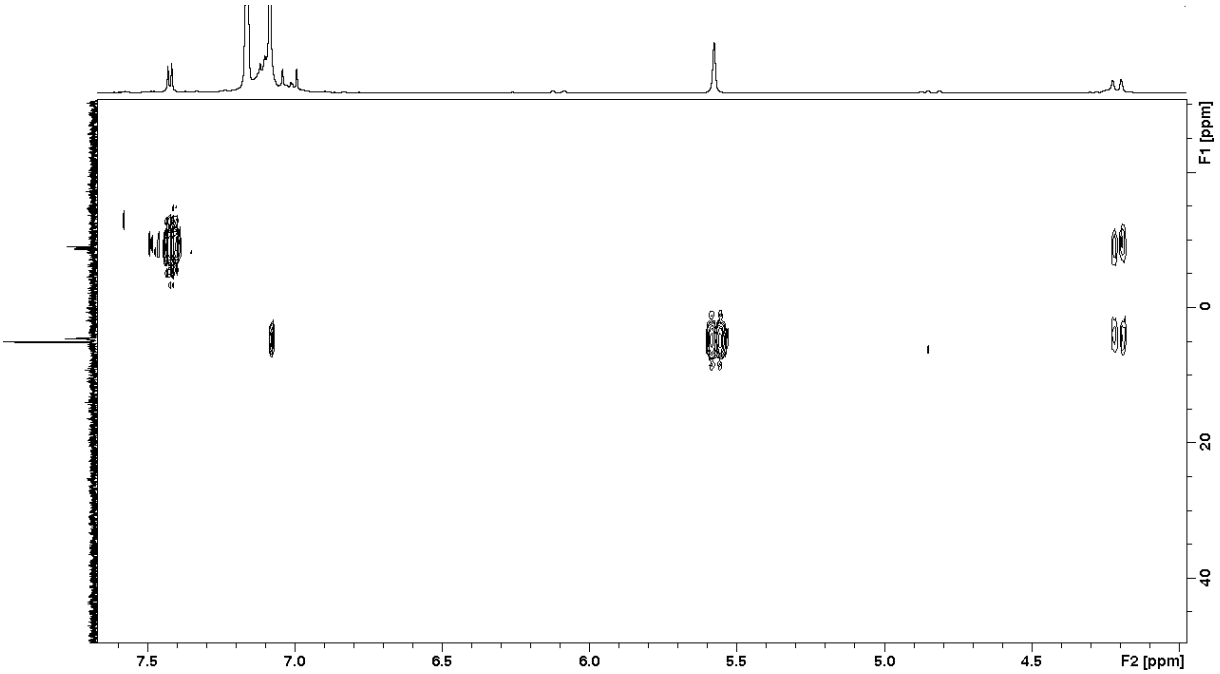

Figure S4. $^{29}Si/^{1}H$ HMBC NMR spectrum of a 1:1.5 mixture of the bis(silylgermane) and the mono(silylgermane) from silane trapping of bis(germylene) **[3]** in benzene-d_6 (selected section).

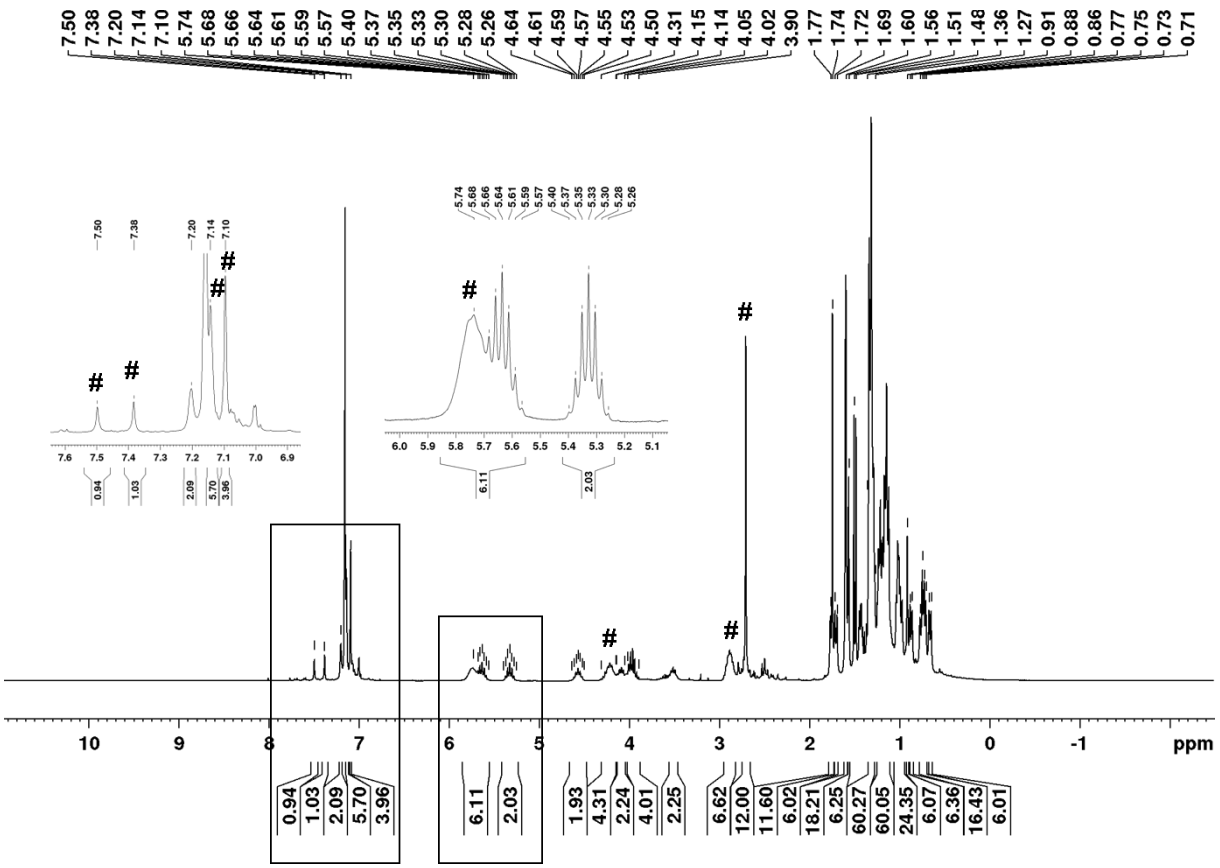

Figure S5. ^{1}H NMR spectrum of the reaction mixture of the reaction of bis(digermene) **1** with four equivalents of Me_2IPr in benzene-d_6 with characteristic resonances of the two products: bis(germylene)/ Me_2IPr adduct **4** (**#**) and $Tip_2Ge{\cdot}Me_2IPr$ in a 1:2 ratio.

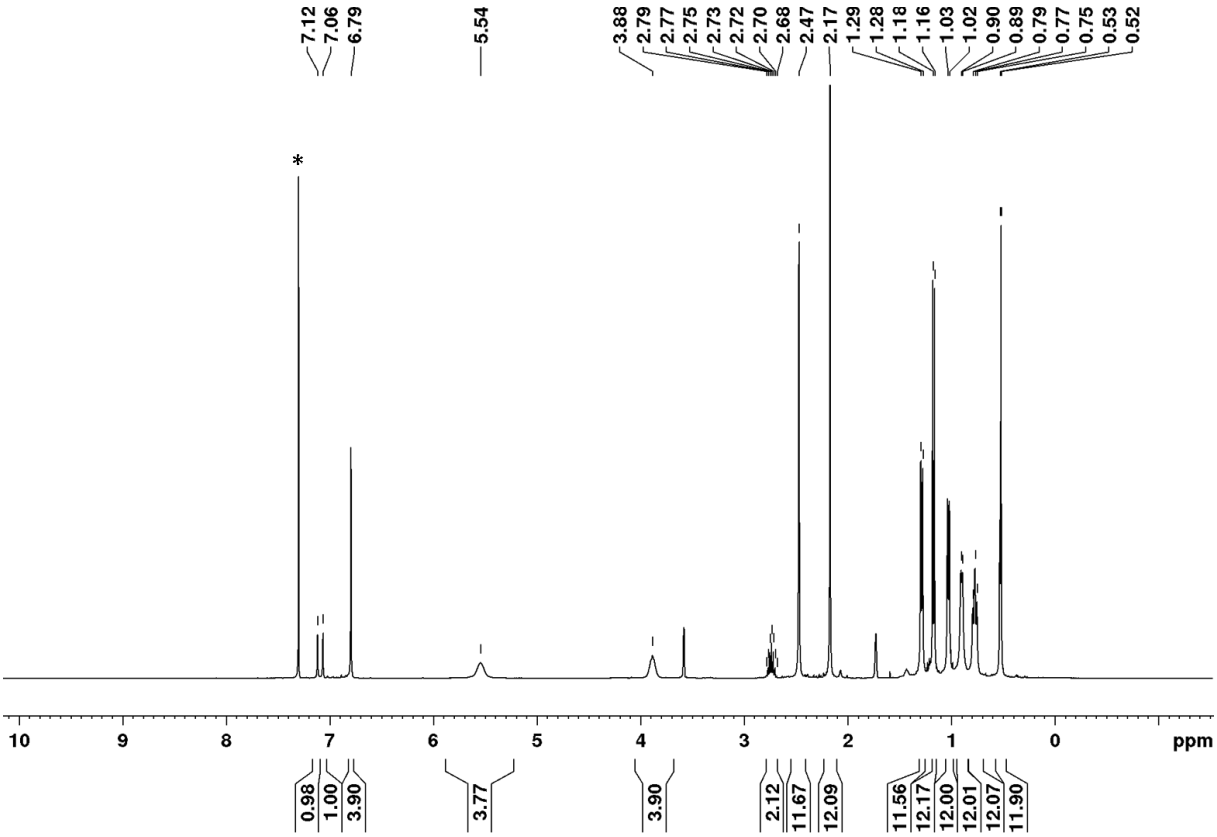

Figure S6. ^{1}H NMR spectrum of bis(germylene)/Me$_2$IPr adduct **4** in thf-d_8.

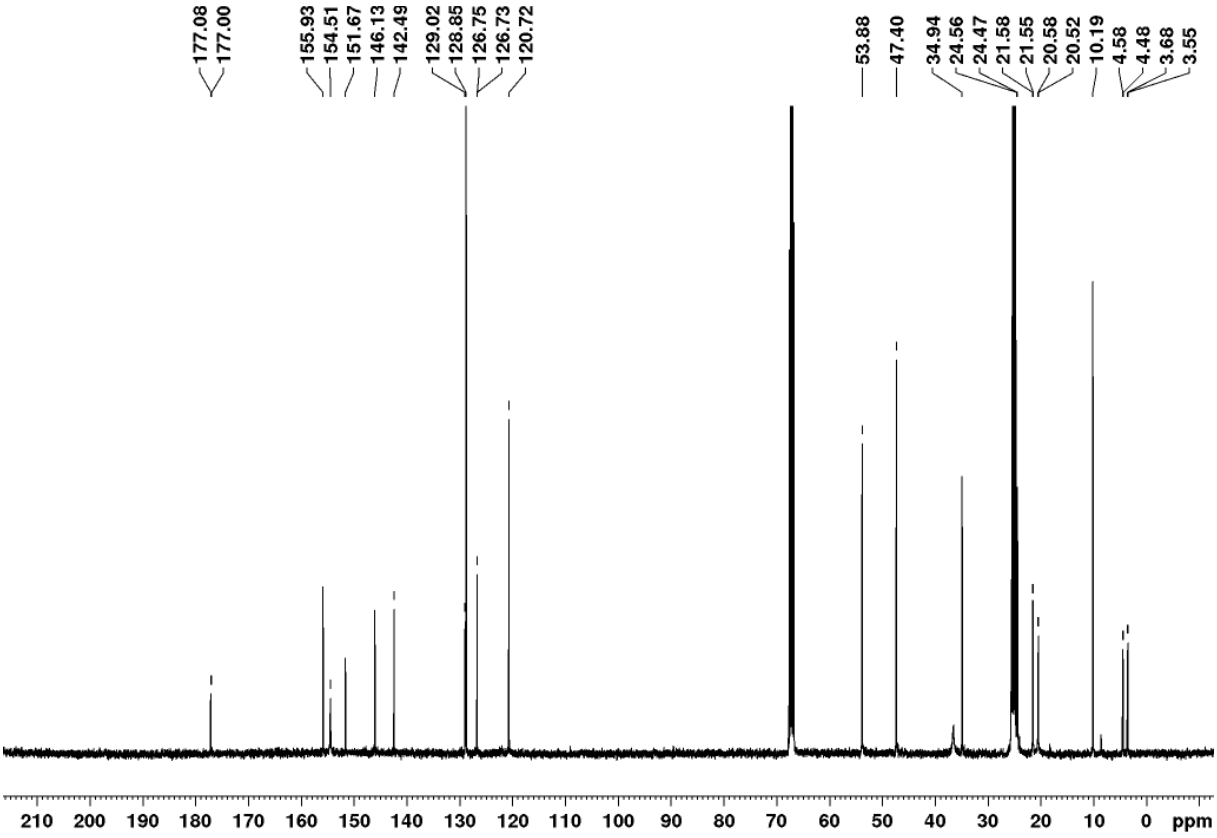

Figure S7. ^{13}C{^{1}H} NMR spectrum of bis(germylene)/Me$_2$IPr adduct **4** in thf-d_8.

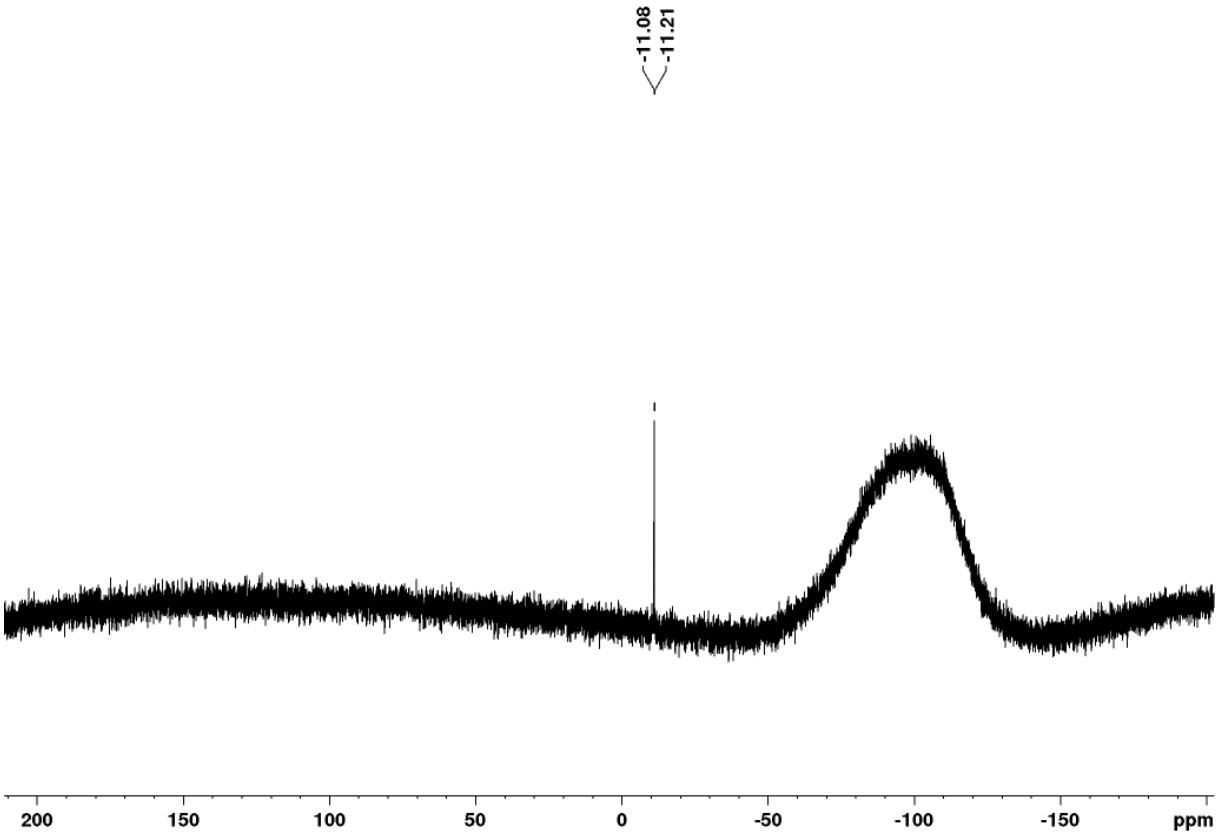

Figure S8. $^{29}Si\{^{1}H\}$ NMR spectrum of bis(germylene)/Me_2IPr adduct **4** in thf-d_8.

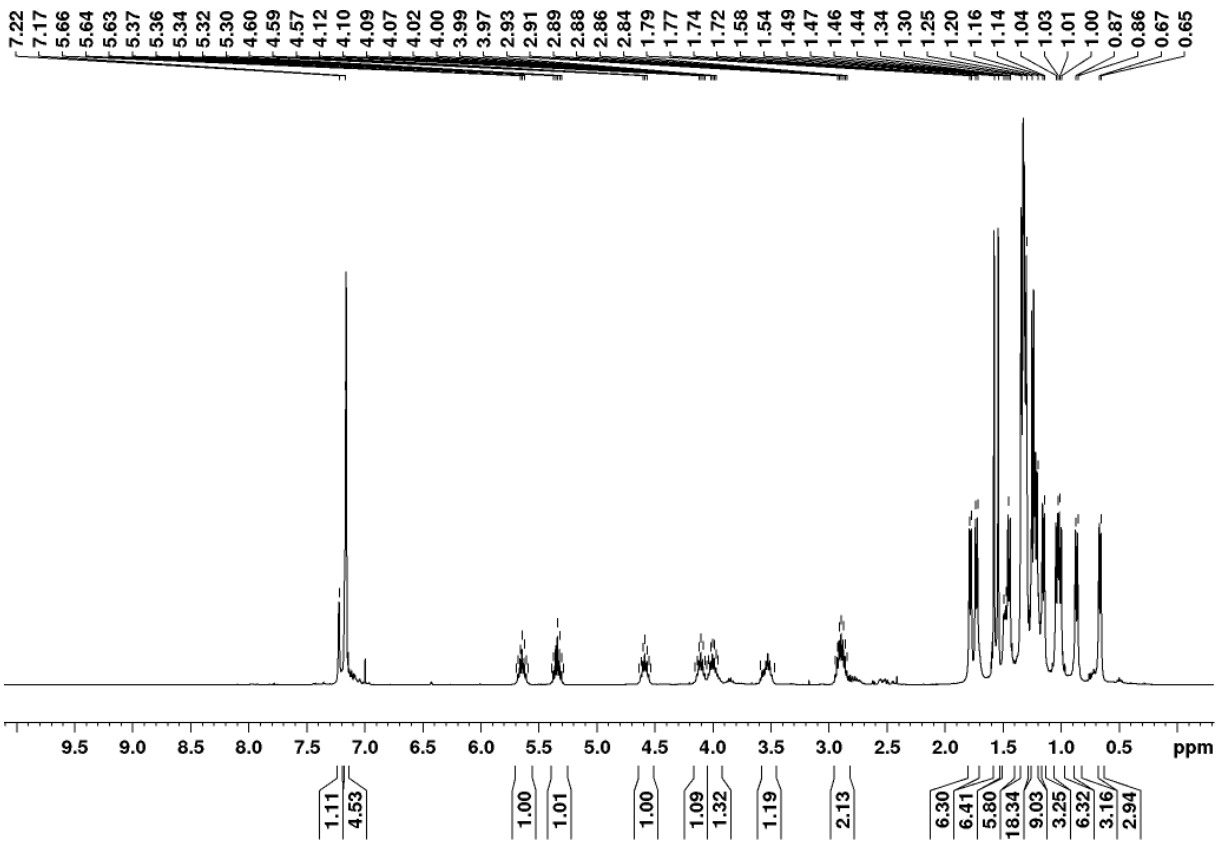

Figure S9. ^{1}H NMR spectrum of $Tip_2Ge{\cdot}Me_2IPr$ in benzene-d_6.

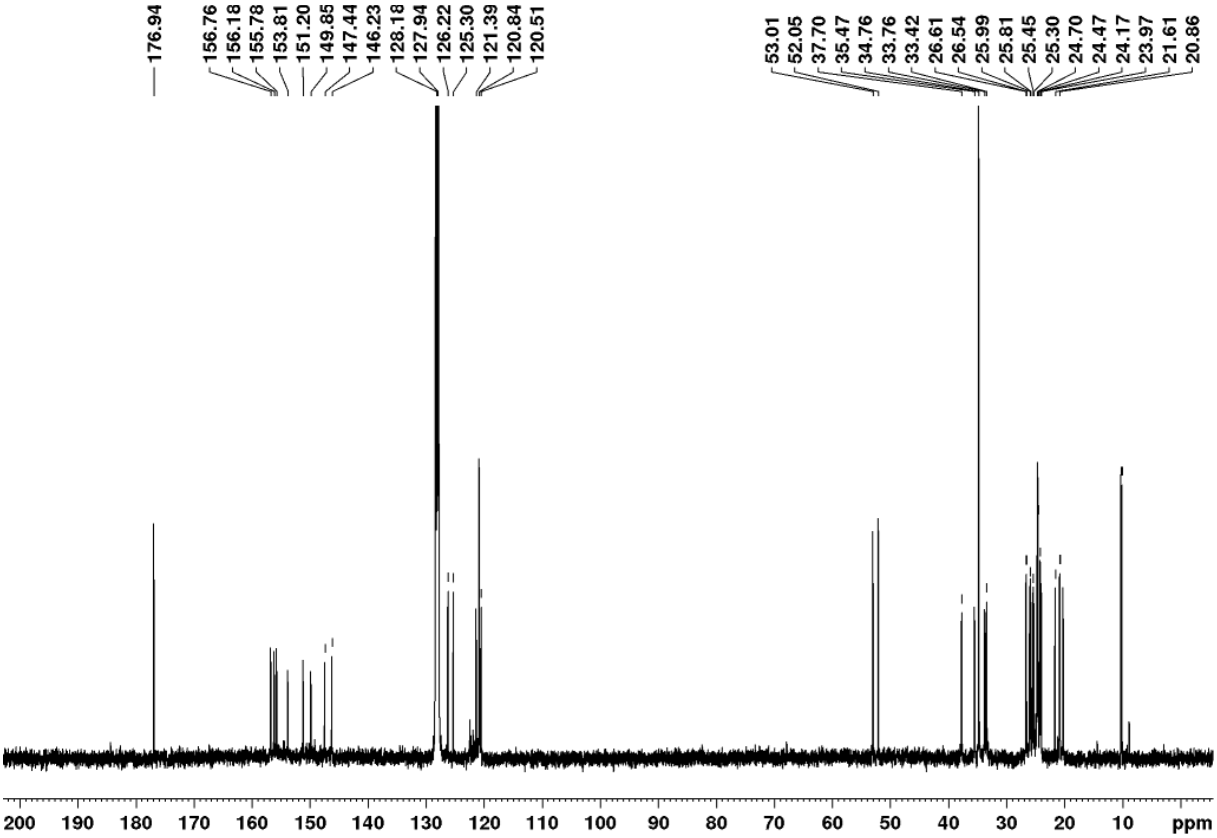

Figure S10. $^{13}C\{^{1}H\}$ NMR spectrum of $Tip_2Ge{\cdot}Me_2IPr$ in benzene-d_6.

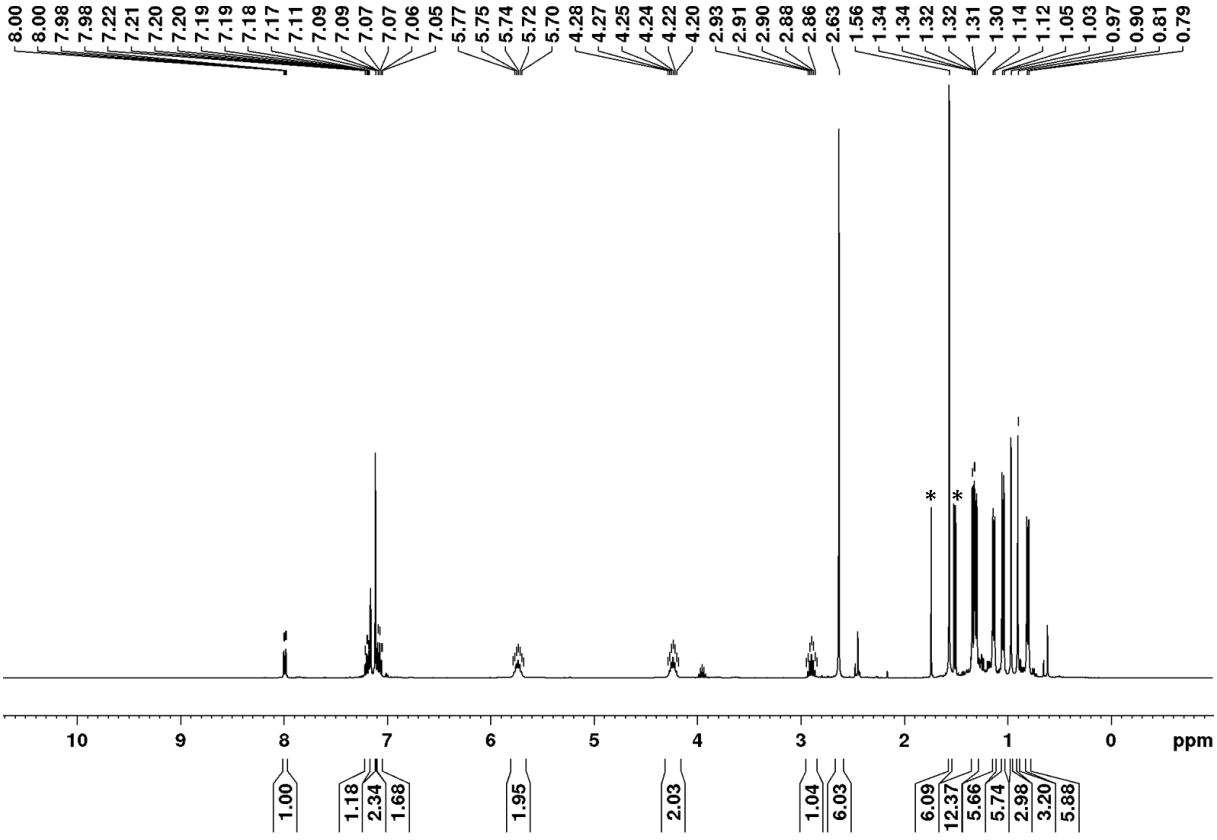

Figure S11. ^{1}H NMR spectrum of germylene/Me_2IPr adduct **6** in benzene-d_6; *residual 5wt% of free Me_2IPr.

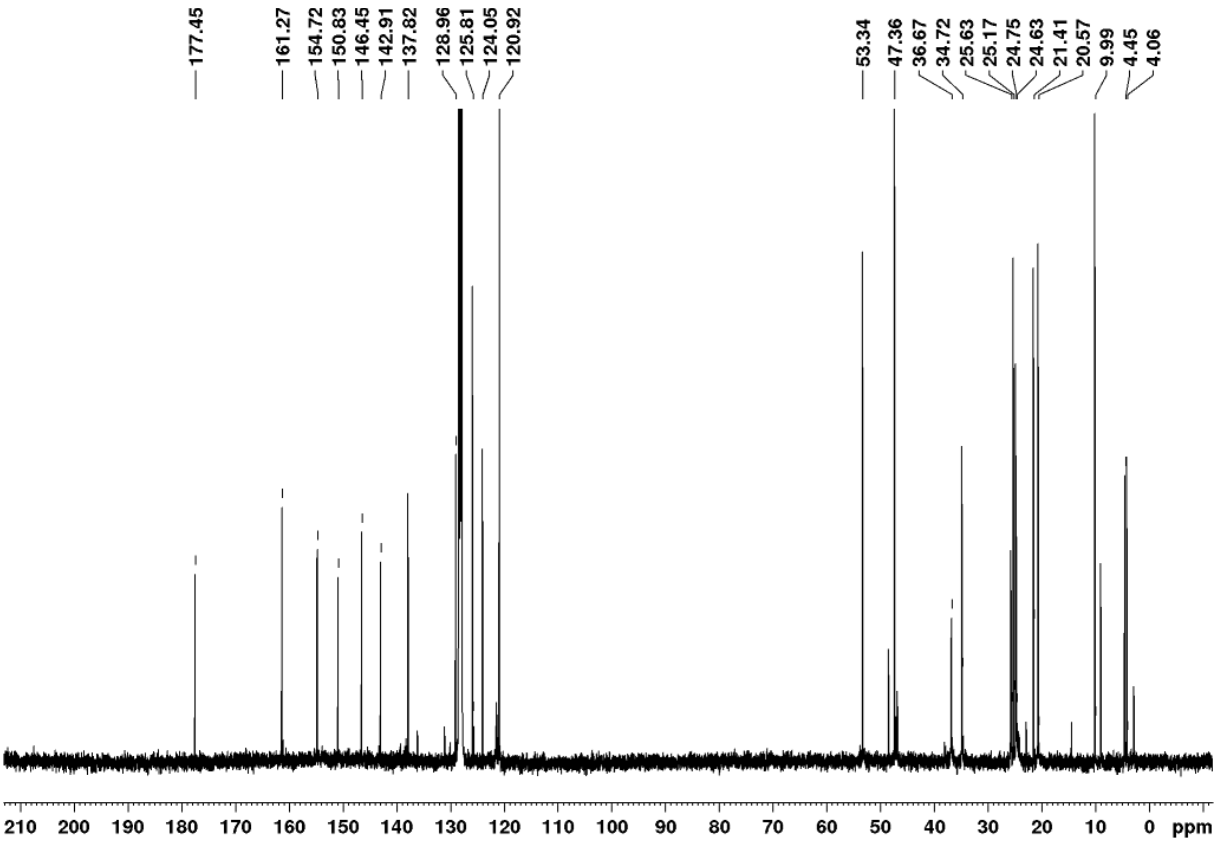

Figure S12. $^{13}C\{^{1}H\}$ NMR spectrum of germylene/Me_2IPr adduct **6** in benzene-d_6.

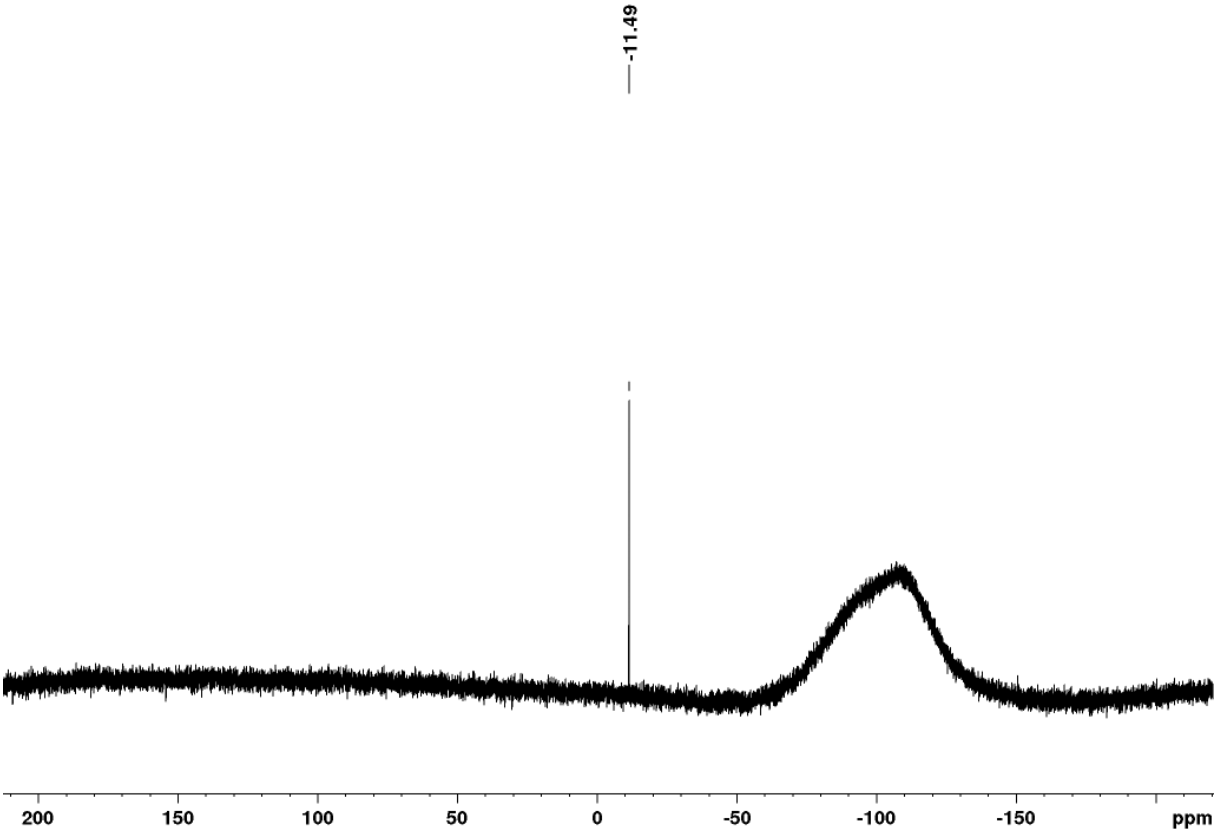

Figure S13. $^{29}Si\{^{1}H\}$ NMR spectrum of germylene/Me_2IPr adduct **6** in benzene-d_6.

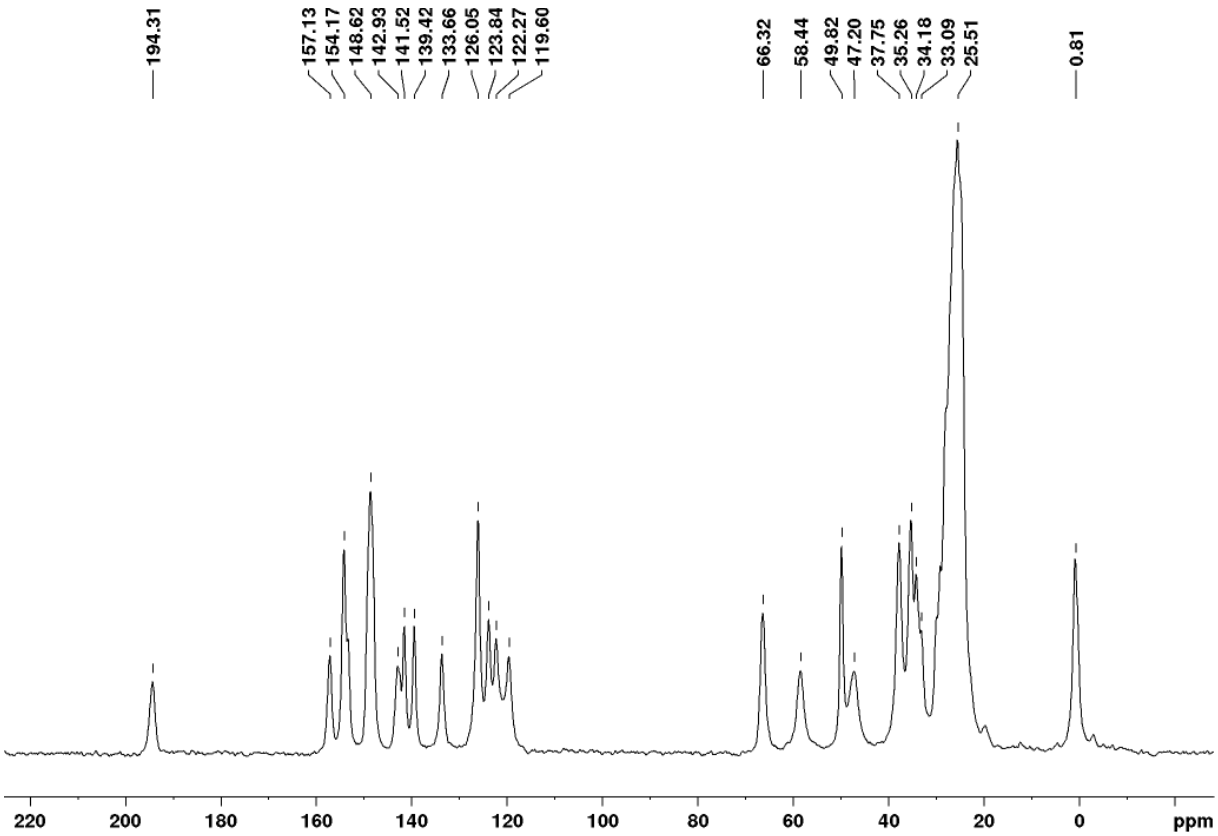

Figure S14. $^{13}C\{^{1}H\}$ CP/MAS NMR spectrum of bis(germene) **7**.

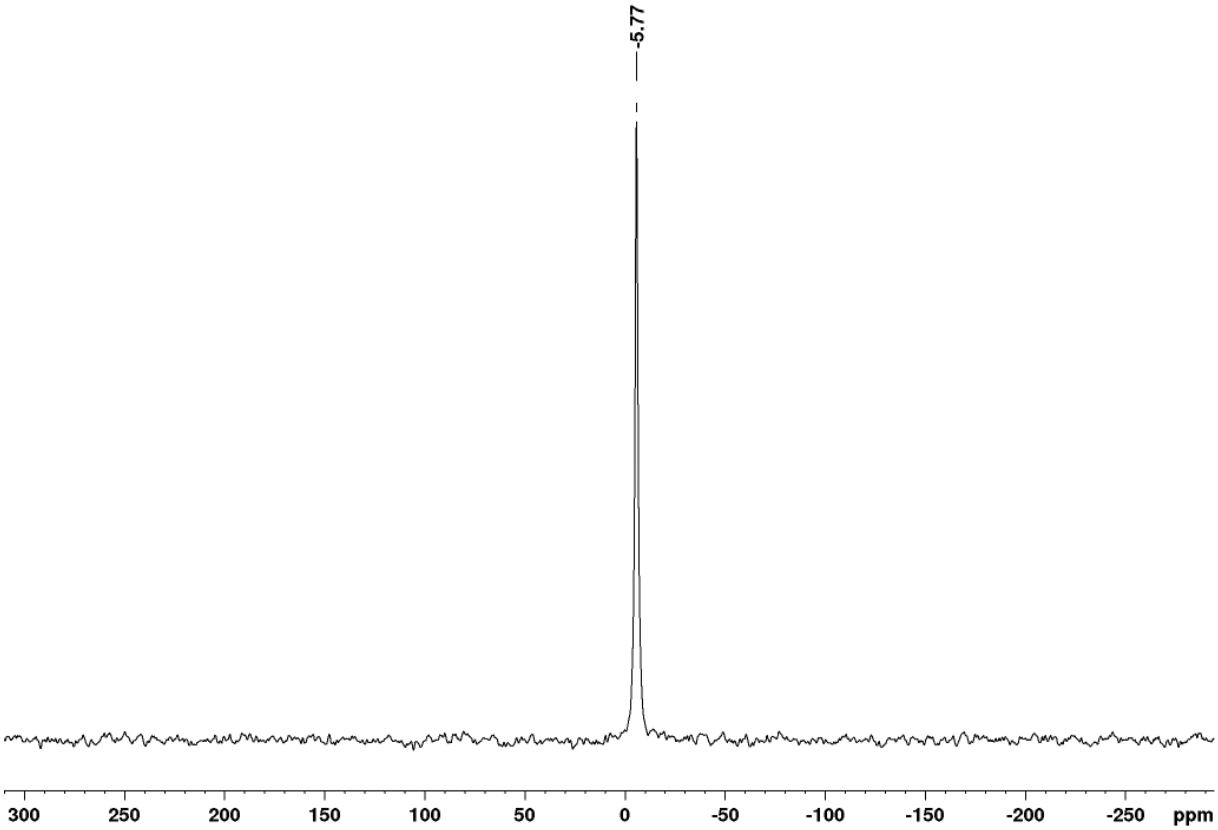

Figure S15. $^{29}Si\{^{1}H\}$ CP/MAS NMR spectrum of bis(germene) **7**.

3. UV/Vis spectra

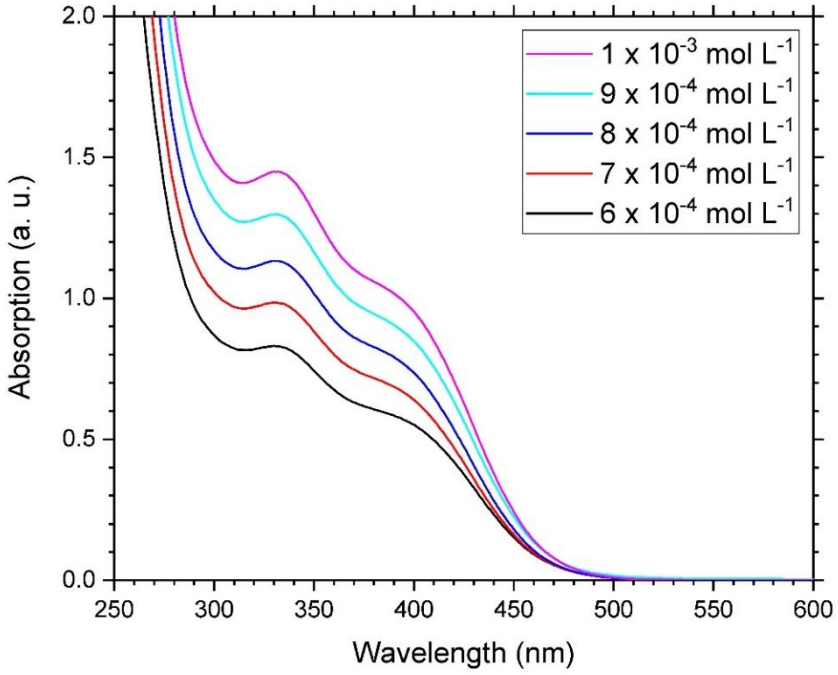

Figure S16. UV/Vis spectrum of bis(germylene)/Me$_2$IPr adduct **4** at different concentrations.

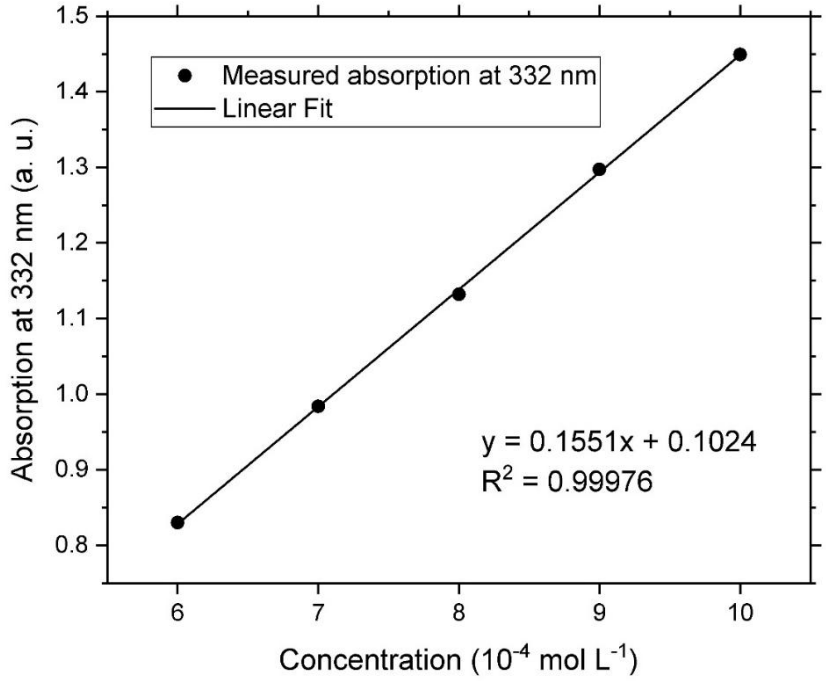

Figure S17. Determination of ε (15500 L mol^{-1} cm^{-1}) of **4** by linear regression of absorbance at 332 nm against concentration.

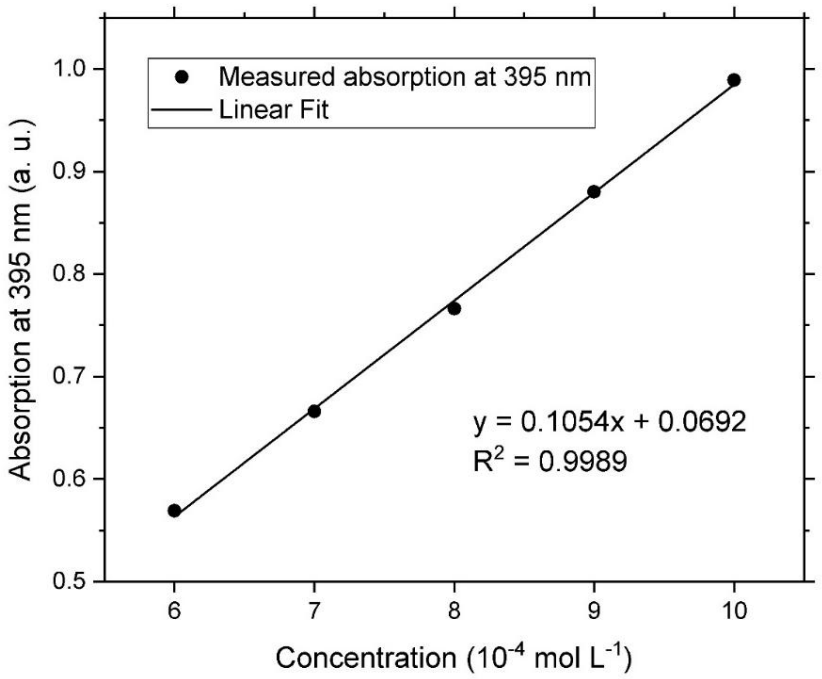

Figure S18. Determination of ε (10500 L mol^{-1} cm^{-1}) of **4** by linear regression of absorbance at 395 nm against concentration.

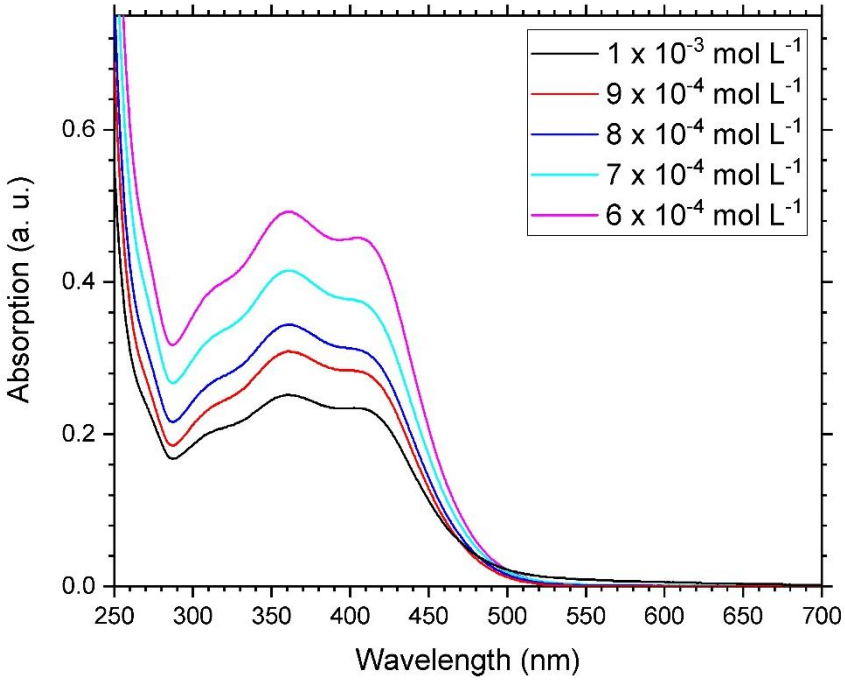

Figure S19. UV/Vis spectrum of $Tip_2Ge{\cdot}Me_2IPr$ at different concentrations.

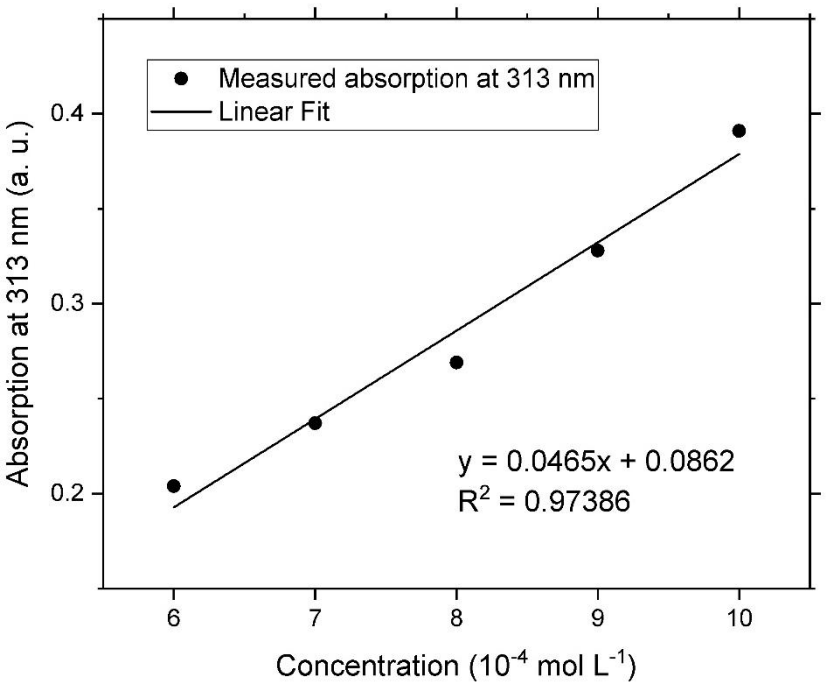

Figure S20. Determination of ε (4700 L mol^{-1} cm^{-1}) of $Tip_2Ge{\cdot}Me_2IPr$ by linear regression of absorbance at 313 nm against concentration.

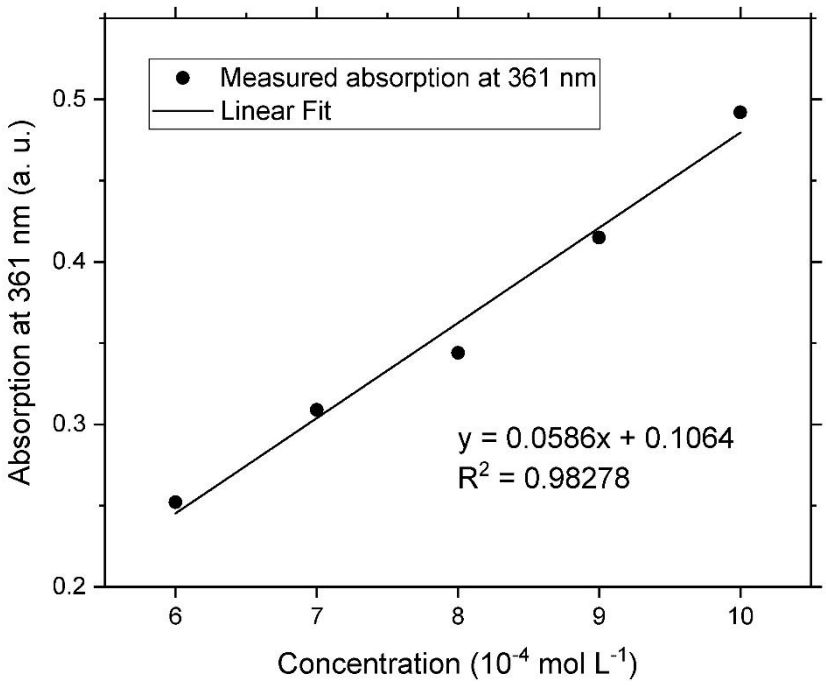

Figure S21. Determination of ε (5900 L mol^{-1} cm^{-1}) of $Tip_2Ge{\cdot}Me_2IPr$ by linear regression of absorbance at 361 nm against concentration.

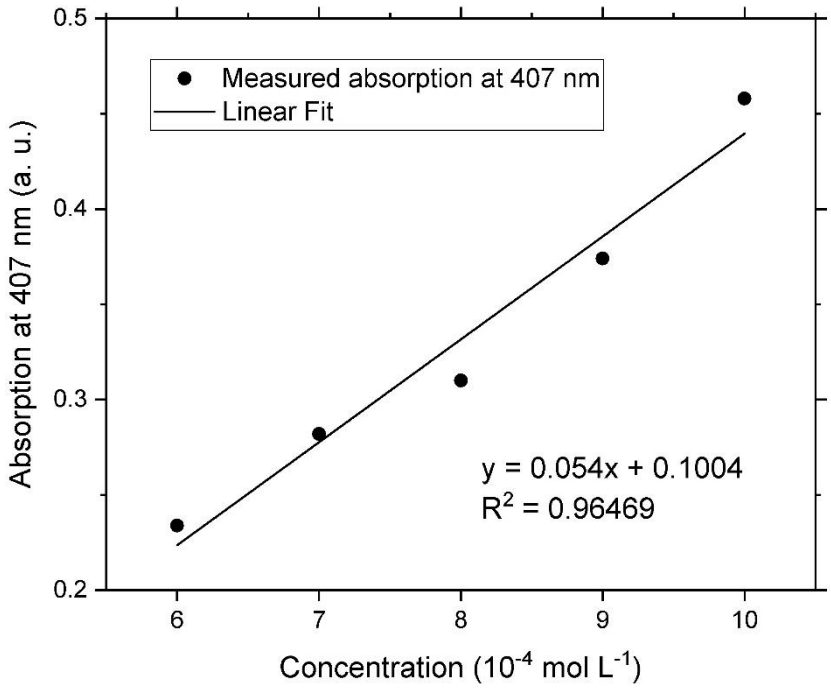

Figure S22. Determination of ε (5400 L mol^{-1} cm^{-1}) of Tip$_2$Ge·Me$_2$IPr by linear regression of absorbance at 407 nm against concentration.

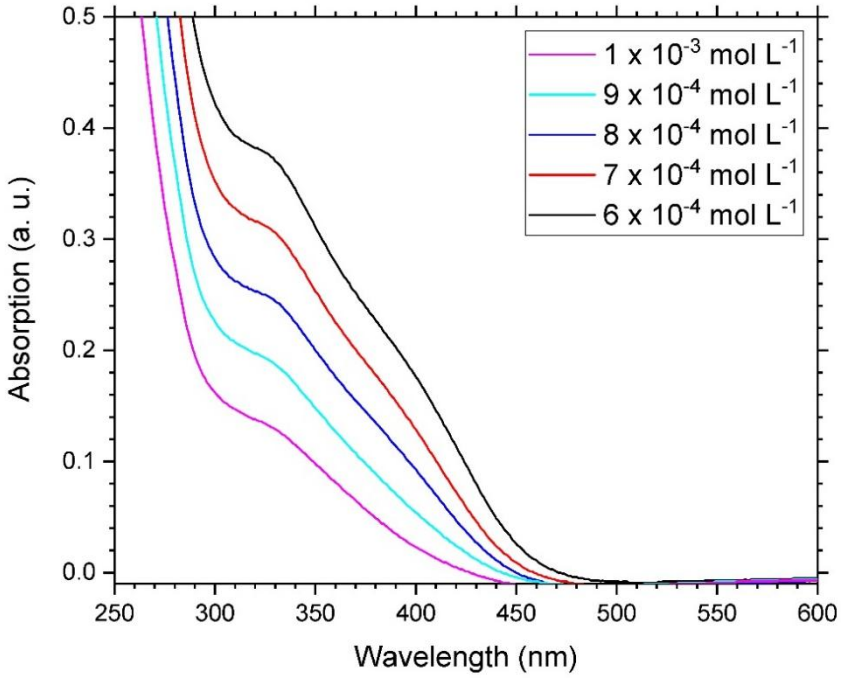

Figure S23. UV/Vis spectrum of germylene/Me$_2$IPr adduct **6** at different concentrations.

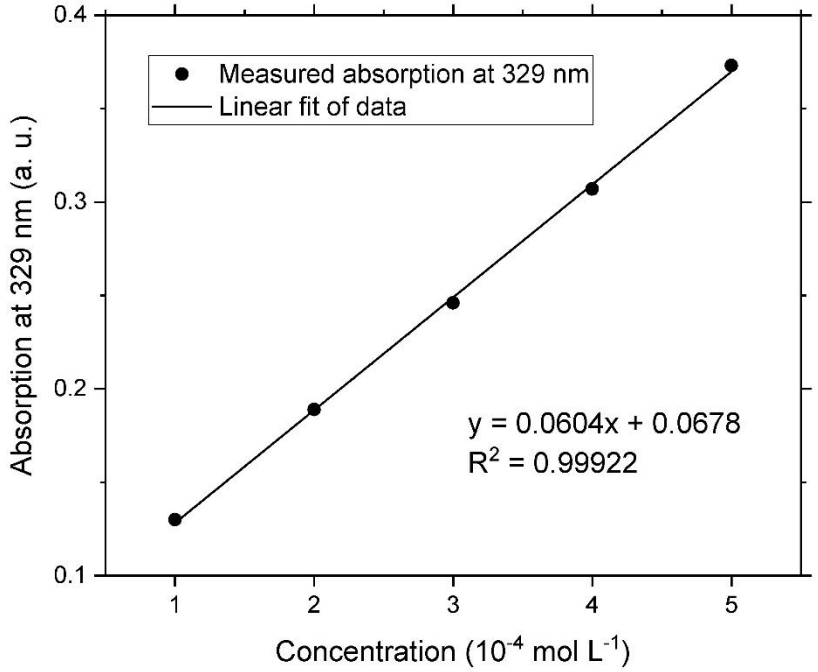

Figure S24. Determination of ε (6000 L mol^{-1} cm^{-1}) of **6** by linear regression of absorbance at 329 nm against concentration.

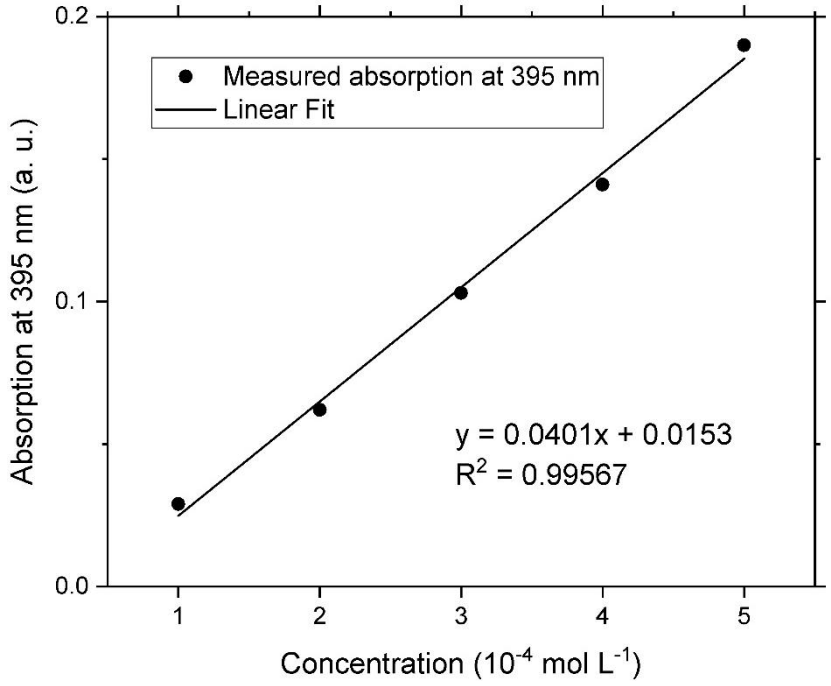

Figure S25. Determination of ε (4000 L mol^{-1} cm^{-1}) of germylene/Me_2IPr adduct **6** by linear regression of absorbance at 395 nm against concentration.

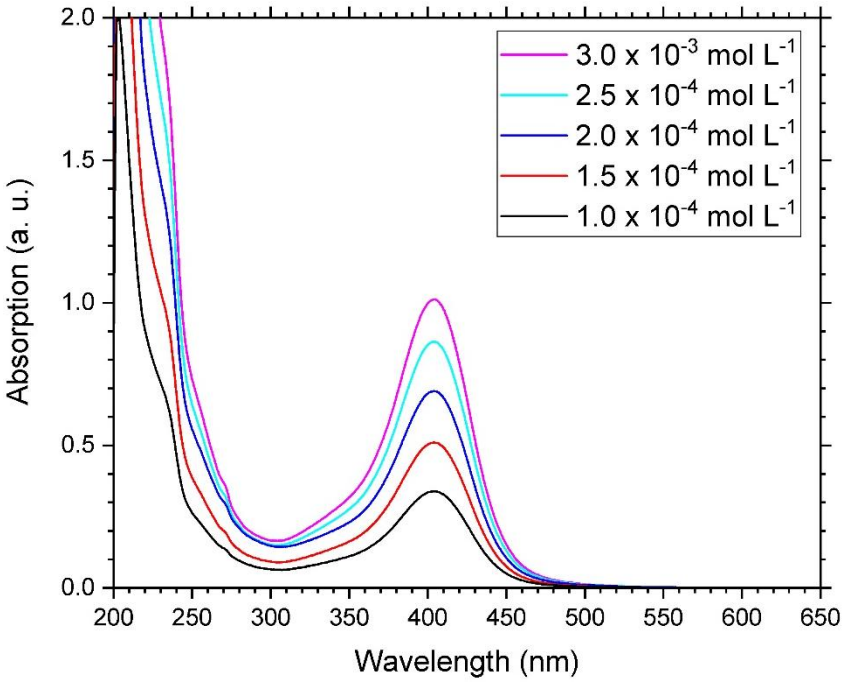

Figure S26. UV/Vis spectrum of **7** at different concentrations.

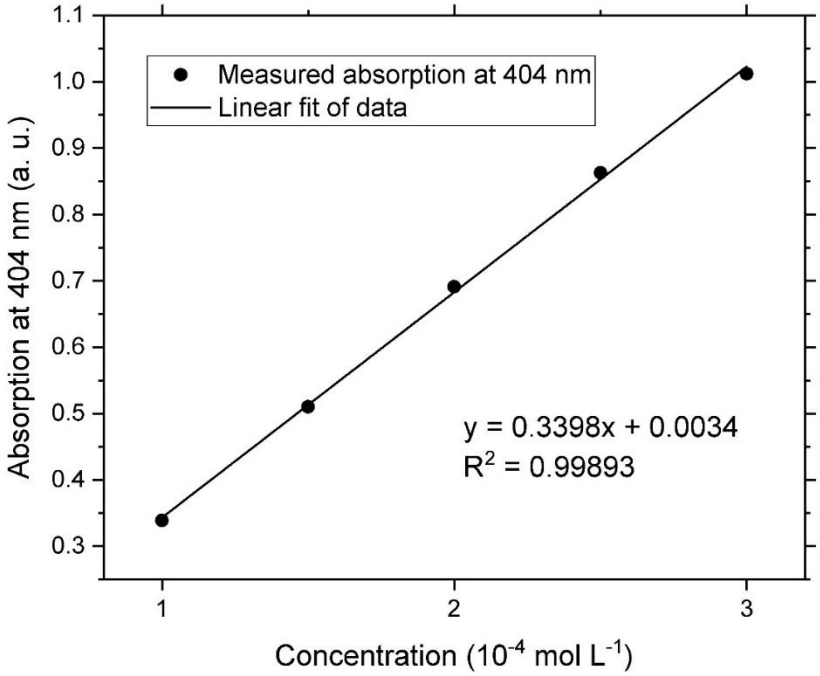

Figure S27. Determination of ε (34000 L mol^{-1} cm^{-1}) of **7** by linear regression of absorbance at 404 nm against concentration.

4. Crystallographic data

Crystallographic data of the structures reported in this paper have been deposited with the Cambridge Crystallographic Data Centre, CCDC, 12 Union Road, Cambridge CB21EZ, UK. Copies of the data can be obtained free of charge on quoting the depository numbers CCDC-2236120 (**6**) and CCDC-2236118 (**7**) (Fax: +44-1223-336-033; E-Mail: deposit@ccdc.cam.ac.uk, http://www.ccdc.cam.ac.uk).

4.1. Me_2IPr-germylene 6 (CCDC-2236120)

Refinement details:

All non H-atoms were located on the electron density maps and refined anisotropically. C-bound H atoms were placed in positions of optimized geometry and treated as riding atoms. Their isotropic displacement parameters were coupled to the corresponding carrier atoms by a factor of 1.2 (CH) or 1.5 (CH3). *Disorder*: One of the isopropyl groups (C46A-C48A, C46B-C48B) was split over two positions. Its occupancy factors refined to 64 % for the major compoent. *Twin refinement*: The structure was solved and refined using the hkl data in the hklf4 format. The last anisotropic refinement cycle without hydrogen atoms resulted in a wR2 of 52 %. The structure was then refined as a two component twin. The twin matrix (2-axis in (1 0 1)) was found to be (-0.003 0.000 0.997 0.000 -1.000 0.000 1.003 0.000 0.003) from TwinRotMat (PLATON [4]). The refinement was operated using the hklf5 routine with all reflections (16133) of component 1, including the overlapping ones (15378) resulting in a BASF value of 0.22. After the first refinement cycle using the hklf5 format the wR2 dropped to 24 %. Finally, the hydrogen atoms were taken into account and the structure was refined to convergence, resulting in a wR2 of 17.8 %.

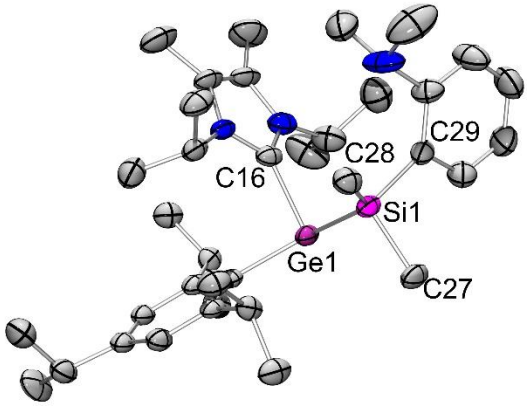

Figure S28. Molecular structure of **6** in the solid state. Second molecule in the asymmetric unit and hydrogen atoms omitted for clarity. Thermal ellisoids are shown at 50% probability.[S18]

Table S1. Crystal data and structure refinement for **6** (CCDC: 2236120).[S18]

The structure was refined as a two component twin.

Identification code	sh4643_a_tw	
Empirical formula	C36 H59 Ge N3 Si	
Formula weight	634.54	
Temperature	133(2) K	
Wavelength	0.71073 Å	
Crystal system	Monoclinic	
Space group	$P2_1/n$	
Unit cell dimensions	a = 26.0882(14) Å	α= 90°.
	b = 10.7042(6) Å	β= 91.212(2)°.
	c = 26.1551(14) Å	γ = 90°.
Volume	7302.3(7) $Å^3$	

Z	8
Density (calculated)	1.154 Mg/m^3
Absorption coefficient	0.898 mm^{-1}
F(000)	2736
Crystal size	0.184 x 0.160 x 0.128 mm^3
Theta range for data collection	2.056 to 25.680°.
Index ranges	-31<=h<=31, -13<=k<=13, -31<=l<=31
Reflections collected	13845
Independent reflections	13845 [R(int) = 0.0738]
Completeness to theta = 25.242°	99.9 %
Absorption correction	Semi-empirical from equivalents
Max. and min. transmission	0.7455 and 0.6274
Refinement method	Full-matrix least-squares on F^2
Data / restraints / parameters	13845 / 81 / 798
Goodness-of-fit on F^2	1.031
Final R indices [I>2sigma(I)]	R1 = 0.0667, wR2 = 0.1499
R indices (all data)	R1 = 0.1034, wR2 = 0.1779
Extinction coefficient	n/a
Largest diff. peak and hole	0.831 and -1.029 $e.Å^{-3}$

4.2. Me_4CAAC-bis(germylene) 7 (CCDC-2236118)

Refinement details:

All non H-atoms were located in the electron density maps and refined anisotropically. C-bound H atoms were placed in positions of optimized geometry and treated as riding atoms. Their isotropic displacement parameters were coupled to the corresponding carrier atoms by a factor of 1.2 (CH) or 1.5 (CH3). Disorder: One isopropyl-group and one solvent benzene molecule is split over two positions. Their occupancy factors refined to 0.76 and 0.53 for the major compound, respectively.

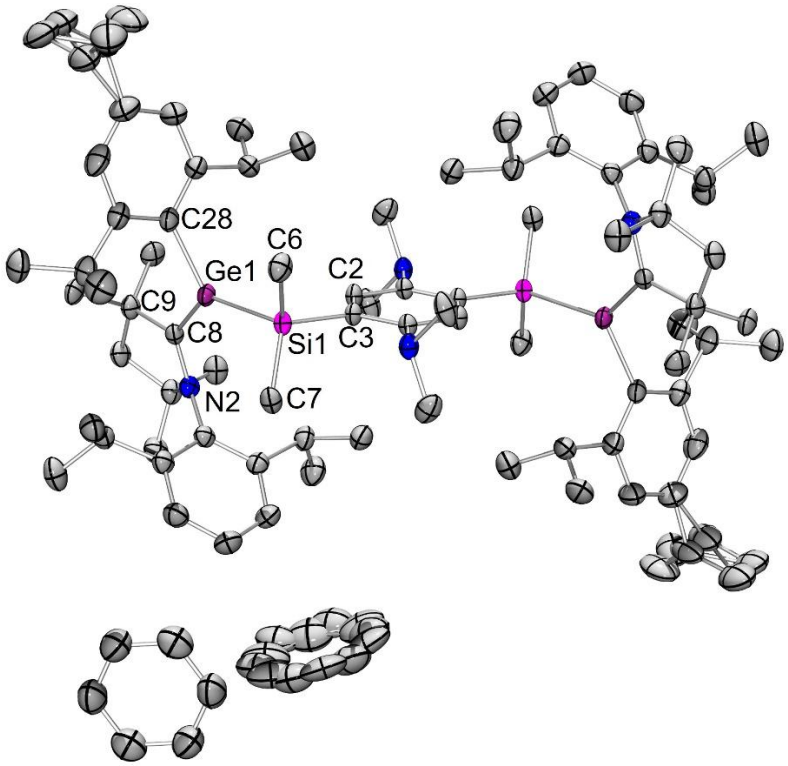

Figure S29. Molecular structure of **7** in the solid state. Hydrogen atoms are omitted for clarity. Thermal ellisoids are shown at 50% probability.[S18]

Table S2. Crystal data and structure refinement for **7** (CCDC: 2236118).[S18]

Identification code	sh4423_a	
Empirical formula	C102 H152 Ge2 N4 Si2	
Formula weight	1635.63	
Temperature	133(2) K	
Wavelength	0.71073 Å	
Crystal system	Triclinic	
Space group	P-1	
Unit cell dimensions	a = 9.8483(4) Å	α= 69.254(2)°.
	b = 14.2480(7) Å	β= 82.099(2)°.
	c = 18.7576(9) Å	γ = 78.804(2)°.
Volume	2407.8(2) $Å^3$	
Z	1	
Density (calculated)	1.128 Mg/m^3	
Absorption coefficient	0.695 mm^{-1}	

F(000)	884
Crystal size	0.189 x 0.137 x 0.078 mm^3
Theta range for data collection	2.114 to 28.732°.
Index ranges	-13<=h<=12, -19<=k<=19, -25<=l<=25
Reflections collected	76927
Independent reflections	12457 [R(int) = 0.0938]
Completeness to theta = 25.242°	100.0 %
Absorption correction	Semi-empirical from equivalents
Max. and min. transmission	0.7458 and 0.6992
Refinement method	Full-matrix least-squares on F^2
Data / restraints / parameters	12457 / 251 / 599
Goodness-of-fit on F^2	1.026
Final R indices [I>2sigma(I)]	R1 = 0.0498, wR2 = 0.1042
R indices (all data)	R1 = 0.0842, wR2 = 0.1202
Extinction coefficient	n/a
Largest diff. peak and hole	0.580 and -0.599 $e.Å^{-3}$

5. DFT calculations

Computations were carried out with the Gaussian 09 program package.[S10] Structural optimizations and frequency analyses were performed at the BP86-D3BJ/def2-SVP level of theory[S11,S12] including the dispersion correction by Grimme.[S13] NBO analyses were run with the NBO 7.0 program[S14] at the BP86/def2TZVPP level of theory.[S11,S12] For TD-DFT calculations, the ORCA quantum chemistry program package[S15] was used and the PBE0/def2-TZVP functional[S16] and basis set[S12] were employed. Pictures of Kohn-Sham and NBO orbitals were displayed with ChemCraft.[S17]

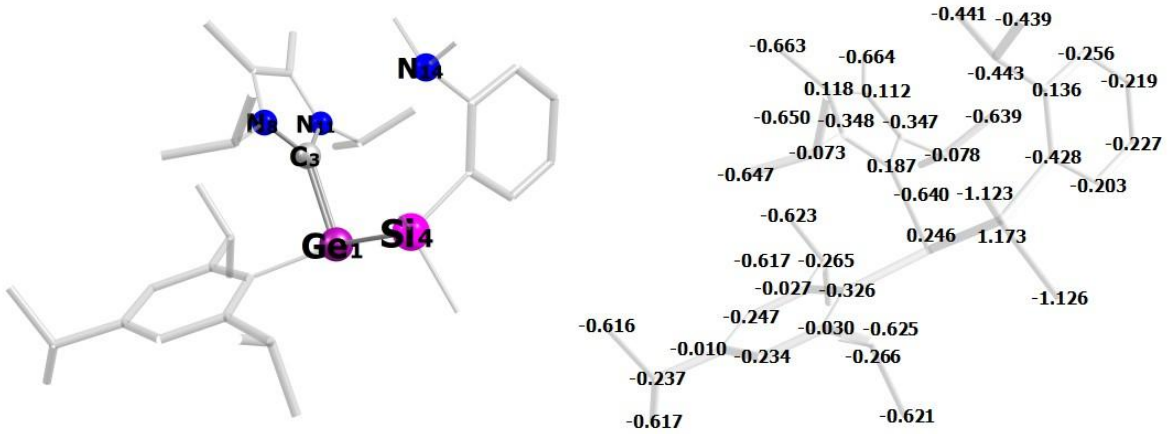

Figure S30. Optimized structure and natural atomic charges of germylene/Me_2IPr adduct **6**.

Table S3. Atomic coordinates of the optimized structure of germylene/Me_2IPr adduct **6**.

32	0.058081000	-0.483791000	-1.322956000
6	-1.923195000	-0.531213000	-0.732602000
6	0.558688000	0.978917000	0.062228000
14	1.515234000	-2.232247000	-0.380398000
6	1.431944000	-3.202937000	1.266554000
6	3.258154000	-1.456259000	-0.604018000
6	1.437520000	-3.625872000	-1.694678000
7	0.145435000	1.159129000	1.355129000
6	0.532175000	2.417870000	1.828720000
6	-0.552171000	0.093744000	2.117906000
7	1.221994000	2.130927000	-0.272473000
6	1.221204000	3.033184000	0.796552000
6	1.832228000	2.322368000	-1.611850000
7	3.488448000	-0.668994000	1.748006000
6	4.057822000	-1.642398000	2.678115000
6	4.018380000	-0.808827000	0.405437000
6	3.578386000	0.690096000	2.270903000
6	-2.618662000	-1.660437000	-0.211927000
6	-2.681375000	0.660442000	-0.953962000
6	-3.981196000	-1.560858000	0.139502000
6	-1.944603000	-3.018477000	-0.073829000
6	-4.712195000	-0.374031000	-0.021165000
6	-4.041081000	0.721456000	-0.590570000
6	-6.168282000	-0.276562000	0.414299000
6	-2.085829000	1.910598000	-1.605446000
6	-2.293424000	-3.913521000	-1.278065000
6	-2.233767000	-3.725710000	1.259055000
6	-2.123547000	3.129324000	-0.666605000
6	-2.761708000	2.211050000	-2.955682000
6	0.208187000	2.970654000	3.178202000
6	1.834477000	4.395514000	0.771958000
6	-1.969366000	0.497564000	2.530080000
6	0.311753000	-0.427184000	3.269219000

6	1.301691000	3.565285000	-2.332456000
6	3.357696000	2.247739000	-1.552134000
6	3.824171000	-1.500721000	-1.904746000
6	5.089609000	-0.967372000	-2.196389000
6	5.844220000	-0.371886000	-1.172845000
6	5.303330000	-0.295016000	0.119048000
6	-7.097499000	0.108574000	-0.752210000
6	-6.326287000	0.693913000	1.601963000
1	-4.498813000	-2.442430000	0.554098000
1	-4.594370000	1.661209000	-0.756902000
1	-0.853383000	-2.820860000	-0.116465000
1	-1.638752000	-4.659288000	1.344957000
1	-3.301764000	-4.013688000	1.357135000
1	-1.978749000	-3.078387000	2.123882000
1	-1.764020000	-4.888766000	-1.222152000
1	-2.011983000	-3.421193000	-2.230936000
1	-3.384872000	-4.119171000	-1.314322000
1	-1.023586000	1.682233000	-1.833416000
1	-2.281565000	3.079929000	-3.455288000
1	-3.839428000	2.448914000	-2.830647000
1	-2.684598000	1.337570000	-3.634531000
1	-1.642688000	4.014561000	-1.135416000
1	-1.598082000	2.923074000	0.287078000
1	-3.167096000	3.417583000	-0.418470000
1	-0.636849000	-0.718298000	1.369898000
1	-2.501830000	-0.399499000	2.903764000
1	-2.540218000	0.878561000	1.661779000
1	-1.978919000	1.255215000	3.339605000
1	-0.148153000	-1.350049000	3.675971000
1	0.399290000	0.293856000	4.107027000
1	1.321340000	-0.676852000	2.888340000
1	0.731399000	3.934857000	3.323209000
1	0.518237000	2.294511000	3.999314000
1	-0.878531000	3.162138000	3.298149000
1	1.908887000	4.793935000	1.801910000
1	1.231912000	5.116306000	0.179889000
1	2.856091000	4.384249000	0.343954000
1	1.467957000	1.423514000	-2.165194000
1	1.603407000	3.514224000	-3.397888000
1	1.707141000	4.510933000	-1.921120000
1	0.196147000	3.609133000	-2.297457000
1	3.767511000	2.237490000	-2.581773000
1	3.684503000	1.318357000	-1.051999000
1	3.807989000	3.112240000	-1.020851000
1	2.320504000	-4.296369000	-1.619616000
1	1.385355000	-3.227384000	-2.728626000
1	0.529565000	-4.243960000	-1.538913000
1	2.297580000	-3.898181000	1.316776000
1	0.513109000	-3.821104000	1.300270000
1	1.451080000	-2.560054000	2.162955000
1	3.250548000	-1.969385000	-2.719255000
1	5.487430000	-1.021964000	-3.222324000
1	6.845032000	0.039886000	-1.379458000
1	5.886156000	0.181620000	0.923160000
1	3.171617000	1.404149000	1.530370000
1	4.619441000	1.011767000	2.536802000
1	2.967542000	0.772201000	3.194619000
1	3.989688000	-2.659324000	2.249359000
1	3.488420000	-1.630636000	3.632893000
1	5.134679000	-1.437928000	2.917657000
1	-6.468748000	-1.289555000	0.765082000

1	-8.160364000	0.116230000	-0.430104000
1	-6.995924000	-0.602859000	-1.596984000
1	-5.680465000	0.392964000	2.452313000
1	-6.036568000	1.726320000	1.311414000
1	-7.377744000	0.726317000	1.958881000
1	-6.859184000	1.122431000	-1.138258000

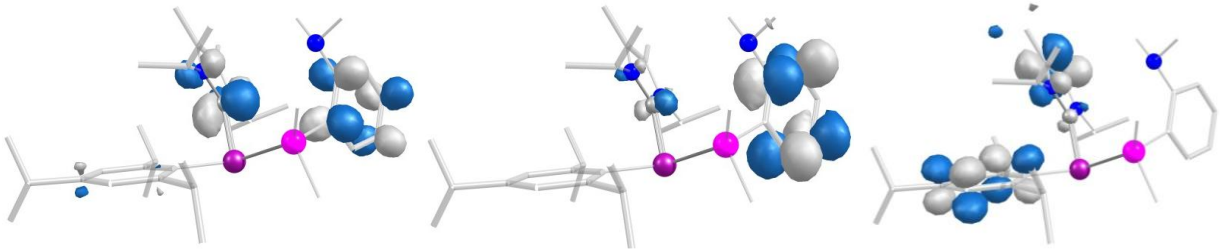

LUMO+1
E = −1.09 eV

LUMO+2
E = −0.96 eV

LUMO+4
E = −0.62 eV

Figure S31. Selected Kohn-Sham molecular orbitals of **6** (contour value 0.052).

Table S4. Selected absorption bands and assigned transitions from the TD-DFT calculation for germylene/Me_2IPr adduct **6**.

λ (nm)	Oscillator strength	Assignment (Contribution)
404.6	0.046575544	HOMO → LUMO (72%)
		HOMO → LUMO+1 (14%)
		HOMO → LUMO+2 (11%)
398.8	0.030037326	HOMO → LUMO+2 (73%)
		HOMO → LUMO+1 (21%)
390.9	0.019535532	HOMO → LUMO+1 (62%)
		HOMO → LUMO (25%)
		HOMO → LUMO+2 (11%)
332.9	0.111958290	HOMO → LUMO+4 (93%)

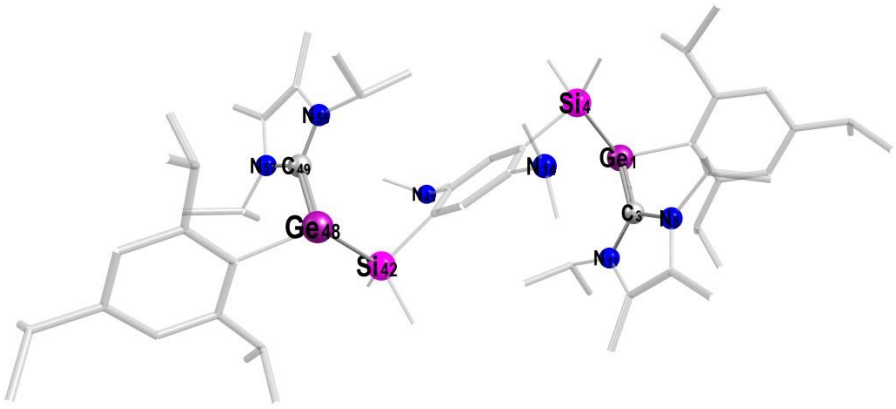

Figure S32. Optimized structure of bis(germylene)/Me_2IPr adduct **4**.

Table S5. Atomic coordinates of the optimized structure of bis(germylene)/Me_2IPr adduct **4**.

32	4.509271000	0.464519000	-1.074076000
6	6.503024000	0.496047000	-0.552665000
6	4.053644000	-1.198573000	0.085880000
14	3.041977000	1.921093000	0.269773000
6	3.235208000	2.609209000	2.044878000
6	1.386951000	0.982612000	0.055536000
6	2.834987000	3.515944000	-0.776593000
7	4.475145000	-1.561991000	1.337717000
6	4.026631000	-2.849445000	1.655887000
6	5.228996000	-0.641716000	2.226952000
7	3.320868000	-2.259917000	-0.375138000
6	3.290522000	-3.290645000	0.569012000
6	2.672946000	-2.261390000	-1.712113000
7	1.147855000	0.094990000	2.383370000
6	0.536681000	1.042935000	3.312285000
6	0.658496000	0.255107000	1.027455000
6	1.049691000	-1.274529000	2.880709000
6	7.171560000	1.592441000	0.066443000
6	7.297048000	-0.628679000	-0.931277000
6	8.540957000	1.500072000	0.389192000
6	6.447083000	2.909299000	0.307140000
6	9.307099000	0.362567000	0.085187000
6	8.666567000	-0.680952000	-0.603959000
6	10.772317000	0.267031000	0.489755000
6	6.719962000	-1.804291000	-1.719442000
6	6.548496000	3.797005000	-0.949298000
6	6.885422000	3.667061000	1.567643000
6	6.751320000	-3.125188000	-0.930841000
6	7.405237000	-1.948922000	-3.090428000
6	4.275531000	-3.561407000	2.945779000
6	2.546521000	-4.578160000	0.420336000
6	6.673752000	-1.090764000	2.461363000
6	4.455533000	-0.360807000	3.518234000
6	3.396753000	-3.181635000	-2.700630000
6	1.171838000	-2.534962000	-1.621486000
6	0.832391000	1.033499000	-1.246160000
6	-0.397319000	0.435397000	-1.603875000
6	-1.137224000	-0.284245000	-0.619598000
6	-0.578791000	-0.323059000	0.676605000
6	11.696769000	0.069132000	-0.726434000
6	10.985409000	-0.839025000	1.542530000
1	9.038758000	2.346516000	0.890619000
1	9.248570000	-1.573230000	-0.890805000
1	5.375520000	2.645146000	0.430182000
1	6.220330000	4.537795000	1.747273000
1	7.918881000	4.065055000	1.480558000
1	6.849128000	3.016733000	2.466244000
1	5.984298000	4.745347000	-0.820201000
1	6.142117000	3.272449000	-1.837995000
1	7.608372000	4.053328000	-1.162892000
1	5.657457000	-1.552460000	-1.923729000
1	6.924174000	-2.750578000	-3.691589000
1	8.479660000	-2.210636000	-2.986097000
1	7.342379000	-1.001927000	-3.664079000
1	6.280011000	-3.947493000	-1.510093000
1	6.211463000	-3.038519000	0.032575000
1	7.793968000	-3.434795000	-0.704083000
1	5.259865000	0.294040000	1.634026000
1	7.219330000	-0.278283000	2.981377000
1	7.195080000	-1.274807000	1.504145000

1	6.741183000	-1.999194000	3.094551000
1	4.919375000	0.503509000	4.034061000
1	4.474786000	-1.214897000	4.223775000
1	3.404993000	-0.104033000	3.275510000
1	4.071547000	-4.642547000	2.822440000
1	3.618419000	-3.191971000	3.761484000
1	5.323420000	-3.455302000	3.285776000
1	2.877351000	-5.292484000	1.198508000
1	2.718998000	-5.053536000	-0.565084000
1	1.450817000	-4.441856000	0.538097000
1	2.820560000	-1.212189000	-2.051986000
1	2.910442000	-3.098704000	-3.693559000
1	3.353029000	-4.247317000	-2.395757000
1	4.457894000	-2.892760000	-2.817401000
1	0.674116000	-2.172285000	-2.542503000
1	0.719710000	-1.988934000	-0.774191000
1	0.939220000	-3.613880000	-1.522284000
1	1.892078000	4.040156000	-0.508963000
1	2.823718000	3.310069000	-1.866330000
1	3.677450000	4.211801000	-0.582961000
1	2.416653000	3.334357000	2.244051000
1	4.191474000	3.159991000	2.147936000
1	3.196404000	1.824242000	2.818278000
1	1.382937000	1.592974000	-2.015185000
1	-1.135475000	-0.860872000	1.461002000
1	1.493337000	-1.969206000	2.140711000
1	0.003431000	-1.611479000	3.098061000
1	1.623475000	-1.364364000	3.828211000
1	0.659249000	2.074753000	2.932000000
1	1.040092000	0.983546000	4.301442000
1	-0.558570000	0.854654000	3.468023000
1	11.040509000	1.238483000	0.962979000
1	12.764317000	0.061416000	-0.419959000
1	11.555491000	0.877614000	-1.472481000
1	10.341186000	-0.674591000	2.430600000
1	10.731176000	-1.837045000	1.126059000
1	12.042577000	-0.874371000	1.882016000
1	11.489229000	-0.895823000	-1.235802000
14	-2.699836000	-1.383933000	-0.815802000
7	-0.880616000	0.545886000	-2.937302000
6	-2.140658000	1.258797000	-3.079420000
6	0.073841000	0.899067000	-3.972854000
1	0.990883000	0.284793000	-3.877973000
1	0.381243000	1.977682000	-3.957661000
1	-0.380222000	0.698917000	-4.966211000
1	-2.008907000	2.371681000	-3.022231000
1	-2.609109000	1.021679000	-4.057946000
1	-2.839797000	0.965246000	-2.275669000
6	-2.185374000	-3.061601000	-0.044369000
6	-3.049792000	-1.814818000	-2.650185000
1	-3.440862000	-2.851441000	-2.709854000
1	-3.789451000	-1.151606000	-3.136151000
1	-2.105461000	-1.753999000	-3.229298000
1	-1.859080000	-2.949637000	1.009278000
1	-1.352104000	-3.514322000	-0.621893000
1	-3.035116000	-3.773391000	-0.057624000
32	-4.142927000	-0.286264000	0.838713000
6	-4.335575000	1.441459000	-0.296291000
6	-6.142307000	-0.764750000	0.827498000
6	-6.978868000	0.060750000	1.640479000
6	-6.749722000	-1.878316000	0.175515000

6	-8.361133000	-0.201959000	1.737899000
6	-8.134902000	-2.105414000	0.294711000
6	-8.967659000	-1.271191000	1.060838000
1	-8.995350000	0.457155000	2.355589000
1	-8.579924000	-2.966404000	-0.231802000
7	-3.657612000	2.598685000	-0.009134000
7	-5.201216000	1.772719000	-1.312159000
6	-4.103089000	3.650977000	-0.813385000
6	-5.084986000	3.129422000	-1.638254000
6	-3.572380000	5.047871000	-0.786205000
1	-4.262022000	5.719626000	-1.332567000
1	-3.471090000	5.439452000	0.244796000
1	-2.577702000	5.126357000	-1.272862000
6	-5.867818000	3.836638000	-2.697324000
1	-6.941364000	3.567342000	-2.671102000
1	-5.795441000	4.931142000	-2.547344000
1	-5.491700000	3.618968000	-3.719316000
6	-6.063241000	0.774461000	-1.992331000
1	-5.722869000	-0.179313000	-1.544943000
6	-5.807619000	0.714577000	-3.503367000
6	-7.547669000	0.947744000	-1.658867000
1	-7.712275000	0.966783000	-0.566646000
1	-7.975659000	1.867048000	-2.108754000
1	-8.110199000	0.081398000	-2.059744000
1	-6.275943000	1.554838000	-4.052222000
1	-6.248510000	-0.221812000	-3.900217000
1	-4.725915000	0.701128000	-3.732394000
6	-2.625030000	2.671374000	1.057580000
1	-2.473632000	1.604110000	1.327858000
6	-3.158442000	3.389132000	2.301163000
6	-1.293089000	3.223637000	0.549796000
1	-0.986845000	2.727273000	-0.390243000
1	-1.304835000	4.320768000	0.399290000
1	-0.506710000	2.998868000	1.295201000
1	-3.376879000	4.460737000	2.114839000
1	-2.398014000	3.335473000	3.106081000
1	-4.080503000	2.900335000	2.669954000
6	-6.435091000	1.263447000	2.414719000
1	-5.325748000	1.215541000	2.328043000
6	-6.760364000	1.182994000	3.916247000
6	-6.896766000	2.600787000	1.806688000
1	-6.586878000	2.696133000	0.746927000
1	-8.003273000	2.697822000	1.841623000
1	-6.468536000	3.461839000	2.363055000
1	-7.851865000	1.253323000	4.110268000
1	-6.272163000	2.014170000	4.468694000
1	-6.401558000	0.225987000	4.346868000
6	-5.937761000	-2.876827000	-0.641558000
1	-4.935286000	-2.418273000	-0.776523000
6	-6.513474000	-3.137606000	-2.042910000
6	-5.746222000	-4.188625000	0.141555000
1	-5.275691000	-3.996361000	1.127061000
1	-6.722296000	-4.686081000	0.327773000
1	-5.103818000	-4.901910000	-0.417954000
1	-7.502294000	-3.641495000	-2.000934000
1	-5.835509000	-3.791327000	-2.630530000
1	-6.644151000	-2.192392000	-2.608938000
6	-10.470349000	-1.506380000	1.140703000
1	-10.878953000	-0.746350000	1.844153000
6	-10.808203000	-2.897777000	1.708788000
6	-11.140039000	-1.281122000	-0.229611000

1	-10.922555000	-0.264990000	-0.618230000
1	-10.767852000	-2.012495000	-0.978410000
1	-12.242619000	-1.398625000	-0.163281000
1	-10.440066000	-3.704843000	1.040371000
1	-11.905727000	-3.029017000	1.816844000
1	-10.341067000	-3.048453000	2.703389000

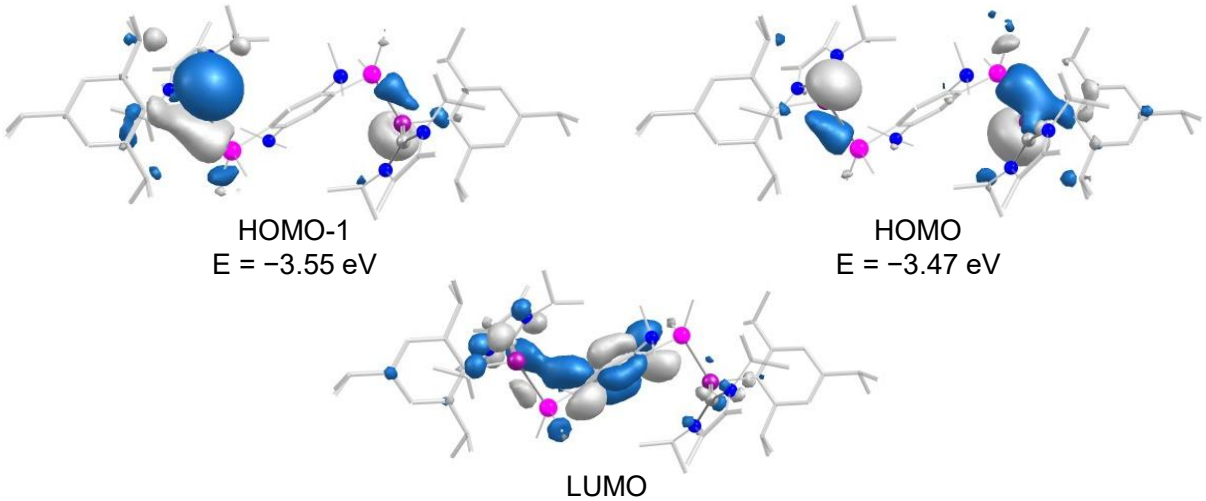

Figure S33. Selected Kohn-Sham molecular orbitals of **4** (contour value 0.036).

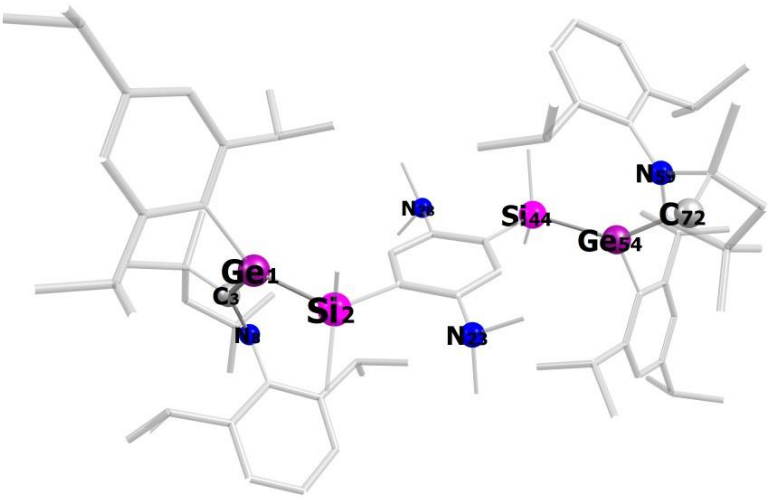

Figure S34. Optimized structure of the *Z*,*Z* isomer of bis(germylene)/Me$_4$CAAC adduct **7** (G = −5164243.21 kcal mol^{-1}).

Table S6. Atomic coordinates of the optimized structure of the *Z*,*Z* isomer of bis(germylene)/Me$_4$CAAC adduct **7**.

32	-4.554049000	-0.055910000	0.023778000
14	-2.845155000	-0.064653000	1.683397000
6	-5.234098000	-1.467487000	-0.967327000
6	-5.537700000	1.672755000	-0.146726000
6	-1.195252000	-0.193447000	0.728496000
6	-2.882215000	1.642416000	2.514302000
6	-3.150900000	-1.408715000	2.979860000
7	-4.792419000	-2.796085000	-0.958189000

6	-6.300003000	-1.290842000	-2.080925000
6	-6.681037000	1.962115000	0.654811000
6	-5.033179000	2.683025000	-1.014244000
6	0.046719000	-0.104023000	1.412699000
6	-1.165502000	-0.245448000	-0.680236000
6	-5.185901000	-3.505081000	-2.229263000
6	-4.374394000	-3.509385000	0.212971000
6	-6.484098000	-2.747707000	-2.582027000
6	-5.830276000	-0.330337000	-3.197012000
6	-7.643326000	-0.747238000	-1.545567000
6	-7.275444000	3.235418000	0.585996000
6	-7.271412000	0.930157000	1.610917000
6	-5.664010000	3.943891000	-1.052798000
6	-3.795988000	2.463439000	-1.881032000
7	0.040373000	-0.111522000	2.853206000
6	1.248287000	-0.015288000	0.685511000
6	0.040600000	-0.196620000	-1.404127000
6	-4.125349000	-3.302283000	-3.333794000
6	-5.443455000	-4.997660000	-2.007300000
6	-3.069143000	-4.083294000	0.304653000
6	-5.316524000	-3.730203000	1.269677000
6	-6.780842000	4.245240000	-0.258896000
6	-6.762137000	1.163209000	3.044950000
6	-8.806995000	0.870550000	1.572470000
6	-2.551654000	3.047498000	-1.193024000
6	-3.947402000	3.001567000	-3.313177000
6	0.141736000	-1.456045000	3.419006000
6	0.981514000	0.803525000	3.484290000
6	1.272858000	-0.061894000	-0.723716000
7	0.057619000	-0.264051000	-2.850589000
6	-2.759297000	-4.901321000	1.413053000
6	-1.964541000	-3.849436000	-0.721193000
6	-4.948802000	-4.543035000	2.356594000
6	-6.728332000	-3.154112000	1.262604000
6	-7.440891000	5.616830000	-0.319421000
14	2.889842000	0.051707000	-1.729938000
6	-0.510970000	0.916070000	-3.492281000
6	-0.506185000	-1.499040000	-3.382843000
6	-3.685216000	-5.142425000	2.431082000
6	-1.688094000	-5.101263000	-1.581029000
6	-0.647641000	-3.429926000	-0.043192000
6	-7.030006000	-2.405253000	2.571424000
6	-7.796928000	-4.231339000	0.997944000
6	-7.383788000	6.333843000	1.043330000
6	-8.886351000	5.523851000	-0.846003000
32	4.680636000	0.147777000	-0.168833000
6	3.195743000	-1.555506000	-2.696756000
6	2.905054000	1.536424000	-2.900320000
6	5.170722000	1.484931000	1.016784000
6	5.681514000	-1.573328000	0.012493000
7	4.656477000	2.786354000	1.083418000
6	6.242997000	1.305103000	2.121435000
6	6.870563000	-1.803871000	-0.741680000
6	5.157921000	-2.632337000	0.807110000
6	5.041500000	3.463236000	2.374285000
6	4.170259000	3.523020000	-0.046296000
6	6.370931000	2.744771000	2.684613000
6	5.804186000	0.275501000	3.187236000
6	7.610392000	0.844126000	1.571299000
6	7.495396000	-3.063054000	-0.693059000
6	7.471393000	-0.719885000	-1.631008000

6	5.818655000	-3.878730000	0.825997000
6	3.875537000	-2.481477000	1.620190000
6	4.009190000	3.188585000	3.491076000
6	5.238609000	4.971123000	2.196847000
6	2.828014000	4.007493000	-0.090723000
6	5.074667000	3.855772000	-1.105904000
6	6.984174000	-4.119133000	0.083147000
6	7.023276000	-0.908400000	-3.091438000
6	9.000731000	-0.612211000	-1.527933000
6	2.686257000	-3.121666000	0.884072000
6	3.995412000	-3.028120000	3.052750000
6	2.436867000	4.845016000	-1.157617000
6	1.775719000	3.662126000	0.955603000
6	4.626668000	4.679847000	-2.153857000
6	6.525918000	3.389437000	-1.145416000
6	7.675560000	-5.475930000	0.122741000
6	3.322177000	5.188893000	-2.182342000
6	1.436672000	4.870115000	1.855246000
6	0.473172000	3.157911000	0.310192000
6	6.818212000	2.626356000	-2.448510000
6	7.518306000	4.552529000	-0.958417000
6	7.700725000	-6.139193000	-1.267982000
6	9.091798000	-5.369909000	0.721188000

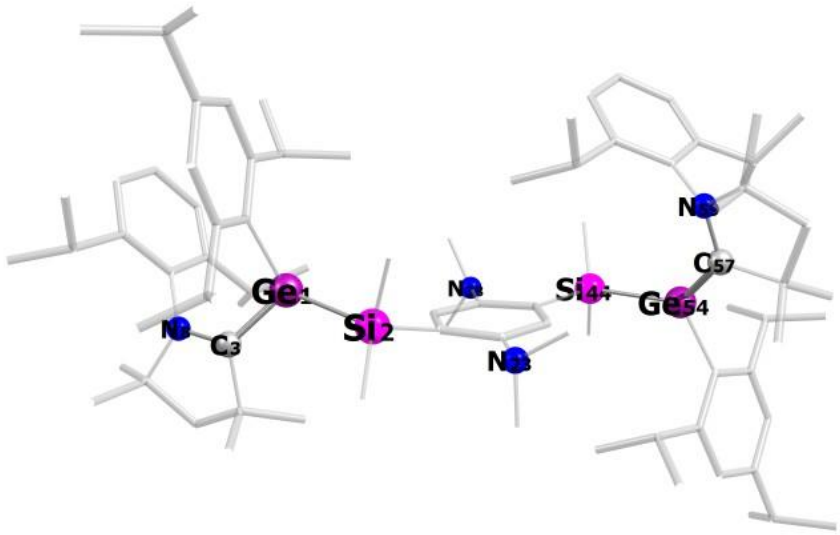

Figure S35. Optimized structure of the *E*,*Z* isomer of bis(germylene)/Me$_4$CAAC adduct **7** (G = −5164241.16 kcal mol^{-1}).

Table S7. Atomic coordinates of the optimized structure of the *E*,*Z* isomer of bis(germylene)/Me$_4$CAAC adduct **7**.

32	-4.082787000	-0.610544000	0.358806000
14	-2.239737000	-0.329881000	1.914069000
6	-5.190622000	-2.147897000	0.423629000
6	-5.118756000	1.100161000	0.523817000
6	-0.613731000	-0.772258000	1.001086000
6	-2.190975000	1.557259000	2.147241000
6	-2.379848000	-1.121329000	3.643428000
7	-6.362585000	-2.336757000	-0.290662000
6	-4.748529000	-3.497759000	1.023914000
6	-5.649709000	1.511103000	1.782446000
6	-5.173413000	1.998237000	-0.577603000
6	0.636700000	-0.422236000	1.586258000
6	-0.607921000	-1.169598000	-0.352695000

1	-1.261163000	1.822237000	2.690484000
1	-3.062961000	1.916908000	2.727210000
1	-2.205260000	2.082632000	1.172174000
1	-1.675582000	-0.603021000	4.323285000
1	-2.136933000	-2.202348000	3.642697000
1	-3.401623000	-0.998796000	4.053929000
6	-6.973975000	-3.698578000	-0.046881000
6	-6.741419000	-1.526608000	-1.421380000
6	-5.719342000	-4.506908000	0.354506000
6	-4.891724000	-3.496237000	2.563672000
6	-3.279908000	-3.818139000	0.674148000
6	-6.234697000	2.786251000	1.903804000
6	-5.628988000	0.593605000	3.004093000
6	-5.780417000	3.259857000	-0.413787000
6	-4.527683000	1.636006000	-1.914376000
7	0.670945000	-0.090100000	2.985146000
6	1.802780000	-0.380403000	0.800374000
6	0.575202000	-1.182095000	-1.121605000
1	-1.567825000	-1.420937000	-0.835659000
6	-8.004893000	-3.639832000	1.102409000
6	-7.659775000	-4.258565000	-1.295211000
6	-7.855662000	-0.645810000	-1.362438000
6	-6.011112000	-1.677217000	-2.643370000
1	-5.251112000	-4.920389000	-0.563525000
1	-5.966082000	-5.362297000	1.014745000
1	-4.596494000	-4.483616000	2.978119000
1	-5.926623000	-3.283910000	2.889563000
1	-4.239525000	-2.723443000	3.007335000
1	-2.995271000	-4.814026000	1.075293000
1	-2.587360000	-3.071058000	1.113683000
1	-3.115202000	-3.820483000	-0.422146000
1	-6.653232000	3.091061000	2.875719000
6	-6.318274000	3.673008000	0.816263000
1	-4.776614000	-0.100786000	2.849630000
6	-5.407723000	1.323589000	4.337396000
6	-6.884665000	-0.291195000	3.062093000
1	-5.833930000	3.953616000	-1.267439000
1	-4.707967000	0.548199000	-2.059262000
6	-3.001370000	1.851496000	-1.854100000
6	-5.122847000	2.368854000	-3.123772000
6	0.860974000	-1.259231000	3.841407000
6	1.566400000	0.995042000	3.353910000
1	2.753713000	-0.039082000	1.243448000
6	1.797752000	-0.756968000	-0.557737000
7	0.573274000	-1.554987000	-2.517915000
1	-8.259142000	-4.668037000	1.432533000
1	-8.940531000	-3.150500000	0.776667000
1	-7.616555000	-3.082663000	1.974323000
1	-8.088034000	-5.253969000	-1.060518000
1	-6.951903000	-4.378738000	-2.134610000
1	-8.484958000	-3.601084000	-1.634062000
6	-8.215122000	0.078244000	-2.518253000
6	-8.714116000	-0.478907000	-0.118490000
6	-6.409639000	-0.926310000	-3.764819000
6	-4.834949000	-2.633160000	-2.819906000
6	-6.998867000	5.028417000	0.956140000
1	-5.239473000	0.589971000	5.153481000
1	-6.286981000	1.935603000	4.630518000
1	-4.527203000	1.996991000	4.297499000
1	-6.849960000	-0.972654000	3.938472000
1	-6.953192000	-0.910458000	2.147575000

1	-7.806658000	0.322412000	3.136556000
1	-2.522541000	1.580876000	-2.818527000
1	-2.531288000	1.226764000	-1.066340000
1	-2.763186000	2.913953000	-1.635311000
1	-4.741710000	1.921202000	-4.064874000
1	-4.842960000	3.444117000	-3.136441000
1	-6.227960000	2.297165000	-3.138340000
1	0.597820000	-1.014942000	4.892877000
1	0.213311000	-2.088657000	3.502972000
1	1.919688000	-1.623746000	3.827963000
1	1.353064000	1.310514000	4.396941000
1	2.653078000	0.722022000	3.304922000
1	1.402235000	1.863282000	2.687621000
14	3.353695000	-0.686949000	-1.660897000
6	-0.134797000	-0.598296000	-3.366197000
6	0.200668000	-2.945245000	-2.746092000
1	-9.076666000	0.761929000	-2.471816000
6	-7.504332000	-0.055320000	-3.713288000
1	-8.202665000	-1.020118000	0.700166000
6	-10.108360000	-1.105722000	-0.324616000
6	-8.844688000	0.994759000	0.300613000
1	-5.850313000	-1.037916000	-4.706912000
1	-4.695926000	-3.178874000	-1.867085000
6	-3.530459000	-1.871236000	-3.103774000
6	-5.085027000	-3.667899000	-3.936768000
1	-6.857433000	5.561575000	-0.010737000
6	-6.357752000	5.887161000	2.062149000
6	-8.515406000	4.862136000	1.179152000
32	5.147823000	0.001005000	-0.264218000
6	3.871008000	-2.412343000	-2.263639000
6	3.178437000	0.471517000	-3.145760000
1	0.021850000	-0.862155000	-4.433839000
1	0.275849000	0.416948000	-3.199408000
1	-1.234406000	-0.552650000	-3.178315000
1	0.339399000	-3.195932000	-3.819334000
1	-0.858262000	-3.188254000	-2.472663000
1	0.858558000	-3.608118000	-2.147774000
1	-7.800857000	0.517347000	-4.605718000
1	-10.694535000	-1.082743000	0.618218000
1	-10.048419000	-2.158533000	-0.668264000
1	-10.683440000	-0.545320000	-1.091798000
1	-9.382387000	1.077896000	1.267909000
1	-9.421557000	1.580167000	-0.445968000
1	-7.854864000	1.470377000	0.416443000
1	-2.683210000	-2.578761000	-3.205717000
1	-3.301849000	-1.176308000	-2.269627000
1	-3.594004000	-1.288232000	-4.046645000
1	-4.262472000	-4.413018000	-3.961481000
1	-5.121857000	-3.183853000	-4.934838000
1	-6.039850000	-4.214903000	-3.803170000
1	-6.484496000	5.418352000	3.060979000
1	-8.720105000	4.329734000	2.132272000
1	-6.825437000	6.893398000	2.105405000
1	-5.269894000	6.017439000	1.889291000
1	-9.024740000	5.848061000	1.226075000
1	-8.976823000	4.270730000	0.362284000
6	5.384111000	1.618479000	0.609458000
6	6.337936000	-1.501103000	0.307391000
1	2.996915000	-2.934838000	-2.698825000
1	4.642153000	-2.314886000	-3.055386000
1	4.300264000	-3.032994000	-1.452081000

1	2.529628000	0.006840000	-3.914158000
1	2.755735000	1.454181000	-2.860863000
1	4.178260000	0.654821000	-3.588486000
7	4.689569000	2.813426000	0.372245000
6	6.442679000	1.856109000	1.714821000
6	7.560779000	-1.742843000	-0.387720000
6	5.924414000	-2.427900000	1.306399000
6	4.955985000	3.828125000	1.455946000
6	4.145158000	3.200649000	-0.897660000
6	6.362274000	3.392385000	1.917561000
6	6.117291000	1.054732000	2.995891000
6	7.871982000	1.464669000	1.279819000
6	8.326405000	-2.882396000	-0.082444000
6	8.046708000	-0.808797000	-1.491600000
6	6.723157000	-3.559437000	1.576372000
6	4.626185000	-2.261508000	2.092105000
6	3.945689000	3.696445000	2.615644000
6	4.946626000	5.262003000	0.918579000
6	2.752384000	3.474677000	-1.052833000
6	5.031703000	3.415064000	-2.002317000
1	7.116087000	3.883732000	1.266758000
1	6.575908000	3.694461000	2.962865000
1	6.803751000	1.339989000	3.821624000
1	5.076172000	1.206279000	3.339506000
1	6.249647000	-0.026606000	2.799511000
1	8.601572000	1.771130000	2.060121000
1	7.961473000	0.370034000	1.144126000
1	8.158895000	1.959624000	0.330311000
1	9.266974000	-3.053745000	-0.630668000
6	7.923394000	-3.810188000	0.895022000
1	7.483796000	0.141298000	-1.358203000
6	7.668042000	-1.366266000	-2.875565000
6	9.546171000	-0.483482000	-1.410270000
1	6.398433000	-4.276232000	2.349101000
1	4.288870000	-1.214676000	1.917357000
6	3.530507000	-3.200854000	1.554991000
6	4.817070000	-2.445852000	3.607617000
1	4.293244000	4.284016000	3.490376000
1	2.946497000	4.070888000	2.334671000
1	3.839655000	2.642700000	2.929869000
1	5.204342000	5.963174000	1.738052000
1	5.682632000	5.393569000	0.103251000
1	3.953242000	5.546883000	0.521043000
6	2.291000000	4.005866000	-2.276830000
6	1.711828000	3.201868000	0.026554000
6	4.513579000	3.924237000	-3.206730000
6	6.532265000	3.149863000	-1.939179000
6	8.762942000	-5.041979000	1.208770000
1	8.006453000	-0.689789000	-3.688058000
1	8.128314000	-2.363380000	-3.041909000
1	6.569095000	-1.484232000	-2.962294000
1	9.810611000	0.304641000	-2.146524000
1	9.830388000	-0.121116000	-0.401577000
1	10.178416000	-1.366949000	-1.642074000
1	2.577281000	-3.059287000	2.104161000
1	3.323250000	-3.006347000	0.485336000
1	3.838048000	-4.263556000	1.657783000
1	3.886466000	-2.176220000	4.149879000
1	5.052941000	-3.498419000	3.871202000
1	5.636228000	-1.808806000	3.998124000
1	1.218464000	4.226960000	-2.389184000

6	3.156147000	4.238024000	-3.348692000
1	2.217666000	2.606593000	0.815144000
6	1.156434000	4.502338000	0.644526000
6	0.532934000	2.375268000	-0.520166000
1	5.200226000	4.099024000	-4.050094000
1	6.744634000	2.671862000	-0.965445000
6	6.953187000	2.154032000	-3.033488000
6	7.362557000	4.444074000	-2.030880000
1	8.224905000	-5.604933000	2.004222000
6	8.887945000	-5.968466000	-0.016280000
6	10.147201000	-4.655112000	1.764836000
1	2.774900000	4.652641000	-4.294953000
1	0.466941000	4.273896000	1.484809000
1	1.950960000	5.175073000	1.022126000
1	0.578645000	5.072867000	-0.112999000
1	-0.116248000	2.027991000	0.306084000
1	-0.100024000	2.974811000	-1.206473000
1	0.879438000	1.480099000	-1.064636000
1	8.026123000	1.890415000	-2.933093000
1	6.360138000	1.220906000	-2.956068000
1	6.806595000	2.574159000	-4.050614000
1	8.445694000	4.216808000	-1.938760000
1	7.208923000	4.960682000	-3.001767000
1	7.098805000	5.161899000	-1.228094000
1	9.427649000	-5.464524000	-0.845987000
1	10.738386000	-4.093565000	1.010602000
1	9.451087000	-6.891328000	0.237751000
1	7.889847000	-6.265348000	-0.398304000
1	10.731013000	-5.557452000	2.044714000
1	10.052899000	-4.010850000	2.662810000

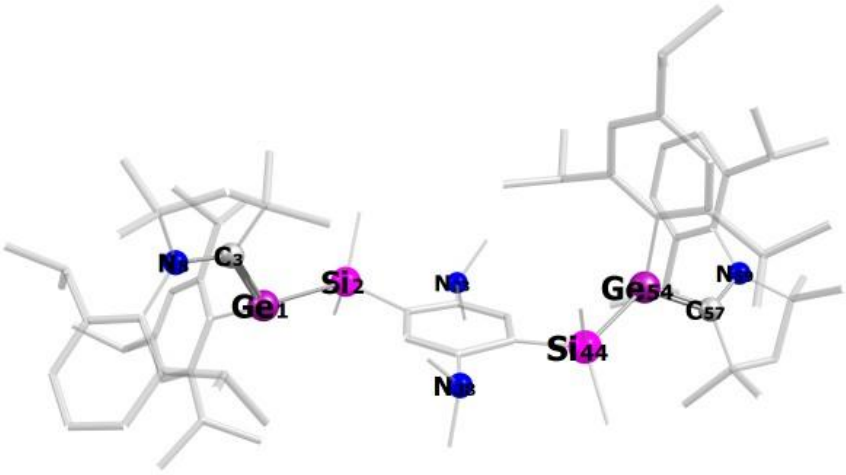

Figure S36. Optimized structure of the *E*,*E* isomer of bis(germylene)/Me$_4$CAAC adduct **7** (G = −5164236.60 kcal mol^{-1}).

Table S8. Atomic coordinates of the optimized structure of the *E*,*E* isomer of bis(germylene)/Me$_4$CAAC adduct **7**.

32	-4.346762000	0.190896000	-0.039635000
14	-2.451126000	1.543069000	0.629647000
6	-4.688086000	-1.469509000	0.823050000
6	-5.928902000	1.425187000	0.100686000
6	-0.960963000	1.027321000	-0.451423000
6	-3.044840000	3.303311000	0.227599000
6	-1.882300000	1.473003000	2.449818000
7	-5.800984000	-2.256575000	0.597830000
6	-3.659722000	-2.283627000	1.632161000

6	-6.254176000	2.045021000	1.343262000
6	-6.623814000	1.830855000	-1.073248000
6	0.276462000	1.693158000	-0.270250000
6	-0.986735000	-0.070250000	-1.339854000
6	-5.769524000	-3.553424000	1.378273000
6	-6.696219000	-2.072647000	-0.516129000
6	-4.248101000	-3.717661000	1.580403000
6	-3.551410000	-1.738757000	3.076901000
6	-2.254651000	-2.249263000	1.004981000
6	-7.255442000	3.035680000	1.384946000
6	-5.585983000	1.646386000	2.657798000
6	-7.621320000	2.822224000	-0.983995000
6	-6.269354000	1.239107000	-2.435349000
7	0.306987000	2.878029000	0.556034000
6	1.445268000	1.201069000	-0.880540000
6	0.182934000	-0.549610000	-1.963698000
6	-6.506568000	-3.417084000	2.729739000
6	-6.389219000	-4.711708000	0.593052000
6	-8.048525000	-1.682789000	-0.311645000
6	-6.228224000	-2.376809000	-1.835313000
6	-7.953172000	3.438599000	0.234237000
6	-5.138154000	2.848549000	3.504757000
6	-6.485504000	0.697393000	3.467512000
6	-5.021044000	1.930879000	-3.018718000
6	-7.419955000	1.254331000	-3.450389000
6	1.279064000	2.838599000	1.642666000
6	0.371976000	4.103559000	-0.235654000
6	1.437870000	0.054744000	-1.700036000
7	0.151605000	-1.669855000	-2.873319000
6	-8.921510000	-1.632670000	-1.418105000
6	-8.611450000	-1.333459000	1.057471000
6	-7.144654000	-2.310031000	-2.901979000
6	-4.794182000	-2.783055000	-2.177246000
6	-9.064091000	4.477922000	0.307662000
14	3.046534000	-0.833593000	-2.235624000
6	-0.286355000	-1.300135000	-4.215296000
6	-0.490634000	-2.869130000	-2.355676000
6	-8.484063000	-1.953966000	-2.704885000
6	-9.661536000	-2.366979000	1.512869000
6	-9.209891000	0.083368000	1.084165000
6	-4.162484000	-1.778181000	-3.159180000
6	-4.708095000	-4.206861000	-2.763912000
6	-8.577096000	5.806476000	0.915150000
6	-10.284576000	3.923419000	1.069637000
32	4.730043000	0.186579000	-0.820267000
6	2.932749000	-2.639832000	-1.645316000
6	3.298269000	-0.798487000	-4.119689000
6	6.318091000	1.033016000	-1.383560000
6	5.091801000	-1.316928000	0.446741000
7	7.267143000	1.513064000	-0.487217000
6	6.669405000	1.509446000	-2.805691000
6	6.040967000	-2.344932000	0.147224000
6	4.177821000	-1.513769000	1.517906000
6	8.509842000	1.978314000	-1.199708000
6	6.928526000	1.907201000	0.860057000
6	7.928398000	2.394075000	-2.575688000
6	6.968583000	0.318865000	-3.744300000
6	5.504216000	2.317180000	-3.418477000
6	6.026100000	-3.531733000	0.902186000
6	7.057705000	-2.235841000	-0.992557000
6	4.221734000	-2.710904000	2.263568000

6	3.134415000	-0.467548000	1.905816000
6	9.496861000	0.801489000	-1.353350000
6	9.199666000	3.135545000	-0.474463000
6	7.336755000	1.145680000	1.989492000
6	6.173543000	3.110561000	1.042843000
6	5.129112000	-3.737475000	1.966606000
6	6.529810000	-2.889457000	-2.282740000
6	8.443965000	-2.805051000	-0.645264000
6	1.696736000	-1.006156000	1.794262000
6	3.428176000	0.111654000	3.300388000
6	6.957016000	1.582289000	3.276371000
6	8.193071000	-0.105211000	1.873344000
6	5.801019000	3.487036000	2.345563000
6	5.778397000	4.032994000	-0.105746000
6	5.165982000	-5.018036000	2.789757000
6	6.183782000	2.731787000	3.461053000
6	9.670206000	0.212155000	2.189770000
6	7.704887000	-1.244559000	2.786002000
6	4.258382000	4.042591000	-0.332941000
6	6.298304000	5.470013000	0.099354000
6	4.925925000	-6.266347000	1.919845000
6	6.482534000	-5.128129000	3.584204000

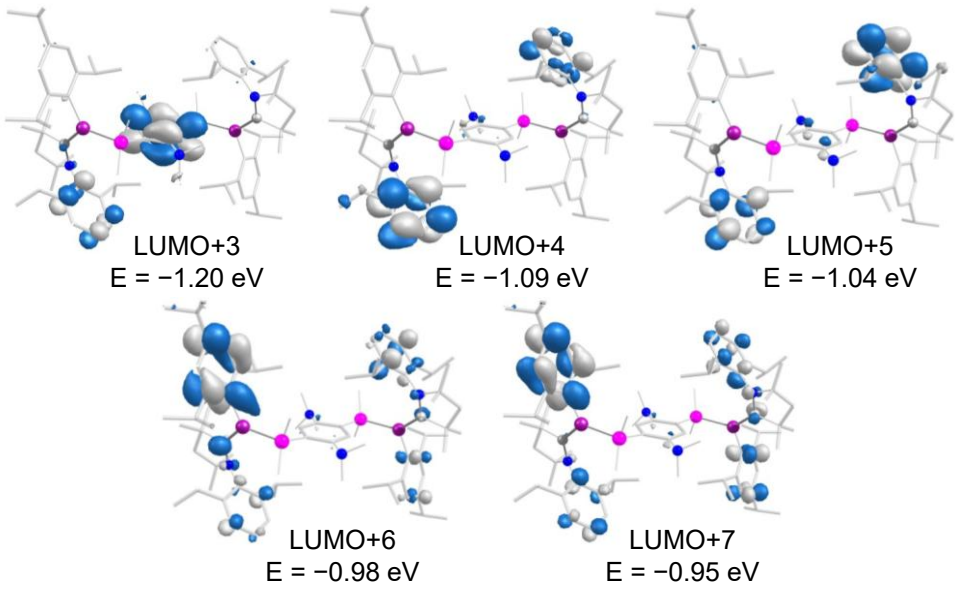

Figure S37. Selected Kohn-Sham molecular orbitals of the *Z*,*Z* isomer of **7** (contour value 0.036).

Table S9. Selected absorption bands and assigned transitions from the TD-DFT calculation for bis(germylene)/Me_4CAAC adduct **7**.

λ (nm)	Oscillator strength	Assignment (Contribution)
436.7	0.072131136	HOMO → LUMO+1 (30%)
		HOMO → LUMO+3 (20%)
		HOMO → LUMO+4 (19%)
		HOMO → LUMO+2 (8%)
426.7	0.081165758	HOMO−1 → LUMO+3 (31%)
		HOMO−1 → LUMO+4 (16%)

		HOMO−1 → LUMO+1 (14%)
		HOMO−1 → LUMO+2 (8%)
		HOMO−1 → LUMO (6%)
		HOMO → LUMO+3 (6%)
397.6	0.022245989	HOMO−1 → LUMO+5 (19%)
		HOMO−1 → LUMO+1 (12%)
		HOMO−1 → LUMO+3 (12%)
		HOMO−1 → LUMO+6 (12%)
		HOMO−1 → LUMO+2 (8%)
397.8	0.079421080	HOMO → LUMO+1 (18%)
		HOMO → LUMO+2 (6%)
		HOMO → LUMO+3 (13%)
		HOMO → LUMO+4 (17%)
		HOMO → LUMO+5 (10%)
398.8	0.061464755	HOMO−1 → LUMO+2 (49%)
		HOMO−1 → LUMO+1 (29%)
		HOMO−1 → LUMO+5 (29%)
		HOMO−1 → LUMO+6 (12%)
421.7	0.037532209	HOMO−1 → LUMO+1 (18%)
		HOMO−1 → LUMO+3 (10%)
405.1	0.013144583	HOMO → LUMO+4 (38%)
		HOMO → LUMO+7 (25%)
		HOMO → LUMO+3 (10%)
398.8	0.031535583	HOMO−1 → LUMO+4 (35%)
		HOMO−1 → LUMO+7 (25%)

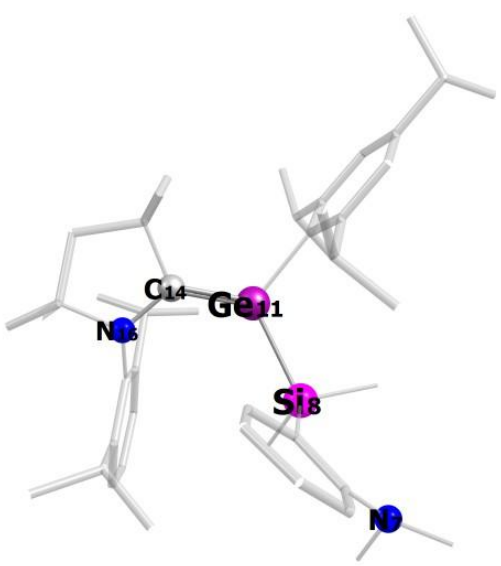

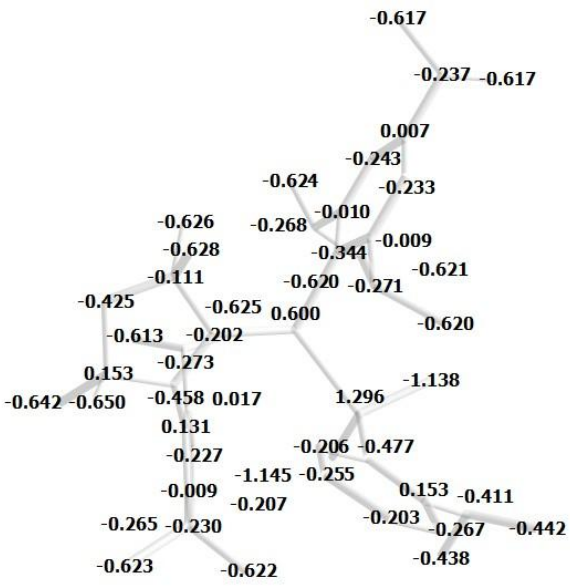

Figure S38. Optimized structure and natural atomic charges of germene **8**.

Table S10. Atomic coordinates of the optimized structure of germene **8**.

6	1.594913000	4.395225000	2.179366000
6	1.520428000	3.006783000	2.373425000
6	1.502753000	4.925649000	0.883521000
6	1.299515000	2.173293000	1.266196000
6	1.323502000	4.080184000	-0.237491000
1	1.593502000	6.012176000	0.739111000
1	1.173640000	1.089405000	1.426852000
6	1.171738000	2.673611000	-0.048795000
7	1.278047000	4.618824000	-1.554977000
14	0.570842000	1.476700000	-1.423782000
6	2.441238000	4.328889000	-2.388321000
6	0.818339000	5.988471000	-1.704024000
32	-0.431298000	-0.391018000	-0.358798000
6	-0.831988000	2.244560000	-2.451426000
6	1.907140000	0.886650000	-2.637461000
1	2.176760000	4.399015000	-3.465412000
1	2.811847000	3.308437000	-2.187736000
1	3.285069000	5.040136000	-2.191160000
1	0.568891000	6.173124000	-2.770454000
1	1.578508000	6.757953000	-1.406841000
1	-0.097612000	6.150169000	-1.102403000
6	0.446335000	-1.445766000	0.907909000
6	-2.392642000	-0.153228000	-0.010488000
1	-0.599342000	3.310367000	-2.647450000
1	-0.914209000	1.710079000	-3.420616000
1	-1.812366000	2.176153000	-1.939179000
1	2.101421000	1.642969000	-3.424769000
1	2.862107000	0.632679000	-2.139973000
1	1.541334000	-0.034993000	-3.134437000
7	1.819600000	-1.711214000	0.964632000
6	-0.281090000	-2.327632000	1.951528000
6	-3.311973000	-0.954063000	-0.753211000
6	-2.903758000	0.832868000	0.880747000
6	2.180964000	-2.502267000	2.199584000
6	2.715404000	-1.618177000	-0.154011000
6	0.857982000	-3.250731000	2.456748000
6	-0.909650000	-1.468648000	3.071151000
6	-1.410276000	-3.186653000	1.340079000
6	-4.695592000	-0.775628000	-0.577620000
6	-2.816569000	-1.971115000	-1.778553000
6	-4.300619000	0.975120000	1.025058000
6	-1.997751000	1.780467000	1.660280000
6	2.517168000	-1.568163000	3.384182000
6	3.342440000	-3.467402000	1.947320000
6	3.862027000	-0.766872000	-0.122386000
6	2.507050000	-2.480449000	-1.280262000
1	0.859679000	-4.186008000	1.858085000
1	0.734348000	-3.535484000	3.521024000
1	-1.310623000	-2.116052000	3.879938000
1	-0.189778000	-0.757876000	3.519532000
1	-1.749078000	-0.879490000	2.655945000
1	-1.807798000	-3.883905000	2.108676000
1	-2.249466000	-2.555937000	0.990309000
1	-1.045384000	-3.791219000	0.485359000
1	-5.392259000	-1.403430000	-1.155773000
6	-5.213595000	0.183718000	0.312527000
1	-1.777784000	-2.231641000	-1.474179000

6	-2.716761000	-1.316352000	-3.168932000
6	-3.629602000	-3.272366000	-1.821976000
1	-4.693497000	1.735441000	1.720898000
1	-0.972150000	1.361483000	1.589298000
6	-1.975696000	3.178210000	1.013661000
6	-2.349977000	1.897258000	3.153204000
1	2.509288000	-2.142795000	4.333287000
1	3.516479000	-1.112193000	3.278079000
1	1.775936000	-0.751621000	3.471259000
1	3.536323000	-4.056819000	2.866333000
1	3.110455000	-4.171059000	1.125546000
1	4.273845000	-2.933095000	1.677915000
6	4.788746000	-0.830127000	-1.185786000
6	4.149641000	0.236025000	0.990103000
6	3.446794000	-2.475380000	-2.326798000
6	1.339110000	-3.456695000	-1.394017000
6	-6.715704000	0.359333000	0.495660000
1	-2.315003000	-2.028717000	-3.920216000
1	-3.713312000	-0.969949000	-3.516339000
1	-2.045772000	-0.433350000	-3.138109000
1	-3.133643000	-4.014142000	-2.482705000
1	-3.729817000	-3.722696000	-0.813135000
1	-4.652800000	-3.115312000	-2.225210000
1	-1.249952000	3.838394000	1.531694000
1	-1.682391000	3.129287000	-0.051281000
1	-2.980409000	3.650228000	1.066634000
1	-1.568898000	2.485560000	3.679025000
1	-3.315936000	2.422853000	3.310055000
1	-2.423390000	0.906145000	3.643284000
1	5.679319000	-0.183569000	-1.153149000
6	4.592939000	-1.672144000	-2.282703000
1	3.251886000	0.271310000	1.637944000
6	5.366975000	-0.181439000	1.841592000
6	4.388733000	1.655159000	0.434698000
1	3.286871000	-3.143518000	-3.187792000
1	0.672625000	-3.282625000	-0.530057000
6	0.513467000	-3.185419000	-2.664240000
6	1.805228000	-4.924700000	-1.347881000
1	-6.856446000	1.171261000	1.243998000
6	-7.396826000	0.806519000	-0.812387000
6	-7.368439000	-0.916615000	1.061942000
1	5.326442000	-1.700411000	-3.103509000
1	5.511649000	0.519299000	2.690723000
1	5.269042000	-1.204752000	2.254233000
1	6.294650000	-0.163866000	1.231330000
1	4.399946000	2.395962000	1.260130000
1	5.361678000	1.724615000	-0.095728000
1	3.589007000	1.959673000	-0.264026000
1	-0.381781000	-3.840529000	-2.696368000
1	0.166337000	-2.131540000	-2.681198000
1	1.101583000	-3.376959000	-3.586283000
1	0.931185000	-5.609049000	-1.377307000
1	2.457180000	-5.175535000	-2.210940000
1	2.378122000	-5.146691000	-0.424773000
1	-7.298520000	0.030238000	-1.600707000
1	-7.268617000	-1.765633000	0.352773000
1	-8.481004000	0.988741000	-0.655142000
1	-6.941495000	1.739435000	-1.203023000
1	-8.452135000	-0.761100000	1.248475000
1	-6.892365000	-1.220565000	2.016571000
1	1.738102000	5.072518000	3.036766000

1	1.603799000	2.574782000	3.382932000

References

(S1) a) C. Müller, D. M. Andrada, I.-A. Bischoff, M. Zimmer, V. Huch, N. Steinbrück, A. Schäfer, *Organometallics* **2019**, *38*, 1052; b) C. M. Weinstein, G. P. Junor, D. R. Tolentino, R. Jazzar, M. Melaimi, G. Bertrand, *J. Am. Chem. Soc.* **2018**, *140*, 9255.

(S2) N. Kuhn, T. Kratz, *Synthesis* **1993**, *1993*, 561.

(S3) A. J. Arduengo, R. Krafczyk, R. Schmutzler, H. A. Craig, J. R. Goerlich, W. J. Marshall, M. Unverzagt, *Tetrahedron* **1999**, *55*, 14523.

(S4) L. Klemmer, A.-L. Thömmes, M. Zimmer, V. Huch, B. Morgenstern, D. Scheschkewitz, *Nat. Chem.* **2020**, *13*, 373.

(S5) G. R. Fulmer, A. J. M. Miller, N. H. Sherden, H. E. Gottlieb, A. Nudelman, B. M. Stoltz, J. E. Bercaw, K. I. Goldberg, *Organometallics* **2010**, *29*, 2176.

(S6) G. M. Sheldrick, *Acta Cryst. A* **2015**, *71*, 3.

(S7) G. M. Sheldrick, *Acta Cryst. C* **2015**, *71*, 3.

(S8) C. B. Hübschle, G. M. Sheldrick, B. Dittrich, *J. Appl. Crystallogr.* **2011**, *44*, 1281.

(S9) H. Cui, J. Zhang, C. Cui, *Organometallics* **2013**, *32*, 1.

(S10) Gaussian 09, Revision A.02, Frisch, M. J.; Trucks, G. W.; Schlegel, H. B.; Scuseria, G. E.; Robb, M. A.; Cheeseman, J. R.; Scalmani, G.; Barone, V.; Petersson, G. A.; Nakatsuji, H.; Li, X.; Caricato, M.; Marenich, A.; Bloino, J.; Janesko, B. G.; Gomperts, R.; Mennucci, B.; Hratchian, H. P.; Ortiz, J. V.; Izmaylov, A. F.; Sonnenberg, J. L.; Williams-Young, D.; Ding, F.; Lipparini, F.; Egidi, F.; Goings, J.; Peng, B.; Petrone, A.; Henderson, T.; Ranasinghe, D.; Zakrzewski, V. G.; Gao, J.; Rega, N.; Zheng, G.; Liang, W.; Hada, M.; Ehara, M.; Toyota, K.; Fukuda, R.; Hasegawa, J.; Ishida, M.; Nakajima, T.; Honda, Y.; Kitao, O.; Nakai, H.; Vreven, T.; Throssell, K.; Montgomery Jr, J. A.; Peralta, J. E.; Ogliaro, F.; Bearpark, M.; Heyd, J. J.; Brothers, E.; Kudin, K. N.; Staroverov, V. N.; Keith, T.; Kobayashi, R.; Normand, J.; Raghavachari, K.; Rendell, A.; Burant, J. C.; Iyengar, S. S.; Tomasi, J.; Cossi, M.; Millam, J. M.; Klene, M.; Adamo, C.; Cammi, R.; Ochterski, J. W.; Martin, R. L.; Morokuma, K.; Farkas, O.; Foresman, J. B. ; Fox, D. J. Gaussian, Inc., Wallingford CT, 2016.

(S11) a) J. P. Perdew, *Phys. Rev. B* **1986**, *33*, 8822; b) A. D. Becke, *Phys. Rev. A* **1988**, *38*, 3098.

(S12) a) A. Schäfer, H. Horn, R. Ahlrichs, *J. Chem. Phys.* **1992**, *97*, 2571; b) A. Schäfer, C. Huber, R. Ahlrichs, *J. Chem. Phys.* **1994**, *100*, 5829; c) F. Weigend, R. Ahlrichs, *Phys. Chem. Chem. Phys.* **2005**, *7*, 3297; d) F. Weigend, *Phys. Chem. Chem. Phys.* **2006**, *8*, 1057.

(S13) S. Grimme, J. Antony, S. Ehrlich, H. Krieg, *J. Chem. Phys.* **2010**, *132*, 154104.

(S14) NBO 7.0. E. D. Glendening, J. K. Badenhoop, A. E. Reed, J. E. Carpenter, J. A. Bohmann, C. M. Morales, P. Karafiloglou, C. R. Landis, and F. Weinhold, Theoretical Chemistry Institute, University of Wisconsin, Madison (2018).

(S15) F. Neese, F. Wennmohs, U. Becker, C. Riplinger, *J. Chem. Phys.* **2020**, *152*, 224108.

(S16) a) J. P. Perdew, M. Ernzerhof, K. Burke, *J. Chem. Phys.* **1996**, *105*, 9982; b) C. Adamo, V. Barone, *J. Chem. Phys.* **1999**, *110*, 6158.

(S17) Chemcraft - graphical software for visualization of quantum chemistry computations. https://www.chemcraftprog.com

(S18) Deposition numbers CCDC 2236120 (for **6**) and 2236118 (for **7**) contain the supplementary crystallographic data for this paper. These data are provided free of charge by the joint Cambridge Crystallographic Data Centre and Fachinformationszentrum Karlsruhe Access Structures service.

Silagermylenation of C=O bonds and radical fragmentation of CO_2-expanded bis(germylene) by a cyclic (alkyl)(amino)carbene

Supporting Information

Anna-Lena Thömmes, Robin Völker, Bernd Morgenstern, Michael Zimmer, Dominik Munz, Christopher W. M. Kay, David Scheschkewitz*

Table of contents

1. General considerations 249
2. Synthetic Procedures 250
2.1 Synthesis of oxycarbonyl NHC-bis(germylene) 2a 250
2.2 Synthesis of aminocarbonyl NHC-bis(germylene) 2b 251
2.3 Reaction of NHC-bis(germylene) 2a with $CAAC^{Me}$ 252
3. Characterization 253
3.1 X-Ray crystallographic data 253
3.2 NMR spectroscopic data 257
3.3 IR spectroscopic data 264
3.4 DFT calculations 265
References 285

1. General considerations

All manipulations were carried out under a protective atmosphere of argon applying standard Schlenk or glovebox techniques. The glassware was pre-dried in an oven at 125 °C and heated in vacuo prior to use. Solvents were taken from solvent purification systems (Innovative technology PureSolv MD7 or MBraun SPS 5/7; hexane, pentane, thf, benzene). Benzene-d_6 and thf-d_8 were dried over a potassium mirror, degassed through freeze-pump-thaw cycles and condensed under argon prior to use. NHC-bis(germylene) **1**,[S1] 1,3-bis(2,6-diisopropyl)imidazol-2-ylidene (NHC)[S2] and 1-(2,6-diisopropylphenyl)-3,3,5,5-tetramethyl-pyrrolidin-2-ylidene ($CAAC^{Me}$)[S3] were prepared according to published procedures. All other chemicals were obtained commercially and used as received. The NMR spectra were recorded on a Bruker Avance III HD 400 spectrometer at 300 K (^{1}H: 400.13 MHz, ^{13}C: 100.61 MHz, ^{29}Si: 79.49 MHz) or on a Bruker Avance III HD 300 at 300 K (^{1}H: 300.13 MHz, ^{13}C: 75.56 MHz, ^{29}Si: 59.6 MHz). The ^{1}H and ^{13}C{^{1}H} NMR spectra were referenced to the residual proton and natural abundance ^{13}C resonances of the deuterated solvents and chemical shifts were reported relative to SiMe4 (benzene-d_6: δH = 7.16 ppm and δC = 128.06 ppm, thf-d_8: δH = 1.72, 3.58 ppm and δC = 67.21, 25.31 ppm).[S4] The ^{29}Si NMR chemical shifts were referenced to external $SiMe_4$. The following abbreviations were used for the multiplicities: s – singlet, d – doublet, t – triplet, sept – septet, m – multiplet, br – prefix broad. IR data of powder samples was acquired on a Bruker Vertex 70 spectrometer in attenuated total reflectance (ATR) mode. X-band continuous wave (cw) EPR spectra were recorded on a Magnettech MiniScope MS 5000 with a microwave frequency of 9.44 GHz using a modulation amplitude of 100 kHz. For least-square fitting of the data, the Nelder-Mead method was applied and the spectra were simulated with the Easyspin toolbox (version 6.0.6)[S5] for Matlab R2024a[S6] using the resulting fit data. Melting points were determined under argon in sealed NMR tubes. The molten samples were examined by NMR spectroscopy to confirm whether decomposition had occurred upon melting. Elemental analyses were performed in triplicate for each sample using Leco CHN900 analyzer and mean values are reported. Single crystal X-ray diffraction (SC-XRD) was performed on a Bruker D8 Venture diffractometer with a microfocus sealed tube and a Photon II detector. Graphite-monochromated Mo Kα radiation (λ = 0.71073 Å) was used. Data were corrected for absorption effects using the multi-scan method. The structures were solved by direct methods using SHELXT[S7] and refined by full matrix least squares calculations on F2 (SHELXL)[S8] in the graphical user interface Shelxle.[S9] Computations were carried out with the Gaussian 16.C01 program package.[S10] Structural optimizations and frequency analyses were performed at the BP86-D3(BJ)/def2-SVP[11,12] or the UB3LYP-D3(BJ)/def2-SVP[12,13] (for paramagnetic compound **3**) level of theory, including the D3 dispersion correction by Grimme with Becke-Johnson damping[S14] and subsequent single-point calculations at the BP86-D3(BJ)/def2-TZVPP[11,12] or the UB3LYP-D3(BJ)/def2-TZVPP[12,13] (for paramagnetic compound **3**) level of theory. For the calculations of EPR parameters, the ORCA quantum chemistry program package (version 5.0.4)[S15] was used at the UB3LYP/def2-TZVPP[12,13] level of theory. Kohn-Sham orbitals and spin densities were visualized with ChemCraft.[S16]

2. Synthetic Procedures

2.1 Synthesis of oxycarbonyl NHC-bis(germylene) 2a

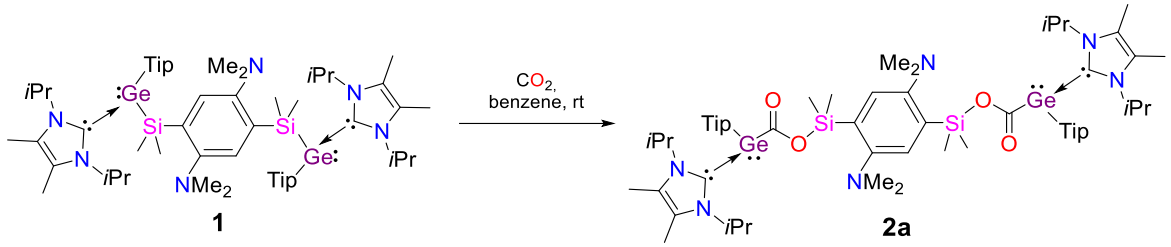

NHC-bis(germylene) **1** (261 mg, 212 µmol, 1 eq.) is suspended in 2.5 mL of benzene. Stirring under CO_2 atmosphere at ambient pressure for 20 minutes results in a colorless solution. The solvent is removed under vacuum to yield NHC-bis(germylene) **2a** (255 mg, 195 µmol, 92%) as a colorless amorphous powder.

^{1}H NMR (400.13 MHz, 300 K, TMS): δ (thf-d_8) = 7.59 (s, 2H, Ph*H*), 6.86 (s, 4H, Tip*H*), 5.69 (m, 4H, C*H*(CH_3)$_2$ of NHC), 3.74 (sept, 4H, C*H*(CH_3)$_2$ of Tip), 2.77 (sept, 2H, C*H*(CH_3)$_2$ of Tip), 2.52 (s, 12H, N(C*H*$_3$)$_2$), 2.24 (s, 12H, NHC-CC*H*$_3$), 1.37 (d, 12H, CH(C*H*$_3$)$_2$ of NHC), 1.19, 1.19 (each d, overall 12H, CH(C*H*$_3$)$_2$ of NHC), 1.11, 1.08 (d, brd, overall 24H, CH(C*H*$_3$)$_2$ of Tip), 0.96 (d, 12H, CH(C*H*$_3$)$_2$ of Tip), 0.41 (s, 12H, Si(C*H*$_3$)$_2$) ppm. δ (C_6D_6) = 8.15, 8.15 (overlapping s, overall 2H, Ph*H*), 7.16 (s, 4H, Tip*H*, overlapping with C_6D_6 peak), 5.93 (m, 4H, C*H*(CH_3)$_2$ of NHC), 4.13 (sept, 4H, C*H*(CH_3)$_2$ of Tip), 2.91 (sept, 2H, C*H*(CH_3)$_2$ of Tip), 2.54, 2.53 (overlapping s, overall 12H, N(C*H*$_3$)$_2$), 1.58 (s, 12H, NHC-CC*H*$_3$), 1.44 (d, 12H, CH(C*H*$_3$)$_2$ of NHC), 1.36, 1.34 (each d, overall 12H, CH(C*H*$_3$)$_2$ of NHC), 1.24, 1.21 (each d, overall 24H, CH(C*H*$_3$)$_2$ of Tip), 0.94 (brd, 12H, CH(C*H*$_3$)$_2$ of Tip), 0.88, 0.86, 0.85, 0.84 (each s, overall 12H, Si(C*H*$_3$)$_2$) ppm. **^{13}C{^{1}H} NMR** (100.61 MHz, C_6D_6, 300 K, TMS): δ = 204.89 (*C*O), 173.44 (NHC-*C*), 158.19, 154.10 (Ph*C*), 149.41, 146.90, 140.07 (Tip*C*), 129.16 (NHC-*C*CH$_3$), 125.48 (Ph*C*), 121.05 (Tip*C*), 52.67 (*C*H(CH_3)$_2$ of NHC), 47.15 (N(*C*H$_3$)$_2$), 35.01, 34.74 (*C*H(CH_3)$_2$ of NHC), 25.60, 25.22, 24.68, 24.59 (CH(*C*H$_3$)$_2$ of Tip), 21.03, 20.96 (CH(*C*H$_3$)$_2$ of NHC), 9.93 (NHC-C*C*H$_3$), 1.40, 1.28 (Si(*C*H$_3$)$_2$) ppm. **^{29}Si{^{1}H} NMR** (79.49 MHz, 300 K, TMS): δ (thf-d_8) = 2.09, 2.05, δ (C_6D_6) = 2.70 ppm. **Elemental analysis:** Calcd. for ($C_{70}H_{114}Ge_2N_6O_4Si_2$): C, 64.42; H, 8.80; N, 6.44. Found: C, 64.69; H, 7.72; N, 6.10. **Mp.:** 164°C (under formation of $Tip_2Ge{=}GeTip_2$ and unidentified decomposition products). **IR:** ν(CO) 1613 cm^{-1}.

In solution, slow decomposition is observed, providing an unidentified mixture of products. A characteristic septet at 4.89 ppm in the ^{1}H NMR spectrum (in thf-d_8), concomitant with the precipitation of a colorless solid, suggests the formation of poorly soluble NHC–CO_2).[S17a]

2.2 Synthesis of aminocarbonyl NHC-bis(germylene) 2b

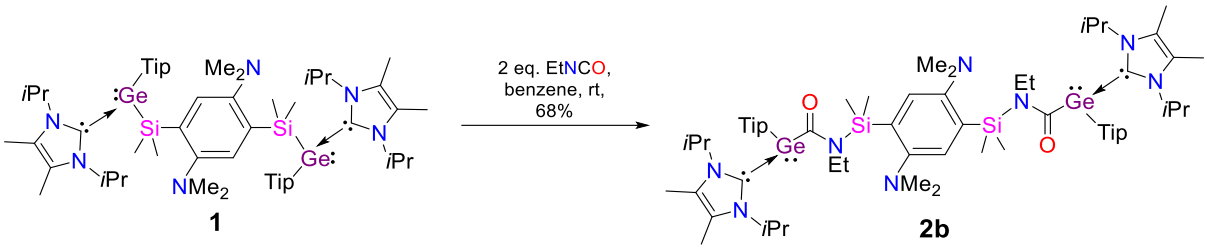

NHC-bis(germylene) **1** (250 mg, 177 µmol, 1 eq.) is suspended in 4 mL of benzene. Dropwise addition of a solution of ethyl isocyanate in benzene (0.41 M, 0.99 mL, 406 µmol, 2.3 eq.) results in complete dissolution of the starting material and subsequent precipitation of a colorless solid. After stirring for one hour, the solvent is removed and the residue is washed with 2 mL of pentane to yield NHC-bis(germylene) **2b** as a colorless powder (176 mg, 121 µmol, 68%). Single crystals of **2b** suitable for SC-XRD anylsis are obtained from a benzene/thf/hexane solution.

^{1}H NMR (400.13 MHz, thf-d_8, 300 K, TMS): δ = 7.41 (s, 2H, Ph*H*), 6.86 (s, 4H, Tip*H*), 5.73 (m, 4H, C*H*$(CH_3)_2$ of NHC), 3.86 (brsept, 2H, C*H*$(CH_3)_2$ of Tip), 3.69 (app. quint, 4H, NCH_2CH$_3$), 3.51 to 3.40 (m, 2H, C*H*$(CH_3)_2$ of Tip), 2.75 (sept, 2H, C*H*$(CH_3)_2$ of Tip), 2.54 (s, 12H, N(CH_3)$_2$), 2.18 (s, 12H, NHC-CCH_3), 1.44 (d, 12H, CH(CH_3)$_2$ of NHC), 1.27 (brtr, 6H, NCH$_2$CH_3), 1.19, 1.18, 1.16 (overlapping d, overall 24H, CH(CH_3)$_2$ of NHC and CH(CH_3)$_2$ of Tip), 0.93 (brd, 24H, CH(CH_3)$_2$ of Tip), 0.53, 0.28 (each s, each 6H, Si(CH_3)$_2$) ppm. **^{13}C{^{1}H} NMR** (100.61 MHz, thf-d_8, 300 K, TMS): δ = 212.19, 211.93 (*C*O), 172.49 (NHC-*C*), 156.54, 154.29, 154.24 (Ph*C*), 149.63, 146.66, 139.92 (Tip*C*), 128.64, 128.45 (NHC-*C*CH$_3$), 126.33 (Ph*C*), 121.41 (Tip*C*), 53.03 (*C*H$(CH_3)_2$ of NHC), 47.39 (N(*C*H$_3$)$_2$), 42.64 (NCH$_2$CH$_3$), 34.93, 34.58 (*C*H$(CH_3)_2$ of NHC), 25.83, 25.09, 24.51, 24.39 (CH(*C*H$_3$)$_2$ of Tip), 21.34, 21.13, 20.88 (CH(*C*H$_3$)$_2$ of NHC), 18.80 (NCH$_2$*C*H$_3$), 10.22, 8.18 (NHC-C*C*H$_3$), 1.44, 0.34, 0.21 (Si(*C*H$_3$)$_2$) ppm. **^{29}Si{^{1}H} NMR** (79.49 MHz, thf-d_8, 300 K, TMS): δ = −6.27, −6.44 ppm. **Elemental analysis:** Calcd. for ($C_{81}H_{131}Ge_2N_8O_2Si_2$): C, 67.07; H, 9.12; N, 7.73. Found: C, 67.13; H, 8.12; N, 7.62. **Mp.:** 110°C (under unselective decomposition to unidentified products). **IR:** ν(CO) 1548 cm^{-1}.

In solution, slow decomposition is observed, providing an unidentified mixture of products. A septet at 5.00 ppm in the ^{1}H NMR spectrum (in thf-d_8), concomitant with the precipitation of a colorless solid (characteristic for poorly soluble NHC–heteroallene adducts),[S17] suggests the formation of NHC–C(O)NEt.

2.3 Reaction of NHC-bis(germylene) 2a with CAAC^{Me}

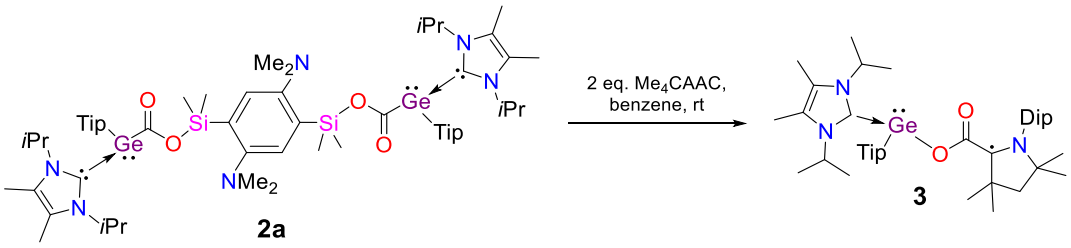

NHC-bis(germylene) **2a** (100 mg, 75.3 µmol, 0.5 eq.) and CAAC^{Me} (43.0 mg, 151 µmol, 1 eq.) are each dissolved in 2 mL of benzene. The germylene solution is added rapidly to the CAAC^{Me} solution *via* syringe. The resulting intensely red solution is concentrated under vacuum and 4 mL of pentane are added prior to filtration. Off-white crystals of germylene **3** (13 mg, 16.7 µmol, 11%) are grown from the concentrated filtrate at +4°C.

EPR (9.44 GHz, 5 dB, 1.5 G modulation amplitude, 100 kHz modulation frequency, C_6D_6, 300 K): *g* 2.0035, *A*(^{14}N) 5.96 G.

*Reasonable elemental analysis and IR spectroscopy of **3** were prevented by its highly sensitive nature.*

3. Characterization

3.1 X-Ray crystallographic data

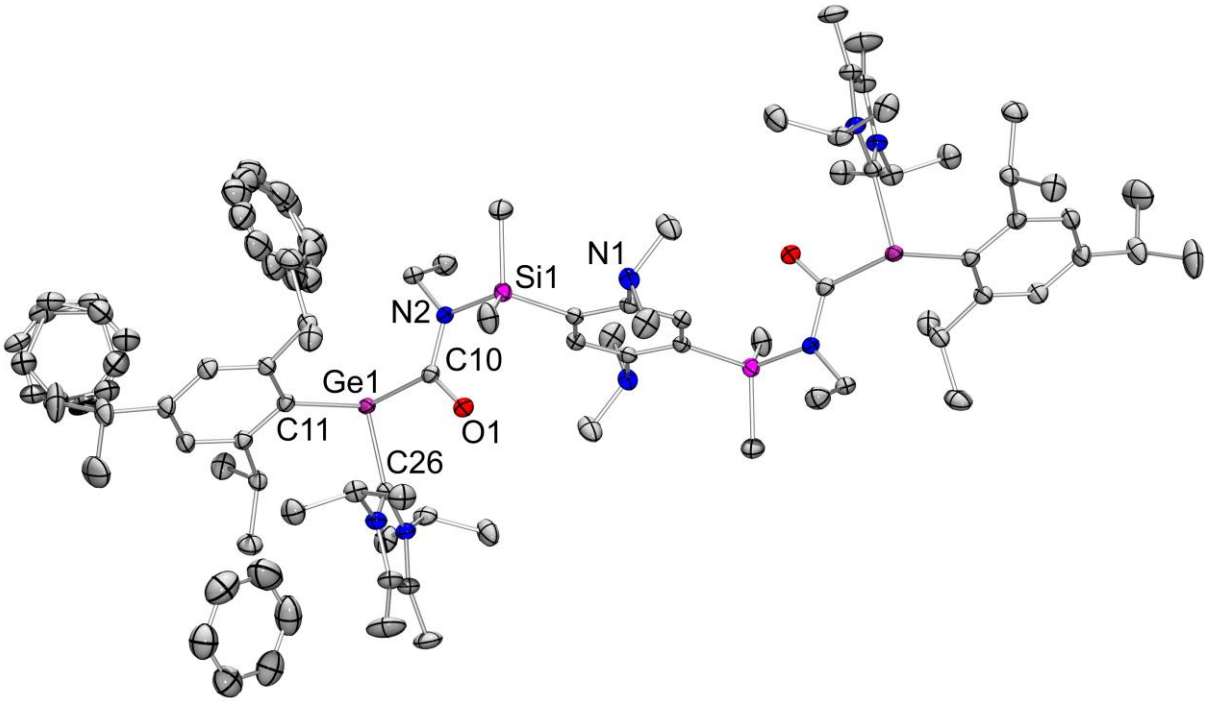

Figure S1. Molecular structure of NHC-bis(germylene) **2b** in the solid state. Hydrogen atoms omitted for clarity. Thermal ellipsoids are shown at 50% probability. Selected bond lengths (in Å) and angles (in °): Ge1–C26 2.078(2), Ge1–C10 2.066(2), N2–C10 1.382(3), C10–O1 1.239(2), Si1–O1 2.788(2), C10-Ge1-C26 90.79(8), C26-Ge1-C11 95.31(8), C11-Ge1-C10 109.92(8), Σ°(Ge1) 296.0(2), C9-N2-Si1 123.8(1), C9-N2-C10 119.6(2), C10-N2-Si1 116.6(2), Σ°(N2) 360.0(5), Si1-N2-C10-O1 9.1(2), C11-Ge1-C10-O1 79.3(2), C26-Ge1-C10-O1 4.8(2).

All non H-atoms were located in the electron density maps and refined anisotropically. C-bound H atoms were placed in positions of optimized geometry and treated as riding atoms. Their isotropic displacement parameters were coupled to the corresponding carrier atoms by a factor of 1.2 (CH, CH_2) or 1.5 (CH_3). *Disorder*: two co-crystallized benzene molecules are disordered across two positions each (fvar 2: 0.60/0.40 and fvar 3: 0.78/0.22).

Table S1. Crystal Data and Structure Refinement for NHC-bis(germylene) **2b** (CCDC 2427550).[S22]

Identification code	sh5583_a	
Empirical formula	C108 H158 Ge2 N8 O2 Si2	
Formula weight	1801.77	
Temperature	133(2) K	
Wavelength	0.71073 Å	
Crystal system	Triclinic	
Space group	P−1	
Unit cell dimensions	a = 12.0604(6) Å	α= 84.472(2)°.
	b = 12.6790(6) Å	β= 73.288(2)°.
	c = 19.5103(10) Å	γ = 66.037(2)°.
Volume	2610.4(2) Å^3	
Z	1	
Density (calculated)	1.146 Mg/m^3	
Absorption coefficient	0.649 mm^{-1}	
F(000)	970	
Crystal size	0.180 x 0.100 x 0.010 mm^3	
Theta range for data collection	1.921 to 27.171°.	
Index ranges	−15≤h≤15, −16≤k≤16, −25≤l≤25	
Reflections collected	95589	
Independent reflections	11547 [R(int) = 0.0796]	
Completeness to theta = 25.242°	99.7 %	
Absorption correction	Semi-empirical from equivalents	
Max. and min. transmission	0.7455 and 0.6765	
Refinement method	Full-matrix least-squares on F^2	
Data / restraints / parameters	11547 / 606 / 677	
Goodness-of-fit on F^2	1.024	
Final R indices [I>2sigma(I)]	R1 = 0.0401, wR2 = 0.0792	
R indices (all data)	R1 = 0.0614, wR2 = 0.0876	
Extinction coefficient	n/a	
Largest diff. peak and hole	0.345 and −0.552 e.Å^{-3}	

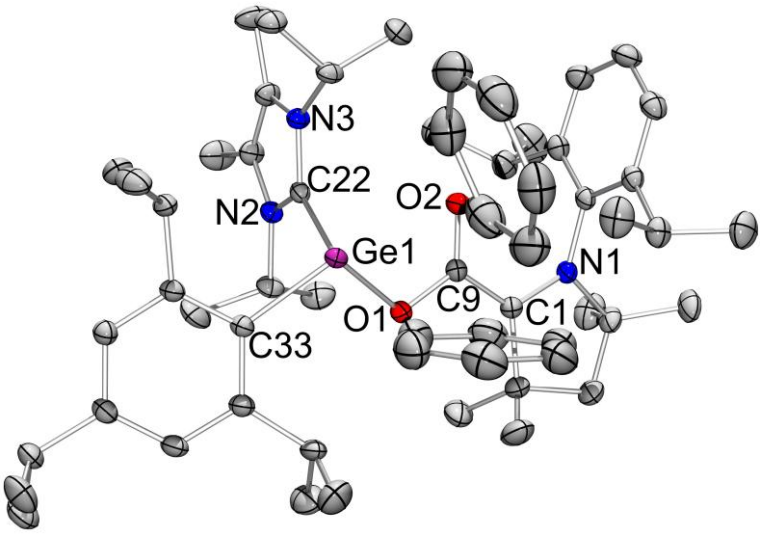

Figure S2. Molecular structure of germylene radical **3** in the solid state. Hydrogen atoms omitted for clarity. Thermal ellipsoids are shown at 50% probability. Selected bond lengths (in Å) and angles (in °): Ge1–C22 2.094(1), Ge1–O1 1.9528(7), Ge1–O2 2.8139(8), C9–O1 1.339(1), C9–O2 1.238(1), C1–N1 1.376(1), C1–C9 1.441(1), O1-Ge1-C22 91.10(3), O1-Ge1-C33 101.76(4), C33-Ge1-C22 95.37(4), Σ°(Ge1) 288.2(1), Ge1-O1-C9-O2 10.5(1).

All non H-atoms were located in the electron density maps and refined anisotropically. C-bound H atoms were placed in positions of optimized geometry and treated as riding atoms. Their isotropic displacement parameters were coupled to the corresponding carrier atoms by a factor of 1.2 (CH, CH_2) or 1.5 (CH_3).

Table S2. Crystal Data and Structure Refinement for germylene radical **3** (CCDC 2427551).[S22]

Identification code	sh5323_a	
Empirical formula	C56 H83 Ge N3 O2	
Formula weight	902.84	
Temperature	143(2) K	
Wavelength	0.71073 Å	
Crystal system	Triclinic	
Space group	P-1	
Unit cell dimensions	a = 12.7231(3) Å	α = 103.0580(10)°.
	b = 12.9550(3) Å	β = 94.8140(10)°.
	c = 16.3893(4) Å	γ = 95.9220(10)°.
Volume	2601.43(11) Å^3	
Z	2	
Density (calculated)	1.153 Mg/m^3	
Absorption coefficient	0.630 mm^{-1}	
F(000)	976	
Crystal size	0.400 x 0.300 x 0.200 mm^3	
Theta range for data collection	2.146 to 28.737°.	
Index ranges	−17≤h≤17, −17≤k≤17, −22≤l≤22	
Reflections collected	114365	
Independent reflections	13482 [R(int) = 0.0358]	
Completeness to theta = 25.242°	99.9 %	
Absorption correction	Semi-empirical from equivalents	
Max. and min. transmission	0.7458 and 0.7150	
Refinement method	Full-matrix least-squares on F^2	
Data / restraints / parameters	13482 / 0 / 579	
Goodness-of-fit on F^2	1.028	
Final R indices [I>2sigma(I)]	R1 = 0.0260, wR2 = 0.0633	
R indices (all data)	R1 = 0.0298, wR2 = 0.0656	
Extinction coefficient	n/a	
Largest diff. peak and hole	0.296 and -0.308 e.Å^{-3}	

3.2 NMR spectroscopic data

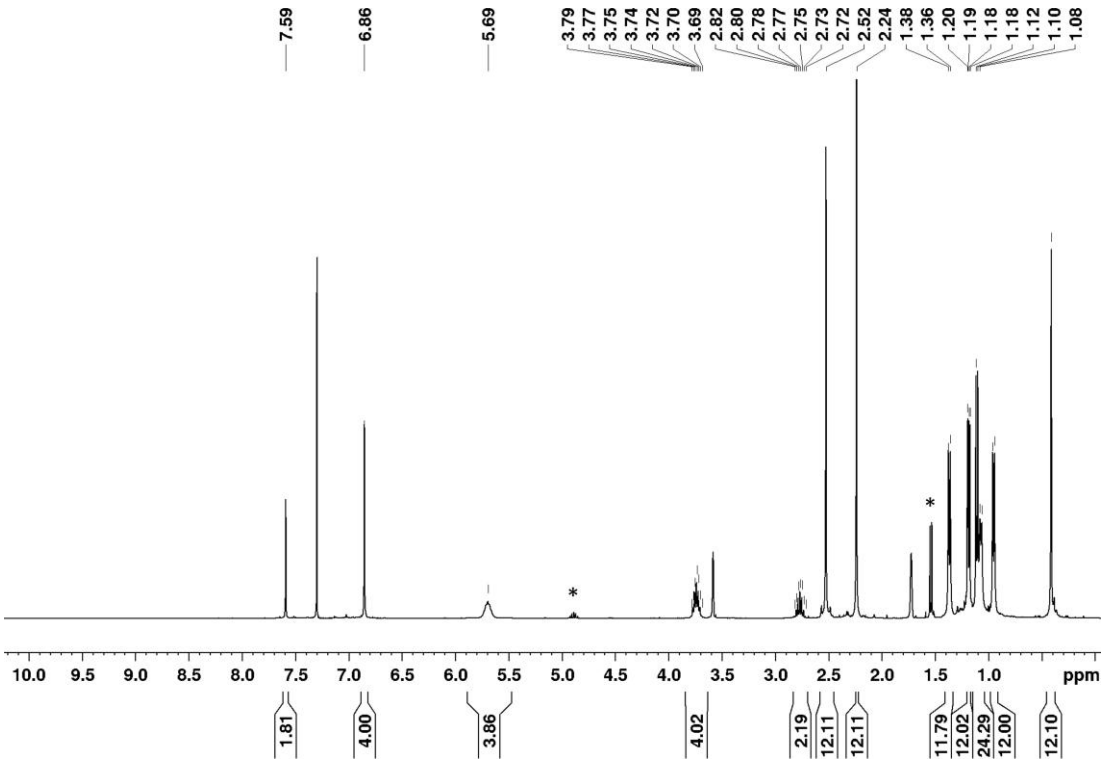

Figure S3. ^{1}H NMR spectrum of oxycarbonyl substituted NHC-bis(germylene) **2a** in thf-d_8 (*: peaks of NHC-CO_2 resulting from beginning decomposition).

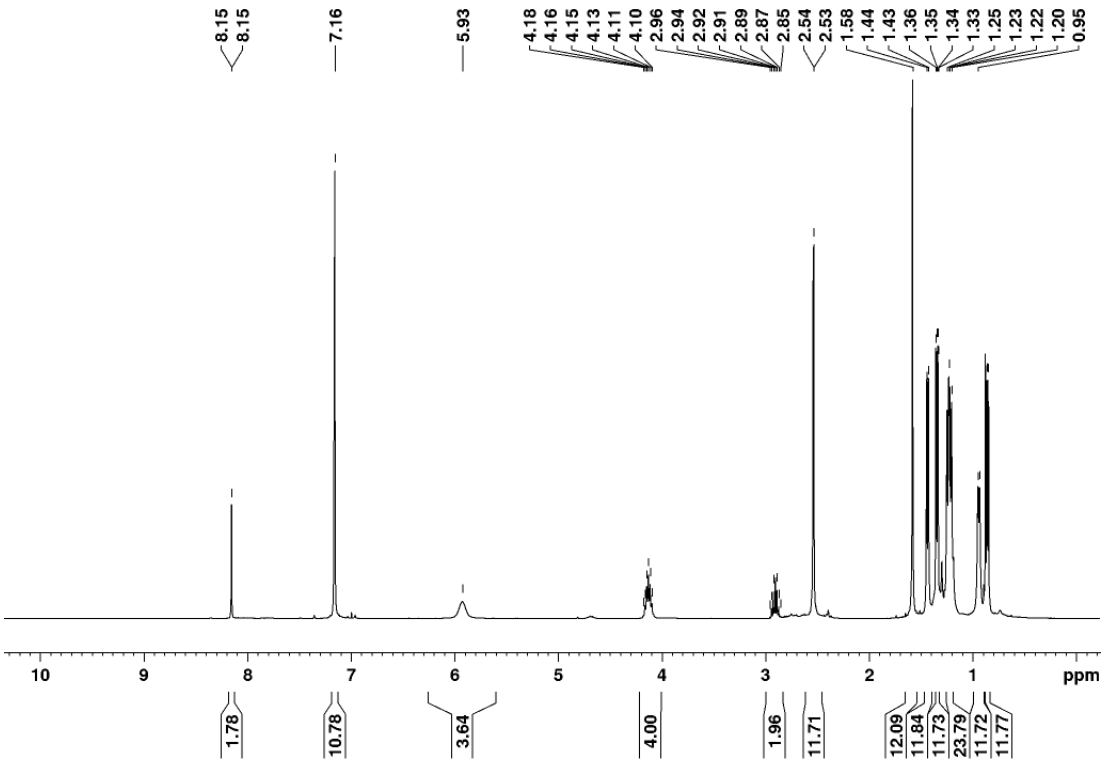

Figure S4. ^{1}H NMR spectrum of oxycarbonyl substituted NHC-bis(germylene) **2a** in C_6D_6.

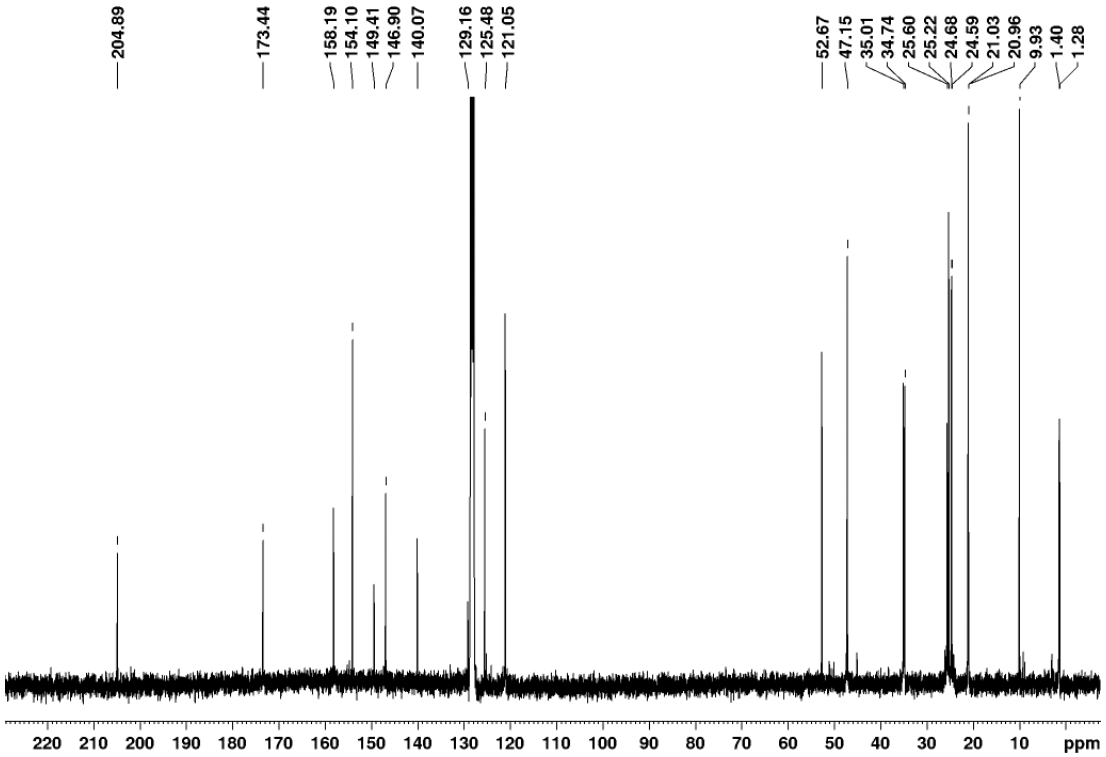

Figure S5. $^{13}C\{^{1}H\}$ NMR spectrum of oxycarbonyl substituted NHC-bis(germylene) **2a** in C_6D_6.

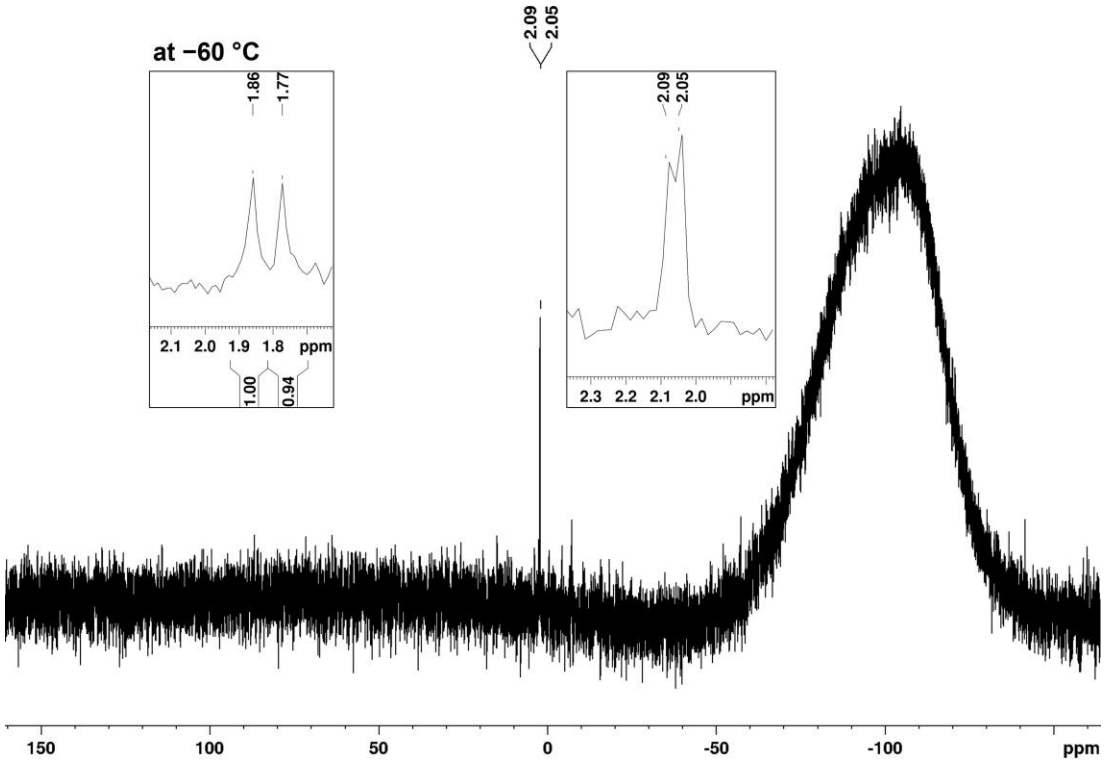

Figure S6. $^{29}Si\{^{1}H\}$ NMR spectrum of a diastereomeric mixture of oxycarbonyl substituted NHC-bis(germylene) **2a** in thf-d_8 and an excerpt from the ^{29}Si NMR spectrum at −60°C.

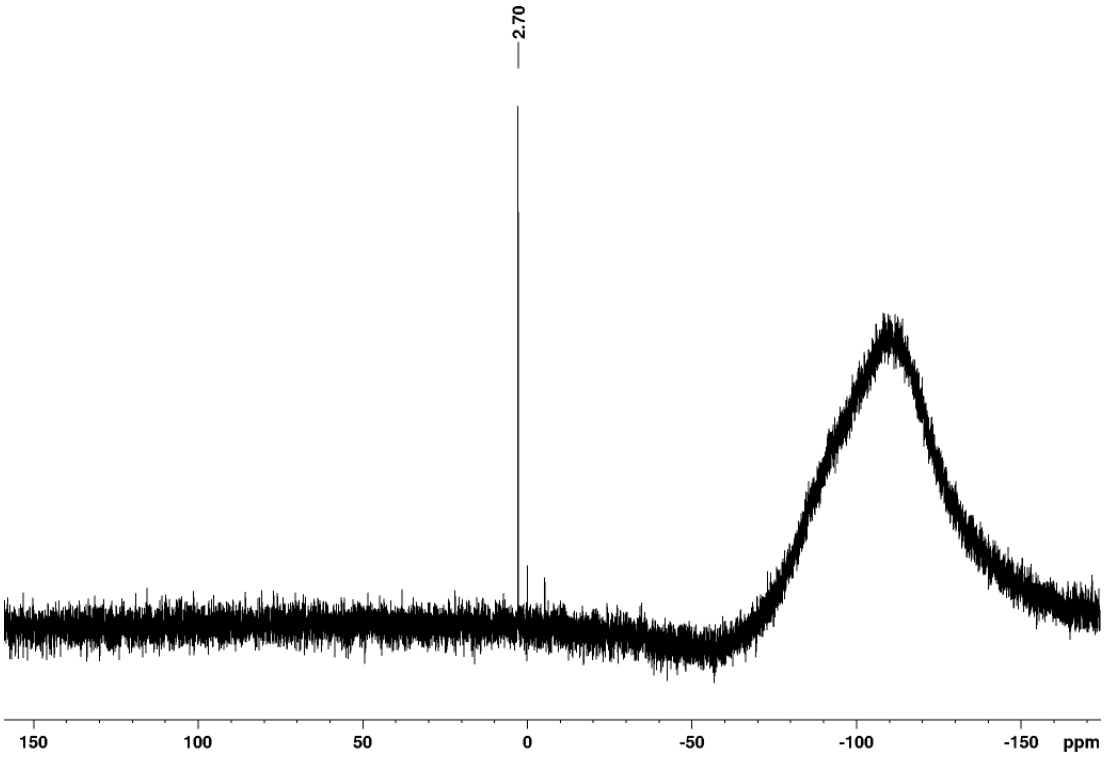

Figure S7. $^{29}Si\{^{1}H\}$ NMR spectrum of oxycarbonyl substituted NHC-bis(germylene) **2a** in C_6D_6.

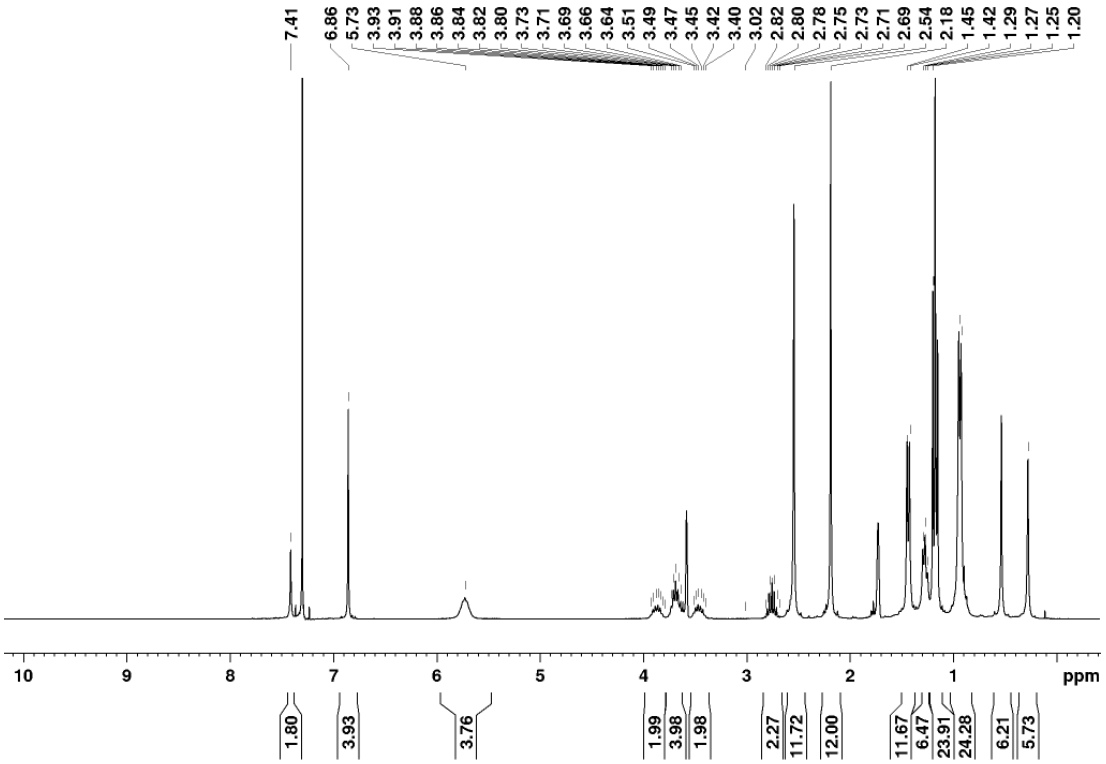

Figure S8. ^{1}H NMR spectrum of aminocarbonyl substituted NHC-bis(germylene) **2b** in thf-d_8.

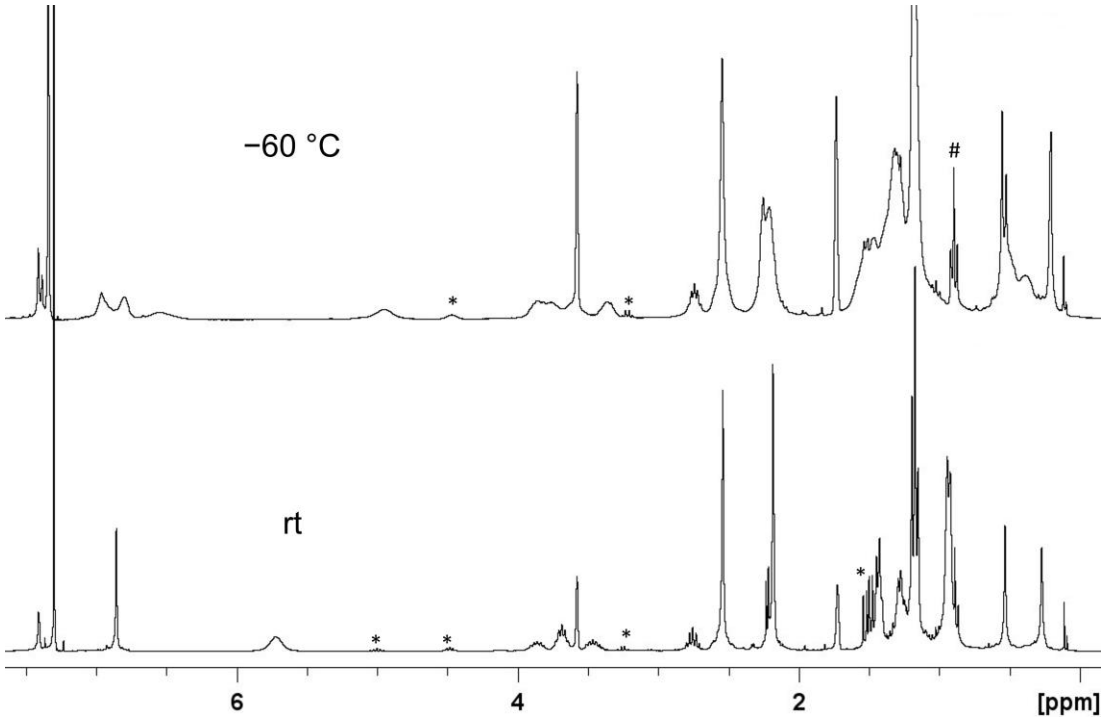

Figure S9. ^{1}H NMR spectra of aminocarbonyl substituted NHC-bis(germylene) **2b** in thf-d_8 at different temperatures (*: peaks of products from beginning decomposition, #: peak of residue hexane).

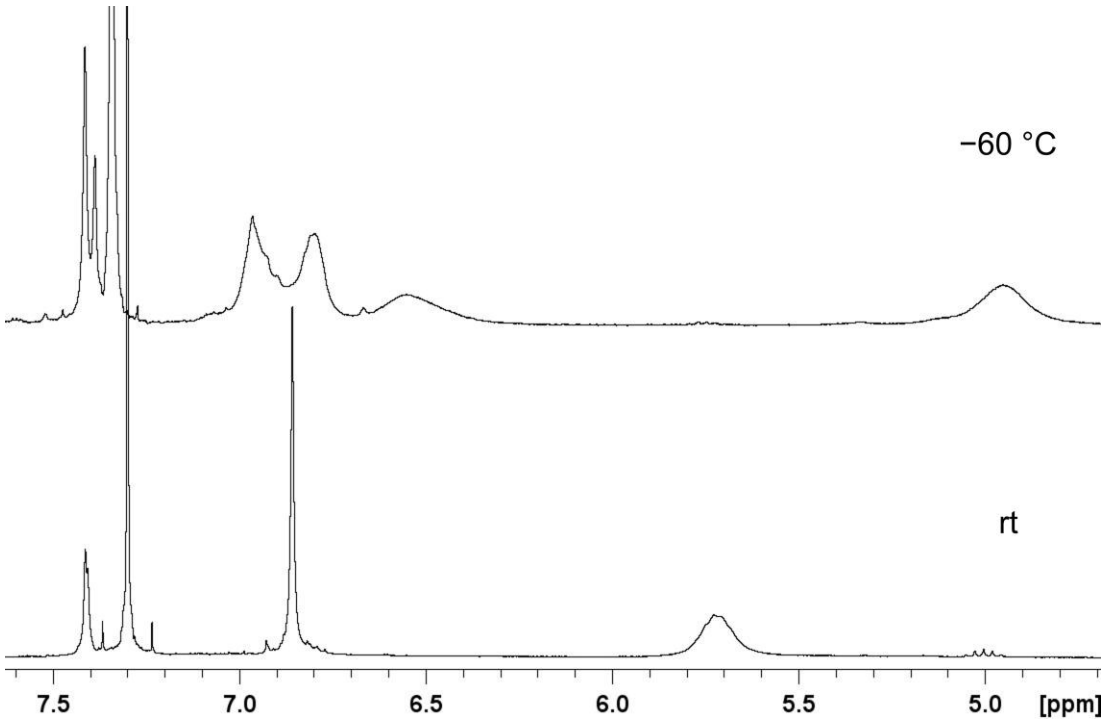

Figure S10. Excerpts of the ^{1}H NMR spectra of aminocarbonyl substituted NHC-bis(germylene) **2b** in thf-d_8 at different temperatures showing the phenylene proton (7.4 ppm at rt), Tip-proton (6.9 ppm at rt) and NHC-methine proton (5.7 ppm at rt) resonances.

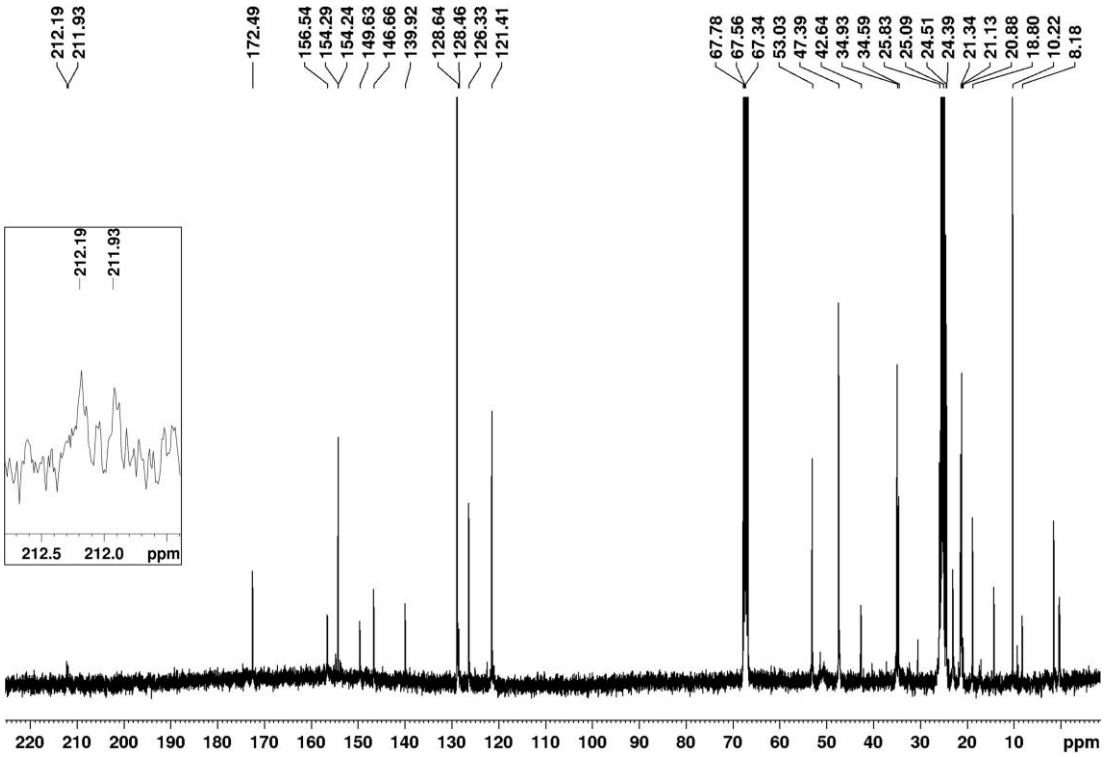

Figure S11. $^{13}C\{^{1}H\}$ NMR spectrum of aminocarbonyl substituted NHC-bis(germylene) **2b** in thf-d_8.

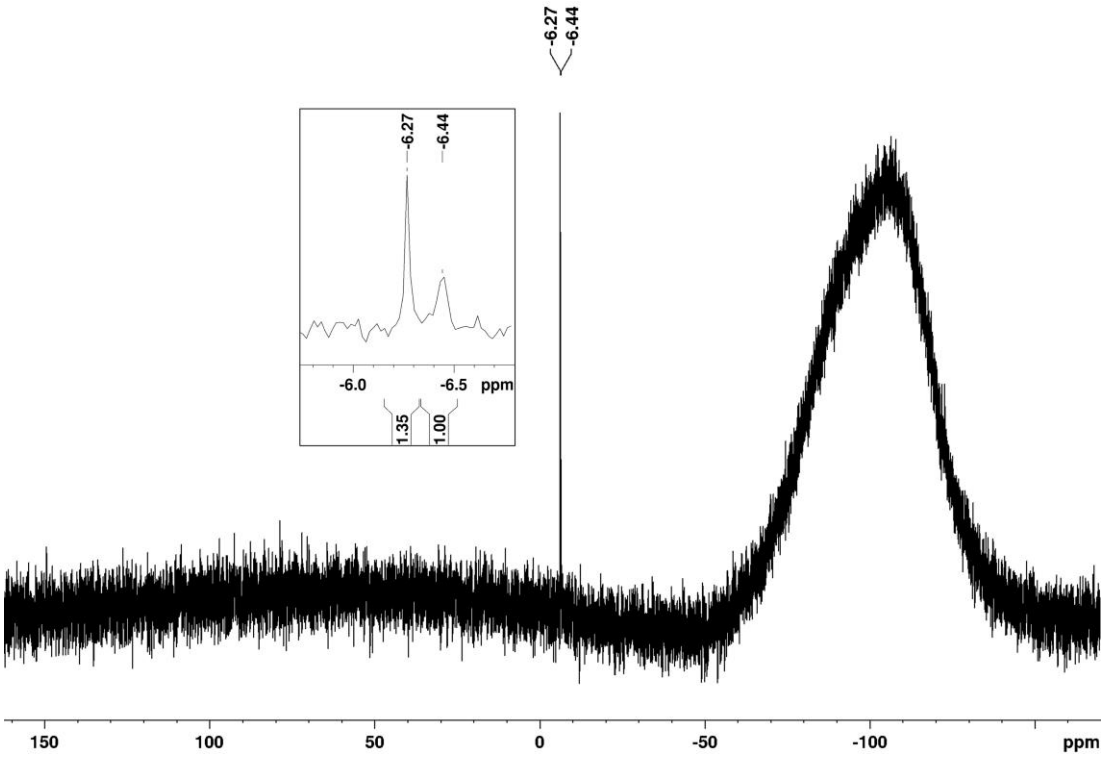

Figure S12. $^{29}Si\{^{1}H\}$ NMR spectrum of aminocarbonyl substituted NHC-bis(germylene) **2b** in thf-d_8.

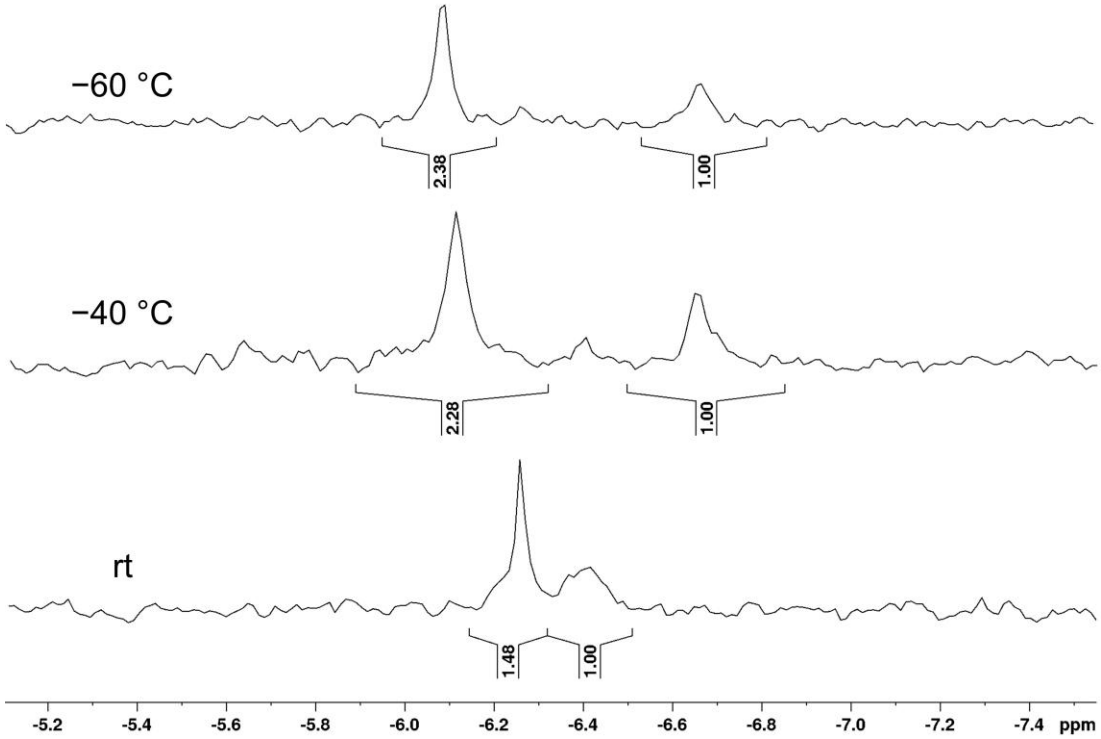

Figure S13. $^{29}Si\{^{1}H\}$ NMR spectra of aminocarbonyl substituted NHC-bis(germylene) **2b** in thf-d_8 at different temperatures.

High temperature experiments for the determination of the coalescence temperature (> rt) were prevented by the limited stability of NHC-bis(germylene) **2b**. Hence, for the determination of the rotational barrier of the C–N bond, the following approach was used according to reference [S20].

The rate constant k_{298} of the conformational change at a temperature below the coalescence temperature (*i.e.* here at 298 K, where the peaks overlap slightly) is estimated *via*:

$$k_{298} = \frac{\pi}{\sqrt{2}} (\Delta\vartheta_0{}^2 - \Delta\vartheta_{298}{}^2)^{1/2}$$

where $\Delta\nu_0$ is the peak separation at slow exchange (*i.e.* at low temperature, here at 213 K) in Hz and $\Delta\nu_{298}$ is the peak separation at 298 K.

The Eyring equation[S21] was used for the determination of the Gibbs free energy barrier $\Delta G^{\ddagger}$ of the rotation:

$$\Delta G^{\ddagger} = -RT\,(\ln\frac{k}{T} - \ln\frac{k_B}{h})$$

where R is the molar gas constant, T the temperature, k the corresponding rate constant, k_B the Boltzmann constant and h the Planck constant.

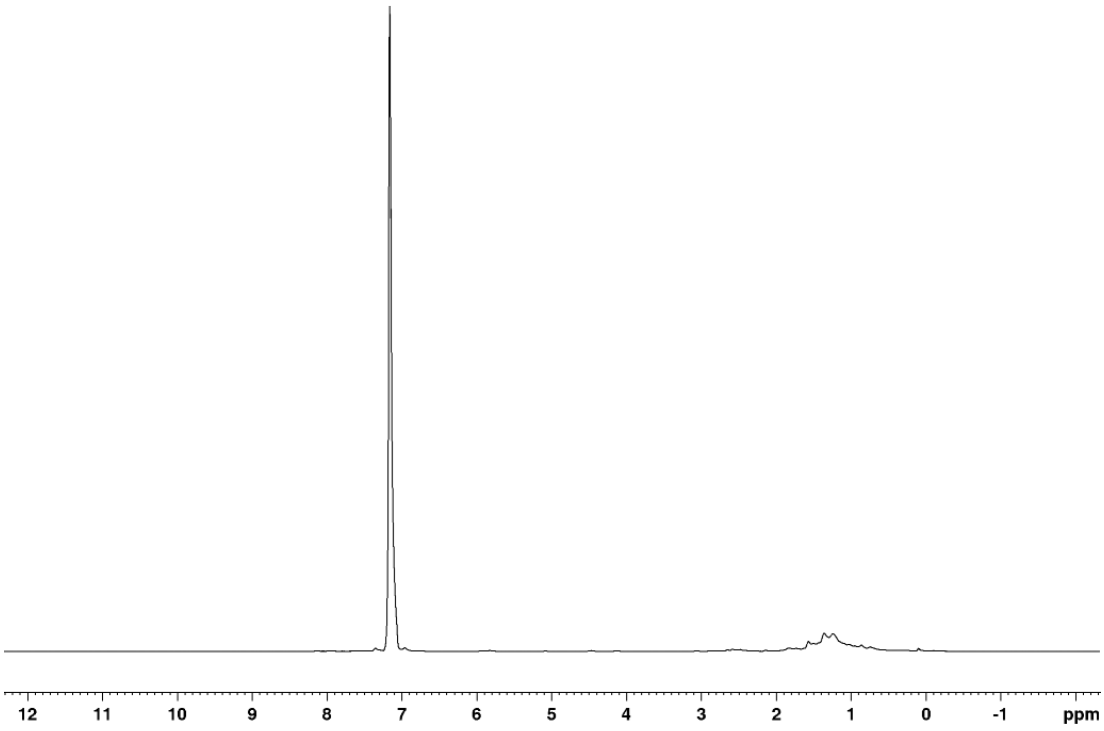

Figure S14. ^{1}H NMR spectrum of germylene radical **3** in C_6D_6.

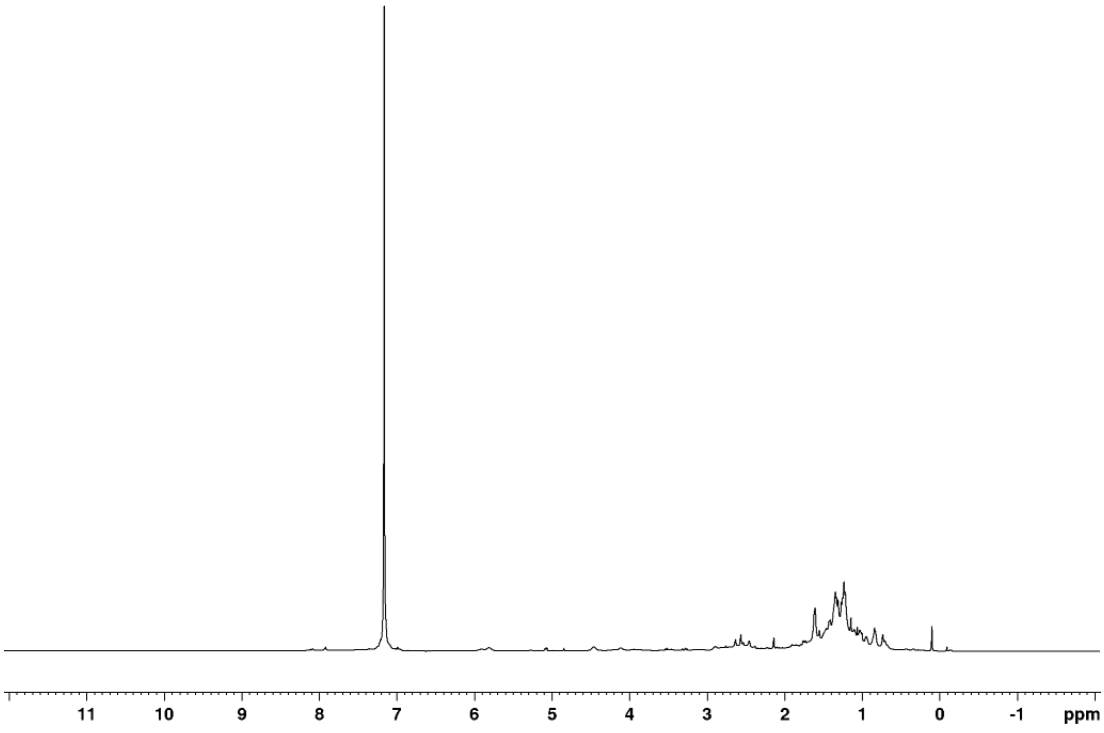

Figure S15. ^{1}H NMR spectrum of the mother liquor of the reaction of NHC-bis(acylgermylene) **2a** with $CAAC^{Me}$ towards germylene radical **3** in C_6D_6.

3.3 IR spectroscopic data

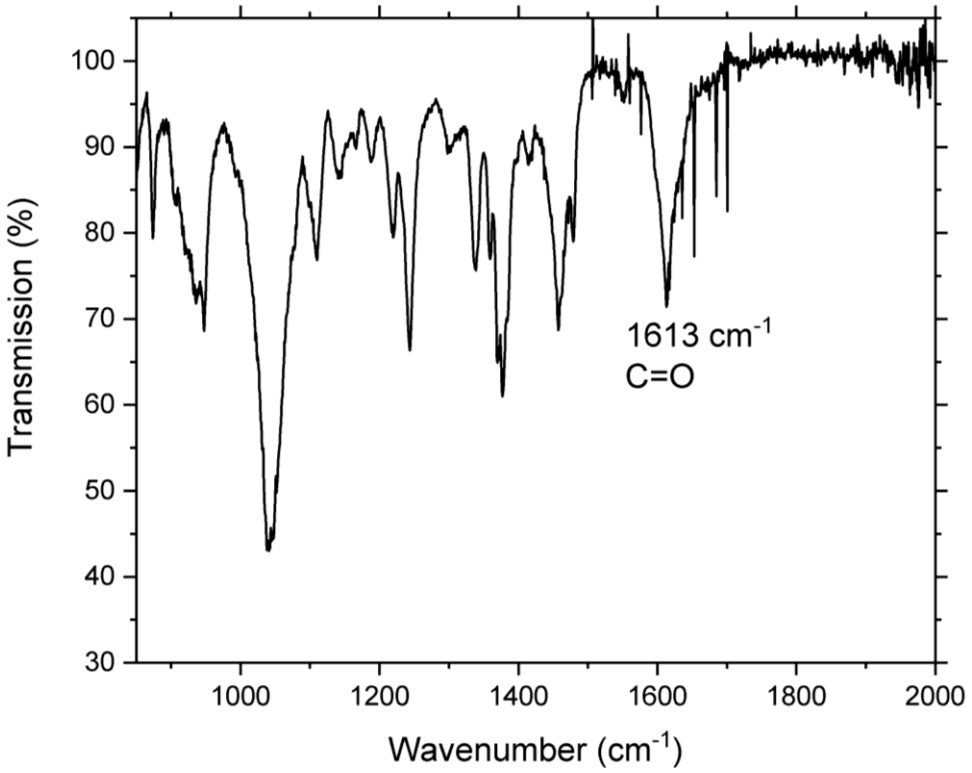

Figure S16. IR spectrum of oxycarbonyl substituted NHC-bis(germylene) **2a**.

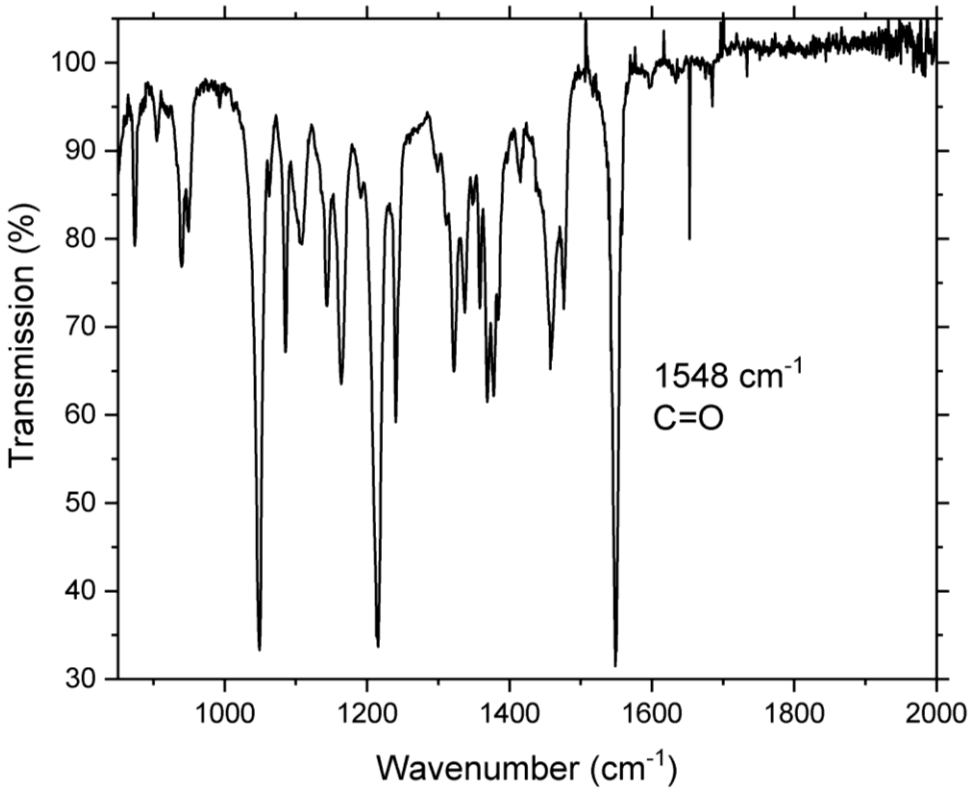

Figure S17. IR spectrum of aminocarbonyl substituted NHC-bis(germylene) **2b**.

3.4 DFT calculations

NHC-Bis(carboxylgermylene) 2a

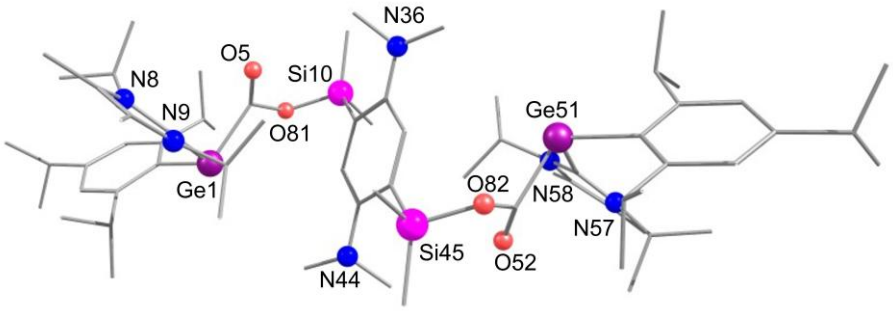

Figure S18. Optimized structure of NHC-bis(germylene) **2a** (Gibbs free energy = −5033900.3832 kcal mol^{-1}). Hydrogen atoms omitted for clarity.

Table S3. Atomic coordinates of the optimized structure of NHC-bis(germylene) **2a**.

32	4.833945000	-0.217993000	-0.517951000
6	3.911781000	-1.077225000	1.100097000
6	6.785158000	-0.783294000	-0.689186000
6	5.205785000	1.483319000	0.625679000
8	3.539722000	-0.451258000	2.100210000
6	7.325420000	-2.016924000	-0.233348000
6	7.648575000	0.132051000	-1.362361000
7	6.225585000	1.831993000	1.462198000
7	4.419923000	2.593001000	0.510904000
14	1.679639000	-2.532113000	1.318575000
6	8.713413000	-2.247341000	-0.332947000
6	6.433512000	-3.090858000	0.386212000
6	9.026859000	-0.140491000	-1.451206000
6	7.113719000	1.381512000	-2.070369000
6	6.097229000	3.170321000	1.860925000
6	7.120458000	0.811274000	2.063339000
6	4.949891000	3.652895000	1.254383000
6	3.053212000	2.503030000	-0.066180000
6	0.759062000	-0.993756000	0.700191000
6	1.594964000	-3.052905000	3.122161000
6	1.158061000	-3.996883000	0.250691000
1	9.134188000	-3.192081000	0.050541000
6	9.588355000	-1.312231000	-0.911984000
1	5.395834000	-2.889917000	0.052546000
6	6.438784000	-3.006122000	1.923990000
6	6.780384000	-4.512306000	-0.089586000
1	9.683144000	0.584572000	-1.962066000
1	6.023097000	1.443721000	-1.858948000
6	7.248937000	1.225353000	-3.597632000
6	7.750681000	2.692368000	-1.579144000
6	7.067722000	3.899074000	2.732297000
1	6.947611000	-0.075078000	1.426067000
6	6.639158000	0.475861000	3.479798000
6	8.608719000	1.150220000	1.958950000
6	4.372272000	5.030066000	1.299260000
1	3.051282000	1.495420000	-0.537598000
6	2.784171000	3.516141000	-1.178813000
6	2.016590000	2.478893000	1.058318000

6	-0.297706000	-0.311349000	1.362692000
6	1.043963000	-0.649336000	-0.641153000
1	2.017492000	-4.075056000	3.218536000
1	0.541958000	-3.065023000	3.469723000
1	2.175123000	-2.371455000	3.770757000
1	1.197539000	-3.743242000	-0.827588000
1	0.121244000	-4.309077000	0.493070000
1	1.829372000	-4.862563000	0.430593000
6	11.088892000	-1.569055000	-0.970532000
1	7.456246000	-3.198184000	2.328249000
1	5.742296000	-3.749560000	2.365175000
1	6.113569000	-2.006009000	2.270922000
1	6.812532000	-4.570587000	-1.197031000
1	6.017651000	-5.233633000	0.271510000
1	7.763521000	-4.857512000	0.295787000
1	6.798064000	2.091148000	-4.128081000
1	6.740204000	0.302899000	-3.944206000
1	8.314632000	1.157563000	-3.903452000
1	8.845775000	2.710855000	-1.765526000
1	7.589616000	2.837752000	-0.492763000
1	7.311259000	3.565174000	-2.106926000
1	8.046463000	4.049482000	2.230491000
1	7.260570000	3.364805000	3.684277000
1	6.666029000	4.898435000	2.986763000
1	7.216281000	-0.385943000	3.871277000
1	5.565789000	0.200613000	3.453888000
1	6.777354000	1.321762000	4.185220000
1	8.875224000	1.447991000	0.926914000
1	9.190000000	0.235846000	2.191372000
1	8.930419000	1.940613000	2.665478000
1	4.912218000	5.642465000	2.046217000
1	3.300542000	5.025048000	1.581425000
1	4.456415000	5.546503000	0.319871000
1	3.606560000	3.516397000	-1.922546000
1	2.641707000	4.549840000	-0.804800000
1	1.855128000	3.214538000	-1.704326000
1	1.914714000	3.459657000	1.567351000
1	2.295003000	1.707257000	1.800922000
1	1.029379000	2.206227000	0.642285000
7	-0.553525000	-0.578844000	2.738737000
6	-1.043392000	0.650453000	0.643109000
6	0.297880000	0.312143000	-1.360981000
1	1.852614000	-1.184660000	-1.162377000
1	11.263939000	-2.566023000	-0.507245000
6	11.866797000	-0.527002000	-0.142987000
6	11.605030000	-1.631870000	-2.420911000
6	0.496468000	-0.087251000	3.636232000
6	-1.879589000	-0.249842000	3.240698000
6	-0.758523000	0.994944000	-0.698282000
1	-1.851978000	1.185827000	1.164392000
7	0.553340000	0.578818000	-2.737122000
1	12.956173000	-0.743721000	-0.144876000
1	11.519419000	-0.511940000	0.910435000
1	11.726344000	0.494788000	-0.555672000
1	11.471326000	-0.657388000	-2.936857000
1	11.058201000	-2.398183000	-3.007283000
1	12.687412000	-1.879273000	-2.449553000
1	1.499497000	-0.265752000	3.204939000
1	0.431147000	-0.599215000	4.619337000
1	0.391947000	1.014647000	3.814758000

1	-2.670237000	-0.587936000	2.541705000
1	-2.033872000	0.848980000	3.402864000
1	-2.031352000	-0.749992000	4.220270000
14	-1.679408000	2.533327000	-1.315909000
6	-0.497667000	0.089158000	-3.634359000
6	1.878730000	0.248413000	-3.239728000
6	-1.591110000	3.056076000	-3.118772000
6	-1.159712000	3.997105000	-0.245680000
1	-1.500330000	0.268584000	-3.202580000
1	-0.432178000	0.601588000	-4.617225000
1	-0.394628000	-1.012761000	-3.813654000
1	2.670141000	0.585775000	-2.541216000
1	2.031730000	-0.850615000	-3.401871000
1	2.030459000	0.748255000	-4.219464000
6	-3.911692000	1.077514000	-1.099841000
1	-2.010732000	4.079429000	-3.214877000
1	-0.537402000	3.065707000	-3.464375000
1	-2.171643000	2.376721000	-3.769230000
1	-1.201224000	3.742573000	0.832315000
1	-0.122409000	4.309445000	-0.485807000
1	-1.830637000	4.862991000	-0.426027000
32	-4.834482000	0.218495000	0.517893000
8	-3.539265000	0.451501000	-2.099781000
6	-6.785985000	0.783345000	0.687844000
6	-5.205322000	-1.483503000	-0.625084000
6	-7.326339000	2.016578000	0.231078000
6	-7.649588000	-0.132004000	1.360763000
7	-6.224486000	-1.832901000	-1.462094000
7	-4.419009000	-2.592787000	-0.509592000
6	-8.714474000	2.246607000	0.329639000
6	-6.434456000	3.090493000	-0.388537000
6	-9.028016000	0.140143000	1.448576000
6	-7.114839000	-1.381064000	2.069545000
6	-6.095390000	-3.171332000	-1.860213000
6	-7.119459000	-0.812787000	-2.064139000
6	-4.948156000	-3.653191000	-1.252910000
6	-3.052777000	-2.502307000	0.068490000
1	-9.135296000	3.191003000	-0.054655000
6	-9.589520000	1.311493000	0.908503000
1	-5.396791000	2.889616000	-0.054807000
6	-6.439710000	3.005585000	-1.926297000
6	-6.781426000	4.511927000	0.087244000
1	-9.684409000	-0.584919000	1.959296000
1	-6.024152000	-1.443297000	1.858518000
6	-7.250525000	-1.224079000	3.596691000
6	-7.751526000	-2.692206000	1.578754000
6	-7.064984000	-3.900825000	-2.731966000
1	-6.947537000	0.073832000	-1.426993000
6	-6.637335000	-0.477548000	-3.480352000
6	-8.607587000	-1.152600000	-1.960707000
6	-4.370013000	-5.030174000	-1.296769000
1	-3.051397000	-1.494493000	0.539499000
6	-2.784431000	-3.514993000	1.181677000
6	-2.015231000	-2.478432000	-1.055134000
6	-11.090175000	1.567898000	0.965904000
1	-7.457185000	3.197496000	-2.330590000
1	-5.743301000	3.749034000	-2.367591000
1	-6.114403000	2.005446000	-2.273071000
1	-6.813520000	4.570163000	1.194692000
1	-6.018763000	5.233320000	-0.273872000

1	-7.764613000	4.857075000	-0.298054000
1	-6.799867000	-2.089596000	4.127777000
1	-6.741814000	-0.301460000	3.942861000
1	-8.316311000	-1.156014000	3.902127000
1	-8.846669000	-2.710758000	1.764828000
1	-7.590147000	-2.838024000	0.492474000
1	-7.312151000	-3.564729000	2.107039000
1	-8.044297000	-4.050666000	-2.231129000
1	-7.256708000	-3.367497000	-3.684715000
1	-6.663082000	-4.900472000	-2.984961000
1	-7.214599000	0.383882000	-3.872443000
1	-5.564119000	-0.201760000	-3.453764000
1	-6.774682000	-1.323708000	-4.185621000
1	-8.874674000	-1.450040000	-0.928723000
1	-9.189277000	-0.238728000	-2.194069000
1	-8.928235000	-1.943548000	-2.667093000
1	-4.908859000	-5.642965000	-2.044200000
1	-3.297970000	-5.024842000	-1.577699000
1	-4.455105000	-5.546364000	-0.317326000
1	-3.607355000	-3.515140000	1.924816000
1	-2.641514000	-4.548790000	0.808107000
1	-1.855811000	-3.213068000	1.707762000
1	-1.912580000	-3.459432000	-1.563567000
1	-2.293218000	-1.707288000	-1.798409000
1	-1.028503000	-2.205190000	-0.638367000
1	-11.265207000	2.564520000	0.501868000
6	-11.867252000	0.525098000	0.138539000
6	-11.607266000	1.631498000	2.415914000
1	-12.956688000	0.741525000	0.139581000
1	-11.519197000	0.509448000	-0.914650000
1	-11.726802000	-0.496389000	0.551975000
1	-11.473597000	0.657387000	2.932571000
1	-11.061059000	2.398360000	3.002145000
1	-12.689744000	1.878580000	2.443694000
8	3.323472000	-2.277574000	0.798113000
8	-3.323824000	2.278128000	-0.797880000

-

NHC-Bis(amidylgermylene) 2b

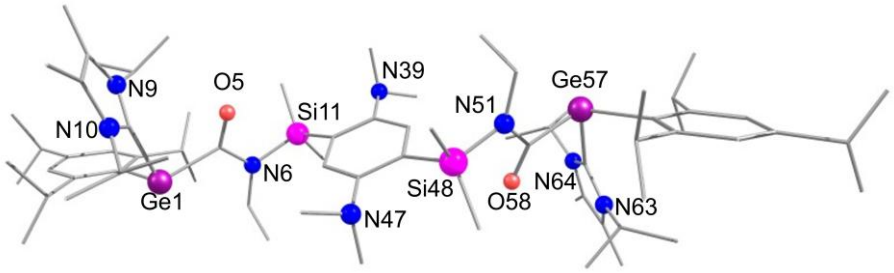

Figure S19. Optimized structure of NHC-bis(germylene) **2b** (Gibbs free energy = −5107565.0053 kcal mol^{-1}). Hydrogen atoms omitted for clarity.

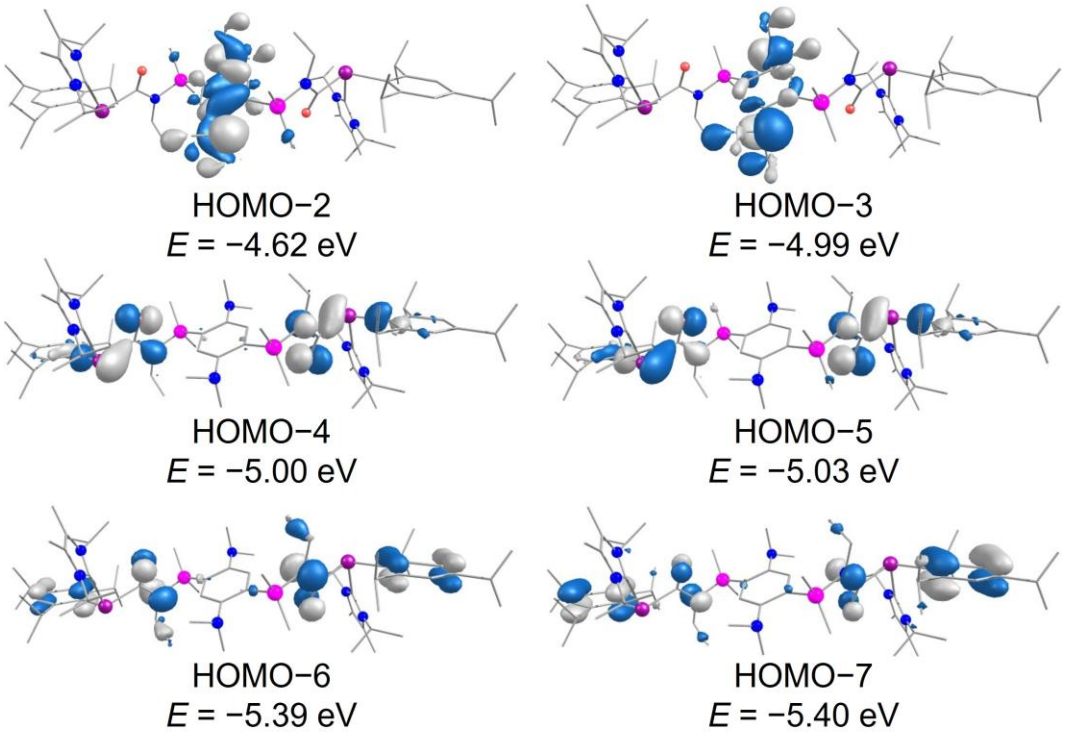

Figure S20. Selected occupied frontier orbitals of NHC-bis(germylene) **2b** (contour value 0.036). Hydrogen atoms omitted for clarity.

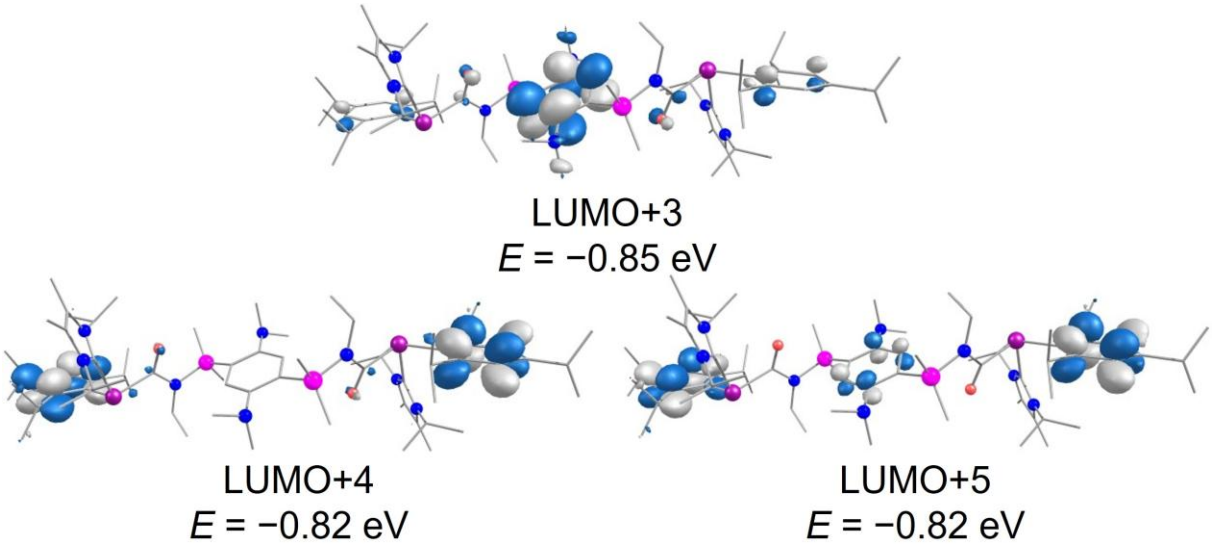

Figure S21. Selected unoccupied frontier orbitals of NHC-bis(germylene) **2b** (contour value 0.036). Hydrogen atoms omitted for clarity.

Table S4. Atomic coordinates of the optimized structure of NHC-bis(germylene) **2b**.

32	-6.273820000	-0.348762000	-1.161343000
6	-4.687336000	0.449637000	-0.072057000
6	-8.015865000	0.724223000	-0.821219000
6	-6.662360000	-1.639973000	0.432719000
8	-4.281762000	-0.105973000	0.973021000
7	-3.918239000	1.467258000	-0.608255000
6	-8.146852000	2.076430000	-0.389051000
6	-9.220220000	-0.002669000	-1.082994000
7	-7.190580000	-1.410055000	1.668469000
7	-6.552782000	-2.996983000	0.326172000
14	-2.558165000	2.044620000	0.449723000
6	-4.176530000	1.973208000	-1.959295000
6	-9.426883000	2.639311000	-0.196673000
6	-6.945637000	2.983101000	-0.133330000
6	-10.477718000	0.593901000	-0.869220000
6	-9.220520000	-1.443506000	-1.602834000
6	-7.427348000	-2.616189000	2.338345000
6	-7.336565000	-0.044477000	2.228357000
6	-7.012972000	-3.626862000	1.487391000
6	-5.879191000	-3.628606000	-0.830786000
6	-1.147531000	0.795483000	0.296023000
6	-3.232057000	2.447426000	2.165412000
6	-1.979248000	3.660608000	-0.352608000
6	-3.288316000	1.328727000	-3.026797000
1	-4.056826000	3.075916000	-1.969030000
1	-5.242800000	1.779306000	-2.208250000
1	-9.508642000	3.685184000	0.146355000
6	-10.609018000	1.917219000	-0.414225000
1	-6.042062000	2.349748000	-0.183352000
6	-6.954544000	3.631428000	1.262770000
6	-6.831885000	4.059370000	-1.230852000
1	-11.387434000	0.000887000	-1.063615000
1	-8.159012000	-1.743936000	-1.742524000
6	-9.879329000	-1.541661000	-2.990702000
6	-9.859598000	-2.419686000	-0.599133000

6	-8.073244000	-2.745177000	3.679886000
1	-7.027118000	0.595810000	1.383274000
6	-6.341582000	0.192873000	3.368877000
6	-8.792102000	0.297619000	2.554193000
6	-7.067398000	-5.104655000	1.702122000
1	-5.805546000	-2.784775000	-1.557193000
6	-6.709364000	-4.734798000	-1.486332000
6	-4.453651000	-4.037400000	-0.448607000
6	0.098565000	1.067394000	0.909842000
6	-1.230124000	-0.287697000	-0.601019000
1	-4.257874000	2.856738000	2.060565000
1	-2.595143000	3.211227000	2.655255000
1	-3.292494000	1.548548000	2.805582000
1	-1.610924000	3.513288000	-1.388078000
1	-1.142599000	4.063333000	0.253233000
1	-2.790145000	4.419406000	-0.370364000
1	-3.476463000	0.235592000	-3.070444000
1	-2.212008000	1.483878000	-2.807615000
1	-3.505049000	1.755135000	-4.028560000
6	-11.974827000	2.535353000	-0.146525000
1	-7.823972000	4.307242000	1.405662000
1	-6.037703000	4.239302000	1.414369000
1	-6.986799000	2.868106000	2.066047000
1	-6.813521000	3.603117000	-2.241037000
1	-5.906768000	4.661421000	-1.104869000
1	-7.696596000	4.756447000	-1.197072000
1	-9.817668000	-2.578151000	-3.386255000
1	-9.375664000	-0.866935000	-3.712467000
1	-10.952948000	-1.258907000	-2.956299000
1	-10.936002000	-2.193331000	-0.443700000
1	-9.362801000	-2.368294000	0.390364000
1	-9.793077000	-3.468034000	-0.962033000
1	-9.154743000	-2.496443000	3.642855000
1	-7.606922000	-2.087332000	4.438544000
1	-7.985321000	-3.787812000	4.040699000
1	-6.345606000	1.270215000	3.632081000
1	-5.325234000	-0.073204000	3.020810000
1	-6.590700000	-0.372151000	4.290047000
1	-9.447335000	0.087601000	1.685992000
1	-8.866357000	1.382802000	2.765119000
1	-9.173604000	-0.243601000	3.443225000
1	-7.288416000	-5.320444000	2.764906000
1	-6.106880000	-5.599963000	1.456039000
1	-7.859731000	-5.588972000	1.093300000
1	-7.751994000	-4.398574000	-1.653767000
1	-6.730492000	-5.673773000	-0.898938000
1	-6.269528000	-4.974736000	-2.475373000
1	-4.434898000	-4.853523000	0.303482000
1	-3.911566000	-3.164814000	-0.032808000
1	-3.911482000	-4.394622000	-1.346866000
7	0.146888000	2.139623000	1.872804000
6	1.229876000	0.287952000	0.601096000
6	-0.098823000	-1.067158000	-0.909737000
1	-2.192303000	-0.501599000	-1.089898000
1	-11.797865000	3.595892000	0.142430000
6	-12.674469000	1.840024000	1.038478000
6	-12.866041000	2.535788000	-1.402816000
6	-0.115754000	1.677649000	3.235665000
6	1.331515000	2.981606000	1.799530000
6	1.147276000	-0.795219000	-0.295959000

1	2.192065000	0.501869000	1.089945000
7	-0.147164000	-2.139424000	-1.872684000
1	-13.646005000	2.324669000	1.273483000
1	-12.042087000	1.870693000	1.949451000
1	-12.877284000	0.772270000	0.808385000
1	-13.093701000	1.500419000	-1.734310000
1	-12.368086000	3.054877000	-2.247062000
1	-13.834204000	3.042942000	-1.205435000
1	-1.019228000	1.039536000	3.248894000
1	-0.292726000	2.546852000	3.904629000
1	0.735314000	1.081089000	3.657150000
1	1.495266000	3.303328000	0.752455000
1	2.269224000	2.483338000	2.159839000
1	1.178692000	3.887702000	2.424419000
14	2.558000000	-2.044207000	-0.449999000
6	0.114866000	-1.677362000	-3.235635000
6	-1.331583000	-2.981673000	-1.798999000
7	3.918086000	-1.467001000	0.608056000
6	3.231753000	-2.446371000	-2.165894000
6	1.979420000	-3.660521000	0.351912000
1	1.018249000	-1.039126000	-3.249199000
1	0.291700000	-2.546525000	-3.904687000
1	-0.736448000	-1.080912000	-3.656779000
1	-1.494898000	-3.303445000	-0.751868000
1	-2.269523000	-2.483596000	-2.158965000
1	-1.178787000	-3.887728000	-2.423952000
6	4.176296000	-1.973113000	1.959052000
6	4.687257000	-0.449340000	0.072046000
1	4.257744000	-2.855334000	-2.061382000
1	2.595002000	-3.210281000	-2.655780000
1	3.291712000	-1.547316000	-2.805857000
1	1.610817000	-3.513512000	1.387329000
1	1.143047000	-4.063431000	-0.254182000
1	2.790584000	-4.419032000	0.369723000
6	3.288018000	-1.328769000	3.026579000
1	4.056597000	-3.075824000	1.968655000
1	5.242550000	-1.779228000	2.208102000
32	6.273922000	0.348653000	1.161382000
8	4.281658000	0.106609000	-0.972842000
1	3.476178000	-0.235644000	3.070415000
1	2.211721000	-1.483859000	2.807309000
1	3.504680000	-1.755337000	4.028289000
6	8.015827000	-0.724510000	0.821077000
6	6.662643000	1.640097000	-0.432450000
6	8.146622000	-2.076676000	0.388699000
6	9.220292000	0.002167000	1.082948000
7	7.190802000	1.410334000	-1.668258000
7	6.553115000	2.997092000	-0.325713000
6	9.426577000	-2.639702000	0.196224000
6	6.945297000	-2.983142000	0.132781000
6	10.477703000	-0.594545000	0.869075000
6	9.220793000	1.442925000	1.603002000
6	7.427853000	2.616567000	-2.337859000
6	7.336650000	0.044840000	-2.228380000
6	7.013517000	3.627133000	-1.486758000
6	5.879513000	3.628607000	0.831302000
1	9.508190000	-3.685534000	-0.146967000
6	10.608814000	-1.917809000	0.413874000
1	6.041804000	-2.349683000	0.182848000
6	6.954202000	-3.631219000	-1.263441000

6	6.831334000	-4.059589000	1.230101000
1	11.387504000	-0.001691000	1.063562000
1	8.159327000	1.743464000	1.742784000
6	9.879686000	1.540820000	2.990842000
6	9.859962000	2.419152000	0.599398000
6	8.074002000	2.745736000	-3.679260000
1	7.027212000	-0.595556000	-1.383381000
6	6.341583000	-0.192271000	-3.368883000
6	8.792138000	-0.297348000	-2.554352000
6	7.068222000	5.104961000	-1.701179000
1	5.805842000	2.784700000	1.557620000
6	6.709703000	4.734721000	1.486948000
6	4.453979000	4.037458000	0.449153000
6	11.974536000	-2.536101000	0.146089000
1	7.823557000	-4.307113000	-1.406401000
1	6.037288000	-4.238942000	-1.415215000
1	6.986612000	-2.867750000	-2.066572000
1	6.812915000	-3.603510000	2.240366000
1	5.906166000	-4.661521000	1.103922000
1	7.695970000	-4.756756000	1.196289000
1	9.818208000	2.577278000	3.386505000
1	9.375954000	0.866099000	3.712565000
1	10.953262000	1.257909000	2.956360000
1	10.936327000	2.192652000	0.443892000
1	9.363110000	2.367965000	-0.390082000
1	9.793612000	3.467466000	0.962430000
1	9.155487000	2.496958000	-3.642057000
1	7.607805000	2.088022000	-4.438110000
1	7.986189000	3.788430000	-4.039929000
1	6.345596000	-1.269549000	-3.632352000
1	5.325262000	0.073742000	-3.020688000
1	6.590623000	0.372970000	-4.289938000
1	9.447485000	-0.087304000	-1.686241000
1	8.866309000	-1.382556000	-2.765171000
1	9.173558000	0.243774000	-3.443482000
1	7.289349000	5.320930000	-2.763904000
1	6.107783000	5.600397000	-1.455054000
1	7.860604000	5.589009000	-1.092204000
1	7.752309000	4.398442000	1.654421000
1	6.730906000	5.673725000	0.899599000
1	6.269826000	4.974627000	2.475978000
1	4.435234000	4.853693000	-0.302813000
1	3.911921000	3.164931000	0.033199000
1	3.911779000	4.394543000	1.347448000
1	11.797413000	-3.596536000	-0.143148000
6	12.674375000	-1.840587000	-1.038688000
6	12.865669000	-2.537008000	1.402439000
1	13.645837000	-2.325345000	-1.273761000
1	12.042043000	-1.870903000	-1.949710000
1	12.877370000	-0.772930000	-0.808306000
1	13.093462000	-1.501761000	1.734223000
1	12.367575000	-3.056243000	2.246514000
1	13.833766000	-3.044260000	1.204989000

Table S5. Reaction enthalpies determined with DFT calculations at the BP86-D3(BJ)/def2-TZVPP//BP86-D3(BJ)/def2-SVP level of theory.

Reaction	ΔG (kcal mol^{-1})
1 + CO_2 → **2a**	−5.996
1 + CO_2 → **2a-iso**	5.391
1 + ^{Et}NCO → **2b**	−18.87

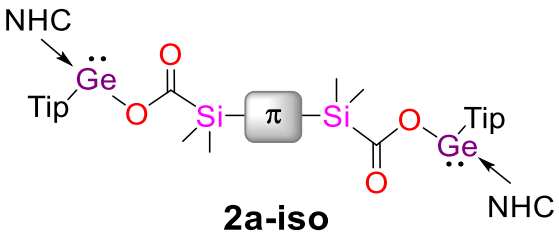

2a-iso

Scheme S1. Structure of the constitutional isomer **2a-iso** with Ge–O and Si–C bonds, which is not formed in the reaction of NHC-bis(germylene) **1** with CO_2 (π = 2,5-(*N*,*N*,*N'*,*N'*-tetramethyldiamino)-*p*-phenylene, Tip = 2,4,6-triisopropylphenyl, NHC = 1,3-diisopropylimidazol-4,5-dimethyl-2-ylidene).

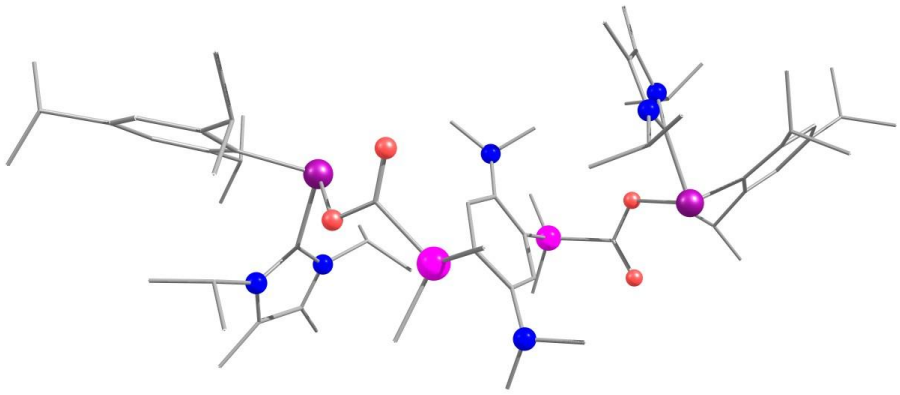

Figure S22. Optimized structure of germylenyl ester **2a-iso** (Gibbs free energy = −5033888.9967 kcal mol^{-1}). Hydrogen atoms omitted for clarity.

Table S6. Atomic coordinates of the optimized structure of the germylenyl ester **2a-iso**.

32	4.457169000	-0.579419000	-0.590818000
6	6.357476000	-1.319876000	-0.870392000
6	5.184676000	1.358504000	-0.129430000
6	6.908592000	-2.415555000	-0.152824000
6	7.144487000	-0.707428000	-1.886947000
7	6.251637000	1.760851000	0.618635000
7	4.609008000	2.502949000	-0.599544000
14	2.086071000	-0.506696000	3.114783000
6	8.260005000	-2.767810000	-0.359517000
6	6.075532000	-3.234461000	0.832132000
6	8.481364000	-1.102299000	-2.082520000

6	6.550750000	0.340807000	-2.832859000
6	6.364010000	3.156630000	0.608154000
6	7.075056000	0.808943000	1.405445000
6	5.320863000	3.629848000	-0.170872000
6	3.330938000	2.485489000	-1.354858000
6	0.892982000	0.340497000	1.899216000
6	3.114476000	0.697723000	4.144609000
6	1.196406000	-1.782820000	4.185690000
1	8.697484000	-3.595268000	0.224994000
6	9.072622000	-2.110779000	-1.298740000
1	5.009343000	-2.970647000	0.678684000
6	6.416599000	-2.898086000	2.295585000
6	6.191480000	-4.747062000	0.567608000
1	9.080114000	-0.608718000	-2.866981000
1	5.502175000	0.529457000	-2.508794000
6	6.460575000	-0.208579000	-4.269538000
6	7.294396000	1.686719000	-2.788425000
6	7.451357000	3.936769000	1.273494000
1	6.702286000	-0.175118000	1.072415000
6	6.772726000	0.932742000	2.900428000
6	8.561589000	0.866879000	1.046082000
6	5.019959000	5.041142000	-0.559964000
1	3.128272000	1.397342000	-1.468458000
6	3.470892000	3.084191000	-2.756725000
6	2.186621000	3.075298000	-0.527882000
6	0.013707000	1.338001000	2.371500000
6	0.805952000	-0.046225000	0.544267000
1	3.979492000	0.169444000	4.597457000
1	2.505096000	1.144851000	4.953672000
1	3.507980000	1.513112000	3.504897000
1	0.805171000	-2.592998000	3.537663000
1	0.356055000	-1.325011000	4.745690000
1	1.895843000	-2.238177000	4.917881000
6	10.537939000	-2.489559000	-1.473369000
1	7.485133000	-3.106360000	2.521533000
1	5.795171000	-3.501577000	2.990481000
1	6.211093000	-1.831977000	2.510972000
1	5.967294000	-4.986583000	-0.492249000
1	5.470734000	-5.301803000	1.204057000
1	7.205909000	-5.139303000	0.795483000
1	5.961597000	0.519176000	-4.944789000
1	5.884972000	-1.155965000	-4.293043000
1	7.469535000	-0.417497000	-4.683602000
1	8.344531000	1.576672000	-3.132313000
1	7.320225000	2.104121000	-1.762366000
1	6.808008000	2.434764000	-3.450258000
1	8.422987000	3.826188000	0.747856000
1	7.605973000	3.627360000	2.325577000
1	7.195028000	5.013466000	1.275728000
1	7.308478000	0.130166000	3.445931000
1	5.688761000	0.798454000	3.071914000
1	7.095435000	1.902849000	3.331111000
1	8.702279000	0.820525000	-0.051192000
1	9.057789000	-0.027065000	1.473377000
1	9.076417000	1.762264000	1.447665000
1	5.625801000	5.736214000	0.051999000
1	3.954984000	5.304892000	-0.408674000
1	5.264932000	5.239169000	-1.624940000
1	4.330686000	2.638031000	-3.295371000
1	3.596638000	4.185150000	-2.743039000

1	2.552053000	2.862735000	-3.335910000
1	2.295856000	4.164942000	-0.354630000
1	2.100970000	2.561615000	0.449933000
1	1.231138000	2.912264000	-1.061172000
7	0.018217000	1.652544000	3.783372000
6	-0.851947000	1.987240000	1.471479000
6	-0.119225000	0.547830000	-0.345243000
1	1.434801000	-0.874170000	0.186801000
1	10.741621000	-3.324078000	-0.765461000
6	11.465784000	-1.318652000	-1.093652000
6	10.834529000	-3.001923000	-2.895700000
6	0.443733000	3.018223000	4.071769000
6	-1.237560000	1.304379000	4.446037000
6	-0.912569000	1.647033000	0.103252000
1	-1.507604000	2.788627000	1.853136000
7	-0.275635000	0.061973000	-1.667856000
1	12.534503000	-1.611675000	-1.169003000
1	11.273756000	-0.975556000	-0.056352000
1	11.307017000	-0.449994000	-1.767794000
1	10.664020000	-2.207030000	-3.652617000
1	10.179968000	-3.858299000	-3.156934000
1	11.891168000	-3.330907000	-2.989520000
1	1.415523000	3.216789000	3.577159000
1	0.581393000	3.143952000	5.167259000
1	-0.284781000	3.799986000	3.730875000
1	-1.494195000	0.249559000	4.223687000
1	-2.107145000	1.936273000	4.130232000
1	-1.119033000	1.408573000	5.545751000
14	-1.993372000	2.820966000	-0.933962000
6	-1.599052000	-0.484886000	-1.962630000
6	0.779987000	-0.783760000	-2.203036000
6	-1.910957000	2.614640000	-2.812653000
6	-1.510926000	4.598493000	-0.500307000
1	-2.395660000	0.095672000	-1.460165000
1	-1.788885000	-0.476391000	-3.056273000
1	-1.686998000	-1.544607000	-1.612276000
1	1.782155000	-0.358089000	-1.997851000
1	0.774565000	-1.821209000	-1.779243000
1	0.649784000	-0.871400000	-3.302092000
1	-2.226313000	3.561042000	-3.298957000
1	-0.875800000	2.373603000	-3.128312000
1	-2.571246000	1.807298000	-3.180480000
1	-1.606020000	4.779462000	0.588303000
1	-0.469762000	4.826307000	-0.809767000
1	-2.191134000	5.307747000	-1.017095000
32	-5.213369000	0.365922000	1.042988000
6	-7.152392000	0.280008000	0.343464000
6	-4.650793000	-1.340159000	-0.093368000
6	-7.809405000	1.341009000	-0.335439000
6	-7.875194000	-0.923646000	0.583643000
7	-4.882207000	-1.684221000	-1.393800000
7	-3.825179000	-2.305935000	0.403209000
6	-9.092782000	1.124404000	-0.882732000
6	-7.168915000	2.719871000	-0.482370000
6	-9.161937000	-1.096850000	0.040583000
6	-7.314115000	-2.025170000	1.488491000
6	-4.200123000	-2.863314000	-1.720253000
6	-5.738186000	-0.871852000	-2.295241000
6	-3.521852000	-3.255822000	-0.577344000
6	-3.298951000	-2.246610000	1.791132000

1	-9.586579000	1.938725000	-1.440453000
6	-9.776969000	-0.093319000	-0.731633000
1	-6.284286000	2.754101000	0.185285000
6	-6.669801000	2.974928000	-1.916228000
6	-8.110466000	3.844070000	-0.011657000
1	-9.702326000	-2.041053000	0.225149000
1	-6.289345000	-1.717261000	1.795838000
6	-8.137134000	-2.130789000	2.787151000
6	-7.192869000	-3.388392000	0.786148000
6	-4.236733000	-3.543843000	-3.049984000
1	-6.151869000	-0.102927000	-1.619043000
6	-4.916784000	-0.148083000	-3.363757000
6	-6.925664000	-1.667050000	-2.845095000
6	-2.628562000	-4.438347000	-0.386042000
1	-3.909591000	-1.438660000	2.252329000
6	-3.554963000	-3.536165000	2.575450000
6	-1.848522000	-1.765021000	1.801655000
6	-11.146901000	-0.310562000	-1.362016000
1	-7.507151000	2.949841000	-2.647203000
1	-6.181411000	3.969810000	-1.990365000
1	-5.922273000	2.214645000	-2.212474000
1	-8.478499000	3.652662000	1.017204000
1	-7.574259000	4.816115000	-0.007999000
1	-8.996701000	3.955384000	-0.672713000
1	-7.690818000	-2.872700000	3.483300000
1	-8.182535000	-1.151413000	3.304891000
1	-9.180143000	-2.448300000	2.576201000
1	-8.185638000	-3.760991000	0.456542000
1	-6.541697000	-3.331347000	-0.108777000
1	-6.766521000	-4.152925000	1.470185000
1	-5.199522000	-4.067596000	-3.226755000
1	-4.084921000	-2.835182000	-3.887206000
1	-3.432573000	-4.302537000	-3.104198000
1	-5.590285000	0.504581000	-3.954185000
1	-4.161330000	0.494225000	-2.875542000
1	-4.413290000	-0.837659000	-4.071582000
1	-7.457678000	-2.192359000	-2.028867000
1	-7.645064000	-0.954527000	-3.295058000
1	-6.638936000	-2.397540000	-3.627761000
1	-2.370588000	-4.874850000	-1.369848000
1	-1.678770000	-4.163900000	0.114455000
1	-3.108079000	-5.238417000	0.215720000
1	-4.602635000	-3.877032000	2.452247000
1	-2.876841000	-4.361952000	2.284515000
1	-3.385582000	-3.338483000	3.652902000
1	-1.156508000	-2.451509000	1.273798000
1	-1.770393000	-0.767656000	1.328214000
1	-1.488028000	-1.672295000	2.844517000
1	-11.412337000	0.633110000	-1.889382000
6	-11.107022000	-1.437223000	-2.413091000
6	-12.232490000	-0.572326000	-0.300444000
1	-12.093729000	-1.560691000	-2.907914000
1	-10.351411000	-1.226835000	-3.197597000
1	-10.841387000	-2.409382000	-1.945650000
1	-12.032300000	-1.513333000	0.254769000
1	-12.273167000	0.251144000	0.441352000
1	-13.234903000	-0.667820000	-0.769089000
8	2.874656000	-2.489638000	1.304222000
6	3.209873000	-1.422070000	1.834080000
8	4.203903000	-0.656415000	1.395252000

8	-4.141778000	3.202048000	0.785604000
8	-4.255716000	1.319447000	-0.466818000
6	-3.718227000	2.482996000	-0.126614000

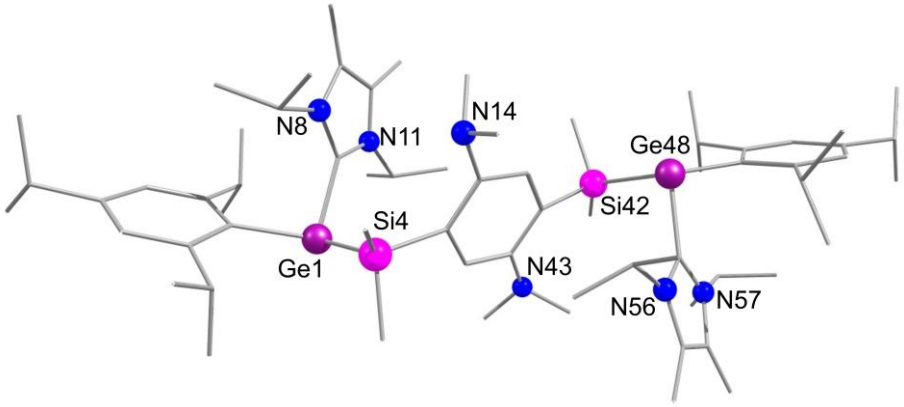

Figure S23. Optimized structure of NHC-bis(germylene) **1** (Gibbs free energy = −4797087.9210 kcal mol^{-1}). Hydrogen atoms omitted for clarity.

Table S7. Atomic coordinates of the optimized structure of NHC-bis(germylene) **1**.

32	4.509271000	0.464519000	-1.074076000
6	6.503024000	0.496047000	-0.552665000
6	4.053644000	-1.198573000	0.085880000
14	3.041977000	1.921093000	0.269773000
6	3.235208000	2.609209000	2.044878000
6	1.386951000	0.982612000	0.055536000
6	2.834987000	3.515944000	-0.776593000
7	4.475145000	-1.561991000	1.337717000
6	4.026631000	-2.849445000	1.655887000
6	5.228996000	-0.641716000	2.226952000
7	3.320868000	-2.259917000	-0.375138000
6	3.290522000	-3.290645000	0.569012000
6	2.672946000	-2.261390000	-1.712113000
7	1.147855000	0.094990000	2.383370000
6	0.536681000	1.042935000	3.312285000
6	0.658496000	0.255107000	1.027455000
6	1.049691000	-1.274529000	2.880709000
6	7.171560000	1.592441000	0.066443000
6	7.297048000	-0.628679000	-0.931277000
6	8.540957000	1.500072000	0.389192000
6	6.447083000	2.909299000	0.307140000
6	9.307099000	0.362567000	0.085187000
6	8.666567000	-0.680952000	-0.603959000
6	10.772317000	0.267031000	0.489755000
6	6.719962000	-1.804291000	-1.719442000
6	6.548496000	3.797005000	-0.949298000
6	6.885422000	3.667061000	1.567643000
6	6.751320000	-3.125188000	-0.930841000
6	7.405237000	-1.948922000	-3.090428000
6	4.275531000	-3.561407000	2.945779000
6	2.546521000	-4.578160000	0.420336000
6	6.673752000	-1.090764000	2.461363000
6	4.455533000	-0.360807000	3.518234000
6	3.396753000	-3.181635000	-2.700630000
6	1.171838000	-2.534962000	-1.621486000
6	0.832391000	1.033499000	-1.246160000

6	-0.397319000	0.435397000	-1.603875000
6	-1.137224000	-0.284245000	-0.619598000
6	-0.578791000	-0.323059000	0.676605000
6	11.696769000	0.069132000	-0.726434000
6	10.985409000	-0.839025000	1.542530000
1	9.038758000	2.346516000	0.890619000
1	9.248570000	-1.573230000	-0.890805000
1	5.375520000	2.645146000	0.430182000
1	6.220330000	4.537795000	1.747273000
1	7.918881000	4.065055000	1.480558000
1	6.849128000	3.016733000	2.466244000
1	5.984298000	4.745347000	-0.820201000
1	6.142117000	3.272449000	-1.837995000
1	7.608372000	4.053328000	-1.162892000
1	5.657457000	-1.552460000	-1.923729000
1	6.924174000	-2.750578000	-3.691589000
1	8.479660000	-2.210636000	-2.986097000
1	7.342379000	-1.001927000	-3.664079000
1	6.280011000	-3.947493000	-1.510093000
1	6.211463000	-3.038519000	0.032575000
1	7.793968000	-3.434795000	-0.704083000
1	5.259865000	0.294040000	1.634026000
1	7.219330000	-0.278283000	2.981377000
1	7.195080000	-1.274807000	1.504145000
1	6.741183000	-1.999194000	3.094551000
1	4.919375000	0.503509000	4.034061000
1	4.474786000	-1.214897000	4.223775000
1	3.404993000	-0.104033000	3.275510000
1	4.071547000	-4.642547000	2.822440000
1	3.618419000	-3.191971000	3.761484000
1	5.323420000	-3.455302000	3.285776000
1	2.877351000	-5.292484000	1.198508000
1	2.718998000	-5.053536000	-0.565084000
1	1.450817000	-4.441856000	0.538097000
1	2.820560000	-1.212189000	-2.051986000
1	2.910442000	-3.098704000	-3.693559000
1	3.353029000	-4.247317000	-2.395757000
1	4.457894000	-2.892760000	-2.817401000
1	0.674116000	-2.172285000	-2.542503000
1	0.719710000	-1.988934000	-0.774191000
1	0.939220000	-3.613880000	-1.522284000
1	1.892078000	4.040156000	-0.508963000
1	2.823718000	3.310069000	-1.866330000
1	3.677450000	4.211801000	-0.582961000
1	2.416653000	3.334357000	2.244051000
1	4.191474000	3.159991000	2.147936000
1	3.196404000	1.824242000	2.818278000
1	1.382937000	1.592974000	-2.015185000
1	-1.135475000	-0.860872000	1.461002000
1	1.493337000	-1.969206000	2.140711000
1	0.003431000	-1.611479000	3.098061000
1	1.623475000	-1.364364000	3.828211000
1	0.659249000	2.074753000	2.932000000
1	1.040092000	0.983546000	4.301442000
1	-0.558570000	0.854654000	3.468023000
1	11.040509000	1.238483000	0.962979000
1	12.764317000	0.061416000	-0.419959000
1	11.555491000	0.877614000	-1.472481000
1	10.341186000	-0.674591000	2.430600000
1	10.731176000	-1.837045000	1.126059000

1	12.042577000	-0.874371000	1.882016000
1	11.489229000	-0.895823000	-1.235802000
14	-2.699836000	-1.383933000	-0.815802000
7	-0.880616000	0.545886000	-2.937302000
6	-2.140658000	1.258797000	-3.079420000
6	0.073841000	0.899067000	-3.972854000
1	0.990883000	0.284793000	-3.877973000
1	0.381243000	1.977682000	-3.957661000
1	-0.380222000	0.698917000	-4.966211000
1	-2.008907000	2.371681000	-3.022231000
1	-2.609109000	1.021679000	-4.057946000
1	-2.839797000	0.965246000	-2.275669000
6	-2.185374000	-3.061601000	-0.044369000
6	-3.049792000	-1.814818000	-2.650185000
1	-3.440862000	-2.851441000	-2.709854000
1	-3.789451000	-1.151606000	-3.136151000
1	-2.105461000	-1.753999000	-3.229298000
1	-1.859080000	-2.949637000	1.009278000
1	-1.352104000	-3.514322000	-0.621893000
1	-3.035116000	-3.773391000	-0.057624000
32	-4.142927000	-0.286264000	0.838713000
6	-4.335575000	1.441459000	-0.296291000
6	-6.142307000	-0.764750000	0.827498000
6	-6.978868000	0.060750000	1.640479000
6	-6.749722000	-1.878316000	0.175515000
6	-8.361133000	-0.201959000	1.737899000
6	-8.134902000	-2.105414000	0.294711000
6	-8.967659000	-1.271191000	1.060838000
1	-8.995350000	0.457155000	2.355589000
1	-8.579924000	-2.966404000	-0.231802000
7	-3.657612000	2.598685000	-0.009134000
7	-5.201216000	1.772719000	-1.312159000
6	-4.103089000	3.650977000	-0.813385000
6	-5.084986000	3.129422000	-1.638254000
6	-3.572380000	5.047871000	-0.786205000
1	-4.262022000	5.719626000	-1.332567000
1	-3.471090000	5.439452000	0.244796000
1	-2.577702000	5.126357000	-1.272862000
6	-5.867818000	3.836638000	-2.697324000
1	-6.941364000	3.567342000	-2.671102000
1	-5.795441000	4.931142000	-2.547344000
1	-5.491700000	3.618968000	-3.719316000
6	-6.063241000	0.774461000	-1.992331000
1	-5.722869000	-0.179313000	-1.544943000
6	-5.807619000	0.714577000	-3.503367000
6	-7.547669000	0.947744000	-1.658867000
1	-7.712275000	0.966783000	-0.566646000
1	-7.975659000	1.867048000	-2.108754000
1	-8.110199000	0.081398000	-2.059744000
1	-6.275943000	1.554838000	-4.052222000
1	-6.248510000	-0.221812000	-3.900217000
1	-4.725915000	0.701128000	-3.732394000
6	-2.625030000	2.671374000	1.057580000
1	-2.473632000	1.604110000	1.327858000
6	-3.158442000	3.389132000	2.301163000
6	-1.293089000	3.223637000	0.549796000
1	-0.986845000	2.727273000	-0.390243000
1	-1.304835000	4.320768000	0.399290000
1	-0.506710000	2.998868000	1.295201000
1	-3.376879000	4.460737000	2.114839000

1	-2.398014000	3.335473000	3.106081000
1	-4.080503000	2.900335000	2.669954000
6	-6.435091000	1.263447000	2.414719000
1	-5.325748000	1.215541000	2.328043000
6	-6.760364000	1.182994000	3.916247000
6	-6.896766000	2.600787000	1.806688000
1	-6.586878000	2.696133000	0.746927000
1	-8.003273000	2.697822000	1.841623000
1	-6.468536000	3.461839000	2.363055000
1	-7.851865000	1.253323000	4.110268000
1	-6.272163000	2.014170000	4.468694000
1	-6.401558000	0.225987000	4.346868000
6	-5.937761000	-2.876827000	-0.641558000
1	-4.935286000	-2.418273000	-0.776523000
6	-6.513474000	-3.137606000	-2.042910000
6	-5.746222000	-4.188625000	0.141555000
1	-5.275691000	-3.996361000	1.127061000
1	-6.722296000	-4.686081000	0.327773000
1	-5.103818000	-4.901910000	-0.417954000
1	-7.502294000	-3.641495000	-2.000934000
1	-5.835509000	-3.791327000	-2.630530000
1	-6.644151000	-2.192392000	-2.608938000
6	-10.470349000	-1.506380000	1.140703000
1	-10.878953000	-0.746350000	1.844153000
6	-10.808203000	-2.897777000	1.708788000
6	-11.140039000	-1.281122000	-0.229611000
1	-10.922555000	-0.264990000	-0.618230000
1	-10.767852000	-2.012495000	-0.978410000
1	-12.242619000	-1.398625000	-0.163281000
1	-10.440066000	-3.704843000	1.040371000
1	-11.905727000	-3.029017000	1.816844000
1	-10.341067000	-3.048453000	2.703389000

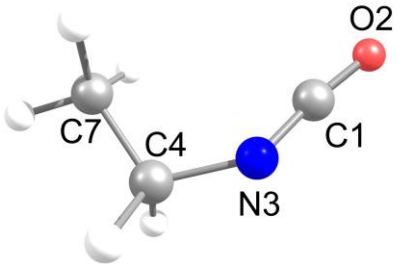

Figure S24. Optimized structure of ^{Et}NCO (Gibbs free energy = −155229.1075 kcal mol^{-1}).

Table S8. Atomic coordinates of the optimized structure of ^{Et}NCO.

6	-1.223249000	0.081888000	0.013500000
8	-2.296363000	-0.423519000	-0.046745000
7	-0.193252000	0.712526000	0.135146000
6	1.228266000	0.629727000	-0.087488000
1	1.458584000	1.056188000	-1.090406000
1	1.725987000	1.297177000	0.648406000
6	1.785809000	-0.792202000	0.025502000
1	1.327459000	-1.460226000	-0.732890000
1	1.583262000	-1.218411000	1.029259000
1	2.883412000	-0.790743000	-0.135512000

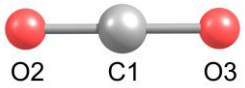

Figure S25. Optimized structure of CO_2 (Gibbs free energy = −118403.2332 kcal mol^{-1}).

Table S9. Atomic coordinates of the optimized structure of CO_2.

6	0.000000000	0.000000000	0.000000000
8	0.000000000	0.000000000	1.175202000
8	0.000000000	0.000000000	-1.175202000

- **Germylene radical 3**

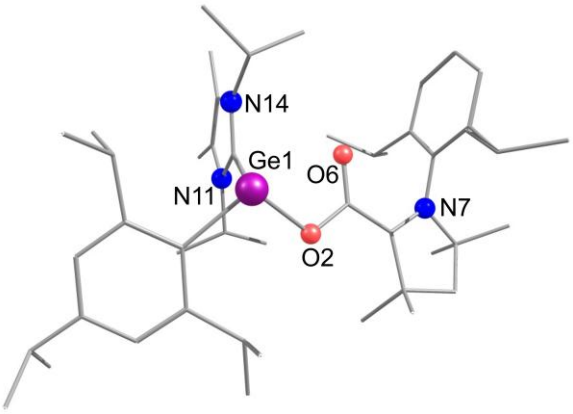

Figure S26. Optimized structure of germylene radical **3**. Hydrogen atoms omitted for clarity.

Table S10. Atomic coordinates of the optimized structure of germylene radical **3**.

32	1.146128000	0.111771000	-1.586309000
8	-0.020748000	-1.116680000	-0.557868000
6	3.008907000	-0.474674000	-0.863791000
6	0.919388000	1.571835000	-0.057362000
6	-1.258155000	-0.675912000	-0.368038000
8	-1.571850000	0.508928000	-0.588798000
7	-3.501253000	-1.307810000	0.441407000
6	-2.207016000	-1.649840000	0.110125000
6	-4.167051000	-0.103781000	0.035745000
6	-4.223192000	-2.437582000	1.101089000
7	1.186038000	1.485181000	1.267031000
6	0.967062000	2.717423000	1.889220000
6	1.533783000	0.206126000	1.924611000
7	0.515054000	2.844437000	-0.277958000
6	0.540421000	3.577287000	0.909884000
6	-0.022063000	3.281822000	-1.586687000
6	-1.968684000	-3.138755000	0.296576000
6	-1.449156000	-3.791425000	-0.998732000
6	-0.979125000	-3.432097000	1.441193000
6	-3.398511000	-3.649357000	0.617592000
6	-5.684126000	-2.523590000	0.657880000
6	-4.180188000	-2.303569000	2.633242000
6	-4.291762000	0.979213000	0.931192000

6	-4.695445000	-0.026459000	-1.274116000
6	-5.405050000	1.122859000	-1.641338000
6	-4.429162000	-1.102332000	-2.317048000
6	-5.583595000	2.176949000	-0.747614000
6	-5.018071000	2.105527000	0.522709000
6	-3.557150000	1.019496000	2.261782000
6	-4.489528000	1.286706000	3.450453000
6	-2.419914000	2.052370000	2.204563000
6	-3.344170000	-0.627347000	-3.300069000
6	-5.693286000	-1.544427000	-3.066318000
6	1.214825000	3.005705000	3.331503000
6	0.203546000	5.025235000	1.031227000
6	0.399845000	-0.288779000	2.822257000
6	2.898371000	0.246093000	2.606635000
6	-1.535231000	3.498914000	-1.532619000
6	0.754062000	4.461933000	-2.168803000
6	4.016214000	0.518428000	-0.895466000
6	3.378310000	-1.775200000	-0.424470000
6	4.671685000	-2.011361000	0.056462000
6	2.404301000	-2.943078000	-0.535854000
6	5.649657000	-1.010009000	0.091970000
6	5.306066000	0.241951000	-0.412861000
6	7.031932000	-1.275730000	0.663138000
6	3.775318000	1.913570000	-1.471738000
6	3.997574000	3.024335000	-0.435703000
6	4.619892000	2.147902000	-2.733170000
6	2.661871000	-4.095420000	0.439047000
6	2.374602000	-3.456707000	-1.985871000
6	7.762338000	-2.399539000	-0.086066000
6	6.963447000	-1.565382000	2.170714000
1	-3.856878000	-4.044716000	-0.301608000
1	-3.395431000	-4.463606000	1.356620000
1	-6.244885000	-1.623305000	0.948001000
1	-6.157030000	-3.392591000	1.140275000
1	-5.772387000	-2.647958000	-0.428499000
1	-3.152914000	-2.173852000	2.999122000
1	-4.597443000	-3.210672000	3.097343000
1	-4.777808000	-1.447636000	2.972123000
1	-2.126524000	-3.580605000	-1.840740000
1	-1.384788000	-4.885459000	-0.875198000
1	-0.457087000	-3.405927000	-1.259779000
1	-0.002373000	-2.983811000	1.221706000
1	-0.842579000	-4.519323000	1.560899000
1	-1.332610000	-3.026083000	2.399278000
1	-5.817421000	1.198162000	-2.649621000
1	-6.146638000	3.063549000	-1.049796000
1	-5.121911000	2.951678000	1.205798000
1	-3.087945000	0.038700000	2.406746000
1	-2.813857000	3.073694000	2.075523000
1	-1.754738000	1.833464000	1.360930000
1	-1.832249000	2.035443000	3.136501000
1	-4.929361000	2.295574000	3.397338000
1	-3.935982000	1.218799000	4.401146000
1	-5.322516000	0.567839000	3.488180000
1	-4.029485000	-1.980915000	-1.794283000
1	-3.716921000	0.210081000	-3.912926000
1	-3.053480000	-1.442323000	-3.982916000
1	-2.451712000	-0.275572000	-2.765868000
1	-6.104052000	-0.732516000	-3.687047000
1	-6.487381000	-1.867348000	-2.375255000

1	-5.463474000	-2.384590000	-3.741106000
1	0.815017000	3.995717000	3.586775000
1	2.289953000	3.009754000	3.571555000
1	0.730638000	2.274099000	3.992501000
1	0.965012000	5.666444000	0.559085000
1	0.146439000	5.306511000	2.090829000
1	-0.765293000	5.264983000	0.572405000
1	1.608183000	-0.496304000	1.092572000
1	0.265564000	0.325965000	3.724083000
1	0.626940000	-1.313821000	3.149395000
1	-0.549022000	-0.313501000	2.270137000
1	3.664780000	0.619035000	1.913352000
1	3.183983000	-0.778234000	2.887868000
1	2.902876000	0.858466000	3.520064000
1	0.153880000	2.411486000	-2.234886000
1	0.446540000	4.612004000	-3.214679000
1	1.836745000	4.270287000	-2.158591000
1	0.561356000	5.401994000	-1.632389000
1	-1.814723000	4.376129000	-0.929896000
1	-2.029222000	2.605240000	-1.132050000
1	-1.906659000	3.670892000	-2.554697000
1	4.931674000	-3.009312000	0.412389000
1	6.066942000	1.027946000	-0.425822000
1	2.726374000	1.976084000	-1.796880000
1	3.754178000	4.013199000	-0.857488000
1	5.048463000	3.057356000	-0.107277000
1	3.373636000	2.872884000	0.456481000
1	4.388664000	3.127724000	-3.183433000
1	4.423117000	1.368763000	-3.485080000
1	5.697453000	2.129670000	-2.504525000
1	1.406401000	-2.550168000	-0.316529000
1	2.732616000	-3.739117000	1.479302000
1	3.588884000	-4.644653000	0.207047000
1	1.835113000	-4.821286000	0.388134000
1	2.099305000	-2.654157000	-2.687410000
1	1.642633000	-4.272892000	-2.100641000
1	3.364708000	-3.838593000	-2.285770000
1	7.618864000	-0.350388000	0.528777000
1	7.971813000	-1.699868000	2.595725000
1	6.390021000	-2.485541000	2.369390000
1	6.468911000	-0.742273000	2.709830000
1	7.829264000	-2.179951000	-1.162749000
1	7.236002000	-3.361245000	0.026140000
1	8.784931000	-2.532791000	0.303499000

References

[S1] A.-L. Thömmes, B. Morgenstern, M. Zimmer, D. M. Andrada, D. Scheschkewitz, *Chem. Eur. J.* **2023**, *29*, e202301273.

[S2] N. Kuhn, T. Kratz, *Synthesis* **1993**, *1993*, 561.

[S3] Synthesized via a procedure described in a) C. Müller, D. M. Andrada, I.-A. Bischoff, M. Zimmer, V. Huch, N. Steinbrück, A. Schäfer, *Organometallics* **2019**, *38*, 1052. This procedure is a modified version of the original synthesis described in b) V. Lavallo, Y. Canac, C. Präsang, B. Donnadieu, G. Bertrand, *Angew. Chem. Int. Ed.* **2005**, *44*, 5705-5709; *Angew. Chem.* **2005**, *117*, 5851-5855. The chloride anion of the iminium salt was exchanged by tetrafluoroborate for purification purposes according to c) C. M. Weinstein, G. P. Junor, D. R. Tolentino, R. Jazzar, M. Melaimi, G. Bertrand, *J. Am. Chem. Soc.* **2018**, *140*, 9255.

[S4] G. R. Fulmer, A. J. M. Miller, N. H. Sherden, H. E. Gottlieb, A. Nudelman, B. M. Stoltz, J. E. Bercaw, K. I. Goldberg, *Organometallics* **2010**, *29*, 2176.

[S5] S. Stoll, A. Schweiger, *J. Magn. Reson.* **2006**, *178*, 42.

[S6] The Mathworks Inc. (2024), version R2024a 24.1.0.2537033, Natick, Massachusetts.

[S7] G. M. Sheldrick, *Acta Crystallogr. A* **2008**, *64*, 112.

[S8] G. M. Sheldrick, *Acta Crystallogr. A* **2015**, 71, 3.

[S9] C. B. Hübschle, G. M. Sheldrick, B. Dittrich, *J. Appl. Crystallogr.* **2011**, *44*, 1281.

[S10] M. J. Frisch, G. W. Trucks, H. B. Schlegel, G. E. Scuseria, M. A. Robb, J. R. Cheeseman, G. Scalmani, V. Barone, B. Mennucci, G. A. Petersson, H. Nakatsuji, M. Caricato, X. Li, H. P. Hratchian, A. F. Izmaylov, J. Bloino, G. Zheng, J. L. Sonnenberg, M. Hada, M. Ehara, K. Toyota, R. Fukuda, J. Hasegawa, M. Ishida, T. Nakajima, Y. Honda, O. Kitao, H. Nakai, T. Vreven, J. J. A. Montgomery, J. E. Peralta, F. Ogliaro, M. Bearpark, J. J. Heyd, E. Brothers, K. N. Kudin, V. N. Staroverov, R. Kobayashi, J. Normand, K. Raghavachari, A. Rendell, J. C. Burant, S. S. Iyengar, J. Tomasi, M. Cossi, N. Rega, J. M. Millam, M. Klene, J. E. Knox, J. B. Cross, V. Bakken, C. Adamo, J. Jaramillo, R. Gomperts, R. E. Stratmann, O. Yazyev, A. J. Austin, R. Cammi, C. Pomelli, J. W. Ochterski, R. L. Martin, K. Morokuma, V. G. Zakrzewski, G. A. Voth, P. Salvador, J. J. Dannenberg, S. Dapprich, A. D. Daniels, O. Farkas, J. B. Foresman, J. V. Ortiz, J. Cioslowski, D. J. Fox, Gaussian 16, Revision C.01. Gaussian, Inc., Wallingford CT, **2016**.

[S11] a) J. P. Perdew, *Phys. Rev. B* **1986**, *33*, 8822; b) A. D. Becke, *Phys. Rev. A* **1988**, *38*, 3098.

[S12] a) A. Schäfer, H. Horn, R. Ahlrichs, *J. Chem. Phys.* **1992**, *97*, 2571; b) A. Schäfer, C. Huber, R. Ahlrichs, *J. Chem. Phys.* **1994**, *100*, 5829; c) F. Weigend, R. Ahlrichs, *Phys. Chem. Chem. Phys.* **2005**, *7*, 3297; d) F. Weigend, *Phys. Chem. Chem. Phys.* **2006**, *8*, 1057.

[S13] a) C. Lee, W. Yang, and R. G. Parr, *Phys. Rev. B* **1988**, *37*, 785; b) A. D. Becke, *J. Chem. Phys.* **1993**, *98*, 5648.

[S14] a) S. Grimme, J. Antony, S. Ehrlich, H. Krieg, *J. Chem. Phys.* **2010**, *132*, 154104; b) S. Grimme, S. Ehrlich, L. Goerigk, *J. Comput. Chem.* **2011**, *32*, 1456.

[S15] F. Neese, F. Wennmohs, U. Becker, C. Riplinger, *J. Chem. Phys.* **2020**, *152*, 224108.

[S16] Chemcraft - graphical software for visualization of quantum chemistry computations. https://www.chemcraftprog.com

[S17] a) B. R. Van Ausdall, J. L. Glass, K. M. Wiggins, A. M. Aarif, J. Louie, *J. Org. Chem.* **2009**, *74*, 7935; b) X. Wang, J. Zhang, L. Wang, L. Deng, *Organometallics* **2015**, *34*, 2775.

[S18] L. Klemmer, A.-L. Thömmes, M. Zimmer, V. Huch, B. Morgenstern, D. Scheschkewitz, *Nat. Chem.* **2020**, *13*, 373.

[S19] K. Chernichenko, B. Kótai, M. Nieger, S. Heikkinen, I. Pápai, T. Repo, *Dalton Trans.* **2017**, *46*, 2263.

[S20] F. P. Gasparro, N. H. Kolodny, *J. Chem. Educ.* **1977**, *54*, 258.

[S21] H. Eyring, *Chem. Rev.* **1935**, *17*, 65.

[S22] Deposition numbers CCDC 2427550 (**2b**) and 2427551 (**3**) contain the supplementary crystallographic data for this paper. These data are provided free of charge by the joint Cambridge Crystallographic Data Centre and Fachinformationszentrum Karlsruhe Access Structures service.